IAEA TECDOC SERIES

IAEA-TECDOC-1857

IAEA-TECDOC-1857

Unconformity-related Uranium Deposits

IAEA
International Atomic Energy Agency

UNCONFORMITY-RELATED URANIUM DEPOSITS

The following States are Members of the International Atomic Energy Agency:

AFGHANISTAN
ALBANIA
ALGERIA
ANGOLA
ANTIGUA AND BARBUDA
ARGENTINA
ARMENIA
AUSTRALIA
AUSTRIA
AZERBAIJAN
BAHAMAS
BAHRAIN
BANGLADESH
BARBADOS
BELARUS
BELGIUM
BELIZE
BENIN
BOLIVIA, PLURINATIONAL STATE OF
BOSNIA AND HERZEGOVINA
BOTSWANA
BRAZIL
BRUNEI DARUSSALAM
BULGARIA
BURKINA FASO
BURUNDI
CAMBODIA
CAMEROON
CANADA
CENTRAL AFRICAN REPUBLIC
CHAD
CHILE
CHINA
COLOMBIA
CONGO
COSTA RICA
CÔTE D'IVOIRE
CROATIA
CUBA
CYPRUS
CZECH REPUBLIC
DEMOCRATIC REPUBLIC OF THE CONGO
DENMARK
DJIBOUTI
DOMINICA
DOMINICAN REPUBLIC
ECUADOR
EGYPT
EL SALVADOR
ERITREA
ESTONIA
ESWATINI
ETHIOPIA
FIJI
FINLAND
FRANCE
GABON
GEORGIA
GERMANY
GHANA
GREECE
GRENADA
GUATEMALA
GUYANA
HAITI
HOLY SEE
HONDURAS
HUNGARY
ICELAND
INDIA
INDONESIA
IRAN, ISLAMIC REPUBLIC OF
IRAQ
IRELAND
ISRAEL
ITALY
JAMAICA
JAPAN
JORDAN
KAZAKHSTAN
KENYA
KOREA, REPUBLIC OF
KUWAIT
KYRGYZSTAN
LAO PEOPLE'S DEMOCRATIC REPUBLIC
LATVIA
LEBANON
LESOTHO
LIBERIA
LIBYA
LIECHTENSTEIN
LITHUANIA
LUXEMBOURG
MADAGASCAR
MALAWI
MALAYSIA
MALI
MALTA
MARSHALL ISLANDS
MAURITANIA
MAURITIUS
MEXICO
MONACO
MONGOLIA
MONTENEGRO
MOROCCO
MOZAMBIQUE
MYANMAR
NAMIBIA
NEPAL
NETHERLANDS
NEW ZEALAND
NICARAGUA
NIGER
NIGERIA
NORWAY
OMAN
PAKISTAN
PALAU
PANAMA
PAPUA NEW GUINEA
PARAGUAY
PERU
PHILIPPINES
POLAND
PORTUGAL
QATAR
REPUBLIC OF MOLDOVA
ROMANIA
RUSSIAN FEDERATION
RWANDA
SAINT VINCENT AND THE GRENADINES
SAN MARINO
SAUDI ARABIA
SENEGAL
SERBIA
SEYCHELLES
SIERRA LEONE
SINGAPORE
SLOVAKIA
SLOVENIA
SOUTH AFRICA
SPAIN
SRI LANKA
SUDAN
SWEDEN
SWITZERLAND
SYRIAN ARAB REPUBLIC
TAJIKISTAN
THAILAND
THE FORMER YUGOSLAV REPUBLIC OF MACEDONIA
TOGO
TRINIDAD AND TOBAGO
TUNISIA
TURKEY
TURKMENISTAN
UGANDA
UKRAINE
UNITED ARAB EMIRATES
UNITED KINGDOM OF GREAT BRITAIN AND NORTHERN IRELAND
UNITED REPUBLIC OF TANZANIA
UNITED STATES OF AMERICA
URUGUAY
UZBEKISTAN
VANUATU
VENEZUELA, BOLIVARIAN REPUBLIC OF
VIET NAM
YEMEN
ZAMBIA
ZIMBABWE

The Agency's Statute was approved on 23 October 1956 by the Conference on the Statute of the IAEA held at United Nations Headquarters, New York; it entered into force on 29 July 1957. The Headquarters of the Agency are situated in Vienna. Its principal objective is "to accelerate and enlarge the contribution of atomic energy to peace, health and prosperity throughout the world".

IAEA-TECDOC-1857

UNCONFORMITY-RELATED URANIUM DEPOSITS

INTERNATIONAL ATOMIC ENERGY AGENCY
VIENNA, 2018

COPYRIGHT NOTICE

All IAEA scientific and technical publications are protected by the terms of the Universal Copyright Convention as adopted in 1952 (Berne) and as revised in 1972 (Paris). The copyright has since been extended by the World Intellectual Property Organization (Geneva) to include electronic and virtual intellectual property. Permission to use whole or parts of texts contained in IAEA publications in printed or electronic form must be obtained and is usually subject to royalty agreements. Proposals for non-commercial reproductions and translations are welcomed and considered on a case-by-case basis. Enquiries should be addressed to the IAEA Publishing Section at:

Marketing and Sales Unit, Publishing Section
International Atomic Energy Agency
Vienna International Centre
PO Box 100
1400 Vienna, Austria
fax: +43 1 26007 22529
tel.: +43 1 2600 22417
email: sales.publications@iaea.org
www.iaea.org/books

For further information on this publication, please contact:

Nuclear Fuel Cycle and Materials Section
International Atomic Energy Agency
Vienna International Centre
PO Box 100
1400 Vienna, Austria
Email: Official.Mail@iaea.org

© IAEA, 2018
Printed by the IAEA in Austria
November 2018

IAEA Library Cataloguing in Publication Data

Names: International Atomic Energy Agency.
Title: Unconformity-related uranium deposits / International Atomic Energy Agency.
Description: Vienna : International Atomic Energy Agency, 2018. | Series: IAEA TECDOC series, ISSN 1011–4289 ; no. 1857 | Includes bibliographical references.
Identifiers: IAEAL 18-01202 | ISBN 978–92–0–108518–4 (paperback : alk. paper)
Subjects: LCSH: Uranium ores — Geology. | Unconformities (Geology) | Geology, Stratigraphic

FOREWORD

Unconformity related uranium deposits are high grade and have among the largest uranium inventories in the world. Historically these deposits have been significant sources of production, and they currently account for around 25% of total world uranium production.

The principal objective of this publication is to provide a summary technical report on unconformity related uranium deposits, including the geology, mineralogy, metallurgy, mining methods, resources, genesis, exploration techniques and exploration strategies and other topics useful for evaluation. The information included in this report will enable users to evaluate the potential to discover and exploit unconformity related deposits.

The targeted audience includes, but is not limited to, decision makers at all levels, government officials in energy and mineral resources, exploration companies, geologists, geological surveys, energy companies, universities and research institutions, and natural resource authorities.

The IAEA acknowledges the contributions of the experts who participated in the consultancy meetings for the planning and editing of this publication, and in particular the contributions of the late K. Kyser (Canada).

The IAEA officer responsible for this publication was A. Hanly of the Division of Nuclear Fuel Cycle and Waste Technology.

EDITORIAL NOTE

This publication has been prepared from the original material as submitted by the contributors and has not been edited by the editorial staff of the IAEA. The views expressed remain the responsibility of the contributors and do not necessarily represent the views of the IAEA or its Member States.

Neither the IAEA nor its Member States assume any responsibility for consequences which may arise from the use of this publication. This publication does not address questions of responsibility, legal or otherwise, for acts or omissions on the part of any person.

The use of particular designations of countries or territories does not imply any judgement by the publisher, the IAEA, as to the legal status of such countries or territories, of their authorities and institutions or of the delimitation of their boundaries.

The mention of names of specific companies or products (whether or not indicated as registered) does not imply any intention to infringe proprietary rights, nor should it be construed as an endorsement or recommendation on the part of the IAEA.

The authors are responsible for having obtained the necessary permission for the IAEA to reproduce, translate or use material from sources already protected by copyrights.

The IAEA has no responsibility for the persistence or accuracy of URLs for external or third party Internet web sites referred to in this publication and does not guarantee that any content on such web sites is, or will remain, accurate or appropriate.

CONTENTS

1. INTRODUCTION

1.1. BACKGROUND

Unconformity-related uranium deposits made up 25% of the total production of uranium in 2016 [1.1], and hence can be considered a significant resource of uranium. In marked contrast to most other deposit types of uranium, unconformity-related ores are both high grade and have among the largest uranium inventories (570 000 tU at a cost <US $260/kg in 2015 [1.2]; Fig. 1.1). While their high grade and significant inventory makes them a highly strategic resource — especially given their low mining cost compared to other deposit types — explorating for these deposits is challenging as they are associated with basal units of Proterozoic basins normally in the subsurface.

Proterozoic unconformity deposits occur below, along or above the unconformable contact between an Archean to Paleoproterozoic crystalline basement with highly reducing lithologic units and oxidized siliciclastic sediments (red beds) of Proterozoic age. The basement rocks immediately below the unconformity are haematized, chlortized and argillized in a transition zone with the fresh basement. This alteration has been attributed to paleoweathering and diagenetic/hydrothermal alteration.

Deposits consist of lenses, pods or veins of massive uranium dioxide commonly with associated strong quartz dissolution and intensive clay alteration. They are mainly found in two major areas — the Athabasca Basin in Canada and the East Alligator River district in Australia. Three sub-types are distinguished by the IAEA uranium deposit classification scheme [1.3]: 1) unconformity-contact deposits such as Cigar Lake that essentially occur in the Athabasca Basin in Canada; 2) basement-hosted deposits such as Ranger and Jabiluka in Australia, Eagle Point, Millennium, the lower pod of Kianna and Arrow in the Athabasca Basin, and Kiggavik and Andrew Lake in the Thelon Basin in Canada; and, 3) stratiform structure-controlled deposits only known in India at Chitrial and Lambapur in the Cuddapah Basin [1.4]. The resources range from medium to large, with very high grades for the Canadian deposits to low grades for the Indian deposits. A recently proposed classification with four end–members, based on lithostructural characteristics, is described in Chapter 2.

An International Atomic Energy Agency (IAEA) publication with reference to unconformity-related deposits was published as TECDOC-315 in 1984, titled “Proterozoic unconformity and stratabound uranium”, edited by J. Ferguson [1.5]. Given the extensive research and exploration that has occurred subsequently for these types of deposits, an update is well overdue on what is now known about their characteristics, formation, evolution and exploration

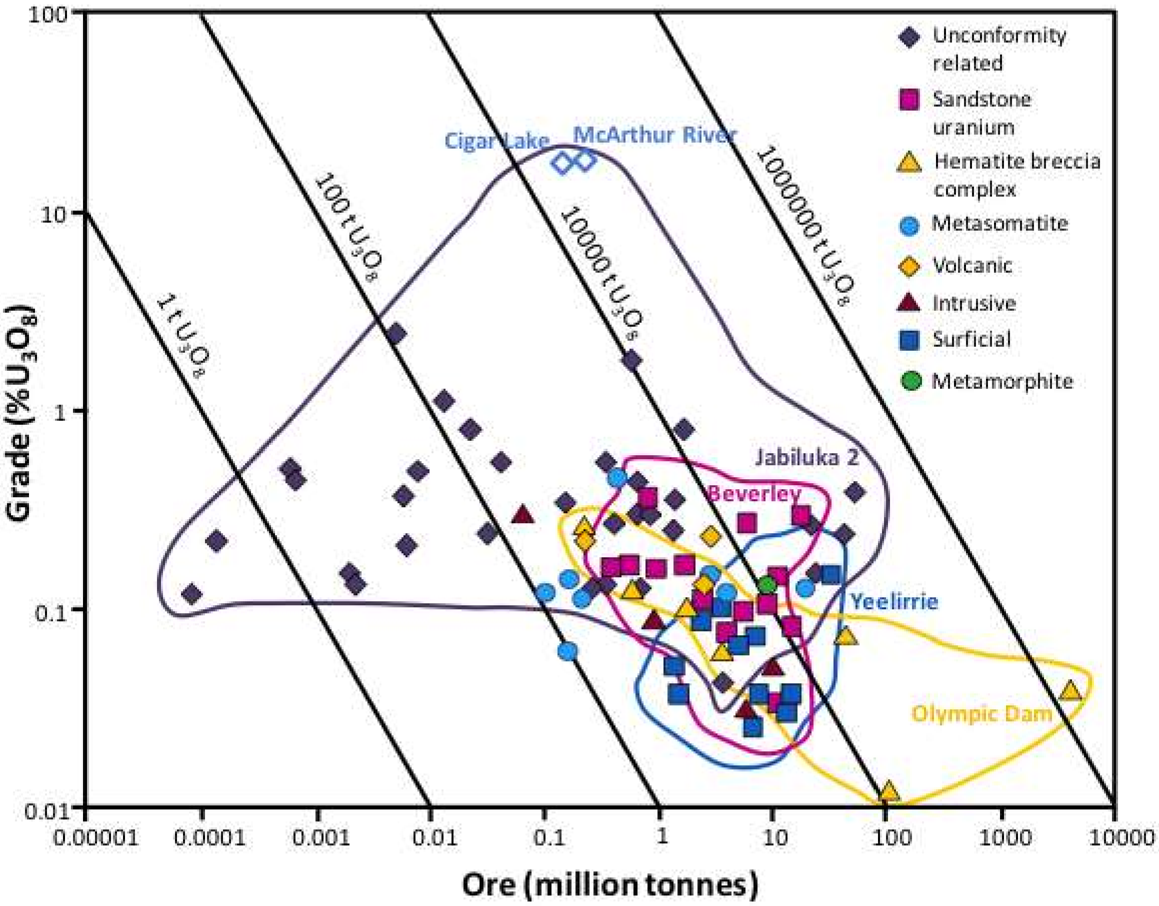

FIG. 1.1. Tonnage vs. grade for eight deposit types (modified from Lambert et al. [1.3]).

1.2. OBJECTIVE

This IAEA TECDOC is intended to be used by IAEA Member States as a guidebook for evaluation and exploration of unconformity-related uranium deposits. Users can utilize this document to better understand the characteristics of unconformity-related deposits and use this information to refine exploration and evaluation strategies.

1.3. SCOPE

The scope of this TECDOC includes a description of existing and emerging technologies to effectively integrate geological, geophysical and geochemical data to recognize the footprint (i.e. the total extent that the mineralizing system has affected its environment) of the deposit and the key vectors to the uranium mineralization. In addition, insights into exploration strategies and risks associated with country and basin selection are discussed, including the role of the IAEA and academia in supporting the exploration process.
The TECDOC has received inputs from diverse sources, including the IAEA, uranium-based and related industries and researchers from governments and universities. The focus is meant to be both basic and applied, with an emphasis on integrating technologies to enhance exploration success. There is a large body of published research on the deposits, as summarized in this TECDOC.

Topics addressed include: how the deposits are classified; descriptions of the deposits and empirical models; current theories on how they form (with an emphasis on critical factors when formulating exploration strategies); exploration processes; and, exploration techniques.

1.4. STRUCTURE

The TECDOC contains descriptions of the empirical models in Chapter 2. Descriptions and empirical models of unconformity-related deposits include those in Australia, Canada (Athabasca Basin, Thelon Basin, Otish Basin), India and the Russian Federation. In Chapter 3, the characteristics of these deposits are compared and contrasted in terms of the genesis of unconformity-related uranium deposits and includes recent research results. The genesis of these deposits also includes a discussion of some other uranium deposits that are proposed to be unconformity-related. The descriptions and models of their formation and evolution set the stage for a discussion of critical factors in the exploration for unconformity-related uranium deposits.

Chapter 4 describes the foundations of exploration methods including the more commonly known exploration techniques. Also addressed are the latest advancements in geophysical and geological exploration methods.

Chapter 5 provides an understanding of the need for future production of uranium and why current known resources, though significant throughout the world, may never be put into production. The need for continuous exploration and related expenditures and a commitment by exploration companies and governmental agencies is required for the long-term sustainability of this industry.

REFERENCES

[1.1] World Nuclear Association, (2017) http://www.world-nuclear.org/information-library/nuclear-fuel-cycle/mining-of-uranium/world-uranium-mining-production.aspx.

[1.2] ORGANISATION FOR ECONOMIC CO-OPERATION AND DEVELOPMENT/ NUCLEAR ENERGY AGENCY–INTERNATIONAL ATOMIC ENERGY AGENCY, Uranium 2016: Resources, Production and Demand, 2016, NEA No. 7301 (2016) 550 pp.

[1.3] IAEA, Geological Classification of Uranium Deposits and Description of Selected Examples, IAEA-TECDOC-1842, IAEA, Vienna (2018) 417 pp.

[1.4] CUNEY, M., URANIUM AND THORIUM: THE EXTREME DIVERSITY OF THE RESOURCES OF THE WORLD'S ENERGY MINERALS, NON-RENEWABLE RESOURCES: GEOSCIENTIFIC AND SOCIETAL CHALLENGES (SINDING-LARSEN, R., WELLMER, F.-W., EDS), SPRINGER (2011).

[1.5] IAEA, PROTEROZOIC UNCONFORMITY AND STRATABOUND URANIUM, IAEA-TECDOC-315, IAEA, VIENNA (1984) 338 PP.

2. EMPIRICAL MODELS

2.1. EMPIRICAL CHARACTERISTICS OF THE WORLD'S PROTEROZOIC UNCOMFORMITY DEPOSITS

The recognition that unconformity-related deposits represented a unique type of uranium concentration, was first made in the 1970s as a result of a number of significant high-grade discoveries that were made in the Athabasca Basin, Canada. In hindsight, the first significant discovery was that of the Rabbit Lake deposit in 1968, by Gulf Minerals Canada Ltd. However, the importance of the Athabasca sandstone and, in particular, the underlying unconformity, went unnoticed and was not appreciated by the exploration community at that time. Meanwhile, at the same time as Gulf Mineral's activity in the late 1960s, exploration by the Compagnie de Mokta in the Carswell Dome area in the western part of the Basin was also returning significant discoveries of high grade uranium mineralization associated with glacial boulders; these eventually led to the discovery of the D-zone orebody in 1970. Yet again, the role of the Athabasca sandstone and the underlying unconformity with older basement rocks and uranium mineralization was not recognized. Subsequent discoveries by Uranerz Exploration and Mining Ltd., of the Gaertner and Deilmann orebodies in the Key Lake area in 1975 and 1976 respectively, were arguably the beginning of an understanding of the basic empirical parameters defining this new and increasingly important type of uranium deposit.

Critical work in the 1970s towards defining the geological setting and possible controls on these deposits was carried out by Ray (Saskatchewan Geological Survey) who was undertaking regional mapping in the Key Lake area and Sibbald (Saskatchewan Geological Survey) and Hoeve (Saskatchewan Research Council) who were jointly mapping the structural and alteration setting of the Rabbit Lake deposit [2.1, 2.2]. In 1976, Ray published some initial observations, noting that the uranium mineralization at the Key Lake deposits showed a spatial association between the intersection of the sub-Athabasca unconformity and sulphide- and graphite-bearing metasedimentary rocks in the underlying basement [2.1]. Hoeve and Sibbald [2.2] published their work in a seminal paper whereby they described the geological controls of the Rabbit Lake deposit and proposed a genetic ore-forming process, dubbed the diagenetic-hydrothermal model. The proposed model involved oxidized diagenetic solutions heated up to 200°C that leach and carry uranium derived from the Athabasca sandstone. This subsequently interacts with a mobile reductant, such as methane (CH_4) generated from graphite-bearing basement gneisses, resulting in the redox-controlled precipitation of uranium.

Following the publication of the work by Ray [2.1] and Hoeve and Sibbald [2.2], a steady stream of discoveries was made in the late 1970s and through the 1980s including: Collins Bay B-zone (1977), West Bear (1977), Maurice Bay (1977), Midwest Lake (1978), Dawn Lake (1978), McClean Lake North and South (1979), Collins Bay-D Zone (1979), Eagle Point (1980), Cigar Lake (1982), McArthur River (1988) and Sue deposits (1988). By the mid-1980s and through to the 2000s, exploration increasingly tested deeper portions of the Basin where sandstone cover exceeded 500 m. Discoveries in the deeper part of the Basin during this period included: Shea Creek deposits (1994–97), Millennium (2000), Centennial (2005), Phoenix (2009) and Fox Lake (2010). More recently, increased exploration activity in the western part of the asin, notably along the immediate SW margin, resulted in several significant discoveries including Triple R (2012) and Arrow (2014) deposits.

The last three decades have seen the emergence of a range of analytical research that has been undertaken to better understand the nature of the fluids involved, as well as pressure, temperature and temporal constraints in the formation of the Athabasca uranium deposits. A small selection of research references includes: oxygen and hydrogen isotopic analysis of alteration halos associated with uranium deposits [2.3–2.6], fluid inclusion analysis of alteration related phases [2.5, 2.7–2.12], dating of uranium mineralization and alteration [2.13–2.17], and numerical modelling of fluid flow conditions [2.18–2.20].

From a purely descriptive perspective, these deposits have been described as high-grade uranium concentrations in pods, veins, and as semi-massive replacements consisting of mainly uraninite located close to basal unconformities between Proterozoic redbed basins and older, generally deformed and metamorphosed Archean and Early Paleoproterozoic 'basement' rocks [2.21]. Further attempts at classifying Athabasca Basin uranium deposits have traditionally been based on characteristics such as host lithologies (basement vs. sandstone), nature of the ore (complex vs. simple), nature of the clay alteration (illite vs. dravite) and fluid flow direction (ingress vs. egress). Previously proposed empirical schemes, with an emphasis on the spatial association of mineralization to the unconformity, include that by Dahlkamp [2.22] in which deposits were divided into: i) unconformity contact; and ii) sub-unconformity-epimetamorphic. The unconformity contact type was further subdivided into Proterozoic unconformity- and Phanerozoic unconformity-related settings, although the latter is no longer recognized in the current IAEA uranium classification. Dahlkamp's [2.22] sub-unconformity-epimetamorphic type also encompassed a large range of uranium occurrences that included those in the current IAEA unconformity-related basement-hosted sub-type, but also included examples now classified as metamorphite and metasomatite deposits in the IAEA uranium deposits scheme.

Unconformity deposits have also been classified or subdivided on the basis of the mineralogical and geochemical make-up of the uranium mineralization. Uraninite and pitchblende form the primary ore mineralogy with two end members recognized based on accessory or subsidiary elements: i) polymetallic or complex ores containing sulphides and arsenides with high contents of Ni, Co, Cu, Pb, Zn, Mo, and locally elevated Au, Ag, Se and platinum-group elements; and ii) monometallic or simple ores which contain minor amounts of Cu and Fe sulphides. Polymetallic deposits are typically developed along the basement-sandstone contact and can extend between 25 and 50 m below the unconformity. From the perspective of a process-related model, the primary debate has been whether the deposits are largely the product of mineralizing fluids that have been derived and ascended from the basement (egress process) or derived and descended from the overlying basinal sediments (ingress process) or some combination of the two (e.g. ingress and egress, or fluid mixing). Precipitation was focused primarily by structural and physiochemical traps that operated in fixed locations; however, these controlling structural characteristics of Proterozoic unconformity deposits have had limited incorporation into classification schemes to date.

The current IAEA classification for uranium deposits is essentially an empirical-based scheme which defines Proterozoic unconformity deposits as uranium concentrations that are associated with and occur immediately above or below, or span an unconformable contact that separates a crystalline basement from overlying, redbed clastic sediments of the Proterozoic age. The IAEA classification further subdivides Proterozoic unconformity deposits into the following sub-types: i) unconformity contact deposits; ii) basement-hosted deposits; and iii) stratiform fracture controlled deposits.

The unconformity contact sub-type is divided into: 1) fracture-bound deposits that occur in metasedimentary rocks immediately below the unconformity. These tend to be marked by monometallic mineralization and are of medium grade; and 2) clay-bound deposits that are associated with, developed along or span the unconformity and are characterized by an intense clay envelope that extends into the overlying sandstone. Mineralization is commonly polymetallic and ranges between high and very high grade.

The basement-hosted sub-type are structurally-controlled infill and replacement type veins, stockworks and breccia mineralization which typically developed subconcordant to the lithostructural setting of the metasedimentary host rocks. These deposits tend to be monometallic with large resources, at low to medium grade.

The third sub-type, the stratiform fracture controlled deposits are characterized by low-grade strata-bound mineralization located along the unconformity between Archean uranium-thorium-rich granites and Proterozoic metasedimentary rocks. The main examples of this type — the Chitrial and Peddagattu deposits — have only been observed in the Srisailam and Palnad Basins in India.

Preserved remnants of Proterozoic sedimentary sequences or basins have a broad global distribution (Chapter 5: Fig. 5.25), however Proterozoic unconformity associated deposits are much more restricted in their occurrence (Fig. 2.1) being identified primarily in Canada (e.g. the Athabasca, Otish and Thelon Basins), Australia (the Bresnahan and McArthur Basins and Rum Jungle), India (the Bhima, Palnad and Srisailam Basins) and in the Russian Federation (the Pasha Ladoga Basin). To date, the Athabasca and McArthur Basins are the only jurisdictions where unconformity associated deposits have been exploited. Although many of the deposits that achieved production in Canada and Australia were discovered in the 1970s through the 1980s, unconformity deposits continued to be found elsewhere in the world through the 1990s as well (e.g. Karku, Russian Federation; Chitrial, Lambapur, Peddagattu, Koppunuru Gogi, India). More recently, very significant, large resource, high grade deposits have been discovered in the Athabasca Basin in the 2010s (e.g. Triple R and Arrow deposits).

In order to properly understand the empirical characteristics of Proterozoic unconformity associated uranium deposits, Table 2.1 and Table 2.2 (Annex 1) represent data from most of the world's deposits as classified by the IAEA at the time of writing (mainly >500 tU).

The table focuses on the following aspects of unconformity uranium deposits:

1) Nature of the mineralization (e.g. resource size and grade, complex or simple mineralogy, age);
2) Geometry of the mineralization (e.g. dimensions, number of pods/orebodies, location in regard to the unconformity, depth below surface, etc.);
3) Structural setting (e.g. unconformity offset, characteristics of the controlling structure);
4) Alteration (e.g. nature and size of basin and basement alteration).

A total of 120 unconformity deposits were compiled and more than half of these deposits can be further grouped into broader systems that define mineralized trends or discrete mineralized geological domains or districts within their respective basins. For example, a few mineralized systems that comprise a series of related, but discrete deposits include: the McArthur River system (seven deposits), Sue system (five deposits), Collins Bay-Eagle system (four deposits), Carswell-Cluff system (eleven deposits), Rum Jungle system (four deposits), Ranger system (three deposits), and the Karku system (three deposits). Table 2.1 cites the specific dimensional, ore tenor, and geological attributes of those individual deposits for which published information is available. In addition, deposits forming a 'system' are grouped together and their dimensional, geological and ore tenor characteristics are cumulatively tabulated.

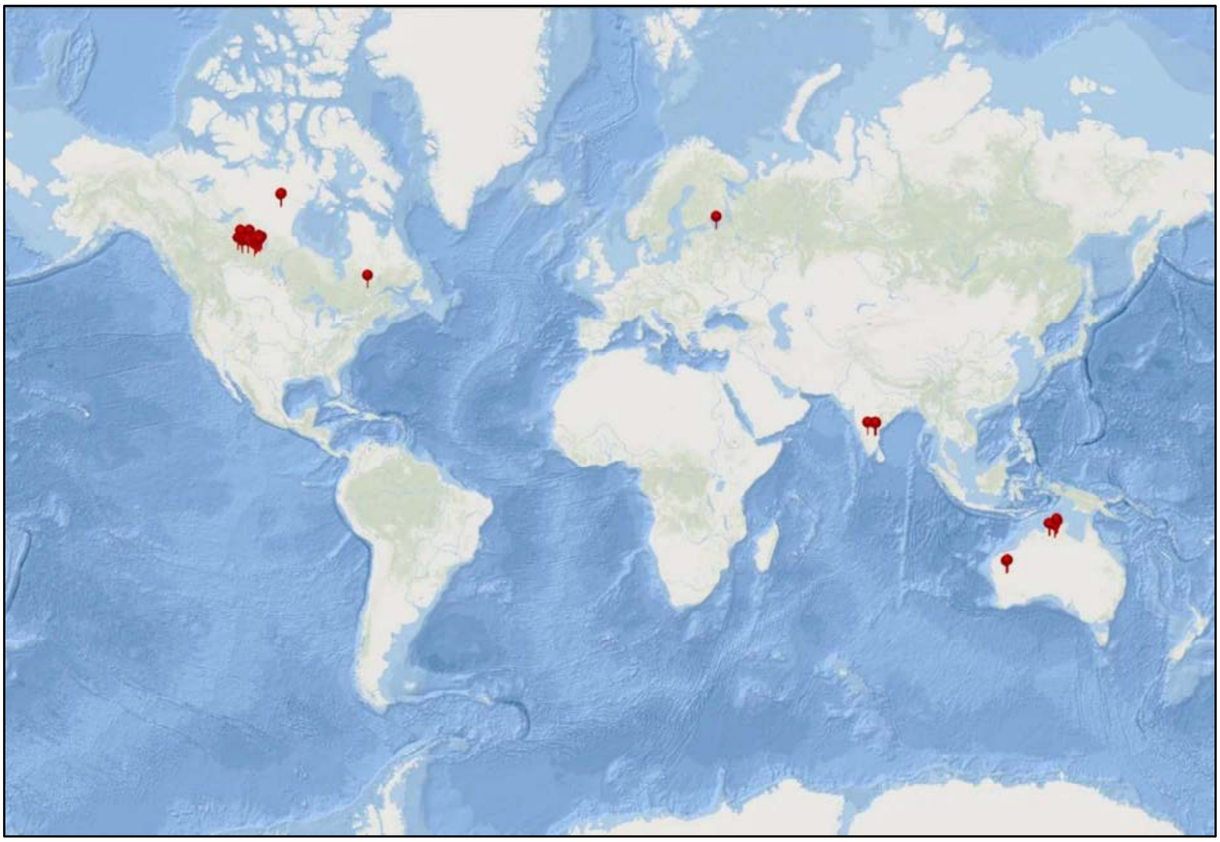

FIG. 2.1. World distribution of the Proterozoic unconformity uranium deposits discussed in Chapter 2 using data from Table 2.1. World base map based on data from ESRI [2.23].

Table 2.1 is divided into four main sections based on geographic location with each being further subdivided in geological regions. The four geographic regions and their geological regions include the following: 1) Canada (the Athabasca, Otish and Thelon Basins); 2) Australia (Bresnahan Basin, Kombolgie Subgroup of the McArthur Basin and the Rum Jungle District); 3) India (the Bhima, Palnad and Srisailam Basins); and 4) the Russian Federation (Pasha Ladoga Basin).

Data within the table was primarily assembled from publicly available information, except for a few examples where the data was provided by companies or by personal communication with researchers or industry consultants. Resource data (e.g. size and grade) is largely in accordance with the data contained in the UDEPO[1] database, with the exception of a few deposits where the data was either missing altogether or deemed to be outdated, or not representative of the authors' understanding of a deposit. Values for the empirical parameters were usually estimated from geological maps or sections, and should be treated as approximate rather than absolute values. Where values for some fields were available as ranges, the authors have converted these into an appropriate mean or average, or in some cases elected to work with the maximum value

[1] World Distribution of Uranium Deposits (UDEPO) is a database of uranium deposits in the world. The database contains information on the classification, geological characteristics, geographical distribution and resources of the deposits. It covers all geographical regions of the world.

as it was more representative of the parameter (e.g. depth extent of the mineralization below the unconformity).

Fields left blank represent information that was not available in the public domain or was unknown to the authors at the time of publication (e.g. deposit mined several decades ago and no descriptive papers published on that deposit). Fields that contain 'n.a.' represent information that is not applicable for a deposit (e.g. depth to the unconformity for deposits where the whole basin cover has been eroded). All the information contained in Table 2.1 was deemed accurate at the time of writing this document (December 2017).

Utilizing the data from Table 2.1, a statistical analysis was conducted in order to look at the distribution of empirical parameters between regions and deposit types (for both deposits and systems).

Based on the 120 deposits tabulated, a number of general observations can be made regarding the resource size and grade, geometric and geological characteristics of an 'average' Proterozoic unconformity uranium deposit. When all the deposits are examined as a whole, regardless of their geographic location, they have an average resource size of about 15 000 tU at 2.64% U. From a dimensional footprint size, they have an average strike length of 571 m, width of 101 m and vertical extent of 100 m, thereby having an elongated prism shape. However, these average values, although statistically valid, reflect a range of deposits with significantly different geometries and grades. Therefore, it is important to examine the data from a number of different perspectives such as geographic region or structural setting type, in order to draw conclusions.

The Athabasca Basin in Canada and the McArthur Basin in Australia clearly stand out as very well endowed with unconformity associated uranium deposits. Each Basin hosts at least one deposit or system containing >200 000 tU, while in the Athabasca Basin, mean average grades are 3.58% U which is at least one order of magnitude higher than all other regions. Deposits in the McArthur Basin rank second in grade with a mean average 0.41% U, while deposits in the Thelon Basin (Canada), rank third with a mean grade of 0.37% U.

The geometry and footprint size of deposits fall into two distinct groups — the Canadian and Australian deposits characterized by relatively small footprints with high contained resource, and the Indian and Russian Federationn deposits characterized by a relatively large footprint, albeit lower contained resource. The Indian deposits in particular, are larger by an order of magnitude from the perspective of the overall strike length and width of the distribution of mineralization. They are of very low grade (<0.1% U) and tend to form very thin (e.g. <10 m thick) sub-horizontal tabular sheets hosted within the basinal sedimentary rocks, while mineralization seldom extends into the underlying basement rocks. The overall geometry of deposit footprints in the Athabasca and McArthur Basins is generally that of an elongated sub-horizontal prism, with a long strike length, more restricted width and limited vertical extent or, an inclined tabular body with a significant down-dip vertical length. The deposits of the Thelon Basin and the Rum Jungle areas are generally of a vertical to plunging equant prismatic shape.

Deposits associated with unconformity offsets are most common in the Athabasca Basin although post-sandstone faulting is locally documented for deposits in the Otish, McArthur and Bhima Basins. As a general observation, deposits that are associated with a dominant post-sandstone vertical displacement component along the controlling fault tend to have mineralization extending into the underlying basement rocks.

A relationship between unconformity displacement and resource size and grade is observed, although it is not proportional — deposits types that exhibit a more significant displacement (mean or maximum) are on average larger than deposit types that show negligible offset. The role that the dip of deposit-associated faults may have on the mineralization from the perspective of footprint orientation and geometry, as well as possibly grade and resource size, is less clear and requires further analysis. However, based on the dip of controlling structures listed for all the deposits in Table 2.1, there appear to be three broad populations: i) faults associated with McArthur Basin deposits have a relatively shallow dip of 39 degrees; ii) Athabasca Basin structures have a more moderate dip of 59 degrees; while, iii) all other regions have somewhat steeper deposit-associated structures ranging between 72 and 87 degrees.

When examining deposits from the perspective of their lithostratigraphic setting, two dominant groups are recognized: 1) basement-hosted; and 2) unconformity contact deposits. A third or intermediate setting is also recognized, herein referred to as wedge type which is typically located within the footwall sandstone wedge of reverse fault structures. Many of these wedge-type deposits may also have a basement root extending below the unconformity. Although only a limited number of deposits are classified as wedge type with basement roots, they are significant from a resource perspective in that they have a mean size of 39 267 tU and a maximum of 108 755 tU (e.g. McArthur River Zone 2 deposit).

Basement-hosted deposits are generally characterized by low average grades of <1% U. However, they can have significant total resource size (e.g. Eagle Point, Arrow, Jabiluka, and Ranger deposits) with a mean size of 17 691 tU. Unconformity-contact deposits have a mean resource size of 8437 tU, which is about half that of basement-hosted deposits, albeit with significantly higher mean grades exceeding 3.0% U.

Fracture-hosted deposits, identified only in India, have the lowest mean resource size at 4518 tU and grades of 0.07% U, despite having very large aerial footprints.

A series of graphs were created in order to identify trends and variability within the data, notably with respect to resource size, grade and relationships and measureable attributes of the footprints of deposits.

Fig. 2.2 shows the distribution of grade vs. tonnage data for Proterozoic unconformity deposits and systems. The data is classified by global region and deposit sub-types. The data emphasizes the extremely high grades that characterize deposits in Athabasca Basin. Only one deposit in the >1% U category occurs elsewhere (the Nabarlek deposit, 1.54% U). In contrast, the majority of deposits outside the Athabasca Basin have grades less than 1% U (Fig. 2.3). From a resource size perspective, the Athabasca Basin and McArthur Basin (Kombolgie Subgroup) are the only Basins containing deposits or systems that have a contained resource of >25 000 tU (Fig. 2.4). The majority of unconformity deposits contain <5000 tU. Although the McArthur Basin deposits can contain significant resources, they have a lower average grade compared to the Athabasca Basin.

At the other end of the spectrum, the Fig. illustrates the low-grade nature of the Indian, Russian Federationn and other Australian deposits, which represent the lowest grade deposits with average grades typically less than 0.2% U. Cumulative frequency diagrams, illustrating the distribution of deposits (Fig. 2.5) and systems (Fig. 2.6) by resource size, emphasize the rareness of very large Proterozoic unconformity deposits. The 90th and 95th percentiles of deposits correspond to 40 000 tU and 85 000 tU respectively, and mainly represent basement-hosted systems within the Athabasca and McArthur Basins. The 75th and 90th percentiles of mineralized systems correspond to 100 000 tU and 165 000 tU respectively, with the former being solely associated with the Athabasca and McArthur Basins. The 75th percentile also represents a variety of geological settings including: unconformity contact, basement- and wedge-hosted deposits.

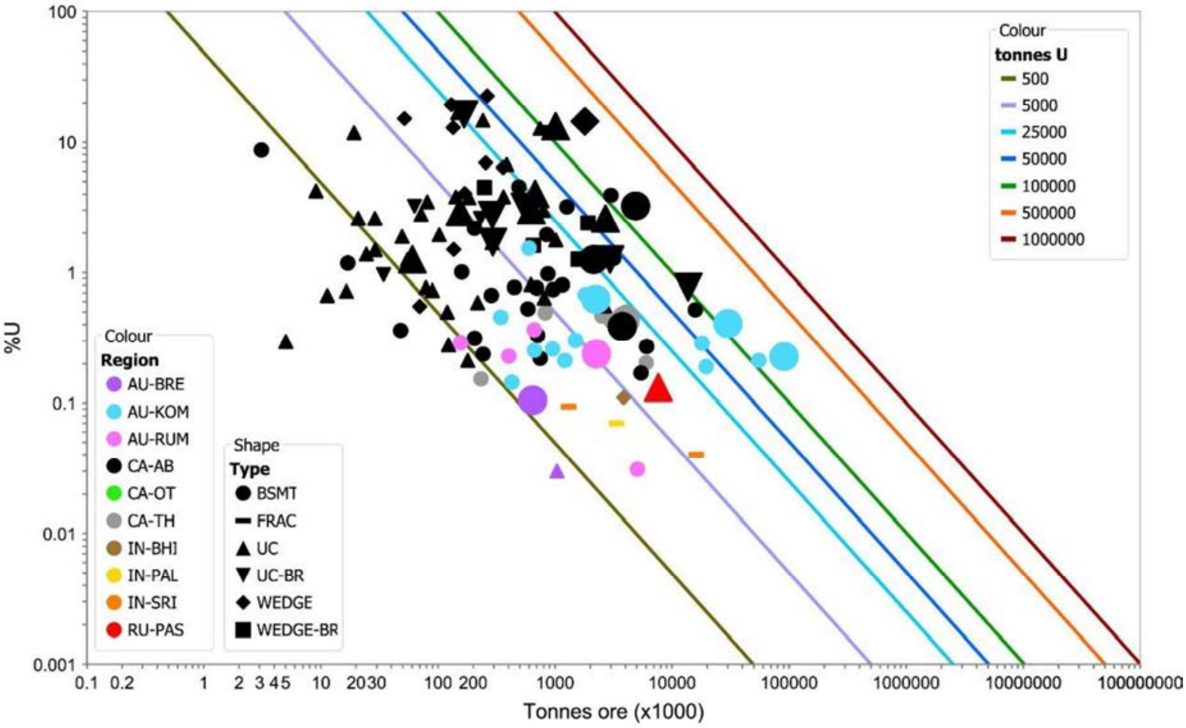

FIG. 2.2. Log/log grade/tonnage diagram for all Proterozoic unconformity uranium deposits and systems listed in Table 2.1. The smaller symbols represent individual deposits and the larger symbols, the mineralized systems. The different shapes represent the different types of deposits within the Proterozoic unconformity classification (BSMT=basement-hosted, FRAC=stratiform fracture controlled, UC=unconformity-hosted, UC-BR=unconformity-hosted with a basement root, WEDGE= structural wedge-hosted, WEDGE-BR=structural wedge-hosted with a basement root), whereas the colours represent the different basins or geographic areas (AU-BRE=Bresnahan Basin, AU-KOM=McArthur Basin, Kombolgie Subgroup, AU-RUM=Rum Jungle area, CA-AB=Athabasca Basin, CA-OT=Otish Basin, CA-TH=Thelon Basin, IN-BHI=Bhima Basin, IN-PAL=Palnad Basin, IN-SRI=Srisailam Basin, RU-PAS=Pasha Ladoga Basin).

Within the context of specific basins, the structural parameters associated with deposits, notably the orientation and dip of the controlling structure, as well as depth of mineralization below the unconformity show some relationship to the resource size and grade (Fig.s 2.7 to 2.11). In the Athabasca Basin, a positive correlation is noted between resource grade, and deposits whose controlling structure trends between 50 and 100 degrees and dips varying from 55 to 70 degrees. The dip of the controlling structures for deposits in the McArthur Basin show a high degree of variability, while structures associated with deposits in the Bresnahan Basin and Rum Jungle deposits exhibit very steep dips. The maximum depth of mineralization below the unconformity has the strongest correlation to the grade of deposits (Fig. 2.11). Deposits with grades >5% U have a maximum depth of mineralization with 100 m below the unconformity, with the majority being less than 25 m of the unconformity. There is a general trend of decreasing average grade with increasing depth below the unconformity.

The strike length, width and vertical extent of the deposits were plotted and aspect ratios calculated in order to characterize the physical dimension of the deposit footprints (Fig.s 2.12 to 2.14). The extensive, thin sheet-like nature of the stratiform fracture-hosted deposits of India is clearly highlighted by their aspect ratios. Similarly, the tabular or prismatic basement-hosted deposits and pipe-like unconformity-contact deposits are well illustrated by the large vertical component and limited width characterizing the former and the dominant sub-horizontal and limited width and vertical dimensions of the latter deposit types.

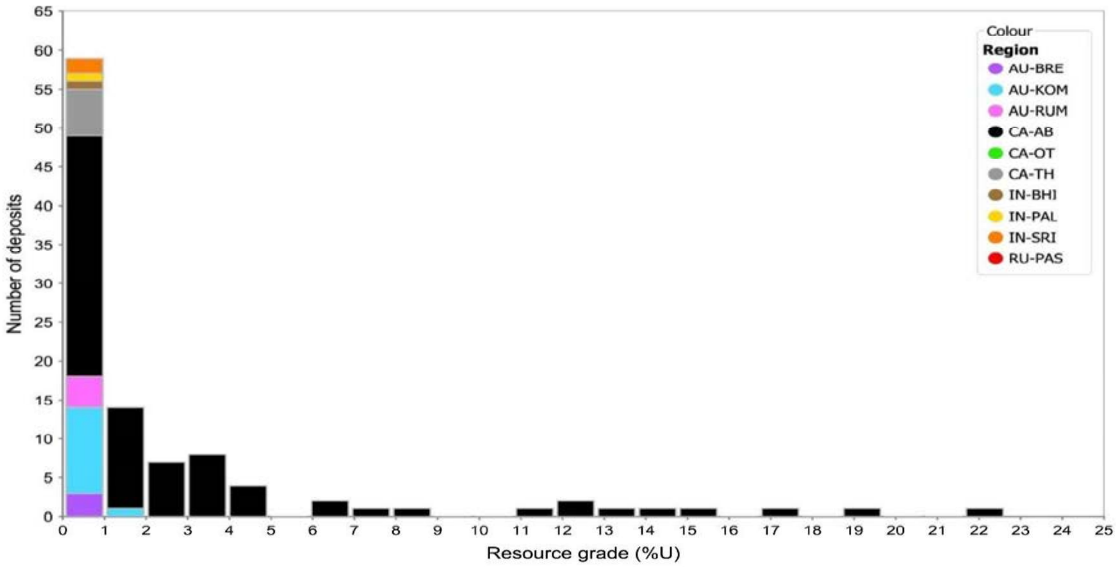

FIG 2.3. Resource grade distribution of individual deposits. The colours represent the different basins or geographic areas (AU-BRE=Bresnahan Basin, AU-KOM=McArthur Basin, Kombolgie Subgroup, AU-RUM=Rum Jungle area, CA-AB=Athabasca Basin, CA-OT=Otish Basin, CA-TH=Thelon Basin, IN-BHI=Bhima Basin, IN-PAL=Palnad Basin, IN-SRI=Srisailam Basin, RU-PAS=Pasha Ladoga Basin).

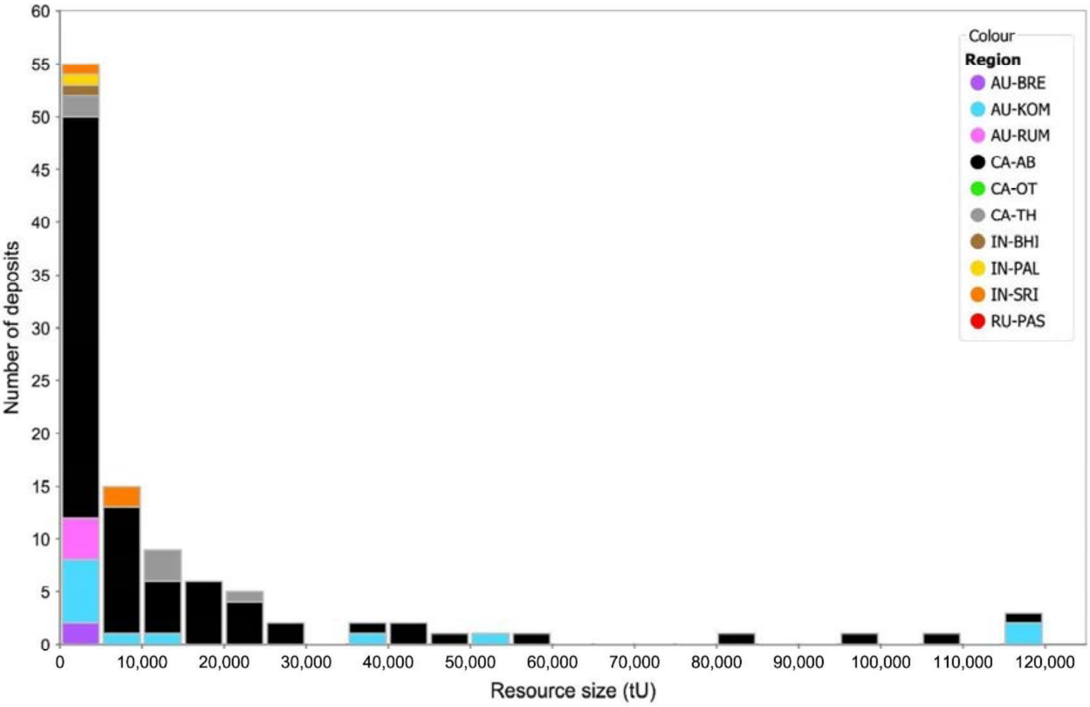

FIG. 2.4. Resource size distribution of individual deposits. The colours represent the different basins or geographic areas (AU-BRE=Bresnahan Basin, AU-KOM=McArthur Basin, Kombolgie Subgroup, AU-RUM=Rum Jungle area, CA-AB=Athabasca Basin, CA-OT=Otish Basin, CA-TH=Thelon Basin, IN-BHI=Bhima Basin, IN-PAL=Palnad Basin, IN-SRI=Srisailam Basin, RU-PAS=Pasha Ladoga Basin).

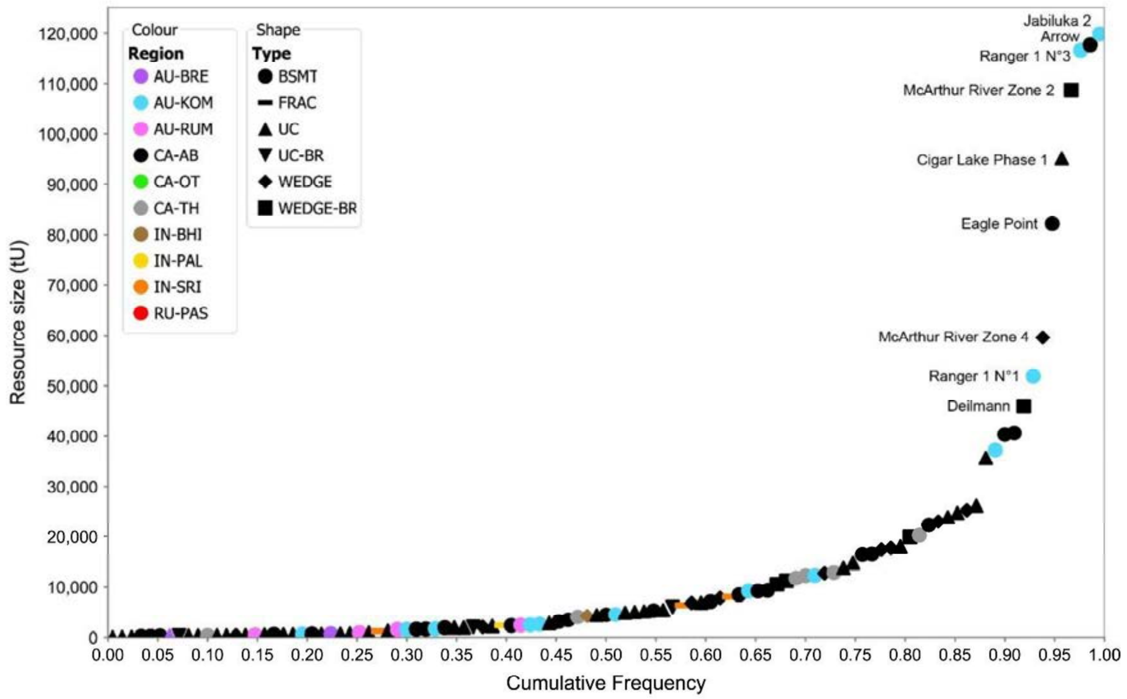

FIG. 2.5. Cumulative frequency diagram of resource size for individual deposits, with the largest deposits labelled. The different shapes represent the different types of deposits within the Proterozoic unconformity classification (BSMT=basement-hosted, FRAC=stratiform fracture controlled, UC=unconformity-hosted, UC-BR=unconformity-hosted with a basement root, WEDGE= structural wedge-hosted, WEDGE-BR=structural wedge-hosted with a basement root) whereas the colours represent the different basins or geographic areas (AU-BRE=Bresnahan Basin, AU-KOM=McArthur Basin, Kombolgie Subgroup, AU-RUM=Rum Jungle area, CA-AB=Athabasca Basin, CA-OT=Otish Basin, CA-TH=Thelon Basin, IN-BHI=Bhima Basin, IN-PAL=Palnad Basin, IN-SRI=Srisailam Basin, RU-PAS=Pasha Ladoga Basin).

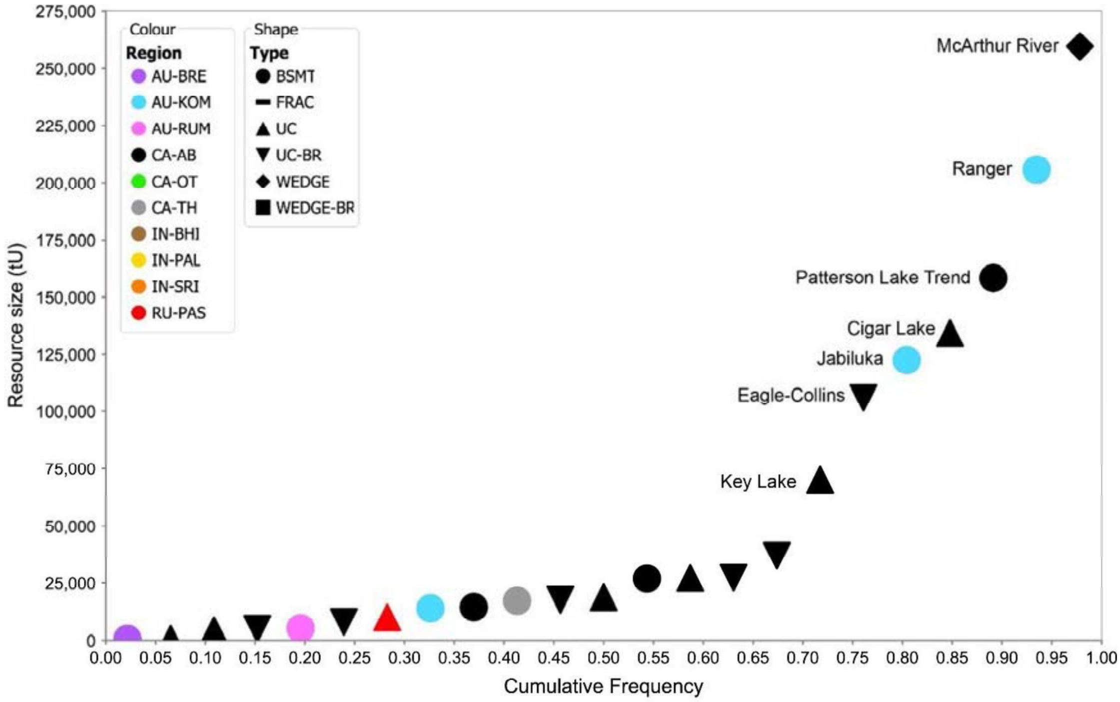

FIG. 2.6. Cumulative frequency diagram of resource size for systems, with the largest systems labelled. The different shapes represent the different types of deposits within the Proterozoic unconformity classification (BSMT=basement-hosted, FRAC=stratiform fracture controlled, UC=unconformity-hosted, UC-BR=unconformity-hosted with a basement root, WEDGE= structural wedge-hosted, WEDGE-BR=structural wedge-hosted with a basement root) whereas the colours represent the different Basins or geographic areas (AU-BRE=Bresnahan Basin, AU-KOM=McArthur Basin, Kombolgie Subgroup, AU-RUM=Rum Jungle area, CA-AB=Athabasca Basin, CA-OT=Otish Basin, CA-TH=Thelon Basin, IN-BHI=Bhima Basin, IN-PAL=Palnad Basin, IN-SRI=Srisailam Basin, RU-PAS=Pasha Ladoga Basin).

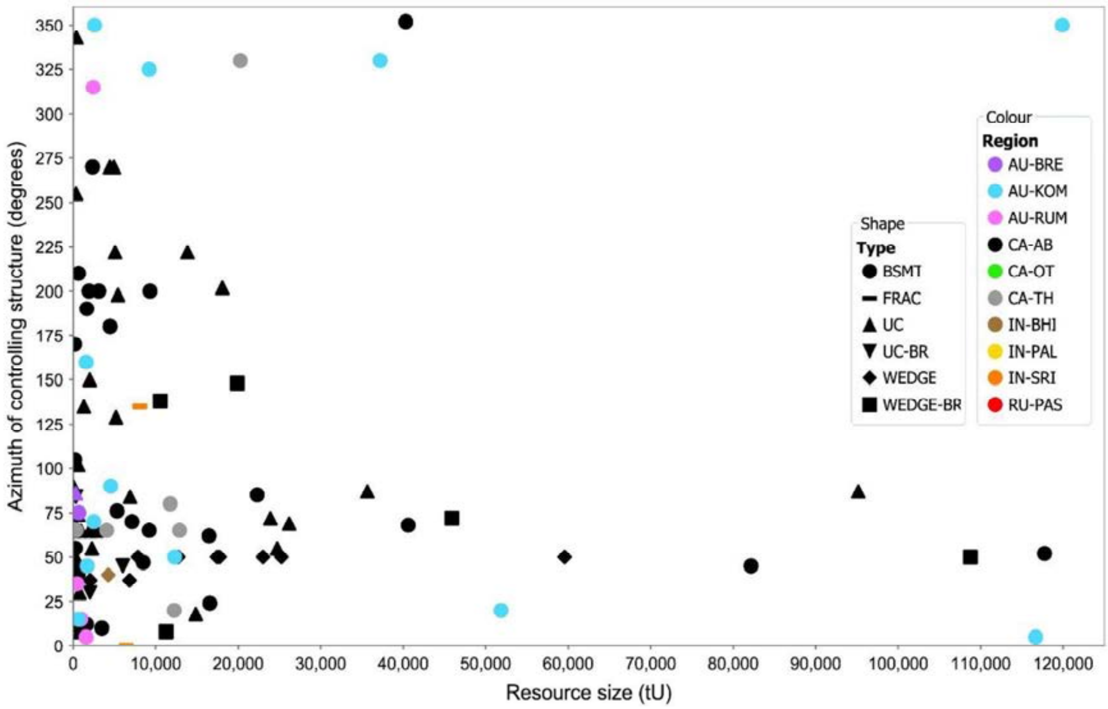

FIG. 2.7. Azimuth of controlling structure (according to the right-hand rule) vs. resource size for individual deposits. The different shapes represent the different types of deposits within the Proterozoic unconformity classification (BSMT=basement-hosted, FRAC=stratiform fracture controlled, UC=unconformity-hosted, UC-BR=unconformity-hosted with a basement root, WEDGE= structural wedge-hosted, WEDGE-BR=structural wedge-hosted with a basement root) whereas the colours represent the different basins or geographic areas (AU-BRE=Bresnahan Basin, AU-KOM=McArthur Basin, Kombolgie Subgroup, AU-RUM=Rum Jungle area, CA-AB=Athabasca Basin, CA-OT=Otish Basin, CA-TH=Thelon Basin, IN-BHI=Bhima Basin, IN-PAL=Palnad Basin, IN-SRI=Srisailam Basin, RU-PAS=Pasha Ladoga Basin).

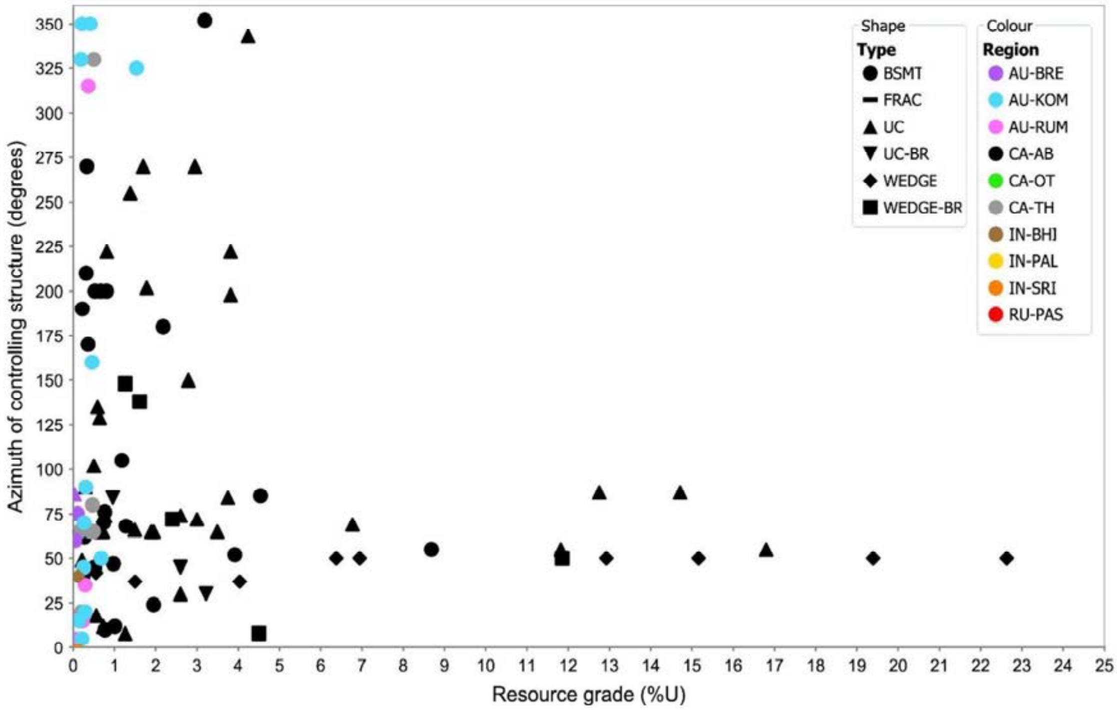

FIG. 2.8. Azimuth of controlling structure (according to the right-hand rule) vs. resource grade for individual deposits. The different shapes represent the different types of deposits within the Proterozoic unconformity classification (BSMT=basement-hosted, FRAC=stratiform fracture controlled, UC=unconformity-hosted, UC-BR=unconformity-hosted with a basement root, WEDGE= structural wedge-hosted, WEDGE-BR=structural wedge-hosted with a basement root) whereas the colours represent the different basins or geographic areas (AU-BRE=Bresnahan Basin, AU-KOM=McArthur Basin, Kombolgie Subgroup, AU-RUM=Rum Jungle area, CA-AB=Athabasca Basin, CA-OT=Otish Basin, CA-TH=Thelon Basin, IN-BHI=Bhima Basin, IN-PAL=Palnad Basin, IN-SRI=Srisailam Basin, RU-PAS=Pasha Ladoga Basin).

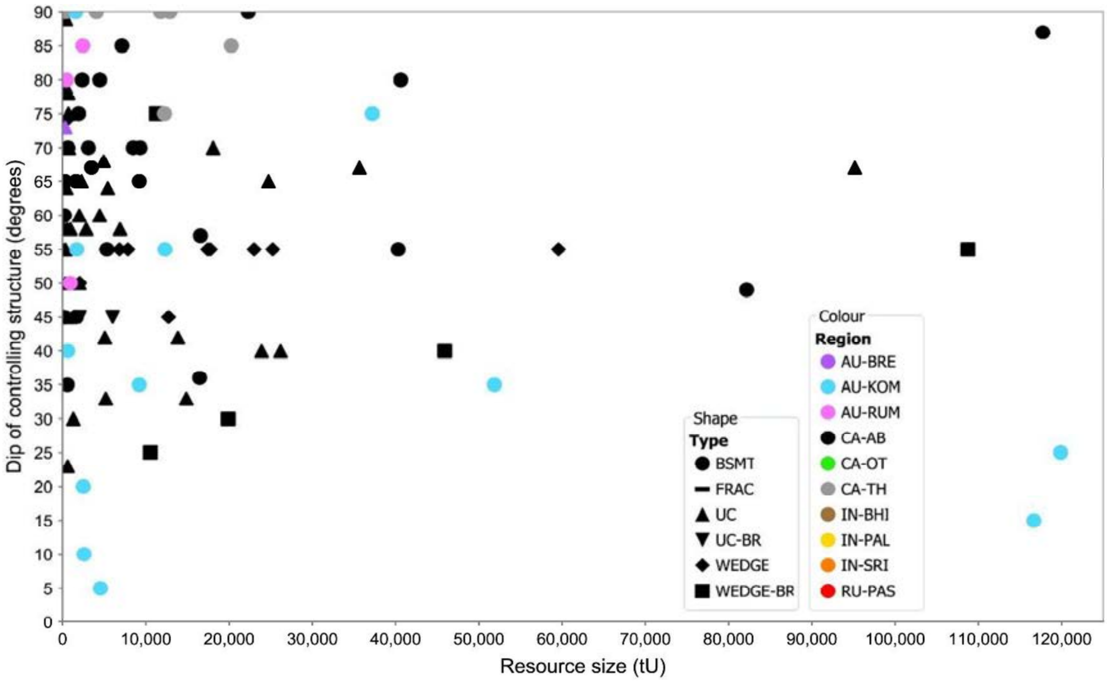

FIG. 2.9. Dip of controlling structure vs. resource size for individual deposits. The different shapes represent the different types of deposits within the Proterozoic unconformity classification (BSMT=basement-hosted, FRAC=stratiform fracture controlled, UC=unconformity-hosted, UC-BR=unconformity-hosted with a basement root, WEDGE= structural wedge-hosted, WEDGE-BR=structural wedge-hosted with a basement root) whereas the colours represent the different basins or geographic areas (AU-BRE=Bresnahan Basin, AU-KOM=McArthur Basin, Kombolgie Subgroup, AU-RUM=Rum Jungle area, CA-AB=Athabasca Basin, CA-OT=Otish Basin, CA-TH=Thelon Basin, IN-BHI=Bhima Basin, IN-PAL=Palnad Basin, IN-SRI=Srisailam Basin, RU-PAS=Pasha Ladoga Basin).

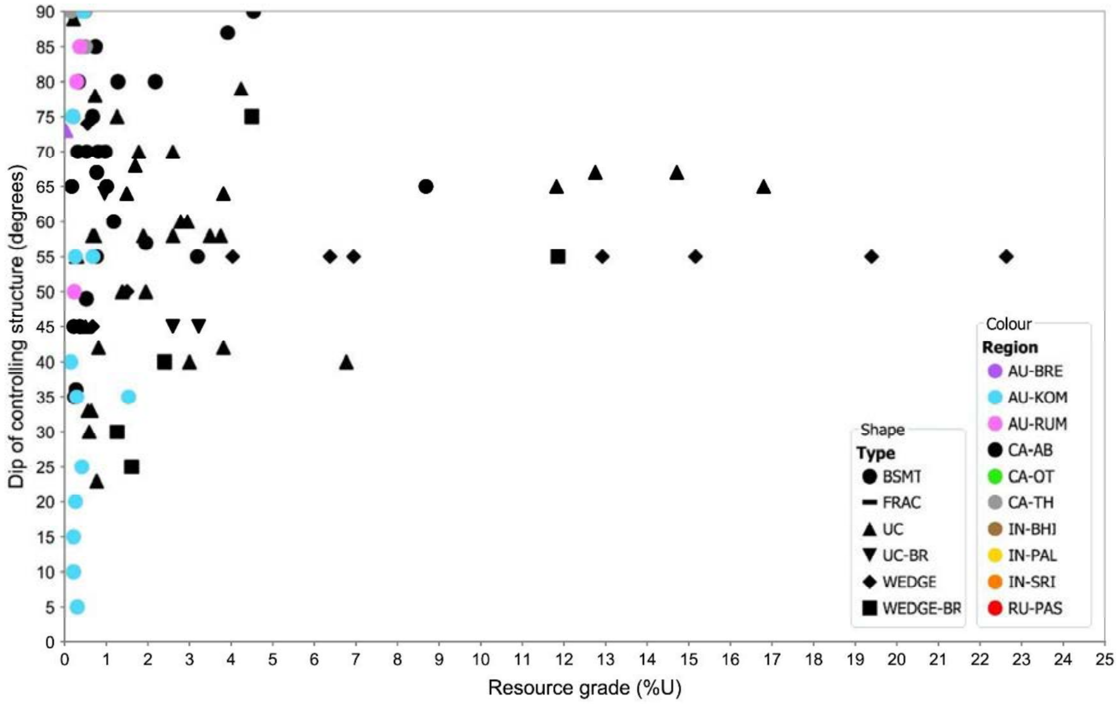

FIG. 2.10. Dip of controlling structure vs. resource grade for individual deposits. The different shapes represent the different types of deposits within the Proterozoic unconformity classification (BSMT=basement-hosted, FRAC=stratiform fracture controlled, UC=unconformity-hosted, UC-BR=unconformity-hosted with a basement root, WEDGE= structural wedge-hosted, WEDGE-BR=structural wedge-hosted with a basement root) whereas the colours represent the different basins or geographic areas (AU-BRE=Bresnahan Basin, AU-KOM=McArthur Basin, Kombolgie Subgroup, AU-RUM=Rum Jungle area, CA-AB=Athabasca Basin, CA-OT=Otish Basin, CA-TH=Thelon Basin, IN-BHI=Bhima Basin, IN-PAL=Palnad Basin, IN-SRI=Srisailam Basin, RU-PAS=Pasha Ladoga Basin).

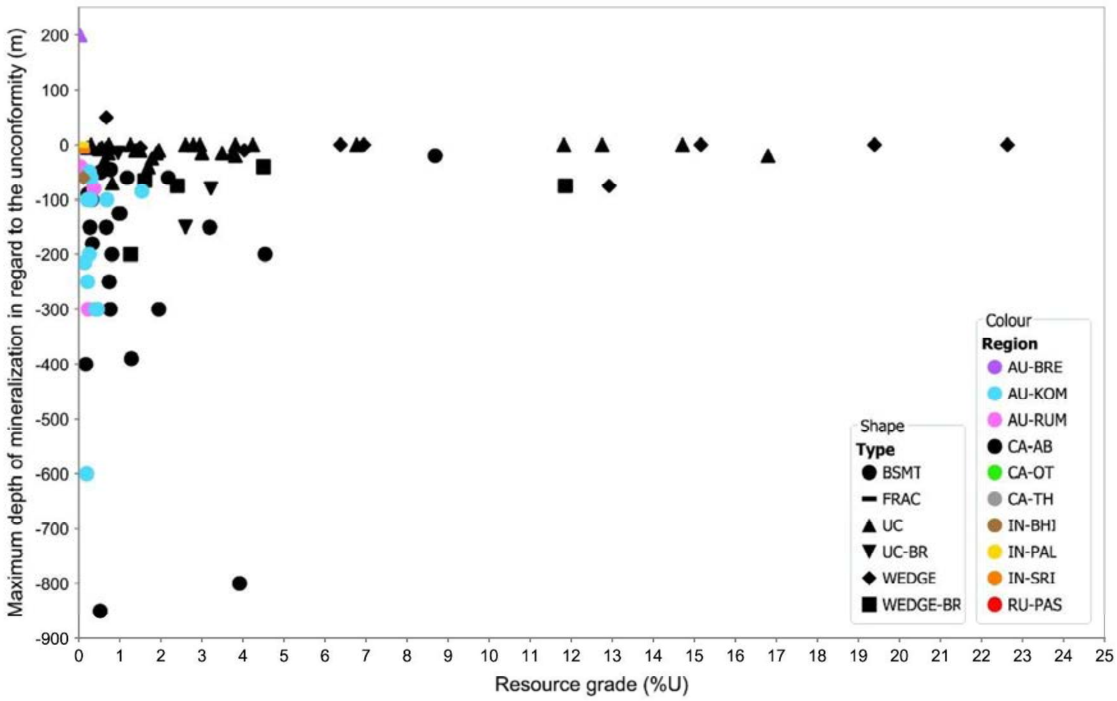

FIG. 2.11. Resource grade of deposits in relation to the maximum extent of the mineralization below the unconformity. The different shapes represent the different types of deposits within the Proterozoic unconformity classification (BSMT=basement-hosted, FRAC=stratiform fracture controlled, UC=unconformity-hosted, UC-BR=unconformity-hosted with a basement root, WEDGE= structural wedge-hosted, WEDGE-BR=structural wedge-hosted with a basement root) whereas the colours represent the different basins or geographic areas (AU-BRE=Bresnahan Basin, AU-KOM=McArthur Basin, Kombolgie Subgroup, AU-RUM=Rum Jungle area, CA-AB=Athabasca Basin, CA-OT=Otish Basin, CA-TH=Thelon Basin, IN-BHI=Bhima Basin, IN-PAL=Palnad Basin, IN-SRI=Srisailam Basin, RU-PAS=Pasha Ladoga Basin).

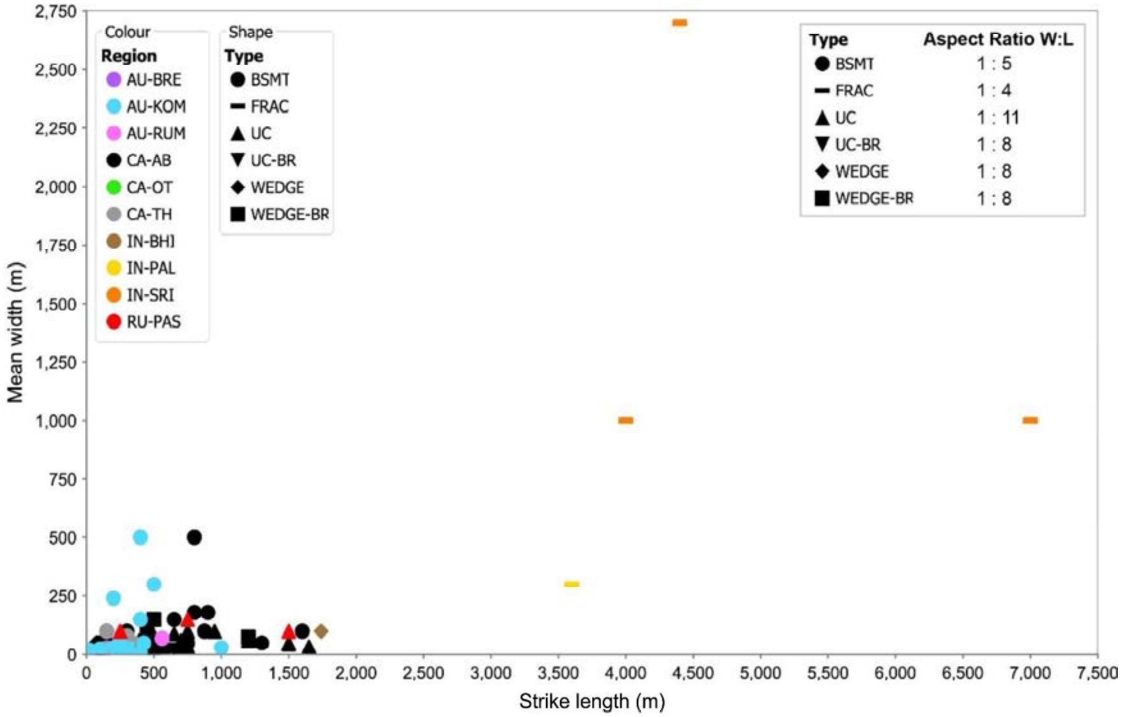

FIG. 2.12. Mean width of mineralization vs. strike length for individual deposits. A summary of aspect ratios by deposit type for the selected parameters is included within the plot area (W=mean width, L=strike length). The different shapes represent the different types of deposits within the Proterozoic unconformity classification (BSMT=basement-hosted, FRAC=stratiform fracture controlled, UC=unconformity-hosted, UC-BR=unconformity-hosted with a basement root, WEDGE= structural wedge-hosted, WEDGE-BR=structural wedge-hosted with a basement root) whereas the colours represent the different basins or geographic areas (AU-BRE=Bresnahan Basin, AU-KOM=McArthur Basin, Kombolgie Subgroup, AU-RUM=Rum Jungle area, CA-AB=Athabasca Basin, CA-OT=Otish Basin, CA-TH=Thelon Basin, IN-BHI=Bhima Basin, IN-PAL=Palnad Basin, IN-SRI=Srisailam Basin, RU-PAS=Pasha Ladoga Basin).

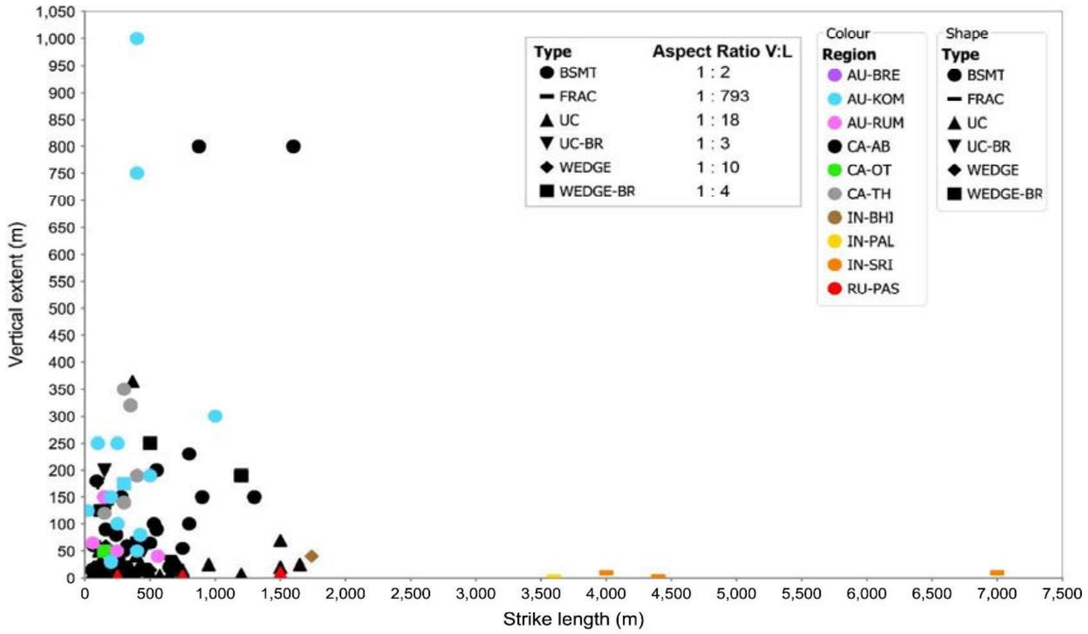

FIG. 2.13. Vertical extent of mineralization vs. strike length for individual deposits. A summary of aspect ratios by deposit type for the selected parameters is included within the plot area (V=vertical extent, L=strike length). The different shapes represent the different types of deposits within the Proterozoic unconformity classification (BSMT=basement-hosted, FRAC=stratiform fracture controlled, UC=unconformity-hosted, UC-BR=unconformity-hosted with a basement root, WEDGE= structural wedge-hosted, WEDGE-BR=structural wedge-hosted with a basement root) whereas the colours represent the different basins or geographic areas (AU-BRE=Bresnahan Basin, AU-KOM=McArthur Basin, Kombolgie Subgroup, AU-RUM=Rum Jungle area, CA-AB=Athabasca Basin, CA-OT=Otish Basin, CA-TH=Thelon Basin, IN-BHI=Bhima Basin, IN-PAL=Palnad Basin, IN-SRI=Srisailam Basin, RU-PAS=Pasha Ladoga Basin).

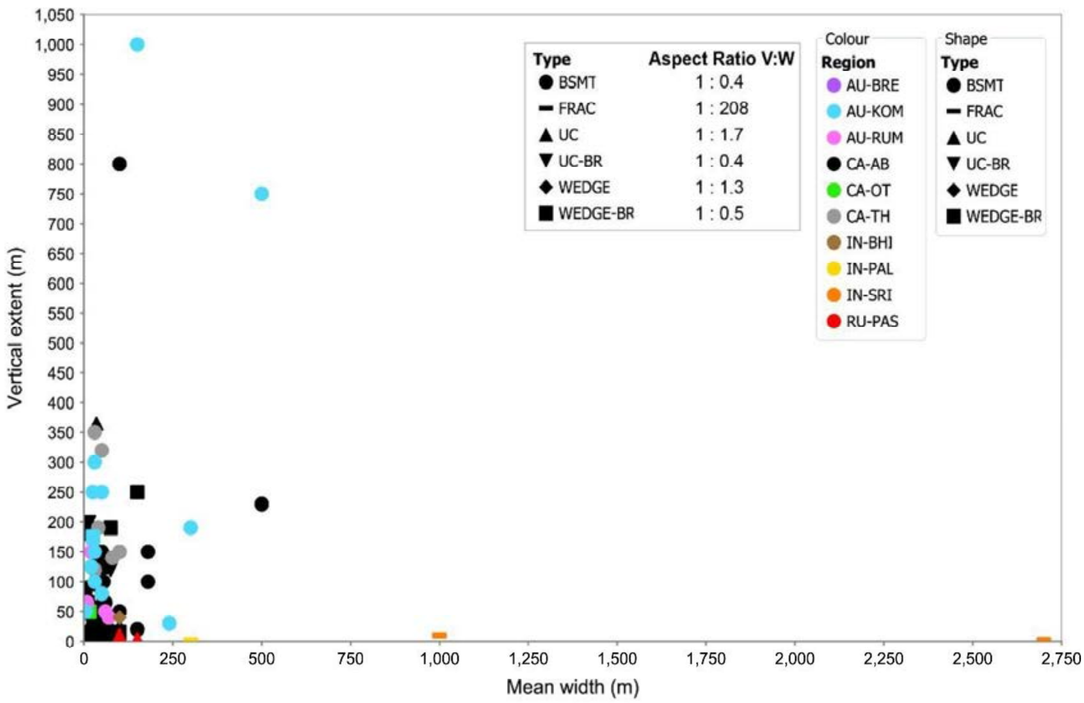

FIG. 2.14. Vertical extent of mineralization vs. mean width for individual deposits. A summary of aspect ratios by deposit type for the selected parameters is included within the plot area (V=vertical extent, W=mean width). The different shapes represent the different types of deposits within the Proterozoic unconformity classification (BSMT=basement-hosted, FRAC=stratiform fracture controlled, UC=unconformity-hosted, UC-BR=unconformity-hosted with a basement root, WEDGE= structural wedge-hosted, WEDGE-BR=structural wedge-hosted with a basement root) whereas the colours represent the different Basins or geographic areas (AU-BRE=Bresnahan Basin, AU-KOM=McArthur Basin, Kombolgie Subgroup, AU-RUM=Rum Jungle area, CA-AB=Athabasca Basin, CA-OT=Otish Basin, CA-TH=Thelon Basin, IN-BHI=Bhima Basin, IN-PAL=Palnad Basin, IN-SRI=Srisailam Basin, RU-PAS=Pasha Ladoga Basin).

Fig. 2.15 compares resource size versus the discovery year for individual deposits. Although many of the large deposits were discovered in the 1970s and 1980s in most basins, the Fig. clearly shows that Proterozoic unconformity deposits continued to be discovered through the 1990s, 2000s and 2010s. Significant deposits from the perspective of contained resource and grades continued to be discovered in the Athabasca Basin in the last decade and include Roughrider (2008), Phoenix (2009), Triple R (2012), Arrow (2014), Gryphon (2014). In Australia, the discovery of Ranger Deeps (2008) and the Angularli deposit (2011) underlined the continued potential for further discoveries in the McArthur Basin. Often, the clustering of discovery dates in specific regions (e.g. Rum Jungle, Kombolgie) and in countries for example, India is more a reflection of the cyclical nature of exploration activity as well as of local political environments (e.g. moratoriums on uranium exploration) rather than whether the area has been fully explored and evaluated. Another contributor to ongoing discoveries, particularly in the Athabasca Basin, has been a result of technological advances in exploration techniques (see Chapters 4 and 5 of this document), notably in geophysics, which can now provide better resolution through greater depths of cover.

The variability in the size and shape of deposit footprints of differing resource size and grades is illustrated in Fig.s 2.16 to 2.18. Only selected deposits are included in these Fig.s in order to provide a visual comparison of the range of resource sizes that can be contained in different footprint sizes and shapes.

Fig. 2.16 shows the footprint, in plan view, of seven deposits including Eagle Point, Cigar Lake, McArthur River, Jabiluka 2, Andrew Lake, Millennium and Koppunuru. The effect of grade is particularly illustrative when comparing the size of the contained resource relative to the aerial size of the footprint (e.g. Eagle Point compared to McArthur River). In particular, the aerial size of the Koppunuru deposits is significantly larger than all the other deposits, however, it contains the smallest resource size of the examples shown.

The two largest deposits in terms of resource size, i.e. >200 000 tU, McArthur River and Jabiluka 2, show a significant difference in their relative widths when illustrated in plan view. However, this is in part a function of the latter reflecting the vertical projection to surface of an inclined tabular deposit as opposed to a sub-vertical tabular deposit as in the former (Fig. 2.17). Similarly, the impact of grade on contained resource size becomes apparent when comparing the footprints of McArthur River (e.g. 14.41% U) and Jabiluka 2 (0.41% U) in plan view. Fig. 2.17, which shows cross-sectional views of these same seven deposits, illustrates the extremely limited thickness of the Koppunuru deposit relative to the other deposits. The cross-sectional footprint view also highlights the three fundamental lithostructural settings of unconformity associated deposits; unconformity contact type (e.g. Cigar Lake), basement-type (e.g. Eagle Point, Millennium, Jabiluka 2 and Andrew Lake) and wedge type (e.g. McArthur River). The cross-section footprint views also highlight the difference in continuity of mineralization within the deposit from narrow discontinuous vein systems (e.g. Eagle Point) through thicker semi-continuous stacked stratabound lenses (e.g. Jabiluka 2, Millennium) to more continuous massive mineralization (e.g. Cigar Lake, Andrew Lake, McArthur River).

Longitudinal footprint sections illustrated in Fig. 2.18 further emphasize the importance of grade in controlling the size of the contained resource when comparing the overall aerial extent of these deposits. The Eagle Point deposit, with a contained resource of 82 161 tU, clearly has the largest longitudinal section footprint, while in comparison, McArthur River and Jabiluka 2, with contained resources of 259 583 tU and 119 884 tU respectively, are relatively modest from the perspective of their longitudinal view. Fig. 2.18 also re-enforces the very thin nature of the Koppunuru deposit compared to the other deposits selected for comparison. The longitudinal view also emphasizes the spatial association of the Millennium, Jabiluka 2, Cigar Lake, McArthur River and Koppunuru deposits to the unconformity. It should be noted that two unconformities are projected for the McArthur River; this is the result of the duplication of the unconformity due to fault repetition when projected in longitudinal section.

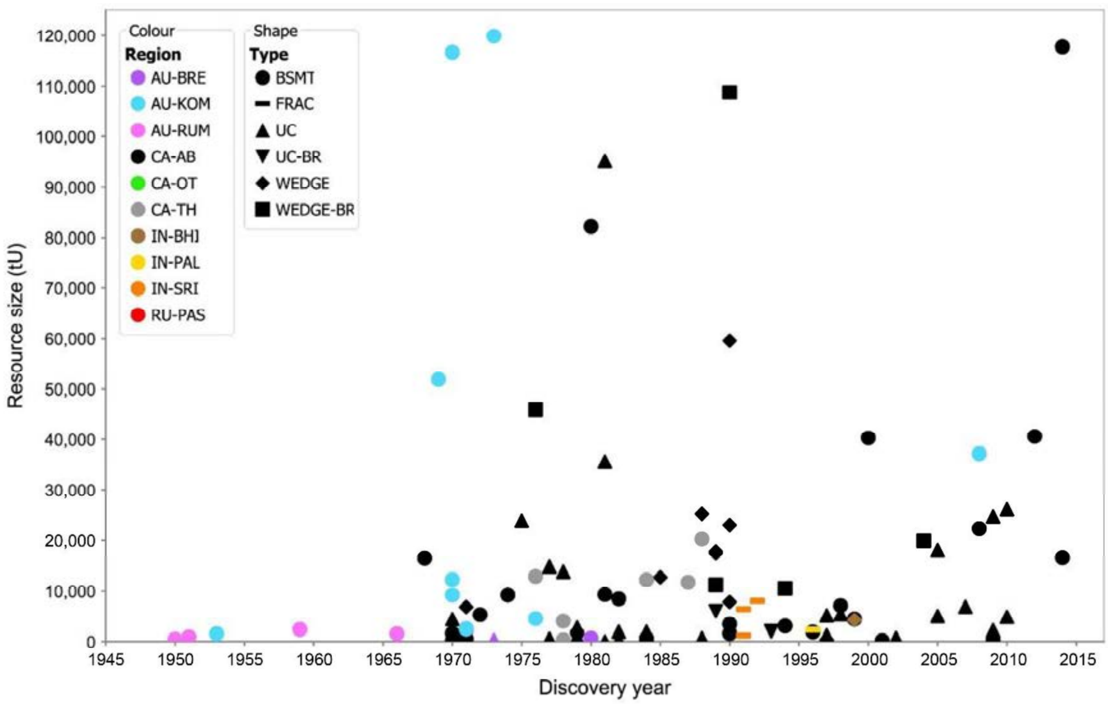

FIG. 2.15. Discovery year of individual deposits. The resource number represents what the deposit size ended up being as of the time of writing. The discovery year is considered the year in which the first significant uranium mineralization was reported for a deposit. The different shapes represent the different types of deposits within the Proterozoic unconformity classification (BSMT=basement-hosted, FRAC=stratiform fracture controlled, UC=unconformity-hosted, UC-BR=unconformity-hosted with a basement root, WEDGE= structural wedge-hosted, WEDGE-BR=structural wedge-hosted with a basement root) whereas the colours represent the different Basins or geographic areas (AU-BRE=Bresnahan Basin, AU-KOM=McArthur Basin, Kombolgie Subgroup, AU-RUM=Rum Jungle area, CA-AB=Athabasca Basin, CA-OT=Otish Basin, CA-TH=Thelon Basin, IN-BHI=Bhima Basin, IN-PAL=Palnad Basin, IN-SRI=Srisailam Basin, RU-PAS=Pasha Ladoga Basin).

Although only seven deposits are selected for visual comparison, the three different views presented illustrate that there is a large range of aerial sizes in deposit footprints. One general observation is that deposits which have a relatively large dimension along one or two axes are usually quite limited in the remaining dimensions. One key observation is that there is little correlation between aerial size of the deposit footprint and the contained uranium resource; it is not surprising that the grade of mineralization becomes a critical parameter when differentiating resource sizes of deposits.

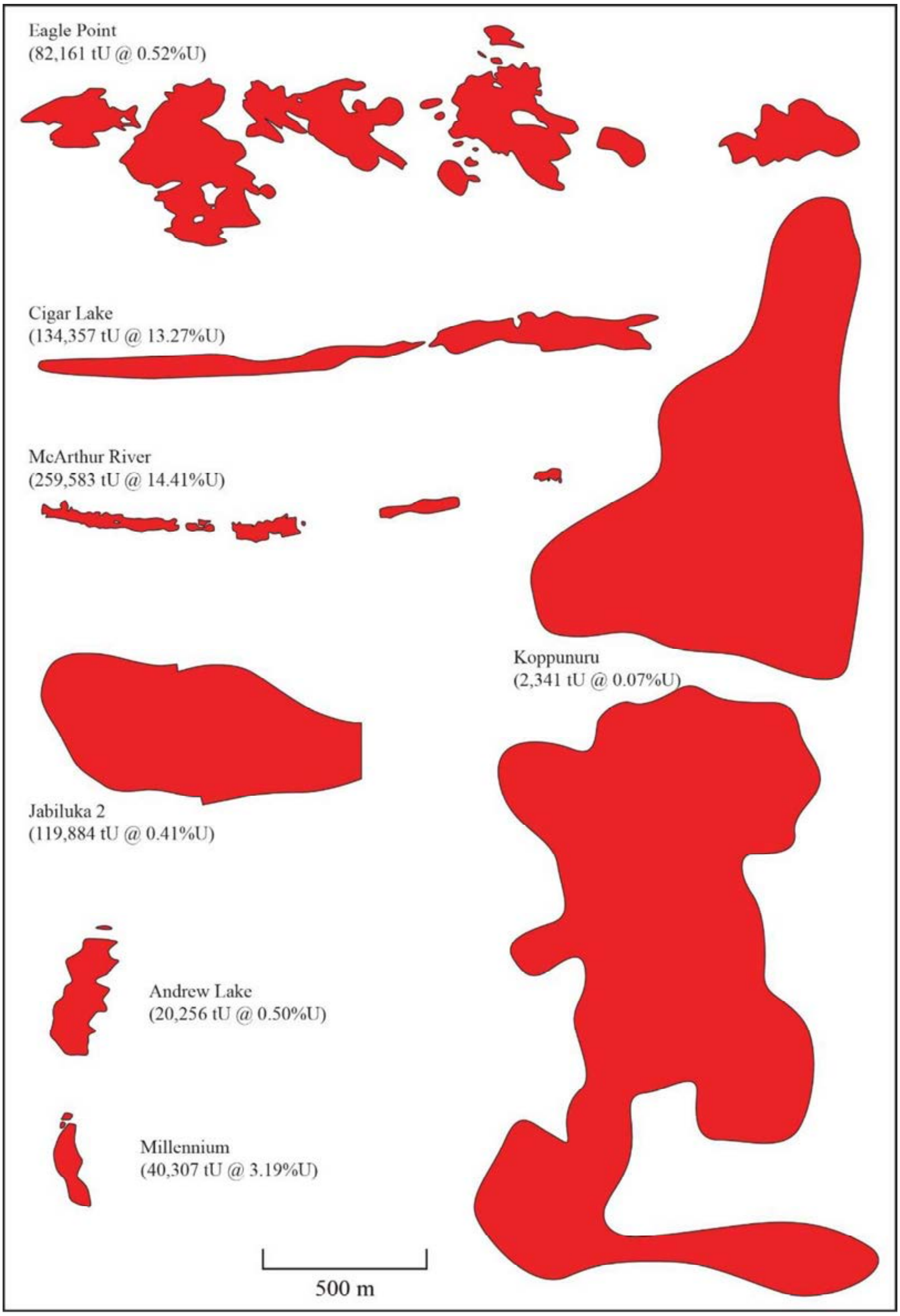

FIG. 2.16. Comparison of individual mineralization footprints for selected deposits in plan view. This is a vertical projection of the mineralization onto a horizontal plane. The footprints are not spatially orientated, but are at the same scale [2.27, 2.47, 2.90, 2.182].

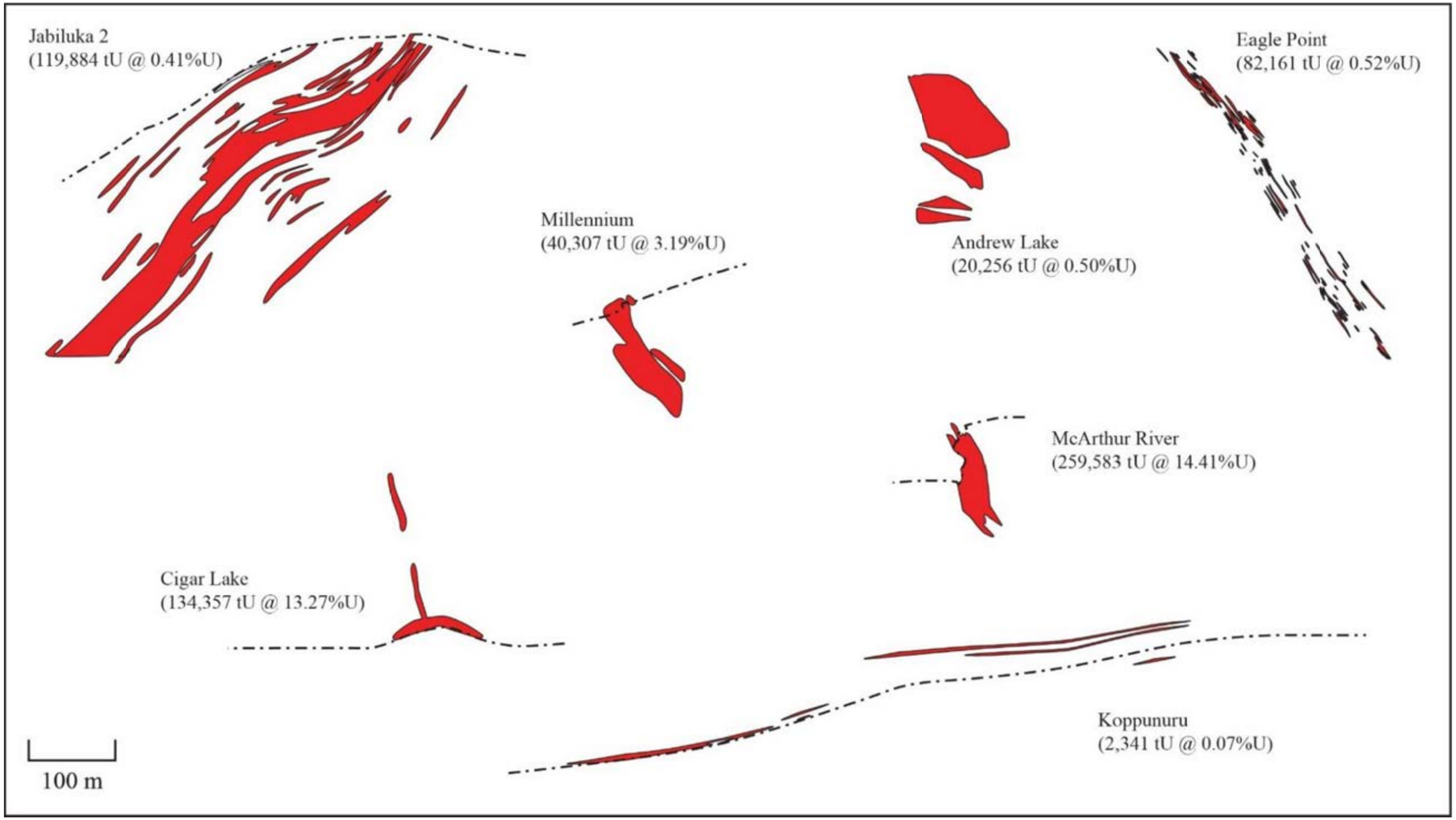

FIG. 2.17. Comparison of individual mineralization footprints for selected deposits in cross-section view (as determined by the short axis of the deposits). This represents schematic or actual cross-section within the specific deposits. The footprints are not spatially orientated, but are at the same scale. Dashed lines represent the unconformity trace [2.27, 2.47, 2.90, 2.182].

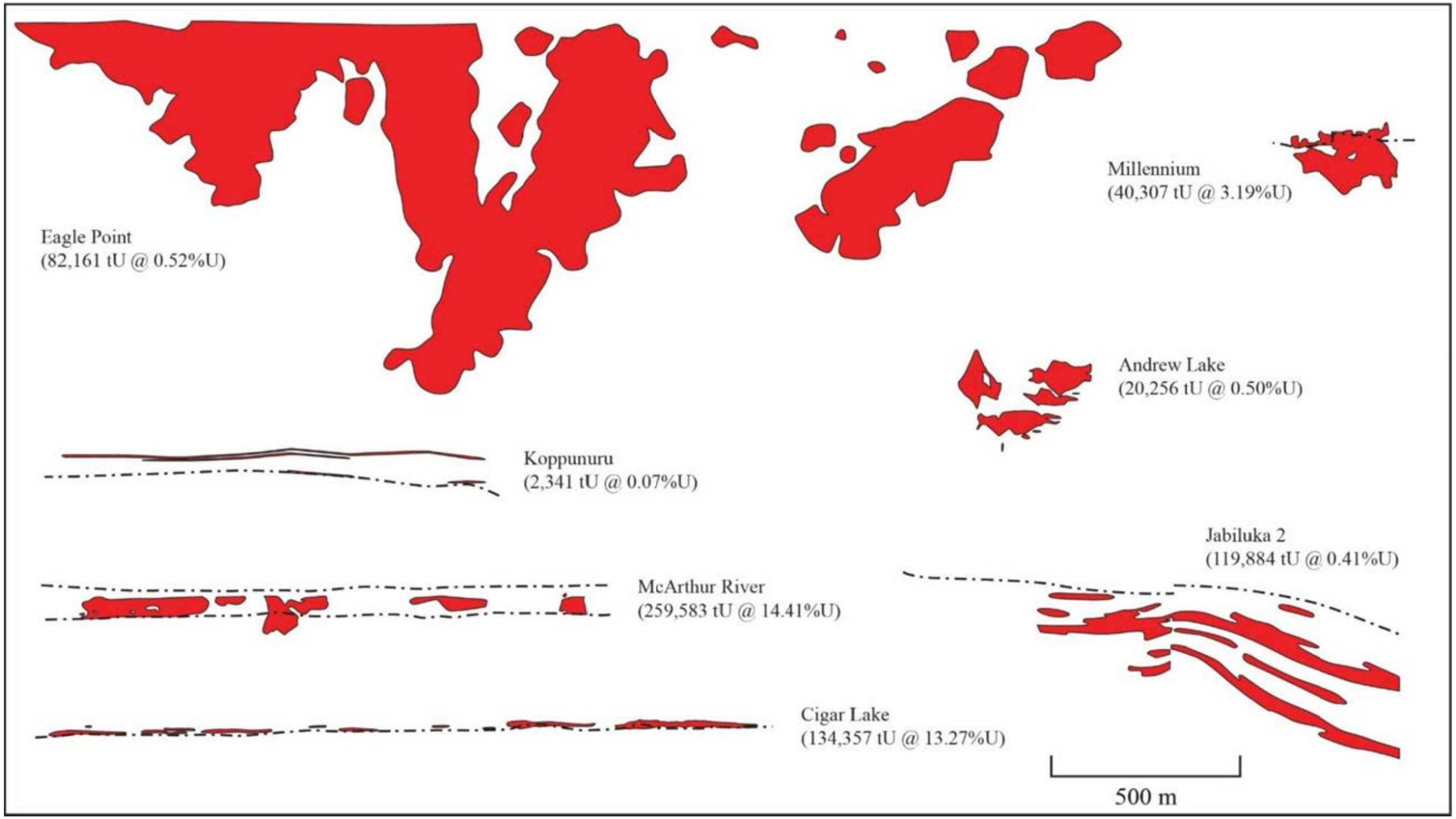

FIG. 2.18. Comparison of individual mineralization footprints for selected deposits in longitudinal section view (as determined by the long axis of the deposits). This is a projection of the mineralization on a vertical plane. The footprints are not spatially orientated, but are at the same scale. Dashed lines represent the unconformity trace [2.27, 2.43, 2.47, 2.90, 2.182].

2.2. EMPIRICAL LITHOSTRUCTURAL END MEMBERS

2.2.1. Introduction

Ongoing analytical research work over the last 30 years has continued to refine the understanding of the physiochemical nature of the ore- and alteration-related fluids and the timing of the mineralization events. However, there has been arguably less advancement in developing a robust exploration-focused empirical model for unconformity-related deposits. Understanding ore-forming processes from the perspective of source of the metals, transport from source to deposition site, critical physical and chemical mechanisms to promote metal precipitation or 'trap', and conditions preserving mineralization, form the cornerstones in the development of ore deposit genetic models. In contrast, in an exploration targeting strategy, whether at a regional, district or drill target scale, the decision process is primarily guided by the empirical criteria that are considered to be critical in defining the ore deposit of interest. The key parameters of a robust empirical model underpinning most exploration targeting strategies, execution tactics and stage-gate decisions typically evolve around: 1) a preferred lithostratigraphic host assemblage; 2) unique structural sites for the localization of mineralization; 3) presence of critical geochemical pathfinder elements and mineralogical assemblages defining alteration zonation; 4) understanding the range of dimensional sizes of orebodies and their enveloping alteration footprints; 5) grade and resource distribution ranges for uneconomic through economic examples; and 6) metallurgical variation of orebodies both in geochemical and mineralogical composition as well as mineralization styles. In the case of blind exploration targets, particularly in deeply covered areas, having sufficient physical property data for many of the geological parameters is critical to build robust geophysical models as a proxy for the empirical deposit model.

An understanding of the range of values characterizing specific empirical parameters of the deposits, especially in the Athabasca Basin, helps delineate potential options or expectations in the exploration decision and planning process. Examples of exploration decisions that are largely driven by a good understanding of the empirical deposit model include area selection at a regional and district scale, drill hole targeting at a property scale, and, depending on the style of mineralization, the optimum drill plan design of a target area. Based on drill hole results, decisions can be made whether the tested area reflects background conditions or alternatively is distal or proximal to mineralization, thereby warranting further work. When drilling mineralization, it is particularly important to understand the specific range of physical dimensions and grades of known orebody footprints, which can help determine whether the results are advancing the prospect to a potentially economic deposit.

2.2.2. New empirical classification and end members

Based on a comprehensive compilation of uranium deposits/pods (85) and systems (16) from the Athabasca Basin (see Table 2.1), an empirical-based classification is proposed which captures the range of structural settings, mineralization styles, as well as the dimensional characteristics of the alteration and orebody footprints. The proposed classification recognizes four Athabasca Basin lithostructural footprint end members which are represented by the Cigar Lake, McArthur River, Eagle Point and Millennium deposits (Fig. 2.19).

The proposed tetragonal-based classification captures the range of structural settings represented by deposits in the basin, in particular the location of mineralization relative to the basin-basement unconformity; whether it is largely developed along the unconformity, or predominantly in the underlying basement gneisses, or in the sandstone footwall wedge along controlling faults. Additionally, the classification captures the maximum extent of the mineralization within the basement from shallow (<10 m) to deep (>10 m).

The four end members of this tetragonal classification exhibit characteristic alteration footprints ranging from extensive broad halos (>100 m) either in the sandstone (e.g. Cigar Lake) or basement (e.g. Millennium) to relatively tight or narrow alteration selvedges (<20 m) enveloping the mineralization (e.g. McArthur, Eagle Point).

A secondary characteristic captured in the tetragonal classification is the relative grade and resource size of the orebody; whether the deposit is high grade and large resource (>10% U, >750 00 tU), low grade and large resource (<2% U, >40 000 tU), or, moderate grade and moderate resource (>2–5% U, <40 000 tU). A corollary of the dimensional data is the aspect ratio or geometric shape of the orebody (e.g. cylindrical, tabular, and prismatic). The classification also captures, in part, the monometallic (simple) or polymetallic (complex) nature of the mineralization.

The Cigar Lake end member is characterized by dominantly sandstone-hosted high-grade mineralization which forms a sub-horizontal cylindrical orebody typically greater than 1000 m in strike length. This end member comprises massive polymetallic mineralization located at the intersection of the sub-Athabasca unconformity and a broad distributed deformation fault zone with minimal vertical displacement of the unconformity. A thick sandstone alteration halo extends up to several hundred metres above the orebody, while intense alteration extends a few tens of metres below the unconformity. The width of the alteration ranges from 10 to 50 m beyond the orebody footprint.

The McArthur River end member represents high-grade, sub-vertically-plunging, narrow prismatic or pod-like orebodies (<100 m strike, up to 100 m vertical thickness) largely developed in the sandstone footwall wedge setting of a dominantly dip-slip reverse fault. The mineralization is dominantly monometallic comprising massive replacement uraninite and pitchblende. The alteration halo in the sandstone extends several 100 m above the unconformity. The width of the alteration halo is relatively tight, typically less than 20 m around sandstone wedge-hosted mineralization and less than 10 m around basement-hosted ore lenses.

The Eagle Point end member forms an extensive system (> 1000 m strike length) of low grade vein-type basement-hosted monometallic uranium mineralization. The mineralization forms moderate to steeply-plunging tabular lenses varying from subconcordant to discordant to the basement lithostratigraphy.

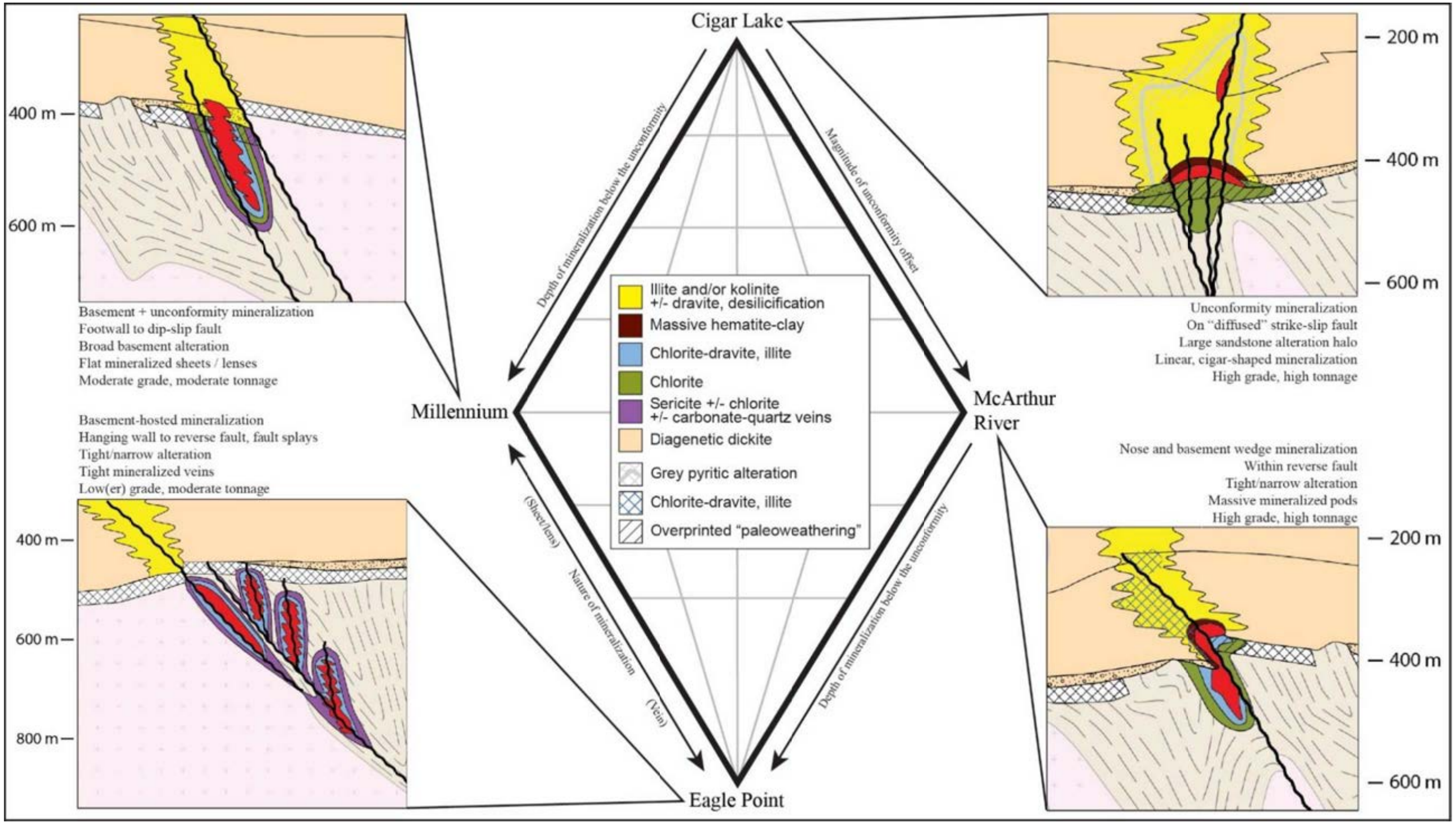

FIG. 2.19. Lithostructural classification diagram with end member summary characteristics.

The orebodies are spatially generally associated with transpressional post-sandstone fault zones developed in metasedimentary rocks although immediately hanging wall to Archean granitoid gneisses. Mineralized zones may occur several hundreds of metres into the hanging wall block of the major controlling faults while individual lenses may extend over several metres down dip. In the case of Eagle Point, uranium mineralization has been traced up to 850 m below surface, indicating this end member represents deeply penetrating ore systems. Alteration is relatively tight to mineralized lenses, ranging between a few metres to several tens of metres in width, however halos associated mineralized lenses within or immediately adjacent to the major controlling faults may be up to 75 m wide.

The Millennium end member is characterized by moderate to high-grade vein- and breccia-associated monometallic mineralization, forming a series of moderately to steeply-plunging stacked basement-hosted tabular lenses. The orebody footprint extends over two hundred metres in strike and up to several hundred metres below the unconformity. Mineralization may also extend to the sandstone-basement unconformity but in general does not form a significant proportion of the overall deposit resources. Individual lenses are broadly subconcordant to concordant to the overall basement lithostratigraphy and may be developed less than a few tens of metres footwall or hanging wall to a major post-sandstone reactivated basement fault. Alteration is intense and forms a broad halo exceeding 50 m around the dominantly basement-hosted mineralization.

This tetragonal classification scheme that focuses on critical empirical parameters — such as, the variations in lithostructural settings, in which the Athabasca deposits occur; the size and shape variation of alteration and mineralization footprints; as well as the range of grades and /tonnages defining the contained resource — will better assist explorationists in developing targeting strategies for uranium mineralization in the Athabasca Basin and possibly worldwide. It is also important to keep in mind that this new classification scheme can be dynamic, and end members could be replaced by new world class discoveries that better exemplify/are better suited as end members.

2.2.3. The Athabasca Basin – Type area for classification

The Athabasca Basin is the premier mineral district for Proterozoic unconformity uranium deposits with an excess of 1 million tU being identified through exploration and mining development since 1968, when the first discovery of high grade uranium mineralization was made at Rabbit Lake by Gulf Minerals Canada Ltd. Since this first discovery, a total of 85 individual deposits or zones have been delineated within the basin. While the majority of discoveries have been made in the eastern part of Athabasca Basin, uranium deposits and significant mineralization have also been identified across much of the basin including the extreme NW at Maurice Bay, to the Maybelle Creek in the west, as well as along the northern margin at Fond du Lac, and along the south-western margin at Patterson Lake. Although most of the deposits have been found at sandstone depths of less than 500 m, significant mineralization has been intersected at unconformity depths exceeding 750 m at the Shea Creek and Centennial deposits, while mineralization has been delineated more than 800 m below the projected unconformity at the Eagle Point and Arrow deposits. Based on the global uranium resource identified to date, and the basin-wide distribution of high grade uranium mineralization, the Athabasca Basin truly represents a world class metallogenic district and its major deposits form the basis deposits.

The Athabasca Basin (Fig. 2.20), located primarily in northern Saskatchewan with a small portion extending into Alberta, is an easterly-elongated basin, approximately 460 km in length and 220 km in width. The basin is infilled by the Athabasca Group, a Late Paleoproterozoic fluvial to marine sequence unconformably deposited between 1760 and 1500 Ma [2.193] on polyphase deformed and metamorphosed Archean and early Paleoproterozoic rocks. The Athabasca Group is predominantly composed of quartz-rich fluvial sandstones and lesser amounts of conglomerate and siltstone which have undergone metamorphism or penetrative deformation. The siliciclastic rocks are subdivided into eight formations (Fair Point, Reilly, Read, Smart, Manitou Falls, Lazenby, Wolverine Point, and Locker Lake formations), having an estimated aggregate thickness of about 3000 m, and which in turn are overlain by a minimum of 800 m of shale (Douglas Formation) and carbonate (Carswell Formation) strata. The Douglas and Carswell formations are preserved in the western part of the basin where they outcrop around the circular Carswell structure, a meteorite impact feature estimated to have formed during the Lower Cretaceous about 115 Ma. Due to erosion, the maximum thickness of the Athabasca Group in any one place in the basin is about 1500 m although the aggregate thickness of all stratotypes is estimated around 3800 m [2.193]. A detailed stratigraphic framework for the Athabasca Basin has been proposed by Ramaekers et al. [2.193] with more recent revisions by Bosman and Ramaekers [2.194].

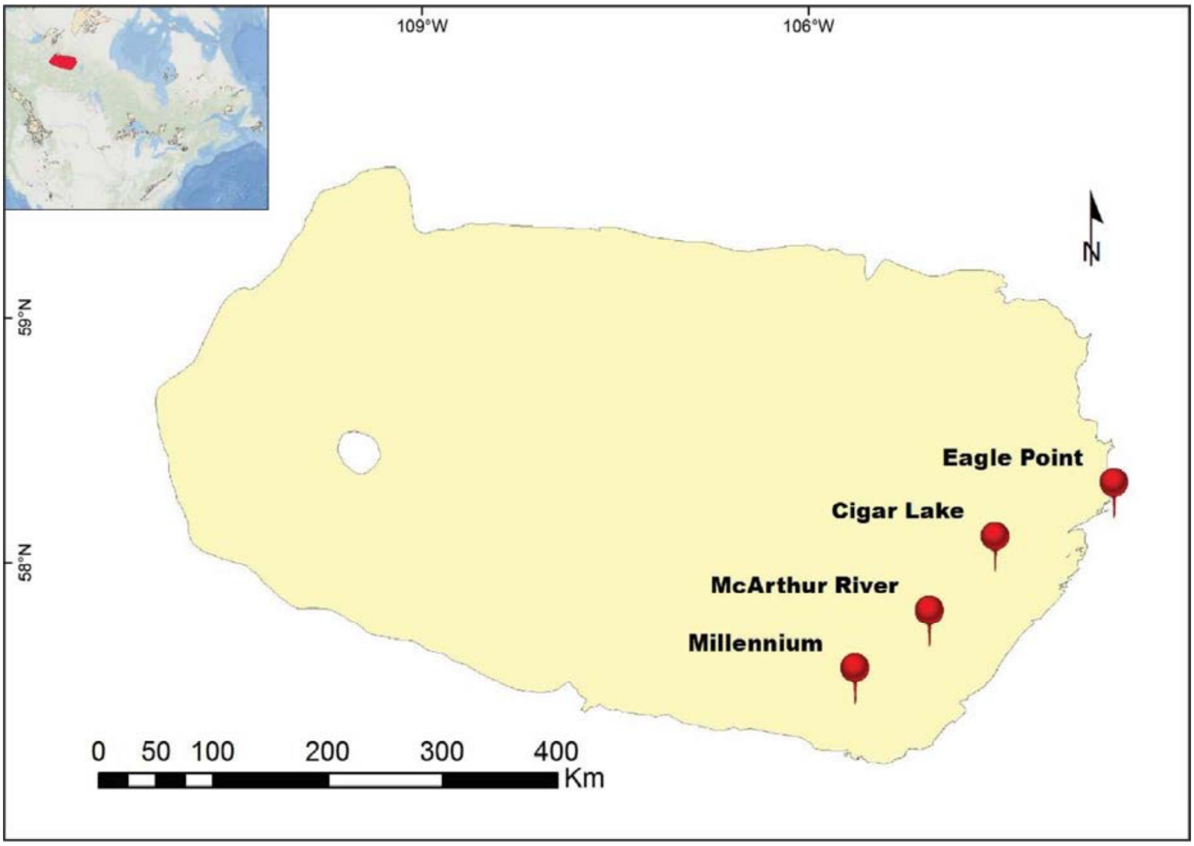

FIG. 2.20. Athabasca Basin with the location of the four lithostructural deposit end-members used in the lithostructural classification introduced in Chapter 2 using the data provided in Table 2.1. Inset represents the location of the Athabasca basin within part of North America [2.23,2.47].

The basin is intruded by sparsely distributed NW-trending sub-vertical diabase 1.267 Ga Mackenzie dykes [2.195] and olivine gabbro sills of the 1.11 Ga Moore Lake Complex located along the SE perimeter of the basin.

The Athabasca Basin and its underlying basement rocks are cut by a variety of semi-brittle to brittle post-sandstone faults varying in orientation from NS, NNE, EW to NW trending. Offsets of the pre-Athabasca unconformity reflect a spectrum of kinematic movements, although dip slip-reverse and transpressional displacements are predominant. Maximum vertical fault displacement documented in the basin is in excess of 250 m where it is observed along the NE-trending Dufferin Fault in the south-central part of the basin. Many post-sandstone faults are interpreted as reactivation of pre-existing, pre-sandstone graphitic ductile to semi-brittle basement structures. Uranium deposits in the basin have a clear spatial relationship to post-sandstone reactivated graphitic basement faults.

2.2.4. Cigar Lake deposit

2.2.4.1. Introduction

The Cigar Lake deposit, located in the eastern Athabasca Basin, is the world's second highest grade uranium mine, behind McArthur River. The deposit is owned by a joint venture between Cameco Corporation (50.025%), AREVA Resources Canada Inc. (37.100%), Idemitsu Canada Resources Limited (7.875%) and TEPCO Resources Inc. (5.000%) and is located on the Waterbury/Cigar Lake property. The site can be accessed via provincial highways as well as an on-site permanent airstrip. Cameco Corporation is the operator of the mine and commercial production started in May 2015.

Since the beginning of production to the end of 2016, Cigar Lake has produced approximately 11 116 tU. As of 31 Dec. 2016, the deposit contained an estimated mineral reserve (proven and probable) of approximately 82 776 tU at an average grade of 13.48% U, with an additional mineral resource (measured and indicated) of 32 541 tU at an average grade of 13.71% U.

2.2.4.2. Exploration history

The current Cigar Lake property was initially staked by Asamera Oil Corporation. In 1980, S.E.R.U. Nucléaire Limitée took over as operator and which later became COGEMA Resources Inc. in 1984, and subsequently AREVA Resources Canada Inc. in 2006. Early fieldwork consisted of airborne and ground geophysical surveys, and lake sediment and water sampling programmes. Drilling on the property began in 1978 with the discovery of the Cigar Lake uranium deposit in 1981.

Following the discovery, a combination of 239 additional exploration diamond drill holes and off-cuts (102 577 m) were completed between 1982 and 1986, on the Waterbury/Cigar Lake property, almost all of which were located on or adjacent to the Cigar Lake deposit. Additional airborne and ground geophysical surveys continued both within and outside of the immediate Cigar Lake deposit area. All exploration activities ceased after the 1986 field season, at which point the Cigar Lake Mining Corporation was formed to develop and control all mining activities.

Exploration activities on the project outside of the deposit mining lease recommenced in 1999 and continue till date.

2.2.4.3. Regional geology

The Cigar Lake deposit is located under sandstones from the Manitou Falls (MF) Formation of the Athabasca Basin, of which three members are present: conglomeratic MFb (Bird Member), sandy MFc (Collins Member), and clay-intraclast rich MFd (Dunlop Member). The sandstone is characterized by 1 to 5% pore space filled with matrix clay, composed of kaolin (dickite and lesser kaolinite) and illite, plus or minus haematite, and variable amounts of quartz overgrowth cement. These sandstones were deposited in alluvial fans and in braided streams with generally horizontally-bedded alternating coarser and finer units, with abundant cross-bedding observed. The sandstone thickness in the area ranges in thickness from 270 to 550 m.

The unconformable contact between the Mesoproterozoic Athabasca Group sandstone and the underlying crystalline basement rocks is typically marked by a few metres of mineral-rich clay, red to green mineralogically-zoned (paleo-weathered) post-Hudsonian regolith that can range in thickness from 0 to >80 m. The thickness of the profile is highly dependent on the composition of the parent rock as well as the presence of basement faults. Below an upper clay-rich (kaolinitic) and hematitic red zone, there is an illitic to chloritic red-green zone that is transitional to a chloritic to illitic, variably light to dark green zone. The weathered basement then grades downward, generally over a few metres, into unaltered basement.

The sub-Athabasca crystalline metamorphic basement is composed of rocks of the Wollaston and Mudjatik lithostructural domains. The Wollaston Domain is a distinctly NE trending fold-thrust belt composed of Paleoproterozoic Wollaston Group metasediments overlying Archean granitoid gneisses. The Mudjatik Domain is a NE trending, shear-bounded belt consisting mainly of Archean felsic gneisses [2.196]. Both domains have undergone complex polyphase deformation and metamorphism during the Trans Hudson Orogeny, including intrusion of metaluminous and peraluminous bodies. The Mudjatik Domain consists of variably reworked Archean granitic orthogneisses, locally charnockitic, and numerous small remnants of polydeformed Aphebian metasedimentary rocks similar to Wollaston Group metasediments. This domain displays a mixed pattern of aeromagnetic highs and lows. To the east, the metasedimentary rocks of the Wollaston Domain rest unconformably on Archean granitoid gneiss. This domain comprises the Wollaston–Mudjatik Transition Zone, the western Wollaston Domain, and the eastern Wollaston Domain. The Wollaston–Mudjatik Transition Zone forms a transition from the linear Wollaston fold and thrust belt to the dome and basin interference-folded Mudjatik Domain.

The western Wollaston Domain and the Wollaston–Mudjatik Transition Zone are structurally complex, consisting of elongated Archean granitoid domes (mega-boudins), dominant thrust- and strike-slip structures, and related duplex structures [2.196]. The western Wollaston Domain is characterized by an overall aeromagnetic low related to the dominant Paleoproterozoic Wollaston Group metasedimentary lithologies. This lower sequence of the Wollaston Group consists mainly of lowermost graphitic pelitic gneiss, followed by garnetite, pelitic gneiss, calc-pelitic gneiss, psammo-pelitic gneiss, psammitic gneiss, and meta-quartzite. The Wollaston Group comprises three metasedimentary supracrustal successions deposited in rift, passive margin, and foreland basin environments [2.197]. These rocks overlie and are locally intercalated with the Archean orthogneisses.

The eastern Wollaston Domain corresponds to an aeromagnetic high and is made up of the upper sequence of the Paleoproterozoic Wollaston Group. It consists of calc-silicate- and magnetite-bearing siliciclastic metasediments overlying a lower Wollaston Group sequence of magnetite-rich to magnetite-poor pelitic to psammitic gneisses. Archean orthogneisses are locally infolded.

The Waterbury/Cigar Lake area is located within both the Mudjatik and Wollaston Domain with a large portion of the centre part of the property being within the Wollaston/Mudjatik transition zone. The sub-Athabasca basement geology is characterized by both a 'dome and basin' setting and long linear granitoids, depending on the location within the property. Within the 'dome and basin' scenario, in plan view, large Archean granitoid 'domes' alternate with stratigraphically-overlying Paleoproterozoic Wollaston Group metasedimentary rocks.

Sub-vertical, N-NE trending ductile and brittle-ductile fault zones that developed during the Hudsonian Orogeny are dominant structural features within the basement rocks of the eastern Athabasca Basin. However, the main Cigar Lake trend is in an EW orientation and represents a peculiar structural system in this general tectonic framework. These faults are commonly reactivated after the deposition of the Athabasca Group and are associated with graphitic stratigraphy. Post Athabasca Group faulting, as recognized within the Wollaston Domain, is characterized as dominantly reverse structures (referred to as D5) with a later dominantly strike-slip component (referred to as D6). The geological setting of the Cigar Lake deposit in regard to basement stratigraphy is illustrated in Fig. 2.21.

2.2.4.4. Deposit geology

Host rocks

The Cigar Lake uranium deposit is located at the unconformity between the Middle Paleoproterozoic Wollaston Group metasedimentary basement rocks and the Late Paleoproterozoic to Mesoproterozoic Athabasca Group, at a depth between 410 and 450 m below surface.

The deposit and host rocks consist of three principal geological and geotechnical elements: 1) the deposit itself; 2) the overlying sandstone; and 2) the underlying metamorphic basement rocks. The Athabasca Group's Manitou Falls Formation is 420–445 m thick. The basement lithological domains consist of: 2) a variably graphitic pelite unit located directly below the deposit, 2) a calc-silicate rich unit labelled as 'Meta-Arkose' locally present to the south of the deposit, and 3) a biotite pelite unit located to the south of the deposit area within which most of the mine access infrastructure is located. The graphitic pelite unit has been further divided into two sub-domains including a graphite and sulphide-rich portion located directly below the uranium mineralization, that has undergone variable and locally significant shear deformation, and a lesser graphite-rich portion that contains significantly less sulphides and exhibits less shear deformation. The dominant foliation in the basement rocks is east striking and moderately to steeply south dipping. Fig. 2.22 presents a generalized geological cross-section of the deposit.

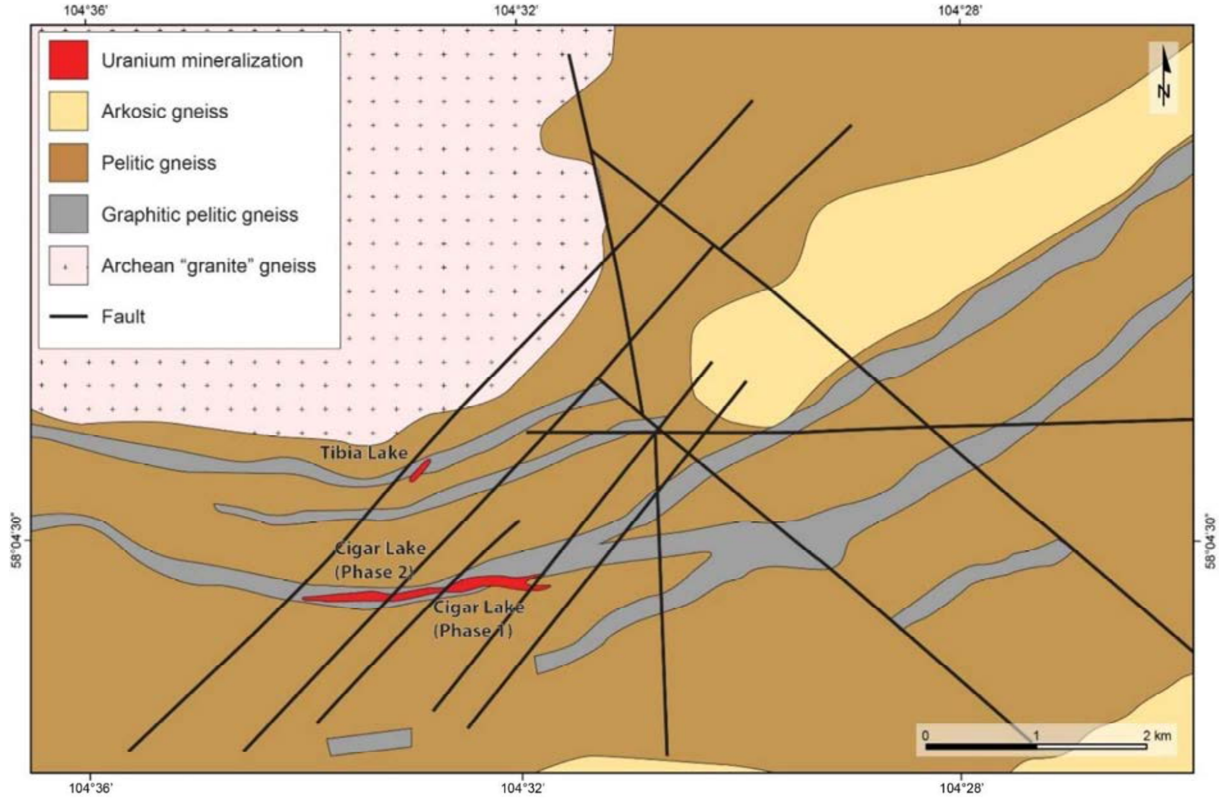

FIG. 2.21. Regional basement geology map of the Cigar Lake area with major lithologies, major faults and uranium deposits. Modified from Bruneton [2.43].

Structure

The structural framework in the Cigar Lake mine area is dominated by variably reactivated east-trending mylonitic corridors. The unconformable contact between these mylonites and the overlying Athabasca sandstone, is considered as the most significant location for the concentration of uranium mineralization, specifically where graphitic basement fault zones were reactivated as brittle faults after sandstone deposition.

The dominant structural control at Cigar Lake is a series of east-trending and south dipping, foliation parallel, semi-brittle to brittle faults within a zone approximately 20–100 m in width. These faults are largely hosted by graphitic pelitic schist and gneiss and are variably defined as crackle to chaotic breccia with lesser cataclasite. Individual faults are less than 4 m in width; commonly less than 0.5 m in width. Within the lower sandstone, discrete fault structures are difficult to identify due to a zone of strong brecciation and quartz dissolution. The density of breccia fractures decreases with elevation above the unconformity surface.

Within the basement, a series of steeply dipping NNW and NE brittle structures have been mapped. These structures appear to have limited strike extent of less than 300 m. Within the Athabasca Group, two dominant discrete fault orientations are defined: east-striking and steeply south dipping and west-striking and steeply north dipping. These faults are defined as 0.5–5 m wide fracture/breccia zones with enhanced permeability.

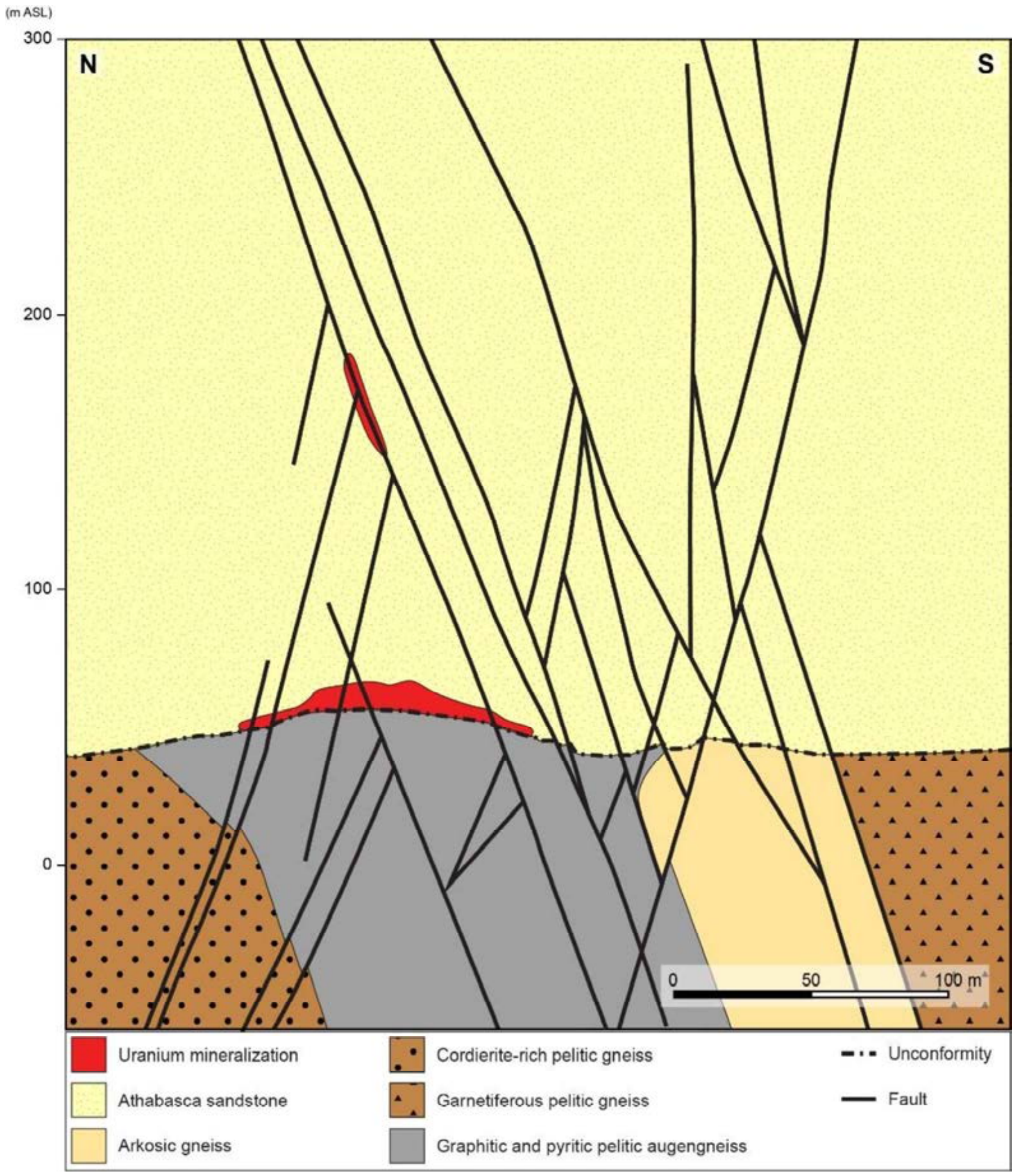

FIG. 2.22. Schematic geological cross-section of the Cigar Lake Phase 1 deposit. Modified from Cameco Corporation [2.47].

Deposit footprint

The Cigar Lake deposit has the morphology of a flat- to cigar-shaped lens approximately 1900 m in length, 30–100 m in width and ranges up to 13.5 m thick, with an average thickness of about 8 m. The deposit is subdivided into the eastern Phase 1 and western Phase 2 zones, Phase 1 being further divided into the east and west pods. The deposits show remarkable longitudinal and lateral geological continuity.

Mineralization style

Three distinct styles of mineralization occur within the Cigar Lake deposit: 1) the first contains all of the mineral resources and reserves which is the high grade mineralization at the unconformity ('unconformity' mineralization); 2) fracture controlled, vein-like mineralization higher up in the sandstone ('perched' mineralization); and 3) fracture controlled, vein-like mineralization in the basement rock [2.38].

The high-grade mineralization located at the unconformity contains most of the total uranium metal and represents the only economically viable style of mineralization considering the specialized mining method and ground conditions. It is characterized by the occurrence of massive clays and very high-grade uranium concentrations.

Alteration

The Cigar Lake deposit is surrounded by a strong alteration halo affecting both sandstone and basement rocks, characterized by extensive development of magnesium-aluminium rich clay minerals (illite-chlorite). This alteration halo in the sandstone is centred on the deposit and reaches up to 200 m in width and 250 m in height tapering with elevation (Fig. 2.23). In the basement, this zone extends in the range of 200 m in width and as much as 100 m in depth below the deposit.

Ore mineralogy and geochemistry

The unconformity mineralization consists of three dominant rock and mineral facies in varying proportions. These are quartz, clay (primarily chlorite with lesser illite), and metallic minerals (oxides, arsenides, sulphides). In the relatively higher-grade Phase 1 area, the ore consists of approximately 50% clay matrix, 20% quartz and 30% metallic minerals, visually estimated by volume. In this area, the unconformity mineralization is overlain by a very weakly mineralized contiguous clay cap 1–10 m thick. In the relatively lower grade Phase 2 zone, the proportion changes to approximately 20% clay, 60% quartz and 20% metallic minerals [2.38].

The internal distribution of uranium mineralization at the unconformity was likely controlled primarily by geochemical processes. However, pre- and post-mineralization faulting played major roles in creating preferential pathways for uranium bearing fluids and, to some extent, in remobilizing uranium. There is good continuity and homogeneity of the mineralization and its geometry, particularly in the eastern part of the deposit. A pronounced separation exists between well mineralized and weakly mineralized rocks at the upper boundary and particularly at the lower surface of the deposit.

Uranium oxide in the form of uraninite and pitchblende occurs in both a sooty form and as botryoidal, metallic masses. It occurs as disseminated grains in aggregates ranging in size from millimetres to decimetres, and as massive metallic lenses up to a few metres thick floating within a matrix of sandstone and clay. Coffinite is estimated to form less than 3% of the total uranium mineralization. The mineralized rock is coloured variably black, red and/or green [2.38].

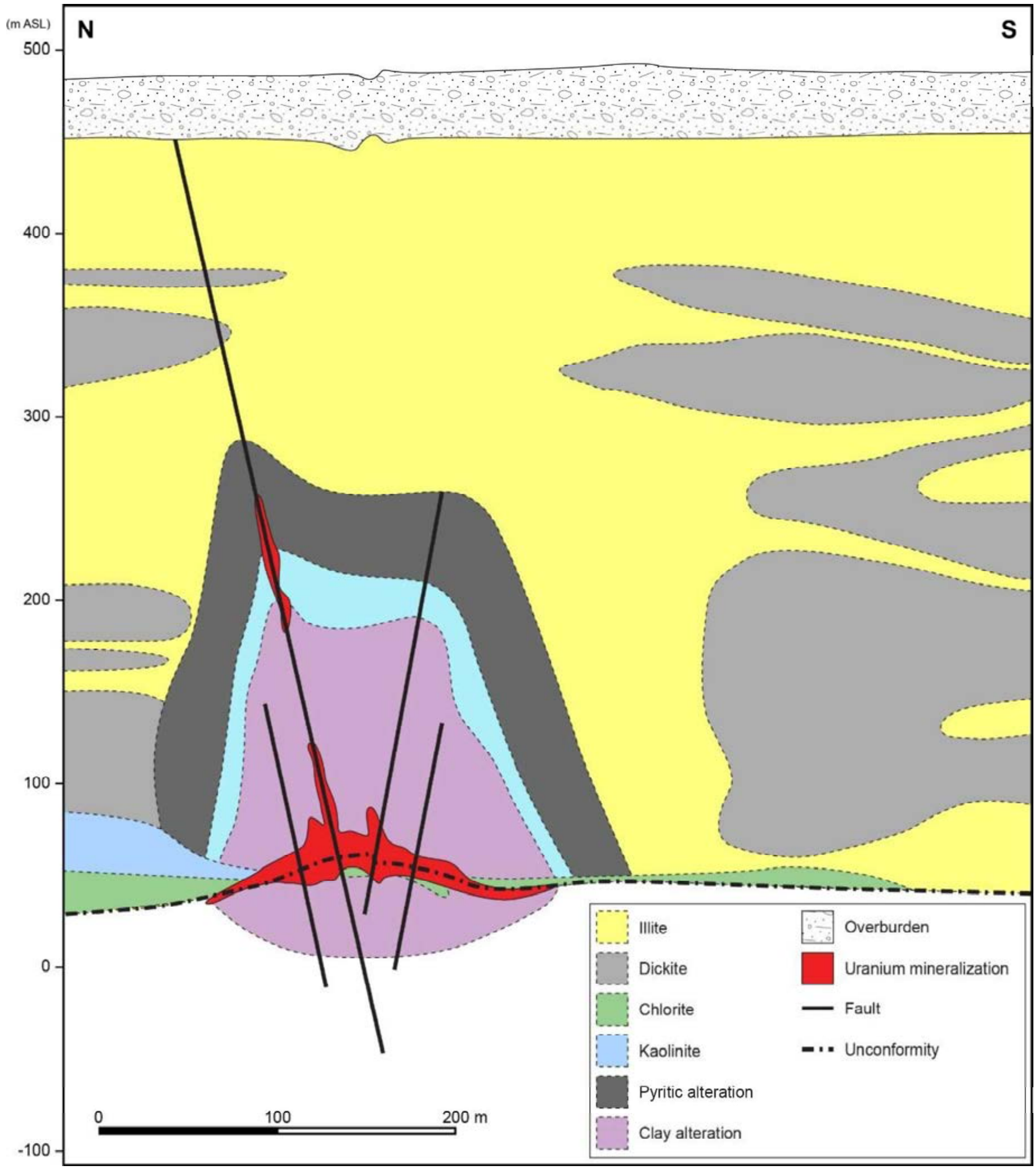

FIG. 2.23. Schematic alteration cross-section of the Cigar Lake Phase 1 deposit. Modified from Cameco Corporation [2.47].

Uranium grades of the unconformity mineralization range up to 70% U for a 0.5 m interval from a single drill hole intersection within the mining area. Geochemically, the deposit contains significant quantities of the elements nickel, copper, cobalt, lead, zinc, molybdenum and arsenic, albeit in non-economic concentrations [2.38]. Higher concentrations of these elements are associated with massive pitchblende or massive sections of arseno-sulphides.

The deposit has been subjected to post formational faulting that has contributed to the formation of vein-type mineralization and has been termed 'perched' when it occurs within the sandstone and is referred to as 'vein-type' mineralization within the basement [2.38]. Volumetrically, these mineralized bodies form only a minor part of the total mineralized rock and currently have no economic significance.

2.2.5. McArthur River deposit

2.2.5.1. Introduction

The McArthur River deposit, located in the southeast part of the Athabasca Basin, is currently the world's largest highest-grade operating uranium mine. The mine is a joint venture between Cameco Corporation (69.805%) and AREVA Resources Canada Inc. (30.195%). Cameco Corporation is the operator of the mine. Access to the mine is by provincial highway 914 to Key Lake, then via the Key Lake to McArthur River mine haul road.

Total resource size including past production is about 259 583 tU at an average grade of 14.1% U. As of 31 Dec. 2016, the deposit contained proven and probable reserves of 142 204 tU at an average grade of 8.1% U [2.46].

2.2.5.2. Exploration history

The McArthur River uranium deposit is situated along the western boundary of the McArthur River project which comprises 21 mineral claims and 1 mineral lease totalling 84 818 ha in area. The property was initially explored by Asamera Inc. from 1976 to 1979 and included airborne induced pulse transient system (INPUT), radiometric, magnetic and very low frequency (VLF) surveys, ground geophysical surveys, lake sediment sampling as well as 3100 m of diamond drilling. Cameco, through its predecessor Saskatchewan Mining Development Corporation (SMDC), became operator of the McArthur River project in 1980.

Initial exploration on the McArthur River project identified sub-economic uranium mineralization at the Volhoffer Lake, BJ, and P2 Main zones in the early- to mid-1980s. Subsequent surface drilling, focused along P2 North conductor, led to the discovery of mineralization of the McArthur River P2 North deposit in 1988. Surface definition drilling of the deposit took place between 1988 and 1992. Approval for underground development was granted in 1993 and uranium production began in late 1999.

2.2.5.3. Regional geology

The McArthur River Project area is underlain by units D, C, B and A of the Manitou Falls Formation of the Athabasca Group. Sandstone thickness varies from 100 m along the SE boundary of the property to more than 620 m over the adjoining Read Lake property to the west. A significant increase in sandstone thickness occurs immediately NW of the P2 fault zone, corresponding to the down-dropped footwall block of the P2 fault zone.

Regional aeromagnetic and electromagnetic data covering the larger McArthur River project area defines a basement complex characterized by NE trending narrow, sinuous magnetic 'lows' which bifurcate around lozenge- and sigmoidal-shaped magnetic 'highs'. The magnetically low areas typically contain conductive units of variable strike lengths while the magnetic highs are commonly bounded in part by strong conductors. Projection of lithostructural domains from outside the Athabasca Basin through the McArthur River area suggests the project lies in the westernmost part of the Wollaston Domain.

Polyphase deformation of basement rocks underlying the McArthur project area resulted in complex fold interference patterns which can be in part discerned in the regional magnetics. Folding of basement lithologies produced initial hook-and mushroom-type interferences structures due to intersecting recumbent D1 and more upright NW-trending D2 axial planes, while later NE-trending D3 axial surface traces resulted in strongly elongated or attenuated 'dome- and Basin-type' patterns. The small-scale lozenge-and arcuate-shaped magnetic highs underlying the McArthur River area probably reflect a structurally transitional region between the broader elongate linear magnetic 'highs' and 'lows' of the eastern Wollaston Domain with the larger arcuate and circular 'dome and basin' magnetic patterns of the Mudjatik Domain to the west.

2.2.5.4. Deposit geology

Host rocks

The McArthur River deposit is directly overlain by 480–560 m of Athabasca Group sandstone including the A, B, C, and D members of the Manitou Falls Formation.

The sub-Athabasca basement stratigraphy comprises of a NE trending (~042 degrees), SE dipping sequence of metasedimentary gneisses of the lower Wollaston Domain Group (Fig. 2.24). Within the deposit area, the basement rock units have been historically subdivided on the basis of their relative structural position to the P2 fault into a hanging wall pelitic sequence, footwall pelitic sequence and a footwall 'quartzite' unit. A graphite-bearing pelitic unit is broadly coincident with the P2 fault while the majority of hanging wall and footwall pelitic rocks are non-graphitic. Pelitic and psammopelitic rocks contain variable amounts of cordierite, garnet and minor sillimanite. A calc-silicate unit, up to 10 m thick, forms a marker unit in the hanging wall to the P2 fault. The calc-silicate unit becomes increasingly interlayered with biotite (±garnet) gneisses along strike to the NE. A high volume of foliated granites and pegmatites have intruded biotite pelitic gneisses structurally above and to the east of the calc-silicate unit. Several narrow (<3.0 m wide) calc-silicate intervals occur in the lower part of the footwall cordierite-bearing pelitic sequences immediately adjacent to the quartzites.

The dominant foliation in the pelitic basement rocks is a moderately to well-developed schistosity (S_1) which is broadly parallel to a variably developed gneissic structure (S_{1g}). The gneissic structure is defined by subtle, variations in biotite, quartz, and feldspar contents and in part probably represents the metamorphic accentuation of the original compositional differences (S_0). Small-scale mesoscopic folds locally deform the gneissic structure (S_{1g}) and schistosity (S_1). A subtle realignment of the early schistosity into an axial planar fabric (S2) is locally distinguished in small-scale fold closures, thereby suggesting that the dominant foliation observed in the core may reflect a composite S_1/S_2 fabric. The S_1/S_2 foliation is relatively constant (~042 degrees), however dips vary from sub-vertical to as shallow as 30 degrees with an overall average dip of about 60 degrees to the SE. A noticeable variation in the inclination of the foliation occurs near the contact between the footwall quartzite and overlying footwall politic sequence.

The pelitic basement rocks hosting the McArthur River deposit are interpreted to have been folded into a steeply-inclined to overturned NW verging antiformal structure cored by the cordierite-bearing (± graphitic) pelitic gneisses.

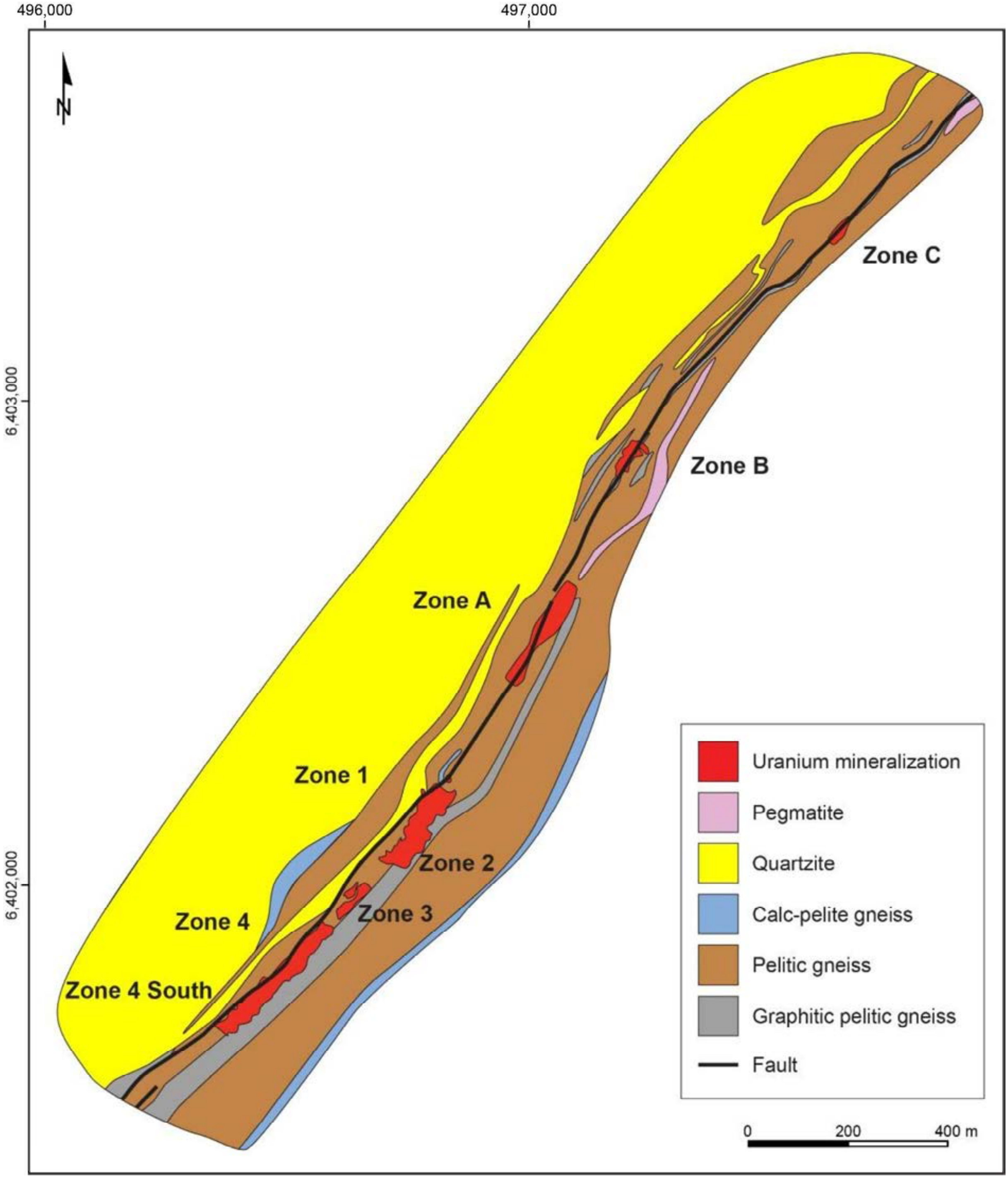

FIG. 2.24. Local basement geology map of the McArthur River area with major lithologies, major faults and uranium deposits. Modified from Cameco Corporation [2.47].

Structure

The main structural feature associated with the McArthur River deposits is the P2 fault, a NE striking and SE dipping, semi-brittle to brittle reverse fault which is coincident with a geophysical-defined feature referred to as the P2 North conductor. The McArthur River deposit is located along a major NW-facing convex flexure in the P2 North conductor; interpreted as a structural salient along the P2 fault. In the basement rocks below the unconformity, the P2 fault is hosted by graphitic gneisses which are characterized by a zone of well-developed schistose fabric overprinted by discrete semi-brittle graphitic shears, and brittle fault gouge and breccias. Displacement along the P2 fault is predominantly reverse dip-slip with a minor dextral horizontal component (Fig. 2.25). Displacement along the fault is distributed across several fault strands, however most of the displacement is typically accommodated along an individual principal strand. The cumulative vertical displacement across the P2 fault zone, as determined from offset of the sub-Athabasca unconformity surface, ranges from about 20–100 m. (Fig. 2.26).

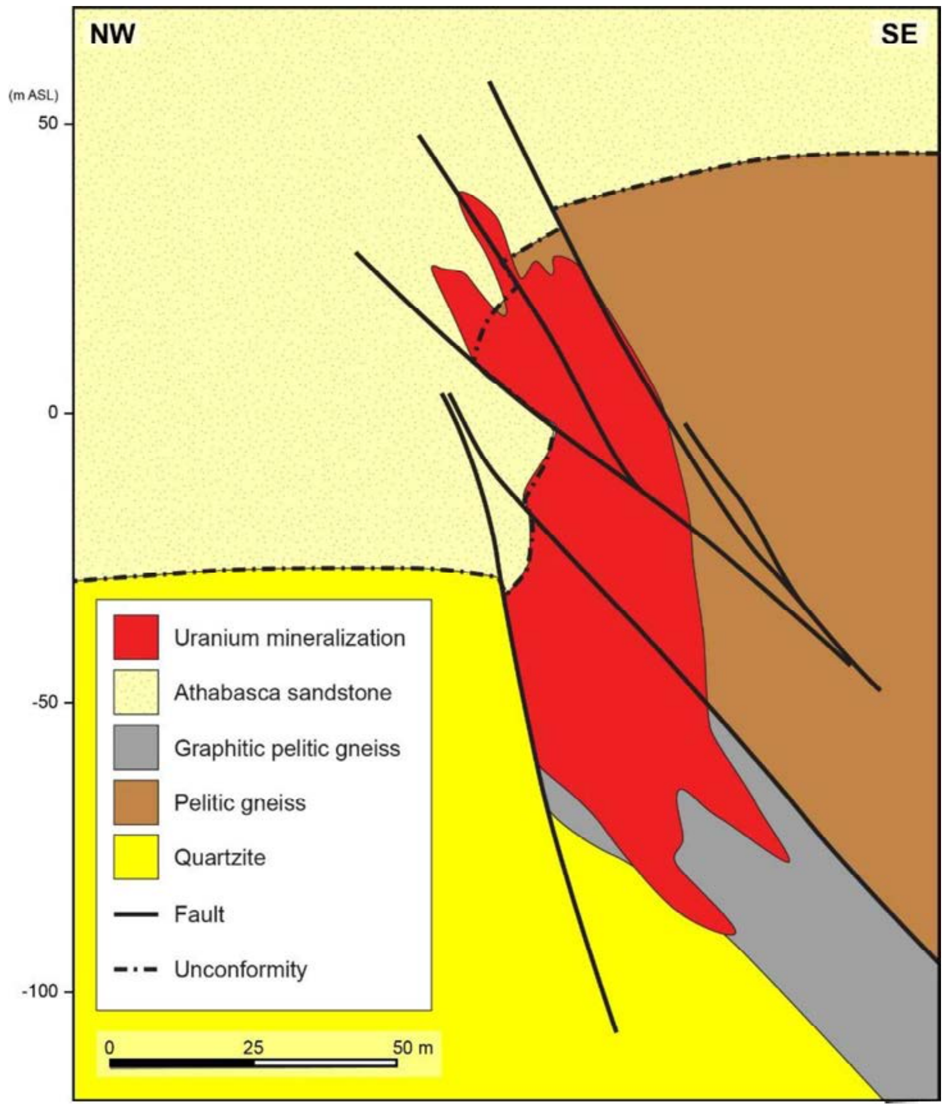

FIG. 2.25. Schematic geological cross-section of the Zone 2 deposit at McArthur River. Modified from Cameco Corporation [2.47].

The P2 fault in the lower sandstone is characterized by a broad zone of fractures, breccias, and gouges. The density of fault-related structures diminishes with increasing distance above the unconformity with the P2 fault, terminating in the sandstone as a broad zone of disbursed fractures and deformation bands in the upper Manitou Falls sandstone members.

The development of the P2 fault zone is proposed to have been initiated prior to the deposition of the Athabasca Group and associated with Hudsonian thermotectonic ductile deformation. The initial high strain deformation associated with the P2 fault zone is interpreted to have developed along the contact between cordierite-bearing and biotite pelitic units on the upper limb of a tight NW verging antiformal structure. Subsequent post-Athabasca semi-brittle to brittle reverse dip-slip reactivation along the fault is responsible for much of the unconformity displacement. The youngest movement is marked by sub-horizontal dextral slickensides.

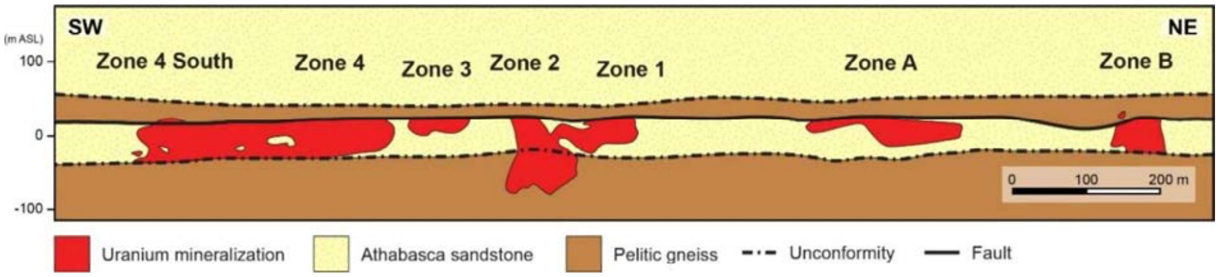

FIG. 2.26. Schematic geological longitudinal cross-section of the McArthur River system, with individual deposits. The two unconformity traces and the fault located in between are the result of a reverse fault creating a basement wedge structural setting [2.47].

A sub-vertical brittle fault of limited vertical displacement is intermittently developed along the upper contact of the footwall quartzite unit over much of the mineralized strike length of the P2 fault. The structure appears to be spatially located near the intersection of the unconformity and the upper contact of the footwall quartzite and pelitic units in the immediate footwall to the P2 fault zone. The fault is best developed where the footwall quartzite is in close proximity (20–50 m) to the P2 fault. The fault is a relatively narrow zone (2–10 m wide) characterized by fracturing, brecciation and clay-rich intervals in the basement rocks which extend up to 70 m below the unconformity, before it appears to terminate in a series of narrow listric splays or horse-tail fracture sets. Up to 50 m vertical displacement is indicated by down-dropped wedges of sandstone and conglomerate along the sub-vertical fault in Zone 2 orebody.

Detailed drilling of mineralized areas indicates the presence of closely-spaced (<10 to 30 m) WNW to NW-trending vertical faults that offset the P2 fault strands and terminate mineralized lenses. Horizontal movement along these structures is predominantly dextral with displacements ranging between less than 5 and 20 m while vertical displacements are in the order of 1 to 10 m. These cross faults have a limited strike extent of less than 100 m and therefore do not represent major property-scale structures features but are considered to reflect localized tear faults probably developed in response to differential movement of fault segments along the P2 structure.

Deposit footprint

Seven separate zones or lenses of uranium mineralization have been identified over a strike length of 1700 m along the P2 fault. They include from NE to SW the B, A, 1, 2, 3, 4, and 4

South zones. Individual mineralized zones range between 50–300 m in strike, 10–50 m in width and 35–125 m in vertical thickness. The two largest ore bodies in terms of contained resources are Zones 2 and 4 which contain resources of 108 755 tonnes and 59 566 tU respectively.

Uranium mineralization tends to be best developed in sandstone in the immediate footwall of the P2 fault, extending from the upper hanging wall unconformity 'nose ore' to the footwall 'sandstone wedge ore', although in the Zone 2 orebody high grade mineralization extends up to 75 m below the footwall unconformity as 'basement-ore'. Zone 2 is also unique in that mineralization extends up to several tens of metres into basement rocks along the hanging wall of the P2 fault.

The abrupt termination of uranium mineralization and alteration in several of the zones, notably Zone 2, correlates with the location of inferred cross faults or tear faults along the P2 fault. In that extensive drilling did not confirm an offset of the ore lenses by these structures, it is proposed that these tear faults may have played a role in compartmentalizing and focusing the ore forming fluids along the P2 fault.

Mineralization style

The McArthur River deposit is dominated by replacement style mineralization which appears to be largely sub-parallel to the foliation in the basement rocks, sub-parallel to the fault strands of the P2 fault or as wholesale replacement of the sandstone. Specific mineralization styles include: i) black metallic, massive pitchblende ranging from a few centimetres to several metres, and locally tens of metres thick; ii) dark grey to black massive uraninite fragments up to several centimetres diameter cemented in a chlorite-dravite matrix which hosts finely disseminated uraninite; iii) black vitreous to sub-metallic aggregates of uraninite forming replacement bands overprinting and weakly preserving the foliation in basement gneiss; and iv) discrete fracture infill veins and veinlets.

Alteration

Alteration in sandstones above the McArthur River deposit is characterized by an early pervasive silicification in the lower sandstone which preserves the regional diagenetic dickite signature of the Athabasca Group (Fig. 2.27). Illite forms a distinctive horizontal layer above the early silicification, particularly in drill holes intersecting the footwall sandstone wedge or hanging wall sandstones to the P2 fault. Kaolinite and magnesiofoitite alteration occurs within shears and fractures crosscutting the silicification in the lower sandstone as well as extensively overprinting the illite-dominated layer in the immediate footwall sandstone to the P2 fault. Kaolinite also is dominant in the more permeable upper sandstone units of the MFc and MFd members and forms a 500-m wide halo in the upper sandstone. The magnesium-chlorite or sudoite is best developed in the lowermost sandstones immediately above the unconformity.

Alteration associated with basement-hosted mineralization is characterized by intense multiphase chloritization and dravitization (magnesiofoitite) occurring as discrete fracture fill veins and massive wholesale replacement. Early 'paleo-weathering' associated kaolinite immediately below the unconformity is typically converted to an illite/chlorite mixture distal from the mineralization. Mineralization developed near the unconformity in the sandstone footwall wedge and in the immediate underlying basement rocks along the P2 fault are commonly associated with extensive multiphase chlorite-dravite breccias. Chlorite phases includes an early pale greyish green iron-magnesium chloritization, followed by dark green to black iron-rich chloritization and a widespread very pale greenish white magnesium-chlorite (sudoite) event, this latter temporally related with widespread dravitization. A 10–30 m wide zone comprising quartz-dravite (magnesiofoitite)-carbonate-sulphide veining forms a crude halo around the more intense multiphase chlorite-dravite breccia. In general, intense basement alteration is quite restricted, typically less than 10 m outboard of uranium mineralization.

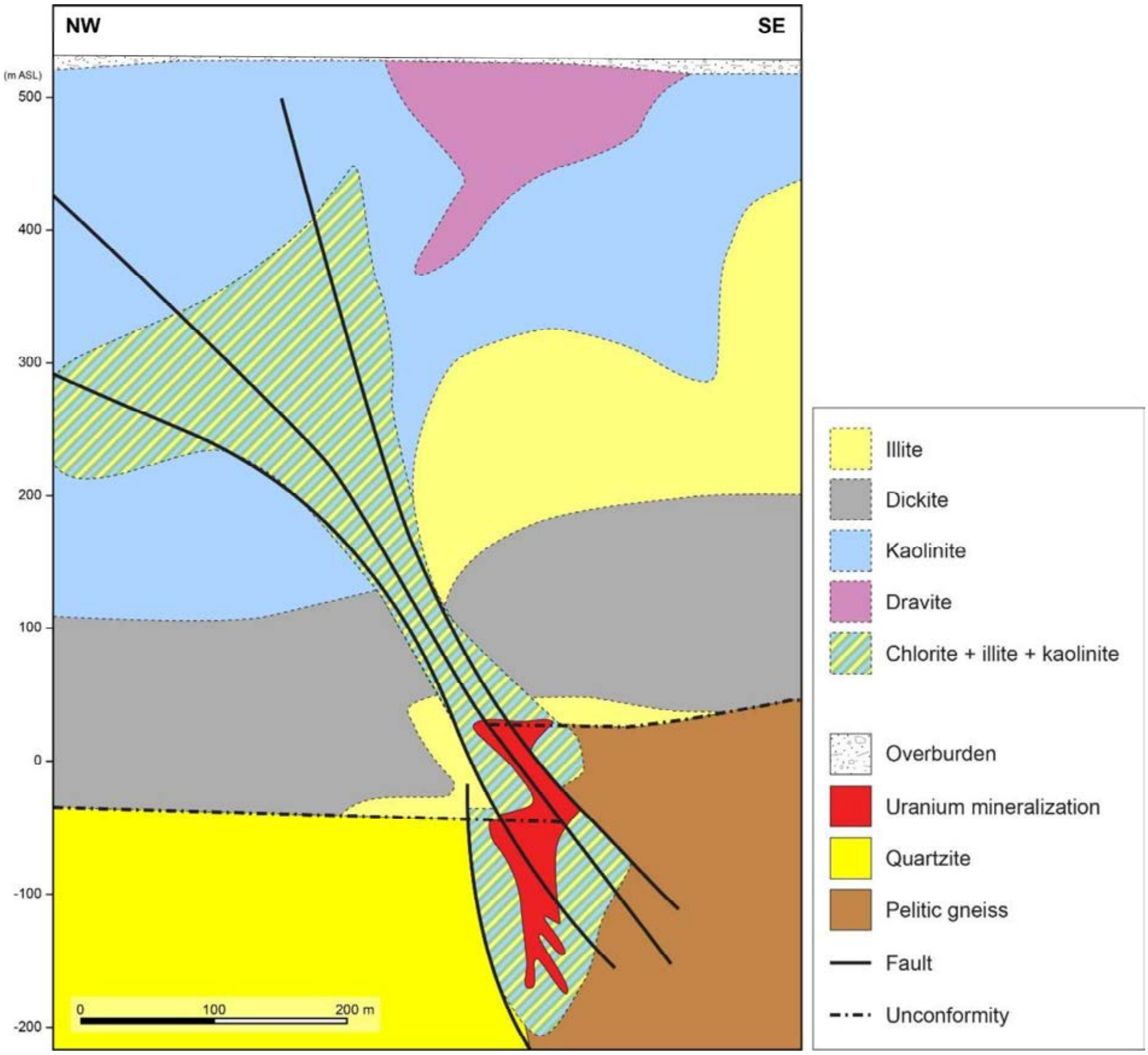

FIG 2.27. Schematic alteration cross-section of the McArthur River system depicting the different clay assemblages associated with the mineralization. Modified from Cameco Corporation [2.47].

Ore mineralogy and geochemistry

Uranium mineralization is predominantly monomineralic, dominated by primary uraninite and lesser amounts of younger coffinite and uranophane. Minor amounts of iron-copper-cobalt-arsenic-nickel sulphides are associated with orebodies.

Uranium enrichment of greater than 1 ppm (partial) extends vertically through much of the 500-m sandstone cover, along the entire 1700 m of mineralized strike length of the P2 North conductor. The uranium and heavy rare earth elements with lesser copper and gold exhibit a very irregular or nugget-like enrichment in the McArthur River deposit. Basement rocks immediately proximal to mineralization exhibit elevated contents in leachable yttrium, manganese, nickel, cobalt, arsenic, and vanadium.

2.2.6. Eagle Point deposit

2.2.6.1. Introduction

The Eagle Point deposit is located along the eastern margin of the Athabasca Basin and underlies Collins Bay situated on the western side of Wollaston Lake. The deposit was exploited as an underground mine, owned and operated by Cameco Corporation with operations ceasing in 2016. The Eagle Point deposit currently ranks as the fourth largest deposit in the Athabasca Basin behind the McArthur River, Cigar Lake and Arrow deposits. Access to the mine is by provincial highways 102 and 905 north of the community of La Ronge in northern Saskatchewan.

Total resource size of Eagle Point including past production is about 82 161 tU at an average grade of 0.52% U.

2.2.6.2. Exploration history

The Eagle Point deposit occurs on the larger Rabbit Lake project which consists of 15 mineral claims and two mining leases totalling 10 169 hectares.

The larger Rabbit Lake property was initially explored by Gulf Minerals Canada Ltd., a subsidiary of Gulf Mineral Resources Company (GMCL), under an option on a series of five permits totalling 3.5 million acres controlled by New Continental Oil Company of Canada Ltd. (NCO). The permits were acquired on the basis of an extensive airborne radiometric survey flown by NCO with an emphasis on the NE edge of the basin. In 1968, GMCL began a programme of geological prospecting and ground geophysics which resulted in discovery of radioactive float immediately near the edge of the Athabasca Basin. Further prospecting, gravity and seismic work in the area of a small lake, referred to as Rabbit Lake, led to a late season drill programme that same year. The last hole on the programme intersected high grade uranium mineralization, while follow-up drilling early in 1969 confirmed the discovery of the Rabbit Lake deposit.

Subsequent exploration by GMCL north of the Rabbit Lake deposit, notably along Collins Bay, included boulder prospecting and electromagnetic surveys. Follow-up diamond drilling commonly targeted the coincidence of the apex of radioactive boulder trains and electromagnetic anomalies. This activity led to the discovery of a series of small deposits beginning with the A-zone (1971), followed by B-zone (1977) and D-zone (1979).

In 1976, GMCL entered a joint venture with Saskatchewan Mining Development Corporation (SMDC) and Noranda Exploration Company Ltd. to explore mineral claims underlying the northern part of the Rabbit Lake property. The southern boundary of the joint venture cut across a peninsula on the eastern shore of Collins Bay now referred to as Eagle Point. The joint venture claims became referred to as Eagle North area while to the south, the 100% GMCL ground was referred to as Eagle South area. Exploration activities during this time included airborne (Triden, INPUT) and ground electromagnetic surveys, with follow-up diamond drilling of conductors, as well as reverse circulation drill programmes targeting uranium-in-basal-till anomalies. In 1980, diamond drilling intersected high-grade mineralization along a conductor on the Eagle North joint venture ground which subsequently became referred to as the Eagle Point fault. At the same time, follow-up reverse circulation drilling on the Eagle South ground intersected mineralization which eventually became part of the overall Eagle Point deposit. In 1982, Eldorado Resources Limited acquired Gulf Minerals Canada Ltd., thereby acquiring the Rabbit Lake project. In 1988, Eldorado Resources Ltd. merged with the Saskatchewan Mining Development Corporation to form Cameco Corporation at which time the new entity became owner and operator of the project and of the Eagle Point deposit. In 1990, Uranerz Exploration and Mining Ltd. (UEM) purchased a one-third interest in the Rabbit Lake property which included the Eagle Point underground operation. In 1998, Cameco purchased UEM, thereby becoming 100% owner and operator of the Rabbit Lake project and the Eagle Point mine.

Underground mining began at Eagle Point in 1992 and continued to 1999 with an average production of 2230 tU per annum (1993–1999). The operation was put on care and maintenance from 2000 to 2002; production resumed in 2003 and continued till mid-2016.

2.2.6.3. Regional geology

The Rabbit Lake property and Eagle Point deposit are underlain by polyphase deformed and metamorphosed Archean and Early Paleoproterozoic rocks of the Wollaston lihostructural domain of the larger Hearne Province of the Canadian Shield (Fig. 2.28). These rocks include granitic gneisses of Archean age overlain and structurally interleaved with early Paleoproterozoic pelitic, psammopelitic, meta-arkosic and calc-silicate metasedimentary gneisses and their anatectic derivatives.

These older deformed and metamorphosed rocks are unconformably overlain by flat-lying, undeformed rocks of the late Paleoproterozoic Athabasca Group consisting mainly of fluvial clastic sedimentary rocks. The Rabbit Lake project straddles the eastern edge of the Athabasca Basin with sandstone covering the western portion while older basement gneisses are exposed within the eastern part of the property.

Four phases of ductile deformation affect metasedimentary rocks of the Wollaston Domain; the first phase (D_1) corresponds to the main regional fabric (S_1) which is largely conformable to primary lithologic layering (S_0) and is interpreted to be associated with relatively shallow to recumbent folds; the second phase (D_2) is an axial planar foliation (S_2) associated with NE-trending, tight to isoclinal folds; the third event (D_3) is manifested by ENE-trending tight folds and associated axial planar foliation (S_3); and last phase (D_4) is associated with open to moderate, upright NW-trending folds with locally developed axial planar cleavages (S_4). Metamorphic grades are predominantly upper amphibolite to lower granulite facies across this part of the Wollaston Domain.

The Wollaston Domain and overlying Athabasca Group are crosscut by a series of brittle to semibrittle faults and shear zones. The dominant faults in the region include: 1) NE-trending semibrittle to brittle oblique-dextral reverse faults which are largely conformable to the regional stratigraphy; 2) NS striking, sinistral strike slip faults of the Tabbernor fault system which extend across much of the eastern part of the Saskatchewan Precambrian shield and; 3) east-trending fault zones which exhibit an apparent dextral displacement although the vertical component of movement is unknown. These major faults exhibit multiple displacement events which post-date regional metamorphism, as well as movements prior to and after deposition of the Athabasca Group.

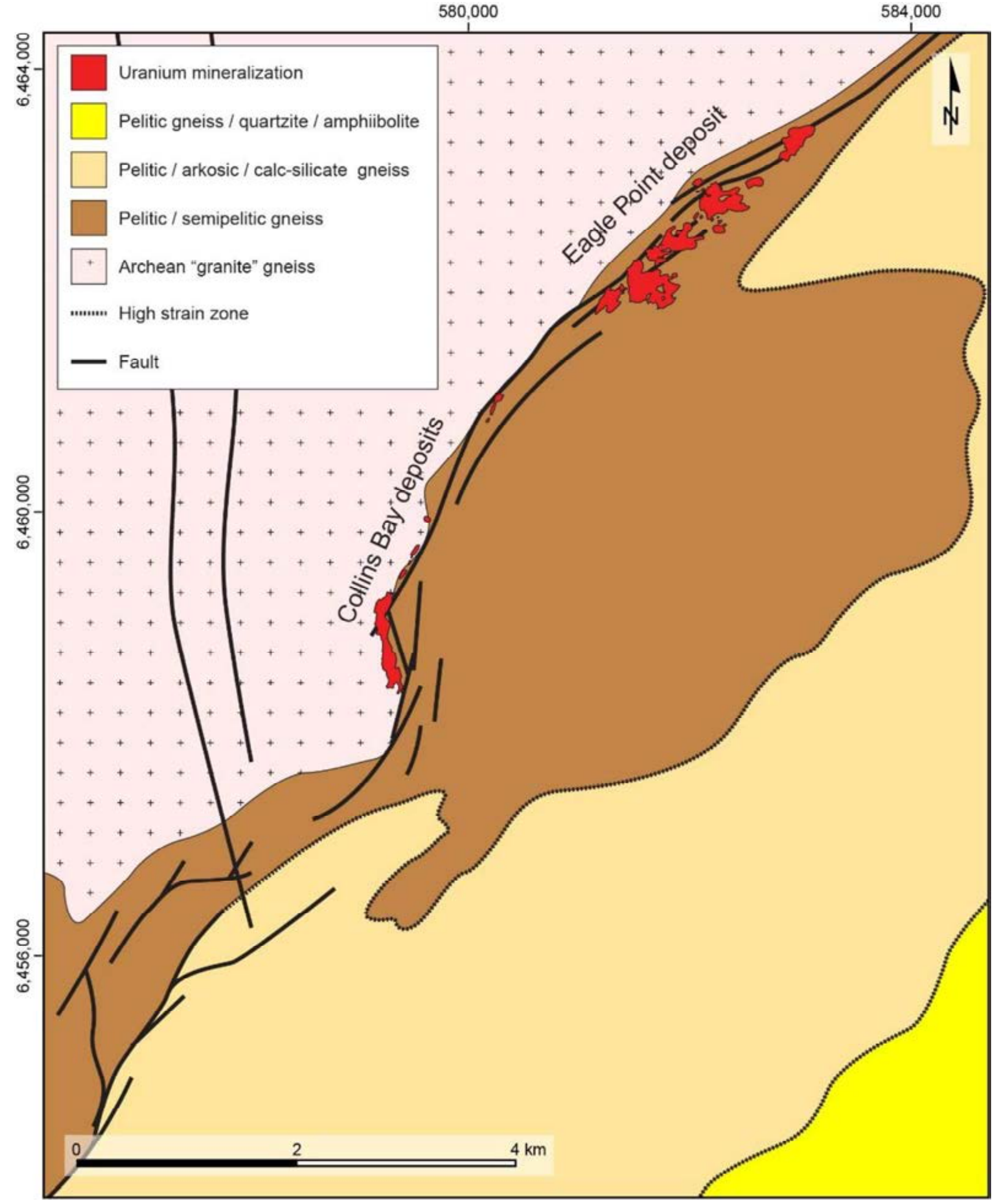

FIG. 2.28. Simplified regional basement geology map of the Collins Bay – Eagle Point area with major lithologies, major faults and uranium deposits. Modified from Cameco Corporation [2.47].

2.2.6.4. *Deposit geology*

Host rocks

The stratigraphy of the Eagle Point deposit comprises an older complex of Archean granodioritic to tonalitic gneisses which occupy what is referred to as the Collins Bay Dome and a younger sequence of early Paleoproterozoic metasedimentary rocks. The metasedimentary rocks are further subdivided into: 1) the Lower Mine Sequence composed predominantly graphitic and non-graphitic pelite and semipelite gneiss and their anatectic derivatives; and 2) the Upper Mine Sequence composed of quartzofeldspathic gneiss and biotite-quartz-feldspar (psammopelite and psammite) gneiss.

Subordinate rock units within the mine sequence include quartzite or siliceous units that are commonly located in the lower part of the Upper Mine Sequence where they are gradational into quartz-rich quartzofeldspathic gneisses. Locally, similar quartz-rich rocks are gradational upwards into pegmatite suggesting some 'quartzites' may represent a siliceous-rich phase of fractionating anatectic melts. The main quartzite interval in the lower part of the Upper Mine Sequence exhibits good strike and dip continuity and is in part discordant to stratigraphic layering and folding, suggesting it may be a zone of siliceous metasomatism associated with a tectonic discontinuity.

Calc-silicate gneisses are uncommon, and occur as massive to weakly schistose rocks exhibiting a centimetre scale gneissic layering defined by alternating micaceous-rich and diopsidic and/or actinolitic-rich layers.

A major pegmatite body, termed the Eagle Point Sill, as well as numerous pegmatite dykes and sills intrudes the metasedimentary sequence along the margin of the Collins Bay Dome. The main part of the pegmatite body, which is the primary host unit of the 144 Zone mineralization, extends for at least 500 m along strike and is up to 200 m wide. A narrow tongue-like apophysis extends up to 600 m NE of the main body of the Eagle Point pegmatite while several relatively large sills/dykes are also intercalated with the stratigraphy within the 02/03 Zones of mineralization. The Eagle Point Sill is dominated by very coarse to pegmatitic grain sizes while textures and wall rock contacts indicate these larger bodies are largely allochthonous and were emplaced by intrusive processes as opposed to in situ anatexis. Nevertheless, these larger sill-like bodies probably reflect wholesale anatectic melting within the lower part of the Wollaston Group supracrustal succession with local migration and coalescence of melt fractions at particular lithostructural sites (e.g. margin of the Collins Bay Dome, axial plane of major fold structures).

In the northern part of the mine, feldspar porphyry dykes and sills are a volumetrically important part of the mine stratigraphy. This distinctive unit is typically medium to light pinkish grey, fine to medium grained with elongated, tabular feldspar laths ranging between 0.5 and 2 cm in length and forming from 10 to 25% of the rock. Biotite is the main mafic mineral and varies from less than a few per cent to 12% of the rock. The rocks vary from weakly foliated with a semi-random alignment of phenocrysts to very strongly foliated with a pervasive preferred orientation of feldspar laths. Based on drill intersections, the distribution of the porphyry appears to have limited aerial or strike extent, although drill intersects indicate individual bodies can locally be up to 50 m thick. The feldspar porphyry generally has sharp wallrock contacts, however more gradational contacts are locally observed with pegmatites and medium-grained 'grey' granites.

Structure

The composite effect of the shallowly inclined to recumbent D_1 folds and NE and ENE-trending tight to isoclinal D_2 and D_3 events respectively, are reflected in the magnetic and EM data for the area underlying the Rabbit Lake – Eagle Point property. The 'grain' of the magnetic maps is interpreted to represent a composite $D_1/D_2/D_3$ regional and property scale fold pattern that becomes increasingly tighter and more attenuated towards the eastern margin of the Collins Bay Dome. The wavelengths of the fold structures may be in the order of only a few hundred metres immediately adjacent to the dome and broadening out to typically about 2000 m wide east of the dome.

Multiphase foliation development and complex polyphase folding are locally observed in an outcrop south of the Eagle Point mine as well as in underground exposures. Fabric relationships illustrate an early-formed penetrative fabric (e.g. S_1 schistosity) developed subconformable to compositional layering (S_0) which is in turn deformed about tight, NE trending D_2 folds which have a well-developed axial planar cleavage (S_2).

The decreasing wavelength and increasing tightness of the D_2/D_3 composite folds towards the Collins Bay Dome also corresponds to multiple conductor axes along the SE margin of the dome. The conductor axes in part reflect fold repetition of graphitic pelite units while the stronger conductor axes also correspond to major semibrittle to brittle graphitic fault structures developed close to the margin of the Collins Bay Dome. Between the A-Zone and the southern part of the Eagle Point mine, these conductors form a series of sub-parallel right stepping or overlapping semi-brittle to brittle faults, referred to as the Collins Bay and Eagle faults. Immediately north of the Eagle Point mine, the conductors display a more complex array of overlapping and fanning features that diverge to the NE; the Collins Bay and Eagle faults are restricted to the most westerly conductor traces developed close to the margin of the Collins Bay Dome. Kinematic data indicates an overall oblique dextral reverse shear couple along the Collins Bay and Eagle faults, although a horizontal component of displacement may become dominant further into the hanging wall from the Collins Bay Dome (e.g. 02/03 Zones).

The multiple conductor array present in the Eagle Point mine area is interpreted to reflect structural reactivation along the limbs of a shallow east-dipping, and shallow NNE plunging tight D_1 structure that folds the variably graphitic basal pelitic unit. This results in a series of fan-like short segment graphitic fault structures that converge to the SW into the area of the tight synformal D_1 fold closure. A corresponding fold closure immediately to the east of the above described D_1 structure, is inferred from the magnetic and drill data to be a NE trending steeply east-dipping D_2 antiformal structure that refolds the D_1 structure. The surface projection of the main Eagle Point ore bodies (e.g. 01, 02, 03, Sump zones) are distributed along the axial surface trace of this inferred D_2 antiformal structure, although individual ore bodies lie at a high angle to the axial plane of this D_2 structure. In detail, the overall easterly orientation of the orebodies may be sub-parallel to the axial surface trace of the earlier, albeit refolded D_1 structures.

The mineralized veins comprising the Eagle Point deposits are broadly consistent with dilational or extensional structures developed in response to a series of right-stepping fault segments comprising the NE trending Collins Bay and Eagle faults as well as subsidiary structures developed further into the hanging wall to these structures.

Deposit footprint

The total reserves and resources of the Eagle Point deposit, including past production, is approximately 82 161 tU at a grade of 0.52% U. The Eagle Point deposit comprises up to 11 discrete zones which are distributed over a strike length of over 1600 m along the SW flank of the Collins Bay Dome. Individual zones vary in width from 25 to 100 m and can extend up to 300 m down-dip. The top of the mineralized system sub-crops below glacial overburden and has been trace to more than 850 m below surface. At a deposit scale, the Eagle Point mineralized system strikes NE (045 degrees) and dips moderately SE (49 degrees) and has an overall shallow NE rake (15 degrees).

Mineralization style

The mineralized lenses forming the Eagle Point deposit are entirely hosted by basement gneisses while the erosional margin of the Athabasca Basin occurs immediately west of the deposit. Based on alteration and mineralization, the Eagle Point deposit can be divided into two distinct mineralization types: 1) the 144-type; and 2) 02 North Extension-type.

The 144 Zone-type is characterized by broad alteration halos, up to several tens of metres wide developed around predominantly foliation-controlled replacement style mineralization that is centred along or immediately adjacent to the main controlling graphitic faults, notably the Collins Bay and Eagle faults. Although centred along major graphitic faults, the foliation-controlled replacement style is commonly developed along major lithologic contacts (e.g. pegmatite-pelite, porphyry-pelite) with mineralization extending along foliation planes. Individual replacement style mineralization typical of the 144-type lenses form narrow semicontinuous irregular lenses varying from a few centimetres up to several metres wide and extending for a few tens to several hundred metres along strike and down-dip. Mineralization comprises uraninite that occurs as concentrations of finely disseminated uraninite along foliation planes which can grade to wholesale massive replacement of country rocks by massive pitchblende.

The 02 North Extension-type lenses (Fig. 2.29) are characterized by relatively narrow zones of alteration, ranging between a few tens of centimetres and several metres wide, developed around steeply-dipping infill veins. These veins tend to be easterly striking and are best developed in the hanging wall above the major NE-striking graphitic faults. The mineralization comprises massive pitchblende infill veins although foliation-controlled replacement selvedges comprising disseminated uraninite may develop up to several tens of centimetres into the wallrock along the veins.

High grade mineralized bodies, up to several metres thick, several tens of metres in strike, and up to 100 m vertically, develop at the intersection of subsidiary faults and shear splays associated with the main graphitic faults, as well as where structures hosting 02 North Extension lenses intersect. These high-grade lenses form elongate rod-or podiform zones coincident with the intersection axis of the structures. Locally, these intersection lenses exhibit breccia textures where uraninite forms both matrix and clasts.

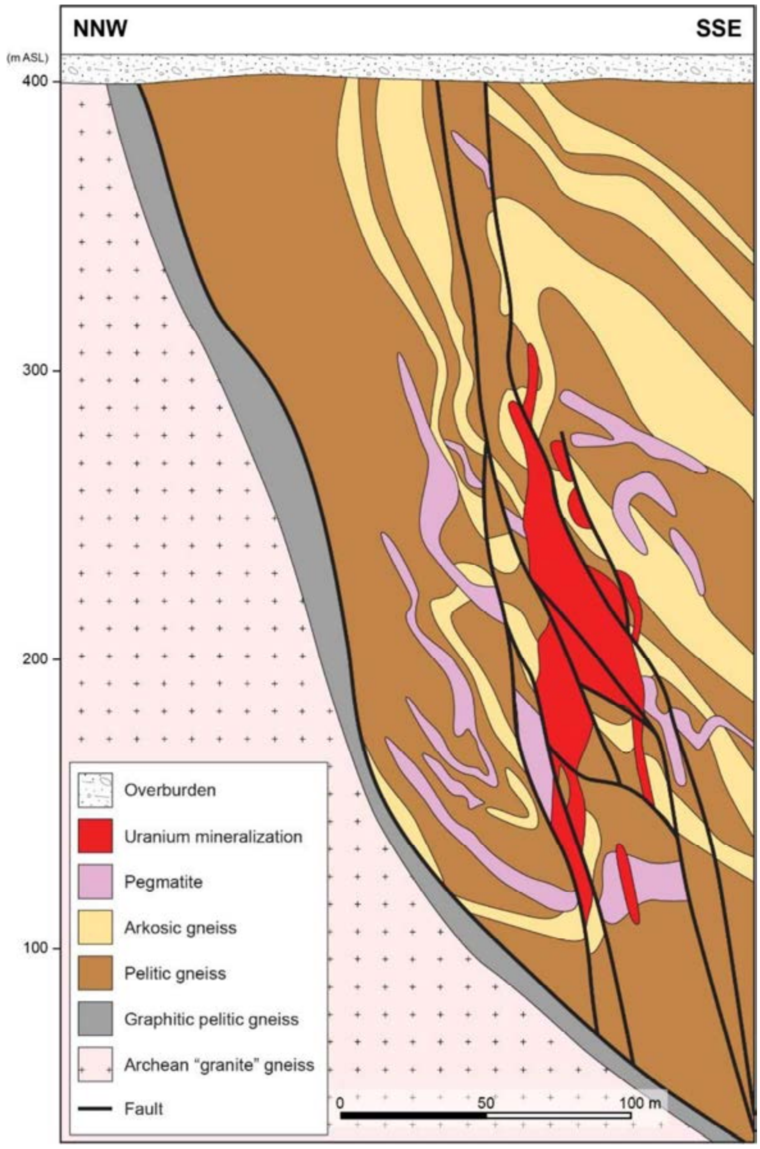

FIG. 2.29. Schematic geological cross-section of the O2 Zone at the Eagle Point deposit. Modified from Cameco Corporation [2.47].

Alteration

Alteration associated with the 144 Zone style of mineralization is characterized by a zone of argillic alteration (illite and sudoite), up to 50 m wide, consisting of moderate to strong bleaching (e.g. loss of iron) and strong to intense clay and magnesium-chlorite replacement. A progressive loss or depletion in graphite content is noted within the pelitic host rocks and graphitic faults with increasing clay alteration. The argillic alteration appears to overprint a broader zone of iron-rich chlorite, up to 75 m wide, which is interpreted to reflect both cataclastic retrograde alteration associated with the fault movement as well as hydrothermal chlorite. This zone of chloritization is commonly marked by strong plagioclase destruction, as well as iron depletion in biotite and sodium depletion. Disbursed pyrite ± quartz veins form a more distal halo on the outer margins of the argillic alteration. Strong sericitic and/or saussuritization is typically developed immediately adjacent major graphitic faults although with increasing argillization these former alteration assemblages are progressively obliterated.

The 02 North Extension-type lenses are characterized by an alteration halo comprising a central bleached and argillic halo (illite and sudoite), which is outwardly enveloped by more proximal silicic (i.e. quartz veins) and iron-rich chlorite halos, followed by increasingly more distal sericitization, carbonate veining and pyritization respectively (Fig. 2.30). The overall width of the enveloping alteration halos ranges from a few metres to several tens of metres in width. The 02 North Extension-type lenses exhibit an apparent asymmetry, in both the intensity and distribution of the alteration halos about the mineralization. The proximal silicification and chloritization as well as the various distal alteration assemblages appear to be strongest developed up-hole and are less intense below the mineralized intercepts. Similarly, the pitchblende mineralization and hematization is generally best developed towards the 'up-hole' side of the argillic halo. The more distal iron-sulphide halo appears to be entirely developed on the up-hole side of mineralization.

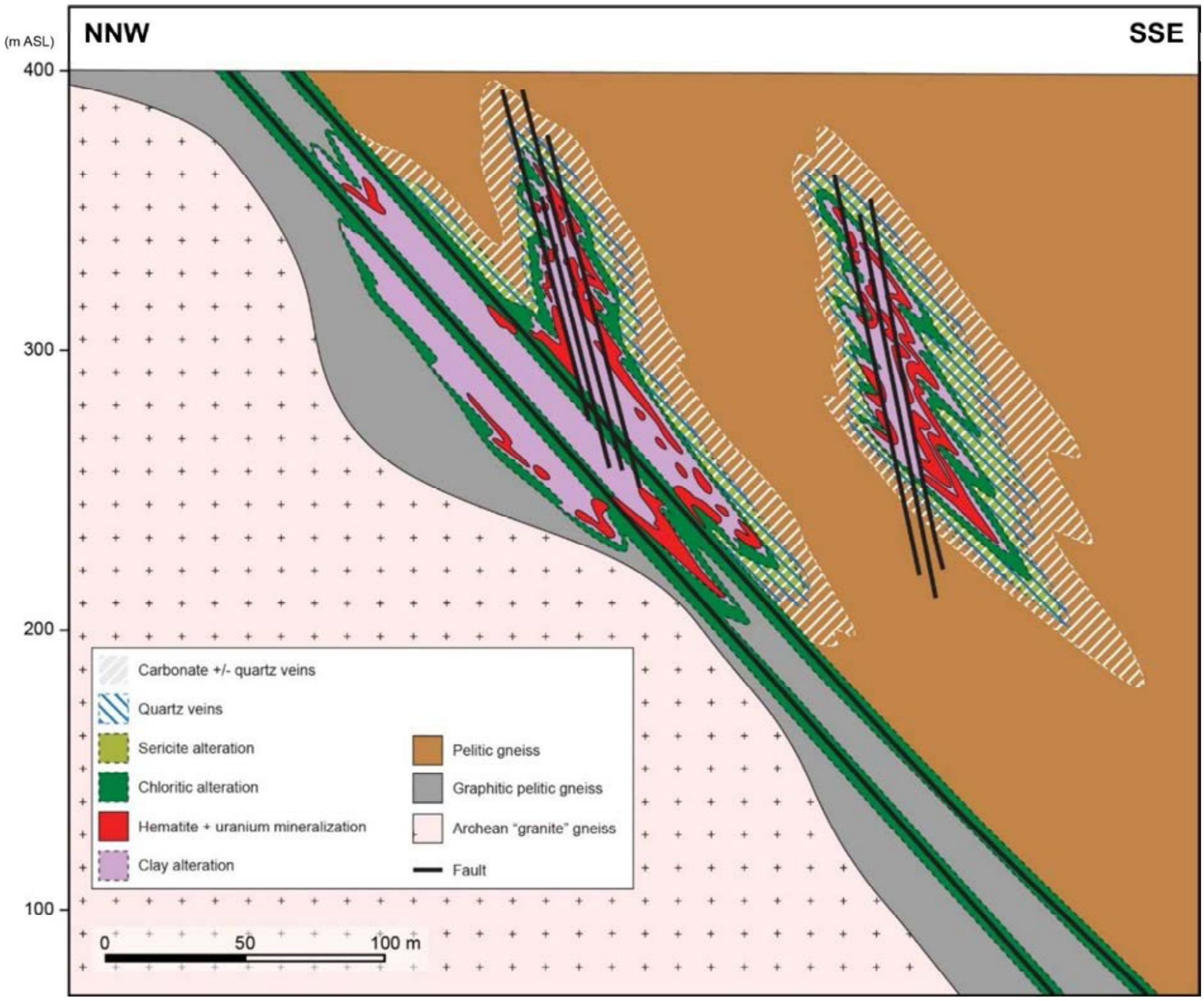

FIG. 2.30. Schematic alteration cross-section of the Eagle Point deposit. Modified from Cameco Corporation [2.47].

Ore mineralogy and geochemistry

Eagle Point mineralization is mineralogically simple, consisting of several generations of uraninite and pitchblende. Boltwoodite has been described as the most common secondary uranium mineral while coffinite occurs rarely [2.142]. Micron scale becquerellite and beta-uranophane is also reported with the uraninite [2.57]. Nickel and molybdenum occur in trace amounts while native copper is restricted to disseminations within and adjacent to uranium minerals. Arsenides are absent with pyrite the most abundant sulphide, although lesser amounts of galena and chalcopyrite are present. Gangue minerals include illite, magnesium chlorite (sudoite), haematite and dravite. Carbonaceous matter with a characteristic odour is associated with higher grade mineralization [2.142].

2.2.7. Millennium deposit

2.2.7.1. Introduction

The Millennium deposit occurs on the Millennium joint venture Project which is a joint venture between Cameco Corporation (69.901%) and JCU (Canada) Exploration Co. Ltd. (30.901%) Cameco Corporation is the operator of the joint venture.

The Millennium deposit is located in the SE part of the Athabasca Basin about 35 km north of the Key Lake mill and 35 km SW of the McArthur River mine. Prior to the formation of the Millennium Project joint venture, the deposit was situated on the larger Cree Extension project which is a joint venture between Cameco Corporation (41.9645%), JCU (Canada) Exploration Co. Ltd. (30.0990%) and AREVA Resources Canada Inc. (27.9365%). Cameco Corporation is also the operator of the Cree Extension project.

Total resources reported for the Millennium deposit, as of December 2015, in the indicated category are 29,195 tU at a grade of 2.03% U.

2.2.7.2. Exploration history

Exploration work on the Cree Extension project and later on the Millennium Project has been active since 1978 and can be divided into three main periods. The first period, between 1978 and 1989, was initially undertaken by SMDC and then by Cameco Corporation, and involved reconnaissance boulder geochemical surveys, airborne INPUT-EM, ground time-domain EM (TDEM) and University of Toronto TDEM System (UTEM) and, gravity and magnetic surveys as well as 20 diamond drill holes.

The second period of exploration was undertaken by Uranerz Exploration and Mining between 1990 and 1998. Work programmes included a range of geophysical surveys including EM, gravity and magnetics, drill core lithogeochemistry and reflectance spectroscopy and 17 diamond drill holes.

Cameco Corporation assumed operatorship of the project in 2000, which marked the third period of exploration (2000–2018). Work programmes continued to include a range of geophysical surveys, including airborne magnetic gradiometer, TDEM and direct current (DC) resistivity and induced polarization (IP) resistivity as well as 74 diamond drill holes.

Total drilling between 1978 and 2012 on the Cree Extension/Millennium projects, including delineation drilling of the Millennium deposit, is approximately 89 000 m.

In 1999, a data compilation and drill core review recognized drill core from CX-38 exhibited significant alteration in the lower 200 m of sandstone as well strong foliation controlled argillic alteration in the underlying basement rocks. Anomalous uranium, lead and boron were also present in both sandstone and basement rocks. The discovery hole for the Millennium deposit, CX-40, was drilled in 2000, on a 40-m step-out to the west of drill hole CX-38. The hole intersected weak to moderate grade basement-hosted uranium mineralization over 153 m which included 29 m averaging over 0.85% U.

2.2.7.3. Regional geology

The Cree Extension and Millennium Project area is underlain by 500 to 750 m of sandstone and conglomerate of the Manitou Falls Formation of the Athabasca Group. The sedimentary sequence increases in thickness towards the north and NW across the property.

The regional basement geology underlying the Cree Extension/Millennium projects is largely inferred from aeromagnetic, gravity, EM data and regional drilling. The regional geophysical pattern characterizing the area underlying the Millennium project area and western part of the Cree Extension project is characterized by a narrow NNE trending magnetic low corridor, ranging between 250 to 750 m wide, which is interpreted to comprise pelitic and psammopelitic rocks. Electromagnetic surveys along the southern portion of this interpreted metasedimentary corridor identified a NNE trending conductive response referred to as the B1 conductor. Exploration drilling along the B1 conductor confirmed graphite-bearing pelitic rocks as well as indications of post-Athabasca faulting and anomalous sandstone lithogeochemistry. The Millennium deposit lies along the southern part of the B1 conductive corridor.

The B1 conductive corridor is bound to the east and west by magnetically high domains inferred to be dominantly Archean granitic gneiss. The more regional 'magnetic' fabrics, particularly exhibited in the 1st vertical derivative products, suggests the B1 corridor is part of a more complex fold interference pattern involving relatively shallow dipping recumbent D_1 folds verging to the NW which are refolded by upright NE-trending D_2 folds that are in part inclined moderately to steeply to the NW. The Millennium deposit is interpreted to lie within a N-NNE-striking D_2 synform located in a structurally transitional region between the broader elongate linear magnetic 'highs' and 'lows' typical of the eastern Wollaston Domain and arcuate to circular 'dome and Basin' magnetic patterns of the Mudjatik Domain to the west.

2.2.7.4. Deposit geology

Host rocks

The project area is underlain by 500 to 750 m of sandstones and conglomerates of the Manitou Falls Formation of the Athabasca Group. The sedimentary sequence, which has a shallow dip to the WNW, consists in ascending order of the Manitou Falls A to D members as defined by Ramaekers [2.198].

Basement rocks underlying the Athabasca Group comprise a north to NNE-striking and steeply east-dipping sequence of graphite and non-graphite-bearing pelitic and psammopelitic gneisses, granite, anatectic pegmatites, and minor calc-silicate rocks. The basement stratigraphy hosting the Millennium deposit has been subdivided into ten lithostratigraphic units [2.152] (Fig. 2.31). The following summarizes the basement lithologic units:

The most easterly hanging wall unit, termed the Granitic Assemblage (I) is composed of a dominantly pegmatite and weakly foliated leucogranite with subordinate intercalations of pelitic gneiss. This unit is gradationally underlain by the Graphitic Metasedimentary Assemblage (II) comprising 40–55 m of variably graphitic pelite and semipelite gneiss and minor leucogranite. The Graphitic Metasedimentary Assemblage (II), which is coincident with the B1 conductor, is further underlain the Heterogeneous Metasedimentary Assemblage (III) consisting of 20–40 m of texturally and compositionally varied, non-graphitic pelite and semipelite gneiss, minor calc-silicate and anatectic pegmatite. Weak uranium accumulations are locally developed along the wallrock contact of the anatectic pegmatites in this unit. The Hanging Wall Pegmatite (IV), a distinct unit defining the lower extent of Assemblage (III), varies between 3 and 20 m thick and generally overlies the main uranium mineralization in the Millennium deposit. The Graphitic Marker unit (V), immediately underlying the hanging wall pegmatite unit, forms a 0.5 and 4.5 m thick, moderately to strongly graphitic cordierite porphyroblastic pelitic schist with locally developed semibrittle shear fabrics. The Marker Unit is spatially coincident with uppermost stratigraphic limits of ore-grade mineralization in the Millennium deposit. The Host Assemblage (VI) is a 25–55 m thick sequence of non-graphitic pelite and semipelite gneiss and schist and forms the main host unit for the Millennium deposit. A mixed unit of calc-semipelite and semipelite gneisses, 9–15 m thick, forms the Upper Calc-Silicate Assemblage (VII). This unit locally contains weak uranium mineralization. The Bracketed Assemblage (VIII) comprises a 15–25 m thick sequence of pelite and semipelite gneiss, that is gradational with, and underlies the Upper Calc-Silicate Assemblage. Disseminated, weak uranium mineralization and elevated background radioactivity occurs over the entire thickness of the Bracketed assemblage (VIII).

In the initial lithostratigraphy proposed by Roy et al. [2.152] a Lower Calc-Silicate assemblage (IX) was defined underlying the Bracketed Assemblage. The unit was defined as a 25–40 m thick sequence composed of interbedded calc-semipelite and calc-pelite gneiss and schist with minor amphibolite. The unit is intensely overprinted by argillic and chlorite alteration with widespread dravite ± quartz-healed breccias. For the most part, the unit is not mineralized. Subsequent investigations have determined that there is likely negligible calc-semipelitic or calc-pelitic material present in this unit and the pale-green colour of the rocks is largely due to chloritic and illitic alteration of semi-pelitic and pelitic rocks, likely contiguous with the lower part of the Bracketed assemblage. The Footwall Assemblage is structurally the lowest unit in the lithostratigraphy. It consists of a series of non-graphitic semipelite gneiss intercalated with massive to well-foliated granite gneiss that occur in the immediate footwall to the Mother Fault. The thickness of this unit is unknown.

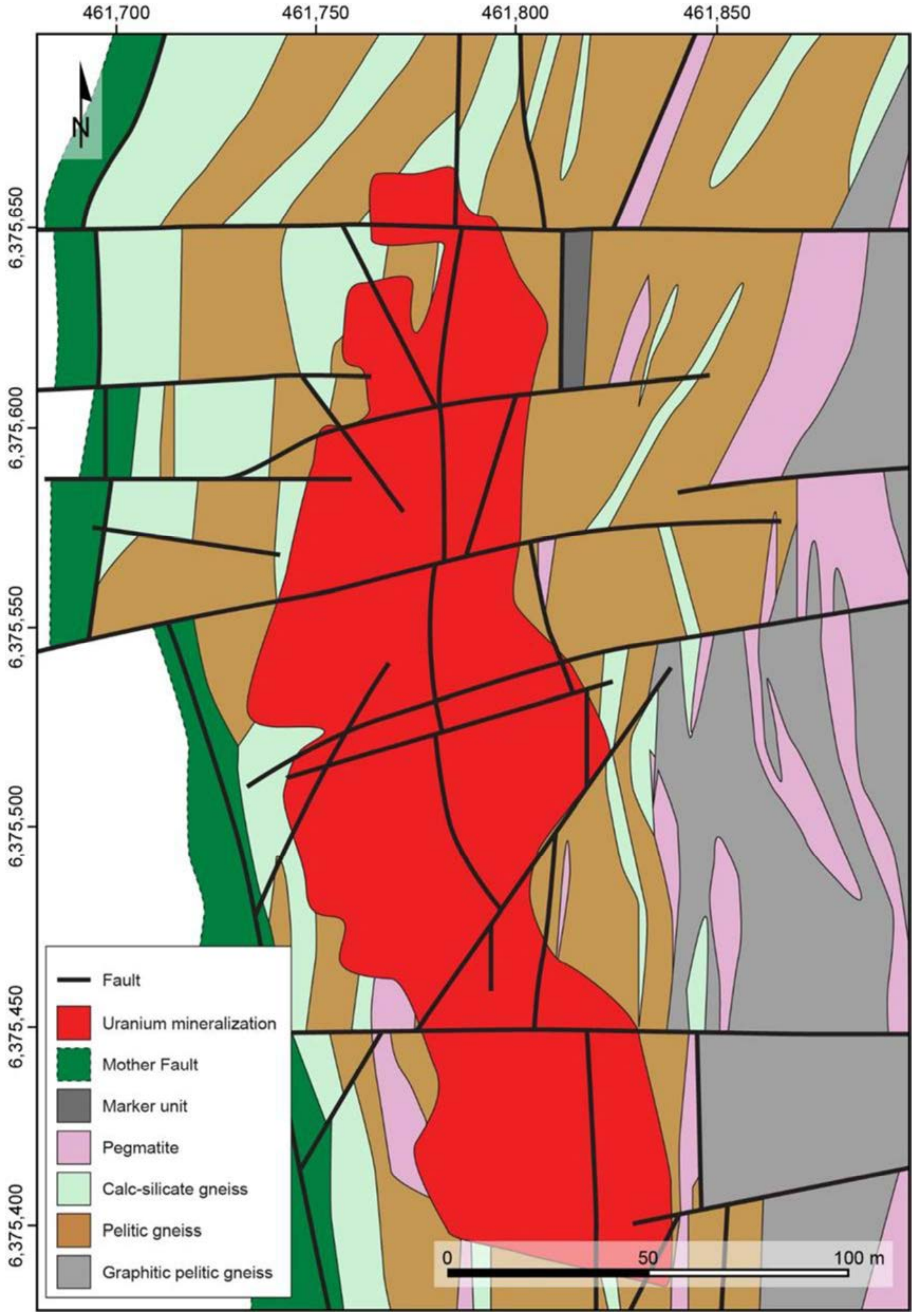

FIG. 2.31. Local basement geology map of the Millennium deposit with major lithologies, major faults and uranium deposits. Modified from Cameco Corporation [2.47].

Structure

Based on structural data from drill core, a pronounced rotation of bedding occurs in the sandstone directly above the Millennium deposit. Rotation and steepening of sandstone bedding, with a consistent westerly dip, begins at approximately 300 m vertical depth and increases in magnitude with depth towards the unconformity. This bedding rotation is interpreted to reflect fault-related structural disruption of the sandstones overlying the Millennium deposit.

Four main fault sets cut the Millennium stratigraphy. They include: 1) a major NNE-trending, moderate east-dipping fault, termed the mother fault, which forms the footwall boundary to the Millennium stratigraphy; 2) a main NS sub-vertical fault with several subsidiary parallel structures interpreted to have a dominantly oblique reverse dextral strike-slip displacement, and which show no evidence of post-sandstone displacement at the unconformity; 3) a stratigraphic conformable semi-brittle cordierite-rich graphitic shear, termed the Marker Unit; and 4) a set of east-striking, sub-vertical faults which locally offset mineralized lenses with limited vertical and horizontal displacement.

Within the deposit area, the most significant structural feature is the presence of a major fault zone, termed the mother fault, located at the base of what was originally defined as the Lower Calc-Silicate Assemblage and is now considered to be intensely altered pelitic and semipelitic gneisses of the Bracketed Assemblage (Fig. 2.32). The mother fault strikes northerly and has a moderate easterly dip; it is characterized by a 10–25 m wide hydraulic breccia zone of silicified angular fragments within an intense clay-dravite matrix. Drill holes in the area of the intersection of the mother fault and the basement-sandstone unconformity have not confirmed any significant offset if the fault has any significant post-Athabasca vertical component of movement.

The cordierite-bearing, graphitic marker unit is largely conformable to the basement stratigraphy and ranges between 0.5 and 10 m in width. The structure is characterized by closely spaced anastomosing sub-millimetres scale slip planes, while none of the unit hosts significant fault breccia or gouge. The marker unit is interpreted to be a pre-sandstone ductile to semi-brittle reverse shear structure, although post-sandstone reactivation has occurred, resulting in localized minor reverse displacement of a few metres of the unconformity.

The majority of the Millennium deposit occurs immediately below the marker unit within pelite and semipelite gneiss of the host assemblage. The main ore lenses are largely developed on the western side of the main north-trending, sub-vertical, dextral strike slip fault. Ore grade mineralization largely terminates against or near the fault, suggesting the structure has acted as a semi-permeable barrier that restricted mineralizing fluids to the western side of the fault, although weak mineralization does extend locally into the eastern block of the north-trending fault. The east-trending faults are interpreted to have initiated as pre-Athabasca structures which have undergone post-Athabasca reactivation as indicated by localized displacement of the unconformity and the ore lenses.

Deposit footprint

Millennium deposit is dominantly basement-hosted deposit containing 29 195 tU at a grade of 2.03% U. The enveloping surface of the deposit footprint has a strike length of 280 m, width of 40–80 m, and vertical extent of 150 m. The top of the deposit is coincident with the sandstone-basement unconformity and occurs at a depth of 550–575 m below surface. Resource modelling has delineated several dozen discrete mineralized lenses that comprise the Millennium deposit; individual lenses are largely conformable with compositional layering of basement units and the S_1 penetrative foliation.

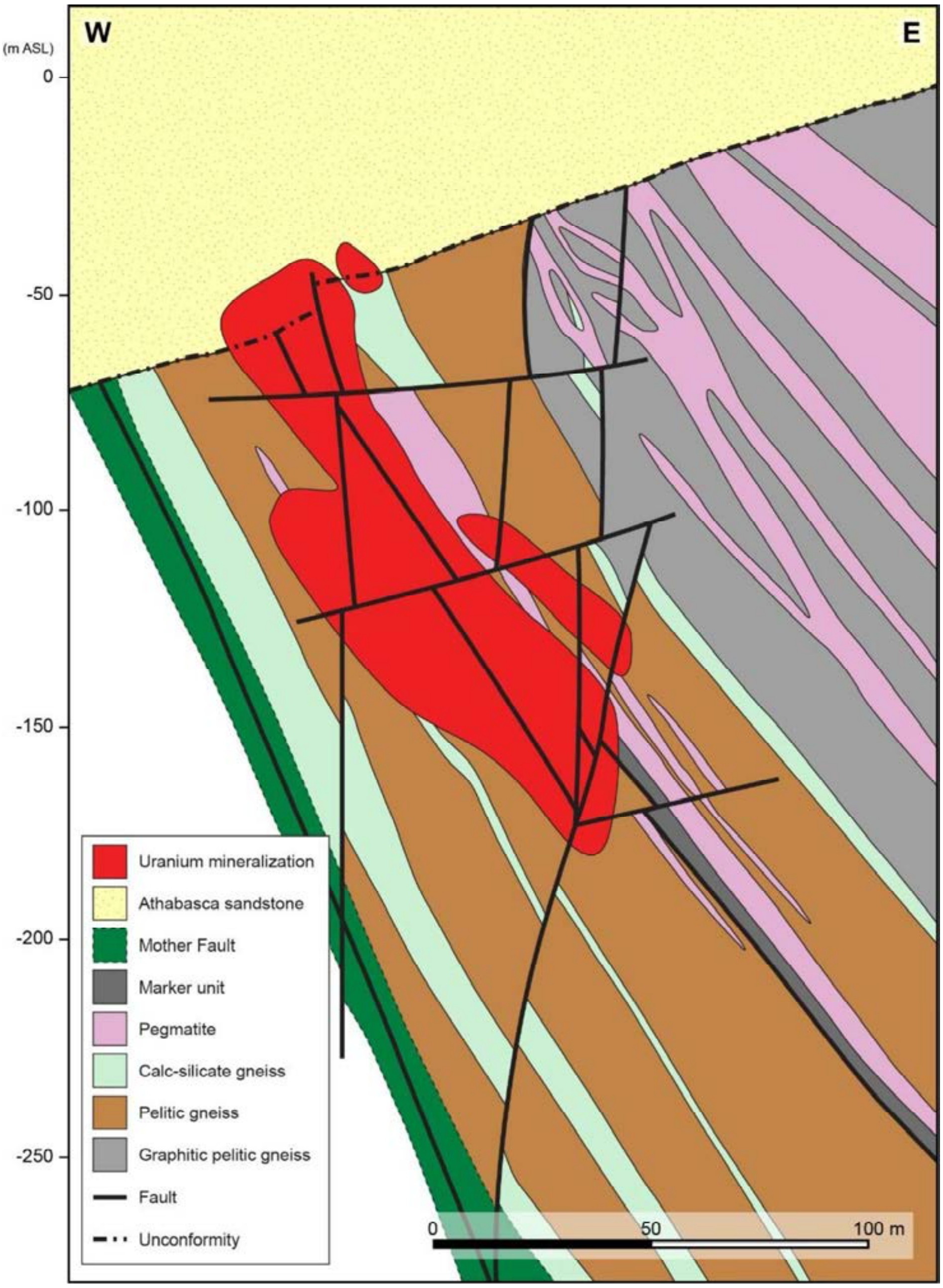

FIG. 2.32. Schematic geological cross-section of the Millennium deposit. Modified from Cameco Corporation [2.47].

Mineralization style

Uranium mineralization occurs in a variety of styles including; massive foliation-controlled replacement, breccia matrix infill, irregular fracture-controlled veins and veinlets, bleb-like aggregates and replacement rims around breccia fragments and along quartz vein selvedges. Massive replacement type mineralization is the dominant style while fracture infilling and vein-type are less well developed. The mineralizing fluids are interpreted to have infiltrated the rocks primarily along the S_1/S_2 foliation as well as lithologic contacts, particularly between pegmatite and pelitic units.

Textures in breccia-hosted mineralization suggest a progression from simple fracture-controlled, through more complex hydraulic fracturing with minor comminution, and finally into corrosive solution breccias. Breccias are oriented at a high angle to the S_0/S_1 foliation while mineralized breccia intervals are generally of limited dimensions and discontinuous, thereby making correlations between drill holes difficult.

Alteration

The Millennium deposit is enveloped by a vertically extensive hydrothermal alteration halo that is most intensely developed in the basement rocks and to a lesser degree in the overlying sandstone (Fig. 2.33). Alteration of the basement rocks includes: i) a distal halo of saussurite and sericite reflecting incipient to moderate feldspar destruction; ii) a more proximal zone dominated by both selective mineral and pervasive chlorite replacement; iii) a central zone of increasing argillic alteration dominated by illite, dravite and lesser kaolinite. The main area of uranium mineralization is coincident with the proximal alteration assemblage and commonly associated with the dark chlorite and haematite. The central facies is marked by strong to intense illite and dravite alteration replacement of basement gneisses over vertical thickness of 100 m or more. This central alteration facies increases in intensity towards the Mother Fault. A broad envelop of quartz ± carbonate ± chlorite veins and veinlets, largely predates central, proximal and distal alteration assemblages.

Textural and overprinting relationships indicate extensive bleaching and argillic alteration continued after the main uranium mineralization and associated hematization event. The lateral zonation and apparent contradictory cross-cutting relationships between alteration types reflects an evolving, fluctuating hydrothermal cell not dissimilar to that described in high level porphyry and epithermal systems. The spatial distribution of the alteration types, their intensities and distribution of the uranium mineralization to the outer proximal chlorite facies as opposed to the more intense central argillic facies, suggests the Millennium deposit is situated in the hanging wall of the hydrothermal system and somewhat separated from the Mother Fault (the main hydrothermal conduit).

Ore mineralogy and geochemistry

The Millennium uranium deposit is essentially monomineralic consisting of pitchblende with lesser amounts of uraninite and coffinite. As only minor amounts of sulphide and arsenide phases are present the overall content in nickel, arsenic, copper and cobalt is general low in orders (e.g. 100 to 200 ppm). Lead and vanadium enrichment are directly associated with and generally proportional to coincident uranium enrichment while light rare earth elements (LREE) and heavy rare earth elements (HREE) along with bismuth, lithium, molybdenum, tungsten and yttrium display elevated concentrations coincident with uranium mineralization.

Geochemically, the overall basement alteration is characterized by boron enrichment and Na_2O and zinc depletion.

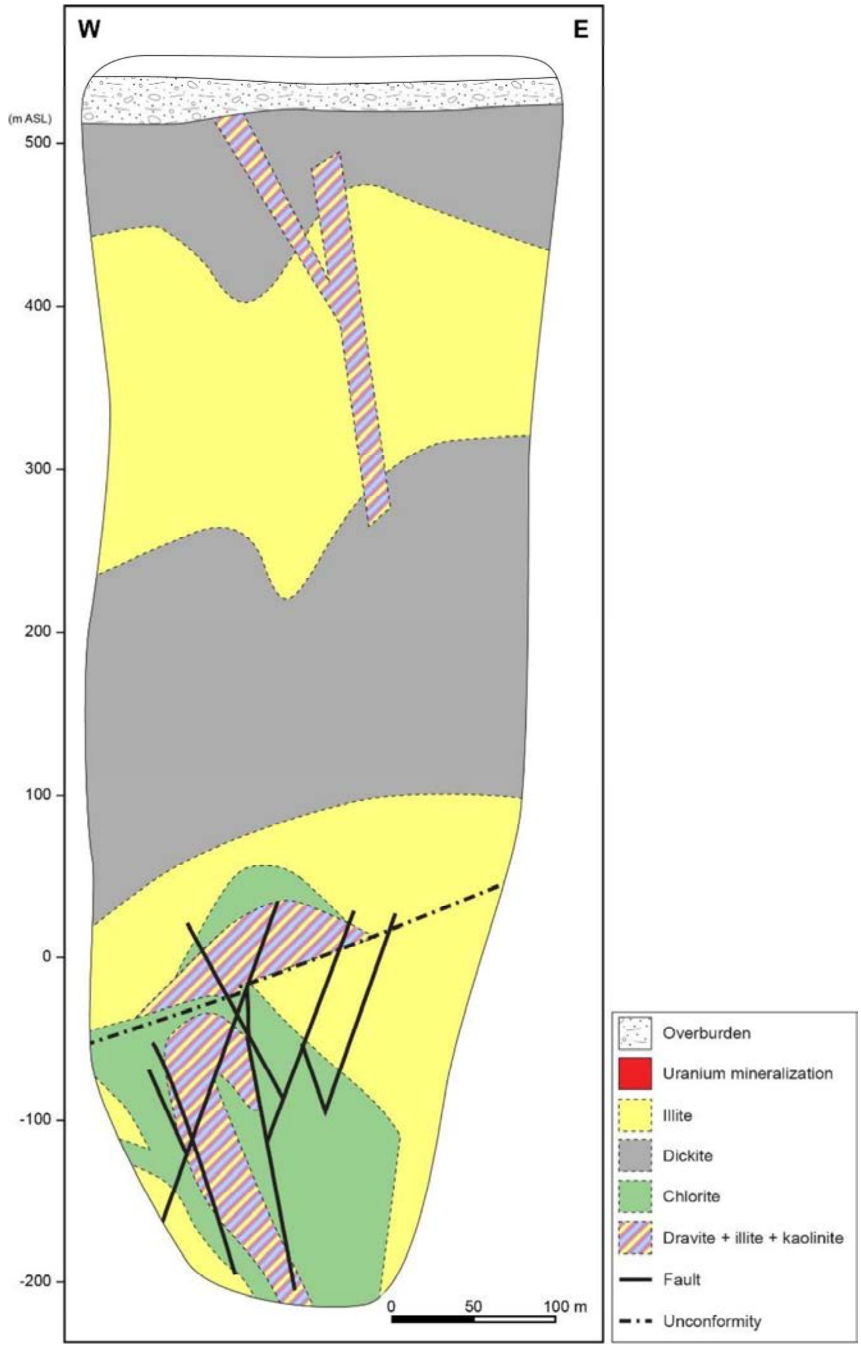

FIG. 2.33. Schematic alteration cross-section of the Millennium deposit depicting the different clay assemblages that characterize the deposit. This non-mineralized section within the deposit best depicts the alteration distribution, especially within the sandstone. As this basement deposit was generally tested with drill holes from the hanging wall side of the deposit (east), sandstone alteration above the deposit was only intersected in a few areas, one of which being this non-mineralized fence within the deposit. Modified from Cameco Corporation [2.47].

2.3. LITHOSTRUCTURAL CLASSIFICATION OF DEPOSITS

All deposits and systems listed in Table 2.1 were classified using the proposed lithostructural classification (Fig.s 2.34 and 2.35). Although the development of the classification was largely based on the geological setting of deposits in the Athabasca Basin, Proterozoic unconformity deposits from other regions of the world can also be accommodated within the parameters of the classification. Deposits not associated with the Athabasca Basin generally cluster together as distinct regionally groupings within this lithostructural classification, therefore exploration would be beneficial to develop modified versions of this classification which incorporates the more specific geological settings of the deposits from these other global regions. Developing a modified version of this classification for other regions would potentially result in a larger differentiation between deposits in specific basins that could better help with local exploration strategies and tactics.

A summary of the classification system as it applies to deposits from the four main global regions (e.g. Australia, Canada, India and Russian Federation) follows.

2.3.1. Australia

Australian deposits plot in four distinct areas of the classification diagram (Fig. 2.34). When the individual deposits are grouped as mineralization systems, they reflect more similarities, particularly from the perspective of their lithostructural setting.

The Turee Creek deposit is classified near the Cigar Lake end member of the classification since the deposit is hosted solely within the sedimentary rocks, while actual unconformity between the Mesoproterozoic Bresnahan Group and underlying basement rocks of the Wyloo Group is estimated to be at least 200 m below the mineralization. Therefore, the Turee Creek deposit is considered to be a sandstone hosted system without any basement component.

The Angularli deposit plots along the line between the Millennium and McArthur River end-members of the classification diagram. The deposit is characterized by high-grade mineralization with values up to 4.41% U over 20.2 m [2.105] associated with a post-Kombolgie fault displacement of the sandstone-basement unconformity. The deposit is associated with significant cataclastic deformation of the sandstone underlying and basement gneisses and extensive basement alteration. The uranium mineralization forms a thick, fault-parallel lens largely hosted within the basement rocks with a smaller amount extending into the overlying sandstone wedge.

The third grouping of deposits lie along the Millennium-Eagle Point line, approximately midway between the end members. These deposits/systems represent entirely basement-hosted mineralization that immediately underlies sandstones of the Kombolgie Sub-group but do not appear to extend into the overlying sedimentary rocks. The mineralization typically occurs as thick tabular lenses of low-grade foliation-controlled disseminated uranium, largely conformable to the basement stratigraphy, and locally as high grade uraninite associated with discordant mineralized breccia lenses. The deposits exhibit strong spatial association to broad zones of conformable semi-brittle shears networks in the host basement gneisses and localized post-Kombolgie brittle faults.

The fourth cluster of deposits lie close to the Eagle Point end member of the classification, and represent deposits of the Rum Jungle and Coronation Hill areas. These deposits are entirely hosted within basement rocks and are characterized by relatively tight alteration envelopes. In the case of the Rum Jungle deposits, the unconformity has been eroded and the distance between the unconformity and the mineralization is unknown. At Coronation Hill, the bulk of the mineralization is hosted hundreds of metres below the unconformity and is spatially associated with a significant unconformity offset of up to 325 m, it is not classified as a wedge type sub-deposit because the mineralization is not associated with the unconformity-offsetting fault. Similarly, there is no mineralization component within the sandstone.

2.3.2. Canada (Athabasca Basin)

Deposits in the Athabasca Basin plot with a bimodal distribution within the classification diagram: i) one population clusters in the area between the Cigar Lake and McArthur River, and ii) another population along the Millennium-Eagle Point side of the diagram. In the former population, most, if not all deposits have a significant component of their mineralization hosted by sandstones along the unconformity while in the latter population, the deposits are predominantly basement hosted.

The mineralizing systems, shown by the ellipsoidal fields, commonly show a large area of coverage relative to the diagram axes. This range of lithostructural characteristics of the sub-deposits comprising the mineralizing system is tentatively interpreted to reflect the overall fluid flow vector in the mineralizing process. For example, the Sue and Collins Bay Systems, both show an overall rake to the system in longitudinal sections from mineralization along the unconformity to progressively straddling both the sandstone and basement, to entirely basement hosted. This range of lithostructural settings from entirely sandstone-hosted unconformity to entirely basement-hosted sub-deposits within a mineralization system is an important consideration when designing exploration programmes along larger mineralized trends. An interesting pattern to note is that the ellipses of some mineralization systems contain deposits that are close to different end members of the classification but do not appear to have any sub-deposits that are transitional between them. One explanation of the absence of transitional sub-deposits within a mineralization system is that they remain undiscovered by exploration efforts to date.

2.3.3. Canada (other basins)

The deposits of the Thelon basin cluster in the area close to the Millennium-Eagle Point line, lying about half-way between the two end-members (see Fig. 2.34). This reflects that the mineralization in the Thelon is entirely basement hosted, and if sandstone-hosted mineralization was present it has been removed by erosion.

The mineralization is structurally controlled by brittle deformation features including steep-dipping fractures, veins, and breccias that form extensive permeability networks within the host gneisses. This extensive permeability network allowed widespread circulation of oxidized uranium-bearing fluids through sulphide-rich rocks. The mineralization style is characterized by small, thin veins of uraninite and pitchblende, and is comparable to that at Eagle point. The widespread fracture and brittle fault network also resulted in an extensive, moderate to strong clay alteration envelope, which is similar to the alteration at the Millennium deposit. There is virtually little difference between empirical characteristics of the various deposits, therefore as a System, these deposits are quite restricted on the classification diagram.

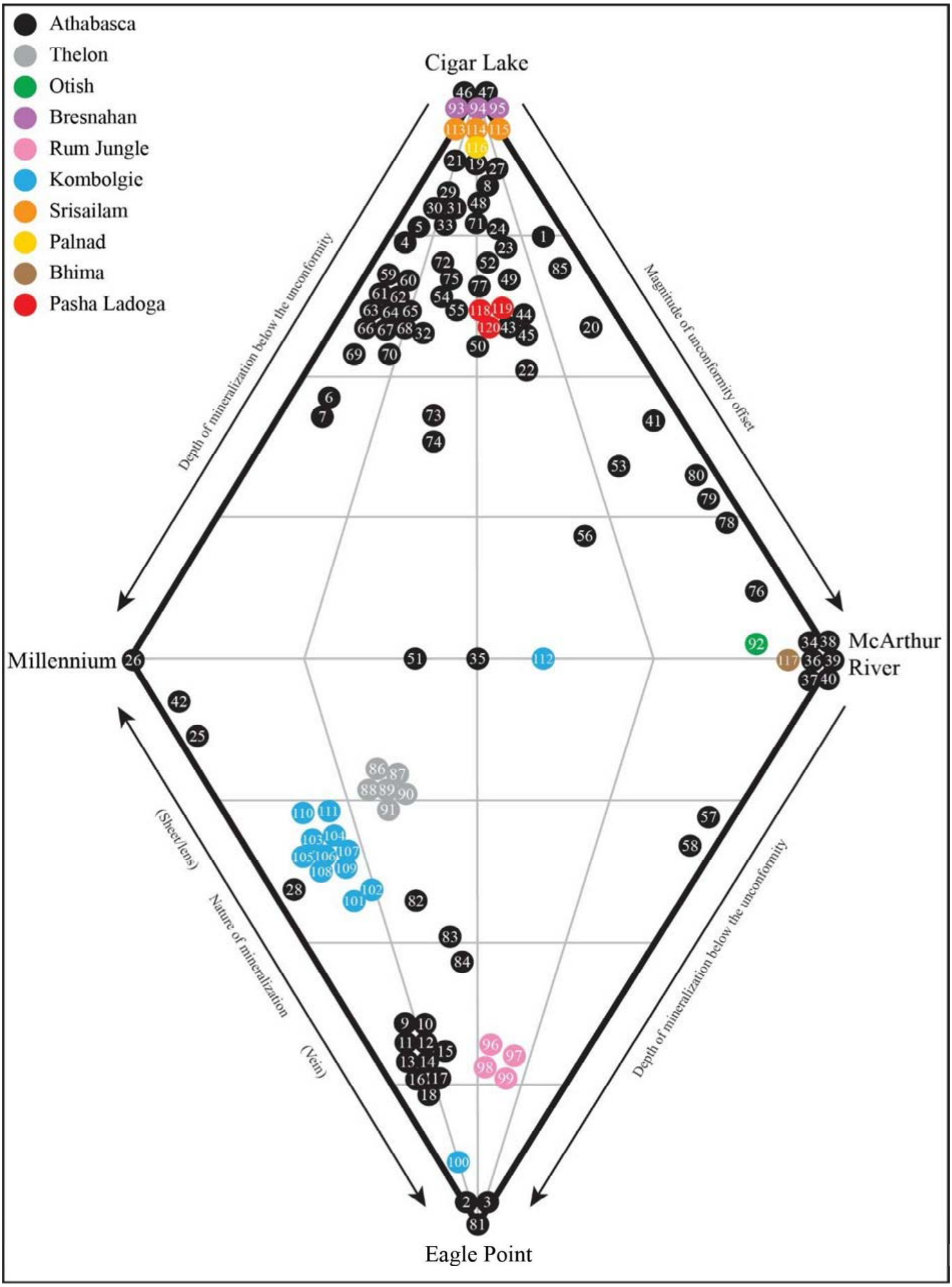

FIG. 2.34. Distribution of Proterozoic unconformity uranium deposits within the lithostructural classification. The numbers correspond to the values in the 'ID' field in Table 2.1.

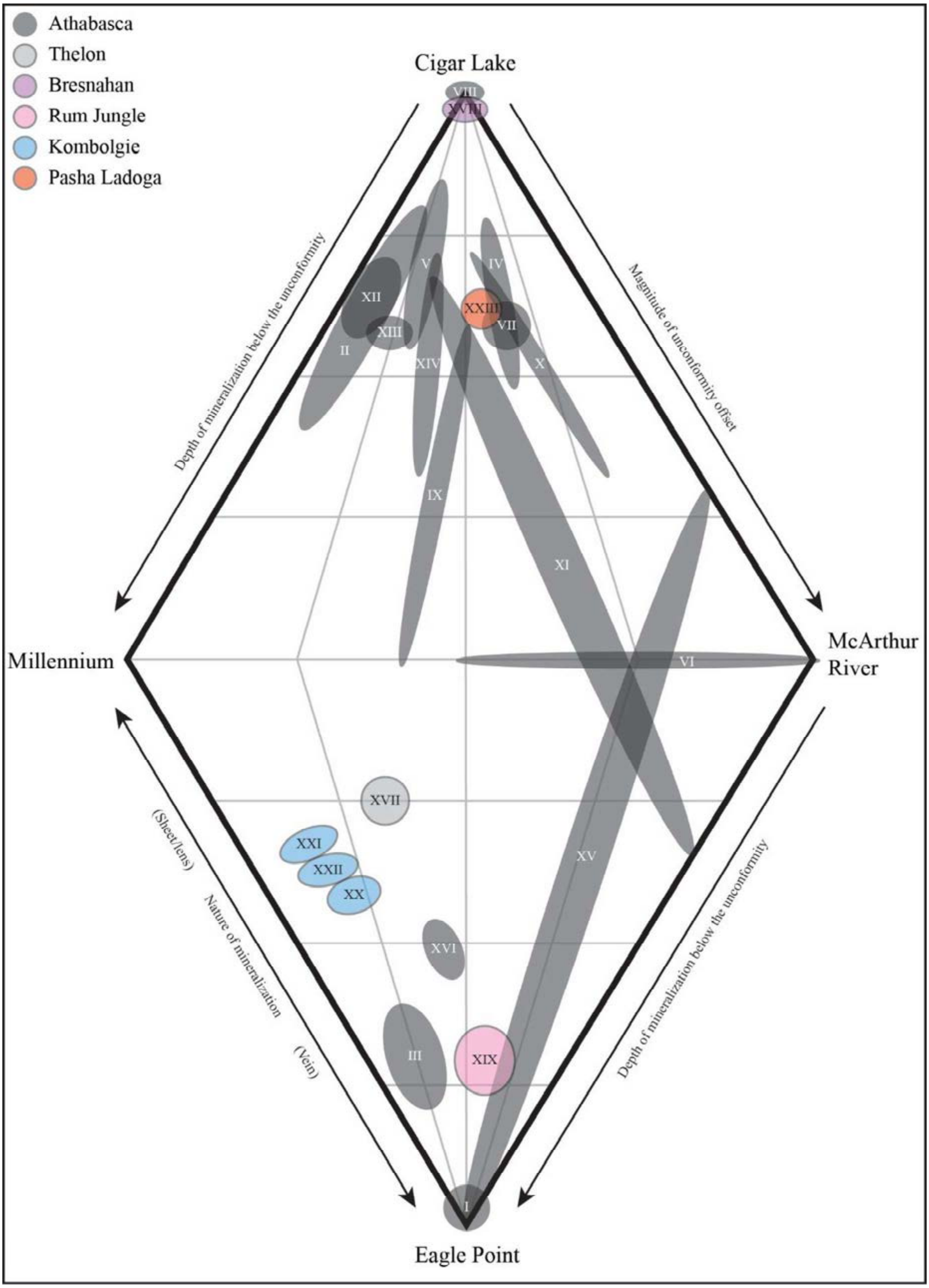

FIG. 2.35. Distribution of Proterozoic unconformity uranium systems within the lithostructural classification. The Roman numerals correspond to the values in the 'ID' field in Table 2.1.

The Camie River deposit, located in the Otish Basin, plots close to the McArthur River end member since uranium mineralization is spatially related to a series of closely-spaced reverse faults that offsets the unconformity into a number of sandstone-basement wedges. The deposit is characterized by high grade mineralization, with a single sample returning up to 22% U [2.28], occurring in both sandstone just above the unconformity and extending up to 25 m into the underlying basement rocks along the controlling fault zone.

2.3.4. India

All but one of the Indian deposits (e.g. Gogi deposit) are plotted towards the Cigar Lake end member of the classification. Although the footprint of these very low grade, aerially extensive deposits contrast significantly with that of the very high grade and more restricted footprint of Cigar Lake, the Indian deposits lie immediately above the basement-basin unconformity. These deposits are characterized forming laterally extensive thin tabular bodies parallel to the sedimentary basin stratigraphy with only minor mineralization extending into the underlying basement rocks.

The Gogi deposit plots in close proximity to the McArthur River end member. Although of much lower grade than McArthur River, this deposit is associated with a reverse fault which has a vertical displacement of >200 m and contains both basin-hosted and basement-hosted mineralization typical of wedge-type sub-deposits.

2.3.5. Russian Federation

The Karku deposit represents the only Proterozoic unconformity system identified to date in Russian Federation. The deposit is located in the Pasha-Ladoga Basin in the Baltic region. These deposits are plotted in proximity to the Cigar Lake end member since the bulk of the mineralization is hosted by Basinal sandstones although a small ‘basement root’ extends up to 10 m below the unconformity. The mineralization is associated with a post-sandstone fault which appears to have a limited component of vertical offset. Within the overlying sandstones, the mineralization extends laterally along bedding planes from the controlling fault while ‘perched’ mineralization occurs higher in the stratigraphy, notably within dolerite sills, that are cut by the controlling fault.

2.4. CONCLUSION

This compilation, of empirical parameters characterizing Proterozoic unconformity deposits provides a valuable format to compare and contrast the range of variability found in this deposit class. Like other deposit model classifications, each individual unconformity deposit can exhibit characteristics unique to itself, nevertheless there is a range of quantifiable limits that can be assigned to these deposits from the perspective of their footprint parameters. Similarly, a number of generalizations can be made in terms of the variations in lithostructural settings observed (e.g. basement, unconformity, wedge-type settings), resource size and grades (e.g. high, moderate, low grade; large, moderate, small resource size), size of associated alteration envelop relative to the orebody and styles of mineralization (e.g. broad vs. narrow), and the spatial relationship to mineralization controlling structures (e.g. footwall, hanging wall, amount of unconformity offset).

An outcome of this compilation is a classification based largely on the lithostructural setting of the mineralization and alteration footprint. The classification is developed around four end members; Cigar Lake, McArthur River, Eagle Point, and Millennium, which reflect the variation in footprint characteristics that is seen in Proterozoic unconformity deposits. The intent of this classification is that it will better assist and guide exploration teams in developing targeting strategies for Proterozoic unconformity associated uranium mineralization, not only in those basins already with identified deposits but hopefully in under-explored basins elsewhere in the world.

2.5. REFERENCES

[2.1] RAY, G.E., Project 5: Foster Lake (NW) – Geikie River (SW) Area Reconnaissance Geological Mapping of 74A-13, 14 and 74H-3, 4, Summary of Investigations 1976, Saskatchewan Geological Survey (1976) pp. 18–23.

[2.2] HOEVE, J., SIBBALD, T.I.I., On the genesis of Rabbit Lake and other unconformity-type uranium deposits in northern Saskatchewan, Canada, Economic Geology **73** (1978) 1450–1473.

[2.3] HALTER, G., SHEPPARD, S.M.F., WEBER, F., CLAUER, N., PAGEL, M., Radiation-related retrograde hydrogen isotope and K–Ar exchange in clays minerals, Nature **330** (1987) 638–641.

[2.4] WILSON, M.R., KYSER, T.K., Stable isotope geochemistry of alteration associated with the Key Lake uranium deposit, Canada, Economic Geology **82** 6 (1987) 1540–1557.

[2.5] KOTZER, T.G., KYSER, T.K., Petrogenesis of the Proterozoic Athabasca Basin, northern Saskatchewan, Canada, and its relation to diagenesis, hydrothermal uranium mineralization and paleohydrogeology, Chemical Geology **120** (1995) 45–89.

[2.6] FAYEK, M., KYSER, T.K., Characterization of multiple fluid-flow events and rare-earth-element mobility associated with formation of unconformity-type uranium deposits in the Athabasca Basin, Saskatchewan, Canadian Mineralogist **35** (1997) 627–658.

[2.7] PAGEL, M., Détermination des conditions physico-chimiques de la silicification diagénétique des grès Athabasca (Canada) au moyen des inclusions fluides, Comptes Rendus Hebdomadaires des Sécances de l'Académie des Sciences, Série D: Sciences Naturelles **280** 3 (1975) 2301–2304.

[2.8] PAGEL, M., JAFFREZIC, H., Analyses chimiques des saumures des inclusions du quartz et de la dolomite du gisement d'uranium de Rabbit Lake (Canada). Aspect méthodologique et importance génétique, Comptes Rendus Hebdomadaires des Sécances de l'Académie des Sciences, Série D: Sciences Naturelles **284** 1 (1977) 113–116.

[2.9] PAGEL, M., POTY, B., SHEPPARD, S.M.F., "Contribution to some Saskatchewan uranium deposits mainly from fluid inclusion and isotope data", Uranium in the Pine Creek Geosyncline (FERGUSON, J., GOLEBY, A., Eds), International Atomic Energy Agency, Vienna (1980) 639–645.

[2.10] DEROME, D., CATHELINEAU, M., CUNEY, M., FABRE, C.L., BANKS, D.A., Mixing of sodic and calcic brines and uranium deposition at McArthur River, Saskatchewan, Canada: a Raman and laser-induced breakdown spectroscopic study of fluid inclusions, Economic Geology **100** 8 (2005) 1529–1545.

[2.11] RICHARD, A. et al., U Concentrations in Ore Fluids: A LA-ICP-MS Investigation of Fluids Associated with Unconformity-Related Uranium Deposits, Québec City (2008) 143.

[2.12] RICHARD, A. et al., Metal-rich fluid inclusions provide new insights into unconformity-related U deposits (Athabasca Basin and Basement, Canada), Mineralium Deposita **51** 2 (2015) 249–270.

[2.13] BAAGSGARD, H., CUMMING, G.L., WORDEN, J.M., U-Pb geochronology of minerals from the Midwest uranium deposit, northern Saskatchewan, Canadian Journal of Earth Sciences **21** (1984) 642–648.
[2.14] CARL, C., VON PECHMANN, E., HONDORF, A., RUHMANN, G., Mineralogy and U/Pb, Pb/Pb, and Sm/Nd geochronology of the Key Lake uranium deposit, Athabasca Basin, Saskatchewan, Canada, Canadian Journal of Earth Sciences **29** (1992) 879–895.
[2.15] PHILIPPE, S., LANCELOT, J.R., CLAUER, N., PAQUET, A., Formation and evolution of the Cigar Lake uranium deposit based on U-Pb and K-Ar isotope systematics, Canadian Journal of Earth Sciences **30** (1993) 720–730.
[2.16] FAYEK, M., HARRISON, T.M., EWING, R.C., GROVE, M., COATH, C.D., O and Pb isotopic analyses of uranium minerals by ion microprobe and U-Pb ages from the Cigar Lake deposit, Chemical Geology **185** (2002) 205–225.
[2.17] ALEXANDRE, P., KYSER, T.K., THOMAS, D.J., POLITO, P.A., MARLATT, J., Geochronology of unconformity-related uranium deposits in the Athabasca Basin, Saskatchewan, Canada, and their integration in the evolution of the Basin, Mineralium Deposita **44** (2009) 41–59.
[2.18] CUI, T., YANG, J.W., SAMSON, I.M., Tectonic deformation and fluid flow: implications for the formation of unconformity-related uranium deposits, Economic Geology **107** (2012) 147–163.
[2.19] LI, Z., CHI, G., BETHUNE, K.M., The effects of basement faults on thermal convection and implications for the formation of unconformity-related uranium deposits in the Athabasca Basin, Canada, Geofluids **16** (2016) 729–751.
[2.20] LI, Z., CHI, G., BETHUNE, K.M., THOMAS, D.J., ZALUSKI, G., Structural Controls on Fluid Flow During Compressional Reactivation of Basement Faults: Insights from Numerical Modeling for the Formation of Unconformity-Related Uranium Deposits in the Athabasca Basin, Canada, Economic Geology **112** (2017) 451–466.
[2.21] JEFFERSON, C.W. et al., "Unconformity-associated uranium deposits of the Athabasca Basin, Saskatchewan and Alberta", Mineral Deposits of Canada: A Synthesis of Major Deposits – Types, District Metallogeny, the Evolution of Geological Provinces, and Exploration Methods, Vol. Special Publication No. 5 (GOODFELLOW, W.D., Ed), Geological Association of Canada, Mineral Deposits Division (2007) 273–305.
[2.22] DAHLKAMP, F.J., Uranium Ore Deposits, Springer-Verlag, New York (1993) 460 pp.
[2.23] ESRI, World Topographic Map, (2018).
[2.24] AHMAD, M., LALLY, J.H., MCCREADY, A.J., Economic Geology of the Rum Jungle Mineral Field, Northern Territory, Report 19, (2006) p. 75.
[2.25] ALEXANDRE, P., KYSER, T.K., JIRICKA, D., WITT, G., Formation and evolution of the Centennial unconformity-related uranium deposit in the South-Central Athabasca Basin, Canada, Economic Geology **107** 3 (2012) 385–400.
[2.26] ANTHONY, P.J., "Nabarlek uranium deposit", Economic Geology of Australia and Papua New Guinea, Vol. 1. Metals (KNIGHT, C.L., Ed), The Australasian Institute of Mining and Metallurgy, Victoria (1975) 304–308.
[2.27] AREVA RESOURCES CANADA INC, Personal Communication, (2017).
[2.28] AUBIN, A., Les Projets Camie-Beaver et Otish South, et Le Potentiel Uranifère Du Bassin Sédimentaire Otish, Énergie et Ressources naturelles Québec, Chibougamau (2011) 11–12.
[2.29] AUBIN, A., ZALUSKI, G., ROGERS, S., KELLER, C., BORT, E., Cameco Corporation 2011 Exploration Report – Camie River Project, (2012) p. 41.

[2.30] AUBIN, A., ZALUSKI, G., ROGERS, S., KELLER, C., BORT, E., Cameco Corporation 2011 Exploration Report – Otish South Project, (2012) p. 54.
[2.31] BATTEY, G.C., MIEZITIS, Y., MCKAY, A.D., Australian Uranium Resources, Department of Resources & Energy, Canberra (1987).
[2.32] BAUDEMONT, D., FEDOROWICH, J., Structural control of uranium mineralization at the Dominique-Peter deposit, Saskatchewan, Canada., Economic Geology **91** (1996) 855–874.
[2.33] BAUDEMONT, D., PACQUET, A., "The Sue D and E uranium deposits, northern Saskatchewan: evidence for structurally controlled fluid circulation in the Athabasca Basin.", MinExpo'96 Symposium - Advances in Saskatchewan Geology and Mineral Exploration, Vol. Special Publication 14 (ASHTON, K.E., HARPER, C.T., Eds), Saskatchewan Geological Survey (1996) 85–94.
[2.34] BAUDEMONT, D., PIQUARD, J.P., EY, F., ZIMMERMAN, J., The Sue uranium deposits, Saskatchewan, Canada., Exploration and Mining Geology **2** 3 (1993) 179–202.
[2.35] BEAUFORT, D., PATRIER, P., LAVERRET, E., BRUNETON, P., MONDY, J., Clay alteration associated with Proterozoic unconformity-type uranium deposits in the East Alligator Rivers uranium field, Northern territory, Australia., Economic Geology **100** (2005) 515–536.
[2.36] BELL, K., "Geochronology of the Carswell area, northern Saskatchewan", The Carswell Structure Uranium Deposits, Saskatchewan, Vol. Geological Association of Canada Special Paper 29 (LAINÉ, R., ALONSO, D., SVAB, M., Eds), Geological Association of Canada (1985) 33–46.
[2.37] BEYER, S.R. et al., Basin Evolution and Unconformity-Related Uranium Mineralization: The Camie River U Prospect, Paleoproterozoic Otish Basin, Quebec, Economic Geology **107** (2012) 401–425.
[2.38] BISHOP, C.S., MAINVILLE, A.G., YESNIK, L.D., Cigar Lake Operation, Northern Saskatchewan, Canada: National Instrument 43–101 Technical Report, Cameco Corporation, Saskatoon (2016) p. 155.
[2.39] BLAISE, J.R., KONING, E., "Mineralogical and structural aspects of the Dominique-Peter uranium deposit.", The Carswell Structure Uranium Deposits, Saskatchewan., Vol. Special Paper 29 (LAINÉ, R., ALONSO, D., SVAB, M., Eds), Geological Association of Canada (1985) 139–151.
[2.40] BOULANGER, R.A., Geological, Petrographic and Geochemical Characterization of the Roughrider West Zone Unconformity-Type Uranium Deposit, Athabasca Basin, Saskatchewan, MSc, University of Regina (2012) 277 pp.
[2.41] BRONKHORST, D., MAINVILLE, A.G., MURDOCK, G.M., YESNIK, L.D., McArthur River Operation, Northern Saskatchewan, Canada: National Instruments 43-101 Technical Report, Cameco Corporation (2012) p. 196.
[2.42] BROWNE, A.L.L., "Ranger 68 uranium deposit", Geology of the Mineral Deposits of Australia and Papua New Guinea, Vol. 1 (HUGHES, E.F., Ed), The Australasian Institute of Mining and Metallurgy, Melbourne (1990) 795–797.
[2.43] BRUNETON, P., "Geology of the Cigar Lake uranium deposit (Saskatchewan, Canada).", Economic Minerals of Saskatchewan, Vol. Special Publication 8 (GILBOY, C.F., VIGRASS, L.W., Eds), Saskatchewan Geological Survey, Regina (1987) 99–119.
[2.44] BRUNETON, P., "IAEA Classification of Uranium Deposits", presented at the URAM 2014: International Symposium on Uranium Raw Material for the Nuclear Fuel Cycle: Exploration, Mining, Production, Supply and Demand, Economics and Environmental Issues Presentations, Vienna (Austria), 2014.

[2.45] BRUNT, D.A., “Miscellaneous uranium deposits in Western Australia”, Geology of the Mineral Deposits of Australia and Papua New Guinea, Vol. 2 (HUGHES, E.F., Ed), The Australasian Institute of Mining and Metallurgy, Melbourne (1990) 1615–1620.
[2.46] CAMECO CORPORATION, Cameco Corporation, Home–Cameco, www.cameco.com.
[2.47] CAMECO CORPORATION, Personal Communication, (2017).
[2.48] CANALASKA URANIUM LTD., NI-43-101 Technical Report on the Fond Du Lac Project, NI 43–101, (2010) p. 78.
[2.49] CARVILLE, D.P., LECKIE, J.F., MOORHEAD, C.F., RAYNER, J.G., DURBIN, A.A., “Coronation Hill gold-platinum-palladium deposit”, Geology of the Mineral Deposits of Australia and Papua New Guinea, Vol. 1 (HUGHES, E.F., Ed), The Australasian Institute of Mining and Metallurgy, Melbourne (1990) 759–762.
[2.50] CHAKI, A., “An overview of uranium exploration strategy in India”, presented at the URAM-2009: International symposium on uranium raw material for the nuclear fuel cycle: Exploration, mining, production, supply and demand, economics and environmental issues, Vienna (Austria), 2009.
[2.51] CHAKI, A., PUROHIT, R.K., MAMALLAN, R., Low grade uranium deposits of India – a bane or boon, Energy Procedia **7** (2011) 153–157.
[2.52] CHAUVET, J.F., LEGUÉRÉ, J., ANDREWS, C., Rapport de Synthèse Des Gisements R et F - Étude Des Ressources Du Gisement R, Internal Report to AREVA, Saskatoon (1982) p. 17.
[2.53] CHEN, S., HATTORI, K., GRUNSKY, E.C., Multielement statistical evidence for uraniferous hydrothermal activity in sandstones overlying the Phoenix uranium deposit, Athabasca Basin, Canada., Mineralium Deposita (2017) 16 p. WITH REGARD TO THE P. AFTER THE 16. THIS SHOULD BE PP IF REFERRING TO TOTAL NUMBER OF PAGES OR p. 16 IF REFERRING TO A SPECIFIC PAGE
[2.54] CHI, G. et al., Petrography, fluid inclusion analysis, and geochronology of the End uranium deposit, Kiggavik, Nunavut, Canada, Mineralium Deposita **52** 2 (2017) 211–232.
[2.55] CLARKE, P.J., FOGWILL, W.D., “Geology of the Dawn Lake uranium deposits, northern Saskatchewan.”, Uranium Deposits of Canada, Vol. Special Volume 33 (EVANS, E.L., Ed), Canadian Institute of Mining and Metallurgy (1986) 184–192.
[2.56] CLOUTIER, J., KYSER, T.K., OLIVO, G.R., ALEXANDRE, P., HALABURDA, J., The Millennium uranium deposit, Athabasca Basin, Saskatchewan, Canada: An atypical basement-hosted unconformity-related uranium deposit, Economic Geology **104** (2009) 815–840.
[2.57] CLOUTIER, J., KYSER, T.K., OLIVO, G.R., BRISBIN, D., Geochemical, isotopic, and geochronologic constraints on the formation of the Eagle Point basement-hosted uranium deposit, Athabasca Basin, Saskatchewan, Canada and recent remobilization of primary uraninite in secondary structures., Mineralium Deposita **46** (2011) 35–56.
[2.58] CUMMING, G.L., KRSTIC, D., The age of unconformity-related uranium mineralization in the Athabasca Basin, northern Saskatchewan, Canadian Journal of Earth Sciences **29** (1992) 1623–1639.
[2.59] CUNEY, M., KYSER, T.K., Recent and Not-So-Recent Developments in Uranium Deposits and Implications for Exploration, Short Course Series, Vol. 39, (2008) 257 p.

[2.60] CURTIS, L., “Post-Kombolgie alteration at Jabiluka II and its significance with regards to the Athabasca – Alligator rivers comparison”, Geology of Uranium Deposits: Proceedings of the CIM-SEG Uranium Symposium, Vol. 32 (SIBBALD, T.I.I., PETRUK, W., Eds), The Canadian Institute of Mining and Metallurgy, Montreal (1981) 231–245.

[2.61] DAHLKAMP, F.J., Geologic appraisal of the Key Lake U-Ni deposits, Northern Saskatchewan, Economic Geology **73** (1978) 1430–1449.

[2.62] DENISON MINES CORP., Denison Mines Corp. - Canada, Denison Mines Corp. - Canada, http://www.denisonmines.com/s/Canada.asp.

[2.63] DENISON MINES CORP., Personal Communication, (2018).

[2.64] DENISON MINES INC., Technical Report on the Midwest Uranium Deposit Mineral Resource and Mineral Reserve Estimates, Saskatchewan, Canada, NI 43-101, (2006) p. 198.

[2.65] DENISON MINES INC., Technical Report on the Sue D Uranium Deposit Mineral Resource Estimate, Saskatchewan, Canada, NI 43-101, (2006) p. 101.

[2.66] DODSON, R.G., PRICHARD, C.E., “Uranium in the Pine Creek Geosyncline”, Economic Geology of Australia and Papua New Guinea, Vol. 1. Metals (KNIGHT, C.L., Ed), The Australasian Institute of Mining and Metallurgy, Victoria (1975) 281–284.

[2.67] DUNN, P.R., BATTEY, G.C., MIEZITIS, Y., MCKAY, A.D., “The distribution and occurrence of uranium”, Geological Aspects of the Discovery of Some Important Mineral Deposits in Australia (GLASSON, K.R., RATTIGAN, J.H., Eds), The Australasian Institute of Mining and Metallurgy, Victoria (1990) 455–462.

[2.68] DUNN, P.R., BATTEY, G.C., MIEZITIS, Y., MCKAY, A.D., “The uranium deposits of the Northern Territory”, Geological Aspects of the Discovery of Some Important Mineral Deposits in Australia (GLASSON, K.R., RATTIGAN, J.H., Eds), The Australasian Institute of Mining and Metallurgy, Victoria (1990) 463–476.

[2.69] ENERGY RESOURCES OF AUSTRALIA LTD., Ranger 3 Deeps Draft Environmental Impact Statement, (2014) p. 702.

[2.70] ENERGY RESOURCES OF AUSTRALIA LTD., 2014 Annual Report, (2015) p. 136.

[2.71] ENERGY RESOURCES OF AUSTRALIA LTD., 2015 Annual Report, (2016) p. 116.

[2.72] ENERGY RESOURCES OF AUSTRALIA LTD., 2016 Annual Report, (2017) p. 120.

[2.73] EUPENE, G.S., FEE, P.H., COLVILLE, R.G., “Ranger One uranium deposits”, Economic Geology of Australia and Papua New Guinea, Vol. 1. Metals (KNIGHT, C.L., Ed), The Australasian Institute of Mining and Metallurgy, Victoria (1975) 308–317.

[2.74] EY, F., Un Exemple de Gisement d’uranium Sous Discordance: Les Minéralisations Protérpzoïques de Cluff Lake, Saskatchewan, Canada, Thèse d’État, Université Louis Pasteur (1984) 165 pp.

[2.75] EY, F., GAUTHIER-LAFAYE, F., LILLIÉ, F., WEBER, F., “A uranium unconformity deposit: the geological setting of the D orebody (Saskatchewan – Canada)”, The Carswell Structure Uranium Deposits, Saskatchewan., Vol. Special Paper 29 (LAINÉ, R., ALONSO, D., SVAB, M., Eds), Geological Association of Canada (1985) 121–138.

[2.76] FAYEK, M., Petrography of Samples from the Fond Du Lac Deposit, Athabasca Basin, Saskatchewan, Canada, Report Prepared for Canalaska Uranium Ltd., (2009).

[2.77] FAYEK, M., KYSER, T.K., RICIPUTI, L., U and Pb isotope analysis of uranium minerals by ion microprobe and the geochronology of the McArthur River and Sue Zone uranium deposits, Saskatchewan, Canada, Canadian Mineralogist **40** (2002) 1553–1569.

[2.78] FERGUSON, J. et al., Uranium in the Pine Creek Geosyncline: Proceedings of the International Uranium Symposium on the Pine Creek Geosyncline, v. 1, International Atomic Energy Agency (1980) 760 pp.
[2.79] FISSION ENERGY CORP., “J-Zone: Discovery and growing high-grade unconformity-type mineralization in the Athabasca Basin”, presented at the Saskatchewan Geological Survey Open House, Saskatoon, 2010.
[2.80] FISSION ENERGY CORP., Mineral Resource Estimate on the J Zone Uranium Deposit, Waterbury Lake Property, NI 43-101, (2013) p. 95.
[2.81] FISSION ENERGY CORP., Revised Resource Estimate on the J Zone Uranium Deposit, Waterbury Lake Property, NI 43-101, (2013) p. 53.
[2.82] FISSION URANIUM CORP., Technical Report on the Patterson Lake South Property, Northern Saskatchewan, Canada: NI 43-101 Report, NI 43-101, (2015) p. 140.
[2.83] FOY, M.F., “South Alligator Valley uranium deposits”, Economic Geology of Australia and Papua New Guinea, Vol. 1. Metals (KNIGHT, C.L., Ed), The Australasian Institute of Mining and Metallurgy, Victoria (1975) 301–303.
[2.84] FOY, M.F., PEDERSON, C.P., “Koongarra uranium deposit”, Economic Geology of Australia and Papua New Guinea, Vol. 1. Metals (KNIGHT, C.L., Ed), The Australasian Institute of Mining and Metallurgy, Victoria (1975) 317–321.
[2.85] FRANKOVICH, F.J., FIRMAN, J.B., Regional Geology of the Rum Jungle District, Northern Territory, Australia, 1954/26, Department of National Development, Bureau of Mineral Resources, Geology and Geophysics, Commonwealth of Australia (1954) p. 13.
[2.86] FRASER, W.J., “The Embayment line of mineralization, Rum Jungle”, Economic Geology of Australia and Papua New Guinea, Vol. 1. Metals (KNIGHT, C.L., Ed), The Australasian Institute of Mining and Metallurgy, Victoria (1975) 271–277.
[2.87] GABOREAU, S., BEAUFORT, D., VIEILLARD, P., PATRIER, P., Aluminium phosphate-sulfate minerals associated with Proterozoic unconformity-type uranium deposits in the East Alligator River uranium field, northern Territories, Australia, The Canadian Mineralogist **43** (2005) 813–827.
[2.88] GEOSCIENCE AUSTRALIA, Australian Mines Atlas, Australian Mines Atlas, http://www.australianminesatlas.gov.au/.
[2.89] GOVERNMENT OF SASKATCHEWAN, Saskatchewan Mineral Deposit Index (SMDI), Mineral Deposit Index – Central Services – Government of Saskatchewan, http://applications.saskatchewan.ca/mineral-deposit-index.
[2.90] HANCOCK, M.C., MAAS, R., WILDE, A.R., “Jabiluka uranium-gold deposits”, Geology of the Mineral Deposits of Australia and Papua New Guinea, Vol. 1 (HUGHES, E.F., Ed), The Australasian Institute of Mining and Metallurgy, Melbourne (1990) 785–793.
[2.91] HARPER, C.T., TAYLOR, R.P., FRYER, B.J., “Geology and lithogeochemistry of the Maurice Bay uranium deposit, northern Saskatchewan”, Uranium Deposits of Canada, Vol. Special Volume 33 (EVANS, E.L., Ed), Canadian Institute of Mining and Metallurgy (1986) 241–249.
[2.92] HARPER, C., The geology of the Cluff Lake uranium deposits, CIM Bulletin **71** 800 (1978) 68–78.
[2.93] HARVEY, S.E., BETHUNE, K.M., “Context of the Deilmann orebody, Key Lake mine, Saskatchewan.”, EXTECH IV: Geology and Uranium EXploration TECHnology of the Proterozoic Athabasca Basin, Saskatchewan and Alberta., Vol. Bulletin no. 588 (JEFFERSON, C.W., DELANEY, G., Eds), Geological Survey of Canada (2007) 249–266.

[2.94] HATHOR EXPLORATION LIMITED, Technical Report for the Roughrider East Zone, Roughrider Uranium Deposit, Midwest Northeast Project, Saskatchewan, NI 43-101, (2011) p. 122.
[2.95] HEGGE, M.R., ROWNTREE, J.C., Geologic setting and concepts on teh origin of uranium deposits in the East Alligator River region, N.T., Australia., Economic Geology **73** (1978) 1420–1429.
[2.96] HEIN, K.A.A., Geology of the Ranger Uranium Mine, Northern Territory, Australia: structural constraints on the timing of uranium emplacement, Ore Geology Reviews **20** (2002) 83–108.
[2.97] HEINE, T.H., "The geology of the rabbit Lake uranium deposit, Saskatchewan", Uranium Deposits of Canada, Vol. Special Volume 33 (EVANS, E.L., Ed), Canadian Institute of Mining and Metallurgy (1986) 134–143.
[2.98] HOMENIUK, L.A., CLARK, R.J., "North Rim Deposits, Athabasca Basin", Uranium Deposits of Canada, Vol. Special volume 33 (EVANS, E.L., Ed), C.I.M.M. (1986) 232–233.
[2.99] HOUSE OF REPRESENTATIVES - STANDING COMMITTEE ON INDUSTRY AND RESOURCES, Australia's Uranium — Greenhouse Friendly Fuel for an Energy Hungry World: A Case Study into the Strategic Importance of Australia's Uranium Resources for the Inquiry into Developing Australia's Non-Fossil Fuel Energy Industry, The Parliament of the Commonwealth of Australia, Canberra (2006) p. 730.
[2.100] IAEA/INFCIS, World Distribution of Uranium Deposits (UDEPO), World Distribution of Uranium Deposits (UDEPO), https://infcis.iaea.org/UDEPO/About.
[2.101] IBRAHIM, H.J., WOO, H.F., "Geochemical and mineralogical alteration at the Midwest uranium-nickel deposit", Geology of Uranium Deposits, Vol. Special Volume 32 (SIBBALD, T.I.I., PETRUCK, W., Eds), CIM (1985) 73–84.
[2.102] KENDALL, C.J., "Ranger uranium deposits", Geology of the Mineral Deposits of Australia and Papua New Guinea, Vol. 1 (HUGHES, E.F., Ed), The Australasian Institute of Mining and Metallurgy, Melbourne (1990) 799–805.
[2.103] KERR, W.C., The discovery of the Phoenix deposit: a new high-grade, Athabasca Basin unconformity-type uranium deposit, Saskatchewan, Canada., Economic Geology **Special Publication 15** (2010) 703–728.
[2.104] KERR, W., WALLIS, R., "Real-World" Economics of the Uranium Deposits of the Athabasca Basin, Northern Saskatchewan: Why Grade Is Not Always King!, SEG Newsletter **99** (2014) 1, 11–15.
[2.105] KING, M., Exploration for Unconformity-Style Uranium Deposits: Geology and Mineralisation of the Angularli Prospect, Wellington Range Project, West Arnhem Land, Vol. Annual Geoscience Exploration Seminar (AGES) 2012. Record of abstracts, Northern Territory Geological Survey, Alice Springs (2012) 19–20.
[2.106] KONING, E., "Uranium deposits of the carswell Structure, Saskatchewan, Canada", presented at the Uranium: Athabasca Deposits and Analogues, 2006 CIM Field Conference, Saskatoon, 2006.
[2.107] KUPSCH, B.G., CATUNEANU, O., "Alteration features and geochemical signatures of the Maybelle River uranium zone, Athabasca Basin, Alberta", EXTECH IV: Geology and Uranium EXploration TECHnology of the Proterozoic Athabasca Basin, Saskatchewan and Alberta, Vol. Bulletin 588 (JEFFERSON, C.W., DELANEY, G., Eds), Geological Survey of Canada (2007) 347–361.
[2.108] LAINÉ, R., ALONSO, D., SVAB, M. (Eds), The Carswell Structure Uranium Deposits, Saskatchewan, Vol. Special Paper 29, Geolocial Association of Canada (1985) 230 pp.

[2.109] LAINÉ, R.T., "Uranium deposits of the Carswell structure", Uranium Deposits of Canada, Vol. Special Volume 33 (EVANS, E.L., Ed), Canadian Institute of Mining and Metallurgy (1986) 155–169.

[2.110] LALLY, J.H., Stratigraphy, Structure and Mineralisation, Rum Jungle Mineral Field, Northern Territory, Record 2002-005, (2002) p. 21.

[2.111] LALLY, J.H., BAJWAH, Z.U., Uranium Deposits of the Northern Territory, Report 20, (2006) p. 87.

[2.112] LESBROS-PIAT-DESVIAL, M., Hydrothermal Alteration and Uranium Mineralization at the Camie River Prospect (Otish Basin, Québec), MSc, Université Laval, Québec (2014) 135 pp.

[2.113] LESBROS-PIAT-DESVIAL, M., BEAUDOIN, G., MERCADIER, J., CREASER, R., Age and origin of uranium mineralization in the Camie River deposit (Otish Basin, Québec, Canada), Ore Geology Reviews **91** (2017) 196–215.

[2.114] LOBAEV, V., Caractéristiques Minéralogiques et Géochimiques Du Bassin Sédimentaire Mésoprotérozoique de Pasha – Ladoga et de Son Socle (Bouclier Balte, Russie). Implications Pour La Genèse Des Gisement d'uranium de Type Discordance, PhD, Université Henri Poincaré Nancy I, Nancy, France (2005) 318 pp.

[2.115] LORILLEUX, G., Les Brèches Associées Aux Gisements d'uranium de Type Discordance Du Bassin Athabasca (Saskatchewan, Canada)., PhD, Université Henri Poincaré Nancy 1, Nancy (2001) 319 pp.

[2.116] MCCLEAN LAKE JOINT VENTURE, Technical Report on the Mineral Resource Estimate for the McClean North Uranium Deposits, Saskatchewan, (2007) p. 105.

[2.117] MCCREADY, A.J., "Hathor Exploration`s Roughrider Zone: one year and a lot of core later", presented at the Saskatchewan Geological Survey Open House, Saskatoon, 2009.

[2.118] MCKAY, A.D., MIEZITIS, Y., Australia's Uranium Resources, Geology and Development of Deposits, Mineral Resource Report 1, AGSO – Geoscience Australia (2001) p. 184.

[2.119] MELLINGER, M., "The Maurice Bay uranium deposit (Saskatchewan): geology, host-rock alteration and genesis", Geology of Uranium Deposits, Vol. Special Volume 32 (SIBBALD, T.I.I., PETRUCK, W., Eds), CIM (1985) 140–150.

[2.120] MERNACH, T.P. et al., Chemistry of low-temperature hydrothermal gold, platinum, and palladium (±uranium) mineralization at Coronation Hill, Northern Territory, Australia, Economic Geology **89** 5 (1994) 1053–1073.

[2.121] MURAOKA, H., HAMAI, T., McClean Lake operation, Midwest deposit & discovery of Midwest-A deposit, Athabasca Basin, Canada, Shigen-Chishitsu **59** 2 (2009) 135–144.

[2.122] NASH, J.T., FRISHMAN, D., "Progress report on geologic studies of the Ranger orebodies, Northern Territory, Australia", Geology of Uranium Deposits: Proceedings of the CIM-SEG Uranium Symposium, Vol. 32 (SIBBALD, T.I.I., PETRUK, W., Eds), The Canadian Institute of Mining and Metallurgy, Montreal (1981) 205–215.

[2.123] NEEDHAM, R.S., "A review of the distribution and controls of uranium mineralization in the Alligator Rivers uranium field, Northern Territory, Australia", Geology of Uranium Deposits: Proceedings of the CIM-SEG Uranium Symposium, Vol. 32 (SIBBALD, T.I.I., PETRUK, W., Eds), The Canadian Institute of Mining and Metallurgy, Montreal (1981) 216–230.

[2.124] NEEDHAM, R.S., Geology of the Alligator Rivers Uranium Field, Northern Territory, Bulletin 224, Department of Primary Industries and Energy, Bureau of Mineral Resources, Geology and Geophysics, Canberra (1988) p. 96.

[2.125] NEXGEN ENERGY LTD., Technical Report on the Rook I Property, Northern Saskatchewan, Canada: NI 43-101 Report, (2016) p. 116.
[2.126] NEXGEN ENERGY LTD., NexGen Energy Ltd. - Arrow, NexGen Energy Ltd. | Arrow, http://www.nexgenenergy.ca/projects/arrow/.
[2.127] NEXGEN ENERGY LTD., Personal Communication, (2018).
[2.128] NG, R., ALEXANDRE, P., KYSER, T.K., Mineralogical and geochemical evolution of the unconformity-related McArthur River Zone 4 orebody in the Athabasca Basin, Canada: implications of a silicified zone., Economic Geology **108** (2013) 1657–1689.
[2.129] NORTHERN TERRITORY GEOLOGICAL SURVEY, Annual Geoscience Exploration Seminar (AGES) 2012. Record of Abstracts, Vol. Record 2012-002 (NORTHERN TERRITORY GEOLOGICAL SURVEY, Ed), Alice Springs (2012) 72.
[2.130] NORTHERN TERRITORY GEOLOGICAL SURVEY, Annual Geoscience Exploration Seminar (AGES) 2015. Record of Abstracts, Vol. Record 2015-002 (NORTHERN TERRITORY GEOLOGICAL SURVEY, Ed), Alice Springs (2015) 127.
[2.131] NUTT, C.J., GRAUCH, R.I., An Introduction to the Jabiluka Project: Regional and Mine Geology of the Unconformity-Type Uranium Deposit at Jabiluka, Northern Territory, Australia, Open-File Report #83-163, U.S. Geological Survey (1983) p. 30.
[2.132] ORTH, K., MEFFRE, S., DAVIDSON, G.J., Age and paragenesis of mineralisation at Coronation Hill uranium deposit, Northern Territory, Australia, Mineralium Deposita **49** 5 (2014) 595–623.
[2.133] PACQUET, A., Carrière Claude: Rapport Pétrographique., Internal Report to AREVA, Amok (1983).
[2.134] PAGEL, M., SVAB, M., "Petrographic and geochemical variations within the Carswell Structure metamorphic core and their implications with respect to uranium mineralization", The Carswell Structure Uranium Deposits, Saskatchewan, Vol. Geological Association of Canada Special Paper 29 (LAINÉ, R., ALONSO, D., SVAB, M., Eds), Geological Association of Canada (1985) 55–70.
[2.135] PARIHAR, P.S., Uranium and Thorium Resources in India: UNFC System, (MINISTRY OF MINES, G. of I., Ed), Ministry of Mines, Government of India, New Delhi (2013).
[2.136] PERKINS, C.T., NORMORE, N., "Basement mineralization at Christie Lake", presented at the Saskatchewan Geological Survey Open House, Saskatoon, 2016.
[2.137] PEVELY, S., HINMAN, M., "Orebody knowledge and its impact on resource modelling at Ranger 3 Deeps", presented at the The AusIMM International Uranium Conference 2014, Perth, Australia, 2014.
[2.138] POLITO, P.A., KYSER, T.K., THOMAS, D., MARLATT, J., DREVER, G., Re-evaluation of the petrogenesis of the Proterozoic Jabiluka unconformity-related uranium deposit, Northern Territory, Australia, Mineralium Deposita **40** 3 (2005) 257–288.
[2.139] POLITO, P.A. et al., Significance of alteration assemblages for the origin and evolution of the Proterozoic Nabarlek unconformity-related uranium deposit, Northern Territory, Australia, Economic Geology **99** (2004) 113–139.
[2.140] POWER, M.J., Geochemical Surface Expression of the Phoenix and Millennium Uranium Deposits, Athabasca Basin, Saskatchewan, MSc, University of Ottawa, Ottawa, Canada (2014) 172 pp.
[2.141] POWNCEBY, M.I., JOHNSON, C., Geometallurgy of Australian uranium deposits, Ore Geology Reviews **56** (2014) 25–44.
[2.142] QUIRT, D., Host Rock Alteration at Eagle Point South, Publication R-855-1-E-89, Saskatchewan Research Council (1989) p. 95.

[2.143] QUIRT, D., "Mineral deposit studies: Raven-Horseshoe uranium deposit - preliminary report", Summary of Investigations 1989, Vol. Miscellaneous Report 89-4 (SASKATCHEWAN GEOLOGICAL SURVEY, S.E. and M., Ed), (1989) 92–94.

[2.144] QUIRT, D., "Geochronological update on the Shea Creek uranium deposits", presented at the Saskatchewan Geological Survey Open House, Saskatoon, 2014.

[2.145] RAMESH BABU, P.V., BANERJEE, R., ACHAR, K.K., Srisailam and Palnad Sub-basins: potential geological domains for unconformity-related uranium mineralisation in India, Exploration and Research for Atomic Minerals **22** (2012) 21–42.

[2.146] REID, K.D., ANSDELL, K., JIRICKA, D., WITT, G., CARD, C., Regional setting, geology, and paragenesis of the Centennial unconformity-related uranium deposit, Athabasca Basin, Saskatchewan, Canada, Economic Geology **109** 3 (2014) 539–566.

[2.147] RHYS, D., Report on Structural Geology and Setting of the Eagle Point Uranium Mine, Rabbit Lake Property, with Exploration Recommendations, Cameco Corporation Internal Report, Panterra Geoservices Inc. (1998) p. 102.

[2.148] RHYS, D., ERIKS, S., VAN DER MEER, L., "Basement mineralization at Christie Lake", presented at the Geology of the Shea Creek uranium deposits: an expanding uranium district in the Western Athabasca Basin, Saskatoon, 2010.

[2.149] RICE, S., Paragenesis and Fluid History of the Karku Unconformity-Uranium Deposit, Pasha-Ladoga Basin, Western Russia, Queen's University, Kingston, Ontario, Canada (2012) 55 pp.

[2.150] ROSCOE, W.E., MATHISEN, M.B., Technical Report on a Mineral Resource Estimate for the Wheeler River Property, Eastern Athabasca Basin, Northern Saskatchewan, Canada, (2015) p. 176.

[2.151] ROWNTREE, J.C., MOSHER, D.V., "Jabiluka uranium deposits", Economic Geology of Australia and Papua New Guinea, Vol. 1. Metals (KNIGHT, C.L., Ed), The Australasian Institute of Mining and Metallurgy, Victoria (1975) 321–326.

[2.152] ROY, C., HALABURDA, J., THOMAS, D., HIRSEKORN, D., Millennium Deposit - Basement-Hosted Derivative of the Unconformity Uranium Model, IAEA, International Atomic Energy Agency (IAEA) (2006).

[2.153] ROY, R. et al., Three-dimensional gravity modelling applied to the exploration of uranium unconformity-related basement-hosted deposits: the Contact prospect case study, Kiggavik, northeast Thelon region (Nunavut, Canada), Canadian Journal of Earth Sciences **54** (2017) 869–882.

[2.154] RUHLMANN, F., "Petrographic and geochemical variations within the Carswell Structure metamorphic core and their implications with respect to uranium mineralization", The Carswell Structure Uranium Deposits, Saskatchewan, Vol. Geological Association of Canada Special Paper 29 (LAINÉ, R., ALONSO, D., SVAB, M., Eds), Geological Association of Canada (1985) 105–120.

[2.155] RUHRMANN, G., "The Gaertner uranium orebody at Key Lake (Northern Saskatchewan, Canada) after three years of mining: an update of the geology.", Economic Minerals of Saskatchewan, Vol. Special Publication 8 (GILBOY, C.F., VIGRASS, L.W., Eds), Saskatchewan Geological Survey, Regina (1987) 120–137.

[2.156] RUZICKA, V., "Uranium deposits in the Rabbit Lake-Collins Bay area, Saskatchewan", Uranium Deposits of Canada, Vol. Special Volume 33 (EVANS, E.L., Ed), Canadian Institute of Mining and Metallurgy (1986) 144–154.

[2.157] SHABAGA, B.M., FAYEK, M., QUIRT, D., JEFFERSON, C.W., CAMACHO, A., Mineralogy, geochronology, and genesis of the Andrew Lake uranium deposit, Thelon Basin, Nunavut, Canada, Canadian Journal of Earth Sciences **54** (2017) 850–868.

[2.158] SHEAHAN, C., FAYEK, M., QUIRT, D., JEFFERSON, C.W., A combined Ingress-Egress Model for the Kianna Unconformity-Related Uranium Deposit, Shea Creek Project, Athabasca Basin, Canada, Economic Geology **111** (2016) 225–257.

[2.159] SHERRINGTON, G.H., BROWNE, A.L.L., DUFFIN, R.H., DANIELSON, M.J., Number Three orebody, Ranger One, Australia – a case history, Journal of Geochemical Exploration **19** (1983) 7–9.

[2.160] SIBBALD, T.I.I., "Geology and genesis of the Athabasca Basin uranium deposits", Summary of Investigations 1985, Vol. Miscellaneous Report 85-4 (SASKATCHEWAN GEOLOGICAL SURVEY; SASKATCHEWAN ENERGY AND MINES, Ed), (1985) 133–156.

[2.161] SIBBALD, T.I.I., QUIRT, D.H., GRACIE, A.J., Uranium Deposits of the Athabasca Basin, Saskatchewan (Field Trip 11), Open File 2166, (1991) p. 56.

[2.162] SKIRROW, R.G., MERCADIER, J., ARMSTRONG, R., KUSKE, T., DELOULE, E., The Ranger uranium deposit, northern Australia: Timing constraints, regional and ore-related alteration, and genetic implications for unconformity-related mineralisation, Ore Geology Reviews **76** (2016) 463–503.

[2.163] SLIMMON, W.L., Saskatchewan Precambrian Geochronology Chart: Athabasca Basin, Saskatchewan Energy and Mines, Saskatchewan Geological Survey (1996).

[2.164] SNELLING, A.A., "Koongarra uranium deposits", Geology of the Mineral Deposits of Australia and Papua New Guinea, Vol. 1 (HUGHES, E.F., Ed), The Australasian Institute of Mining and Metallurgy, Melbourne (1990) 807–812.

[2.165] SNELLING, A.A., Alligator Rivers Analogue Project: Final Report, Volume 2, INIS-mf-14377, OECD/NEA (1992) p.118.

[2.166] TAPANINEN, K., Edmonton '76 GAC-MAC Annual Meeting May 19-21, 1976, Field Trip No. A-1, Cluff Lake, Saskatchewan, Vol. Field Trip Guidebook (GAC-MAC, Ed), Edmonton (1976) 50–71.

[2.167] THOMAS, D., Preliminary Observations on the Karku Uranium Deposit, Lake Ladoga Region, Russia., Internal Report, (2004) p. 46.

[2.168] THOMAS, D.J., Preliminary Observations on the Structural Setting of Uranium Mineralization and Alteration – Eagle Point Deposit, Internal Report, Cameco Corporation (2003) p. 85.

[2.169] THOMAS, P.K. et al., Role of hydrothermal activity in uranium mineralisation in Palnad Sub-basin, Cuddapah Basin, India, Journal of Asian Earth Sciences **91** (2014) 280–288.

[2.170] TOURIGNY, G. et al., "Geological and structural features of the Sue C uranium deposit, McClean Lake area, Saskatchewan.", EXTECH IV: Geology and Uranium EXploration TECHnology of the Proterozoic Athabasca Basin, Saskatchewan and Alberta., Vol. Bulletin no. 588 (JEFFERSON, C.W., DELANEY, G., Eds), Geological Survey of Canada (2007) 229–247.

[2.171] TOURIGNY, G., WILSON, S., BRETON, G., PORTELLA, P., "Structural setting of the Sue C uranium deposit, McClean Lake mine, northern Saskatchewan", Summary of Investigations 2000, Misc. Report 2000-4.2, Vol. 2, Saskatchewan Geological Survey, Saskatchewan Energy and Mines (2000) 146–159.

[2.172] TREMBLAY, L.P., Geology of the Uranium Deposits Related to the Sub-Athabasca Unconformity, Saskatchewan, Paper 81-20, Geological Survey of Canada (1982) p. 56.

[2.173] UEX CORPORATION, Preliminary Assessment Technical Report on the Horseshoe and Raven Deposits, Hidden Bay Project, NI 43-101, (2009) p. 292.

[2.174] UEX CORPORATION, Technical Report on the Hidden Bay Property, Saskatchewan, Canada, Including Mineral Resource Estimates for Horseshoe, Raven and West Bear Deposits, NI 43-101, (2009) p. 300.

[2.175] UEX CORPORATION, Technical Report on the Shea Creek Property, Northern Saskatchewan, NI 43-101, (2009) p. 157.
[2.176] UEX CORPORATION, UEX Corporation – Projects, Region Overview | UEX Corporation, https://www.uex-corporation.com/projects/overview.
[2.177] UEX CORPORATION, Personal Communication, (2018).
[2.178] URI, F., Altération et Minéralisation d'uranium à Shea Creek (Ouest Athabasca, Saskatchewan, Canada): Vers Un Nouveau Modèle Génétique de Gisement, PhD, Université de Poitiers, Poitiers (2012) 338 pp.
[2.179] VELICHKIN, V.I. et al., Geology and formation conditions of the Karku unconformity-type deposit in the Northern Ladoga region (Russia), Geology of Ore Deposits **47** 2 (2005) 87–112.
[2.180] VELICHKIN, V.I. et al., Geology and Formation Conditions of Karku Deposit – the First Uranium Unconformity Deposit in Russia, Vol. Proceedings of International Conference Uranium Geochemistry 2003 (CUNEY, M., Ed), Nancy (2003) 371–374.
[2.181] VERMA, M.B. et al., Ore body characterization of Koppunuru uranium deposit in Palnad Sub-basin, Guntur district, Andhra Pradesh, The Indian Mineralogist **45** 1 (2011) 51–61.
[2.182] VERMA, M.B., MAITHANI, P.B., CHAKI, A., NAGESHWAR RAO, P., KUMAR, P., Srisailam sub-basin, an uranium province of unconformity-related deposits in Andhra Pradesh – case study of Chitrial uranium exploration, Nalgonda District, Current Science **96** 4 (2009) 588–591.
[2.183] WALLIS, R.H., SARACOGLU, N., BRUMMER, J.J., GOLIGHTLY, J.P., "The geology of the McClean uranium deposits, northern Saskatchewan.", Uranium Deposits of Canada, Vol. Special Volume 33 (EVANS, E.L., Ed), Canadian Institute of Mining and Metallurgy (1986) 193–217.
[2.184] WARD, D.M., "Rabbit Lake project - history of exploration and general geology", The Rabbit Lake Story, 932, Vol. 82 (CANADIAN INSTITUTE OF MININD AND METALLURGY, Ed), Canadian Institute of Minind and Metallurgy (1989) 40–48.
[2.185] WHEATLEY, K., "Geology and exploration history of the Key Lake and McClean Lake areas", presented at the Saskatchewan Geological Survey Open House, Saskatoon, 2005.
[2.186] WHEATLEY, K., BELL, G., KINAR, D., CALAYAN, N., "Geology of the Key Lake deposits", presented at the Uranium: Athabasca Deposits and Analogues, 2006 CIM Field Conference, Saskatoon, 2006.
[2.187] WHEATLEY, K., CUTTS, C., Overview of the Maybelle River Uranium Mineralization, Alberta, Canada, IAEA, International Atomic Energy Agency (IAEA) (2006) 14 pp.
[2.188] WHEATLEY, K., WILLIAMSON, A., WILSON, S., TOURIGNY, G., BRETON, G., "Geology of the McClean / Sue deposits", presented at the Uranium: Athabasca Deposits and Analogues, 2006 CIM Field Conference, Saskatoon, 2006.
[2.189] WILDE, A.R., NOAKES, J.S., "Nabarlek uranium deposit", Geology of the Mineral Deposits of Australia and Papua New Guinea, Vol. 1 (HUGHES, E.F., Ed), The Australasian Institute of Mining and Metallurgy, Melbourne (1990) 779–783.
[2.190] WILDE, A.R., WALL, V.J., Geology of the Nabarlek uranium deposit, Northern Territory, Australia, Economic Geology **82** 5 (1987) 1152–1168.
[2.191] WORDEN, J.M., "Geochronology of the host rocks and mineralization of the Midwest uranium deposit, northern Saskatchewan", Geology of Uranium Deposits, Vol. Special Volume 32 (SIBBALD, T.I.I., PETRUCK, W., Eds), CIM (1985) 67–72.

[2.192] WRAY, E.M., AYRES, D.E., IBRAHIM, H.J., "Geology of the Midwest uranium deposit, northern Saskatchewan", Geology of Uranium Deposits, Vol. Special Volume 32 (SIBBALD, T.I.I., PETRUCK, W., Eds), CIM (1985) 54–66.
[2.193] RAMAEKERS, P. et al., "Revised geological map and stratigraphy of the Athabasca Group, Saskatchewan and Alberta", EXTECH IV: Geology and Uranium EXploration TECHnology of the Proterozoic Athabasca Basin, Saskatchewan and Alberta, Vol. Bulletin 588 (JEFFERSON, C.W., DELANEY, G., Eds), Geological Survey of Canada (2007) 155–191.
[2.194] BOSMAN, S.A., RAMAEKERS, P., Athabasca Group + Martin Group = Athabasca Supergroup? Athabasca Basin Multiparameter Drill Log Compilation and Interpretation, with Updated Geological Map, Miscellanneous Report 2015-4.2 section: Paper A-5, Summary of Investigations 2015, Saskatchewan Ministry of the Economy (2015) p. 13.
[2.195] LECHEMINANT, A.N., HEAMAN, L.M., Mackenzie igneous events, Canada: Middle Proterozoic hotspot magmatism associated with ocean opening, Earth and Planetary Science Letters **96** (1989) 38–48.
[2.196] ANNESLEY, I.R., MADORE, C., PORTELLA, P., Geology and thermotectonic evolution of the western margin of the Trans-Hudson Orogen: evidence from the eastern sub-Athabasca basement, Saskatchewan., Canadian Journal of Earth Sciences **42** (2005) 573–597.
[2.197] TRAN, H.T., ANSDELL, K., BETHUNE, K.M., ASHTON, K.E., HAMILTON, M.A., Provenance and tectonic setting of Paleoproterozoic metasedimentary rocks along the eastern margin of Hearne craton: Constraints from SHRIMP geochronology, Wollaston Group, Saskatchewan, Canada, Precambrian Research **167** 1–2 (2008) 171–185.
[2.198] RAMAEKERS, P., Geology of the Athabasca Group (Helikian) in Northern Saskatchewan, Report 195, Saskatchewan Energy and Mines (1990) p. 49.

3. GENESIS OF UNCONFORMITY-RELATED URANIUM DEPOSITS

Three critical steps are required for an ore deposit to form: 1) a source of the elements involved, in particular a relatively uranium-rich source; 2) an effective transporting process to move the elements from their source, which normally involves a fluid with high salinities capable of complexing with uranium; and 3) an effective trapping mechanism, which in the case of unconformity-related deposits normally involves a reductant to fix the uranium in the fluid (U^{6+}) as uraninite ($U^{4+}O_2$).

3.1. SOURCES OF URANIUM FOR THE DEPOSITS

Important parameters for the unconformity-related uranium deposits in a genetic model are: the nature of, and possible uranium concentration in potential source rocks; and, whether the source rocks and the mineral phases that host the uranium can liberate their uranium into an ore-forming fluid. Although the ultimate origin of all uranium is the earth's mantle, the most important concentrations near the surface involve transport of oxidized uranium in fluids as well as reduction reactions or changes in solubility. As a consequence, important deposits of uranium did not occur until the Proterozoic age. This was when the oxygen content of the atmosphere finally became high enough in surficial fluids to mobilize uranium as U^{6+} and the biosphere evolved to become a significant quantity of reductant.

The Paleoproterozoic era (2500–1600 million years ago (Ma)) is characterized by substantial orogens associated with the assemblage of the megacontinents of Arctica (Canada, Siberia and parts of Greenland) and Atlantica (Africa and South America). The growth of Arctica occurred during the Paleoproterozoic and through the beginning of the Mesoproterozoic with the accretion of Baltica, North America and East Antarctica into the larger continent of Nena (also named Nuna, or Columbia) [3.1–3.3]. These orogens gave rise to enhanced uranium concentrations as high-heat flow granites. These granites characterized the basement rocks of unconformity-related uranium deposits, the eventual erosion of which would supply uranium-rich minerals to sedimentary basins that would form in response to down-warping due to plate loading and rifting.

The end of the Paleoproterozoic and beginning of the Mesoproterozoic is marked by the general termination of orogens, and a period of continental readjustment and relative tectonic quiet for about 500 Ma, during which several large intracratonic basins formed and evolved. During this period, the basins and the fluids they contained would be affected by tectonic events that resulted in changes in hydraulic gradients within the basins, causing basinal brines to flow. Atlantica and other continental blocks would be accreted to Nena during the Grenville event at c. 1.0 Ga to form the supercontinent Rodinia.

Earth became active once again near the termination of the Proterozoic, and the megacontinent Rodinia was tectonically dissected into several fragments, mainly along suture zones formed previously [3.1]. Many of the basins that formed remained intact, and would remain so unless deformed by later tectonic events. The formation of economic uranium deposits shifted to the subsurface of intracratonic and rift basins, as oxidized basinal brines mobilized and transported U^{6+} that could be concentrated by effective reductants and give rise to unconformity-related uranium deposits.

Two main uranium sources for the unconformity-related deposits have been proposed: basement rocks that floor the basin (e.g. [3.4–3.9]), and uranium-bearing clastic components in platform-cover sandstones that fill the basin (e.g. [3.10–3.12]). The controversy about which of these two sources dominates unconformity-related deposits arises in large part because in most Proterozoic basins, the basin fill is derived from rocks that are similar to the basement rocks.

3.1.1. Potential uranium sources in the basement

3.1.1.1. Archean rocks

The Athabasca Basin in Canada hosts much of the known unconformity-related deposits. Here, the Archean in the basement is mainly represented by U-poor magnetite-bearing tonalities. These rocks do not represent a significant uranium source, not just because of their low uranium content, but also because the uranium is hosted primarily in refractory accessory minerals. However, local potassic orthogneisses with high uranium and potassium contents also comprise the basement. For example, at Key Lake, the average K_2O content of 24 samples of high-potassium granitic gneisses is 5.37 wt%, along with 6.8 parts per million (ppm) U_{total} and 4.1 ppm leachable uranium, and 27 ppm thorium [3.13].

In the East Alligator River area in the Kombolgie sub-Basin in Australia's Northern Territory, high potassium-thorium-uranium Archean granites are present in the basement and surrounding rocks as domes. The Rum Jungle, Waterhouse and Nanambu complexes (2675–2500 Ma) have anomalously high uranium (2.9–39.9 ppm; median = 12.5 ppm; number of samples = 60) and thorium (8.6–123.3 ppm; median = 57.9 ppm) contents and Th/U ratios varying from 0.51 to 14.16 (median = 5.83) [3.14–3.16]. The highly variable Th/U ratios indicate that uranium has been depleted or enriched relative to average ratio of 3.8 in most crustal rocks, and thus should be present in an easily leachable phase such as uraninite. In fact, this mineral has been identified in bitumens of the Rum Jungle complex [3.14] as well as in the Nanambu Complex, together with high uranium zircon, monazite, xenotime and uranothorite [3.17]. An Nd-Sr isotope study confirms that the Nanambu granites may have been involved in the hydrothermal system at the origin of the Ranger 1-1 deposit [3.18].

3.1.1.2. Paleoproterozoic sediments

The Paleoproterozoic Cahill Formation is host to nearly all the uranium deposits and most of the uranium showings of the East Alligator River district in Australia, in a similar way to the Wollaston-Mudjatick transition zone in the Athabasca Basin of Canada. The Nabarlek deposit is hosted by the Myra Falls Formation, which has been correlated to the Cahill Formation. The Cahill Formation in Australia and the Wollaston-Mudjatick transition zone in Canada both correspond to Paleoproterozoic epicontinental sedimentary successions typically enriched in uranium [3.19], with carbonaceous schist, metacarbonate rock, calc-silicate rock, micaschist, feldspathic quartzite, para-amphibolite and evidence of the prior presence of evaporites as halite and gypsum casts. Tran et al. [3.20] used the uranium-lead ages of detrital zircons as evidence that the first sequence of the Wollaston Group in Canada would have been deposited from c. 2100 to 1920 Ma as a passive margin sequence along the Hearne craton, although most of the Group would have been deposited in a basin adjacent to a magmatic arc between 1920–1880 Ma. Metacarbonate rocks of the Cahill Formation close to the Jabiluka, Ranger and Koongarra deposits in Australia were associated with evaporates. The carbonaceous schists of the Cahill Formation have the highest uranium content (7 ppm, [3.21]).

3.1.1.3. Granites/pegmatites

In the eastern part of the Athabasca Basin, leucogranites and anatectic pegmatites are particularly abundant. They occur as syn- to late-orogenic plutons, sheets, dykes, and stockworks within the metasediments of the Wollaston Group [3.22, 3.23]. These intrusions are interpreted as deriving from the partial melting of the U-rich lithologies of the Wollaston Group metasediments along the Wollaston-Mudjatik domain boundary. They are variably enriched in uranium, thorium, zirconium, rare earth elements, and niobium (e.g. [3.5, 3.6, 3.22–3.36]). Their mineralogy consists of quartz, feldspars, and biotite with disseminated monazite, apatite, garnet, xenotime, zircon, allanite, uraninite, uranothorite, and titanium-oxide crystals. The uranium content of these pegmatites, generally in the order of some hundreds of ppm, may reach several thousands of ppm. For example, in the Way Lake occurrence, uranium content could reach 2500 ppm. A uranium resource of 8121 tU has been estimated from a 3-D model over an area of 1300 × 630 × 200 m, assuming a mean uranium content of 250 ppm; and 16 242 tU assuming a mean uranium content of 500 ppm. The Charlebois Lake district represents a sub-economic resource of 17 500 tU at about 600 ppm uranium.

In the Millenium deposit, Fayek et al. [3.37] have discovered disseminated uraninite with $^{207}Pb/^{206}Pb$ ages of 1770 to 1650 Ma older than the age of deposition for the Athabasca sandstone (~1710 Ma). They compare these ages to those from the disseminated uraninite from the Wollaston metasedimentary rocks, such as those of the Karpinka Lake having provided uraninite U-Pb ages ranging from 1770 to 1730 Ma [3.38]. From these data, Fayek et al. [3.37] suggest that the basement lithologies may represent a possible source of uranium for unconformity related uranium deposits, in addition to the Athabasca sandstone.

3.1.1.4. Paleoproterozoic granitoids and volcanics

An important felsic magmatism event, the Cullen Event, occurred at about 1850–1820 Ma in the Northern Territory. It corresponded mainly to high-potassium granites significantly enriched in uranium and thorium such as Jim Jim (8 ppm U, 43 ppm Th, median = 12), Tin Camp (11 ppm U, 63 ppm Th, median = 2) Creek and Nabarlek (25 ppm U, 50 ppm Th, median = 10) [3.16]. In the southern part of the Alligator River district in Australia, a spatial association exists between uranium deposit fields and felsic rocks enriched in uranium — such as the volcanic rocks of the Malone Creek Granite (23 ppm U, 84 ppm Th, median = 2) and Edith River Group especially with the Tennysons leucogranite — where uranium mineralization in veins is known.

In the basement of the Athabasca, Paleoproterozoic granitoids are mainly known in its western part [3.39] and they belong to an extension of the Taltson Belt below the Athabasca Basin. They correspond mainly to high-potassium granitoids enriched in thorium and uranium. A porphyritic granite, with anomalously high uranium contents (3700 to 1700 ppm), was also reported in the Wheeler River district of the eastern part of the Athabasca basement and dated at 1824 Ma [3.31]. A potassic feldspar porphyry granite is also known in the Eagle Point Mine [3.40].

3.1.1.5. Late Hudsonian vein type U-deposits (e.g. Beaverlodge, Gunnar)

The Beaverlodge area was an important uranium-mining district in northern Saskatchewan for ~30 years, where 25 939 tonnes were mined between 1953 and 1982 [3.41–3.45]. Uranium mineralization occurs in breccias and veins associated with faults and fractures, with grades up to 0.4% [3.42, 3.43, 3.45, 3.46]. The host rocks are c. 2.33–1.9 Ga granitic rocks and c. 2.33 Ga Murmac Bay group amphibolite. Minor amounts of uranium are hosted in redbeds of the c. 1.82 Ga Martin group that unconformably overly the amphibolite and granitic rocks.

The Beaverlodge uranium district has been extensively studied. Studies include deposit-scale geologic characteristics [3.41, 3.47–3.51], the regional geology [3.42, 3.43, 3.52, 3.53], structural geology [3.54, 3.55], ages of mineralization [3.56, 3.57], and geochemistry and fluid inclusions [3.49, 3.58–3.60]. More recent studies focused on the geochronology of mineralization [3.61–3.63], and re-examination of geologic features related to uranium mineralization, including deformation and albitization [3.64–3.68].

Uranium mineralization is associated with major deformation zones [3.42, 3.43, 3.54, 3.55], and albitized leucogranites and amphibolites [3.50, 3.65–3.70] that are in close proximity to the redbed-filled Martin Lake Basin [3.41–3.43, 3.46, 3.49, 3.52, 3.53, 3.58].

A number of studies have attempted to document the fluid history associated with the uranium mineralization from the Beaverlodge district. Koeppel [3.56] interpreted the main phase of uranium mineralization as epigenetic, in contrast to the earlier pegmatite- and granite-hosted syngenetic mineralization. Beck [3.42] concluded that epigenetic deposits evolved, transitionally, from the syngenetic deposits during the late stages of the Hudsonian orogeny based on K/Ar geochronology of potassium-rich alteration minerals. Tremblay [3.43] suggested that the first phase of uranium mineralization was syngenetic and related to the formation of the granitic rocks in the area, whereas the epigenetic deposits formed from late hydrothermal fluids that leached and transported uranium from the earlier syngenetic deposits.

Early petrographic and geochemical studies suggested that the mineralizing fluids were mainly metamorphic in origin and evolved from ~440°C to ~80°C and from c. 1950 Ma to <270 Ma [3.41, 3.56, 3.58]. In contrast, Tortosa and Langford [3.49] reported that uranium mineralization substantially postdated metamorphism and was emplaced during a late shearing event that coincided with uplift, erosion and deposition of the Martin group. More recent geochemical and geochronological studies have shown that uranium mineral deposition occurred in several stages, at relatively constant temperatures (~300°C) and from highly saline fluids [3.59, 3.62, 3.63]. Deposition occurred over 2290 Ma to 1620 Ma [3.62, 3.63].

A more recent study proposed that the vein-type uranium mineralization in the Beaverlodge uranium district was coeval with, or postdated deposition of the Martin group, and the mineralizing fluid was mainly derived from the Martin Lake Basin, similar to unconformity-related uranium mineralization in the Athabasca Basin. Uraninite was precipitated mainly as a result of mixing between a basin-derived, oxidizing, uranium-bearing fluid and reducing fluids that were in equilibrium with basement rocks [3.60].

3.1.2. Potential sources of uranium in the sedimentary cover

Several authors consider sandstones to be a major source of uranium because they host oxidized fluids able to transport uranium. Also, the main prejudice against the basement being a major source of uranium is that the observation of the drill core does not seem to indicate sufficiently large volume and permeability of hydrothermally altered basement, to generate the quantity of uranium needed to form the largest deposits [3.71]. Visual observations show that the transitions between altered and unaltered basement rocks seem to be sharp outside of fault zones, and deeper alteration along some fault zones is generally attributed to paleoweathering.

However, a detailed study of the environment of the fractured zones shows that diagenetic fluids have percolated and leached uranium over a much larger thickness than the alteration zone observed visually. Microcracks with highly saline fluid inclusions and incipient monazite alteration, have been observed at least 100 m on each side of the fractured zones [3.72]. Also deep drilling in the basement, to evidence the continuity of hydrothermal alteration at depth, is lacking. But deep seismic profiles suggest that a large volume of basement rock may have been percolated along structures such as the P2 fault to considerable depth [3.73].

If sandstone is considered a major source of uranium, it is necessary to envisage that the initial uranium content in it was significantly higher than the present average uranium content, which is regionally close to 1 ppm away from the mineralized areas. Moreover, 50 to 80% of the uranium is presently hosted by zircon. Fayek and Kyser [3.12] and Kyser et al. [3.74] proposed that the original uranium content of sandstone was much higher (70 ppm), and has over time been leached by the diagenetic fluids, most likely from detrital fluorapatite and zircon. Their initial estimate of 70 ppm is based on the uranium content of lake sediments in the region. If one assumes that uranium only comes from zircons, the Athabasca sandstone currently has an average zirconium concentration of 200 ppm, which corresponds to a zircon concentration of 400 ppm. According to Belousova et al. [3.75], the average uranium content of zircons from granites is 764 ppm. However, zircons from the Athabasca sandstone originated from different sources. Assuming that the average content of these zircons is 500 ppm uranium — and there is 400 ppm zircon — then, 0.2 ppm uranium is hosted by zircons in the sandstone. If the presumed initial 70 ppm of uranium in the sandstone were essentially all hosted in zircon, then the amount of zircon should have been 70/0.2, i.e. 350 times greater than the 400-ppm zircon in the previous estimation; that is 70/0.2 would correspond to 140 000 ppm zircon, i.e. 14% zircon, on average in the Athabasca sandstone. This value is unreasonable and the same argument can be made for zircons in basement rocks. However, zircon is not the only source of uranium in sandstones.

Let us consider the major possible sources that may have hosted uranium in the sandstone. Four major sites are considered: 1) in detrital accessory minerals; 2) adsorbption on clay minerals and tianium-iron oxides; 3) organic matter; and 4) acidic volcanic ash. Among the detrital accessory minerals, the monazite is the richest in uranium and destroyed during the diagenesis [3.82, 3.83], but its abundance is generally low on average in the sandstone, except in some heavy mineral layers. Zircon cannot be a significant source because this mineral is enriched in uranium in the altered zones (see discussion below and Cuney et al. [3.7]. Some uranium can be adsorbed on clays and titanium-oxides, but Athabasca sandstone is characteristically very quartzose and poor in clay minerals as well as titanium-oxides. Uranium could not have been present as uranium oxides, because it was not possible in continental highly oxidized Paleoproterozoic siliciclastic rocks, to have organic matter to reduce it. Also, it would be difficult to evaluate its importance, in case volcanic ash had been locally present.

Apatite contains only a few tens of ppm uranium and under most natural conditions, is considered a negligible source of uranium. However, in the Athabasca Basin, crandallite group minerals (Al-phosphates-sulphate (APS) minerals) occur basin-wide and are an alteration product of phosphate minerals such as apatite and monazite. Therefore, the Athabasca Basin may have had an abundance of phosphate minerals that were altered during diagenesis and released their uranium content into the fluid. Another possibility is that detrital uraninite was encapsulated in quartz and thus survived the oxiding atmosphere [3.12]. Rainbird et al. [3.76, 3.77] have shown that much of the eastern Athabasca Basin fill comes from the erosion of rocks that lie SE of the Basin. These rocks contain numerous uranium showings [3.12, 3.36]. Therefore, it is not unconceivable that the detritous that filled the eastern Athabasca Basin contained phosphate minerals and detrital uraninite grains derived from these uraniferous rocks SE of Athabasca Basin.

Jefferson et al. [3.45] suggested that the lack of base metals associated with unconformity-related uranium ores is consistent with fluids leaching uranium only from the Athabasca Group because these metals are typically derived from feldspar that is absent from the Athabasca Group, but still present in the basement. However, LA ICP-MS analyses of the fluid inclusions have revealed high concentration of base metals, comparable to those observed in Mississippi Valley type (MVT) deposits [3.78, 3.79]. Therefore, the mature sediments that filled the Athabasca Basin may have had feldspars that were altered during diagenesis. Other researchers have suggested that inflowing surficial and ground waters carried uranium into the Athabasca Basin [3.10, 3.71, 3.74, 3.80]. However, these fluids have never been observed in the deposits.

The Athabasca and Kombolgie Basins filled with mature quartzose sandstone and very little clay, had very high permeabilities, represented a huge fluid reservoir in which intensive fluid/mineral interaction occurred due to the importance of the reactive surfaces around the clastic grains, permitting large element transfer, such as rare earth elements [3.12, 3.74, 3.81], but the amount of uranium the basins may have provided remains difficult to evaluate. There is limited direct knowledge about the importance of the fluid circulations within basement lithologies, due to the lack of deep drilling. However, element budget calculations for the basin would apply equally to the basement rocks. Therefore, it is likely that source of uranium comes from both the basin and basement rocks, and may have been fine-grained uraninite.

3.2. EFFICIENCY OF URANIUM EXTRACTION

Fluid inclusion and mineralogical studies have shown that the diagenetic brines have readily altered uranium-bearing accessory minerals in the Athabasca and Kombolgie Basins [3.81–3.85], and in basement lithologies along major structures [3.8, 3.83, 3.86, 3.72]. Similar accessory mineral alteration by diagenetic brines has been also been observed in the Franceville Basin [3.87–3.89]. Monazite suffers incongruent dissolution with new formation of a Th-U silicate and Ca-REE-Sr APS minerals, both in the clastic sediments and in the altered sections of the basement with the liberation of uranium into the fluid. Zircon crystals are also strongly altered, but are enriched in uranium together with calcium, rare earth elements, aluminium, and phosphorus [3.82, 3.83]. If the diagenetic fluids were able to extract uranium from monazite and to alter zircon, considered as some of the most refractory minerals, then it follows that uranium adsorbed on clay minerals or present as uraninite in the basement lithologies could have been leached even more easily during the circulation of diagenetic hydrothermal fluids.

The former abundance of detrital monazite can be evaluated from the thorium content of the sandstone. The average thorium content of 264 samples from across the Athabasca Basin is 9 ppm (Cuney M, University of Lorraine, France, personnel communication, 2017). The highest thorium contents are observed in the eastern part of the Basin with an average value of 18 ppm in the lower Manitou Falls Formation [3.90], and 40 ppm around the Midwest Deposit [3.91], with one value reaching 730 ppm [3.92]. Taking average contents of 9% thorium and 3000 ppm uranium in monazite and 9 ppm thorium in the average sandstone, about 100 ppm monazite can be calculated in the sandstone, representing only 0.3 ppm uranium in the whole rock. Thus, the amount of uranium liberated during monazite alteration remains limited. At the same time, zircon is also altered but contrastingly, it is enriched in uranium from a few hundreds to several thousands ppm [3.83], trapping a significant part of the uranium leached from monazite.

3.3. EFFICIENCY OF URANIUM TRANSPORT

3.3.1. Fluid characteristics

The initial studies of the fluids associated with the Athabasca Basin were done by Pagel [3.93–3.96]. Most authors agree that uranium was transported by highly saline basinal brines. Uranium solubility was favoured by their high fO_2 (well within the haematite field), high chlorinity (up to 6 molal), low pH, and elevated temperature (150–200°C). High fO_2 resulted from the lack of organic matter in the sandstone and the widespread occurrence of haematite. The pH, controlled by the kaolinite-illite paragenesis, was acidic (<4.5 at 200°C) because of the lack of feldspar in highly mature quartzose sandstones, or from its complete alteration during diagenesis. Richard et al. [3.78] estimated from experimental solubility data and uranium content of the brine measured by LA ICP-MS in the fluid inclusions from a series of Athabasca deposits, that the brines had a pH between 2.5 and 4.5.

Early diagenetic brines (Lw1, Lw2 and Lwh) are the first fluids trapped within detrital quartz overgrowths, but also exist in the later quartz generations. They are sodium-rich (20–25 wt% salts) and are presumed to derive from evaporitic layers in presently eroded upper part of the basin. The Lw’ and Lwh’ brines are trapped later in pervasively silicified zones and drusy quartz, close to the ore zones. They have higher salinities (25–40 wt% salts) and are enriched in calcium-magnesium relatively, as compared to the early brines. The calcium-magnesium enrichment is interpreted as resulting from their interaction with calcium-magnesium rich basement lithologies [3.79, 3.97–3.100]. The compositions of these fluids are summarized in Table 3.1 and Fig. 3.1.

TABLE 3.1. FLUID INCLUSION NOMENCLATURE AND SYNTHESIS OF FLUID INCLUSION MICROTHERMETRIC CHARCTERISTICS AND COMPOSITION DATA FOR THE MCARTHUR RIVER DEPOSIT [3.98, 3.100]

ppm	**NaCl-rich brine**			**$CaCl_2$-rich brine**	
Na	80 to 100 000			20 to 40 000	
Ca	20 to 50 000			80 to 130 000	
Mg	2000 to 10 000			30 to 70 000	
K	1000 to 5000			10 to 35 000	
U	1 to 10			100 to 500	
Fluid inclusion types	**Lw1**	**Lw2**	**Lwh**	**Lw′**	**Lwh′**
NaCl at room T	No	No	Yes	No	Yes
Last phase to melt	Ice	Hyd.	Hyd.	Ice	Ice
Eutectic: Te (°C)	-75 to -50	-75 to-50	-75 to -50	-75 to -60	-75 to -60
Tm ice (°C)	-25 to -11.2	-28.8 to -21	-27.7 to -24	-60 to -30	-58 to -36
Tm hyd (°C)	/	-7 to -21.9	-3.2 to 19.2	/	/
Ts NaCl (°C)	/	/	99.5 to 208	/	115 to 235
Th (°C) mode	165	165	135	115	115
Cl (molal)	3 to 45	5.5 to 6.5	6.5	6	6.5
Na/Ca (mole)	4.6	3 to 7.7	3.8	0.5	0.8
Ca/Mg (mole)	1	1 to 17.9	/	1.5	1.7
wt.% NaCl	14	22 to 24	25	5	8
wt.% $CaCl_2$	6	6 to 12	13	20	19
wt.% $MgCl_2$	4	0 to 0.9	0	11.5	9.5

LA-ICP-MS = laser ablation-inductively coupled plasma-mass spectrometry, LIBS = laser-induced breakdown spectroscopy hyd. = hydrohalite, Te = eutectic melting, Tm ice = ice melting, Tm hyd = hydrohalite melting, Ts = NaCl halite dissolution, Th = homogenization to the vapour phase.

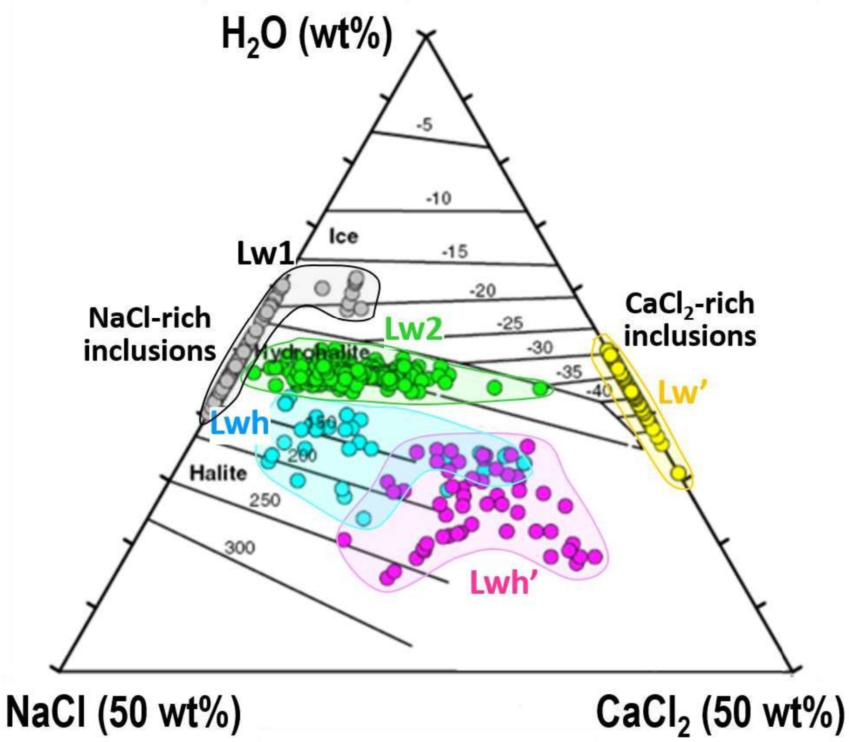

FIG. 3.1. Compositions of the fluid inclusions in the H_2O-NaCl-$CaCl_2$ diagram from the Rabbit Lake, Eagle Point, Shea Creek, P-Patch, Millennium deposits (Richard et al. [3.79]), and McArthur River deposit (Derome et al. [3.98]). Compositional fields have been drawn for the different fluid inclusion types in the right triangle. The left triangle shows that data points for each fluid inclusion type shown in the triangle on the right.

The Lw1 inclusions are liquid + vapour inclusions. Their microthermometric behaviour indicates that they probably have high Na/Ca molar ratios but they are suspected to be metastable Lw2 inclusions that failed to nucleate hydrohalite during cooling. The Lw2 inclusions are liquid + vapour inclusions that exhibit a wide range of molar Na/Ca ratios, but most values centre on the 3–4 range. The Lwh inclusions are liquid + vapour + halite inclusions which are more saline with up to five mole chloride salts. The Lw′ inclusions are liquid + vapour inclusions with molar Na/Ca ratios ranging from to 0.3 to near zero. The Lwh′ inclusions are liquid + vapour + NaCl inclusions with molar Na/Ca ratios mostly ranging from 0.3 to 1. The same types of fluids have been identified in the Kombolgie Basin in Australia [3.101].

Low salinity Lw″ inclusions are found sporadically in the environment of the uranium deposits in the Athabasca district and have been interpreted as late fluids, unrelated to the brines [3.98]. This type of fluid is more common in the Kombolgie Basin area and methane-bearing [3.101].

3.3.2. Fluid characteristics

The concentrations of the elements in the fluid inclusions analysed by La ICP-MS are highly variable: 40<Li<16 000 ppm, 5400<Na<140 000 ppm, 930<K<52 000 ppm, 640<Ca<96 000 ppm, 590<Mg<53 000 ppm, 32<Fe<16 000 ppm, 38<Mn< 2800 ppm, 6<Zn<4400 ppm, 2<Cu<6300 ppm, 3<Pb<8100 ppm, 11<Ba<2100 ppm, 9<Sr<2800 ppm, and 0.2<U<610 ppm. By defining a sodium-rich brine end member for the fluid inclusions that have sodium concentrations higher than 80 000 ppm sodium, and a calcium-rich brine end member that has sodium concentrations lower than 30 000 ppm [3.100], the element concentrations in each end member have been calculated. The calcic brine is up to one order of magnitude enriched in K, Mg, Ca, Fe, Cu, Zn, Pb, Ba, Sr, and U compared to the sodic brine (Fig. 3.2).

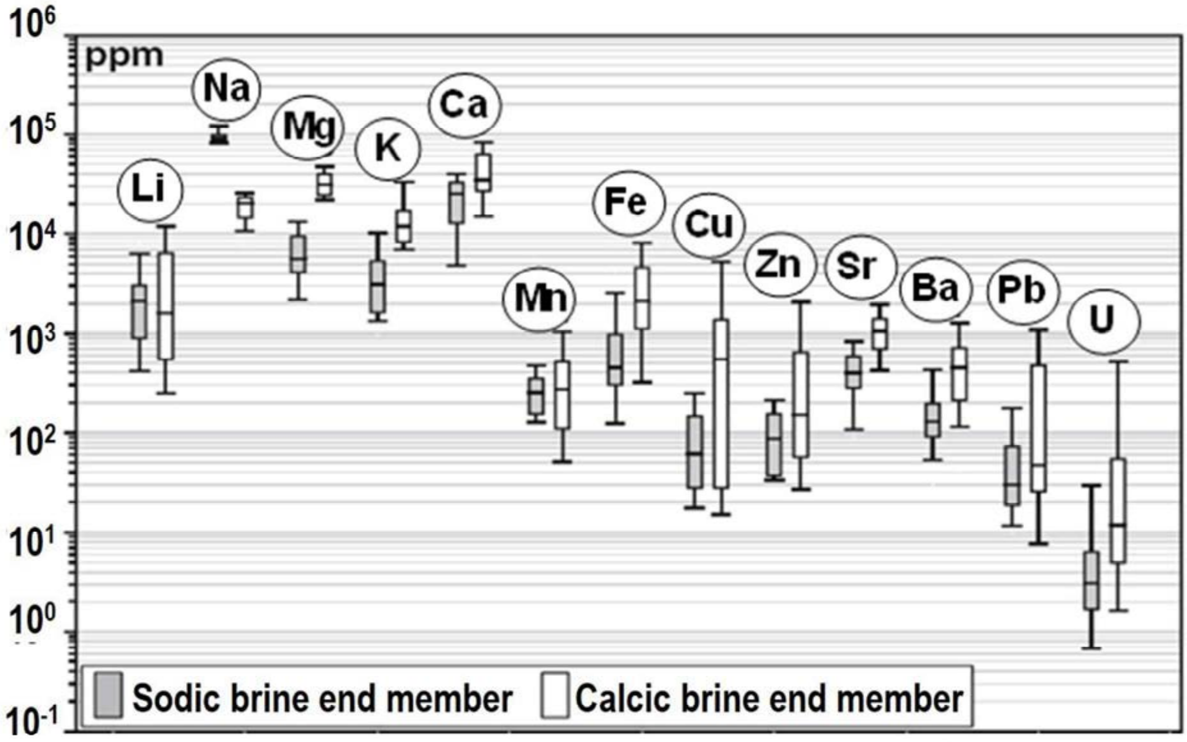

FIG. 3.2. Element concentration ranges for the sodic and calcic brine end members (LA-ICP-MS data. The whiskers represent the 10th and 90th percentiles, and the box edges, the 25th and 75th percentiles. The inner bar is the median (modified from Richard et al. [3.79]).

Uranium concentrations were measurable in 104 fluid inclusions among the 166 analysed in quartz veins from the McArthur River, Eagle Point, Rabbit Lake, Millennium, and P-Patch uranium deposits [3.78, 3.100]. The uranium concentrations vary from 10^{-6} to 2.8 10^{-3} mol/l^{-1} (Fig. 3.2). These concentrations are much higher than the uranium solubilities of 30 ppm estimated by Raffensperger and Garven [3.102] for five molal Na-Ca chloride solutions at 200°C for a fO_2 of –20 and used in their hydrochemical modelling of the fluid circulations in the Athabasca Basin.

However, experimental solubility measurements of U(VI) at 155°C, Psat, in a H_2O-NaCl fluid with variable concentrations (0.3–6:0 mol l^{-1} NaCl) and variable pH (1.9–6.8) show that values up to ~10^{-1} mol l^{-1} for a pH of 2.43. The solubility does not significantly depend on the salinity for NaCl concentrations below 4.4 mol l^{-1}. For sodium concentrations higher than 4.4 mol l-1 and pH lower than 4.3, the solubility of U(VI) decreases by two orders of magnitude.

The microthermometric and Raman analyses have shown that chloride is the dominant anion in the brines from unconformity-related deposits. Hence, chloride can be assumed to be the main uranium complexing anion. Consequently, a maximum pH value can be estimated from the experimental results, for the ore-forming brines (Fig. 3.2). A pH between 2.5 and 4.5 is obtained using the salinity and the range of uranium concentrations measured in the fluid inclusions (Fig. 3.3). A similar pH range is obtained from a $\log a_{K+}/a_{H+}$ versus log aH_4SiO_4 activity diagram at

150°C, in the H_2O-HCl-K_2O-SiO_2-(Al_2O_3) system. The brines plotting within the stability field of illite, in the vicinity of the kaolinite stability field, and along the line for quartz saturation, with ~10^3<K<~$3x10^4$ ppm, the estimated pH lies between 2.5 and 4.5 [3.78]. The low pH of the brines appears to be the key parameter explaining their high uranium content. Higher pH values have been previously proposed by Komninou and Sverjensky [3.103] and Kister et al. [3.104], but only from thermodynamic estimations. The origin of high pH values remains difficult to explain.

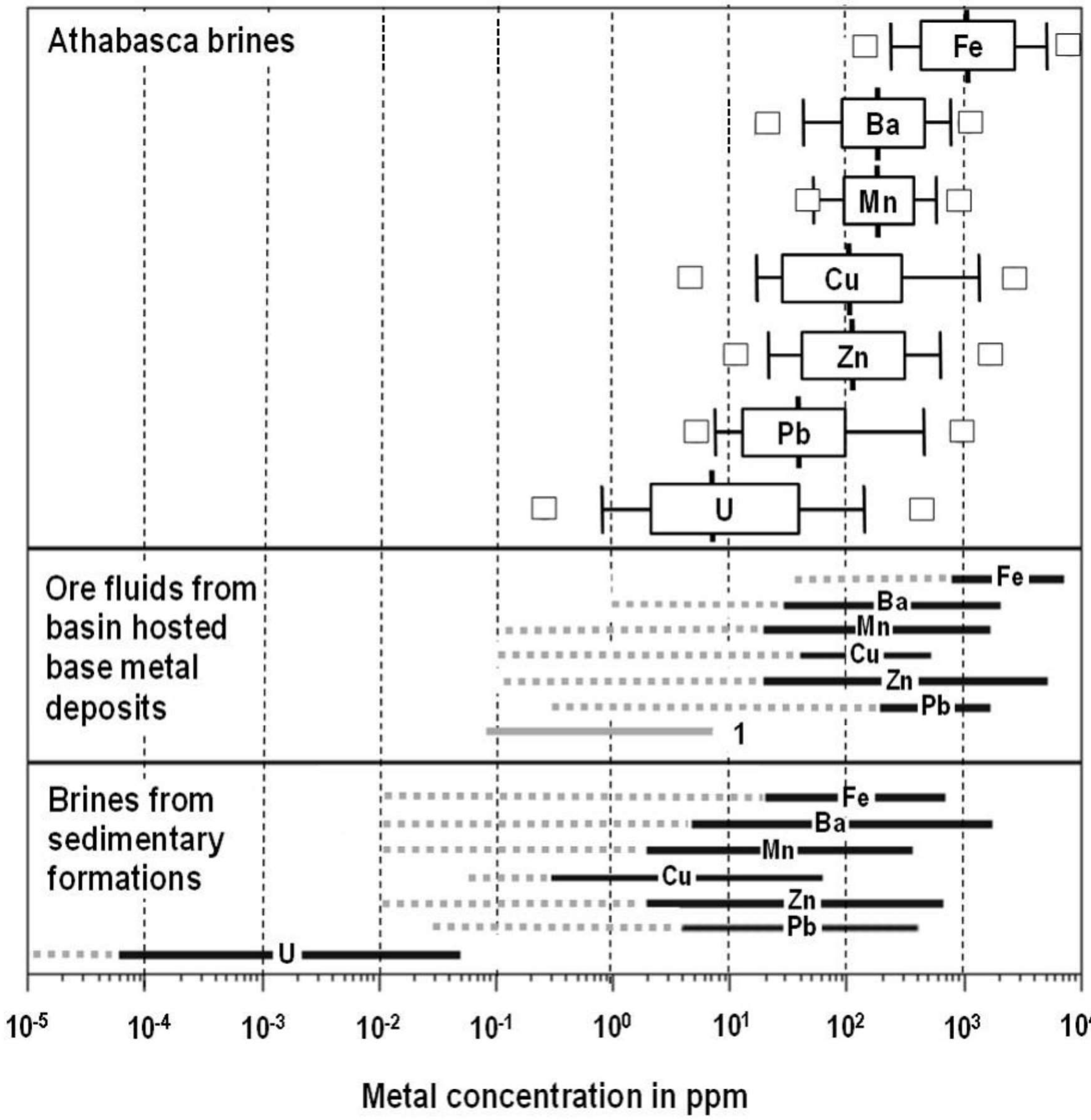

FIG. 3.3. Range of metal concentrations in brines from sedimentary formation (boreholes: [3.105-3.115]) and ore fluids from Pb, Zn, Ba deposits hosted in basins (LA-ICP-MS data of fluid inclusions: [3.116-3.124]) and Athabasca fluid inclusions [3.79]. The circles represent the 5th and 95th percentiles, the whiskers the 10th and 90th percentiles, the box edges the 25th and 75th percentiles, and the inner bar is the median. 1: Detection limits for LA-ICP-MS analyses in fluid inclusions (modified from [3.79]). Black solid lines represent the ranges of the highest values for metal concentrations in each of the selected studies. Gray dotted lines represent the lower ranges of metal concentrations in the selected studies.

Similar uranium concentrations as those measured in the Athabasca brines (~10^{-6} to ~10^{-3} mol l^{-1}) have been reported for high temperature (>400°C) acidic magmatic-hydrothermal brines

(>40 wt% equivalent NaCl) (Fig. 3.3). Uranium concentrations in other types of geological fluids such as basement and basin formation waters, mid-ocean ridge or geothermal fluids do not generally exceed 10^{-6} mol l^{-1}. The exceptional capacities of the Athabasca brines for uranium transport result from a combination of favourable parameters: high fO_2, low pH, high concentration of chlorides, and high uranium availability in the source lithologies [3.78].

3.3.3. Pressure–temperature regime

The homogenization temperatures (Th) range from ~60 to ~200°C for of all fluid inclusions in quartz and carbonate minerals from Rabbit Lake, Eagle Point, Shea Creek, P-Patch, Millennium, and McArthur River deposits. The melting temperature of ice (Tm ice) for these inclusions defines a continuum between ~-15 and ~-60°C. For each range of Tm ice, temperature is variable (± 70°C). For inclusions hosted in quartz, the majority of them have Tm ice values around -25°C and less commonly Tm ice values below -30°C. In quartz- and dolomite- hosted inclusions, there is a slight tendency for a decrease in thorium with the decrease in Tm ice. The two end members of the continuum are the sodic fluid with Tm ice = ~-20 to -30°C and most thorium values between 100 and 150°C, and the calcic fluid with Tm ice = ~-50 to -60°C and most thorium values between 80 and 130°C. However, the sodium chloride-rich fluid inclusions from McArthur River have a higher thorium range distribution (120<Th<170°C). The scatter in the homogenization temperatures is interpreted to be the result of gas contamination in the two brines, possibly leading to homogenization temperatures higher than 150°C [3.79, 3.97]. Trace amounts of CO_2, CH_4, H_2, and O_2 have been detected irregularly in the brine inclusions by Raman spectroscopy [3.97]. The Lwh and Lwh′ fluid inclusions present a Δ(Ts NaCl-Th) continuum between 107 and 216°C indicating that the calcic-rich brine was saturated with respect to halite at the time of trapping. Therefore, they were not taken into account for temperature estimation.

Isochores selected by Richard et al. [3.79] in Fig. 3.4 correspond to the thorium range of the fluid inclusions hosted either in quartz or dolomite and considered as the most representative of the two brine end members: 100–150°C for the sodic brine and 80–130°C for the calcic brine. The P-T fields of fluid trapping defined by the combined use of the isochores and presumed hydrostatic and lithostatic thermal gradients (30 and 40°C/km) are 180 ± 30°C and 800 ± 400 bars for the sodic brine, assumed to correspond to the early diagenesis, and 120 ± 30°C, and 600 ± 300 bars for the calcic brine, assumed to represent the ore stage (Fig. 3.4). Such pressures correspond to a former thickness of ~3 to 6 km for the Athabasca Basin. These values are comparable to the P-T reconstruction proposed by Derome et al. [3.98] only based on the fluid inclusions from the McArthur River deposit: 160–220°C and 1–1.25 kbar for the sodic brine, 140–160°C and 0.6 kbar for the calcic brine.

The temperature estimate of 180 ± 30°C for the sodic brine is also compatible with the temperatures of about 200°C deduced from illite and chlorite chemistry and oxygen isotope composition of quartz-tourmaline pairs [3.125, 3.126]. However, the temperature of 120 ± 30°C estimated for the calcic brine differs largely from that derived from the mineral geothermometers. Kotzer and Kyser [3.125] consider that the temperature at the base of the basin during the ore-forming event was higher than during early diagenesis at about 200–250°C, but such high temperatures require high thermal gradients of 40–50°C/km considering a 5 km thick basin. The hydrostatic pressure regime proposed by Cui et al. [3.127, 3.128] and Chi et al. [3.129] for the Athabasca Basin fluids correspond to the lowest temperature and pressure estimations.

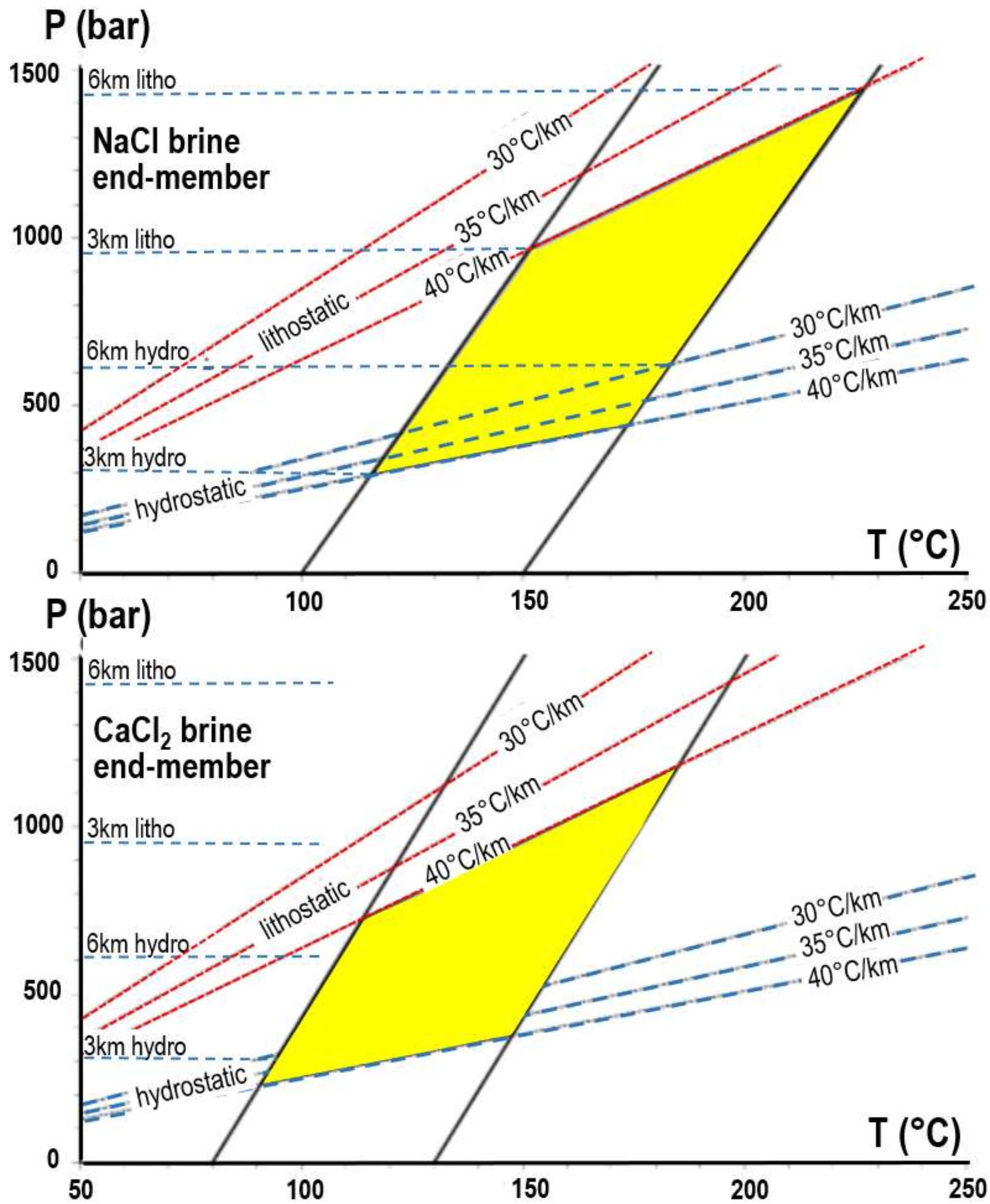

FIG. 3.4. Pressure–temperature field estimation for the conditions of trapping of the brines in the Athabasca Basin. The hydrostatic and lithostatic thermal gradients of 30°C/km, 35°C/km, and 40°C/km and hydrostatic and lithostatic pressures at a depth of 3 km and 6 km are reported (modified from Richard et al. [3.79].

The low temperature calcic brine may indicate that this fluid was not significantly involved in the development of the illite-sudoite-dravite alteration. However, this low-temperature event is not very late, because the calcic brine is already present in the pervasively silicified sandstone prior to the UO_2 deposition [3.98], whereas the higher temperature sodic brine was present before and after the UO_2 stage. The lower temperature of the calcic brine has been tentatively explained by Derome et al. [3.98] by its infiltration from upper levels in the Athabasca Basin along basement structures without any significant temperature re-equilibration, but with a strong chemical re-equilibration. The occurrence of sodic brines and cooler calcic brines seems to be common in Proterozoic basins [3.130]. However, the temperature difference between the two brines is not well understood. Hydrogeochemical modelling such as that performed by Raffensperger and Garven [3.102] and Cui et al. [3.128, 3.129] may help.

The continuity of the chemical properties between the end members of the two brines and the trend of temperature decrease between them suggests an anisothermal mixing process [3.131]. The mixing may have been induced by multiple reactivation of the basement faults controlling the alteration and ore deposition.

Although the mixing between the two brines has been always observed in the mineralized zones, this process cannot explain the reduction of U(VI) to U(IV) necessary for uranium oxide deposition as none of these brines present reducing characteristics and present relatively high uranium content.

The basal sandstones of the Athabasca Group as well as part of the Athabasca Basement can be considered as a giant brine aquifer, and probably larger than the present-day extent of the Athabasca Basin. The deepest known uranium mineralization hosted in the basement (850 m below the unconformity at Eagle Point, but more than 1000 m at Jabiluka in Australia), represents a minimal evaluation of the depth at which the brines have percolated. The presently preserved maximum thickness of sediments in the Basin is about 1.5 km at Rumpel Lake. The past extent of the Basin could have been much greater as suggested by the observation of the following factors: 1) the same brines having registered similar P-T conditions in deposits located at the margin of the basin (Rabbit Lake and Eagle Point); 2) the new discoveries of deposits outside of the Basin (Arrow and Triple R), which seem to present similar characteristics as those located in the basement below the Basin; and 3) the alteration features typical of unconformity-related uranium deposits (e.g. such as the presence of illite-sudoite alteration associated with aluminium-phophate-sulphates and uraninite boxworks) described by Mercadier et al. [3.36] in uraninite-rich pegmatoids, 20 km east of present day Athabasca Basin margins.

3.3.4. Origin of the fluids and metals

The chemistry of basinal brines depends on a series of factors, such as the composition of seawater, the rate of evaporation of seawater, the dissolution of evaporate, the dilution of the brines by seawater and/or meteoric water, the mixing between waters with different chemical compositions, and buffering by minerals [3.132–3.134].

The origin of the parent brine, from which the sodic and calcic brines were derived, has been constrained by a series of geochemical indicators [3.98, 3.135–3.138]. The halogen signature (Cl-Br-I) shows that the two brines derived from the evolution of an initial brine resulting from seawater evaporation having reached epsomite saturation, which also explains their high salinity. The dravites associated with the hydrothermal diagentic fluid circulation have a high B isotopic composition ($\delta^{11}B$ = 19.6‰ to 36.5‰), which contrasts with the low B isotopic composition of tourmalines from basement lithologies ($\delta^{11}B$ = -8.1‰ to 3.3‰), indicating that boron was essentially derived from the basinal brines of marine origin.

It is well known, that the chemistry of seawaters has changed from the Neoproterozoic to the Phanerozoic, between Cretaceous type $CaCl_2$ seas and modern type $BMgSO_4$ seas [3.139, 3.140], but not for Paleoproterozoic seas. Evaporation of $BCaCl_2$ seas enriches the brine in calcium, but is still sodium-dominated [3.141]. However, the sodic and calcic brine end member compositions do not plot between $BMgSO_4$ and $BCaCl_2$ sea compositions having reached epsomite saturation, because their composition has been modified through different types of fluid-fluid and/or fluid-rock interactions during:

- Their migration from the evaporitic layers presumably situated in presently eroded upper lithologic unit of the basin;
- Their storage in the basal sandstone unit; and,
- During their interaction with basement lithologies.

To explain the evolution of their composition, the following interactions mechanisms have been considered [3.79]:

- Dissolution of halite or mixing with a fluid deriving from halite dissolution, both giving sodium-rich compositions;
- Dolomitization of calcite, decreasing the magnesium content of the brine and increasing its calcium content;
- Albitization of the anorthite component of plagioclase decreasing the sodium content of the brine and increasing its calcium content;
- Albitization of potassium-feldspar decreasing the sodium content of the brine and increasing its potassium content; and
- Magnesium-alteration of the basement with sudoite and dravite new formation decreasing the mg content of the brine associated with an intake of calcium, sodium, or potassium depending on the mineral composition of the lithologies submitted to alteration.

Taking a parent brine derived from the evaporation of a $BMgSO_4$ sea, the sodic brine composition can be explained by mixing the initial brine with a fluid derived from halite dissolution, in association with dolomitization, magnesium-alteration, and albitization reactions. The calcic brine composition is best explained by dolomitization and albitization reactions. Taking a parent brine derived from the evaporation of a $BaCaCl_2$ sea, the composition of the brines can be simply explained. The sodic brine composition would be best explained by its mixing with a fluid derived from halite dissolution, requiring to maintain a spatial connection to the evaporitic-bearing layers. The calcic brine can be explained by albitization in the basement lithologies [3.79].

The brines from the Athabasca Basin have concentrations of zinc, lead, barium, and manganese typical of brines from other sedimentary basins, but their copper, iron, and uranium concentrations are much higher (Fig. 3.3). The brines from the Athabasca have also iron, copper, zinc, lead, barium, and manganese concentrations comparable to those measured in fluid inclusions from base metal deposits hosted in basins (Fig. 3.3). The uranium concentrations in the Athabasca brines are among the highest ever recorded for geological fluids [3.78]. High uranium concentrations of tens of ppm have also been measured in the brines associated with the hydrothermal metamorphic deposits of Zambia [3.142] and in the volcanic-related deposit of Maureen in Australia [3.143].

A series of sulphide and arsenide minerals (of iron, nickel, copper, lead, cobalt, zinc, molybdenum), and less commonly gold, silver, and platinoids occur very irregularly in the unconformity-related deposits, and seem to be more abundant in basin-hosted than in basement-hosted deposits [3.12, 3.144, 3.145]. However, despite the high concentration of base metal in the brines, most of these minerals do not seem to have been deposited simultaneously with the main uranium mineralization stage. The ages of these minerals are uknown. Base metal sulphides in basinal settings are generally deposited following production of H_2S by thermochemical sulphate reduction or bacterial sulphate reduction [3.146], and/or by mixing the saline and hot ore-bearing fluids with low saline and/or colder fluids. The Athabasca brines contain negligible sulphate content [3.135], despite the new formation of aluminium-phosphate-sulphate minerals in the basin [3.81, 3.84], and Raman analyses of the gas phase of fluid inclusions have never detected H_2S [3.97]. Furthermore, no evidence of mixing of the Athabasca brines with low-saline fluids has been observed. Therefore, it appears that the typical conditions controlling the deposition of base metals were not present in the Athabasca Basin at the time of uranium deposition.

3.4. MODELS OF FLUID CIRCULATION

3.4.1. Alteration patterns

3.4.1.1. District scale alteration

In addition to paleoweathering, there are two types of regional scale alteration associated with unconformity-related uranium deposits: 1) basin-wide pre-ore diagenetic sandstone alteration; and 2) alteration halos associated with uranium deposits. For example, pre-ore, quartz overgrowths that encapsulate haematite-coated detrital quartz grains are among the earliest recognizable regional diagenetic events in the Athabasca Basin [3.45, 3.147]. This event is closely followed by a complex diagenetic sequence of alteration minerals that differs between basins that host unconformity-related uranium deposits (i.e., Athabasca, Thelon, and Kombolgie basins; Fig 3.5, [3.74]). Hoeve and Quirt [3.71] showed that the alteration mineral assemblage in the Athabasca Basin was dominantly kaolinite with small amounts of montmorillonite, a range of chlorite minerals, and a low magnesium-iron illite [3.148]). Regional diagenesis converted the minerals to dickite and minor amounts of illite and chlorite [3.149–3.152]). In the eastern Athabasca Basin, higher concentrations of illite occur along a 10 to 20 km wide, 100 km NE-trending corridor from Key Lake to Cigar Lake. The illite anomaly encompasses all known uranium deposits including Key Lake, P-Patch, McArthur River and the Millennium deposit, and is discontinuous around the Cigar Lake mine and the Dawn Lake and Rabbit Lake areas. Up to five types of chlorite have been documented in basement rocks [3.149].

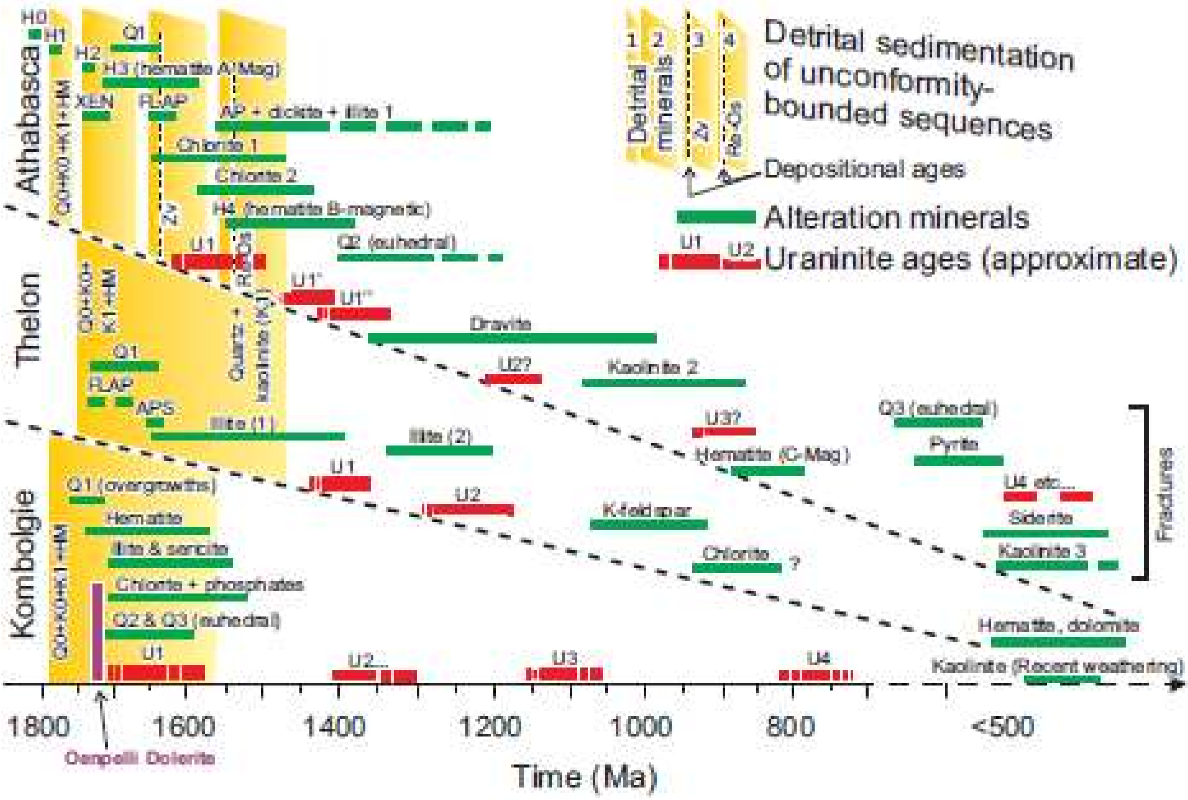

FIG. 3.5. Simplified mineral paragenesis of the Paleo- to Mesoproterozoic Athabasca, Thelon, and Kombolgie basins, modified after Kyser et al. [3.74] and Polito et al. [3.153–3.155]. Depositional ages in the Athabasca Group are Zv: U-Pb on volcanic zircon in Wolverine Point Formation [3.77], and Os-Re: primary organic matter in Douglas Formation [3.156]. The 1723 Ma age of the Oenpelli Dolerite is by 40Ar/39Ar [3.74] and U-Pb [3.157]. AP=aluminum phosphate; APS=aluminum sulphate phosphate; FLAP=fluorapatite; H0 is primary haematite in the paleoweathered regolith; H1 and H2 are very early diagenetic haematite in basal red mudstone beds; XEN=xenotime.

Late silicification fronts consisting of quartz veins and druzy quartz are associated with quartz-dissolution alteration systems (e.g. Cigar Lake [3.158]) and in the McArthur River area [3.159]. Drusy quartz (euhedral quartz crystals) is mostly developed at the periphery of the ore systems [3.160].

Phosphate minerals occur throughout the basins and are related to saline fluid diagenesis [3.12, 3.71]. Minerals include xenotime, apatite, and Ca-Sr-LREE-Al-phosphate minerals (AP). Xenotime in the Athabasca Basin typically forms 1 to 10-micron euhedral overgrowths on detrital zircon, and is overgrown by quartz and fluorapatite [3.12, 3.76]. The AP minerals are intergrown with illite, dickite, anatase, and haematite, and are most abundant in the lower Manitou Falls Formation around the eastern Athabasca Basin. In the Thelon, Hornby Bay, and Elu Basins, aluminum phosphate sulphate (APS) minerals are described as concentrated at the base and in the regolith [3.161].

Purple to maroon, late diagenetic haematite transects sandstone and conglomerate beds in the Athabasca Basin. Hydrothermal, red to black haematite forms dense cements in Athabasca Group subunits that overlie the basal unconformity and are near uranium deposits. Recent oxidation resulted in limonitic alteration zones along faults [3.45].

A number of studies using clay mineral crystallinity [3.71], fluid inclusions [3.94] and equilibrium isotope fractionation factors [3.12, 3.125, 3.162, 3.163] showed that fluid temperatures in the Athabasca Basin reached >200°C. The dominant clay mineral analysed by Kyser et al. [3.74], Renac et al. [3.164] and Riegler et al. [3.165] in the Thelon and Kombolgie basins is illite. Sharpe et al. [3.166] show that fluid temperatures associated with the Bong deposit, Kiggavik region (Thelon Basin) were ~180°C. Dravite overprints the illite illite, chlorite, and kaolinite [3.45].

3.4.1.2. Deposit scale alteration

Alteration zones associated with egress and ingress deposit sub-types are related spatially, but not necessarily temporally, to the ore deposits. Egress-type alteration halos occur mainly in the sandstone overlying unconformity-related uranium deposits [3.12, 3.71, 3.125]. Egress style uranium mineralization can be basement-hosted and sandstone-hosted. Alteration mineral assemblages range between two distinctive end member types: i) quartz dissolution and illite, and ii) quartz-later illite-kaolinite-chlorite-dravite [3.160, 3.167].

Ingress-type alteration zones are very narrow and occur along structures that transect basement rocks. These alteration zones grade outwards where illite and sudoite zones are proximal to the fault, through sudoite and illite, to iron-magnesium chlorite and sudoite against fresh basement rock (Fig. 10; [3.145]), [3.71]. Some deposits have both ingress and egress characteristics (e.g. McArthur River), suggesting a complex and protracted fluid history (e.g. [3.71, 3.168].

3.4.2. Hydrodynamic models

Bons et al. [3.169], using the example of hydrothermal ore deposits of Schwarzwald in Germany, showed that simultaneous upward and downward circulation of fluids cannot occur with fluid overpressure necessary to explain the fractures and brecciation associated with uranium deposits. They proposed an intial downward percolation of the fluids, their evolution within the pores, followed finally by their upward percolation. The descending fluids reach great depths, increase their temperature and have a long residence time. This permits their equilibration with enclosing rock, the acquisition of high salinities, and leaching of metals. A second fluid would only penetrate at shallow depth and retain part of its original chemistry. Mixing between upward migrating fluids and downward migrating fluids would occur at shallow depths.

Characteristics such as the location of the ore zone in relation to the unconformity and the alteration mineral assemblages of unconformity-related uranium deposits in the eastern part of the Athabasca Basin (e.g. Midwest, Collins Bay, Rabbit Lake, McClean Lake, McArthur River, Cigar Lake, and Key Lake) have been used to develop diagenetic-hydrothermal models for uranium mineralization [3.10, 3.71, 3.125, 3.170–3.176; among others]. Basement-hosted deposits (e.g. Eagle Point, Rabbit Lake, Sue C, Millennium, and several of the Cluff Lake deposits) have been categorized as ingress-style deposits, whereas sandstone-hosted deposits (e.g. Cigar Lake, Key Lake, Collins Bay, McClean Lake, and Midwest) are considered to be egress-style deposits [3.45, 3.145, 3.177]. In the ingress model, uraninite precipitated from fluid-rock interaction in which oxidized basinal brine percolated down into basement structures and reacted with the basement rocks, resulting in physiochemical changes to the fluid (e.g. lower fO_2, leaching and deposition of metals). The ingress-style uraninite is commonly fracture-controlled and breccia-hosted replacement uranium mineralization and is hosted in the metamorphic basement. In the egress model, uraninite precipitated as a result of fluid-fluid interactions involving a relatively reduced basement-derived fluid and oxidized basinal brine at/around the unconformity. Egress-style uraninite is commonly a clay-bounded, massive uranium mineralization deposited along/around the unconformity and perched above the unconformity in the overlying sandstone. Egress-style deposits may also contain pods of mineralization in the shallow basement rocks, such as at the Midwest deposit and the Deilmann deposit at Key Lake.

The Kianna deposit, which is located in the western Athabasca Basin consists of three distinct mineralized pods, similar to those of various eastern Athabasca uranium deposits. These are: 1) deep, basement-hosted mineralization, (e.g. Millennium deposit); 2) sandstone-hosted and upper basement-hosted mineralization occurring at the unconformity (e.g. Midwest, Cigar Lake, Key Lake, and McArthur River deposits); and 3) in pods perched above the unconformity (e.g. McClean Lake and Cigar Lake deposits; [3.10, 3.37, 3.45, 3.71, 3.176, 3.178; among others]. Therefore, the Kianna deposit has characteristics of both ingress and egress style deposits [3.163].

The ingress style mineralization at the Kianna deposit was a result of tectonic activity, which caused fault propagation to form a jog along the Kianna transverse fault. Opening of the fault jog created a drop-in pressure, which allowed oxidized marine brines to move down the fault and into the basement rocks. Fault activation caused localized, high-geothermal gradients that superheated the fluids moving along the faults. The oxidized brine interacted with the basement rocks, which caused physiochemical changes to the fluid, which resulted in uranium mineralization to precipitate in upper and lower basement rocks. Mineral precipitation in the basement-rooted fault increased frictional strength and caused the fault to self-seal. Compression and high fluid pressure in the basement rocks caused the equilibrated and reduced basement fluids to move upward along the fault, and interact with oxidized basinal fluids at the unconformity, which resulted in the precipitation of egress-style mineralization. Some of the reduced fluids continued up the fault above the unconformity within the sandstone where they interacted with the APS mineral-bearing intervals and precipitated perched mineralization [3.163].

3.5. EFFICIENCY OF TRAPPING CONDITIONS

Accumulation of such massive, high-grade orebodies requires the creation of large open spaces, an efficient reaction to destabilize the uranium complexes and reduce the uranyl ions in solution.

3.5.1. Tectonic reactivation

It is apparent from the cluster of ages from ~1500 Ma to ~250 Ma for minerals associated with unconformity-related uranium deposits that several tectonic events have influenced fault movement and fluid transport within the basins that host these deposits [3.74, 3.163, 3.179–3.183]. The minimum age of ~1500 Ma for primary uraninite is likely related to the far-field affects of accretion of juvenile crust to the south- and east-facing margins of Laurentia. This event and the associated Granite-Rhyolite province accreted between 1.55–1.40 Ga. Between 1.48–1.35 Ga, granites and associated anorthosites intruded the Granite-Rhyolite province as well as the Paleoproterozoic crust farther to the west [3.184]. Magmatism also occurred c. 1500 Ma in the Thelon Basin. The Thelon Basin's Kuungmi Formation basalt has an age of 1540 Ma [3.185].

From 1.3 to 0.9 Ga, continent-continent collisions and the assembly of supercontinent Rodinia affected Laurentia. During the Grenville orogeny, a NW-directed contraction at Laurentia's southern margin was accompanied by intracratonic extension and extensive mafic magmatism [3.184]. The 1.27 Ga (uranium-lead) Mackenzie dyke swarm [3.186] was a significant magmatic event, which caused movement along deep structures and opened faults [3.187, 3.188]. In addition, the Douglas River dike that outcrops several kilometres north of the Shea Creek project was dated, using the rubidium-strontium mineral isochron method, at 1236 Ma [3.189].

Far-field tectonic stresses related to the Grenville orogeny and assembly of Rodinia have long been postulated to have caused fault movement and resetting of uraninite ages around 1100 Ma (e.g. [3.71]). In addition to this event, a more proximal event, the NNE-trending Moore Lakes Complex in the southeastern Athabasca Basin, may have also influenced fault movement in the western Athabasca Basin c. 1100 Ma [3.163]. The complex is comprised of extensive diabase intrusions in the surrounding Athabasca Group and has an age of 1100 Ma [3.190, 3.191].

The break-up of supercontinent Rodinia began in western Laurentia between 850 and 750 Ma as east Gondwana and south China rifted from western Laurentia [3.192]. The far-field effects of the rifting appear to have reactivated the fault systems, resulting in precipitation of uraninite ~ between 900–850 Ma [3.180, 3.193]. Further rifting of Rodinia led to the opening of the western margin of Laurentia c. 750–570 Ma [3.194]. Some uranium mineralization is concordant at ~300 Ma. This event is ascribed to the break up of supercontinent Pangea (~250 Ma [3.195]).

3.5.2. Quartz dissolution

Another process for creating space for the formation of the high-grade deposits is through quartz dissolution associated with uranium mineralization and associated breccia bodies. According to Hoeve and Quirt [3.71], in the Athabasca Basin, a halo of quartz dissolution surrounds the orebodies and extends along the unconformity and into sandstone overlying ore. For example, at the Cigar Lake deposit, there is no offset of the unconformity by the basement-hosted structures. Therefore, extensive dissolution of quartz within the sandstone is required to create enough open space to allow for massive uraninite to precipitate. Silica dissolution has been also reported for the unconformity-related uranium deposits from the Northern Territory in Australia (e.g. [3.196]).

At Cigar Lake, permeable sandstone allows acidic fluids to flow, which leads to a pervasive dissolution of quartz and the precipitation of clay minerals above the deposit. When the sandstone is silicified or in the tight basement lithologies, breccias are observed and are initiated by hydraulic fracturing. Petrologic, mineralogical and geochemical studies, and mass balance calculations indicate that hydraulic fracturing is followed by quartz dissolution and finally, gravitational collapse of the breccia fragments. These events result from increasing fluid–rock interactions and correspond to increasing quartz dissolution and an increasing proportion of matrix material, consisting mainly of newly formed minerals (dravite, sudoïte and illite; [3.197]). Such breccias surrounding or hosting the high-grade unconformity-related deposits of the Athabasca Basin are common, but they have been previously interpreted as being formed as a result of tectonic activity [3.198, 3.199], meteoritic fluid percolation at Cluff Lake [3.198, 3.200–3.202] or dissolution [3.174]. Recent studies have shown that they are initiated by hydraulic fracturing followed by quartz dissolution [3.197, 3.203, 3.204]. Taking the Anne deposit of the Shea Creek area (Western Athabasca) as an example, and using 3-D modelling on GOCAD, Le Carlier et al. [3.204] have estimated that the dravite-sudoite breccias associated with the uranium mineralization have a volume of c. 166 000 m^3. Assuming a silica saturation of 90% for the diagenetic fluid and an average proportion of quartz dissolution in the breccia, a fluid rock ratio of c. 10^4 is obtained, leading to a quantity of fluid necessary to generate the amount of dravite-sudoite breccias reaching about 1.7 km^3. To explain the tonnage of c. 10 000 tU of the Anne deposit, the amount of uranium in solution has to be at least of 8 ppm for a 100% efficiency of the deposition mechanism. The average uranium concentration measured in the diagenetic brines being ten times larger [3.78], either the efficiency of uranium deposition was very weak and/or the silica undersaturation of the fluid was much more important. Assuming fault permeability of 10 m/yr and a connected porosity of 1 to 5%, the estimated duration of the hydrothermal system ranges from 2.5 Ma to 0.5 kyr.

Hoeve and Quirt [3.71], for the Athabasca deposits, and Wilde and Wall [3.168] for the Nabarlek deposit have respectively attributed the dissolution of quartz to an increase in fluid temperature. For Wilde and Wall, [3.168] the temperature increase occurs during the downward percolation of the fluid, whereas, for Hoeve and Quirt [3.71] heating results from ascending hot fluids deriving from the basement. However, no significant temperature increase has been determined during the ore stage [3.79, 3.98]. Therefore, there is no current mechanism that can explain the undersaturation of the fluids leading to massive quartz dissolution associated with unconformity-related uranium deposits.

3.5.3. Reduction mechanism

The redox processes at the origin of UO_2 deposition are still poorly understood [3.45, 3.172, 3.205–3.207] but they were probably active only at the ore deposit sites because the brines associated with mineralization were present, not only in mineralized zones but also in non-mineralized areas such as Rumpel Lake.

The structures controlling most unconformity-related uranium deposits in the Athabasca Basin are rooted in gneisses rich in graphite [3.208–3.210] and many deposits present small amounts of carbonaceous matter (hydrocarbon buttons or bitumen) within altered ore zones in the basement and in the sandstone. Bitumen may occur as more or less massive layers along fractures, patches or millimetre size nodules. When bitumen is present, the total organic carbon contents may range from 0.06 wt% to 25 wt% [3.211]. Graphite disseminated in graphitic schists in basement rocks has generally been leached out by the basinal hydrothermal fluids in the upper part of the regolith, in the vicinity of most Athabasca uranium deposits [3.212–3.214] and in the East Alligator River uranium deposits in Australia.

Hoeve and Sibbald [3.10] suggested that at temperatures of about 200°C, oxidizing basinal fluids carrying uranium reacted either with reducing fluids coming from reactivated basement shear zones, or directly with the reduced basement lithologies to precipitate uranium.

It has been proposed that the graphite has either directly reducted the uranyle ions [3.178], or has been converted to CH_4 during its interaction with basinal fluids [3.10, 3.102, 3.215]. For Bray et al. [3.215] the interaction of basinal fluids with sulphide- and graphite-bearing pelites could have produced not only CH_4, but also CO_2 plus or minus H_2S and plus or minus H_2 gases. In fact, variable amounts of CH_4, C_2H_6, or H_2 were detected by Raman spectroscopy sporadically in fluid inclusions from unconformity-related uranium deposits [3.97, 3.98, 3.101, 3.216]. H_2S deriving from sulphide mineral alteration, is also a potential reducing agent of uranyle ions [3.217–3.219].

The graphitic gneisses contain high-crystallinity high-temperature (>600°C) graphite resulting from the prograde metamorphism in amphibolite to granulie facies conditions of organic matter from biogenic origin, initially deposited within the sedimentary layers ($\delta^{13}C$ = -26 ± 3‰).

During the uplift of the basement, at shallow crustal level (2–5 km) and cooling down to 500-450°C, C-O-H-N metamorphic fluids have progressively evolved toward a H_2O-CH_4-N_2 composition, and H_2O has been consumed by hydration reactions, finally leading to carbon oversaturation of the fluid and graphite precipitation [3.220]. This newly deposited graphite of hydrothermal-metamorphic origin is poorly ordered and isotopically light ($\delta^{13}C$ = -28 ± 2‰) and forms masses in the core of the shear zones. The graphite enrichment of these shear zones is probably one of the major reasons for the specific spatial relationships between the most unconformity-related uranium deposits and the late-Hudsonian graphite-rich structures.

However, the $\delta^{13}C$ values of graphite analysed by Kyser et al. [3.221], from unaltered and altered gneisses of the Key Lake uranium deposit do not support graphite consumption as a mechanism for uranium precipitation. The $\delta^{13}C$ values of the graphite are relatively constant and the variations do not present any correlation with the distance to the mineralization or with the intensity of deformation or alteration. Therefore, the isotopic data favours complete destruction of graphite by the strongly oxidized basinal fluids deriving from the sandstone and indicate that the graphite in the bleached zones below the unconformity has not reacted to form significant quantities of hydrocarbons such as methane, which should have been enriched in ^{12}C. However, if it is considered that methane could have been produced at deeper levels along the reactivated shear zones at temperatures at which the graphite may have been more reactive, then the possibility remains.

Fluid inclusion studies in the Dufferin Lake Zone, south-central Athabasca Basin, along the graphite-bearing structure, have shown that fluids rich in CO_2, CH_4 and N_2, circulated through fresh graphitic rocks from the basement, while high saline basinal brines circulated through graphite-rich bleached rocks immediately underlying the unconformity. The C–O–H–N fluids may have been generated in the basement prior to the time of deposition of the uranium mineralization. The C–O–H probably resulted from graphite breakdown to form $CO_2 + CH_4$ according to the reaction proposed by Huizenga [3.222], whereas N_2 may have been produced by the breakdown of biotite to chlorite during retrograde metamorphism of the basement lithologies. The brines, observed in the basement rocks are similar to those related to uranium ore deposits [3.72, 3.98, 3.99]. They have infiltrated the basement, and may be responsible for the destruction of graphite in the bleached zone. Based on P-T conditions of the trapping of the carbon- and nitrogen-rich fluids, these fluids may have been also been generated during the ore stage hydrothermal alteration process, which could have led to reduction of the uranyles ions from the mineralizing fluid and deposition of the uranium mineralization. For example, biotite from graphitic schists may be enriched in ammonium because in the black shale protolith, thermal maturation of organic matter leads to the liberation of ammonium, which is initially trapped in clay minerals [3.223] or potassium-micas and potassium-feldspar [3.224, 3.225]. The alteration of these minerals to chlorite and/or illite during the diagenetic hydrothermal event could have led to the liberation of ammonium to form H_2- and N_2-rich fluids, and reaction of H_2 with CO_2 may have led to the production of methane.

Several hypotheses have been proposed for the origin of the hydrocarbon buttons or bitumen nodules associated with the uranium deposits, (e.g. [3.210, 3.226–3.229]). Potential source-rocks for the hydrocarbons in the Athabasca Basin are either the Late Devonian–Early Missippian black shales that originated from bitumen occurring in the Early Cretaceous Athabasca tar sands, or Mesoproterozoic black shales of the Douglas Formation. The stratigraphic location of these potential hydrocarbons source-rocks in the Basin requires a downward migration of the hydrocarbons, which may have formed in the 1500 m thick sandstones of the Athabasca Group and mobilized by the dense highly saline diagenetic brines, thus reaching the base of the basin and the basement. However, numerical modelling by Chi et al. [3.230] shows that hydrocarbons could have migrated from the overlying Douglas black shales to the unconformity and may have participated in the reduction during the uranium mineralizing process.

These results constrast with the observations made in the Franceville Basin where hydrocarbon migration has been clearly evidenced from the black shales of Formation B, the oil impregnates only the uppermost part of the sandstone of the underlying Formation A [3.231]. According to Wilson et al. [3.228] all pyrobitumens in the Athabasca deposits were introduced after mineralization, because they cross-cut the uranium ore, and have had no role in the reduction of uranium.

The carbon isotopic compositions of the bitumen nodules from the Athabasca, determined at the micrometre scale by ion microprobe, are strongly variable ($\delta^{13}C$ = -51‰ to -23‰) [3.229] and within the same range of values obtained on macroscopic samples from different uranium deposits ($\delta^{13}C$ = -53‰ to -23‰) [3.166, 3.221, 3.232, 3.233]. The distribution of the $\delta^{13}C$ values follows a well-defined zonation at the scale of bitumen nodules with $\delta^{13}C$-rich centres. These isotopic values positively correlate with the aliphaticity ratios. By comparison, the $\delta^{13}C$ values of organic matter from the Lodève and Oklo uranium deposits are higher and very homogeneous, -20.5 ± 1.1‰ and -18.6 ± 0.7, respectively and no correlation exists between the isotopic composition and alphatic ratios in these deposits. The isotopic fractionation of carbon related to the catalytic conversion of CO_2 to hydrocarbons by abiogenic mechanisms is similar to the Fisher Tropf process, and may explain the range of $\delta^{13}C$ values and their correlation with the aliphaticity ratios measured in bitumen from the Athabasca uranium deposits.

Recently, Aghbelagh and Yang [3.234] examined two different reducing mechanisms by using reactive mass transport modelling for the precipitation of uraninite in a typical unconformity-related deposit; methane produced by graphite alteration and reduction of the oxygen fugacity. In their model using the two reducing mechanisms, uraninite orebodies can form parallel to the unconformity surface but at some distance into the basement, and away from the graphite fault zone, even without the involvement of methane. In their model, a drop-in oxygen fugucaity does not result in uraninite precipitation in the graphite fault zone. However, methane produced by graphite alteration appears to precipitate larger amounts of uranium oxide in a shorter period of time. Their numerical simulations are based on a thermodynamic and kinetic data from the EQ3/6 database, which are very limited for chloride complexes, the main ligand in the brines from unconformity-related deposits. In addition, many of the values from such databases are not derived from experimental measurements.

The Aghbelagh and Yang [3.234] model also incorporates unrealistic parameters such as the continuation of the graphite bearing structure into the overlying sandstone, a feature which has never been observed in the Athabasca or Kombolgie sandstones. The location and shape of the orebodies as sheets parallel to and at some distance from the unconformity does not exemplify any of the ore systems or orebody geometries observed in the Athabasca Basin or those of the East Alligator River Basin in Australia. The parameters used by Aghbelagh and Yang [3.234] are more akin to the uranium orebodies hosted in basement rocks from the Srisailam sub-basin in the northern part of the Cuddapah Basin in India [3.235]. In addition, the absence of mineralization within the graphitic fault zones in the Aghbelagh and Yang [3.234] model, using both reducing mechanisms, does not explain the common presence of uranium mineralization within the graphitic faults in the Athabasca or East Alligator River Basins.

The reduction of uranyl ions to precipitate uranium oxides UO_2 by Fe^{2+}-bearing minerals (e.g. chlorite or iron sulphides) has also been frequently proposed [3.98, 3.178, 3.236]. Initial calculations made by Privalov et al. [3.237] show that this reaction is possible in the aqueous phase. The experiments of Liger et al. [3.238] and Jeon et al. [3.239] show that U^{6+} reduction by Fe^{2+} may occur through surface-catalyzed reactions using Fe^{3+} mineral species such as haematite and ferrihydrite. Also, the experimental study of Taylor et al. [3.240] shows that Fe^{2+} in aqueous solution can reduce U^{6+} to U^{4+} but U^{6+} is only partly reduced to U^{4+}, but preliminary calculations by the same authors show that the reduction of U^{6+}aq by Fe^{2+}aq does not occur. Moreover, all these experiments were conducted at room temperature and a neutral pH (7.2). More recently, the experimental work of Dargent et al. [3.241] shows that Fe^{2+} was not able to reduce the uranyle ions at 150°C in a one molal LiCl solution. They further support this result using the Phreeqc software and the LLNL database for thermodynamic calculations, which confirm that at 150°C dissolved Fe^{2+} cannot reduce U^{6+} in an acidic brine with pH of 1.

Hydrogen represents another potential reducing agent, which is known to form, together with oxygen, by water radiolysis induced by the radioactive decay of uranium in uranium deposits [3.242–3.245]. However, it is now known if this hydrogen production can play the role of a self-induced reduction process for uranyle ion reduction. That said, hydrogen can be produced by a variety of mechanisms, such as: hydrothermal alteration of Fe^{2+}-bearing minerals [3.246–3.249], reactions of Fe^{2+}-bearing minerals with H_2S [3.250–3.253], or metamorphism of graphitic rocks [3.254–3.257].

The efficiency of the main possible reductants of uranyle ions in the conditions prevailing in unconformity-related uranium deposits have been tested experimentally by Dargent et al. [3.241]. They have shown that H_2, CH_4 and graphite may act as efficient reductants even at temperatures as low as 100–250°C, a range similar to the one recorded in the unconformity-related uranium deposits whereas dissolved Fe^{2+} does not reduce the uranyle ions under similar conditions. The kinetics of the reduction are highest for hydrogen and slowest for graphite. The efficiency of the reduction with these species increases with temperature and the partial pressure of hydrogen, and decreases with increasing pH and chlorinity. Using these experimental results, calculations show that the duration of the formation of a uranium deposit will dominantly depend on the concentration of uranium in the ore fluid and the kinetics of the generation of gaseous reductants, rather than on the kinetics of uranyle ion reduction to uraninite.

The high mobility of the dissolved or gaseous H_2 and CH_4 species represent one of the parameters to consider for explaining the massive nature of the unconformity-related uranium deposits and their location within the oxidized sandstone in many deposits, where no reductants exist, and their occurrence in basement structures devours the graphite. However, further analytical and experimental work is still needed to constrain the origin of hydrogen and methane in the conditions prevailing during the genesis of unconformity-related deposits.

3.6. THE AGE OF THE URANIUM DEPOSITS

3.6.1. History of dating techniques and results

Application of radiogenic isotope systematic to ascertain the timing of geologic and fluid events in basins is tenuous, because many sediments contain mixtures of chemically heterogeneous detrital minerals and inseparable mixtures of detrital and diagenetic mineral phases, both of which are susceptible to later chemical and isotopic alteration (e.g. [3.258–3.262]. Sediments which have had their rubidium and strontium isotopic compositions homogenized during diagenesis and have not undergone substantial post-diagenetic alteration can yield meaningful rubidium-strontium ages [3.258, 3.263–3.265], whereas radiogenic argon in phyllosilicate minerals is labile and much more sensitive to later alteration events [3.264]. Clay and silicate minerals in the Athabasca Basin have formed at temperatures below their typical closure temperatures. Therefore, if the minerals behaved as closed systems since crystallization, their rubidium-strontium, potassium-argon, argon-argon ages should effectively reflect the timing and sources of the fluids from which they formed.

The study of the uranium-lead isotopic system in uraninite is difficult because uraninite undergoes substantial lead-loss during alteration, often resulting in highly discordant data. Additionally, mineral grains are often heterogeneous at the micrometre scale [3.12, 3.266] and zones within a single grain are irregular in shape and size. This is further complicated because multiple generations of uraninite are often present within a single sample. Traditionally, techniques used to study the uranium-lead isotopic system in uraninite, have involved the use of grain separation or micro-drilling prior to dissolution in acid and analysis by isotope dilution thermal ionization mass spectrometry (ID-TIMS) [3.267–3.269].

The major downfall of these techniques is that they have to assume that the entire sample is of primary origin and homogeneous, as they do not have the spatial resolution to avoid altered areas or distinct — yet closely spaced — generations of uraninite. Attempts have been made to separate closely spaced generations by plotting all the data on a Concordia diagram and adding lines of best fit through points that appeared to be of the same generation [3.269]. However, bulk techniques often resulted in mixed ages with little or no geologic meaning (i.e. do not correspond to specific thermal or tectonic events) that add a degree of uncertainty in the geochronology of uranium deposits, thus highlighting the need for in situ techniques.

Bowles [3.270] summarized the various methods that can be used to obtain in situ chemical Pb ages from uraninite using the electron microprobe (EMP). Techniques that use the EMP measure the total amount of uranium, thorium, and lead in uraninite and ages are calculated based on decay constants of uranium and thorium [3.270]. All the lead that is measured is assumed to be the result of radioactive decay of uranium and thorium, and common ^{204}Pb cannot be differentiated from radiogenic ^{206}Pb, ^{207}Pb, and ^{208}Pb. More recently, LA-HR-ICP-MS (Laser Ablation High-Resolution Inductively Coupled Plasma Mass Spectrometry) was used successfully to measure uranium-lead ratios in uraninite and davidite [3.271].

Secondary ion mass spectrometry (SIMS) has several advantages over TIMS and EMP because they combine the measurement of isotope ratios with in situ micro-analytical capability. This allows the researcher to target specific generations of uraninite and avoid altered regions within a sample, while obtaining the necessary measurements to distinguish between common and radiogenic lead [3.193, 3.272]. Matrix effects and heterogeneity of available reference material (RM) produced large errors and erroneous results, ultimately limiting the earliest studies by SIMS [3.193, 3.272–3.282]. Fayek et al. [3.281] used a CAMECA 4f SIMS instrument to develop a correction factor for ^{206}Pb/^{238}U and ^{207}Pb/^{235}U ratios. They observed that the ion-yield normalizing coefficient (αSIMS) varied as a function of wt% PbO. This observation prompted the development of several standards and calibration curves to accurately calculate a uranium-lead age using SIMS [3.283].

3.6.2. Most probable age(s)

Previous field and petrographic observations indicate the Athabasca sandstones and underlying metasedimentary rocks have been altered by several fluid events [3.10, 3.71]. Wide ranges in uranium-lead, potassium-argon and rubidium-strontium ages on contemporaneous uranium, silicate and clay minerals reported in previous studies [3.284–3.289]. Mudstones and clay pebbles in Manitou Falls sandstones and in weathered paleoregolith, believed to be recording the ages of deposition and diagenesis, have rubidium-strontium and potassium-argon whole-rock isochron and mineral ages ranging from 1350 to 1630 Ma [3.284–3.286]. Similar results were obtained from an argon-argon and a potassium-argon study on illites from McClean Lake [3.215].

Kotzer and Kyser [3.125] reported a rubidium-strontium isochron age of 1477 ± 57 Ma and a model age of 900 Ma for well characterized diagenetic illites. They interpreted these ages to represent major high-temperature, diagenetic fluid events, which are similar to the oldest uranium-lead and lead-lead ages of 1400 to 1500 Ma measured on paragenetically early, high-grade uranium mineralization [3.12, 3.193, 3.266, 3.288, 3.289] and paleomagnetic ages of 1450 to 1600 Ma and 900 Ma on diagenetic haematite formed at 200°C [3.180]. Kotzer and Kyser [3.125] also reported rubidium-strontium and potassium-argon ages as young as 400 Ma for illites along reactivated fault zones hosting uranium mineralization that are interpreted to represent late-stage (Phanerozoic to Recent) fluid migration.

More recent studies for the Athabasca Basin uranium deposits reported similar ages. Alexandre et al. [3.162] reported an age c. 1750 Ma for post-peak metamorphic cooling during the Trans-Hudson Orogen, which is the maximum age for the formation of the overlying Athabasca Basin. They propose that there is a pre-ore alteration event that occurred that simultaneously affected both basement and sandstone cover at c. 1675 Ma, as indicated by the $^{40}Ar/^{39}Ar$ dating of pre-ore alteration illite. Alexandre et al. [3.162] and Cloutier et al. [3.40, 3.290, 3.291] suggest that uranium mineralization precipitated c. 1590 Ma, based on LA-ICP-MS uranium-lead dating of uraninite and argon-argon dating of syn-ore illite, and is the same throughout the basin and in both basement- and sandstone-hosted deposits. Several fluid circulation events that subsequently affected all minerals are identified and correspond to far-field, continent-wide tectonic events such as the metamorphic events in Wyoming and the Mazatzal Orogeny (c. 1.6–1.5 Ga), the Berthoud Orogeny (c. 1.4 Ga), the emplacement of the McKenzie mafic dyke swarms (c. 1.27 Ga), the Grenville Orogeny (c. 1.15–1 Ga), the assemblage and break-up of Rodinia (c. 1–0.85 Ga), and the breakup of Pangea at ~250 Ma.

Very few recent studies have focused on the metallogenesis of the western Athabasca Basin deposits. Laverret et al. [3.188] reported argon-argon ages for several generations of authigenic illite at 1453 ± 2, 1330 ± 20 and at about 1235 Ma. Sheahan et al. [3.163] reported several ages for uranium mineralization from the Kianna Deposit in the western Athabasca Basin. Primary basement-hosted ingress-style mineralization has a minimum uranium-lead isotopic age of 1495 ± 26 Ma. A lower basement pod of uraninite gives an age of 1280 ± 30 Ma whereas uraninite from the upper basement gives an age of 1088 ± 22. This latter age is interpreted to represent recrystallization of basement uraninite at ~1100 Ma. Late basement uraninite precipitated at 855 ± 27 Ma. Egress-style mineralization at the unconformity and perched uraninite in the sandstone, intergrown with alumino-phosphate sulphate (APS) minerals and chalcopyrite, formed at 739 ± 58 Ma. Later unconformity and perched uraninite precipitated with haematite, pyrite, and chalcopyrite at 482 ± 11 Ma.

3.6.3. Importance of radiogenic lead loss

The uranium oxides in the uranium deposits from the Athabasca Basin have generally experienced significant episodic and continuous lead loss [3.74, 3.162, 3.178, 3.187, 3.193, 3.269, 3.281, 3.292–3.295], evidenced in Concordia diagrams from the rarity of concordant data, the large degree of discordance of most samples, and the common lower intercepts largely different from zero. Part of the mobilized radiogenic lead has been trapped within the orebodies, as shown for example by the extremely radiogenic lead isotopic composition of galenas measured in mineralized samples from the Shea Creek uranium deposit [3.296] and from the Midwest deposit [3.297]. Moreover, 3-D modelling of the lead distribution in the Shea Creek deposit [3.296] shows anomalously high lead content in the sandstone above the deposit and an increase of the Pb/U ratios from the centre to the margins of the orebody (Fig. 3.6), where galena crystals have been observed, and suggest radiogenic lead migration outward from the deposit. However, those galenas present significant amounts of common and thorogenic lead indicating that the lead does not derive exclusively from the uranium oxides because the Th, ^{208}Pb and ^{204}Pb concentrations are very low in the uranium oxides ($38.3<^{208}Pb/^{204}Pb<43$; [3.187]). Therefore, ^{204}Pb in these galenas was likely derived from the alteration of the feldspars from basement lithologies; ^{208}Pb was likely derived from the alteration of monazite in the heavy-mineral-rich layers of the sandstone. Similar lead isotopic compositions have been also measured in 'basement-type' galena in the vicinity of the Midwest deposit [3.297], and were interpreted to be from regolith alteration.

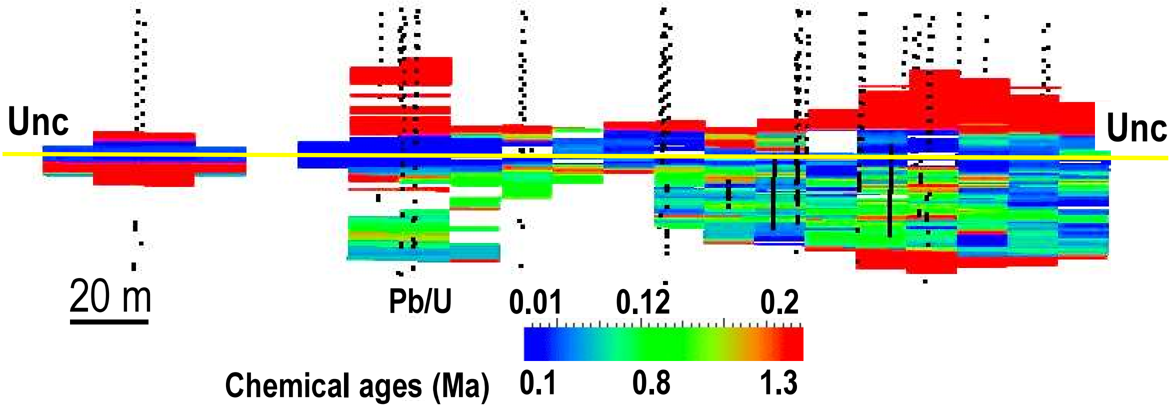

FIG. 3.6. Cross-section through a 3-D model of Pb/U ratio distribution in the Anne deposit (Shea Creek district, W Athabasca Basin). The dotted lines represent the drill core that was sampled for uranium and lead analysis. Unc = unconformity surface (modified from Kister [3.298]).

The essentially radiogenic origin of lead concentrations in the ore zone used in the 3-D model is supported by: 1) the low contents of ^{204}Pb and ^{208}Pb in the uranium oxides of all uranium deposits of the Athabasca region (e.g. [3.193, 3.269]); 2) galenas rich in ^{204}Pb and ^{208}Pb have been only observed in the sandstone outside of the ore zone; 3) the highly radiogenic nature of the galena crystals associated within the uranium oxides of the orebodies; and 4) the positive correlation observed between the lead and uranium content for uranium content above 500 ppm (Fig. 3.7).

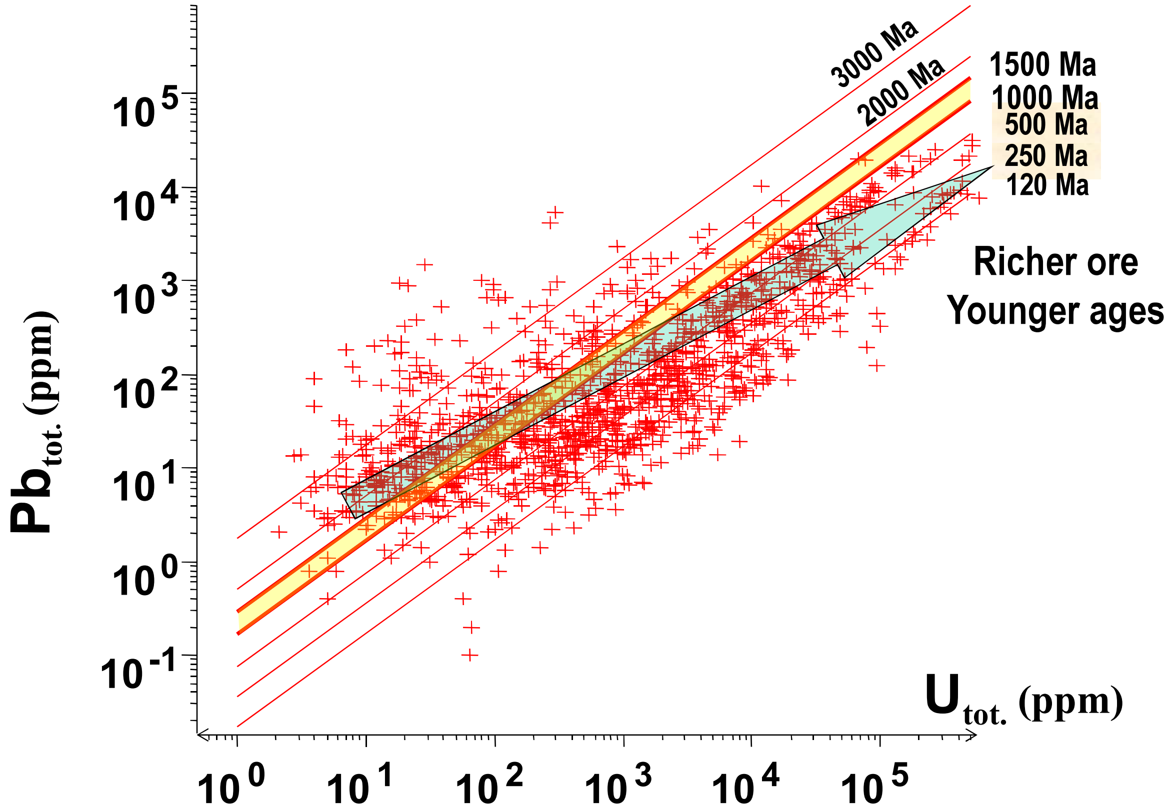

FIG. 3.7. A plot of uranium vs. lead concentrations for the Shea Creek uranium mineralization and enclosing sandstone (modified from Kister [3.298]). The red lines represent the chemical age isochrones. The yellow domain represents the field of uranium-lead compositions for chemical ages between 1500 and 1000 Ma.

Assuming a closed system, and using the two ages for uranium oxides at Shea Creek as the two main uranium deposition events, Kister et al. [3.296] suggested that the average Pb/U ratio of 0.071 ± 0.015 measured in the deposit can be generated by deposition of 9 ± 9% of uranium at 1315 Ma and 91 ± 9% at 391 Ma. Regardless of additional uranium depositional events, the hypothesis of a closed system requires that more than 50% of uranium in the deposit be deposited before 485 ± 97 Ma. If the presence of common and thorogenic lead is considered in the system, the proportion of uranium that has been deposited recently is greater. A recent deposition of the main part of the mineralization seems to be very unlikely, as lead loss at the scale of the uranium oxide crystals is systematically observed and the lead isotopic compositions of uranium oxides are generally strongly discordant. Upper intercept or Concordant ages in the range of 200–500 Ma have been only obtained for uranium oxides representing minor ore lenses and generally small rims or intergranular filling around older uraninites [3.163, 3.269, 3.293, 3.299]. Assuming the age of 1315 Ma as a main depositional event at Shea Creek, and considering that no uranium has been lost since, Kister et al. [3.296] have calculated that a minimum of 53 to 64% of the radiogenic lead has been lost from the Anne orebody in the Shea Creek district. A similar calculation has been obtained by Cumming et al. [3.297] on the Key Lake deposit. The anomalous lead contents measured in the Athabasca sandstone above the Anne deposit are not sufficient (generally Pb<6 ppm) to account for the amount of lead missing in the Anne orebody. Therefore, a major partion of the radiogenic lead has to have migrated over more than 700 m (the average thickness of the analysed sandstone above the orebody). The 3-D images of the distribution of uranium and lead in the sandstone above the Anne deposit at Shea Creek [3.296, 3.298] show lead anomalies that are not supported by uranium anomalies following structures extending from the basement into the sandstone, indication that ^{204}Pb has migrated, at least partly, along fractures. Also, it can be observed in Fig. 3.6, that the lowest lead/uranium ratios are localized along the unconformity, which indicates that ^{204}Pb has been preferentially leached there, and that ^{204}Pb has migrated massively along the unconformity, in accordance with the higher permeability of the regolith and the coarser grain size of the basal siliciclastic sediments of the Athabasca Basin. Although the calculations above are an effective method for modelling lead loss associated with a uranium system, they rely heavily on the ages of the ore, which do not necessarily represent the age of ore deposition. For example, the recent study by Sheahan et al. [3.163] on a Shea Creek deposit gives a much older age of ~1500 Ma, which is not considered to be the initial age of ore deposition.

Regardless of how lead loss is modeled, most researchers working on unconformity-related uranium agree that a significant amount of radiogenic lead loss has occurred and that this phenomenon can be used to explore for these types of orebodies. Lead isotopes have been used extensively for decades in exploration geochemistry, primarily in lithogeochemistry, to assess metallogeny (e.g. [3.300–3.302], but also for tracing secondary migration of lead from ores with unique isotope ratios. A rapid and inexpensive lead isotope analytical method using ICP-MS has been developed for uranium exploration [3.303]. The distal migration of lead can be detected up to several kilometres from the uranium deposits in the Athabasca and Thelon basins [3.303] because of the U/Pb ratios in the ores — therefore, the lead isotope ratios are dramatically different from the host rock. Recent studies have used lead isotopes in surficial media to reflect buried ore deposits [3.304, 3.305], but the anthropogenic contribution to the surface must be assessed for each medium to effectively use lead isotopes as a definitive tracer of the origin of lead associated with uranium ore systems (e.g. [3.306–3.308]).

3.7. OTHER DEPOSITS REFERRED AS UNCONFORMITY RELATED

3.7.1. Deposits associated with the Thelon Basin (Canada)

The uranium deposits of the eastern Thelon region (Fig. 3.8) display many similarities, but also some dissimilarities to the basement-hosted unconformity-related uranium deposits of the Athabasca region. The Thelon Basin is similar to the Athabasca Basin in size, geology, and geometry. It has been suggested that uranium deposits located adjacent to the Thelon Basin, in the Kiggavik region, are also unconformity-related deposits [3.309–3.313]. However, while the Athabasca Basin has been thoroughly studied in terms of its stratigraphic, sedimentological, diagenetic, fluid, and metallogenic histories (e.g. [3.10, 3.12, 3.125, 3.138, 3.163, 3.172, 3.178, 3.290, 3.314, 3.315]), the Thelon Basin has a much smaller body of literature documenting such characteristics.

Most previous publications on the Thelon Basin have focused on understanding the sedimentology and lithostratigraphy (e.g. [3.76, 3.316–3.318], sequence stratigraphy and hydrostratigraphy [3.76, 3.319–3.321), and the diagenetic fluid history [3.164, 3.322, 3.323]. Fewer studies have focused on the uranium metallogeny and genesis of the Kiggavik-Andrew Lake trend deposits (e.g. [3.165, 3.166, 3.309, 3.311, 3.313, 3.324, 3.325].

The uranium deposits from the Kiggavik region occur along the NE-SW Kiggavik-Andrew Lake structural trend (KALST), which is ~30 km long and is located near the NE edge of the Thelon Basin. Overall, the quartzo-feldspathic metasediments that host the uranium deposits along the KALST have undergone retrograde metamorphism and contain chlorite after biotite, coarse-grained muscovite, and pyrite. Uranium mineralization generally occurs in three textural forms: 1) disseminated grains; 2) along fractures (vein-style); and 3) along mini roll-fronts. Uranium minerals include uraninite, coffinite, boltwoodite, and uranophane. Uraninite appears to be the only primary uranium mineral. Illite is the dominant clay mineral associated with uranium mineralization, with lesser sudoite. Organic matter is only occasionally associated with uranium mineralization.

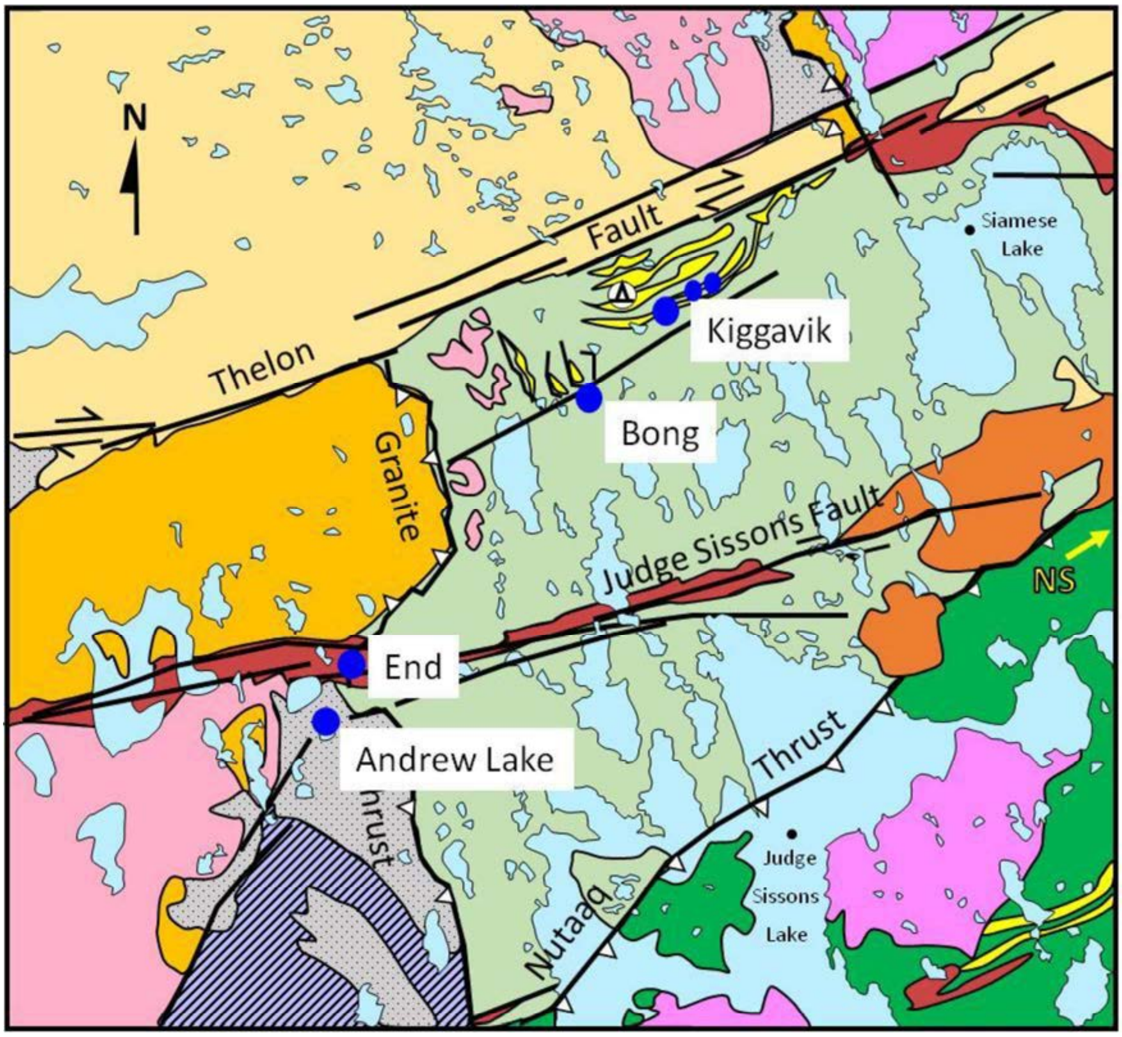

FIG. 3.8. Simplified geologic map of the Kiggavik project area located in Nunavut, Canada, showing known uranium deposits along the NE-SW Kiggavik—Andrew Lake structural trend (modified from [3.165, 3.166, 3.326–3.328]).

Using the oxygen and hydrogen isotopic composition of clay minerals associated with uranium mineralization and the oxygen isotopic composition of uraninite, the temperature of formation for the KALST deposits was calculated to be ~200°C. This is similar to the temperatures of formation calculated for the uranium deposits in the Athabasca Basin region (e.g. [3.125]). The calculated isotopic composition of the fluids associated with the KALST deposits have $\delta^{18}O$ and δD values between -1‰ and +8‰, and -130‰ and -40‰, respectively. These values are slightly lower compared to the fluids associated with the Athabasca Basin uranium deposits, which have values $\delta^{18}O$ and δD values between +2‰ and +10‰, and -10‰ and -100‰, respectively (e.g. [3.163]).

Farkas [3.329] separated pitchblende, coffinite, and galena using a microscope, analysed the minerals for their uranium-lead isotopic ratios, and reported ages that group around 1400 Ma and 1000 Ma. Fuchs et al. [3.310] reported whole rock potassium-argon ages from relatively unaltered and altered Woodburn Lake group metasedimentary rocks and from the Lone Gull Granite. The unaltered samples gave ages of 1648 Ma and 1563 Ma, whereas the altered samples gave ages of 1358 Ma and 1073 Ma. They interpreted the older ages to be related to the uplift and erosion of Woodburn Lake group and Lone Gull basement rocks after the Hudsonian Orogeny. Alternatively, the older ages may represent deep burial and diagenesis, especially because they are close to the 1667 ± 5 Ma ages of the Thelon fluorapatite [3.323] and the 1540 Ma Kuungmi Lavas [3.185] respectively. The younger ages, 1358 Ma and 1073 Ma, were interpreted by Fuchs et al. [3.310] to be related to the age of primary mineralization and the age of a late fluid event that remobilized uranium, respectively (i.e. similar to the 1403 Ma primary uraninite age and the 1000 Ma remobilization age of Farkas [3.329]. Weyer [3.330] reported potassium-argon ages from illite at the Kiggavik Main and Centre deposits that group around 930 Ma, 1166 Ma, 1230 Ma and 1290 Ma.

More recently, Riegler [3.331] analysed alteration illite that is coeval uraninite from the Bong deposit and reported an argon-argon age of 1124 ± 9 Ma. Sharpe et al. [3.166] reported ages for uranium minerals from the Bong deposit at 1520 ± 79 Ma, 1114 ± 8 Ma, and 982 ± 19 Ma. The 1114 ± 8 Ma for uraninite is the same, within error, as the argon-argon age reported by Riegler [3.331] for coeval illite. Riegler [3.331] also reported uranium-lead ages of 1293 ± 6 Ma and 1187 ± 19 Ma from uraninite in the End deposit. The older age was corroborated by Chi et al. [3.325] where they reported an age of 1295 ± 12 Ma for uraninite from the End deposit.

Shabaga et al. [3.328] reported an age for uraninite from Andrew Lake deposit of 1031 ± 23 Ma and 528 ± 34 Ma. The older age is similar to ages obtained by Farkas [3.329], who reported an age of 1000 ± 10 Ma for uranium minerals from the Kiggavik deposit, by Sharpe et al. [3.166] who reported an age of 982 ± 19 Ma for uraninite from the Bong deposit, and Weyer [3.330] who reported a 930 Ma potassium-argon age from illite at the Kiggavik deposit. The ~500 Ma age for altered uraninite from the Andrew Lake deposit records a fluid event that has not been observed in previous studies from the Kiggavik region. However, the 500 Ma age is similar to the age obtained by Sheahan et al. [3.163] for perched and late unconformity-related mineralization at the Kianna deposit in the Shea Creek area of the western Athabasca Basin.

Shabaga et al. [3.28] also analysed muscovite and illite from the Andrew Lake deposit. They report argon-argon ages that rise monotonically from ~1600 Ma to a plateau-like segment at 1782 ± 18 Ma for metamorphic muscovite. However, alteration illite gave much younger ages at 941 ± 31 and 1330 ± 36 Ma. The ~1780 Ma argon-argon age obtained for muscovite is interpreted to be the age of a fluid event associated with the second phase Nueltin intrusion and metasomatism of the primarily Hudson (~1.83 Ga) Lone Gull granite, which was reset by the Kivalliq Igneous event at about 1759 Ma. The younger low temperature age of ~1600 Ma from muscovite does not correlate with any other reported ages in the Kiggavik region. The ~940 Ma age obtained for illite is similar to the oldest reported age for uranium mineralization from the Andrew Lake deposit (1031 Ma), and similar to ages reported for uraninite from the Bong deposit (982 Ma; [3.166]), Kiggavik region (1000 Ma; Farkas [3.329]), and alteration minerals (913–1073 Ma; Weyer [3.330]; Fuchs et al. [3.310]). These ages suggest that there was a major fluid event that re-set primary uraninite in the Kiggavik region at ~1000 Ma. Similar ages have been reported in the Athabasca and McArthur basins (e.g. [3.153, 3.193, 3.281], Kyser et al. [3.332]) and can be correlated with the Grenville orogeny (980–1120 Ma; Rivers [3.333]).

3.7.2. Yeneena Basin, Western Australia

3.7.2.1. Geological setting

The Mesoproterozoic Yeneena Basin (Fig. 3.9) comprises the Throssell and Lamil Group that form the Yeneena Supergroup. The Throssell Group consists of a sandstone-shale-carbonate succession. The basal member of the Throssell Group is represented by the Coolbro sandstone. According to the youngest age of detrital zircons in the basal Coolbro Formation, deposition in the Yeneena Basin occurred after ~910 Ma [3.334], and before ~830 Ma, the age of mafic intrusives emplaced in the lower part of the basin (D. Maidment, unpub. data, in [3.335]). This time range is compatible with a carbonate rock Pb–Pb isochron age for the Isdell Formation at ~860 Ma (R. Maas and D.L. Huston, University of Melbourne, Australia, unpub. data, 2017, [3.335]), and is interpreted as a diagenetic age.

The Coolbro sandstone is a fluviatile-deltaic succession, deposited in an intra-continental basin or continental margin setting, that includes discontinuous conglomerate, thin carbonaceous mudstone and shale beds [3.336]. The sandstone succession is up to four km thick and unconformably overlies the Paleoproterozoic Rudall complex. The Rudall Complex was metamorphosed up to granulite facies conditions with partial melting, during two Palaeoproterozoic events (c. 2015–1800 Ma and 1790–1760 Ma; [3.337]). The complex is composed dominantly of metamorphosed monzogranites and metasediments. The Yeneena Basin has been deformed and faulted during the Miles (~840 to ~810 Ma) and Paterson Orogenies (c. 650 Ma) [3.338].

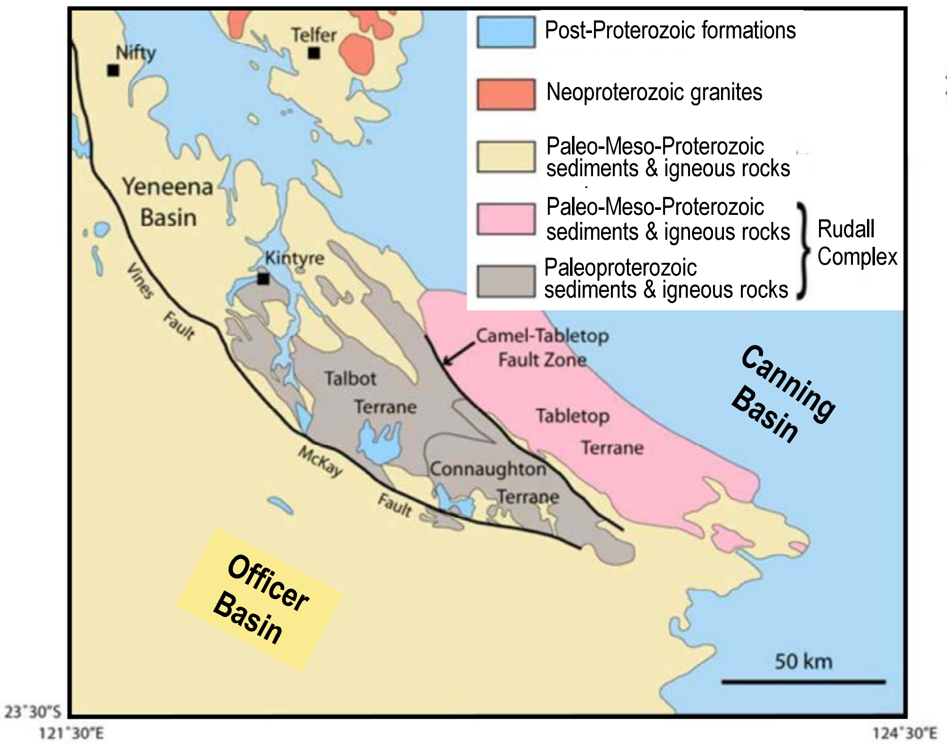

FIG. 3.9. Regional geology of the Rudall Complex and the Yeneena Basin, and locations of uranium deposits and prospects (modified from Hickman and Bagas [3.336]).

The Coolbro sandstone is a moderate to well sorted fine-medium grained quartz arenite having an average detrital composition of 90–98% quartz, 0–5% K-feldspar, 0–1% plagioclase, and with zircon, monazite, muscovite, tourmaline, haematite and iron-titanium oxides as the main accessory minerals. Matrix components generally account for less than 5% of the volume and include metamorphic muscovite and chlorite and late kaolinite and haematite. Chlorite is a minor phase that occurs primarily in sandstones closest to the unconformity and is coeval with fine-grained muscovite. Detrital quartz shows variable degrees of polygonization and weak to strong undulose extinction due to metamorphic overprinting [3.339].

3.7.2.2. The Kintyre deposit

Kintyre uranium deposit has been described as an unconformity-related uranium deposit [3.340] because it is a vein-type deposit that occurs in the vicinity of the unconformity between the Rudall Metamorphic Complex and the overlying sedimentary rocks of the Coolbro Formation (Fig. 3.10). The deposit is entirely hosted in the metasediments of the Yandagooge Formation, initially deposited in an epicontinental setting and typically comprising black shale, silt, sandstone, limestone, and iron formation [3.341]. At the deposit, the Rudall Complex is tightly folded and consists of chlorite–garnet–quartz schists, graphitic schist and dolomitic marbles. The probable uranium resource of the Kintyre deposit has been estimated at 25 000 tU at 0.477% uranium, with an inferred resource of about 10 000 tU [3.342].

Mineralization occurs as narrow closely spaced NW striking veins and dipping 60ºNE. These veins follow a major NW shear zone also affecting the Coolbro sandstone.

The veins are dominantly hosted within chlorite schist and chert layers and tend to occur in the hinges of folds with an orientation sub-parallel to the axial fold planes. The main mineralized zone comprises a tabular mylonitic unit rich in biotite, 300 m along strike with a thickness of less than 10 to 15 m, and reaching a maximum depth of 175 m. The structure hosting the deposit crosscuts the Coolbro Sandstone and therefore the Kintyre mineralization should be younger than the maximum age of the Coolbro Sandstone (i.e. 1070 Ma). The deposit comprises five orebodies: Kintyre and East Kintyre, Pioneer, Whale, East Whale, and Nerada. Pitchblende is the main uranium mineral and is associated with minor amounts of native bismuth, bismuthinite, bornite, chalcopyrite, galena and gold. The main gangue minerals are magnesium-iron chlorite, dolomite, calcite, and ankerite [3.340].

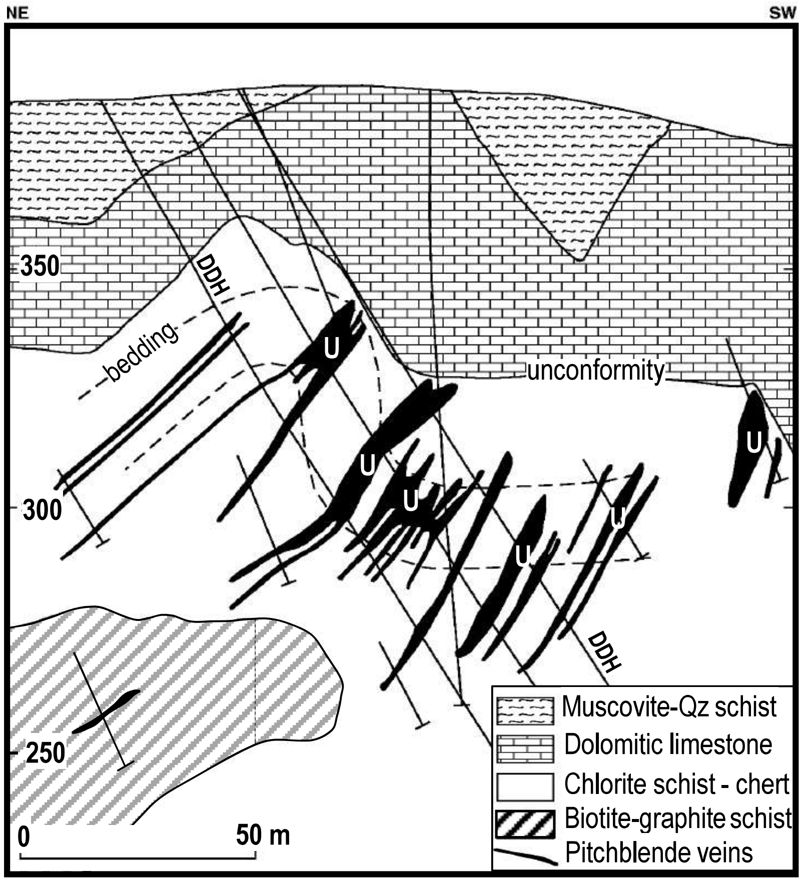

FIG. 3.10. Cross-section through the Kintyre uranium deposit (modified from Gauci [3.343]). DDH = diamond drill holes.

Cross et al. [3.335] obtained a chemical lead age of 837 +35/-31 Ma for uraninite from the Kintyre deposit. They interpreted this age as the crystallization age because it is similar to the ~845 Ma age proposed by R. Maas of the University of Melbourne for uranium deposition [3.344]. It confirms that uranium mineralization is younger than the Paleoproterozoic Yandagooge Formation that hosts the deposit. Cross et al. [3.335] suggest that the Kintyre mineralization was formed during or soon after the latest period of sedimentation in the Yeneena Basin, probably during the ~850 to ~800 Ma Miles Orogeny.

Fluid inclusions observed in quartz veins that crosscut the Coolbro sandstone close to the unconformity, which are presumed to have survived the metamorphism, are generally highly saline and consists of variable mixtures of H_2O, NaCl, $MgCl_2$, and $CaCl_2$ with variable homogenization temperatures (163–347°C). There is only one fluid inclusion generation that has low salinities and high homogenization temperatures (250–378°C) (Fig. 3.11; [3.339]). The highest temperatures recorded for the high saline inclusions are attributed to re-equilibration of some of the inclusions during metamorphism. However, Hanly [3.339] suggests that significant amounts of fluids were not generated during metamorphism and as a result, many fluid inclusions from the diagenetic evolution of the basin have been preserved as well as the diagenetic fluid isotopic compsotions of the clay minerals.

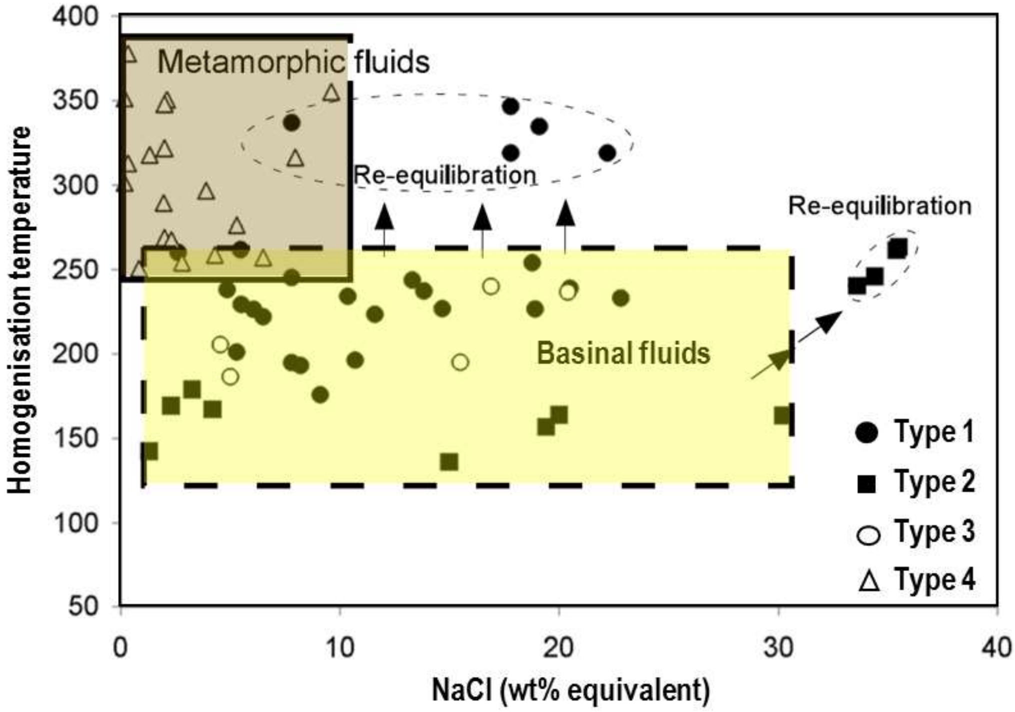

FIG. 3.11. Salinity versus homogenization temperatures for the fluid inclusions from quartz veins in the Coolbro sandstone (Reproduced courtesy of Hanly [3.339]).

The depth of burial during quartz vein deposition was estimated by adding the maximum thickness currently preserved in the Throssell Group of 6 km to that of the Lamil Group which is up to 6 km thick [3.341], thus indicating a depth range of 6 to 12 km. The homogenization temperatures of presumably preserved fluid inclusions, which would represent the diagenetic fluid, range from 176 to 262° C. Assuming a thermal gradient of 30°C/km and neglecting the pressure effect on the homogenization temperatures, this corresponds with a burial depth of c. 6–9 km, which is in agreement with the thickness estimates for the basin fill of 6 km.

The δD values of the fluids in equilibrium with fine-grained muscovite (M1) in the Coolbro Formation range from –33 to –56‰, consistent with a dominantly meteoric water source with a contribution from evaporated seawater. The salts may derive from the evaporites occurring in the overlying Broadhurst Formation [3.345] Haynes et al. A mixing between seawater and a meteoric fluid for the basinal fluids is also consistent with the wide salinity range (3 to 23 wt% eq. NaCl) recorded in fluid inclusions in some of the quartz veins. The $\delta^{18}O$ values of the fluids in equilibrium with fine-grained muscovite in the Coolbro sandstone matrix (+5.1 to +6.2 ‰) show a $\delta^{18}O$ enrichment away from the meteoric water line, typical of basinal waters that have exchanged oxygen with the host sedimentary rocks or mixed with evaporated seawater (Fig. 3.12; Hanly [3.339]).

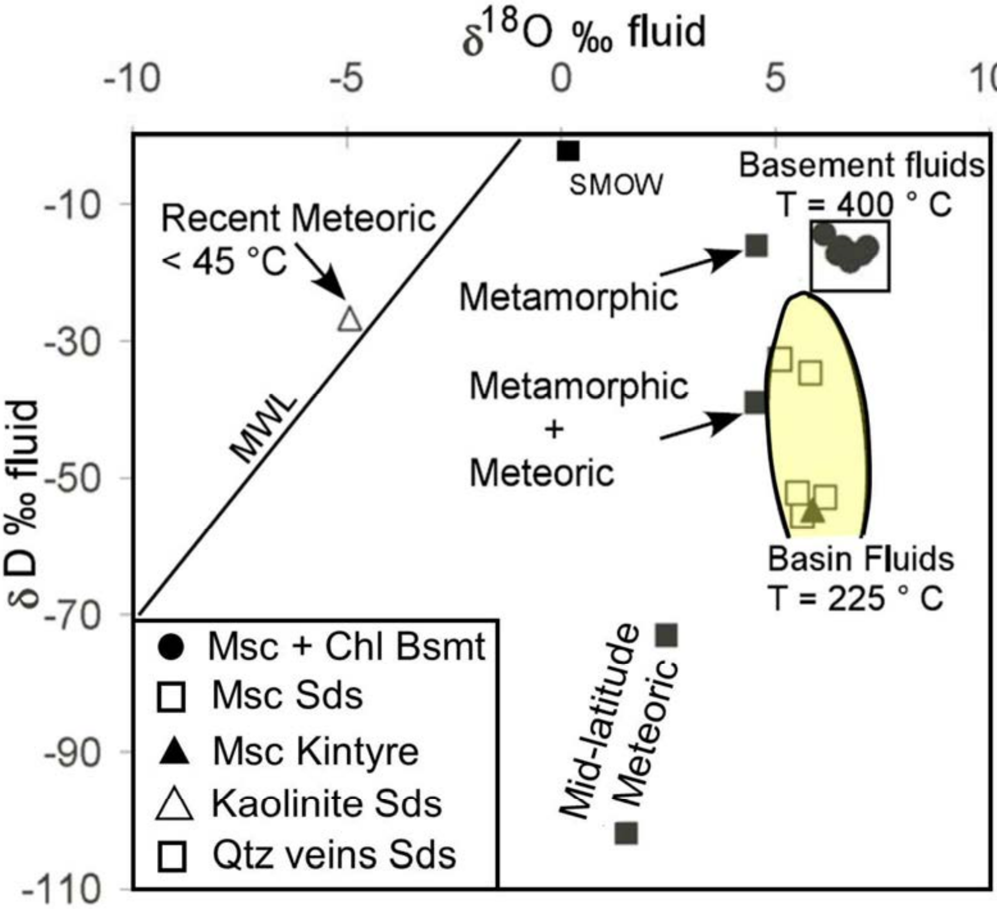

FIG. 3.12. $\delta^{18}O$ and δD diagram for the basinal fluids calculated at 225°C for the Coolbro Formation sandstones and at 400°C for the basement fluids of the Rudall Metamorphic Complex. Squares = measured δD values of fluids extracted from fluid inclusions and calculated $\delta^{18}O$ values of fluids from quartz veins. Msc=muscovite; Chl=chlorite; Sds=sandstone, SMOW= Standard Mean Ocean Water; MWL= Meteoric Water Line (Reproduced courtesy of Hanly [3.339]).

The lead isotopic ratios obtained from the Coolbro Formation are typical of regional values in the Yeneena Basin and do not record radiogenic lead mobilized from the Kintyre deposit. The absence of post-diagenetic fluid circulation able to mobilize radiogenic lead from a uranium-rich source is attributed to the metamorphic events, which have decreased the porosity and permeability of the sandstones [3.339].

The lack of alteration of zircon and monazite in the Coolbro Formation sandstones indicates that the fluids in the Yeneena Basin have been chemically less reactive than the fluids in the Athabasca Basin and suggests that the existence of large high-grade uranium deposits similar to those of the Athabasca Basin are less likely in the Yeneena Basin [3.339].

3.7.2.3. Comparison with unconformity-related deposits

The Kintyre deposit shares two main features with classical unconformity-related uranium deposits: 1) its location relative to an unconformity with overlying Proterozoic sandstones; and 2) the identification of highly saline fluids, which may represent diagenetic fluids preserved from the overprinting metamorphic event.

However, several typical features of unconformity-related deposits are lacking or debatable.

- No regolithic type alteration has been described at the top of basement below the unconformity with the Coolbro sandstone;
- The mineralization is not hosted in graphite schists, but graphtic schists have been intersected at few tens of metres below the main orebody;
- Typical alteration minerals such as the magnesium-rich chlorite (sudoïte) and magnesium-rich tourmaline (dravite) are lacking;
- The association of carbonate with the uranium oxides in the veins at Kintyre is not typical of unconformity related deposits, the ore forming fluids having a low pH;
- The fluid inclusions have been observed in quartz veins in the overlying sandstone, but not directly in the vicinity of the deposit in the basement;
- Despite the identification of highly saline fluids, the accessory minerals (especially monazite) are relatively unaltered compared to similar minerals in the Athabasca and Kombolgie sandstones, indicating that either these fluids have not percolated significantly in the basin or that the diagenetic fluids were not highly saline fluids;
- The available chemical age on the uranium oxide from Kintyre may reflect the overprint of the Patterson orogeny. In the absence of precise dating of the uranium deposit, it is not possible to ascertain that the Coolbro sandstone were present above the Rudall metamorphic rock when the uranium deposit was formed.

3.7.3. Westmoreland District, Australia

3.7.3.1. Geological setting

The Westmoreland uranium field is 100 km south of the coastline of the Gulf of Carpentaria and straddles the boundary between the Northern Territory and Queensland (Fig. 3.13). Total resources of the five discovered deposits were estimated in 2009 at 19.980 tU at 0.07% uranium. Additionally, gold associated with the uranium mineralization may be of economic significance in some of the deposits. The uranium deposits of Westmoreland District are spatially associated with the large intracratonic McArthur Basin of Paleo- to Meso-Proterozoic age (1800–1575 Ma, [3.346]. The Basin was up to 10 km thick and predominantly filled with sedimentary and volcanic rocks.

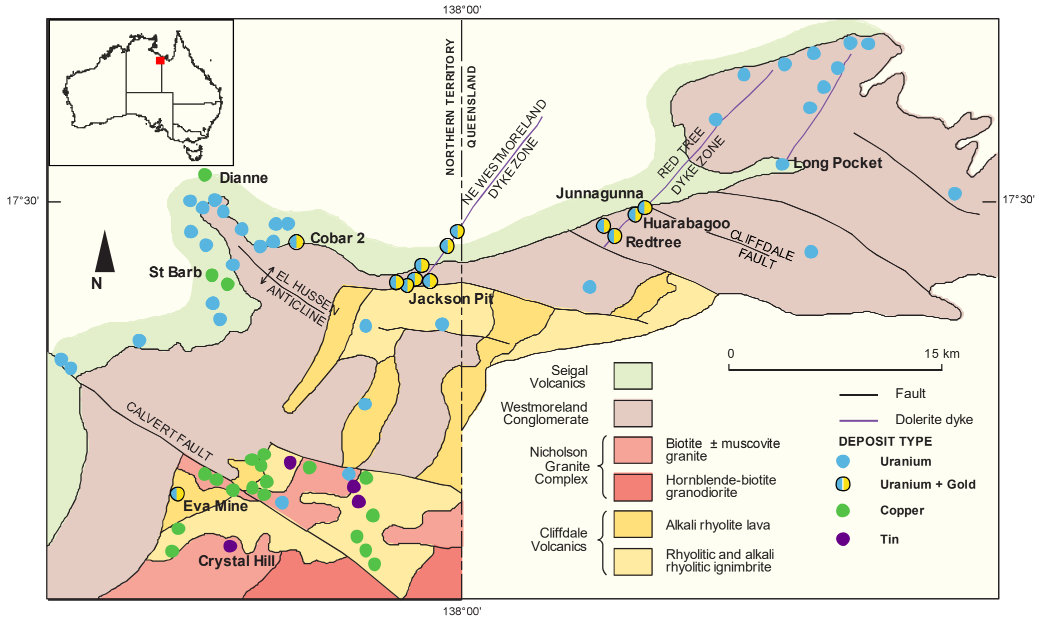

FIG. 3.13. Geological setting for the Westmoreland uranium field (modified from Lally and Bajwah [3.347]).

The basement rocks in the Westmoreland region are Paleoproterozoic quartz-feldspar-mica schists and gneisses of the Murphy Metamorphics. The protoliths of these metamorphics correspond to siltstone, shale, greywacke and volcanics. A maximum age of deposition of the sediments at 1853 ± 4 Ma is from detrital zircons [3.348]. The Murphy metamorphic rocks are covered unconformably by the Paleoproterozoic Cliffdale Volcanics. The metamorphic and the volcanic rocks are intruded by the Nicholson granites and adamellites. All these units are covered by the sedimentary rocks of the McArthur Basin. The basal unit, the Westmoreland Conglomerate, is a ~1200 m thick fluvial siliciclastic sequence subdivided into four stratigraphic units [3.349]. The uranium-lead dating of detrital zircons have constrained the maximum ages of deposition of the lower and upper sections respectively at 1865 ± 7 Ma and 1843 ± 4 Ma [3.348] Wygralak and Mernagh). The Westmoreland Conglomerate is covered by basalts, dolomite, sandstone and finally by mafic and felsic volcanic rocks. The NE-trending dolerite dykes and minor sills intrude the Westmoreland Conglomerate. The Redtree dyke zone extends over 15 km. Individual dykes are less than 20 m wide. The Redtree, Junnagunna and Huarabagoo uranium deposits lie along the Redtree dyke zone.

3.7.3.2. Uranium mineralization

The uranium (gold) veins are mainly hosted by the porous, coarse-grained sandstone and conglomeratic 80–90 m thick upper unit of the Westmoreland Conglomerate (Fig. 3.14). The deposits occur in the following four geological settings [3.350].

- Stratabound uranium mineralization in the sandstone unit, nearly parallel with the overlying mafic volcanic layers and to the contact with mafic sills;
- Discordant, steeply dipping uranium mineralization, at the contact with mafic dykes; the steeply dipping mineralization may grade into stratabound mineralization;
- Uranium mineralization within fractures cross-cutting altered mafic volcanics;
- Uranium mineralization along shear zones in altered felsic volcanics.

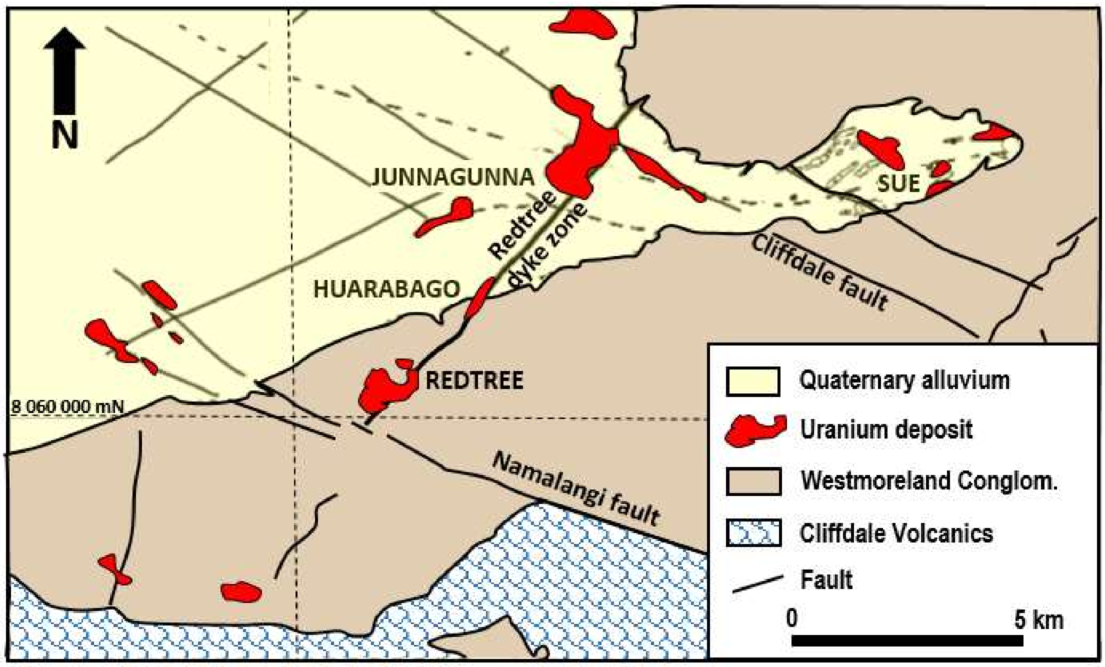

FIG. 3.14. Geology of the Westmoreland uranium field (modified from Rheinberger et al. [3.351]).

Pitchblende is the main uranium mineral, generally associated with haematite, within the quartz or clay matrix in the sandstone. In the volcanic rocks, pitchblende occurs along the edges of the quartz veins. Up to 10 µm grains of gold are associated. Marcasite, pyrite chalcopyrite, bornite, safflorite, and gersdorffite grains are locally observed [3.349]. Resource estimations come from a Press Release from Laramide Resources [3.352].

The Redtree uranium mineralization occurs in both horizontal and vertical ore zones (Fig. 3.15). Indicated resources are 12.86 Mt of ore at 0.076% uranium and inferred resources are 4.47 Mt of ore at 0.06% uranium. The horizontal mineralization is entirely hosted by sandstone, up to 15 m thick, and associated with a chlorite-haematite alteration. With the steepening of the orebody near the dyke, the mineralization is upto 30–40 m thick.

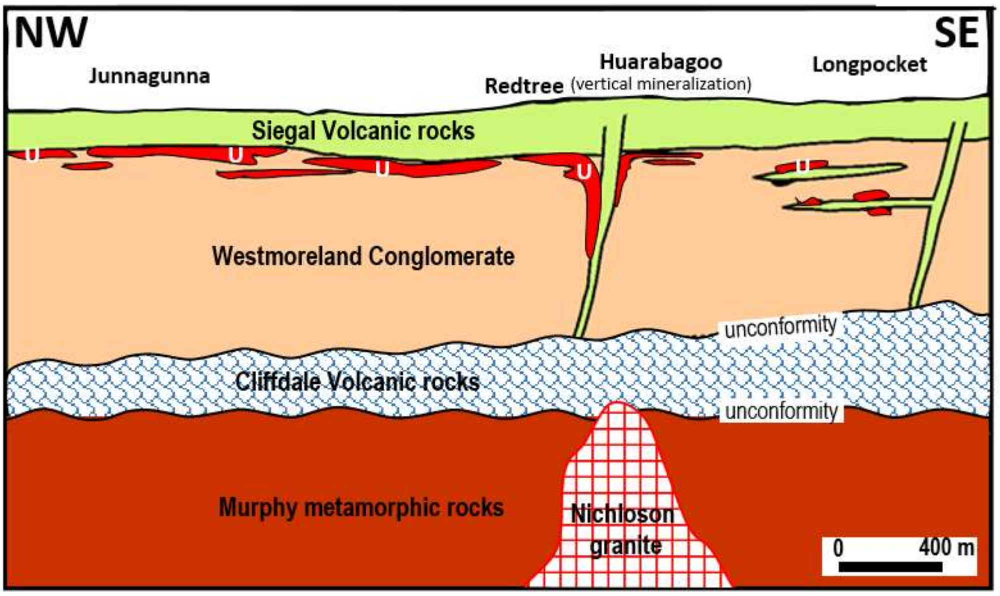

FIG. 3.15. Simplified cross-section of uranium deposits in the Westmoreland uranium field (modified from Fuchs and Schindlmayr [3.353]).

The Junnagunna uranium deposit occurs at the intersection between two faults. The mineralization is essentially flat-lying within the upper unit of the Westmoreland Conglomerate and below overlying volcanics. Steeply dipping mineralization occurs in the vicinity of the Redtree dyke. Indicated resources are 4.36 Mt of ore at 0.068% uranium, inferred resources are 2.15 Mt at an average grade of 0.068% uranium.

The Huarabagoo uranium mineralization is hosted by the Westmoreland Conglomerate. Most of the mineralization is adjacent to the two main vertical dykes and some mineralization occurs within the dykes. Indicated resources are 1.46 Mt of ore at 0.076% uranium and inferred resources are 2.41 Mt at 0.10% uranium.

The Long Pocket prospects form 0.5–5 m thick horizontal lenses, where 90% of the mineralization occurs within sandstones along the lower and upper contacts of a 5-m thick horizontal dolerite sill and 10% occurs within the sill.

3.7.3.3. Metallogenic model

The mineralization is clearly epigenetic and occurs in Proterozoic sandstones and formed under conditions similar to those of unconformity related deposits. Temperatures of the hydrothermal fluids determined from fluid inclusion studies are 190 ± 70 ºC [3.354]. Hydrogen and oxygen isotopic compositions of illite associated to the mineralization indicate that uranium was transported by basinal brines deriving from evolved evaporated seawater [3.154]. The age of 1655 ± 83 Ma determined by $^{40}Ar/^{39}Ar$ in illite and $^{207}Pb/^{206}Pb$ ratios in uraninite are similar to those of the east Alligator River unconformity related deposits. Remobilization events have also been dated at 1150 and 850 Ma [3.154]. The Fe^{2+} from the mafic dykes and volcanics is proposed as a potential reductant of the uranyle ions to precipitate uraninite.

3.7.4. Karku, Pasha Lodoga, Russian Federation

3.7.4.1. Geological setting

The Karku uranium deposit is located in a sub-basin to the NE of the Pasha-Ladoga basin called the Salmi depression (Fig. 3.16). The unconformity gently dips (~4°) to the WSW with local paleoelevations of the basement surface. The main basement structure is a NW striking and steeply dipping (70–80°) Ruskeala tectonic zone. The N-S and EW faults produce local uplifts of the depression. The Karku deposit is located within one of the most prominent uplifts called the Central Block.

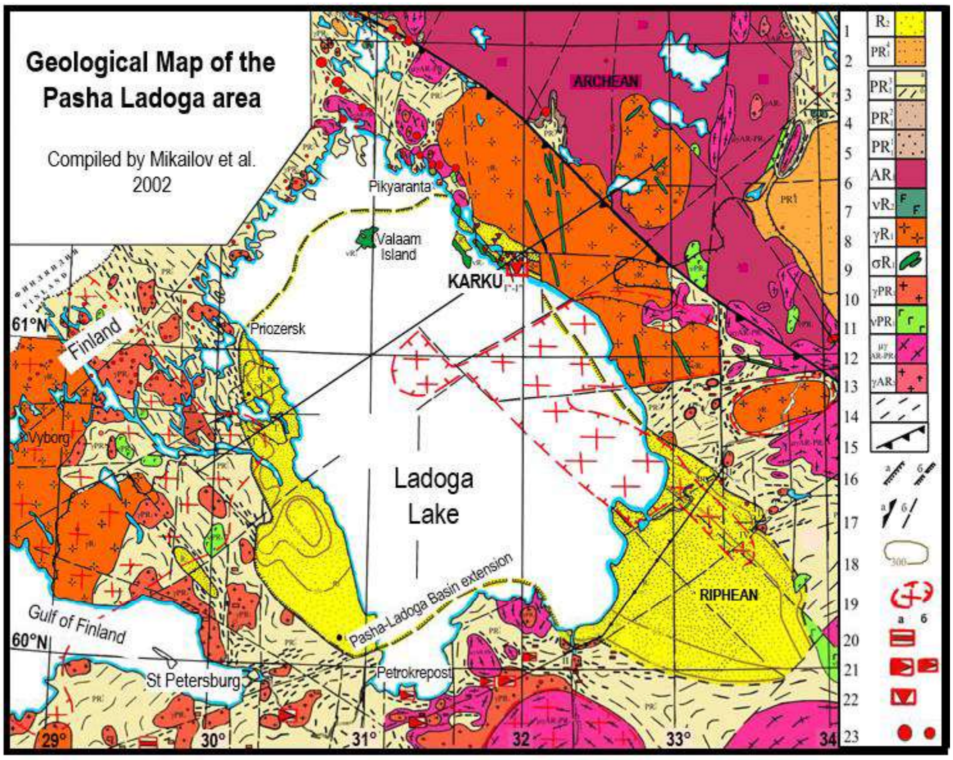

FIG. 3.16. Geological map of the Ladoga area with the present extension of the Pasha Ladoga Basin and the location of the main uranium occurrences (modified from Mikhailov et al. [3.355]).

The local basement is composed of Archean and Paleoproterozoic granitic-gneissic domes surrounded by Paleoproterozoic marbles and amphibole schists of the Ludicovian Pitkjaranta suite and metapelites, sometimes graphitic with pyrite and pyrrhotite, of the Kalevian Impilakhti suite with anataxis (Fig. 3.17). The metasedimentary and metavolcanic basement units have been dated at 2100–1880 Ma [3.356, 3.357]. All rocks were folded and metamorphosed up to granulite facies [3.357], with migmatization and injection by plagioclase-microcline and microcline granite and pegmatite veins during the 1910–1820 Ma Svecofennian orogeny [3.358]. Basement rocks were also intruded by the Mesoproterozoic (Lower Riphean) Salmi Rapakivi Salmi anorthosite-mangerite-charnockite-granite (AMCG) plutonic complex at the NE edge of the basin [3.359]. The pluton is dated at 1547–1530 Ma [3.360].

The intensity of the regolithic alteration of the upper part of the basement formations at contact with the Riphean sediments is variable. Its thickness is generally 5–20 m, but may reach up to 70 m. Leucocratic coarse-grained rocks are more altered than melanocratic ones. The alteration of the upper part of the basement is attributed to paleoweathering, but probably also results at least partly from hydrothermal alterations, especially along the faults. Intensive kaolinitization and chloritization with sporadic ferruginization occur. It is important to note that a zoning from a red to a green regolith, typical for the Athabasca Basin, has not been observed in the Karku area.

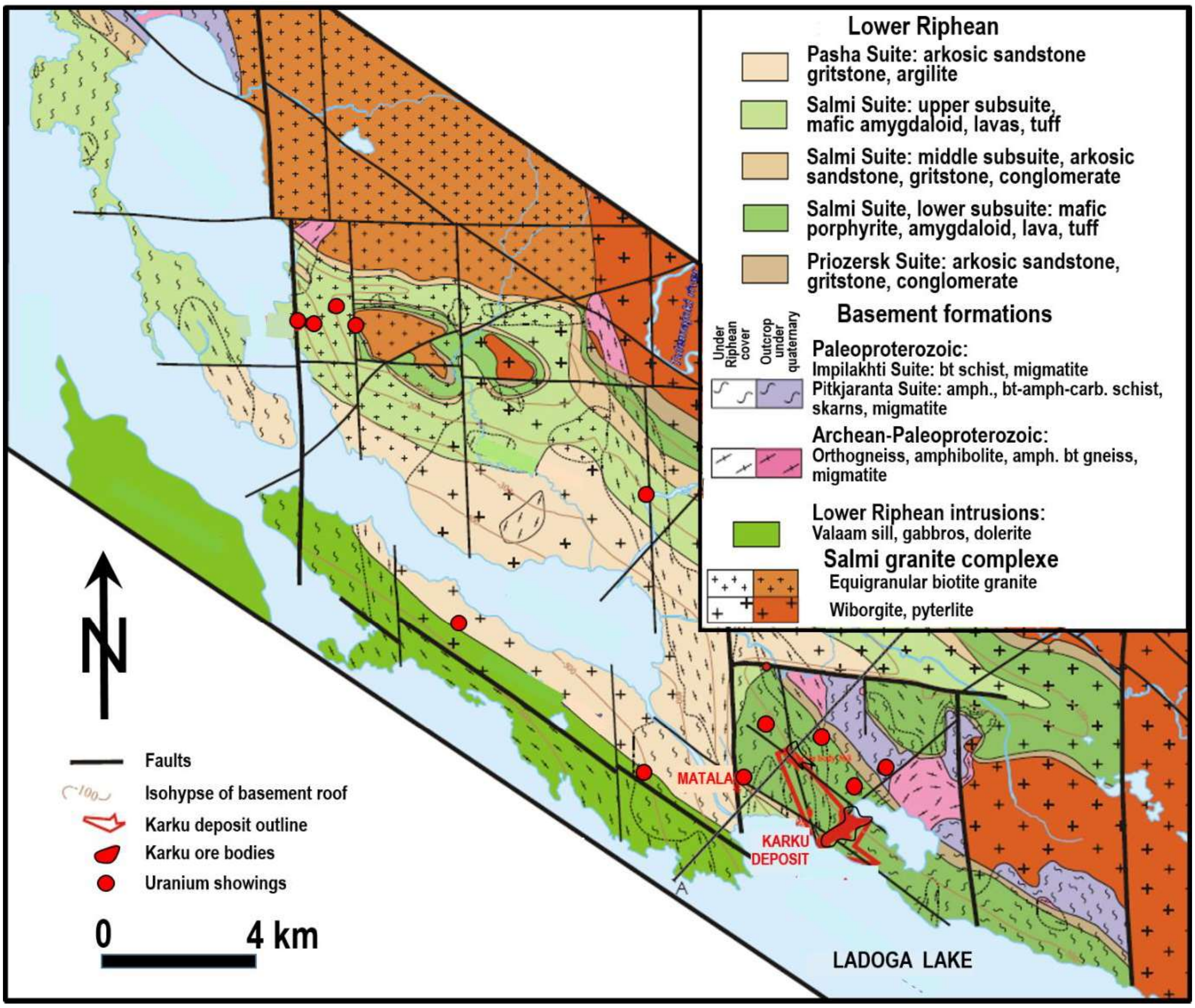

FIG. 3.17. Geology of the NE part of Ladoga lake (Salmi area) with the location the Karku deposit (modified from Mikhailov et al. [3.355]).

The Mesoproterozoic (Middle and Upper Riphean) volcanic-sedimentary basin in the Salmi depression extends for 40 km parallel to the Lake Ladoga coastline and with a width of 10–12 km (Fig. 3.17). Its present thickness reaches up to 360 m. The basement surface below the Salmi sub-basin was a very hilly landscape. Many elongated depressions represent former paleo-valleys. The basal units are affected by several faults formed during the subsidence and post-depositional tectonic movement related to the Danopolonian orogeny c. 1500–1460 Ma [3.361]. Three suites with variable thickness have been distinguished (Fig. 3.18).

- *The Priozersk (Priozerskaya) formation* is 5–80 m thick and is composed of coarse polymictic conglomerates occurring locally at the base and pink- or beige-coloured coarse-grained arkosic sandstones with subordinated gritstones; detrital minerals include 20–50% quartz, 10–35% potassium-feldspar and plagiocalse, and highly corroded lithic fragments; the cement is composed clay minerals (illite, illite/smectite, kaolinite and subordinated iron-chlorite); calcite and chlorite enrichments occur near the contact with overlying effusives with a small layer of dark-gray tuffaceous-sandstone at the contact; diagenetic alteration is represented by the replacement of detrital minerals by kaolinite and to a lesser extent by illite, chlorite, carbonate and haematite. Diagenetic overgrowths associated with detrital quartz are uncommon [3.362, 3.363]; clear quartz overgrowths only occur in the vicinity of the uranium orebodies [3.364]; the most common accessory minerals are: amphibole, biotite, muscovite, garnet, zircon, tourmaline, apatite, and sporadic epidote and monazite;
- *The Salmi (Salminskaya) formation* has a total thickness up to 250 m; it comprises a lower (130 m) and an upper effusive mafic volcanites suite (up to 90 m thick), with a up to 1 m thick layer of strongly altered brecciated dark-gray effusive ash at the bottom of each effusive suite. The two suites are separated by a up to 35 m thick sedimentary layer composed of quartz-feldspar or polymictic coarse-grained beige to pink sandstones, with subordinate gritstones and conglomerates; the lower and the upper effusive layers are composed each of two to five more or less regular rhythms; a complete rhythm is composed of a basal thin to thick layer of gray vesicular basalt (with small chlorite amygdalae), a basalt porphyry (main part of the rhythm), a vesicular basalt (with chlorite and carbonate amygdalae), volcanogenic breccias and tuffs at the roof. The basalts of the lower subsuite have given a Sm-Nd isochron at 1499 ± 68 Ma [3.365].;
- *The Pasha (Pashskaya) formation* is up to 290 m thick and is composed of interlayered polymictic sandstones, siltstones and mudstones with predominance of the fine-grained varieties; the detrital grains are cemented by illite with minor kaolinite.

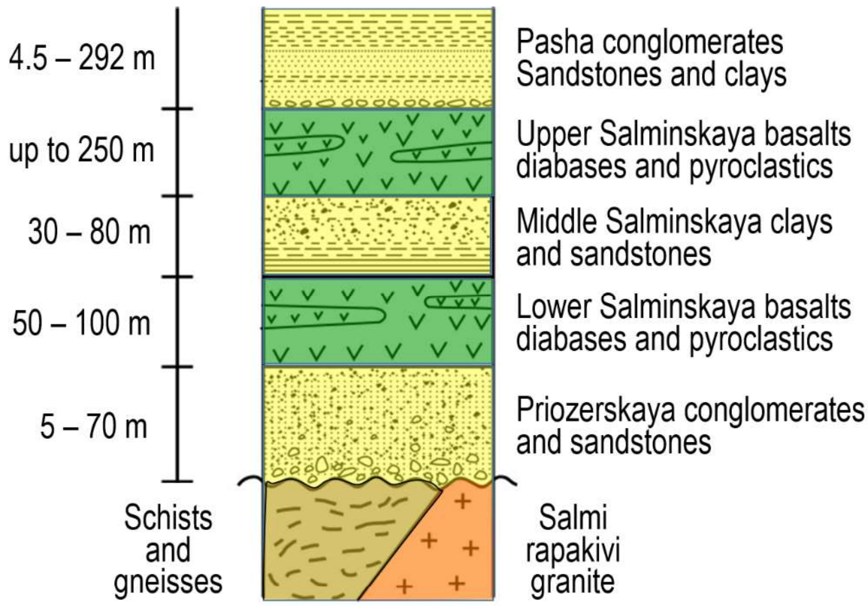

FIG. 3.18. Stratigraphic cross-section of the Pasha-Ladoga volcanic-sedimentary Group in the Salmi depression area.

The Mesoproterozoic volcanic-sedimentary basin is cut by the gabbroic Valaam sill to the west. It is dated at 1457 ± 3 Ma by uranium-lead on baddeleyite, using thermal ionization mass spectrometry [3.366].

The basement below the Mesoproterozoic volcanic-sedimentary basin is enriched in uranium, molybdenum, lead and zinc. The orthogneisses of the domes and the amphibolites of the Pitkjaranta suite are enriched in lead (20 ppm) and zinc (200 ppm) [3.367]. The biotite gneiss and schist of the Impilakhti suite are weakly enriched in molybdenum (3.6 ppm), lead (28 ppm) and zinc (180 ppm). The graphite-schist of the Impilakhti suite is enriched in uranium (5.8 ppm) and molybdenum (5.6 ppm). The potassic granites of the Salmi intrusion in the Salmi area have 4–5 ppm uranium, 18–20 ppm thorium and 3.3–3.5 ppm molybdenum. Svecofennian uranium mineralization is widespread in the basement rocks of the Raahe-Ladoga [3.368]. Similar uranium occurrences are expected to occur under the Riphean sediments. The regolith is depleted in uranium, molybdenum, and lead compared with the unaltered rocks. The sedimentary rocks of the basin are slightly enriched in uranium: 4.8–6.5 ppm in the Priozersk formation sandstone and gritstone, 3.9 ppm in the Salmi formation sandstone, and 4.6–5.6 ppm in the Pasha Formation siltstone. They also have slightly enhanced molybdenum contents (2–3.9 ppm) and the Pasha suite is also enriched in lead (up to 30 ppm) and zinc (up to 170 ppm) [3.367]. A few uranium occurrences are hosted by the Riphean sediments in the Salmi depression: the Karku deposit and the Matala and Kotalakhti showings.

3.7.4.2. The Karku deposit

The ore is localized above a locally uplifted tectonic block called the Central Block. The total amplitude of the uplift of the basement roof is up to 200 m. The low-density gravimetric anomaly in this area probably indicates the presence of the Salmi granite intrusion at depth (Fig. 3.19).

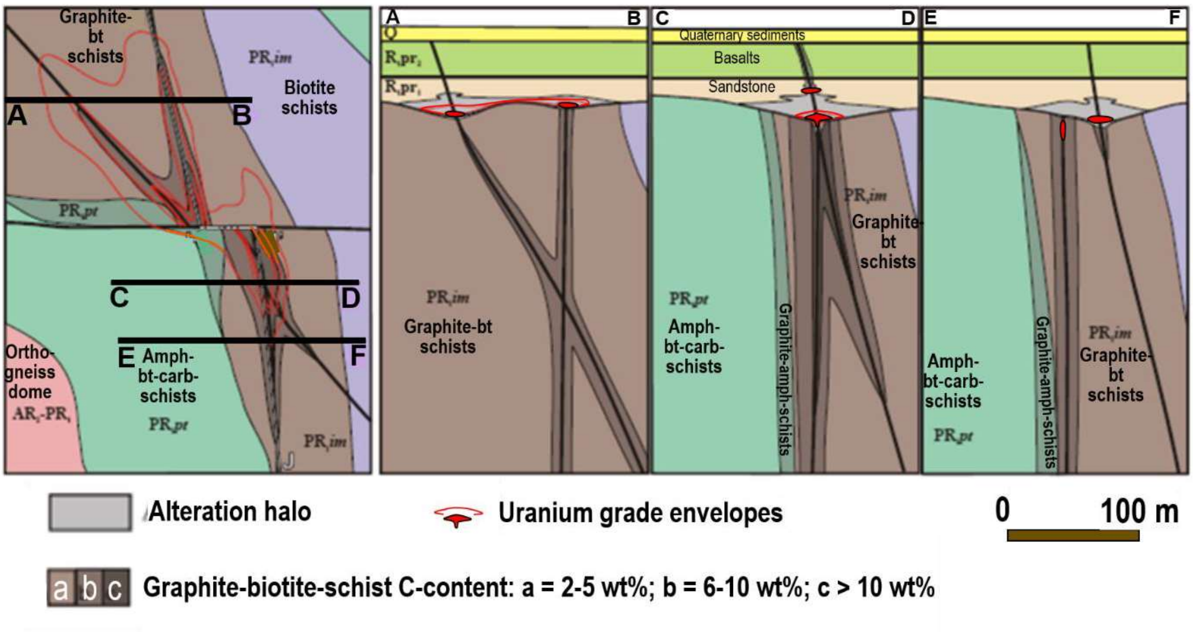

FIG. 3.19. Map (upper left) and a series of EW cross-sections through the Karku deposit (modified from Shurilov [3.368]).

The basement surface present local elevations corresponding to the granitic-gneiss domes and valley-like depressions composed of Palaeoproterozoic schists. The basement roof dips to the west, and the depth of the unconformity varies from 77 to 190 m in the Karku deposit area (Fig. 3.20).

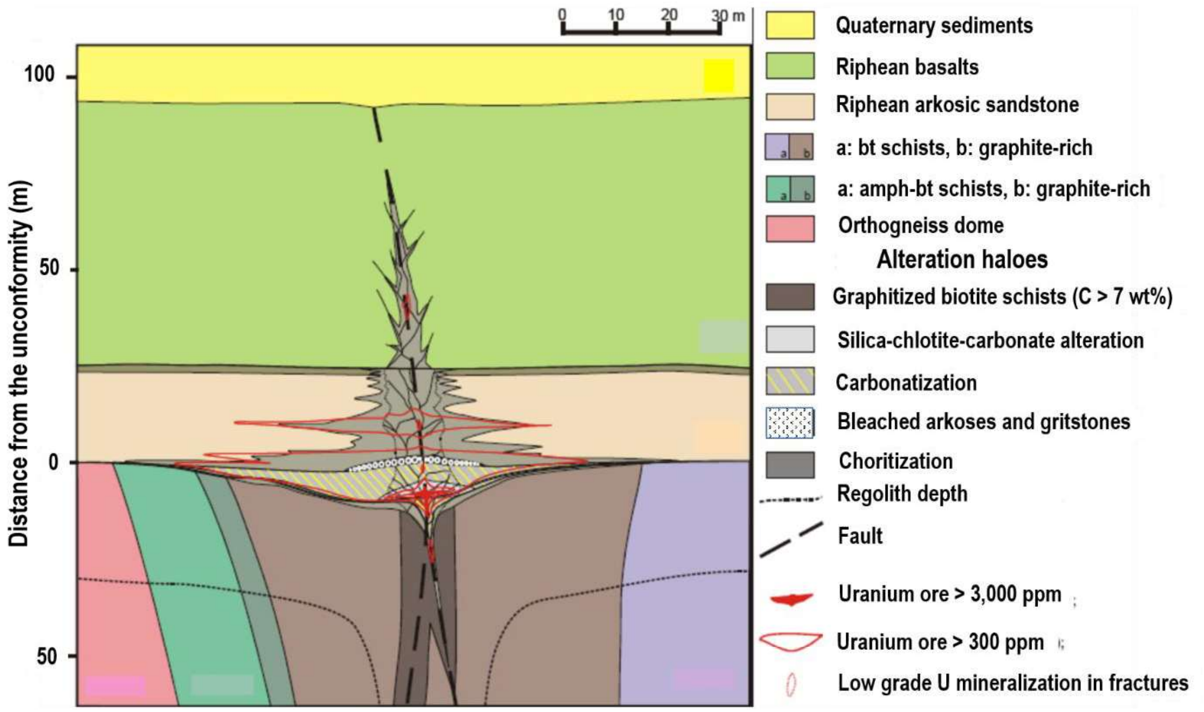

FIG. 3.20. Simplified cross-sections through the Karku deposit with alteration envelopes (modified from Shurilov [3.368]).

The Riphean sequence in the Karku deposit area consists of the Priozersk suite and the lower volcanogenic subsuite of the Salmi suite. All of the Central Block is covered by 25–140 m thick Quaternary moraine sediments. The Karku deposit comprises three separated orebodies located in the south-eastern part of the Central Block along the unconformity.

Orebody 1 is the largest and occurs in a valley-like depression corresponding to a biotite schist of the interdome Impilakhti suite. The ore zone ~1.5 km long and ~ 2 km wide. The ore lens has an average thickness of 8.2 m, but may reach up to 20.5 m based on a 300-ppm cut-off. At a 1000 ppm cut-off, its thickness is up to 5.6 m. Its average uranium content is 840 ppm, with up to 3.46 wt% over 0.5 m. Estimated resources of orebody 1 is about 6600 tU [3.369]. The highest-grade ore concentrations occur at the intersection of NE and NW faults rooted in graphite-rich biotite schists of the Impilakhti suite. The orebody is essentially hosted by the Priozersk suite sediments, with minor amounts in the very upper part of the regolith. Rare low-grade uranium mineralization (up to 470 ppm) also occurs in fracture zones in the basalts of the Salmi suite. Anomalous thorium content (>300 ppm and up to 1840 ppm) occurs locally in the sandstones at the unconformity.

Orebody 2 is the smallest (250 × 150 m at a 300-ppm cut-off) and located at the intersection between the NW and NS faults. The average thickness of the orebody at a 300-ppm cut-off is 1.2 m, but can be up to 6.5 m in thickness. At a 1000 ppm cut-off, its average thickness is 3.2

m, and its size is 90 × 140 m. Its average uranium content is 1040 ppm for a resource of about 400 tU [3.369].

Orebody 3, at a 300-ppm cut-off, is 220 × 620 m and only 50 × 430 m at a 1000 ppm cut-off. The orebody thickness increases southwards up to 7 m. Average uranium content is 1800 ppm, with a maximum of 16.62 wt% uranium over 0.25 m. The resource of the orebody is about 1300 tU [3.367]. The orebody has a wedge shape with two lenses corresponding to the NW and NS faults rooted in graphite-bearing biotite schist of the Impilakhti suite. The eastern flank of the orebody partly occurs above the graphite-bearing amphibole-biotite schist of the Pitkjaranta suite. The highest-grade ores occur at the intersection of this zone with graphitized schists (with 6–10 vol.% graphite) of the Impilakhti suite. The high-grade ore is enveloped by a wide halo of low-grade mineralization located in a valley-like depression of the basement surface with corresponding increase of the above lying sandstone thickness. An EW fault in the central part of Orebody 3 is a sinistral strike-slip and displaces the orebody by over 40 m. The vertical displacement is 3 m and the fault is late because it has no influence on the uranium distribution. The main part of the ore is elongated along the unconformity and hosted by the Priozersk formation. Lenses of low-grade ores occur in the upper and middle part of the Priozersk formation. In the southern part of the orebody, uranium mineralization occurs within the regolith down to 4 m below the unconformity. A unique low-grade ore intersection has been discovered 50 m to the south of orebody 3, in a breccias zone at a depth of 9.8–10.8 m below the unconformity.

The Karku deposit is ~8300 tU. High-grade ore with uranium content over 3000 ppm represent a resource of about 1300 t [3.367, 3.369]. Prognosticated resource of the Karku deposit is estimated at 11 000 tU, and 22 000 t for whole the Central Block (V. Kushnerenko personal comment).

3.7.4.3. Alteration

The alteration halo is poorly characterized in orebody 1. The alteration is weak in orebody 2, and mostly represented by dickite and haematite and minor chlorite. In orebody 3, the following succession of alteration zones from external to internal have been observed: 1) bleaching; 2) chloritization; 3) porous sandstones; 4) chlorite-carbonate alteration; and+ 5) sulphide-carbonate alteration hosting high-grade ore, with the following charcteristics.

- *The bleached alteration zone* is the most external and extends over hundreds of metres from the orebodies. It is characterized by the replacement of the clayey cement and partially the clasts by dickite, with dissolution of iron-oxides and hydroxides leading to bleaching of the pink and beige background sandstone. Significant quartz overgrowths occur in this zone. The contact between the overgrowth and the detrital grain is defined by brownish clinochlore and Fe-hydroxides aggregates;
- *The dark-grey intensively chloritized zone* is the largest alteration zone. Its lateral extension has "pine-tree" edges reflecting the variability of the permeability of the enclosing sandstone and is developed most extensively along the unconformity. Its thickness increases above the orebodies. Along the faults, chloritization penetrates into the effusive layer for a distance of 50 m. Chloritization also extends down 8 m below the unconformity and below the high-grade ores. In this alteration zone, the cement mainly consists of dark-gray chlorite with FeO/MgO = 5.4–7.5, mixed layer illite/smectite, illite with subordinated amounts of leucoxene, Fe-hydroxides, dickite and calcite. Calcite is also abundant in the cement;

- *The porous sandstone zone* (1–2 m thick) is dark-gray to black because of the intense chloritization of the cement and occurs above the high-grade orebodies. A specific feature of this zone is the presence of quartz overgrowths but also euhedral crystals, forming tiny druse-like aggregates in the pores. Calcite content is low;
- *The chlorite-carbonate alteration zone* is characterized by an increase of calcite content. The zone has a lens-like profile with a maximum thickness of 22 m above the high-grade uranium orebody. It occurs mostly in the sandstone layer, but also in the upper part of the regolith, usually less than 1.5 m below the unconformity. Along the ore-controlling faults this alteration may extend 12 m below the unconformity. Quartz overgrowths are partly resorbed. Carbonatization increases toward the orebodies;
- *The sulphide-carbonate alteration* zone is intimately associated with the high-grade uranium mineralization in the sandstone along the unconformity. Its thickness reaches up to 5 m. The same kind of alteration occurs locally in the uppermost part (< 0.4 m) of the regolith below the high-grade mineralization. This alteration zone is characterized by intensive carbonatization with calcium oxide contents exceeding 15 wt%. Its colour varies from light to dark-gray, depending on the relative calcite, chlorite and pitchblende contents. The zone may become yellowish where sulphides are abundant in the cement. Haematite may be locally present. The amount of feldspar is much lower than in the non-altered sandstones and disappears in the centre of this alteration zone. Quartz is also corroded and partially replaced by calcite and becomes smoky when associated with the high-grade uranium mineralization. Chlorite FeO/MgO ratio varies from 0.24 up to 10. The zone’s magnesium content increases towards the central part of the alteration halo where high-grade ores occur. Small amounts of newly formed apatite, fluorite, Al-lizardite, ilmenite, rutile and sulphides (pyrite, marcasite, pyrrhotite, pentlandite, chalcopyrite, bornite, sphalerite, and molybdenite) have been documented. Bitumens are also locally association with a molybdenum-rich mineral and pitchblende. The amount of sulphides increases toward to the central part of the halo and often form the main part of the sandstone cement close to high-grade ore.

The SiO_2 and Al_2O_3 content decreases towards the centre of the alteration halo because of quartz and feldspar dissolution. The magnesium content in the whole rock and chlorite increases with increasing chloritization of the rock. However, the central part of the halo is depleted in magnesium because of the low chlorite content of the dominantly sulphide-carbonate composition of the most internal mineralized zone. Dickite is replaced by the chlorite and calcite towards the centre of this alteration zone.

Chlorite geothermometers of Kranidiotis and MacLean [3.370] and Zang and Fyfe [3.371] used by Rice [3.372] on the newly formed iron-rich chlorite of the ore zone, give temperatures between 190ºC and 240ºC. These temperatures are similar to fluid inclusion homogenization temperatures from the syn-ore calcite [3.363]. No temperatures were obtained from magnesium-rich chlorite because its composition falls outside of the calibration ranges of the geothermometers.

3.7.4.4. Other uranium occurrences in the Riphean sandstone

The most significant occurances are the Matala and the Kotalakhti showings. The Matala showing is located in the Central Block, 1 km west of orebody 3 on the other flank of the Ilyarantskii granitic-gneiss dome. The uranim mineralization has similar characteristics as at

Karku deposit: it is also hosted by the Priozersk suite sandstone, occurs above graphite-enriched biotite schist of the Impilakhti suite, is developed at the unconformity and has a halo in the middle part of the sandstone layer. The uranium content is up to 1800 ppm over a thickness of 1.75 m, and elevated concentrations of lead, zinc, arsenic and silver.

The Kotalakhti showing is located in the NW part of the Salmi depression and is hosted by a fracture zone in the basalts of the Salmi lower subsuite. Pitchblende and coffinite occur within quartz-haematite-carbonate veinlets. The uranium contents are up to 890 ppm over 0.4 m. Two generations of pitchblende and late coffinite are accompanied by increased lead, molybdenum and arsenic content.

Several uranium anomalies are located at the northern part of the Central Block and related to thrust structures (Surjamyaki showing). The uranium mineralization occurs at different levels of the Riphean sequence — in the sandstones and in the basalts, and are related to fracture zones. Uranium contents reach up to 350 ppm. Most uranium anomalies are localized close to the unconformity, but there are a few uranium anomalies in the basement rocks.

3.7.4.5. Ore mineralogy

The high-grade uranium ore is associated with the sulphide-carbonate alteration and consists of pitchblende with subordinated coffinite (Fig. 3.21). Calcite overgrowths replace quartz grains, and enclose brannerite, zircon, garnet and secondary pyrite. Pitchblende-1 forms 2 to 30 μm large nodules and has PbO contents from 1.5 to 16.5 wt%, SiO_2 contents from 1.6 to 16.5 wt%, TiO_2 up to 1.9 wt%, MnO up to 1.8 wt%, Al_2O_3 up to 1.1 wt%, FeO up to 2.2 wt%, CaO up to 5.4 wt% and locally ThO_2 up to 5.4 wt%.

The highest-grade mineralization is mainly composed of clastic quartz relics cemented by pitchblende, carbonate and galena mainly associated with pitchblende-2. Pitchblende-2 and coffinite replace Pitchblende-1, and they are usually associated with disseminated fine-grained radiogenic galena. Pitchblende-2 has a PbO content which varies from 0.7 to 13.0 wt%, SiO_2 varies from 4.3 to 12.8 wt%, Y_2O_3 is up to 3.9 wt%, BaO up to 1.3 wt% and SrO up to 1.0 wt% [3.373]. Galena, Cd-sphalerite, greenockite, howlite, a molybdenum-phase, copper-arsenides, iron, nickel, cobalt arsenides and sulphoarsenides are associated with the uranium mineralization. Late uranium mineralization (pitchblende 3 and 4) occurs in the quartz-chlorite-carbonate veinlets cutting the lower volcanic layer. Pitchblende-3 is associated with galena, pyrite, marcasite and chalcopyrite. Its PbO content is lower ($0.7<PbO<8.1$wt%), as well as its silica content ($3.7<SiO_2<6.4$ wt%. Pitchblende-3 is replaced by pitchblende-4 and coffinite and has lower PbO contents (up to 3.7 wt%), with SiO_2 content up to 6.4 wt% [3.373]. Uncommon brannerite-like minerals have been also described.

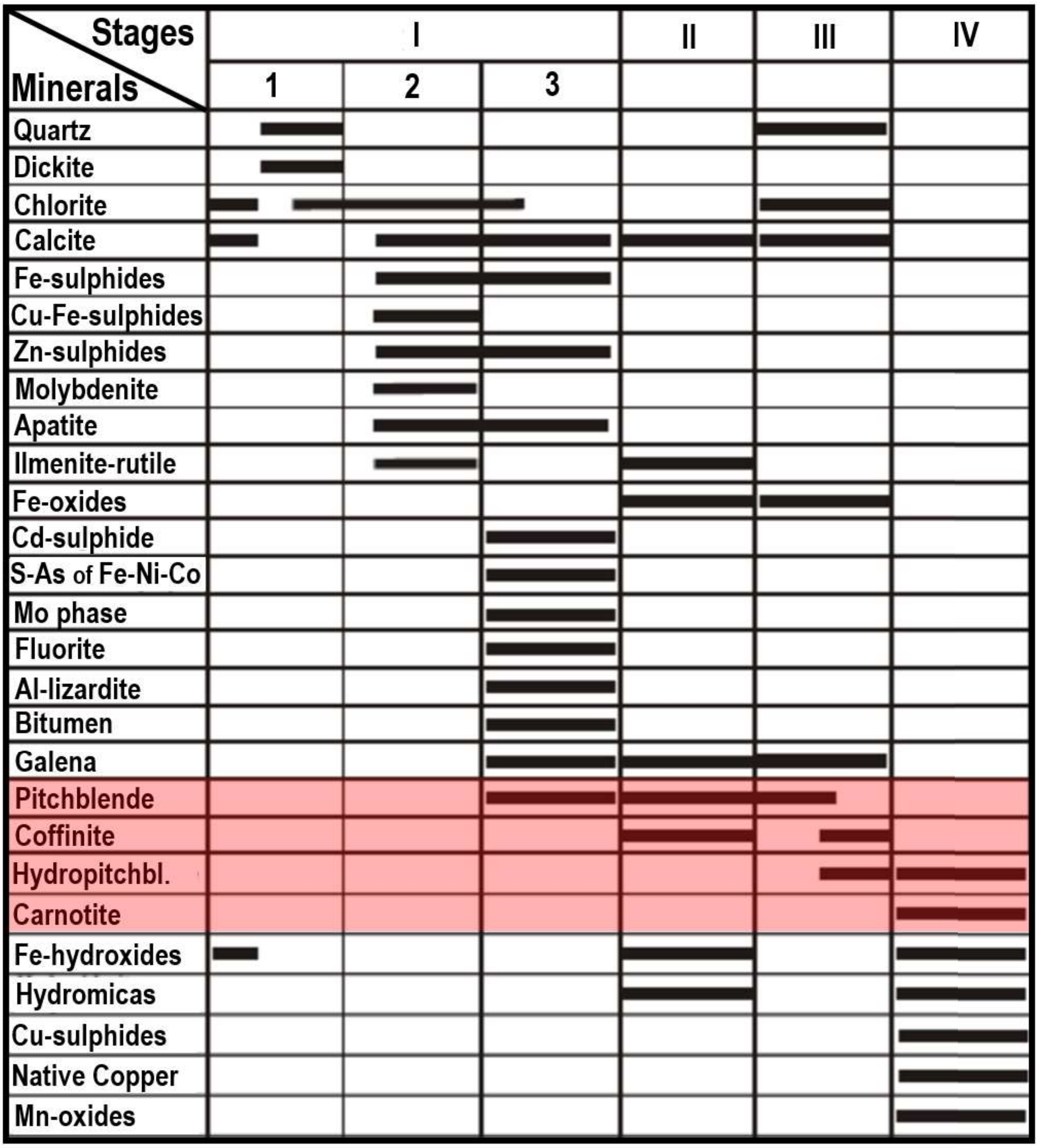

FIG. 3.21. Mineral paragenesis for the Karku deposit (modified from Shurilov [3.368]).

3.7.4.6. Geochronology

Interpretation of the isotopic data for pitchblende is difficult because of strong alteration and heterogeneity of the uranium minerals. The SIMS uranium-lead isotopic analyses of pitchblende from the Karku deposit have an upper intercept at 1496 ± 340 Ma and a lower intercept at 525 ± 310 Ma. These results are similar to previous isotopic data giving Lower-Middle Riphean ages [3.368].

Three isotopic analyses of a pitchblende from a vein at the Kotalakhti [3.368] give an upper intercept at 412 ± 730 Ma. This age may correspond to a remobilization during the Caledonian orogeny. By constraining the data from Karku to fit with a lower intercept at about 400 Ma, a better upper intercept of 1405 ± 76 Ma is obtained [3.368]. This age is close to the age calculated using lead isotopic data obtained by LA MC-ICP-MS [3.374], which gave an age of 1371 ± 46 Ma for pitchblende-1 and 1131 ± 32 Ma for pitchblende-2.

The uranium-lead isotope ratios determined on uranium oxides by LA-MC-ICP-MS by Rice [3.372] give a better-defined Concordia upper intercept of 1467 ± 39 Ma with a high MSWD (11.7). The lead-lead ages reveal several resetting events and indicate a maximum age of 1505 ± 20 Ma, consistent with the upper intercept uranium-lead age.

3.7.4.7. REE distribution in uranium oxides

The real earth elements patterns of pitchblende from the uranium ore of Karku are atypical for unconformity-related uranium deposits. The chondrite normalized real earth elements patterns of pitchblende from the high-grade ore of the Karku deposit is weakly bell-shaped, centred on samarium and europium, instead of terbium and dysprosium, with a significant enrichment in the lightest rare earth elements. The absolute rare earth elements content is also much lower than in uranium oxides from typical unconformity-related deposits.

The chondrite normalized rare earth elements patterns of pitchblende from the Kotalakhti ore-showing, are weakly fractionated from the light to the heavy rare earth elements, but its absolute amount of rare earth elements is relatively high. No europium anomaly is present. The completely different rare earth elements patterns obtained for the Kotalakhti uranium mineralization relative to Karku ore suggests that the Kotalakhti uranium mineralization has a different origin and results from a distinct Palaeozoic uranium mineralization event.

3.7.4.8. Fluid characteristics

Fluid inclusions have homogenization temperatures from 148–261°C in quartz and 105– 238°C in calcite from the ore zones, and 134–202°C in calcite from the post-ore veinlets [3.363]. Three types of fluids during the ore stage have been identified, NaCl-rich fluid (0.2 –12.8 wt%), a $MgCl_2$-rich fluid (1.8–19.5 wt%), and $CaCl_2$-rich fluid (16–42 wt%). The NaCl–rich fluid is only observed in quartz. Salt concentration in the fluid inclusions increases with the decreasing homogenization temperatures. Molecular H_2 and O_2 has been identified in the gas phase of the inclusion hosted in quartz by Raman spectroscopy. Sporadically, CO_2 and CH_4 have been identified, along with carbonaceous material. A pressure of less than 50 bars during ore deposition is proposed by Velichkin et al. [3.363], but the method of estimation is not precise.

3.7.4.9. Stable isotopes

Oxygen and hydrogen isotopic compositions have been measured in five samples from different alteration zones (A to C, from the most internal to the most internal external zones of the deposit) of the Karku deposit by Rice [3.372]. The $\delta^{18}O$ values of matrix clays from the <2µm size fraction of four samples range from 8.9‰ to 9.1‰ in zone A and 11.2‰ to 15.5‰ in zone B, whereas δD ranges from –58‰ to –46‰ throughout both zones. In zone C, $\delta^{18}O$ values range from 14.6‰ to 16.9‰ and δD ranges from –72‰ to –62‰.

Using a formation temperature of 210ºC for the syn-ore event deduced from fluid inclusion studies on syn-ore carbonates [3.363] and chlorite geothermomentry [3.372] and 130ºC for the pre-ore event in Zone C, based on the smectite-illite transition identified in Pollastro [3.375], and the lower fluid inclusion homogenization temperatures from calcite from the external alteration zones [3.363], calculated $\delta^{18}O$ values of the fluids range from 6.0‰ to 12.7‰ and

δD from –8‰ to 4‰ in zones A and B, and $\delta^{18}O$ ranges from 3.3‰ to 6.0‰ and δD from –55‰ to –44‰ in zone C.

The $\delta^{18}O$ increase of ~3‰ and δD of ~40‰ from the pre-ore to the syn-ore fluids indicate a different origin of these fluids. The data for pre-ore fluids are consistent with their derivation from low-latitude meteoric waters and those for the syn-ore fluids correspond to modified seawater. Both have become richer in ^{18}O through their interaction with the sedimentary rocks of the basin, with minor effect on the δD values if the water-rock ratios were low [3.376].

3.7.4.10. Metallogenic model of the Karku deposit

The Paleoproterozoic metasediments surrounding the granitic-gneiss domes typically originate from epicontinental sedimentation with meta-arkoses, limeston, marls and black shales deposited between 2.1 and 1.0 Ga. They were probably significantly enriched in uranium as shown by the widespread Svecofennian uranium mineralization occurring in migmatites, pegmatoids and skarns described in the basement rock, carbonate rocks and sodium-metasomatites of the Raahe-Ladoga basement by Shurilov [3.368].

Erosion of the basement uranium-enriched rocks led to a uranium enrichment of the Riphean sediments. The earliest radioactive anomalies in the Priozersk sediments correspond to heavy mineral layers with uranium- and thorium-bearing minerals such as monazite, zircon and ferrithorite. They represent one of the possible uranium sources for the deposits, because they have been partly altered during the diagenesis [3.377]. Altered zircon are uranium and thorium enriched from 0.04 wt% uranium and 0.06 wt% thorium in unaltered grains up to 1.5 wt% and 2.0 wt% in altered grains, respectively.

The first stage of diagenesis in the Riphean sediments corresponds to the replacement of the sandstone cement and clasts by dickite. Quartz and especially feldspar clasts are corroded, but compared to the huge quartz dissolution occurring in unconformity-related deposits, this process was relatively weak in Karku. While feldspar clasts disappear in the central part of the alteration halo, quartz — although partially corroded — remains present everywhere.

The second stage of alteration is represented by intense carbonatization of the sandstone and of the upper part of the regolith. This alteration is associated with a wide development of Fe-chlorite (FeO/MgO = 5.4 ÷ 7.5), local sulphidization and new formation of apatite, rutile and ilmenite. The third stage corresponds to the deposition of the earliest generation of uranium mineralization, i.e. pitchblende-1, at about 1405 ± 76 Ma. This stage of alteration consists of aluminium-magnesium-chlorite, aluminium-lizardite, sulphides (galena, cadmium-sphalerite, cobalt-nickel arsenides), and minor fluorite and apatite. Bitumen has been observed but the paragenesis is unknown. During the fourth stage, pitchblende-1 is replaced by pitchblende-2, coffinite, haematite and illite. Low-grade coffinite mineralization at the periphery of the main orebodies is often associated with sulphides and haematite. The fifth stage consists of several generations of veinlets cutting the primary ore and the whole sequence. Late chlorite, calcite, quartz, chalcedony, barite, fluorite, galena, chalcopyrite, pyrite, marcasite, haematite, coronadite, hollandite and romanechite also occur in the veinlets during this stage. The sixth stage corresponds to supergene alteration, represented by limonitiztion and kaolinitization with hexavalent uranium minerals developed along late fractures.

3.7.4.11. Main parameters controlling the uranium mineralization

- The lower part of the Priozersk Riphean sequence located below the first basaltic layer controls the main uranium orebodies probably because of the presence of conglomerates and coarse-grained arkoses having a higher permeability for the circulation of the fluids. Low grade uranium mineralization may also occur in the middle and upper levels of the sediments;
- The wide sulphide-chlorite-carbonate alteration halo enveloping the orebodies is evidence for the permeability of the Priozersk sequence;
- The upper part of the regolith may also have had higher permeability because it hosts some uranium mineralization. Basement rocks that are devoid of a regolith do not host uranium mineralization;
- Graphite- and sulphide-rich schists may have played a role as reductants because high-grade ores are localized above the Impilakhti suite biotite schists with more than 10% graphite. The grade of the ore correlates with graphite content;
- The Riphean unconformity also represents a preferential fluid circulation zone as the main orebodies occur along the unconformity;
- Valley-like topographic depressions of the unconformity surface also control uranium mineralization, because the graphite- and sulphide-rich schists were more susceptible to erosion, which created interdome depressions when the basement was outcropping, and especially along the faulted zones of the basement;
- Reactivation of the NW- to NE-striking Palaeoproterozoic basement faults is the main control on the occurrence of the uranium mineralization by creating pathways for fluid circulation. These faults intersect, but rarely offset the Riphean sediments. The highest graphite and sulphide enrichments occur along these faults. The highest-grade ores in orebody 2 and 3 are related to the intersection of NW and NS faults, and NW and NE-striking faults for orebody 1;
- The basalts of the lower subsuite of the Salmi suite have played a minor role in controlling several small uranium occurrences in fractured basalts;
- The fluid circulation around the Karku deposit has created geochemical anomalies, which can be used for exploration. The sediments have higher background uranium content and a higher proportion of labile uranium, as well as higher molybdenum, silver, lead, zinc, arsenic and manganese content [3.378]. A 1200 × 400 m halo with lower thorium content (<12 ppm) is associated with orebody 3 [3.379]. The basalts of the Salmi suite lower layer are also enriched with up to 5 ppm uranium, above orebodies compared to background values of 2 ppm uranium [3.378]. The Quaternary sediments above the orebodies also contain radon anomalies [3.380].

3.7.4.12. Comparison between the Karku deposit and unconformity-related deposits

The Karku deposit has the following similarities and differences with the unconformity related deposits.

- The uranium orebodies extend mainly along a regional unconformity between Archean to Paleoproterozoic basement rocks and non-metamorphosed clastic sediments, similar to Cigar Lake, Canada. The extension of the mineralization into the basement is very limited compared to many other unconformity related deposits in Canada and Australia;
- The basement rocks have a similar age and composed of similar lithologies as the rocks from the Athabasca Basin, Canada and Kombolgie Basin, Australia;

Paleoproterozoic metasediments were deposited in an epicontinental environment significantly enriched in uranium;

- The Pasha Ladoga Basin is Mesoproterozoic with sedimentation starting at 1470 MA whereas the Athabasca and Kombolgie Basins formed during the Paleoproterozoic (1740 to 1730 Ma, [3.77, 3.381]) and continue at least until 1541 ± 13 Ma [3.156];
- The Riphean siliciclastic sediments of the Pasha Ladoga Basin are much less mature in comparison with the highly quartzose sediments of the Athabasca Group. The Ripheansediments are rich in potassium-feldspar, plagioclase, which have been altered by alkaline pH during diagenesis. The alteration of the feldspar during the diagenetic-hydrothermal event has created large amounts of clays, which rapidly decreased the initial permeability of the siliciclastic sediments. Also, the thickness of the Priozersk formation through which the main hydrothermal diagenetic fluid circulation has occurred was much thinner (<40 m) than in the Athabasca Basin (several hundreds of metres and probably no more than 1 km). The Priozersk formation is covered by two continuous layers of basalts, with a cumulative thickness of more than 200 m which has focussed diagenetic fluid flow in the upper part of the basin. A 'free convection' model [3.102] cannot be applied to the Karku deposit because a convection cell could have formed in the confined space between the sedimentary cover and basalts;
- The weak development of diagenetic overgrowths on detrital quartz and the presence of kaolinite in the cement of the non-altered sandstones in the Karku area, rather than dickite, which is common in the Athabasca Basin, is likely related to lower water/rock ratios because Riphean sediments in the Salmi depression are relatively thin at the time of the diagenesis;
- The intensity of the alteration in the regolith is relatively moderate and the regolith thickness is much thinner in the Karku deposit area compared to the regolith associated with the Athabasca Basin. Regolith alteration zones characteristic of the Athabasca Basin (upper oxidized red zone and lower reduced greenish one) have not been identified in the Karku area. If this alteration dominantly results from the circulation of oxidized basinal brines [3.382], its absence at Karku is an indication of a lower water/rock ratios or less reactive brines;
- The chemical (highly saline fluids with high calcium content) and physiochemical characteristics of the fluids (homogenization temperatures varying from 105 to 261°C) in the Karku deposits are similar to those identified with regard to the Athabasca and Kombolgie Basins [3.97, 3.98, 3.101] except for the pressure conditions which are lower (less than 50 bars at Karku);
- Alteration of zircon has been observed in all basinal and basement lithologies of the Pasha Ladoga region and are, similar altered zircons observed in the Athabasca basin and basement. These zircons may be a source for the uranium. However, the observed weaker alteration of monazite suggests that fluids were less aggressive than the fluids from the Athabasca and Kombolgie Basins;
- Uranium mineralization is controlled by Paleoproterozoic fault zones rooted in the basement, which were reactivated during the ore stage. These faults extend into the siliciclastic sediments of the overlying basin similar to the Athabasca Basin;
- The mineralized fault zones are essentially rooted in graphite- and sulphide-rich metasediments in the basement at Karku and in the Athabasca Basin;
- Breccias frequently associated with uranium mineralization in the Athabasca basin [3.203] have not been observed in the Karku area; only a relatively weak cataclasis is associated with the ore hosted in the sandstones at the Karku deposit;

- The uranium mineralization at Karku is surrounded by a chlorite alteration halo in the host rocks, but the chlorite at Karku is very rich in iron, whereas the chlorite associated with other unconformity-related deposits is aluminium-magnesium rich sudoite. The most intense alteration is associated with high-grade uranium mineralization in the Karku deposit. This alteration is rich in carbonates, which are rare and paragenetically late in the Athabasca Basin. The presence of carbonates with the uranium mineralization confirms the pH of the diagenetic-hydrothermal fluids in the Karku area was relatively higher than the pH of the fluids associated with the unconformity-related uranium deposits from Canada and Australia;
- Uranium ore at Karku is composed mainly of pitchblende and coffinite similar to the ore from the Athabasca Basin. High-grade ore from the Karku deposit is surrounded by a wide halo of low-grade mineralization forming the main part of the deposit resource, whereas the ore zones in the Athabasca Basin consist mainly of high-grade ores lenses with sharp decrease of the uranium grade in the host rocks. uranium oxides from all unconformity-related deposits have a bell shape rare earth elements pattern and high total rare earth elements, whereas ore from the Karku deposit have rare earth elements patterns similar to those of vein type deposits and much lower rare earth elements content;
- Epigenetic thorium enrichment of the sandstone and basement rocks in the vicinity of the uranium orebodies in the Karku deposit has not been observed at other unconformity-related deposits;
- The estimated age of the uranium mineralization at Karku is similar to Athabasca Basin ore deposits (1500–1100 Ma);
- Sulphides, sulphoarsenides and arsenides also accompany the uranium mineralization at Karku.

3.7.5. Bertholène, France

3.7.5.1. Regional geology

The Bertholène deposit located in the northern Rouergue (Fig. 3.22), southern part of the Massif Central, has been considered by Pagel [3.383] as an example in France of a uranium orebody spatially related to an unconformity. Resources have been estimated at 2000 tU at 0.11% uranium, recognized to a depth of 200 m.

The basement is of Variscan age and consists of a pile of thrusted metamorphic units comprising micaschists, paragneisses, orthogneisses, metabasic rocks and migmatites. This basement is covered by sedimentary basin filled with Carboniferous to Jurassic sediments (Fig. 3.23). The Bertholène uranium deposit is hosted in the Palanges monzonitic orthogneiss (542 ± 50 Ma, [3.384]) close to the unconformity with the Carboniferous sedimentary formations, which consists of alternating sandstone and coal layers. The northern part of the Palange orthogneiss presents mylonitic bands. Wrench faulting leads to brittle structures trending N160°E, N20°E and N50°E. During Permian times, these faults are responsible for the formation of the Rodez basin in a WNW-ESE oriented graben. During the Pyrenean tectonic event WNW-ESE, normal Permian faults were reactivated, which led to the overthrusting of both the metamorphic basement and the Carboniferous sedimentary cover onto the Jurassic sedimentary formations of the Rodez basin.

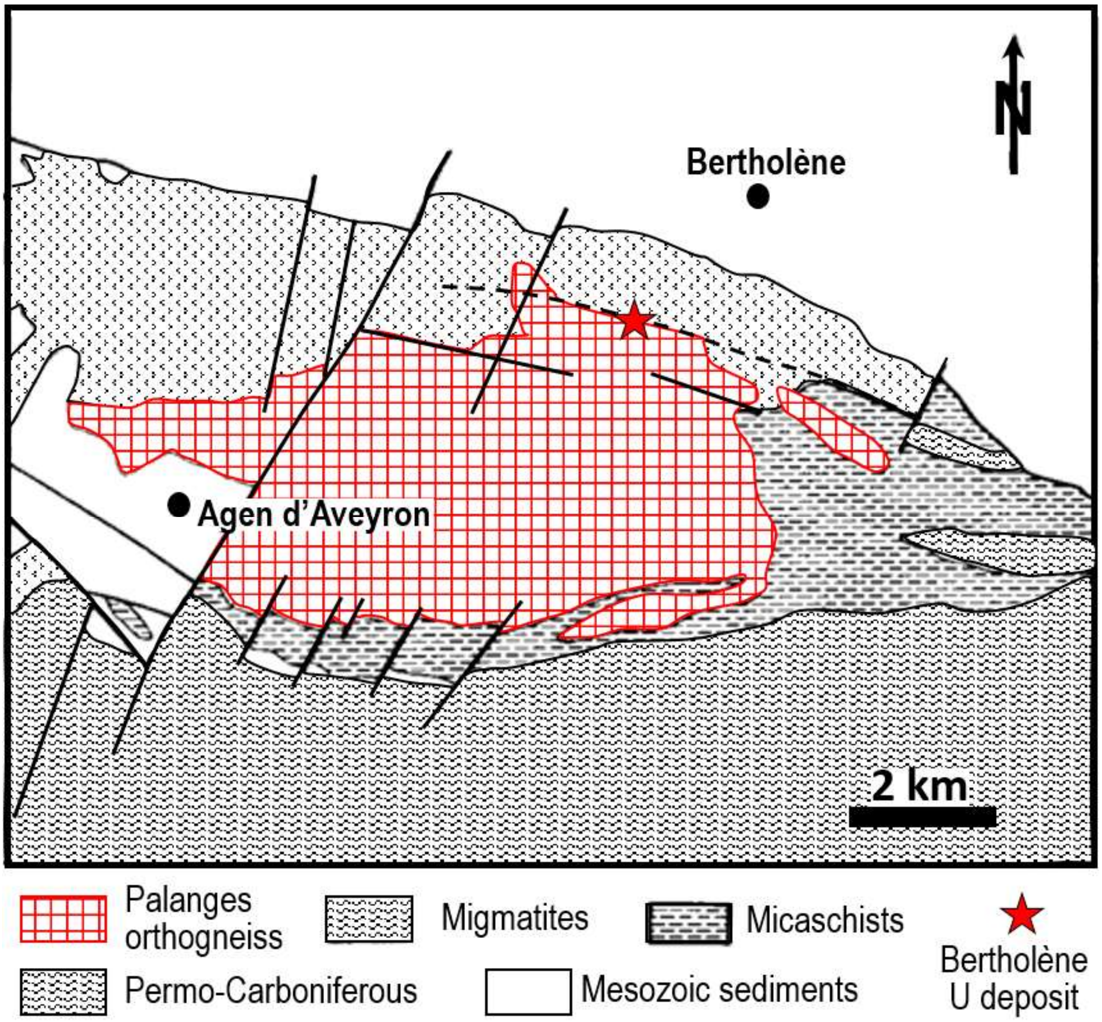

FIG. 3.22. Simplified geologic map of the northern Rouerge area (modified from Levêque et al. [3.384]).

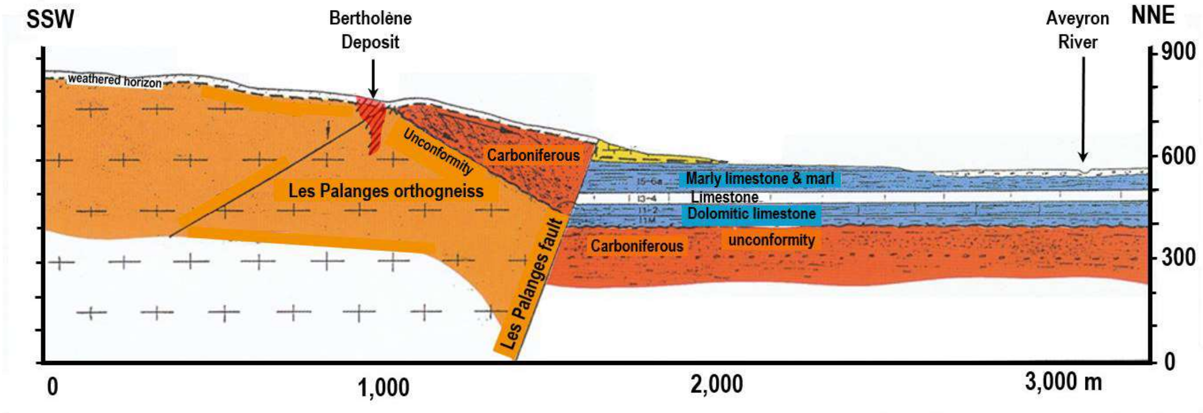

FIG. 3.23. Geologic cross-section showing the position of the Bertholène uranium deposit (modified from SCUMERA unpublished document).

3.7.5.2. The Bertholène uranium deposit

In the Bertholène uranium deposit, the mineralized veins have an average N40°E direction with a 45°SE to NW dip. The first hydrothermal alteration event which corresponds to albitization has a regional extension and is locally associated with crystallization of adularia [3.385]. Adularia has been dated by K/Ar at about 210–200 Ma. The mineralized zones are typically associated with the early stage of albitization, followed by argillization, silicification and carbonatization, which extends into the Permian-Carboniferous sediments [3.386]. The primary uranium mineralization consists of uranium oxides crystallized with the cube and octahedron faces as well as spherolites deposited on euhedral quartz crystals and in veinlets filled with pyrite and uranium oxide. Small amounts of marcasite, chalcopyrite, sphalerite and galenaare also observed. The uranium oxides have high ZrO_2 contents (1 wt% in the average). A lead-lead isotopic age of 173 ± 9 Ma was calculated for uranium oxide deposition [3.384].

The fluid inclusions in the albite crystals are monophased, which indicate low-temperature crystallization. During the second stage, albite is altered to smectite and illite, and is followed by the crystallization of quartz. The fluid inclusions in the quartz crystals are filled with an aqueous sodium chloride-rich fluid (8–14 eq wt% NaCl) and give homogenization temperatures comprised between 135 to 140° C, and corresponding to trapping temperatures of about 160°C [3.386]. The fluid associated with carbonate deposition (dolomite and Fe-dolomite) has a low salinity (1 eq wt% NaC1) and a homogenization temperature of 110°C [3.386]. Primary uranium minerals have been largely replaced by coffinite during an Oligocene event (~30–40 Ma; [3.384]).

3.7.5.3. Comparison with unconformity deposits

The Bertholène deposit occurs close to an unconformity with a sedimentary basin and saline fluids of possible basinal origin are associated with ore deposition. These features led Pagel [3.383] to propose that it belongs to the unconformity-related deposit types. However, the following differences can be underlined.

- The alteration associated with the mineralization is very different, with an early albitization followed by low temperature clay minerals, instead of the characteristic magnesium-rich alteration minerals (sudoïte and dravite) in typical unconformity-related deposits. The fluids were probably more alkaline at Bertholène deposit;
- Lower temperature and salinities of the fluids, together with their more alkaline character indicate that these fluids were much less aggressive than the ones associated to unconformity related deposits, and probably explain the much lower grades and tonnage of the deposit;
- Absence of strongly reducing component in the basement: the host rock is a hematized orthogneiss instead of graphitic schists;
- Oxidized sandstones are absent and organic matter-bearing Carboniferous sediments are present. Oxidized sandstones are common at other unconformity-related deposits.

3.7.6. Cuddapah Basin, India

3.7.6.1. Geological setting

The Paleoproterozoic Cuddapah Basin is located in the eastern Dharwar Craton. Several low grade – low tonnage uranium deposits, Lambapur (1370 tU at 0.094% uranium), Peddagattu (6.000 tU at 0.04% uranium), Chitrial (between 5000 and 10 000 tU at 0.05 to 0.10% uranium) and Koppunuru (700 tU at 0.07% uranium), have been discovered at the unconformity contact between basement granitic rocks and the Palnad sub-basin, at the northern part margin of the Cuddapah Basin (Fig. 3.24).

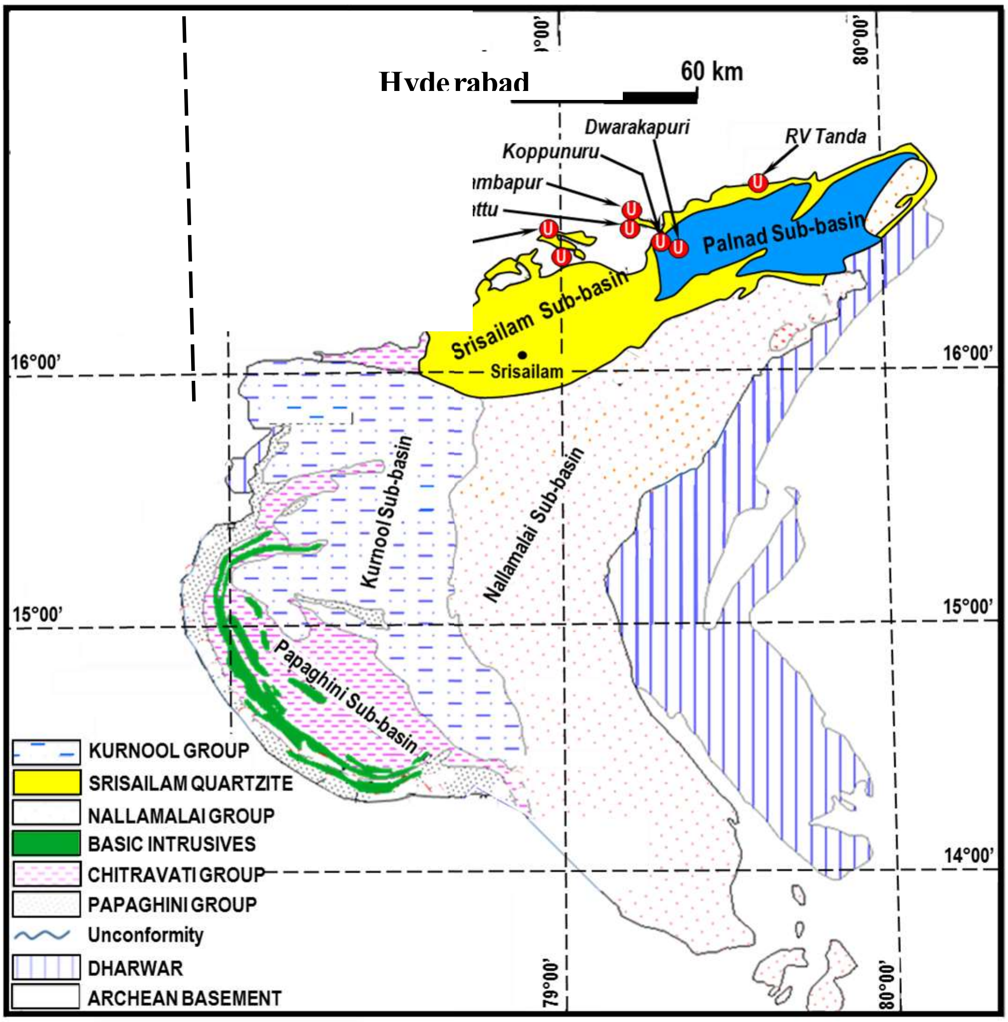

FIG. 3.24. Geological map of the Cuddapah Basin with the different sub-basins and the uranium deposits associated to the Srisailam-Palnad sub-Basin (modified from GSI [3.387], Bhoopathi et al. [3.388]).

The Cuddapah Basin presently extends over an area of 44 500 km^2 and is filled with a 12-km thick pile of unmetamorphosed Paleo- to Neo-proterozoic sedimentary and volcanic rocks subdivided into the Cuddapah Supergroup and the Kurnool Group. The Cuddapah Basin comprises six sub-basins: Papaghni, Chitravati, Nallamalai, Srisailam, Kurnool and Palnad. In the western part of the basin, the sedimentary formations unconformably overlies Archean to

Palaeoproterozoic gneisses, greenstone belts and granites. The sediments of the Cuddapah Basin predominantly consist of siliciclastic to argillaceous sediments with calcareous and dolomitic limestone layers. In the northern part of the Basin, the major faults are striking NNE-SSW and ENE-WSW. Mafic dyke swarms radiating over the whole Dharwar craton are interpreted by French et al. [3.389] as resulting from a ~30 Ma (2.21–2.18 Ga) stationary mantle plume, tentatively linked to a major rifting episode at the western margin of the craton. This rifting episode lead to the breakup of a larger Paleoproterozoic continent and possibly initiated the formation of the Cuddapah Basin. A summary of the available geochronological (K–Ar and $^{40}Ar/^{39}Ar$ ages) and geochemical data for the mafic dykes surrounding the Cuddapah basin by Mallikarjuna et al. [3.390] indicates three major ages of emplacement at 1.9–1.7, 1.4–1.3, 1.2–1.0 Ga, with a minor event at 650 Ma.

The uranium deposits are spatially related to the Neoproterozoic Srisailam and Palnad sub-Basins, which form the northern part of the Cuddapah Basin and extend over 6400 km^2. The Srisailam sub-Basin (3000 km^2) is filled with the Neoproterozoic Srisailam Formation, which is the youngest unit of the Cuddapah Supergroup, and consists mainly of siliciclastic sediments with minor shale intercalations. The sediments reach a maximum thickness of 300 m and dip very gently SE (3–10°). The underlying basement rocks consist of Archean to Paleoproterozoic gneisses and granites (2482 ± 70 Ma to 2268 ± 32 Ma [3.391, 3.392]; 2659 ± 120 Ma [3.393–3.395]). To the south, the Srisailam Formation unconformably overlies the Nallamalai Group sediments. In the northern part of the Srisailam sub-Basin, the sediments form a series of 100–150 m high outliers. The uranium deposits are located below these outliers. The Srisailam Formation starts with a pebbly gritty arenite layer, overlain by pyritic black shale and shale/quartzite intercalations, followed by massive quartzite and limestone. The quartzite is highly silicified and displays primary sedimentary structures: bedding, laminations, cross-stratification, ripple marks, with pyrite, haematite and goethite.

The Palnad sub-Basin extends over 3400 km^2, dips gently to the east, and unconformably overlies gneisses and granites. The sedimentary succession (10–450 m thick) comprises the Banganapalle quartzite/shale, the Narji limestone/calcareous shale, the Owk shale and the Paniam quartzite.

The basement is made entirely of a leuco to mesocratic, equigranular, medium to coarse-grained porphyritic highly potassic granite. It is composed of quartz, potassium-feldspar, plagioclase, with minor amounts of biotite, rare hornblende. Iron-titanium oxides are ilmenite and magnetite, and radioactive accessory minerals are zircon, allanite, and monazite. Uraninite also occurs as inclusions in biotite and feldspar and has syn-magmatic characteristics. Fractures are filled with chlorite, titanite, epidote, and locally uranophane. The granite is enriched in thorium ($11 < Th < 61$ ppm, m = 35 ppm) and uranium ($10 < U < 116$ ppm, m = 27 ppm), and has relatively low Th/U ratios ($2.9 < Th/U < 0.43$) [3.396]. Mafic dikes intrude both the basement and the sedimentary rocks and may be locally mineralized.

3.7.6.2. Ore deposits

The uranium deposits of the Srisailam and Palnad sub-basins are referred to as ‘unconformity proximal’ by local geologists, because they occur as thin, tabular orebodies, along the unconformity between the Archean granitic basement and the Middle Proterozoic Srisailam sediments (Fig. 3.25). They occur at shallow depths (1–60 m).

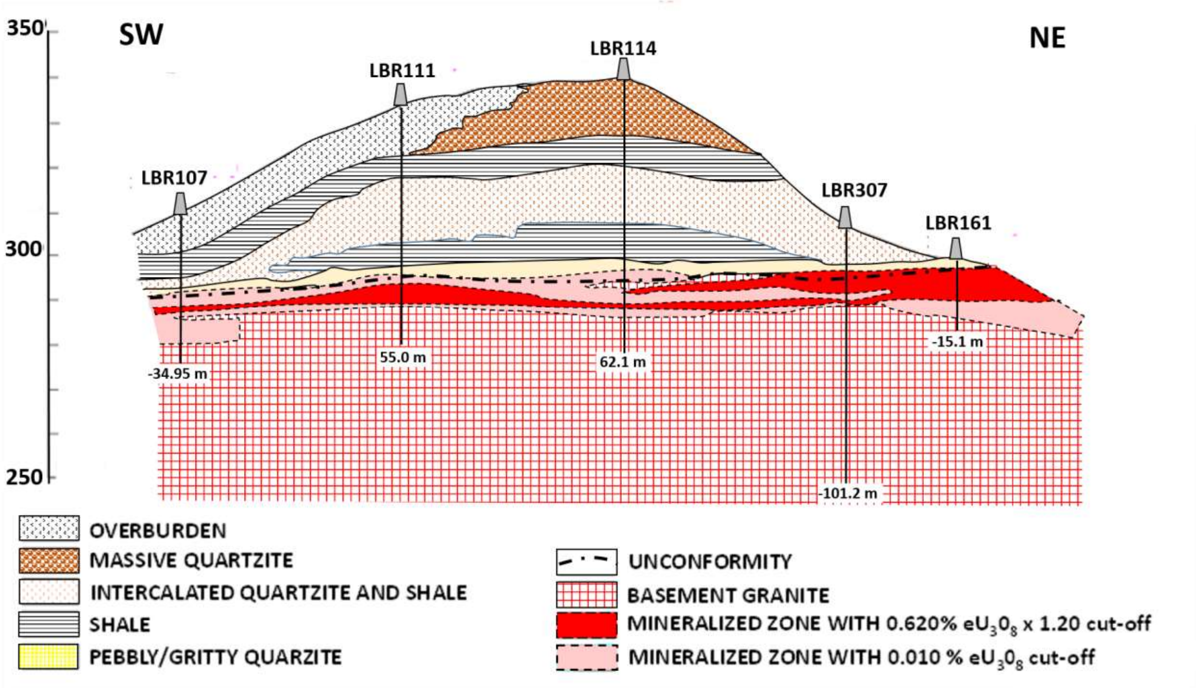

FIG. 3.25. Cross-section through the Lambapur uranium deposit in the Srisailam sub-Basin, where the uranium mineralization straddles the unconformity (modified from Sinha [3.235]).

In the Lambapur deposit, the Srisailam sediments vary from feldspathic sandstone to arkose. The alkali feldspar content may reach 40% in some samples. Mafic dikes and quartz veins intruding the granitic basement rocks may be mineralized in the vicinity of the unconformity. The uraninite and secondary uranophane is hosted by chloritized granites and partly in the feldspathic sandstone at the base of the Srisailam Formation. Occasionally, small quartz veins may bear some lead and copper minerals. The intensity of fractures within the granite, and their intersection with the unconformity, seems to control the location, shape and grade of the orebodies. The uranium enrichment occurs along NNESSW and NW-SE fractures in the basement.

The main uranium minerals in the Peddagattu and Lambapur deposits are pitchblende, uranophane, kasolite, with small amounts of galena, pyrite and chalcopyrite. Organic matter blebs have been locally observed in granite fractures. The primary uranium mineralization is interpreted as epigenetic hydrothermal [3.397].

The Koppunuru uranium deposit is located in the Palnad sub-Basin. Uranium mineralization is mainly confined to the Banganapalle sediments, the basal unit of the Kurnool Group (Fig. 3.26). The Banganapalle Formation (10–173 m thick) consists of a basal conglomerate, quartz arenites with intercalation of grey shales, and is overlaid by the massive limestone and calcareous shale of the Narji Formation (100–260 m thick). The thickness of the sedimentary pile to the SE ranges from 10 to 450 m [3.398]. The uranium mineralization that occurs, has horizontal lenses concordant with the sedimentary bedding, mainly in the basal conglomerate horizon and also in the upper quartzite unit intercalated with carbonaceous shale. Organic matter and pyrite commonly occur with the uranium mineralization, which suggest that they may have been involved in the reduction of uranium [3.399]. The orebodies occur between 5 and 40 m above the unconformity [3.400]. The resources estimated at Koppunuru correspond to a small tonnage at a medium grade.

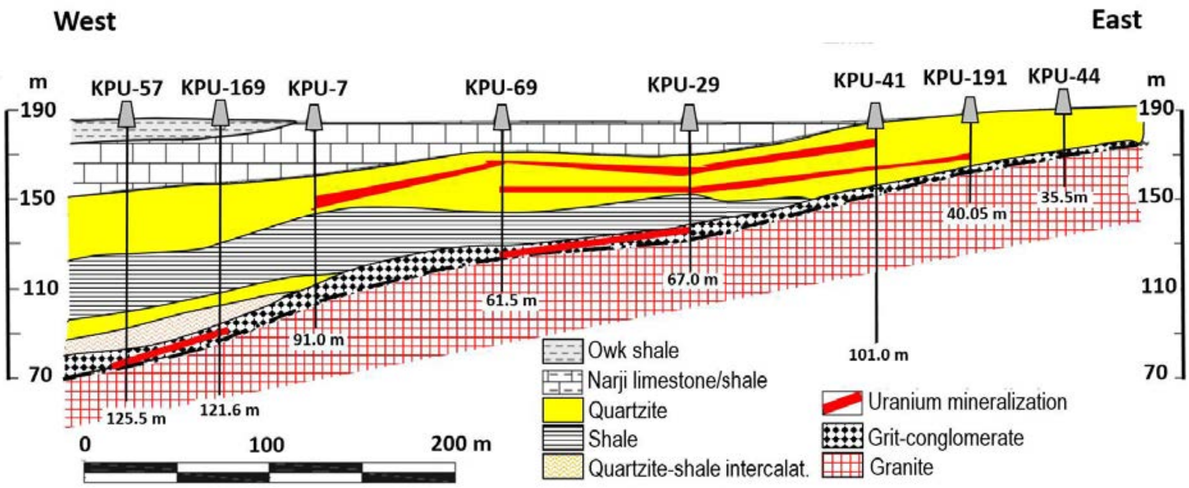

FIG. 3.26. Cross-section through the Koppunuru deposit in the Palnad sub-Basin, where uranium mineralization is hosted in the basal sedimentary formation above the unconformity (modified from Ramesh Babu et al. [3.401], Thomas et al. [3.402]).

Both the granite and the sediments are pervasively hydrothermal altered and are crosscut by several generations of veins. Quartz occurs in veins, chlorite is essentially developed in the granite and rarely in sediments, epidote only occurs in the granite away from the unconformity, illite is pervasively developed in the granite and the arkosic quartzite up to a few metres on each side of the unconformity.

3.7.6.3. Ore deposit model

The Lambapur-Peddagattu, Chitrial and Koppunuru uranium deposits have a similar lithostructural setting, with comparable geological and geochemical controls. They all form elongated sheets parrallel to the Archaean-Proterozoic unconformity surface either mostly at the top of the granitic basement in the Lambapur-Peddagattu-Chitrial deposits, or at three different horizons of Banganapalle quartzite above the unconformity and less mineralization in basement granite in the Koppunuru deposit.

The hydrothermal alteration is developed mainly in the granitic basement associated with the Lambapur-Peddagattu, Chitrial and Koppunuru uranium deposits. Illitization and chloritization can extend into the lower sedimentary layers of the basin. The epidote observed in the deeper part of the basement may be related to postmagmatic alteration of high-potassium calc-alklaine granites. Quartz veins with illite in the basement and chlorite in the sandstone is common and straddles the unconformity. The development of illite and chlorite requires the percolation of relatively acidic fluids. Carbonaceous matter occurs as colloform aggregates and discrete euhedral crystals of pyrite commonly occur in illitized zones.

Primary biphase aqueous inclusions have a wide range of salinity (1.9 to more than 23.2 wt% NaCl eq.) in the quartz veins near to the unconformity, with lower salinities (0.2 to 11.7 wt% NaCl eq.) away from the unconformity These inclusions are NaCl–KCl dominant in veins located in the sediments and granite close to unconformity and their composition becomes $MgCl_2$ dominant with increasing depth below the unconformity contact. In the R.V. Tanda deposit, $CaCl_2$-rich inclusions have been observed. Homogenization temperatures (Th) of the inclusions range from 81.7 to 226.4°C, where the higher Th are observed at the deepest levels. In the Palnad sub-Basin, the maximum thickness of preserved cover sediments reaches 633 m and in the Koppunuru and R.V. Tanda area, the thickness of the cover is only 60–200 m. Thomas et al. [3.402] consider that the thickness of the sedimentary cover has never exceeded 650 m, and they conclude that pressure correction on Th is not necessary and that Th values can be considered as representing temperature of the hydrothermal fluid. However, other lithological units, presently eroded, may have been present above the Kurnool Group, and a temperature correction of the Th may be necessary.

The large variation in salinity relatively to the narrow range of homogenization temperatures of the fluid inclusions has been interpreted by Thomas et al. [3.402] as a mixing of two fluids. The low to moderate saline fluid would correspond to the basinal brine, whereas the hypersaline inclusions would correspond to evolved brines formed as a result of hydrothermal alteration. However, there is an alternate interpretation for the origin of the saline fluids. As commonly observed at the margin of the sedimentary basins [3.130, 3.403], the brines may derive from deeper part of the Cuddapah basin to the SE, which explains the temperature reaching more than 200°C, and could have migrated along the unconformity surface producing the illitic alteration of the upper part of the granite and in some sedimentary layers, and then mixing with low saline surficial fluids.

The source of the uranium for the deposits is most probably the granite from the basement which is significantly enriched in uranium, has highly variable thorium/uranium ratios, and contains uraninite as an accessory mineral. The reductants may be the organic matter in the pyritic black shale layers. The degree of maturation of this organic matter is not known, but the oil window may have been reached because of the burial of the sedimentary series, which may have been covered by a thicker pile of sediments presently eroded. The origin of the carbonaceous matter associated with the pyrite crystal is not known. The carbonaceous nodules may derive from the black shale layers but may also result from an abiogenic process as shown by Sangély et al. [3.229] in the Athabasca deposits. An age of 1327 ± 170 Ma has been obtained from a samarium-neodymium isochron on uranium oxides from the Lambapur deposit by [3.404].

3.7.6.4. Comparison with unconformity related uranium deposits

Compared to unconformity-related uranium deposits, the Chitrial-Lambapur-Peddagattu-Koppunuru deposits have the following differences and simlarities.

- Graphite-bearing Paleoproterozoic metasedimentary rocks and associated shear zones controlling the ore bearing structures do not exist in the basement, the basement is only granitic;
- The overlying basin as a varied lithology (meta-arkoses, massive quartzite, black shales, limestone), which is different from the mature quartzose sandstone of the Athabasca or Kombolgie basins. The siliciclastic rocks in the Srisailam and Palnad sub-basins are generally highly silicified and the feldspar in the arkoses may be preserved close to the unconformity. Therefore, the permeability of the Srisailam and Palnad sub-basins was very low, the redox variations were very important, with the presence of strong reductants in the black shale layers, the siliciclastic rocks were much less mature (abundance of preserved feldspars), and the initial thickness of the basins where the uranium deposit occur was probably less important;

- The uranium mineralization form elongated sheets parallel to the Archaean-Mesoproterozoic unconformity either mostly in the granitic basement in the Lambapur-Peddagattu-Chitrial deposits, or at the base of the sedimentary formations in the Koppunuru deposit, with minor structural controls, whereas in unconformity-related deposits are structurally controlled and occur within reactivated structures rooted in basement rocks;
- The fluids have similar temperature as those of the Athabasca and Kombolgie Basins, but their salinity is generally lower;
- The alteration paragenesis is different where iron-rich chlorite is associated with illite in the Indian deposits instead of dominantly magnesium-rich alteration minerals (sudoite and dravite) in the Athabasca and Kombolgie Basins;
- In the Chitrial-Lambapur-Peddagattu-Koppunuru deposits, the reductants are absent in the basement of the Srisailam and Palnad sub-Basins, but are present in the sedimentary sequence above the unconformity.

3.7.7. The Lufilian Belt, DRC

3.7.7.1. Regional geology

The Lufilian Belt overlaps the external fold-and-thrust belt to the south of the Democratic Republic of Congo (DRC) and the northern part of Zambia in the Domes region. Folding and metamorphism occurred during the Pan-African orogeny. The Lufilian belt is essentially known for its sediment hosted copper-cobalt deposits and is commonly called the Central African Copper Belt [3.405–3.408]. This belt also hosts about 42 uranium showings and deposits [3.409] (Fig. 3.27).

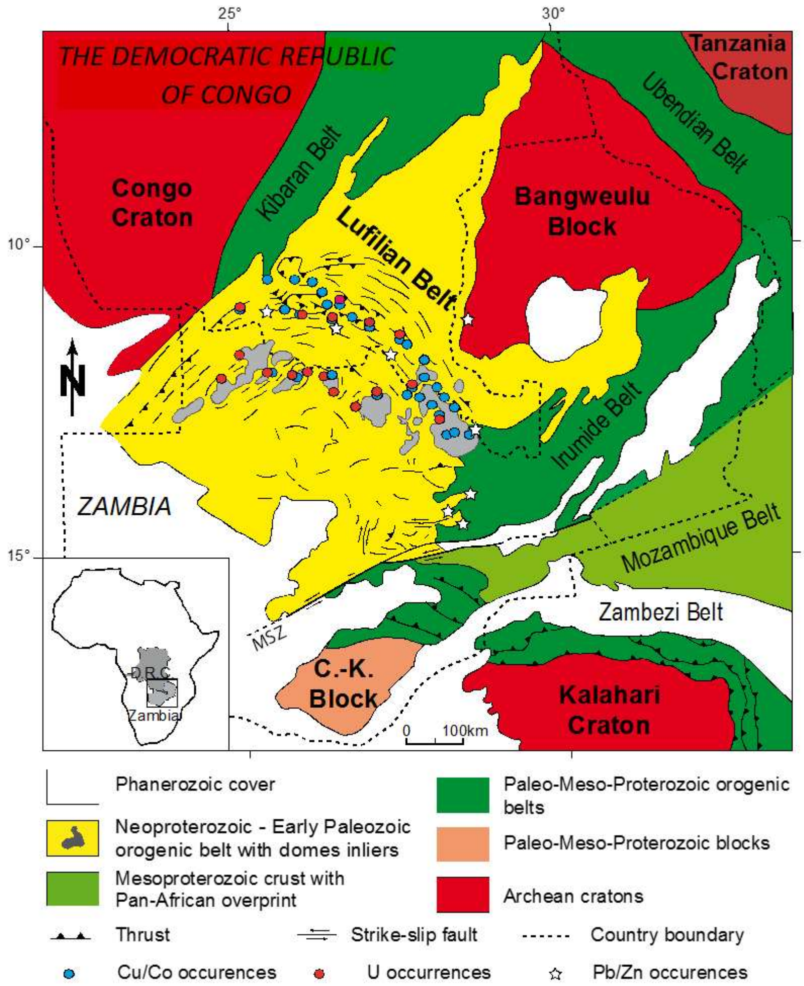

FIG. 3.27. Geological map of the Lufilian Belt with the main tectonic structures trends and U, Cu-Co and Pb-Zn deposits (modified from De Waele et al. [3.411]). C.-K. = Choma Kalomo block, Kbp = Kabompo Dome; Kfu = Kafue Anticline; Lwh = Luiswishi Dome; Mbz = Mwombezhi Dome; MSZ = Mwembeshi Shear Zone; Slz = Solwezi Dome.

The Lufilian Belt formed during the Pan-African orogeny as a result of the collision between the Kalahari and the Congo cratons participating in the amalgamation of the Gondwana supercontinent [3.411]. The external zone of the belt consists of the Neoproterozoic Katanga Supergroup metasediments, comprising the Roan, Nguba and Kundelungu Groups (Fig. 3.27), which have been folded, thrusted and metamorphosed to low greenschist facies. The internal zone of the belt corresponds to the higher-grade metamorphosed Domes region comprising a folded nappe pile of metasediments overlying migmatitic gneisses forming the core of dome-shaped structures (e.g. [3.412]).

3.7.7.2. The uranium deposits

Uranium mineralization occurs mainly within the basal Roan Group [3.413, 3.414]. In the external zone of the belt, dolomitic shale is the prevalent host rock, whereas in the Domes region carbonaceous quartzite and quartz mica-schists prevail [3.415]. Initially, the Shinkolobwe uranium deposit, located in the external zone of the belt, has been interpreted as being of magmatic origin [3.416]. Many authors have agreed that this deposit is syngenetic to early diagenetic in origin, because of the strong control on mineralization by the lithostratigraphy, similar to copper-cobalt deposits from the same area [3.409, 3.417–3.419]. More recently, Loris et al. [3.420] have proposed a re-concentration of the uranium during the Lufilian orogeny with an epigenetic origin for the mineralization. Ages ranging from 706 to 235 Ma have been attributed to these deposits (e.g. [3.409, 3.418, 3.421]). Recent uranium-lead in situ dating of uranium oxides by SIMS by Decrée et al. [3.422], yields two distinct sets of ages: 652 ± 7 Ma for the Shinkolobwe, Kalongwe, and Swambo deposits located within the most external zone of the belt, and 530 ± 6 Ma for uranium oxides from Kolwezi and Luiswishi deposits from the external zone of the belt, and Musoshi and Nkana deposits from the Domes region. An age of 542 ± 12 Ma has been also obtained by SIMS Cathelineau et al. [3.278] on the Kawanga occurrence in the Domes region. The c. 650 Ma mineralization event coincides with the formation of a proto-oceanic rift, whereas the 530–540 Ma one corresponds to the final collision stage of the Lufilian Belt [3.422].

The rare earth element concentration by SIMS on uranium oxides from the external zone of the Lufilian belt, dated at 650 Ma, has ‘bell-shape’ rare earth element patterns, [3.423] (Fig. 3.28) similar to rare earth element patterns of uranium oxides from unconformity-related –uranium deposits [3.424], whereas the 530–540 Ma uranium oxides have rare earth element patterns typical of synmetamorphic deposits [3.423] (Fig. 3.28). More specifically, the rare earth element patterns of the uranium oxides from Shinkolobwe are identical to those of the unconformity-related Shea Creek uranium deposit from the Athabasca Basin.

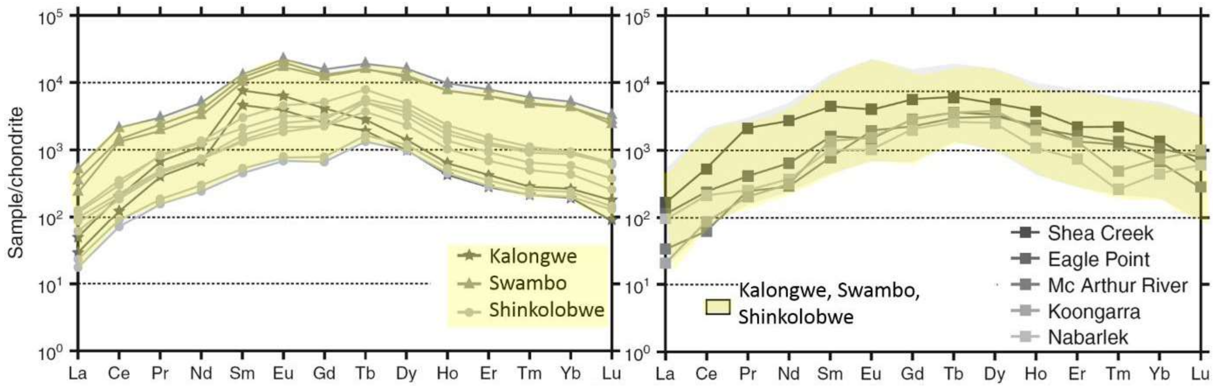

FIG. 3.28. REE patterns for the deposits of the external fold and thrusted belt of DRC, compared with typical unconformity related deposits from Canada and Northern Territory, Australia (modified from Eglinger et al. [3.424]).

3.7.7.3. Comparison with unconformity related uranium deposits

In addition to the rare earth element patterns for uranium oxides, the Shinkolobwe deposit with a Cu–Co–Ni–Fe–(Mo)–(Pb)–(Se)–(Au) sulphide assemblage has a similar mineralogical paragenesis relative to unconformity-related deposits [3.45]. Evaporitic layers known in the upper and lower part of the Katanga Supergroup were likely the source of the $MgCl_2$–$CaCl_2$–NaCl–KCl-rich fluids associated to the Shinkolobwe deposit. In the Shinkolobwe deposit, these fluids were trapped at temperature slightly higher than the classical unconformity related deposits (between 200 and 350°C) and at pressures of 1.00–1.25 kbar [3.425]. Moreover, hydrothermal alteration is characterized by late Mg-rich chlorite (26–33 wt% MgO, and 7 wt% FeO). The magnesium-rich diagenetic rims associated with detrital tourmaline grains are associated with haematite in the dolomitic siltstones of the Roan Group [3.413, 3.425, 3.426]. Eginger et al. [3.423] have proposed that the 650 Ma uranium mineralizing event in the external zone of the Lufilian Belt corresponds to a diagenetic hydrothermal circulation prior to the Pan-African metamorphic event, with conditions similar to those prevailing during the formation of the Proterozoic Canadian and Australian unconformity-related uranium deposits [3.205]. A minor difference between the Shinlolobwe deposit and the unconformity-related deposits is the origin of the brine.

For Australian and Canadian deposits, the brines are interpreted as having been expelled directly from evaporite layers [3.135, 3.427], whereas for the deposits in the external zone of the Lufilian belt they represent secondary brines derived from the dissolution of evaporate layers [3.428, 3.429]. A more important difference is the location of the redox boundary. In unconformity-related deposits, the redox boundary is between the base of oxidized basinal sandstone and reduced basement lithologies. In the external zone of the Lufilian Belt, the redox boundary is between the oxidized basal R.A.T. (R.A.T. = Roches Argio-Talqueuses = Clay mineral – talc –rocks) Subgroup (red R.A.T.) of the Roan Group and the upper reduced organic matter- and sulphide-bearing R.A.T. subgroup (gray R.A.T.; [3.405]). Eglinger et al. [3.423] speculate that the source of uranium could be the basement rocks, and/or the Katanga Supergroup sediments in agreement with Koziy et al. [3.430] who proposed a similar source for copper for the stratiform copper deposits of the Zambian copper belt.

3.7.8. Maureen, Australia

Maureen deposit is the largest of a series of uranium-molybdenum-fluorine deposits and showings of Late Permian age occurring in a Paleozoic volcanic-sedimentary sequence of the Georgetown area in northern Queensland. Hurtig et al. [3.143] show mineralization occurs along fractures that intersect the unconformity between a reduced Proterozoic basement and a largely oxidized Paleozoic cover. The mineralized structures are steeply dipping EW fractures. The uranium mineralization is essentially hosted within the Lower clastic sequence of the Fiery Creek Formation (Fig. 3.29), as pencil-shaped orebodies. About 2% of the ore is hosted by the basement rocks within narrow fractures a few tens of metres below the unconformity surface. The high-grade ore is composed of pitchblende, arsenopyrite, As-pyrite, molybdenite, dickite, chlorite, goyazite, plus or minus graphite or haematite and is surrounded by a fluorite-rich halo. Brecciation and quartz dissolution are also commonly observed.

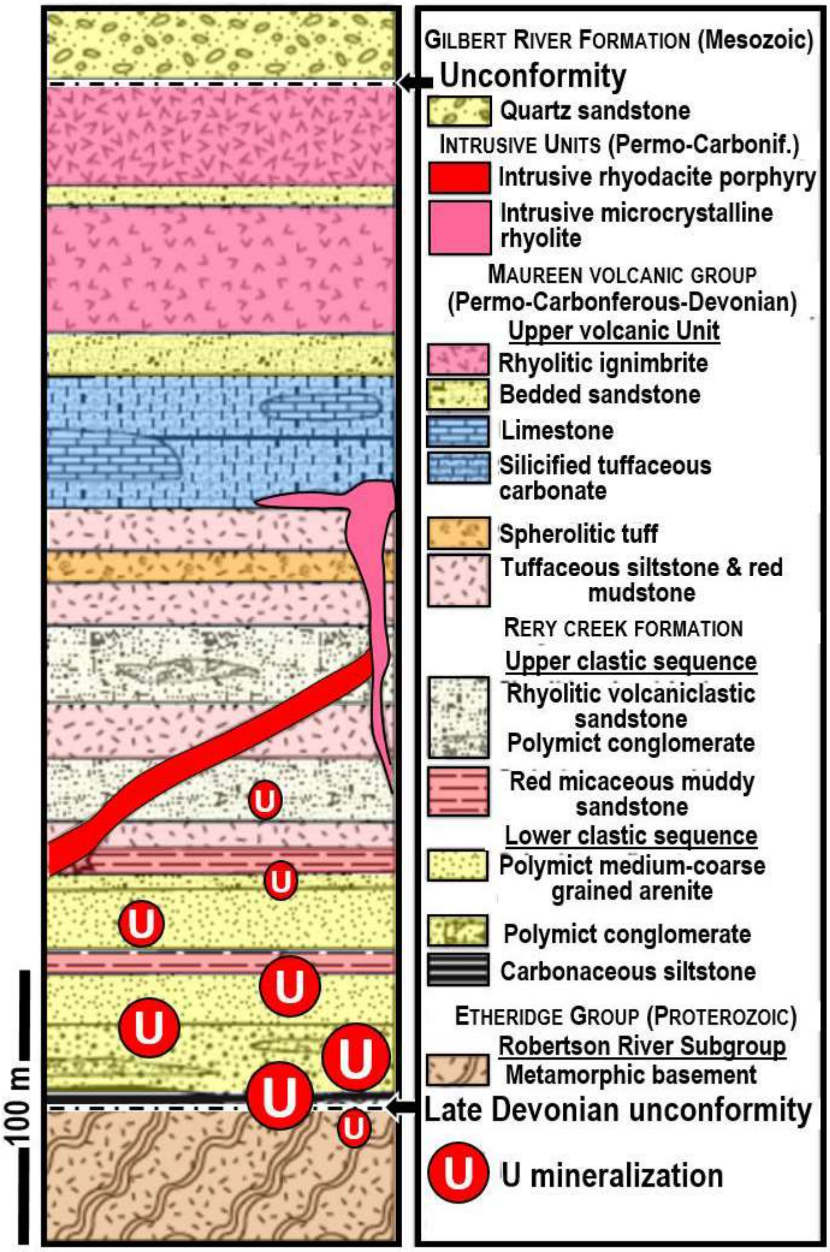

FIG. 3.29. Stratigraphic column of the Maureen U-Mo-F deposit, Queensland, Australia. The stars indicate locations of mineralization within the stratigraphic column and their size indicates relative grade of uranium mineralization (modified from Hurtig et al. [3.143]).

Three fluids have been identified at Maureen deposit (Fig. 3.30):

- L1: an aqueous fluid;
- L2: an oxidized moderately saline fluid;
- L3: a U-Mo-As-rich saline and presumably oxidized fluid, trapped in fluorite and quartz veins associated to dickite ([$10<U<47$ ppm], [$489<Mo<888$ ppm], [$318<As<777$ ppm]);
- (cV): a vapour-rich fluid with CO_2 and CH_4 which is responsible for the reduction and the precipitation of U- and Mo-rich minerals.

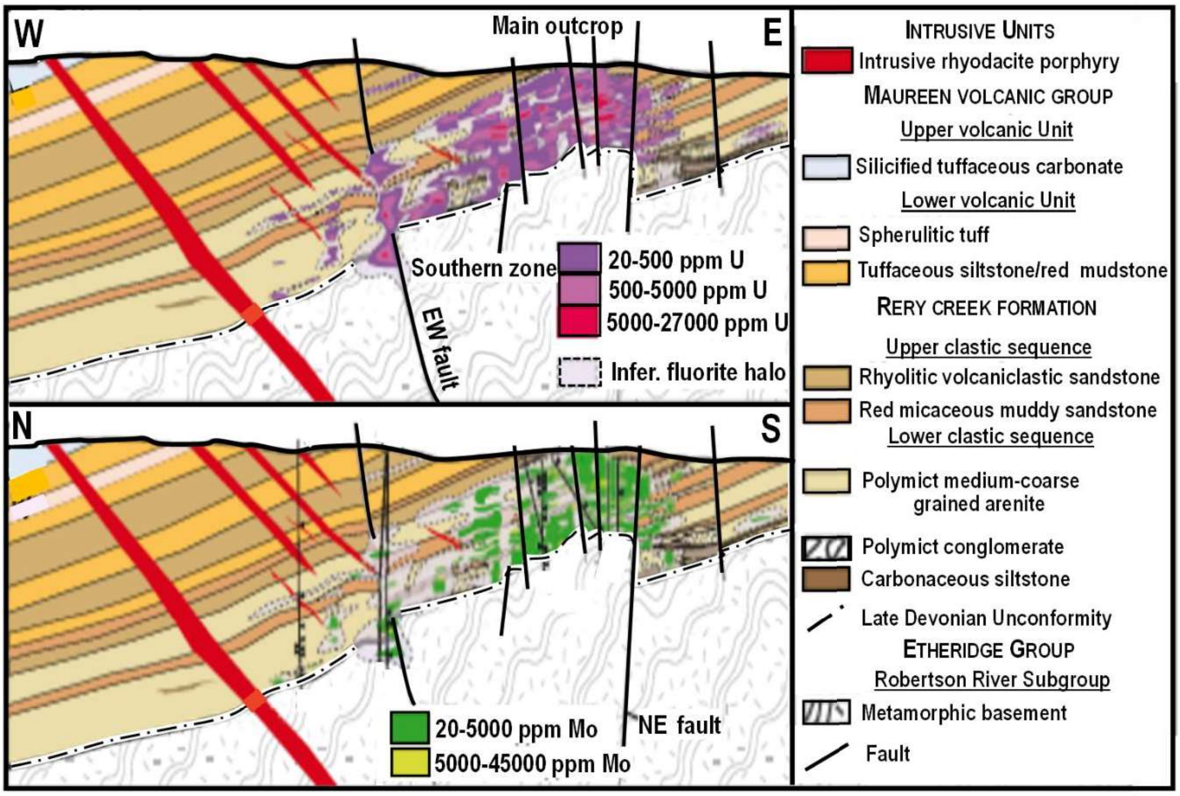

FIG. 3.30. EW and NS geologic sections of the Maureen deposit with the distribution of U (A, C) and Mo (B, D), and associated fluorite halo (modified from Hurtig et al. [3.143]).

Hurtig et al. [3.143] stated that "the Maureen deposit shares essential geologic characteristics and hydrothermal processes with Proterozoic unconformity-related uranium deposits, and owes its unusual element association of uranium with molybdenum and abundant fluorine to a source region in the volcano-sedimentary cover sequence". However, this deposit lacks most of the basic features of typical unconformity related deposits.

- No regolithic alteration is present at the top of the basement, below the unconformity;
- Lack of a thick, regional scale, homogeneous, entirely oxidized, feldspar free, highly quartzose fluid reservoir in the overlying basin sequences; the Fiery Creek Formation is highly heterogeneous, and contains a significant proportion of siltstone and shale, with tuffaceous, carbonaceous, and carbonate-bearing sedimentary layers;
- The presence of a carbonaceous siltstone at the unconformity in the Fiery Creek Formation may have generated reduced fluids within the overlying sedimentary formation;
- The carbonate units in the Fiery Creek Formation would not generate highly acidic brines similar to brines observed in the Athabasca Basin;
- The saline fluid is much less saline than the brines of the Athabasca and Kombolgie basins and calcic brine fluid inclusions with halite crystals are rare;
- Compared to the Athabasca ore forming fluid, the L3 saline fluid considered as the ore metal transporting fluid, is dominantly sodic rather than calcic, has lower uranium content (10–47 ppm) and significantly higher temperature (>300°C);

- The much higher geothermal gradients of 60 to 100°C (300°C for a depth of 3 to 5 km) at Maureen are explained by coeval emplacement of granites, which does not occur in the environment of the classical unconformity-related uranium deposits;
- The deposit is mostly hosted by sediments and forms discontinuous lenses partly controlled by vertical structuress, but mineralization is controlled by stratigraphy, which is not observed in unconformity-related uranium deposits (Fig. 3.29);
- The structures associated with the uranium lenses do not seem to be rooted along specific basement lithologies such as graphitic layers in unconformity-related deposits, even though graphitic mica schists occur in the basement of the western part of the Maureen deposit;
- The alteration mineral paragenesis (fluorite, dickite, chamosite, pyrophyllite, donbassite, sulphides, is different from unconformity related depsoits characterized by illite and magnesium-rich minerals (dravite and sudoïte);
- Fluorine-rich goyazite and gorceixite are the main aluminium-phosphate at Maureen whereas the APS minerals associated with unconformity-related deposits are a solid solution between florencite close to the deposits and svanbergite away from the deposits [3.84];
- Quartz dissolution is observed at Maureen, but seems to be very weakly developed compared to unconformity-related deposits from the Athabasca Basin [3.197, 3.203].

3.7.9. Southern Siberia

Uranium mineralization occurring along the SW Siberian Platform at the contact between folded formations of the Yenisei Ridge and Eastern Sayan are deemed to be unconformity-related deposits [3.431]. More specifically, the Stolbovoye and Anzakh deposits of Eastern Sayan formed in a pre-Sayan trough developed within the granite-gneissic basement between the Archean- Paleoproterozoic Biryusa block and the Siberian Platform. The trough is filled with Mesoproterozoic terrigenous sediments. The sediments of the trough have been folded and intruded by granitoids of the Sayan complex during the middle Riphean (Mesoproterozoic). The sediments are overlain by Late Riphean-Vendian (Neoproterozoic) sediments of the Siberian Platform. During Late Riphean, the peralkaline gabbro-granite Biryusa complexes were emplaced and included abundant pegmatite veins and development of a quartz-sericite-ankerite-pyrite alteration. Pitchblende is associated with this alteration. The uranium mineralization is localized in collapse breccia cements, which are characterized by microcrystalline haematite-bearing quartz, sericite, chlorite and copper, lead, zinc, arsenic, bismuth, and molybdenum sulphides. The breccias are distributed irregularly along structures that are 400–600 m in width and have a strike length of 2 km.

In the North-Yenisei region, the Vorogovo trough was formed during the Mesoproterozoic between the North-Yenisei Archean to Paleoproterozoic block and the Siberian Platform. The trough is filled with Mesoproterozoic terrigenous sediments and covered by Upper Riphean (Neoproterozoic) terrigenous-effusive formations. By the end of the Mesoproterozoic, the trough sediments were folded, metamorphosed and intruded with the Posolnensky complex granitoids. During the Late Riphean-Vendian (Neoproterozoic), the midly peralkaline Tatar-Ayakhta granitic complex was emplaced. Intense quartz-sericite-ankerite-pyrite alteration and graphitization is associated with the instruction of the granitic complex. This alteration assemblage is close to the unconformity with overlying Neoproterozoic sedimentary cover, and is associated with the deposition of uranium (Polyarnoye showing with 0.1 to 1.0% uranium), gold-uranium (Kutukasskoye showing with 0.05–1.0 % uranium and 1–25 ppm gold rarely up to 65 ppm), and gold-uranium-polymetallic (Zakhrebetnoye with 0.1% and up to 2 ppm Au + Ag, Pb, Zn) mineralization.

Despite the limited amount of data, the uranium occurrences of South Siberia are considered to be unconformity-related deposits because of the proximity to the unconformity between an Archean-Paleoproterozoic basement sedimentary cover.

3.7.10. The Otish Basin (Québec, Canada)

3.7.10.1. The Otish Basin

The Otish Basin is located in north-central Québec, Canada, about 250 km NE of Chibougamau. It belongs to the intracontinental part of the Otish-Mistassini Basin deposited on the margin of the Superior Province [3.433]. The Otish Basin is over 150 km in length and 50 km in width (Fig. 3.31) [3.433].

The basement is Archean and comprises two high-grade metamorphic units: the Epervanche Complex and the metavolcano-sedimentary Tichegami Group, both intruded by younger granitic intrusions. A locally-developed regolith is visible [3.434]. It is unconformably overlain by the Otish Supergroup. Its maximum age is constrained by the uranium-lead baddeleyite age of 2515 ± 3 Ma of the Mistassini diabase dykes [3.435], whereas its minimum age is fixed by another uranium-lead baddeleyite age of 2172–2162 Ma of gabbro sills and dikes that intrude the Otish Supergroup [3.435, 3.436].

The basin consists of the Otish Supergroup, which has been subdivided into the Indicator Group (225–1200 m thick) comprising essentially greenish clastic fluvial poorly sorted sedimentary rocks, and the overlying Peribonca Group (>1200 m) consisting of reddish clastic deltaic sedimentary rocks, Genest [3.432]. The Indicator Group comprises the Matoush and the overlying Shikapio formations. The Peribonca Group consists of the Laparre, Gaschet and Marie-Victorin formations, which contain features consistent with deposition in a typical coastal sabkha.

The gabbro sills and dikes have thicknesses from <300 m to >500 m and from 30 to 200 m, respectively. They are variably altered and metamorphosed to the greenschist facies [3.436]. At the Matoush deposit, the Matoush dyke, has a lamprophyric chemistry, different from the other gabbros, but its age is not known [3.436].

During the Grenville Orogeny (1090–980 Ma), the Otish Basin and basement rocks were faulted but without significant folding [3.437]. Brittle deformation associated to low grade greenschist facies metamorphism recorded in fault zones occurs in the NW part of the Otish Basin, whereas brittle to ductile deformation and greenschist to the amphibolite facies metamorphic grade is observed in the SE part of the Basin closer to the Grenville Front [3.438].

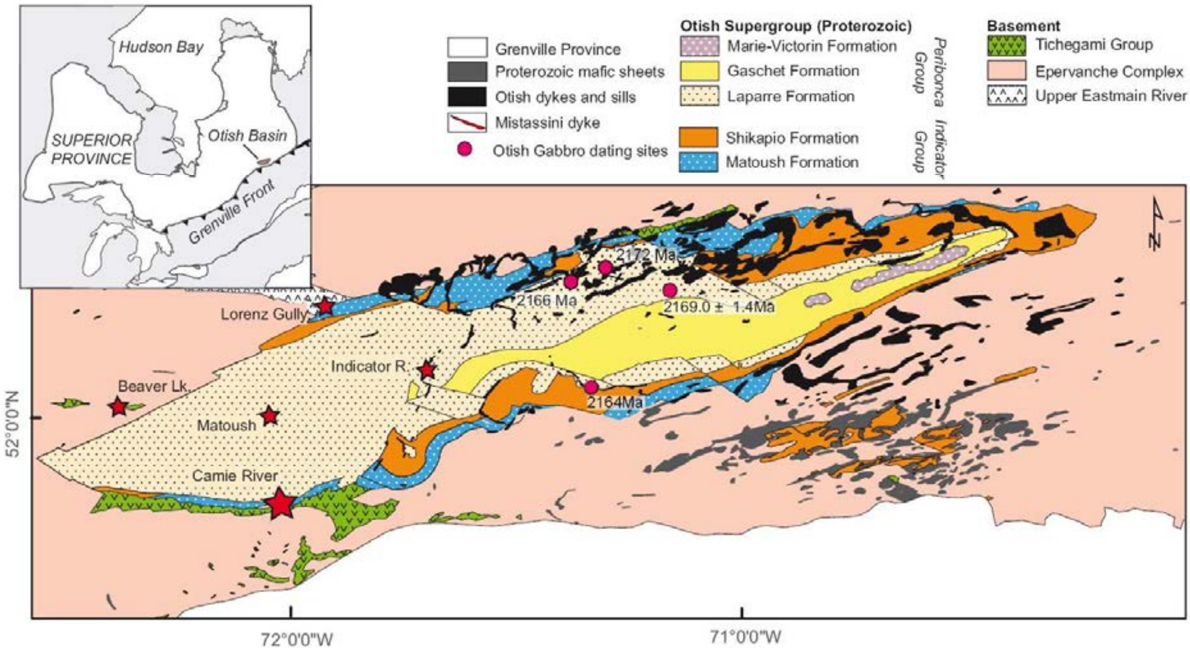

FIG. 3.31. Simplified geological map of the Otish Basin (modified from Lesbros-Piat-Desvial et al. [3.439]). Red stars represent the location of selected uranium occurences.

3.7.10.2. The uranium deposits

More than 30 uranium occurrences are known in the Otish Basin and underlying basement. Höhndorf et al. [3.440] and Gatzweiler [3.433] defined four types of deposits according to their geological setting (Fig. 3.32).

- Stratiform mineralization in the basement (Takwa River mineralized boulders);
- Vein-type mineralization in the basement (Beaver Lake and Lorenz Gully);
- Mineralization related to the unconformity (Camie River);
- Vein-type mineralization in the sediments of the Otish Supergroup associated with mafic dykes and faults (Matoush and Indicator Lake).

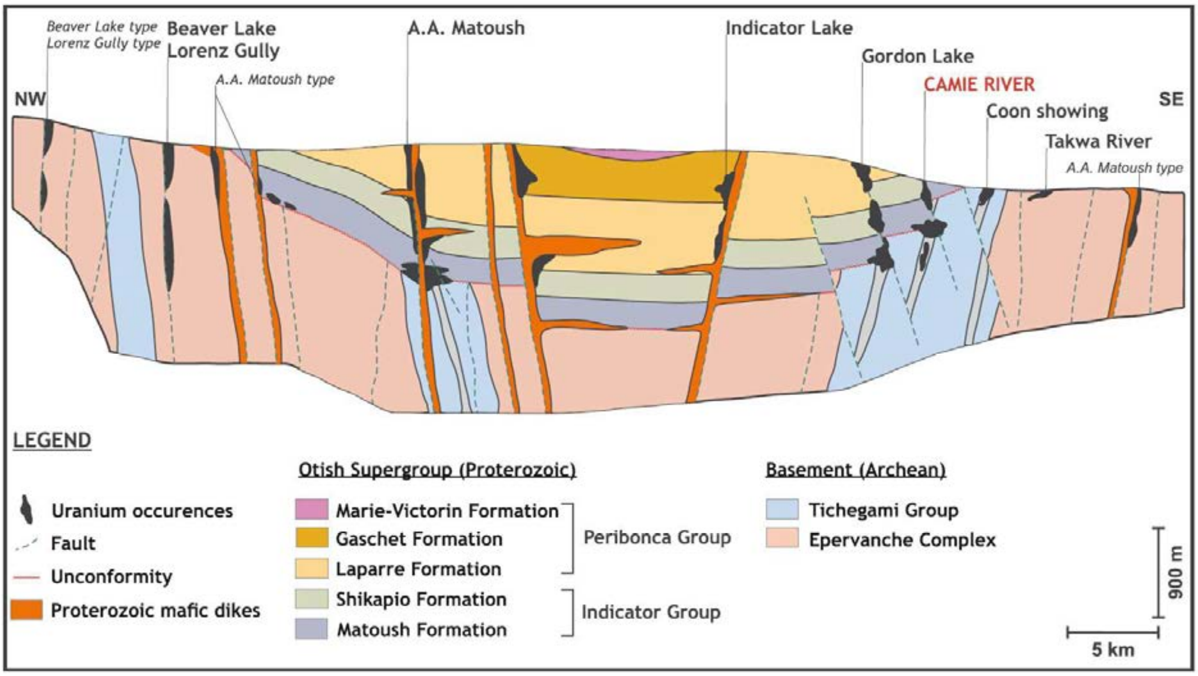

FIG. 3.32. Cross-section through the Otish Basin with location of known and presumed uranium occurrences (modified from Gatzweiler [3.433]; Genest [3.432]).

The Camie River uranium mineralization is the main occurrence presenting some of the typical characteristics of classical unconformity-related deposits [3.441]. The deposit is located along the SW rim of the Otish Basin (Fig. 3.31). The mineralization is associated with alteration comprising an external zone with disseminated albite, chlorite and pyrite and an inner zone with iron-magnesium chlorite and carbonate.

Basement lithologies comprise subvertically dipping metavolcanic and metavolcaniclastic rocks of the Tichegami Group. The EW-striking, steeply south-dipping reverse faults affect the southern part of the Otish Basin. They are cross-cut by NE-trending normal faults [3.433, 3.440]. The two fault systems offset the unconformity and are localized along graphitic metapelite units in the basement [3.433], and extend into the sedimentary cover.

The Matoush A-member directly lying on basement rocks, consists of polymictic conglomerate with quartz pebbles and mafic lithic fragments, overlain by a monomictic conglomerate. Both conglomerates are poorly sorted and matrix supported. The Matoush B-member, consists of sandstones with interbedded conglomeratic sandstones, followed by the arkosic conglomeratic sandstones and sandstones of the Laparre Formation. At Camie River, feldspar makes up to 25% of the detrital minerals in the Indicator Group [3.442]. Detrital minerals also include rutile, zircon, pyrite, rare muscovite, apatite and monazite.

The Camie River uranium mineralization occurs near a reverse fault offsetting the unconformity between the Matoush fluviatile sandstones and conglomerates and the Tichegami Group basement rocks (Fig. 3.33). The uranium mineralization is hosted by subvertical faults rooted in graphite-sulphide-bearing metapelites [3.433]. The main mineralized zone forms an EW elongated body, 550 m long, dipping to the east and extending up to 30–50 m in overlying sediments, and 20–30 m into the basement [3.433]. The uranium grades may reach 10 to 20% uranium locally. Colloform pitchblende is the main uranium mineral, associated to lesser amounts of brannerite [3.434, 3.441, 3.444]. The uranium mineralization is polymetallic with Mo, Cu, Ni, Co, As, Se, V, Nb, Ag, Au (± Th) [3.433, 3.440].

The metamorphic chlorite in basement rocks yields temperatures (~360°C) consistent with the greenschist grade rocks. Post-diagenetic chlorite associated with hematization in basin sedimentary rocks yields temperatures near 210°C. The uranium is paragenetically late and associated with chlorite, which yields temperatures near 320°C both in basement rocks and the sedimentary cover [3.439]. This suggests an increase in temperature, from ~210°C after diagenesis, to ~320°C at the time of the uranium mineralization, as reported by Beyer et al. [3.442].

Chlorite and sulphides alteration in the basement and cover rocks has been attributed by Beyer et al. [3.442] to a late stage diagenetic fluid event associated with uranium deposition. The higher temperature of that stage (>300°C) is related to the thermal anomaly created by the intrusion of the Otish Gabbro Suite dated previously at ~1730 Ma. However, recent dating of the gabbros between 2172 to 2162 Ma [3.435, 3.436], do not support such an interpretation. Consequently, chlorite, carbonate, and sulphides veins alteration is probably not related to diagenesis and has been interpreted by Lebros-Piat-Desvial [3.439] as a post-ore alteration event. Interpretation of the oxygen and hydrogen isotope data on alteration minerals associated with the uranium mineralization indicates a mixing between seawater-derived basinal brines of metamorphic origin [3.442].

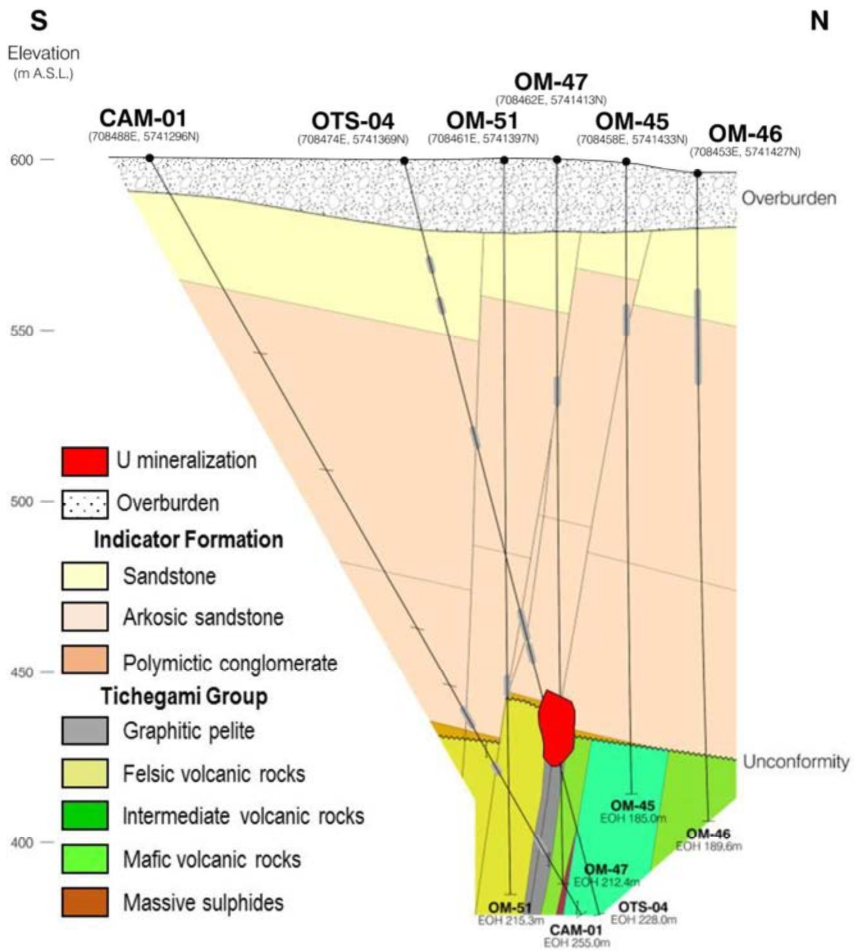

FIG. 3.33. Cross-section through the Camie River deposit (modified from Aubin [3.444]).

Höhndorf et al. [3.440] obtained a uranium-lead age by TIMS of 1723 ± 16 Ma for uranium oxides from the Camie River deposit and Beyer et al. [3.442] reported lead-lead age of 1721 ± 20 Ma by LA-ICP-MS. These ages are similar, to the more recent SIMS uranium-lead uraninite age of 1724 ± 29 Ma and rhenium-osmium molydenite age of 1724 ± 5 Ma [3.439]. These data show that the uranium mineralization formed at ~1724 Ma at least 440 Ma after the Otish Group deposition. This result is consistent with deposition of the uranium mineralization during a late paragenetic stage. The uranium mineralized veins and associated chlorite, cut diagenetic and hydrothermal feldspathic and muscovite alteration. The Camie River uranium mineralization has a similar age to that of the Lorenz Gully (1717 ± 20 Ma) and L (1711 ± 2 Ma) occurrences [3.440].

The hydrothermal alteration associated with the uranium mineralization also occurs about 440 Ma after the emplacement of the Otish Gabbro suite. Therefore, the Gabbro emplacement cannot be related to the formation of the uranium mineralization as proposed initially [3.440, 3.442], except for the Matoush uranium deposit which has not been dated and presents a uranium mineralization intimately associated to a chromium-rich alteration [3.445].

3.7.10.3. Comparison with unconformity- related deposits

The location of the deposit at the unconformity between basement and basin, the structural control by reverse faulting, the age of the uranium oxides and associated alteration, the oxygen and hydrogen isotopic compositions obtained for the ore-forming fluids, and the polymetallic paragenesis associated with uranium mineralization, have led several researchers to classify these deposits as unconformity-related uranium deposits [3.433, 3.440, 3.442]. However, several major differences exist with the classical model of unconformity-related uranium mineralization, even for the Camie River deposit.

- The sedimentary rocks of the Otish Basin have been deposited between 2515 and 2162 Ma and thus are much older than other sedimentary basins hosting unconformity-related uranium deposits;
- The basal units of the Otish Basin have reducing characteristics and are not oxidized as in the siliciclastic units overlying the basement in the classical unconformity-related settings, and they may have been deposited before the great oxygenation event;
- The siliciclastic basal units of the Otish Basin are also immature with significant amounts of detrital feldspars compared to the mature quartzose sandstones of the Athabasca or Kombolgie Basins, indicating more alkaline diagenetic brines in the Otish sediments in accordance with the albitic alteration;
- The early feldspar cementation of the basal clastic sedimentary sequence at Camie River have occluded its porosity and permeability preventing massive fluid flow of the diagenetic fluids within the Basin. The uranium mineralization at Camie River formed almost 440 Ma after deposition of the sedimentary rocks after the porosity of the rocks was reduced;
- The temperature of the uranium ore stage, both in the basement and the basin from chlorite geothermometry (320°C), is much higher than temperatures proposed for typical unconformity-related uranium deposits (140 and 220°C);
- The composition of chlorite (clinochlore to chamosite instead of sudoite) and lack of the typical unconformity-related mineralogical association (i.e. dravite, APS) in the alteration paragenesis of the Camie River, and other uranium deposits in the Otish

Basin, preclude a major role for basinal brines in the genesis of the uranium mineralization there;

- The high rare earth element concentrations and flat patterns of the Camie River uranium oxides (Fig. 3.34) are typical of high temperature, syn-metamorphic uranium mineralization [3.439], such as the syn-metamorphic uranium deposits of Mistamisk, Canada and of the Lufilian Belt) formed at similar temperatures [3.423, 3.446], and different from the bell-shape patterns depleted in light rare earth elements of unconformity-related uranium deposits [3.424].

According to Lebros-Piat Desvial [3.439], the uranium deposits from the Otish Basin, with temperatures of genesis higher than 300°C, more likely formed during a metamorphic event at c. 1724 Ma long after sedimentation and diagenesis in the Otish Basin.

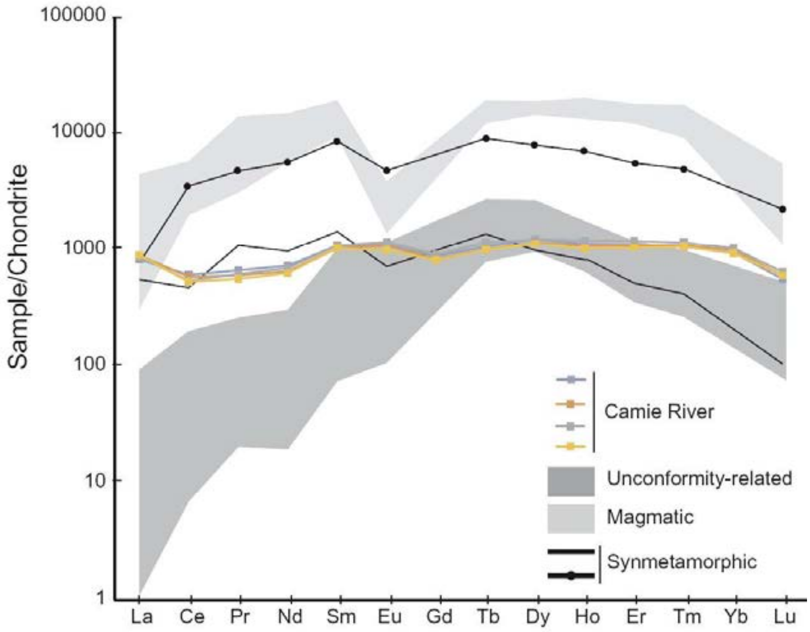

FIG. 3.34. Rare earth element patterns for Camie River uranium oxides, and from other uranium deposit types (modified from [3.440]).

3.8. CONCLUSIONS

1. Unconformity-related uranium deposits are hydrothermal-diagenetic ore systems that form along fracture zones, proximal to an unconformity commonly between mature sandstone and dominantly reduced older metamorphosed basement rocks. Fault zones hosting mineralization are often rooted in graphite-rich metamorphosed rocks. The uranium mineralization may extend hundreds of metres into the sandstone cover and may extend to more than a kilometre into the basement rocks (e.g. Jabiluka). However, knowledge of the extent of fluid circulation into basement rocks is greatly hampered by the lack of deep drill holes;

2. A thick regolith (several tens of metres) is typically developed at the top of the basement, just below the sandstone. Its importance and origin is debated. The regolith may have

formed from lateritic weathering prior to deposition of the sandstone, from the alteration of the basement by the percolation of diagenetic brines or both weathering and alteration;

3. Primary mineralization is commonly in the form of massive accumulations of uranium dioxide (with euhedral or collomorph shape), which is readily altered to uranium silicate minerals and oxidized uranyl oxyhydroxide minerals. A great variety of other ore minerals (mainly sulphides and arsenides) can be associated, but their abundance is quite variable from one deposit to the other and their deposition seems to be late in the paragenetic succession;

4. Mineralization is commonly hosted in moderately reactivated Proterozoic ductile structures and often is associated with large, clay-rich alteration halos and quartz dissolution. However, it is not known what chemical or physical mechanism has led to quartz undersaturation of the ore forming fluid;

5. Typical alteration minerals associated to the unconformity-related uranium mineralization are illite, sudoite (magnesium-rich chlorite), dravite (magnesium-rich tourmaline), and alumino-phosphate-sulphate (APS) minerals;

6. Several mechanisms have been suggested for the reduction of U^{6+} to U^{4+} and the precipitation of uranium dioxide. These include graphite consumption, oxidation of Fe^{2+}, and interaction with hydrocarbons (e.g. CH_4) and dissolved gases (e.g. H_2). However, the mechanism of the reduction of the uranyl-bearing fluid has not been unambiguously identified;

7. The fluids associated with these deposits are acidic, highly oxidized, chloride-sodium and/or calcium-rich (diagenetic) brines of probable evaporitic origin. These fluids are hosted in aquifers at the base of a 4–7 km thick sandstone-rich intracontinental basin and commonly range in temperature from ~100–300°C at pressures that range from 0.5–1.5 kbars;

8. The age of these deposits is controversial because radiogenic lead readily diffuses from the uranium-oxide structure. However, most researchers agree that initial uranium mineral precipitation began at ~1600–1500 Ma. Numerous post-depositional fluid events have impacted these deposits, resulting in ages for mineralization that range from recent, very young ages, and up to 1600 Ma, but it is not known if these later fluids events have led to any significant addition of new uranium to the ore systems. It is also difficult to evaluate the duration of hydrothermal circulations associated to the initial formation of the uranium deposits;

9. The source of uranium is debated, but was likely accessory minerals in both basement rocks and the sedimentary cover. The extremely reactive diagenetic brines were able to consume monazite and alter zircon, which are generally considered as refractory minerals;

10. Uranium oxides from Proterozoic unconformity-related uranium deposits (Athabasca, East Alligator River and Kiggavik) have a unique bell-shaped pattern, regardless of style of mineralization (e.g. at the unconformity, hosted entirely in basement rocks);

11. There are numerous uranium deposits worldwide that were classified as unconformity-related in the literature largely because they are located at or near an unconformity, between

basement rocks and basin fill. However, many of these deposits do not share the main structural, mineralogical, fluid, and genetic characteristics that are typical of the classical, Proterozoic unconformity-related uranium deposits from Canada and Australia. The classification of an ore occurrence as unconformity-related in some cases has been rather broadly and liberally applied, therefore some deposits designated as unconformity-related are better interpreted as a different uranium model type.

3.9. REFERENCES

[3.1] ROGERS, J., SANTOSH, M., Configuration of Columbia, a Mesoproterozoic supercontinent, Gond. Res. **5** (2002) 5–22.

[3.2] ZHAO, G., CAWOOD, P.A., WILDE, S.A., SUN, M., Review of global 2.1–1.8 Ga orogens: implications for a pre-Rodinia supercontinent, Earth Sci. Rev. **59** (2002) 125–162.

[3.3] CAWOOD, P.A., JOHNSON, M.R., NEMCHIN, A.A., Early Palaeozoic orogenesis along the Indian margin of Gondwana: tectonic response to Gondwana assembly, Earth Planet. Sci. Lett. **255** (2007) 70–84.

[3.4] TREMBLAY, L.P., Geology of the Uranium Deposits Related to the Sub-Athabasca Unconformity, Saskatchewan, Geological Survey of Canada Paper **81–20** (1982).

[3.5] ANNESLEY, I.R., MADORE, C., SHI, R., KROGH, T.E., U-Pb Geochronology of Thermotectonic Events in the Wollaston Lake Area, Wollaston Domain: A Summary of 1994–1996 Results, Rep. 97-4, Saskatchewan Geological Survey (1997) 162–173.

[3.6] MADORE, C., ANNESLEY, I.R., WHEATLEY, K., "Petrogenesis, age, and uranium fertility of peraluminous leucogranites and pegmatites of the McClean Lake/Sue and Key Lake deposit areas, Saskatchewan", Proc. Conf. GAC–MAC, Calgary **25** (2000) 1041.

[3.7] CUNEY, M., BROUAND, M., CATHELINEAU, M., DEROME, D., FREIBERGER, R., HECHT, L., KISTER, P., LOBAEV, V., LORILLEUX, G., PEIFFERT, C., BASTOUL, A.M., "What parameters control the high grade-large tonnage of the Proterozoic unconformity related uranium deposit?" Proc. Conf. Uranium Geochemistry 2003 (CUNEY, M., Ed.), Université Henri Poincaré, Nancy, France (2003) 123–126.

[3.8] FREIBERGER, R., CUNEY M., "New evidence for extensive fluid circulations within the basement in relation to unconformity type uranium deposit genesis in the Athabasca Basin, Saskatchewan, Canada", Proc. Conf. Uranium Geochemistry 2003 (CUNEY, M., Ed.), Université Henri Poincaré, Nancy, France (2003) 151–154.

[3.9] HECHT, L., CUNEY M., "Tracing the sources of unconformity-type uranium deposits", Proc. Conf. Uranium Geochemistry 2003 (CUNEY, M., Ed.), Université Henri Poincaré, Nancy, France (2003) 177–180.

[3.10] HOEVE, J., SIBBALD, T.I.I., On the genesis of the Rabbit Lake and other unconformity-type uranium deposits in Northern Saskatchewan, Canada, Econ. Geol. **73** (1978) 1450–1473.

[3.11] RUZICKA, V.R., "Unconformity-associated uranium", Geology of Canadian Mineral Deposit Types (ECKSTRAND, O.R., SINCLAIR, W.D., THORPE, R.I., Eds), Geological Survey of Canada, Geology of Canada **8** (1996) 197–210.

[3.12] FAYEK, M., KYSER, T.K., Characterization of multiple fluid-flow events and rare-earth-element mobility associated with formation of unconformity-type uranium deposits in the Athabasca Basin, Saskatchewan, Can. Min. **35** (1997) 627–658.

[3.13] HÖHNDORF, A., STRNAD, J.G., CARL, C., “Age determination of basement units in the Key Lake uranium deposit area, Saskatchewan, Canada”, Uranium Resources and Geology of North America, IAEA-TECDOC-500, IAEA, Vienna (1989) 381–410.
[3.14] MCCREADY, A.J., STUMPFL, E.F., MELCHER, F., U/Th-rich bitumen in Archean granites and Palaeoproterozoic metasediments, Rum Jungle Mineral Field, Australia: implications for mineralizing fluids, Geofluids **3** (2003) 147–159.
[3.15] FERGUSON, J., WINER, P., “Pine Creek geosyncline: Statistical treatment of whole rock data”, Uranium in the Pine Creek Geosyncline (FERGUSON, J., GOLEBY, A.B., Eds), IAEA, Vienna, (1980) 191–208.
[3.16] FERGUSON, J., CHAPPELL, B.W., GOLEBY, A.B., “Granitoids in the Pine Creek geosyncline”, Uranium in the Pine Creek Geosyncline (FERGUSON, J., GOLEBY, A.B., Eds), IAEA, Vienna, (1980) 73–90.
[3.17] MCANDREW, J., FINLAY, C.J., “The nature and significance of the uranium occurrence in the Nanambu Complex of the Pine Creek geosyncline”, Uranium in the Pine Creek Geosyncline (FERGUSON, J., GOLEBY, A.B., Eds), IAEA, Vienna, (1980) 357–363.
[3.18] MAAS, R., Nd–Sr isotopic constraints on the age and origin of unconformity-type uranium deposits in the Alligator Rivers uranium field, Northern Territory, Australia, Econ. Geol. **84** (1989) 64–90.
[3.19] CUNEY, M., Evolution of uranium fractionation processes through time: driving the secular variation of uranium deposit types, Econ. Geol. **105** (2010) 553–569.
[3.20] TRAN, H.T., ANSDELL, K.M., BETHUNE, K.M., ASHTON, K., HAMILTON, M.A., Provenance and tectonic setting of Paleoproterozoic metasedimentary rocks along the eastern margin of Hearne craton: Constraints from SHRIMP geochronology, Wollaston Group, Saskatchewan, Canada, Precamb. Res. **167** (2008) 171–185.
[3.21] NEEDHAM, R.S., Geology of the alligator uranium field, Northern Territory, Australia, BMR Bull. **284** (1988).
[3.22] ANNESLEY, I.R., MADORE C., “Leucogranites and pegmatites of the sub-Athabasca basement, Saskatchewan: U protore?” Mineral Deposits: Processes to Processing (STANLEY, C.J. et al., Eds), Balkema, **1** (1999) 297–300.
[3.23] ANNESLEY, I.R., MADORE C., KROGH, T.E., KWOK, Y.Y., and KAMO, S.L., New U-Pb Zircon and Monazite Geochronological Results for Archean and Paleoproterozoic Basement to the Southeastern Part of the Athabasca Basin, Saskatchewan, Misc. Rep. 99-4.2, Saskatchewan Geological Survey (1999) 90–99.
[3.24] MAWDSLEY, J.B., Uraninite-bearing deposits, Charlebois Lake area, northeastern Saskatchewan, Can. Inst. Min. Metal. Bull. **482** (1952) 366–375.
[3.25] MAWDSLEY, J.B., Uraninite-bearing fine-grained pegmatite of the Charlebois Lake area northeastern Saskatchewan, Geol. Soc. Am. Bull. **64** (1953) 1550.
[3.26] MAWDSLEY, J.B., Radioactive pegmatites of northern Saskatchewan, Can. Min. **76** (1955) 53–56.
[3.27] MAWDSLEY, J.B., The Geology of the Middle Foster Lake Area, Northern Saskatchewan, Rep. 26, Saskatchewan Department of Mineral Resources (1957) 1–45.
[3.28] PARSLOW, G.R., THOMAS, D.J., Uranium occurrences in the Cree Lake Zones, Saskatchewan, Canada, Min. Mag. **46** (1982) 163–171.
[3.29] VON PECHMANN, E., HÖHNDORF, A., VOULTSIDIS, V., “Synmetamorphic uranium mineralization in the Needle Lake-Keefe Lake area, Wollaston fold Belt, Saskatchewan, Canada”, Syngenesis and Epigenesis in the Formation of Mineral Deposits (WAUSCHKUHN, A., ET AL., Eds), Springer, Berlin (1984) 160–169.

[3.30] PARSLOW, G.R., BRANDSTÄTTER, F., KURAT, G., THOMAS, D.J., Chemical ages and mobility of U and Th in anatectites of the Cree Lake Zone, Saskatchewan, Can. Min. **23** (1985) 543–551.

[3.31] ANNESLEY, I.R., MADORE, C., KROGH, T.E., KAMO, S.L., "Anomalous U-Pb values in monazites from peraluminous leucogranites and pegmatites near unconformity-type uranium mineralization, eastern Athabasca, Saskatchewan", Proc. Conf. GAC–MAC, Sudbury **23** (1999).

[3.32] MCKECHNIE, C.L., ANNESLEY, I.R., ANSDELL, K., Radioactive abyssal granitic pegmatites and leucogranites in the Wollaston Domain, northern Saskatchewan, Canada: mineral compositions and conditions of emplacement in the Fraser Lakes area, Can. Min. **50** (2012a) 1637–1667.

[3.33] MCKECHNIE, C.L., ANNESLEY, I.R., ANSDELL, K., Medium to low-pressure pelitic gneisses of Fraser Lakes Zone B, Wollaston Domain, northern Saskatchewan, Canada: mineral compositions, metamorphic P–T–t path, and implications for the genesis of radioactive abyssal granitic pegmatites, Can. Min. **50** (2012b) 1669–1694.

[3.34] MCKECHNIE, C.L., ANNESLEY, I.R., ANSDELL, K., Geological setting, petrology and geochemistry of granitic pegmatites hosting the Fraser Lakes Zone B U–Th–REE mineralization, Wollaston Domain, northern Saskatchewan, Canada, Explor. Mining Geol. **21** (2013) 1–26.

[3.35] MCKEOUGH, M.A., LENTZ, D.R., MCFARLANE, C.R.M., BROWN, J., Geology and evolution of pegmatite-hosted U–Th ± REE–Y–Nb mineralization, Kulyk, Eagle, and Karin Lakes region, Wollaston Domain, northern Saskatchewan, Canada: examples of the dual role of extreme fractionation and hybridization processes, J. Geosci. **58** (2013) 321–346.

[3.36] MERCADIER, J., ANNESLEY, I.R., MCKECHNIE, C.L., BOGDAN, T.S., CREIGHTON, S., Magmatic and metamorphic uraninite mineralization in the western margin of the Trans-Hudson Orogen (Saskatchewan, Canada): A uranium source for unconformity-related uranium deposits? Econ. Geol. **108** (2013) 1037–1065.

[3.37] FAYEK, M., CAMACHO, A., BESHEARS, C., JIRICKA, D., HALABURDA, J., "Two sources of uranium at the Millennium uranium deposit, Athabasca Basin, Saskatchewan, Canada", Proc. Conf. GAC–MAC, Calgary (2010) 5 pp.

[3.38] WILLIAMS-JONES, A.E., SAWIUK, M., The Karpinka Lake uranium prospect, Saskatchewan–a possible metamorphosed Middle Precambrian sandstone-type uranium deposit, Econ. Geol. **80** (1985) 1927–1941.

[3.39] BROUAND, M., CUNEY, M., DELOULE, E., "Eastern extension of the Taltson orogenic belt and eastern provenance of Athabasca sandstone: IMS 1270 ion microprobe U/Pb dating of zircon from concealed basement plutonic rocks and from overlying sandstone (northwestern Saskatchewan, Canada)", Proc. Conf. Uranium Geochemistry 2003 (CUNEY, M., Ed.), Université Henri Poincaré, Nancy, France (2003) 91–94.

[3.40] CLOUTIER, J., KYSER, T.K., OLIVO, G., BRISBIN, D., Geochemical, isotopic, and geochronologic constraints on the formation of the Eagle Point basement-hosted uranium deposit, Athabasca Basin, Saskatchewan, Canada and recent remobilization of primary uraninite in secondary structures, Miner. Dep. **46** (2011) 35–56.

[3.41] ROBINSON, S.C., Mineralogy of uranium deposits, Goldfields, Saskatchewan, Can. Bull. Geol. Surv. Can. **31** (1955) 32–35.

[3.42] BECK, L.S., Uranium Deposits of the Athabasca Region, Saskatchewan, Rep. 1969–169, Saskatchewan Department of Mineral Resources (1969) 126–139.

[3.43] TREMBLAY, L.P., Geology of the Beaverlodge mining area, Saskatchewan, Geol. Surv. Can. Mem. **367** (1972) 1–265.

[3.44] SIBBALD, T.I.I., Geology and Genesis of the Athabasca Basin Uranium Deposits, Rep. 1985-4, Saskatchewan Geological Survey, Sask. Energy and Mines (1985) 133−155.
[3.45] JEFFERSON, C.W., THOMAS, D.J., GANDHI, S.S., RAMAEKERS, P., DELANEY, G., BRISBIN, D., CUTTS, C., PORTELLA, P., OLSON, R.A., “Unconformity associated uranium deposits of the Athabasca Basin, Saskatchewan and Alberta”, EXTECH IV: Geology and Uranium Exploration Technology of the Proterozoic Athabasca Basin, Saskatchewan and Alberta (JEFFERSON, C.W., DELANEY, G., Eds), Bull. Geol. Surv. Can. **588** (2007) 23–67.
[3.46] RUZICKA, V., “Vein uranium deposits,” Vein-type Ore Deposits (HAYNES, S.J., Ed.), Ore Geol. Rev. **8** (1993) 247–276.
[3.47] TUREK, A., Geology of the Lake Cinch mine, Uranium City, Saskatchewan, Can. Min. **58** (1965) 183–192.
[3.48] SIBBALD, T.I.I., Uranium Metallogenic Studies: Nicholson Bay Area, Rep. 1982-4, Saskatchewan Geological Survey, Sask. Energy and Mines (1982) 40–42.
[3.49] TORTOSA, D.J.J., LANGFORD, F.F., “The geology of the Cenex U deposit, Beaverlodge, Saskatchewan”, Uranium Deposits of Canada (EVANS, E.L., Ed.), Can. Inst. Min. Metall. Petrol. (1983) 110–119.
[3.50] EVOY, E.F., “The Gunnar uranium deposit”, Uranium Deposits of Canada, (EVANS, E.L., Ed.), Can. Inst. Min. Metall. Petrol. (1986) 250—260.
[3.51] PEIRIS, E., PARSLOW, G., Geology and Geochemistry of the Uranium Gold Mineralization in the Nicholson Bay Fish Hook Bay Area, Rep. 1988–4, Saskatchewan Geological Survey, Sask. Energy and Mines (1988) 70–77.
[3.52] TREMBLAY, L. P., “Geologic setting of the Beaverlodge–type vein-uranium deposit and its comparison to that of the unconformity-type”, Uranium Deposits: their Mineralogy and Origin (KIMBERLY, M.M., Ed.), Min. Assoc. Can. Short Course **3** (1978) 431–456.
[3.53] MAZIMHAKA, P.K., HENDRY, H.E., The Martin Group, Beaverlodge Area, Rep. 1984—-4, Saskatchewan Geological Survey, Sask. Energy and Mines (1984) 53–62.
[3.54] CHAMBERLAIN, J.A., Structural Control of Pitchblende Orebodies, Eldorado, Saskatchewan, PhD Thesis, Harvard University, Cambridge (1958).
[3.55] ALLAN, J.F., Structural Control of the 01 and 09 Orebodies Ace and Fay Mines, Beaverlodge, Saskatchewan, PhD Thesis, Queen’s University, Kingston (1963).
[3.56] KOEPPEL, V., Age and History of Uranium Mineralization of the Beaverlodge Area, Saskatchewan, Geological Survey of Canada Paper **67–31** (1967) 111 pp.
[3.57] VAN SCHMUS, W.R., PERSONS, S.S., MACDONALD, R., SIBBALD, T.I.I., Preliminary Results from U-Pb Zircon Geochronology of the Uranium City Region, Northwest Saskatchewan, Rep. 1986–4, Saskatchewan Geological Survey, Sask. Energy and Mines (1986) 108–111.
[3.58] SASSANO, G.P., FRITZ, P., MORTON, R.D., Paragenesis and isotopic composition of some gangue minerals from the uranium deposits of Eldorado, Saskatchewan, Can. J. Earth Sci. **9** (1972) 141–157.
[3.59] REES, M.I., History of the Fluids Associated with Lode-gold Deposits, and Complex U-PGE-Au Vein Type Deposits, Goldfields Peninsula, Northern Saskatchewan, Canada, MSc Thesis, University of Saskatchewan, Saskatoon, (1992).
[3.60] LIANG, R., CHI, G., ASHTON, K., BLAMEY, N., FAYEK, M., Fluid compositions and P-T conditions of vein-type uranium mineralization in the Beaverlodge uranium district, northern Saskatchewan, Canada, Ore Geol. Rev. **80** (2017) 460–483.
[3.61] DIENG, S., KYSER, T.K., GODIN, L., “Fluid evolution and structural control on uranium deposits in the Beaverlodge successor basin, Saskatchewan, Canada”, Proc. Conf. GAC–MAC, Calgary (2010) 5 pp.

[3.62] DIENG, S., KYSER, T.K., GODIN, L., Tectonic history of the North American shield recorded in uranium deposits in the Beaverlodge area, northern Saskatchewan, Canada, Precamb. Res. **224** (2013) 316–340.

[3.63] DIENG, S., KYSER, T.K., GODIN, L., Genesis of multifarious uranium mineralization in the Beaverlodge area, northern Saskatchewan, Canada, Econ. Geol. **110** (2015) 209–240.

[3.64] TRACEY, G.M., LENTZ, D.R., OLSON, R.A., ASHTON, K.E., Geology and Associated Vein or Shear Zone-hosted Uranium Mineralization of the 46 Zone and Hab Mine Areas, Beaverlodge Uranium District, Northern Saskatchewan, Rep. 2009–4, Saskatchewan Geological Survey, Sask. Energy and Mines (2009) 1–18.

[3.65] ASHTON, K.E., The Gunnar Mine: An Episyenite-hosted, Granite-related Uranium Deposit in the Beaverlodge Uranium District, Rep. 2010-4, Saskatchewan Geological Survey, Sask. Energy and Mines (2010) 1–21.

[3.66] ASHTON, K.E., A New Look at Selected Deposits in the Historic Beaverlodge Uranium District: Variations on the Vein-type Uranium Theme, Rep. 2011-4, Saskatchewan Geological Survey, Sask. Energy and Mines (2011) 1–23.

[3.67] ASHTON, K.E., NORMAND, C., Bedrock Geology of the Ace-Fay-Verna-Dubyna Mines Area, Beaverlodge Uranium District, Rep. 2012-4, Saskatchewan Geological Survey, Sask. Energy and Mines (2012) 1–21.

[3.68] KENNICOTT, J., CHI, G., ASHTON, K., Field and Petrographic Study of Albitization Associated with Uranium Mineralization in the Beaverlodge Uranium District of Northern Saskatchewan, Rep. A4 2015-4.2, Saskatchewan Geological Survey, Sask. Ministry of the Economy (2015) 1–24.

[3.69] EVOY, E.F., Geology of the Gunnar Uranium Deposit, Beaverlodge Area, Saskatchewan, PhD Thesis, University of Wisconsin, Madison (1961).

[3.70] HOEVE, J., Uranium Metallogenic Studies: Relationship between Hudsonian Soda Metasomatism and Beaverlodge Vein-type Mineralization, Saskatchewan Geological Survey (1982) 57–59.

[3.71] HOEVE, J., QUIRT, D., Mineralization and Host Rock Alteration in Relation to Clay Mineral Diagenesis and Evolution of the Middle Proterozoic Athabasca Basin, Northern Saskatchewan, Canada, Tech. Rep. 187, Saskatchewan Research Council (1984).

[3.72] MERCADIER, J., RICHARD, A., BOIRON, M.C., CATHELINEAU, M., CUNEY, M., Brine migration in the basement rocks of the Athabasca Basin through microfracture networks (P-Patch U deposit, Canada), Lithos **115** (2010) 121–136.

[3.73] HAJNAL, Z., TAKÁCS, E., WHITE, D.J., GYÖRFI, I., POWELL, B., KOCH, R., “Regional seismic signature of the basement and crust beneath the McArthur River mine district, Athabasca Basin, Saskatchewan”, EXTECH IV: Geology and Uranium Exploration Technology of the Proterozoic Athabasca Basin, Saskatchewan and Alberta (JEFFERSON, C.W., DELANEY, G., Eds), Geological Survey of Canada Bulletin **588** (2007) 389–396.

[3.74] KYSER, T.K., HIATT, E., RENAC, C., DUROCHER, K., HOLK, G., DECKART, K., “Diagenetic fluids in Paleo- and Mesoproterozoic sedimentary basins and their implications for long protracted fluid histories”, Fluids and Basin Evolution (KYSER, T.K., Ed.), Min. Assoc. Can. Short Course **28** (2000) 225–262.

[3.75] BELOUSOVA, E.A., GRIFFIN, W.L., O’REILLY, S.Y., FISHER, N.I., Igneous zircon: trace element composition as an indicator of source rock type, Contrib. Min. Pet. **143** (2003) 602–622.

[3.76] RAINBIRD, R.H., RAYNER, N., STERN, R.A., SHRIMP U-Pb Geochronology of Apatite Cements and Zircon-bearing Tuff Clasts in Sandstones from the Athabasca Group, Athabasca Basin, Northern Saskatchewan and Alberta, Rep. 6, Saskatchewan Geological Survey (2003).

[3.77] RAINBIRD, R.H., STERN, R.A., RAYNER, N., JEFFERSON, C.W., "Age, provenance, and regional correlation of the Athabasca Group, Saskatchewan and Alberta, constrained by igneous and detrital zircon geochronology", EXTECH IV: Geology and Uranium Exploration Technology of the Proterozoic Athabasca Basin, Saskatchewan and Alberta (JEFFERSON, C.W., DELANEY, G., Eds), C **588** (2007) 193.

[3.78] RICHARD, A., ROZSYPAL, C., MERCADIER, J., BANKS, D.A., CUNEY, M., BOIRON, M.C., CATHELINEAU, M., Giant uranium deposits formed from exceptionally uranium-rich acidic brines, Nature **5** (2012) 142–146.

[3.79] RICHARD, A., CATHELINEAU, M., BOIRON, M.C., MERCADIER, J., BANKS, D., CUNEY, M., Metal-rich fluid inclusions provide new insights into unconformity-related U deposits (Athabasca Basin and Basement, Canada), Mineral. Dep. **51** (2015) 249–270.

[3.80] MACDONALD, C., Mineralogy and Geochemistry of a Precambrian Regolith in the Athabasca Basin, MSc Thesis, University of Saskatchewan, Saskatoon (1980).

[3.81] GABOREAU, S., CUNEY, M., QUIRT, D., BEAUFORT, D., PATRIER, P., MATHIEU, R., Significance of aluminium phosphate-sulfate minerals associated with U unconformity-type deposits: the Athabasca Basin, Canada, Am. Min. **92** (2007) 267–280.

[3.82] HECHT, L., M. CUNEY, M., "The role of diagenetic fluids in the mobilisation of LREE-U-Pb-Zr Mechanism of uranium mobilization in the Athabasca basin and basement by hydrothermal and/or diagenetic fluids", Proc. Conf. GAC–MAC, Calgary **25** (2000a).

[3.83] HECHT, L., CUNEY, M., Hydrothermal alteration of monazite in the Precambrian basement of the Athabasca basin: implications for the genesis of unconformity related deposits, Mineral. Dep. **35** (2000b) 791–795.

[3.84] GABOREAU, S., BEAUFORT, D., VIEILLARD, P., PATRIER, P., BRUNETON, P., Aluminum phosphate-sulfate minerals associated with Proterozoic unconformity-type uranium deposits in the East Alligator River Uranium Field, Northern Territories, Australia, Can. Min. **43** (2005) 813–827.

[3.85] MWENIFUMBO, C.J., PERCIVAL, J.B., BERNIUS, G., ELLIOTT, B., JEFFERSON, C.W., WASYLIUK, K., DREVER, G., "Comparison of geophysical, mineralogical and stratigraphic attributes in drill holes MAC 218 and RL 88, McArthur River uranium camp, Athabasca Basin, Saskatchewan", EXTECH IV: Geology and Uranium Exploration Technology of the Proterozoic Athabasca Basin, Saskatchewan and Alberta (JEFFERSON, C.W., DELANEY, G., Eds), Bull. Geol. Surv. Can. **588** (2007) 507–520.

[3.86] CUNEY, M., BROUAND, M., HECHT, L., BRUNETON, P., "Contrasted rare earth mobility during hydrothermal alteration in the Jabiluka U-deposit (Alligator Rivers district, Northern Territory, Australia)", Proc. Conf. GAC–MAC, Calgary **25** (2000).

[3.87] CUNEY, M., MATHIEU, R., Extreme light rare earth element mobilization by diagenetic fluids in the geological environment of the Oklo natural reactor zones, Franceville basin, Gabon, Geology **28** (2001) 743–746.

[3.88] MATHIEU, R., CUNEY, M., CATHELINEAU, M., Geochemistry of paleofluids circulation in the Franceville Basin and around Oklo natural reaction zones (Gabon), J. Geochem. Explor. **69–70** (2000) 245–249.

[3.89] MATHIEU, R., ZETTERSTRÖM, L., CUNEY, M., GAUTHIER-LAFAYE, F., HIDAKA, H., Alteration of monazite and zircon and lead migration as geochemical tracers of fluid paleocirculations around Oklo-Okélobondo and Bangombé natural nuclear reaction zones (Gabon), Chem. Geol. **171** (2001) 147–171.

[3.90] QUIRT, D.H., Lithogeochemistry of the Athabasca Group: Summary of Sandstone Data, Rep. 85–4, Saskatchewan Geological Survey, Sask. Energy and Mines (1985) 128–132.

[3.91] IBRAHIM, H.J., WU, H.F., "Geochemical and mineralogical alteration at the Midwest uranium-nickel deposits", Geology of Uranium Deposits: Canadian Institute of Mining and Metallurgy (SIBBALD, T.I., PETRUK, W., Eds), Special Volume **32** (1985) 73–84.

[3.92] MWENIFUMBO, C.J., BERNIUS, G., "A Th rich crandallite group mineral: a source of thorium enrichment in the Athabasca Group, Saskatchewan", EXTECH IV: Geology and Uranium Exploration Technology of the Proterozoic Athabasca Basin, Saskatchewan and Alberta (JEFFERSON, C.W., DELANEY, G., Eds), Bull. Geol. Surv. Can. **588** (2007) 521–532.

[3.93] PAGEL, M., Cadre Géologique des gisements d'uranium dans la structure Carswell (Saskatchewan, Canada) Etude des phases fluides, PhD Thesis, Université de Nancy 1, (1975a).

[3.94] PAGEL, M., Détermination des conditions physico-chimiques de la silicification diagénétique des grès Athabasca (Canada) au moyen des inclusions fluides, C.R. Acad. Sci. Paris **280** (1975b) 2301–2304.

[3.95] PAGEL, M., JAFFREZIC, M., Analyses chimiques des saumures des inclusions du quartz et de la dolomite du gisement d'uranium de Rabbit Lake (Canada): Aspect méthodologique et importance génétique, C. R. Acad. Sci. Paris **284** (1977) 113–116.

[3.96] PAGEL, M., POTY, B., SHEPPARD, S.M.F., "Contribution to some Saskatchewan uranium deposits mainly from fluid inclusion and isotopic data", Proc. Symp. International Uranium Symposium on the Pine Creek Geosyncline, IAEA, Vienna, (1980) 639–654.

[3.97] DEROME, D., CATHELINEAU, M., LHOMME, T., CUNEY, M., Fluid inclusion evidence of the differential migration of H_2 and O_2 in the McArthur River unconformity-type uranium deposit (Saskatchewan, Canada): possible role on post-ore modifications of the host rocks, J. Geochem. Explor. **78–79** (2003a) 525–530.

[3.98] DEROME, D., CATHELINEAU, M., CUNEY, M., FABRE, C., LHOMME, T., BANKS, D.A., Mixing of sodic and calcic brines and uranium deposition at the McArthur River, Saskatchewan, Canada: A Raman and laser induced breakdown spectroscopic study of fluid inclusions, Econ. Geol. **100** (2005) 1529–1545.

[3.99] RICHARD, A., Brine migration at the basement/sedimentary cover unconformity and formation of Proterozoic uranium mineralizations (Athabasca Basin, Canada), PhD Thesis, Institut National Polytechnique de Lorraine, Nancy, France, (2009).

[3.100] RICHARD, A., PETTKE, T., CATHELINEAU, M., BOIRON, M.C., MERCADIER, J., CUNEY, M., DEROME, D., Brine-rock interaction in the Athabasca basement (McArthur River U deposit, Canada): consequences for fluid chemistry and uranium uptake, Terra Nova **22** (2010) 303–308.

[3.101] DEROME, D., CUNEY, M. CATHELINEAU, M., DUBESSY, J., BRUNETON, P., A detailed fluid inclusion study in silicified breccias from the Kombolgie sandstones (Northern Territory, Australia): application to the genesis of Middle-Proterozoic unconformity-type uranium deposits, J. Explor. Geochim. **80** (2003b) 259–275.

[3.102] RAFFENSPERGER, J.P., GARVEN, G., The formation of unconformity-type uranium ore deposits II: Coupled hydrochemical modeling, Am. J. Sci. **295** (1995) 639–696.

[3.103] KOMNINOU, A., SVERJENSKY, D.A., Geochemical modeling of the formation of an unconformity-type uranium deposit, Econ. Geol. **91** (1996) 590–606.

[3.104] KISTER, P., LAVERRET, E., QUIRT, D., CUNEY, M., PATRIER, P., BEAUFORT, D., BRUNETON, P., Mineralogy and geochemistry of the host-rock alterations associated to the Shea Creek unconformity-type uranium deposits (Saskatchewan, Canada), part 2: Spatial distribution of the Athabasca Group sandstone matrix minerals, Clay Min. **54** (2006) 295–313.
[3.105] CARPENTER, A.B., TROUT, M.L., PICKETT, E.E., Preliminary report on the origin and chemical evolution of lead- and zinc-rich brines in central Mississippi, Econ. Geol. **69** (1974) 1191–1206.
[3.106] KRAEMER, T.F., KHARAKA, Y.K., Uranium geochemistry in geopressured-geothermal aquifers of the US Gulf Coast, Geochim. Cosmochim. Acta **50** (1986) 1233–1238.
[3.107] KHARAKA, Y.K., MAEST, A.S., CAROTHERS, W.W., LAW, L.M., LAMOTHE, P.J., FRIES, T.L., Geochemistry of metal-rich brines from central Mississippi Salt Dome basin, USA, Appl. Geochem. **2** (1987) 543–556.
[3.108] CONNOLLY, C.A., WALTER, L.M., BAADSGAARD, H., LONGSTAFFE, F., Origin and evolution of formation waters, Alberta Basin, Western Canada Sedimentary Basin I: isotope systematics and water mixing, Appl. Geochem. **5** (1990) 397–413.
[3.109] BANNER, J.L., WASSERBURG, G.J., CHEN, J.H., MOORE, C.H., 234U-238U-230Th-232Th systematics in saline groundwaters from central Missouri, Earth Planet. Sci. Lett. **101** (1990) 296–312.
[3.110] STUEBER, A.M., WALTER, L.M., Origin and chemical evolution of formation waters from Silurian-Devonian strata in the Illinois basin, USA, Geochim. Cosmochim. Acta **55** (1991) 309–325.
[3.111] LAND, L.S., MACPHERSON, G.L., Origin of saline formation waters, Cenozoic section, Gulf of Mexico sedimentary basin, Am. Assoc. Pet. Geol. Bull. **76** (1992) 1344–1362.
[3.112] PLUTA, I., ZUBER, A., Origin of brines in the Upper Silesian Coal Basin (Poland) inferred from stable isotope and chemical data, Appl. Geochem. **10** (1995) 447–460.
[3.113] HODGE, V.F., JOHANNESSON, K.H., STETZENBACH, K.J., Rhenium, molybdenum, and uranium in groundwater from the southern Great Basin, USA, Geochim. Cosmochim. Acta **60** (1996) 3197–3214.
[3.114] HITCHON, B., PERKINS, E.H., GUNTER, W.D., Recovery of trace metals in formation waters using acid gases from natural gas, Appl. Geochem. **16** (2001) 1481–1497.
[3.115] AQUILINA, L., LADOUCHE, B., DOERFLIGER, N., SEIDEL, J.L., BAKALOWICZ, M., DUPUY, C., LE STRAT, P., Origin, evolution and residence time of saline thermal fluids (Balaruc springs, southern France): implications for fluid transfer across the continental shelf, Chem. Geol. **192** (2002) 1–21.
[3.116] STOFFELL, B., WILKINSON, J.J., JEFFRIES, T,E., Metal transport and deposition in hydrothermal veins revealed by 213 nm UV laser ablation microanalysis of single fluid inclusions, Am. J. Sci. **304** (2004) 533–557.
[3.117] APPOLD, M.S., NUMELIN, T.J., SHEPHERD, T.J., CHENERY, S.R., Limits on the metal content of fluid inclusions in gangue minerals from the Viburnum Trend, Southeast Missouri, determined by laser ablation ICP-MS, Econ. Geol. **99** (2004) 185–198.
[3.118] HUIZENGA, J.M., GUTZMER, J., BANKS, D.A., GREYLING, L., The Palaeoproterozoic carbonate-hosted Pering Pb-Zn deposit, South Africa II: fluid inclusion, fluid chemistry and stable isotope constrains, Mineral. Dep. **40** (2006) 686–706.

[3.119] BOUCH, J.E., NADEN, J., SHEPHERD, T.J., MCKERVEY, J.A., YOUNG, B., BENHAM, A.J., SLOANE, H.J., Direct evidence of fluid mixing in the formation of stratabound Pb–Zn–Ba–F mineralisation in the Alston Block, North Pennine Orefield (England), Mineral. Dep. **41** (2006) 821–835.
[3.120] STOFFELL, B., APPOLD, M.S., WILKINSON, J.J., MCCLEAN, N.A., JEFFRIES, T.E., Geochemistry and evolution of Mississippi Valley-type mineralizing brines from the Tri-State and Northern Arkansas districts determined by LA-ICP-MS microanalysis of fluid inclusions, Econ. Geol. **103** (2008) 1411–1435.
[3.121] Piqué, A., Canals, A., Grandia, F., Banks, D.A., Mesozoic fluorite veins in NE Spain record regional base metal-rich brine circulation through basin and basement during extensional events, Chem. Geol. **257** (2008) 139–152.
[3.122] WILKINSON, J.J., STOFFELL, B., WILKINSON, C.C., JEFFRIES, T.E., APPOLD, M.S., Anomalously metal-rich fluids form hydrothermal ore deposits, Science **323** (2009) 764–767.
[3.123] SÁNCHEZ, V., VINDEL, E., MARTIN-CRESPO, T., CORBELLA, M., CARDELLACH, E., BANKS, D.A., Sources and composition of fluids associated with fluorite deposits of Asturias (N Spain), Geofluids **9** (2009) 338–355.
[3.124] APPOLD, M.S., WENZ Z.J., Composition of ore fluid inclusions from the Viburnum Trend, Southeast Missouri district, United States: implications for transport and precipitation mechanisms, Econ. Geol. **106** (2011) 55–78.
[3.125] KOTZER, T., KYSER, T.K., Petrogenesis of the Proterozoic Athabasca Basin, northern Saskatchewan, Canada, and its relation to diagenesis, hydrothermal uranium mineralization and paleohydrogeology, Chem. Geol. **120** (1995) 45–89.
[3.126] NG, R., ALEXANDRE, P., KYSER, T.K., Mineralogical and geochemical evolution of the unconformity-related McArthur River Zone 4 Orebody in the Athabasca Basin, Canada: implications of a silicified zone, Econ. Geol. **108** (2013) 1657–1689.
[3.127] CUI, T., YANG, J., SAMSON, I., Tectonic deformation and fluid flow: Implications for the formation of unconformity-related uranium deposits, Econ. Geol. **107** (2012a) 147–163.
[3.128] CUI, T., YANG, J., SAMSON, I., Solute transport across basement/cover interfaces by buoyancy driven thermohaline convection: implications for the formation of unconformity-related uranium deposits, Am. J. Sci. **312** (2012b) 994–1027.
[3.129] CHI, G., BOSMAN, S., CARD, C., Numerical modeling of fluid pressure regime in the Athabasca basin and implications for fluid flow models related to the unconformity-type uranium mineralization, J. Geochem. Explor. **125** (2013) 8–19.
[3.130] BOIRON, M.C., CATHELINEAU, M., RICHARD, A., Fluid flows and metal deposition near basement/cover unconformity: lessons and analogies from Pb–Zn–F–Ba systems for the understanding of Proterozoic U deposits, Geofluids **10** (2010) 270–292.
[3.131] DUBESSY, J., DEROME, D., SAUSSE, J., Numerical modelling of fluid mixings in the H_2O-NaCl system: applications to the North Caramal uranium prospect (Australia), Chem. Geol. **194** (2003) 25–39.
[3.132] HANOR, J.S., "Origin of saline fluids in sedimentary basins", Geofluids: Origin, Migration and Evolution of Fluids in Sedimentary Basins (PARNELL, J., Ed.), Geol. Soc. Spec. **78** (1994) 151–174.
[3.133] DAVISSON, M.L., CRISS, R.E., Na-Ca-Cl relations in basinal fluids, Geochim. Cosmochim. Acta **60** (1996) 2743–2752.
[3.134] HOUSTON, S., SMALLEY, C., LAYCOCK, A., YARDLEY, B.W.D., The relative importance of buffering and brine inputs in controlling the abundance of Na and Ca in sedimentary formation waters, Mar. Pet. Geol. **28** (2011) 1242–1251.

[3.135] RICHARD, A., BANKS, D.A., MERCADIER, J., BOIRON, M.C., CUNEY, M., CATHELINEAU, M., An evaporated seawater origin for the ore-forming brines in unconformity-related uranium deposits (Athabasca Basin, Canada): Cl/Br and $\delta^{37}Cl$ study of fluid inclusions, Geochim. Cosmochim. Acta **75** (2011) 2792–2810.
[3.136] RICHARD, A., KENDRICK, M.A., CATHELINEAU, M., Noble gases (Ar, Kr, Xe) and halogens (Cl, Br, I) in fluid inclusions from the Athabasca Basin (Canada): implications for unconformity-related U deposits, Precamb. Res. **247** (2014) 110–125.
[3.137] LEISEN, M., BOIRON, M.C., RICHARD, A., DUBESSY, J., Determination of Cl and Br concentrations in individual fluid inclusions by combining microthermometry and LA-ICPMS analysis: implications for the origin of salinity in crustal fluids, Chem. Geol. **330–331** (2012) 197–206.
[3.138] MERCADIER, J., RICHARD, A., CATHELINEAU, M., Boron- and magnesium rich marine brines at the origin of giant unconformity-related uranium deposits: $\delta^{11}B$ evidence from Mg tourmalines, Geology **40** (2012) 231–234.
[3.139] LOWENSTEIN, T.K., TIMOFEEFF, M.N., BRENNAN, S.T., HARDIE, L.A., DEMICCO, R.V., Oscillations in Phanerozoic seawater chemistry: Evidence from fluid inclusions, Science **294** (2001) 1086–1088.
[3.140] KOVALEVYCH, V.M., MARSHALL, T., PERYT, T.M., PETRYCHENKO, O.Y., ZHUKOVA, S.A., Chemical composition of seawater in Neoproterozoic: results of fluid inclusion study of halite from Salt Range (Pakistan) and Amadeus Basin (Australia), Precamb. Res. **144** (2006) 39–51.
[3.141] LOWENSTEIN, T.K., TIMOFEEFF, M.N., Secular variations in seawater chemistry as a control on the chemistry of basinal brines: test of the hypothesis, Geofluids **8** (2008) 77–92.
[3.142] EGLINGER, A., FERRAINA, C., TARANTOLA, A., ANDRÉ-MAYER, A.S., VANDERHAEGHE, O., BOIRON, M.C., DUBESSY, J., RICHARD, A., BROUAND, M., Hypersaline fluids generated by high-grade metamorphism of evaporites: fluid inclusion study of uranium occurrences in the Western Zambian Copper belt, Contrib. Min. Pet. **167** (2014) 1–28.
[3.143] HURTIG, N.C., HEINRICH, C.A., DRIESNER, T., HERRMANN, W., WALL, V., MATHISON, I., Fluid evolution and uranium (-Mo-F) mineralization at the Maureen Deposit (Queensland, Australia): unconformity-related hydrothermal ore formation with a source in the volcanic cover sequence, Econ. Geol. **109** (2014) 737–773.
[3.144] RUZICKA, V.R., Monometallic and polymetallic deposits associated with sub-Athabasca unconformity in Saskatchewan, Geological Survey of Canada Paper **1–C** (1989) 67–79.
[3.145] QUIRT, D., “Athabasca unconformity-type uranium deposits: one type of deposit with many variations”, Proc. Conf. Uranium Geochemistry 2003 (CUNEY, M., Ed.), Université Henri Poincaré, Nancy, France (2003) 309–312.
[3.146] MACHEL, H.G., Bacterial and thermochemical sulphate reduction in diagenetic settings - old and new insights, Sediment. Geol. **140** (2001) 143–165.
[3.147] HIATT, E.E., KYSER, T.K., “Sequence stratigraphy, hydrostratigraphy, and mineralizing fluid flow in the Proterozoic Manitou Falls Formation, eastern Athabasca Basin, Saskatchewan” EXTECH IV: Geology and Uranium Exploration Technology of the Proterozoic Athabasca Basin, Saskatchewan and Alberta (JEFFERSON, C.W., DELANEY, G., Eds), Bull. Geol. Surv. Can. **588** (2007) 489–506.
[3.148] NICKEL, E.H., NICHOLS, M.C., Mineral Reference Manual, Van Nostrand Reinhold, New York (1991) 250 pp.

[3.149] QUIRT, D., WASYLIUK, K., "Kaolinite, dickite, and other clay minerals in the Athabasca Group, Canada, and the Kombolgie Formation, Australia", Proc. Conf. 11th International Clay Conference, Ottawa, (1997).
[3.150] EARLE, S., WHEATLEY, K., WASYLIUK, K., "Application of reflectance spectroscopy to assessment of alteration mineralogy in the Key Lake area" Proc. Symp. MinExpo96 Symposium–Advances in Saskatchewan Geology and Mineral Exploration (ASHTON, K.E., HARPER, C.T., Eds), Saskatchewan Geological Society, Special Publication **14** (1999) 109–123.
[3.151] QUIRT, D.H., Kaolinite and Dickite in the Athabasca Sandstone, Northern Saskatchewan, Canada, Pub. No. 10400-16D01, Saskatchewan Research Council (2001) 1–27.
[3.152] WASYLIUK, K., Petrogenesis of the Kaolinite-group Minerals in the Eastern Athabasca Basin of Northern Saskatchewan: Applications to Uranium Mineralization, MSc Thesis, University of Saskatchewan, Saskatoon (2002).
[3.153] POLITO, P.A., KYSER, T.K., MARLATT, J., ALEXANDRE, P., BAJWAH, Z., DREVER, G., Significance of the alteration assemblages for the origin and evolution of the Proterozoic Nabarlek unconformity-related uranium deposit, Northern Territory, Australia, Econ. Geol. **99** (2004) 113–139.
[3.154] POLITO, P.A., KYSER, T.K, RHEINBERGER, G., A paragenetic and isotopic study of the Proterozoic Westmoreland uranium deposits, southern McArthur Basin, Northern Territory, Australia, Econ. Geol. **100** (2005a) 1243–1260.
[3.155] POLITO, P.A., KYSER, T.K., THOMAS, D., MARLATT, J., DREVER, G., Re-evaluation of the petrogenesis of the Proterozoic Jabiluka unconformity-related uranium deposit, Northern Territory, Australia, Mineral. Dep. **40** (2005b) 257–288.
[3.156] CREASER, R.A., STASIUK, L.D., "Depositional age of the Douglas Formation, northern Saskatchewan, determined by Re-Os geochronology", EXTECH IV: Geology and Uranium Exploration Technology of the Proterozoic Athabasca Basin, Saskatchewan and Alberta (JEFFERSON, C.W., DELANEY, G., Eds), Bull. Geol. Surv. Can. **588** (2007) 341–346.
[3.157] EDGECOMBE, S.M., HAZELL, M., PAGE, R.W., BLACK, L.P., SUN, S-S., OZCHRON National Geochronology Database Canberra, Geoscience Australia, http://www.ga.gov.au/databases/20010926_27.jsp (2002).
[3.158] ANDRADE, N., "Geology of the Cigar Lake uranium deposit", The Eastern Athabasca Basin and its Uranium Deposits (ANDRADE, N., BRETON, G., JEFFERSON, C.W., THOMAS, D.J., TOURIGNY, G., WILSON, S., YEO, G.M., Eds), GAC–MAC 2002, Saskatoon, Field Trip Guidebook A1, (2002) 53–72.
[3.159] MCGILL, B., MARLATT, J., MATTHEWS, R., SOPUCK, V., HOMENIUK, L., HUBREGTSE, J., The P2 North uranium deposit Saskatchewan, Canada, Explor. Mining Geol. **2** (1993) 321–331.
[3.160] PERCIVAL, J.B., Clay Mineralogy, Geochemistry and Partitioning of Uranium within the Alteration Halo of the Cigar Lake Uranium Deposit, Saskatchewan, Canada, PhD Thesis, Carleton University, Ottawa (1989).
[3.161] GALL, Q., DONALDSON, J.A., Diagenetic fluorapatite and aluminum phosphate-sulphate in the Paleoproterozoic Thelon Formation and Hornby Bay Group, northwestern Canadian Shield, Can. J. Earth Sci. **43** (2006) 617–628.
[3.162] ALEXANDRE, P., KYSER, T.K., THOMAS, D., POLITO, P., MARLAT, J., Geochronology of unconformity-related uranium deposits in the Athabasca Basin, Saskatchewan, Canada and their integration in the evolution of the basin, Mineral. Dep. **44** (2009) 41–59.

[3.163] SHEAHAN, C., FAYEK, M., QUIRT, D., A Combined ingress-egress model for the Kianna unconformity-related uranium deposit, Shea Creek project, Athabasca Basin, Canada, Econ. Geol. **111** (2016) 225–257.
[3.164] RENAC, C., KYSER, T.K., DUROCHER, K., DREAVER, G., O'CONNOR, T., Comparison of diagenetic fluids in the Proterozoic Thelon and Athabasca Basins, Canada: implications for protracted fluid histories in stable intracratonic basins, Can. J. Earth Sci. **39** (2002) 113–132.
[3.165] RIEGLER, T., LESCUYER, J-L., WOLLENBERG, P., QUIRT, D., BEAUFORT, D., Alteration related to uranium deposits in the Kiggavik-Andrew Lake structural trend, Nunavut Canada: New insights from petrography and clay mineralogy, Can. Min. **52** (2014) 27–45.
[3.166] SHARPE, R., FAYEK, M., QUIRT, D., JEFFERSON, C.W., Geochronology and genesis of the Bong uranium deposit, Thelon Basin, Nunavut, Canada, Econ. Geol. **110** (2015) 1759–1777.
[3.167] MATTHEWS, R., KOCH, R., LEPPIN, M., POWELL, B., SOPUCK, V., "Advances in integrated exploration for unconformity uranium deposits in western Canada", Geophysics and Geochemistry at the Millennium (GUBINS, A.G., Ed.), Proc. Conf. Fourth Decennial International Conference on Mineral Exploration, PDAC, Toronto (1997) 993–1002.
[3.168] WILDE, A. R., WALL, V. J., Geology of the Nabarlek uranium deposit, Northern Territory, Australia, Econ. Geol. **82** (1987) 1152–1168.
[3.169] BONS, P.D., FUSSWINKEL, T., GOMEZ-RIVAS, E., MARKL, G., WAGNER, T., WALTER, B., Fluid mixing from below in unconformity-related ore deposits, Geology **42** (2014) 1035–1038.
[3.170] HOEVE, J., SIBBALD, T.I.I., RAMAEKERS, P., LEWRY, J.F., "Athabasca Basin unconformity type uranium deposits: A special class of sandstonetype deposits?" Uranium in the Pine Creek Geosyncline (FERGUSON, J., GOLEBY, A.B., Eds), IAEA, Vienna, (1980) 575–594.
[3.171] HOEVE, J., QUIRT, D., "A stationary redox front as a critical factor in the formation of highgrade, unconformity-type uranium ores in the Athabasca Basin, Saskatchewan", Proc. Conf. Concentration Mechanisms of Uranium in Geological Environments, Nancy, France, (1985) 219–224.
[3.172] HOEVE, J., QUIRT D., A stationary redox front as a critical factor in the formation of high-grade, unconformity-type uranium ores in the Athabasca Basin, Saskatchewan, Canada, Bull. Mineral. **110** (1987) 151–171.
[3.173] HOEVE, J., QUIRT, D., "A common diagenetic-hydrothermal origin for unconformity-type uranium deposits and stratiform copper deposits", Geological Association of Canada, Special Paper **36** (1989) 151–172.
[3.174] WALLIS, R.H., SARACOGLU, N., BRUMMER, J.J., GOLIGHTLY, J.P., "Geology of the McClean uranium deposits", Uranium Exploration in the Athabasca Basin, Saskatchewan, Canada (CAMERON, E.M., Ed.), Geological Survey of Canada Paper **82-11** (1983) 71–110.
[3.175] BRUNETON, P., Geology of the Cigar Lake Uranium Deposit (Saskatchewan, Canada), Spec. Pub. 8, Saskatchewan Geological Society (1987) 99–119.
[3.176] BRUNETON, P., 1993, Geological environment of the Cigar Lake uranium deposit, Can. J. Earth Sci. **30** (1993) 653–673.
[3.177] QUIRT, D., Host Rock Alteration at Eagle Point South, Pub. No. R-855-1-E-89, Saskatchewan Research Council (1989) 95 pp.

[3.178] ALEXANDRE, P., KYSER, T.K., POLITO, P., THOMAS, D., Alteration mineralogy and stable isotope geochemistry of Paleoproterozoic basement hosted unconformity-type uranium deposits in the Athabasca Basin, Canada, Econ. Geol. **100** (2005) 1547–1563.
[3.179] YOUNG, G.M., Late Proterozoic stratigraphy and the Canada-Australia connection, Geology **20** (1992) 215–218.
[3.180] KOTZER, T.G., KYSER, T.K., IRVING, E., Paleomagnetism and the evolution of fluids in the Proterozoic Athabasca Basin, northern Saskatchewan, Canada, Can. J. Earth Sci. **29** (1992) 1474–1491.
[3.181] LI, Z. X., ZHANG, L., POWELL, C., Positions of the East Asian cratons in the Neoproterozoic supercontinent Rodinia, Austral. J. Earth Sci. **43** (1996) 593–604.
[3.182] HOFFMAN, P.F., Did the breakout of Laurentia turn Gondwanaland inside-out, Science **252** (1991) 1409–1412.
[3.183] KYSER, T.K., "Controls on fluids and basins", Fluids and Basin Evolution (KYSER, T.K., Ed.), Min. Assoc. Can. Short Course **28** (2000) 1–18.
[3.184] WHITMEYER, S.J., KARLSTROM, K.E., Tectonic model for the Proterozoic growth of North America, Geosphere **3** (2007) 220–259.
[3.185] CHAMBERLAIN, K.R., SCHMITT, A.K., SWAPP, S.M., HARRISON, T.M., SWOBODA-COLBERG, N., BLEEKER, W., PETERSON, T.D., JEFFERSON, C.W., KHUDOLEY, A.K., In situ U-Pb SIMS (IN-SIMS) micro-baddeleyite dating of mafic rocks: method with examples, Precamb. Res. **183** (2010) 379–387.
[3.186] LECHEMINANT, A.N., HEAMAN, L.M., MacKenzie igneous events, Canada: Middle Proterozoic hotspot magmatism associated with ocean opening, Earth Planet. Sci. Lett. **96** (1989) 38–48.
[3.187] CUNEY, M.L., CHABIRON, A., KISTER, P., GOLUBEV, V., DELOULE, E., "Chemical versus ion microprobe isotopic dating (CAMECA IMS 3f) of the Shea Creek unconformity-type uranium deposit (West Athabasca, Saskatchewan, Canada)", Proc. Conf. GAC–MAC, Saskatoon, **27** (2002) 25.
[3.188] LAVERRET, E., CLAUER, N., FALLICK, A., MERCADIER, J., PATRIER, P., BEAUFORT, D., BRUNETON, P., K-Ar dating and $\delta^{18}O$-δD tracing of illitization within and outside the Shea Creek uranium prospect, Athabasca Basin, Canada, App. Geochem. **25** (2010) 856–871.
[3.189] ARMSTRONG, R.L., QUIRT, D., HOEVE, J., Rb-Sr Dating of Diabase Dikes in the Athabasca Basin, Northern Saskatchewan, Pub. No. R-855-3-A-88, Saskatchewan Research Council (1988) 20 pp.
[3.190] MACDOUGALL, D.G., WILLIAMS, D.H., The Moore Lakes Complex, Neohelikian olivine diabase lopoliths in the Athabasca Group (part of NTS 74H-6 and -7), Saskatchewan Geological Survey, Sask. Energy and Mines, Summary of Investigations (1993) 86–91.
[3.191] FRENCH, J.E., HEAMAN, L.M., CHACKO, T., Feasibility of chemical U-Th-total Pb baddeleyite dating by electron microprobe, Chem. Geol. **188** (2002) 85–104.
[3.192] CONDIE, K.C., Supercontinents, Superplumes and Continental Growth: The Neoproterozoic Record, Special Publication no. 206, Geological Society of London (2002) 1–22.
[3.193] FAYEK, M., KYSER, T.K., RICIPUTI, L.R., U and Pb isotope analysis of uranium minerals by ion microprobe and the geochronology of the McArthur River and Sue Zone uranium deposits, Saskatchewan, Canada, Can. Min. **40** (2002a) 1553–1569.
[3.194] NELSON, J., COLPRON, M., Tectonics and metallogeny of the British Columbia, Yukon, and Alaskan Cordillera, 1.8 Ga to the present, Spec. Pub. No. 5, Geological Association of Canada, Mineral Deposits Division (2007) 755–791.

[3.195] ROGERS, J.J., A history of continents in the past three billion years, Geology **104** (1996) 91–107.
[3.196] SKIRROW, R.G., MERCADIER, J., ARMSTRONG, R., KUSKE, T., DELOULE, E., The Ranger uranium deposit, northern Australia: Timing constraints, regional and ore-related alteration, and genetic implications for unconformity-related mineralization, Ore Geol. Rev. **76** (2016) 463–503.
[3.197] LORILLEUX, G., JÉBRAK, M., CUNEY, M., BAUDEMONT, D., Polyphase hydrothermal breccia associated with unconformity-related uranium mineralizations (Canada): From fractal analysis to structural significance, J. Struct. Geol. **24** (2002) 323–338.
[3.198] EY, F., GAUTHIER-LAFAYE, F., LILLIÉ, F., WEBER, F., "A uranium unconformity deposit: The geological setting of the D orebody (Saskatchewan, Canada)", The Carswell Structure Uranium Deposits, Saskatchewan, (LAINÉ, R., ALONSO, D., SVAB, M., Eds), Spec. Pub. **29,** Geological Association of Canada (1985) 121–138.
[3.199] BAUDEMONT, D., PIQUARD, J.P., EY, F., ZIMMERMAN, J., The Sue uranium deposits, Saskatchewan, Canada, Explor. Min. Geol. **2** (1993) 179–202.
[3.200] VON EINSIEDEL, C.A., Petrography and Geochemistry of the Cluff Lake Breccias, Carswell Structure, Northern Saskatchewan, BSc Thesis, Carleton University, Ottawa (1981).
[3.201] HARPER, C.T., The Geology and Uranium Deposits of the Central Part of the Carswell Structure, Northern Saskatchewan, Canada, PhD Thesis, Colorado School of Mines, Golden, CO (1983).
[3.202] PAGEL, M., WHEATLEY, K., EY, F., "The origin of the Carswell circular structure", The Carswell Structure Uranium Deposits, Saskatchewan, (LAINÉ, R., ALONSO, D., SVAB, M., Eds), Spec. Pub. **29,** Geological Association of Canada (1985) 213–223.
[3.203] LORILLEUX, G., CUNEY, M., JEBRAK, M., RIPPERT, J.C., PORTELLA, P., Hydrothermal processes in an unconformity type uranium deposit in the eastern Athabasca Basin (Canada), J. Geochem. Explor. **80** (2003) 241–258.
[3.204] LE CARLIER DE VESLUD, C.H., CUNEY, M., LORILLEUX, G., ROYER, J.J., JÉBRAK, M., 3D modeling of uranium-bearing solution-collapse breccias in Proterozoic sandstones (Athabasca Basin, Canada–metallogenic interpretations, Comp. Geosci. **35** (2009) 92–107.
[3.205] KYSER, T.K., CUNEY, M., "Unconformity-related uranium deposits", Recent and Not-So-Recent Developments in Uranium Deposits and Implications for Exploration (CUNEY, M., KYSER, T.K., Eds), GAC–MAC 2008, Quebec, Short Course **39** (2008) 161–219.
[3.206] RICHARD, A., CAUZID, J., CATHELINEAU, M., BOIRON, M.C., MERCADIER, J., CUNEY, M., Synchrotron-XRF and XANES investigation of uranium speciation and element distribution in fluid inclusions from unconformity-related uranium deposits, Geofluids **13** (2013a) 101–111.
[3.207] YEO, G.M., POTTER, E.G., "Review of reducing mechanisms potentially involved in the formation of unconformity-type uranium deposits and their relevance to exploration", Paper A-12, Saskatchewan Geological Survey, Summary of Investigations, Vol. **2** (2010).
[3.208] MADORE, C., ANNESLEY, I.R., "Graphitic pelitic gneisses of the Paleoproterozoic Wollaston Group, Hearne province, Saskatchewan", Mineral Deposits, Research and Exploration:Where do they Meet? (PAPUNEN, H., Ed.), Balkema (1997) 79–82.

[3.209] THOMAS, D., MATTHEWS, R.B., SOPUCK, V., “Athabasca Basin (Canada) unconformity-type uranium deposits: exploration model, current mine developments and exploration directions”, Proc. Symp. Geology and Ore Deposits 2000: The Great Basin and Beyond (CLUER, J.K., PRICE, J.G., STRUHSACKER, E.M., HARDYMAN, R.F., MORRIS, C.L., Eds), Geological Society of Nevada, Reno, NV (2000) 103–126.
[3.210] ANNESLEY, I.R., MADORE, C., CUTLER, J., Synchrotron X-ray analysis of graphitic pelitic gneisses in the vicinity of unconformity-type uranium mineralization, Rep. 2001–4.2, Saskatchewan Geological Survey, Sask. Energy and Mines (2001) 132–140.
[3.211] LEVENTHAL, J.S., GRAUCH, R.I., THRELKELD, C.N., LICHTE, F.E., Unusual organic matter associated with uranium from the Claude deposit, Cluff Lake, Canada, Econ. Geol. **82** (1987) 1169–1176.
[3.212] WANG, A., DHAMENINCOURT, P., DUBESSY, J., GUERARD, D., LANDAIS, P., LELAURAIN, M., Characterization of graphite alteration in an uranium deposit by micro-Raman spectroscopy, X-ray diffraction, transmission electron microscopy and scanning electron microscopy, Carbon **27** (1989) 209–218.
[3.213] PASCAL, M., ANSDELL, K.M., ANNESLEY, I.R., “Graphite-bearing and graphite-depleted Basement Rocks in the Dufferin Lake Zone, South-central Athabasca Basin, Saskatchewan”, Targeted Geoscience Initiative 4: Unconformity-related Uranium Systems (POTTER, E.G., WRIGHT, D.M., Eds), Geological Survey of Canada, open file 7791 (2015) 91–100.
[3.214] PASCAL, M., BOIRON, M.C., ANSDELL, K., ANNESLEY, I.R., KOTZER, T., JIRICKA, D., CUNEY, M., Fluids preserved in variably altered graphitic pelitic schists in the Dufferin Lake zone, south-central Athabasca Basin, Canada: implications for graphite loss and uranium deposition, Mineral. Dep. **51** (2016) 619–636.
[3.215] BRAY, C.J., SPOONER, E.T.C., LONGSTAFFE, F.J., Unconformity-related uranium mineralization, McClean deposits, North Saskatchewan, Canada: hydrogen and oxygen isotope geochemistry, Can. Min. **26** (1988) 249–268.
[3.216] WILDE, A.R., MERNACH, T.P., BLOOM, M.S., HOFFMAN, C.F., Fluid inclusion evidence on the origin of some Australian unconformity-related uranium deposits, Econ. Geol. **84** (1989) 1627–1642.
[3.217] SPIRAKIS, C.S., The possible role of sulfate-reduction kinetics in the formation of hydrothermal uranium deposits, Econ. Geol. **76** (1981) 2236–2239.
[3.218] CHENEY, E.S., “Similarities between roll-type and Athabasca unconformity-type uranium deposits and the possible role of sulfides in their origin”, Geology of Uranium Deposits (SIBBALD, T.I.I., PETRUK, W., Eds) Canadian Institute of Mining, Spec. Vol., **32** (1985) 159–163.
[3.219] BEYER, S.R., KYSER, T.K., HIATT, E.E., FRASER, I., “Geological evolution and exploration geochemistry of the Boomerang Lake unconformity-type uranium prospect, Northwest Territories, Canada”, The Challenge of Finding New Mineral Resources: Global Metallogeny, Innovative Exploration, and New Discoveries (GOLDFARB, R.J., MARSH, E.E., MONECKE, T., Eds), Society of Economic Geology Spec. Pub. **15** (2010) 675–702.
[3.220] MARTZ, P., CATHELINEAU, M., MERCADIER, J., BOIRON, M.C., JAGUIN, J., TARANTOLA, A., DEMACON, M., GERBEAUD, O., QUIRT, D., DONEY, A., LEDRU, P., C-O-H-N fluid circulations and graphite precipitation in reactivated Hudsonian shear zones during basement uplift of the Wollaston-Mudjatik Transition Zone: Example of the Cigar Lake U deposit, Lithos **294-295** (2017) 222–245.

[3.221] KYSER, T.K., WILSON, M.R., RUHRMANN, G., Stable isotope constraints on the role of graphite in the genesis of unconformity-type uranium deposits, Can. J. Earth Sci. **26** (1989) 490–498.
[3.222] HUIZENGA, J. M., Thermodynamic modelling of a cooling C–O–H fluid–graphite system: implications for hydrothermal graphite precipitation, Mineral. Dep. **46** (2011) 23–33.
[3.223] BOTTRELL, S.H., CARR, L.P., DUBESSY, J., A nitrogen-rich metamorphic fluid and coexisting minerals in slates from North Wales, Min. Mag. **52** (1988) 451–457.
[3.224] HURAI, V., JANAK, M., LUDHOVA, L., HORN, E.E., THOMAS, R., MAJZLAN, J., Nitrogen-bearing fluids, brines and carbonate liquids in Variscan migmatites of the Tatra Mountains, Western Carpathians; heritage of high-pressure metamorphism, Eur. J. Mineral. **12** (2000) 1283–1300.
[3.225] SADOFSKY, S.J., BEBOUT, G.E., Ammonium partitioning and nitrogen isotope fractionation among coexisting micas during high temperature fluid-rock interactions: examples from the New England Appalachians, Geochim. Cosmochim. Acta **64** (2000) 2835–2849.
[3.226] MCCREADY, A.J., ANNESLEY, I.R., PARNELL, J., RICHARDSON, L.C., “Morphology, chemistry, and origin of carbonaceous matter from the McArthur River deposit, Saskatchewan, Canada”, Mineral Deposits, Processes to Processing (STANLEY, C.H., ET AL., Eds), A.A. Balkema (1999a) 251–254.
[3.227] MCCREADY, A.J., ANNESLEY, I.R., PARNELL, J., RICHARDSON, L.C., Uranium Bearing Carbonaceous Matter, McArthur River Uranium Deposit, Saskatchewan, Rep. 99–4.2, Saskatchewan Geological Survey, Sask. Energy and Mines (1999b) 110–120.
[3.228] WILSON, N.S.F., STASIUK, L.D., FOWLER, M.G., Post-mineralization Origin of Organic Matter in Athabasca Unconformity Uranium Deposits, Saskatchewan, Canada, Saskatchewan Geological Survey, Summary of Investigations **2** (2002).
[3.229] SANGÉLY, L., CHAUSSIDON, M., MICHELS, R., BROUAND, M., CUNEY, M., HUAULT, V., LANDAIS, P., Micrometer scale carbon isotopic study of bitumen associated with Athabasca uranium deposits: Constraints on the genetic relationship with petroleum source-rocks and the abiogenic origin hypothesis, Earth Planet. Sci. Lett. **258** (2007) 378–396.
[3.230] CHI, G., LI, Z., BETHUNE, K.M., Numerical modeling of hydrocarbon generation in the Douglas Formation of the Athabasca Basin (Canada) and implications for unconformity-related uranium mineralization, J. Geochem. Explor. **144** (2014) 37–48.
[3.231] GAUTHIER-LAFAYE, F., WEBER, F., The Francevillian (Lower Proterozoic) uranium ore deposits of Gabon, Econ. Geol. **84** (1989) 2267–2285.
[3.232] LANDAIS, P., DEREPPE, J.M., “A chemical study of the carbonaceous material from the Carswell structure”, The Carswell Structure Uranium Deposits, Saskatchewan, (LAINÉ, R., ALONSO, D., SVAB, M., Eds), Spec. Pub. **29,** Geological Association of Canada (1985) 165–174.
[3.233] LANDAIS, P., Organic geochemistry of sedimentary uranium ore deposits, Ore Geol. Rev. **11** (1996) 33–51.
[3.234] AGHBELAGH, Y.B, YANG, J., Effect of graphite zone in the formation of unconformity-related uranium deposits: Insights from reactive mass transport modeling, J. Geochem. Explor. **144** (2014) 12–27.
[3.235] SINHA, R.M., SHRIVASTAVA, V.K., SHARMA, G.V.G., PARTHASARATHY, T.N., Geological favourability for unconformity related uranium deposits in northern parts of the Cuddapah basin: evidence from Lambapur uranium occurrence, Andhra Pradesh, India, Explor. Res. Atomic Min. **8** (1995) 111–126.

[3.236] ALEXANDRE, P., KYSER, T.K., Effects of cationic substitutions and alteration in uraninite, and implications for the dating of uranium deposits, Can. Min. **43** (2005) 1005–1017.
[3.237] PRIVALOV, T., SCHIMMELPFENNIG, B., WAHLGREN, U., GRENTHE, I., Reduction of uranyl (VI) by iron (II) in solutions: an ab initio study, J. Phys. Chem. A **107** (2003) 587–592.
[3.238] LIGER, E., CHARLET, L., VAN CAPPELLEN, P., Surface catalysis of uranium (VI) reduction by iron (II), Geochim. Cosmochim. Acta **63** (1999) 2939–2955.
[3.239] JEON, B.H., DEMPSEY, B.A., BURGOS, W.D., BARNETT, M.O., RODEN, E.E., Chemical reduction of U (VI) by Fe (II) at the solid− water interface using natural and synthetic Fe (III) oxides, Enviro. Sci. Tech. **39** (2005) 5642–5649.
[3.240] TAYLOR, S.D., MARCANO, M.C., ROSSO, K.M., BECKER, U., An experimental and ab initio study on the abiotic reduction of uranyl by ferrous iron, Geochim. Cosmochim. Acta **150** (2015) 154–172.
[3.241] DARGENT, M., TRUCHE, L., DUBESSY, J., GILLES BESSAQUE, G., MARMIER, H., Reduction kinetics of aqueous U(VI) in acidic chloride brines to uraninite by methane, hydrogen or C-graphite under hydrothermal conditions: Implications for the genesis of unconformity-related uranium ore deposits, Geochim. Cosmochim. Acta **167** (2015) 11–26.
[3.242] KISH, L., CUNEY, M., Uraninite-albite veins from the Mistamisk Valley of the Labrador Trough, Quebec, Min. Mag. **44** (1982) 471–483.
[3.243] DUBESSY, J., PAGEL, M., BENY, J.-M., CHRISTENSEN, H., HICKEL, B., KOSZTOLANYI, C., POTY, B., Radiolysis evidenced by H_2–O_2 and H_2-bearing fluid inclusions in three uranium deposits, Geochim. Cosmochim. Acta **52** (1988) 1155–1167.
[3.244] KRYLOVA, T.L., ALESHIN, A.P., VELICHKIN, V.I., CUNEY, M., PIRONON, J., CHABIRON, A., POTY, B., "Uranium-bearing fluid composition at the Streltsovskoye and Antei deposits (Eastern Transbaikalia, Russia)", Proc. Conf. Uranium Deposits: from their Genesis to their Environmental Aspects International Workshop (KRIBEK, B., ZEMAN, J., Eds), Prague, Czech Republic (2002) 69–72.
[3.245] LIN, L.-H., SLATER, G.F., SHERWOOD LOLLAR, B., LACRAMPE-COULOUME, G., ONSTOTT, T.C., The yield and isotopic composition of radiolytic H2, a potential energy source for the deep subsurface biosphere, Geochim. Cosmochim. Acta **69** (2005) 893–903.
[3.246] HAWKES, H.E., Free hydrogen in genesis of petroleum, AAPG Bulletin **56** (1972) 2268–2270.
[3.247] SALVI, S., WILLIAMS-JONES, A.E., Fischer-Tropsch synthesis of hydrocarbons during sub-solidus alteration of the Strange Lake peralkaline granite, Quebec/Labrador, Canada, Geochim. Cosmochim. Acta **61** (1997) 83–99.
[3.248] SHERWOOD LOLLAR, B., WESTGATE, T.D., WARD, J.A., SLATER, G.F., LACRAMPE-COULOUME, G., Abiogenic formation of alkanes in the Earth's crust as a minor source for global hydrocarbon reservoirs, Nature **416** (2002) 522–524.
[3.249] SHERWOOD LOLLAR, B., LACRAMPE-COULOUME, G., VOGLESONGER, K., ONSTOTT, T.C., PRATT, L.M., SLATER, G.F., Isotopic signatures of CH_4 and higher hydrocarbon gases from Precambrian Shield sites: a model for abiogenic polymerization of hydrocarbons, Geochim. Cosmochim. Acta **72** (2008) 4778–4795.
[3.250] DROBNER, E., HUBER, H., WACHTERSHAUSER, G., ROSE, D., STETTER, K.O., Pyrite formation linked with hydrogen evolution under anaerobic conditions, Nature **346** (1990) 742–744.

[3.251] WÄCHTERSHÄUSER, G., The cradle chemistry of life: on the origin of natural-products in a pyrite-pulled chemoautotrophic origin of life, Pure Appl. Chem. **65** (1993) 1343–1348.
[3.252] GRAHAM, U.M., OHMOTO, H., Experimental study of formation mechanism of hydrothermal pyrite, Geochim. Cosmochim. Acta **58** (1994) 2187–2202.
[3.253] RICKARD, D., Kinetics of pyrite formation by the H_2S oxidation of iron (II) monosulfide in aqueous solution between 25 and 125 C: the rate equation, Geochim. Cosmochim. Acta **61** (1997) 115–134.
[3.254] FRENCH, B.M., Some geological implications of equilibrium between graphite and a C-H-O gas phase at high temperatures and pressures, Rev. Geophys. **4** (1966) 223–253.
[3.255] LEVINSON, A.A., Hydrogen — a reducing agent in some uranium deposits, Can. J. Earth Sci. **14** (1977) 2679–2681.
[3.256] DUBESSY, J., Simulation des équilibres chimiques dans le systèmme C–O–H : Conséquences méthodologiques pour les inclusions fluides, Bull. Minéral. **107** (1984) 155–168.
[3.257] CONNOLLY, J.A.D., CESARE, B., C–O–H–S fluid composition and oxygen fugacity in graphitic metapelites, J. Metamorph. Geol. **11** (1993) 379–388.
[3.258] MORTON, J.P., Rb-Sr dating of diagenesis and source age of clays in Upper Devonian black shales of Texas, Geol. Soc. Am. Bull. **96** (1985) 1043–1049.
[3.259] FAURE, G., Principles of Isotope Geology, John Wiley and Sons, New York, NY (1986) 589 pp.
[3.260] MACDOUGALL, J.D., "Radiogenic isotopes in seawater and sedimentary systems", Applications of Radiogenic Isotope Systems to Problems in Geology (HEAMAN, L., LUDDEN, J.N., Eds), Min. Assoc. Can. Short Course **19** (1991) 337–364.
[3.261] CLAUER, N., CHAUDHURI, S., KRALIK, M., BONNOT-COURTOIS, C., Effects of experimental leaching on Rb–Sr and K–Ar isotopic systems and REE contents of diagenetic illite, Chem. Geol. **103** (1993) 1–16.
[3.262] ROBINSON, A.G., COLEMAN, M.L., GLUYAS, J.G., The age of illite cement growth, Village Fields area, southern North Sea: Evidence from K-Ar ages and $^{18}O/^{16}O$ ratios, AAPG Bulletin **77** (1993) 68–80.
[3.263] CLAUER, N., "A new approach to Rb–Sr dating of sedimentary rocks", Lectures in Isotope Geology (JÄGER, E., HUNZIKER, J.C., Eds) Springer, Berlin, Heidelberg (1979) 30–51.
[3.264] CLAUER, N., Rb–Sr and K–Ar dating of Precambrian clays and glauconies, Precamb. Res. **15** (1981) 331–352.
[3.265] CLAUER, N., The Rubidium-Strontium Method Applied to Sediments: Certitudes and Uncertainties, Numerical Dating in Stratigraphy, John Wiley, New York, (1982) 245.
[3.266] KOTZER, T.G., KYSER, T.K., O, U and Pb isotopic and chemical variations in uraninite: implications for determining the temporal and fluid history of ancient terrains, Am. Min. **78** (1993) 1262–1274.
[3.267] HILLS, J.H., RICHARDS, J.R., The age of uranium mineralization in northern Australia, Search **3** (1972) 382–385.
[3.268] LUDWIG, K.R., GRAUCH, R.I., NUTT, C.J., NASH, J.T., FRISHMAN, D., SIMMONS, K.R., Age of uranium mineralization at the Jabiluka and Ranger uranium deposits, Northern Territory, Australia: New U-Pb isotope evidence, Econ. Geol. **82** (1987) 857–874.
[3.269] CUMMING, G.L., KRSTIC, D., The age of unconformity-related uranium mineralization in the Athabasca Basin, northern Saskatchewan, Can. J. Earth Sci. **29** (1992) 1623–1639.

[3.270] BOWLES, J.F.W., Age dating of individual grains of uraninite in rocks from electron microprobe analyses, Chem. Geol. **83** (1990) 47–53.
[3.271] CHIPLEY, D., POLITO, P.A., KYSER, T.K., Measurement of U-Pb ages of uraninite and davidite by laser ablation-HR-ICP-MS, Am. Min. **92** (2007) 1925–1935.
[3.272] HOLLIGER, P., Ages U-Pb définis in-situ sur la pitchblende à l'analyseur ionique, C.R. Acad. Sci. Paris **307** (1988) 367–373.
[3.273] MEDDAUGH, W.S., Age and Origin of Uraninite in the Elliot Lake, Ontario Uranium Ores, PhD Thesis, Harvard University, Cambridge (1983).
[3.274] HOLLIGER, P., CATHELINEAU, M., Le Chronométre U-Pb en milieu uranifère : application aux gisements hydrothermaux d'uranium liés spatialement au batholithe de Mortagne (Vendée, France), Chron. Rech. Min. **485** (1986) 33–43.
[3.275] HOLLIGER, P., CATHELINEAU, M., Ion-microprobe lead isotopic measurements on U ore minerals: application for in-situ determined Pb-Pb apparent ages, Terra Cognita **7** (1987) 230.
[3.276] HOLLIGER, P., CATHELINEAU, M., In situ U-Pb age determination by secondary ion mass spectrometry, Chem. Geol. **70** (1988) 173.
[3.277] FOUREL, F., LANCELOT, J.R., ALLÈGRE, C.J., DUPRÉ, B., Isotopic analyses of uraniferous minerals by both U-Pb and Sm-Nd methods, Chem. Geol. **70** (1988) 134.
[3.278] CATHELINEAU, M., BOIRON, M.C., HOLLIGER, P., POTY, B., Metallogenesis of the French part of the Variscan orogen. Part II: Time–space relationships between U, Au and Sn–W ore deposition and geodynamic events – Mineralogical and U–Pb data, Tectonophys. **177** (1990) 59–79.
[3.279] FAYEK, M., HARRISON, T.M., GROVE, M., COATH, C.D., A rapid in situ method for determining the ages of uranium oxide minerals, Inter. Geol. Rev. **42** (2000) 163–171.
[3.280] EVINS, Z.L., SUNDE, T., SCHÖBERG, H., FAYEK, M., U and Pb isotope calibration of uraninite and galena standards for SIMS, SKB Tech. Rep. TR-01-35 (2001) 49 pp.
[3.281] FAYEK, M., HARRISON, T.M., EWING, R.C., GROVE, M., COATH, C.D., O and Pb isotopic analyses of uranium minerals by ion microprobe and U–Pb ages from the Cigar Lake deposit, Chem. Geol. **185** (2002b) 205–225.
[3.282] STERN, R.A., RAYNAR, N., DAVIS, W., AMELIN, Y., ANNESLEY, I.R., BONLI, T., A method of determining uraninite U-Pb ages by SHRIMP II ion microprobe, Proc. Conf. Goldschmidt 2002, Davos, Switzerland (2002) A741.
[3.283] SHARPE, R.W., FAUYEK, M., Mass bias corrections for U-Pb isotopic analysis by secondary ion mass spectrometry: implications for U-Pb dating of uraninite, Rap. Comm. Mass Spec. **30** (2016)1601–1611.
[3.284] RAMAEKERS, P.P., DUNN, C.E., Geology and geochemistry of the eastern margin of the Athabasca Basin, Saskatchewan Geological Society Spec. Pub. **3** (1977) 297–322.
[3.285] FAHRIG, W.F., LOVERIDGE, W., Rubidium–strontium isochron age of weathered pre-Athabasca basement gneiss, northern Saskatchewan, Geol. Surv. Can. (1981) 1–6.
[3.286] ARMSTRONG, R.L., RAMAEKERS, P., Sr isotopic study of Helikian sediment and diabase dikes in the Athabasca Basin, northern Saskatchewan, Can. J. Earth Sci. **22** (1985) 399–407.
[3.287] HOEHNDORF, A., CARL, C., STRNAD, J.G., Age Determination of Basement Units in the Key Lake Uranium Deposit Area, Saskatchewan, Canada, IAEA–TECDOC–500, Vienna (1989).
[3.288] CARL, C., HOEHNDORF, F., VON PECHMANN, E., STRNAD, J.G., RUHRMANN, G., Geochronology of the Key Lake uranium deposit, Saskatchewan, Canada, Chem. Geol. **70** (1988) 133.

[3.289] CUMMING, G. L., KRSTIC, D., Geochronology at the Namew Lake Ni–Cu deposit, Flin Flon area, Manitoba, Canada: a Pb/Pb study of whole rocks and ore minerals, Can. J. Earth Sci. **28** (1991) 1328–1339.
[3.290] CLOUTIER, J., KYSER, T.K., OLIVO, G.R., ALEXANDRE, P., HALABURDA, J., The Millennium uranium deposit, Athabasca Basin, Saskatchewan, Canada: An atypical basement-hosted unconformity-related uranium deposit, Econ. Geol. **104** (2009) 815–840.
[3.291] CLOUTIER, J., KYSER, T.K., OLIVO, G.R., ALEXANDRE, P., Contrasting patterns of alteration at the Wheeler River area, Athabasca Basin, Saskatchewan, Canada: insights into the apparently uranium-barren zone K alteration system, Econ. Geol. **105** (2010) 303–324.
[3.292] TROCKI, L.K., CURTIS, D.B., GANCARZ, A.J., BANAR, J.C., Ages of major uranium mineralization and lead loss in the Key Lake uranium deposit, Northern Saskatchewan, Canada, Econ. Geol. **79** (1984) 1378–1386.
[3.293] PHILIPPE, S., LANCELOT, J.R., CLAUER, N., PACQUET, A., Formation and evolution of the Cigar Lake uranium deposit based on U–Pb and K–Ar isotope systematics, Can. J. Earth Sci. **30** (1993) 720–730.
[3.294] ALEXANDRE, P., KYSER, T.K., "Geochronology of the Paleoproterozoic basement-hosted unconformity-type uranium deposits in northern Saskatchewan, Canada", Proc. Conf. Uranium Geochemistry 2003 (CUNEY, M., Ed.), Université Henri Poincaré, Nancy, France (2003) 37–40.
[3.295] ALEXANDRE, P., KYSER, T.K., JIRICKA, D., WITT, G., Formation and evolution of the Centennial unconformity-related uranium deposit in the South-Central Athabasca Basin, Canada, Econ. Geol. **107** (2012) 385–400.
[3.296] KISTER, P., CUNEY, M., GOLUBEV, V.N., ROYER, J.J, LE CARLIER DE VESLUD, C., RIPPERT, J.C., Radiogenic lead mobility in the Shea Creek unconformity-related uranium deposit (Saskatchewan, Canada): migration pathways and Pb loss quantification, C.R. Geosci. **336** (2004) 205–215.
[3.297] CUMMING, G.L., KRSTIC, D., WORDEN, J.M., BAADSGAARD, H., Isotopic composition of lead in galena and Ni-arsenides of the Midwest deposit, northern Saskatchewan, Can. J. Earth Sci. **21** (1984) 649–656.
[3.298] KISTER, P., Mobilité des Eléments Géochimiques dans un Bassin Sédimentaire Clastique, du Protérozoïque à nos jours : Le Bassin Athabasca (Saskatchewan, Canada). PhD Thesis, INPL, Nancy France, (2003).
[3.299] BELL, K., "Geochronology of the Carswell area, Northern Saskatchewan", The Carswell Structure Uranium Deposits, Saskatchewan, (LAINÉ, R., ALONSO, D., SVAB, M., Eds), Spec. Pub. **29,** Geological Association of Canada (1985) 33–45.
[3.300] BOWIE, S.H.U., DARNLEY, A.G., Uranium-thorium-lead-isotope ratios as an aid to mineral exploration, Advanc. Sci. **20** (1975) 446–447.
[3.301] CANNON, R.S., Jr., PIERCE, A.P., Lead isotope guides for Mississippi Valley lead-zinc exploration, US Geol. Surv. Bull. (1969) G1–G20.
[3.302] DOE, B.R., "Lead isotopes applied to mineral exploration", US Geol. Surv. Prof. Paper (1979) 12 pp.
[3.303] HOLK, G.J., KYSER, T.K., CHIPLEY, D., HIATT, E.E., MARLATT, J., Mobile Pb-isotopes in Proterozoic sedimentary basins as guides for exploration of uranium deposits, J. Geochem. Explor. **80** (2003) 297–320.
[3.304] LEYBOURNE, M.I., COUSENS, B.L., GOODFELLOW, W.D., Lead isotopes in ground and surface waters; fingerprinting heavy metal sources in mineral exploration, Geochem. Explor. Enviro. Anal. **9** (2009) 115–123.

[3.305] SITNONETTI, A., BELL, K., HALL, G.E.M., Pb isotopic ratios and elemental abundances for selective leachates from near-surface till: implications for mineral exploration, App. Geochem. **11** (1996) 721–734.
[3.306] BEYER, S.R., KYSER, T.K., KOTZER, T., ANSDELL, K., WASYLIUK, K., QUIRT, D., "Expression of the McArthur River U deposit footprint in diverse surficial sampling media", Proc. Conf. GAC–MAC 2017, Kingston, ON **40** (2017) 47.
[3.307] KYSER, T.K., LAHUSEN, L., DREVER, G., DUNN, C., LEDUC, E., CHIPLEY, D., Using Pb isotopes in surface media to distinguish anthropogenic sources from undercover uranium sources, C.R. Geosci. **347** (2015) 215–226.
[3.308] STEWART, P., KYSER, T.K., GRIFFITHS, D., LAHUSEN, L., Dendrochemistry and soil clay geochemistry applied to exploration for deep U mineralization at the Halliday Lake Prospect, Athabasca Basin, Canada, Geochem. Explor. Enviro. Anal. **17** (2016) 164–181.
[3.309] MILLER, A.R., LECHEMINANT, A.N., Geology and uranium metallogeny of Proterozoic supracrustal successions, central District of Keewatin, N.W.T. with comparisons to northern Saskatchewan, Can. Inst. Min. Metall. Spec. Pub. **32** (1985) 167–185.
[3.310] FUCHS, H.D., HILGER, W., PROSSER, E., Geology and exploration history of the Lone Gull property, Can. Inst. Min. Metall. Spec. Pub. **33** (1986) 286–292.
[3.311] WEYER, H.J., FRIEDRICH, G., BECHTEL, A., BALLHORN, R.K., "The Lone Gull uranium deposit: New geochemical and petrological data as evidence for the nature of the ore bearing solutions", Rep. TC542/19, IAEA, Vienna (1987) 293–306.
[3.312] FRIEDRICH, G., WEYER, H.J., BECHTEL, A., "The Lone Gull uranium deposit: New geochemical and petrological data as evidence for the nature of the ore-bearing solutions", Proc. Conf. International Atomic Energy Agency Technical Committee Meeting on Metallogenesis of Uranium Deposits, IAEA TC-542 (1987).
[3.313] FUCHS, H., HILGER, W., "Kiggavik (Lone Gull): An unconformity related uranium deposit in the Thelon Basin, Northwest Territories, Canada", Proc. Conf. International Atomic Energy Agency Technical Committee Meeting, Saskatoon, Canada, 1987, IAEA TECDOC-**500** (1989) 429–454.
[3.314] RAMAEKERS, P., JEFFERSON, C.W., YEO, G.M., COLLIER, B., LONG, D.G.F., DREVER, G., et al., "Revised geological map and stratigraphy of the Athabasca Group, Saskatchewan and Alberta", EXTECH IV: Geology and Uranium Exploration Technology of the Proterozoic Athabasca Basin, Saskatchewan and Alberta (JEFFERSON, C.W., DELANEY, G., Eds), Bull. Geol. Surv. Can. **588** (2007) 155–192.
[3.315] RICHARD, A., BOULVAIS, P., MERCADIER, J., BOIRON, M.C., CATHELINEAU, M., CUNEY, M., FRANCE-LANORD, C., From evaporated seawater to uranium mineralizing brines: isotopic and trace element study of quartz dolomite veins in the Athabasca system, Geochim. Cosmochim. Acta **113** (2013b) 38–59.
[3.316] DONALDSON, J.A., The Dubawnt Group, districts of Keewatin and Mackenzie, Geological Survey of Canada Current Research Paper (1965) 64–20.
[3.317] JACKSON, M.J., PIANOSI, J.G., DONALDSON, J.A., "Aeolian dunes in early Proterozoic Thelon formation near Schultz Lake, central Keewatin", Geological Survey of Canada Current Research Paper **84-1B** (1984) 53–56.
[3.318] GALL, Q., PETERSON, T.D., DONALDSON, J.A., "A proposed revision of early Proterozoic stratigraphy of the Thelon and Baker Lake Basins, Northwest Territories", Geological Survey of Canada Current Research Paper **92-01C** (1992) 129–137.

[3.319] HIATT, E.E., KYSER, T.K., DALRYMPLE, R.W., Relationships among sedimentology, stratigraphy, and diagenesis in the Proterozoic Thelon Basin, Nunavut, Canada: implications for paleoaquifers and sedimentary-hosted mineral deposits, J. Geochem. Explor. **80** (2003) 221–240.
[3.320] PALMER, S.E., KYSER, T.K., HIATT, E.E., Provenance of the Proterozoic Thelon Basin, Nunavut, Canada, from detrital zircon geochronology and quartz detrital oxygen isotopes, Precamb. Res. **129** (2004) 115–140.
[3.321] BEYER, S., HIATT, E.E., KYSER, T.K., DALRYMPLE, R.W., PETTMAN, C., Hydrogeology, sequence stratigraphy and diagenesis in the Paleoproterozoic western Thelon Basin: influences on unconformity-related uranium mineralization, Precamb. Res. **187 (**2011) 293–312.
[3.322] HIATT, E.E., PALMER, S.E., KYSER, T.K., O'CONNOR, T.K., Basin evolution, diagenesis and uranium mineralization in the Paleoproterozic Thelon Basin, Nunavut, Canada, Basin Res. **22** (2010) 302–323.
[3.323] DAVIS, W.J., GALL, Q., JEFFERSON, C.W., RAINBIRD, R.H., Fluorapatite in the Paleoproterozoic Thelon basin: structural-stratigraphic context, in situ ion microprobe U-Pb ages, and fluid-flow history, Geol. Soc. of Am. Bull., **123** (2011) 1056–1073.
[3.324] MILLER, A.R., CUMMING, G., KRSTIC, D., U–Pb, Pb–Pb and K–Ar isotopic study and petrography of uraniferous phosphate bearing rocks in the Thelon Formation, Dubawnt Group, Northwest Territories, Canada, Can. J. Earth Sci. **26** (1989) 867–880.
[3.325] CHI, G., HAID, T., QUIRT, D., FAYEK, M., BLAMEY, N., CHU, H., Petrography, fluid inclusion analysis and geochronology of the End uranium deposit, Kiggavik, Nunavut, Canada, Mineral. Dep. **52** (2016) 211–232.
[3.326] ROBINSON, S.V.J., PAULEN, R.C., JEFFERSON, C.W., MCCLENAGHAN, M.B., LAYTON MATTHEWS, D., QUIRT, D., WOLLENBERG, P., Till geochemical signatures of the Kiggavik uranium deposit, Nunavut, Geological Survey of Canada open file 7550 (2014).
[3.327] SCOTT, J.M.J., PETERSON, T.D., DAVIS, W.J., JEFFERSON, C.W., COUSENS, B.L., Petrology and geochronology of Paleoproterozoic intrusive rocks, Kiggavik uranium camp, Nunavut, Can. J. Earth Sci. **52** (2015) 495–518.
[3.328] SHABAGA, B.M., FAYEK, M., QUIRT, D., JEFFERSON, C.W., CAMACHO, A., Mineralogy, geochronology, and genesis of the Andrew Lake uranium deposit, Thelon Basin, Nunavut, Canada, Can. J. Earth Sci. **54** (2017) 850–868.
[3.329] FARKAS, A., Mineralogy and host rock alteration of the Lone Gull deposit, Urangesellschaft Internal Report (1984) 44 pp.
[3.330] WEYER, H.J., Die Uranlagerstatte Kiggavik, Nordwestterritorien, Kanada. Genehmigte dissertation, Rheinisch-Westfalischien Technischen Hochschule, Aachen, Deutchland (1992) 212 pp.
[3.331] RIEGLER, T., Systeme D'alteration et Mineralisation en Uranium le Long du Faisceau Structural Kiggavik-Andrew Lake (Nunavut, Canada): Modele Genetique et Guides D'exploration, PhD Thesis, Poitiers, France, Universite de Poitiers (2013).
[3.332] KYSER, T.K., KOTZER, T., SIBBALD, T.I.I., "Oxygen, U-Pb and Pb-Pb isotope systematics in uraninite from complex U-Au-PGE vein-type and unconformity-type uranium deposits in northern Saskatchewan", Rep. 90-4, Saskatchewan Geological Survey (1990) 64–69.
[3.333] RIVERS, T., Assembly and preservation of lower, mid, and upper orogenic crust in the Grenville province–implications for the evolution of large hot long-duration orogens, Precamb. Res. **167** (2008) 237–259.

[3.334] BAGAS, L., NELSON, D.R., “Provenance of Neoproterozoic sedimentary rocks in the northwest Paterson Orogen, Western Australia”, Central Australian Basins Symposium Spec. Pub., Northern Territory Geological Survey (2007).
[3.335] CROSS, A., JAIRETH, S., RAPP R., ARMSTRONG, R., Reconnaissance style chemical U-Th-Pb dating of uraninite, Austral. J. Earth Sci. **58** (2011) 675–683.
[3.336] HICKMAN, A.H., BAGAS, L., Geology of the Rudall 1:100 000 sheet. Western Australia Geological Survey, 1:100 000 Geological Series Explanatory Notes (1998) 30 pp.
[3.337] BAGAS, L., SMITHIES, R.H., Geology of the Connaughton 1:100 000 sheet, Western Australia, Western Australia Geological Survey, 1:100 000 Geological Series, Explanatory Notes (1998) 38 pp.
[3.338] HUSTON, D.L., FRASER, G., CROSS, A., KOSITCIN, N., “Oasis U deposit, Queensland”, Uranium Mineralisation Events in Australia: Geochronology of the Nolans Bore, Kintyre, Oasis, Mt Gee-Armchair, and Maureen Deposits (SKIRROW, R.G., Ed.), Geosci. Austral. (2011) 12 pp.
[3.339] HANLY, A.J, The uranium mineralization potential and diagenetic fluid histories of the Proterozoic Yeneena, Sibley and Sioux Basins, PhD Thesis, Queen’s University, Kingston, Canada (2005).
[3.340] JACKSON, D.G., ANDREW, R.L., “Kintyre uranium deposit”, Geology of the Mineral Deposits of Australia and Papua New Guinea (HUGHES, F.E., Ed.), Australasian Institute of Mining and Metallurgy, Melbourne, Mono. **14** (1990) 653–658.
[3.341] HICKMAN, A.H., CLARKE, G.L., Geology of the Broadhurst 1:100 000 sheet, Western Australia, Western Australia Geological Survey (1994).
[3.342] GAUCI, G.C., CUNNINGHAM, C.C., A holistic approach to project design for cost effective yellowcake production at Kintyre, The Uranium Institute Annual Symposium (1992).
[3.343] GAUCI, G., The Kintyre Advancement Program. Twenty-Second Annual Symposium, Uranium Institute, London (1997) 1–6.
[3.344] HUSTON, D.L., MAAS, R., MIGGINS, D., MAIDMENT, D.W., CZARNOTA, K., PREISS, W., CASSIDY, K., “Neoproterozoic mineralisation in Australia: timing and geodynamic setting”, Proc. Conf. 10th Biennial SGA Meeting, Townsville, Australia (2009) 285–287.
[3.345] HAYNES, D.W., BROOKE, W.J.L., MAZZONI, P.P., “Application of conceptual models for sediment-hosted ore deposits in the discovery of the Nifty copper and adjacent zinc-lead deposits, Yeneena Basin, Western Australia”, Mineral Deposit Modeling (KIRKHAM, R.V., SINCLAIR, W.D., THORPE, R.I., DUKE, J.M., Eds), Geological Association of Canada Special Paper **40** (1993) 75–88.
[3.346] PAGE, R.W., JACKSON, M.J., KRASSAY, A.A., Constraining sequence stratigraphy in the north Australian basins: SHRIMP U-Pb zircon geochronology between Mt. Isa and McArthur River, Austral. J. Earth Sci. **47** (2000) 431–459.
[3.347] LALLY, J.H., BAJWAH, Z.U., Uranium Deposits of the Northern Territory, Northern Territory Geological Survey, Report **20** (2006).
[3.348] WYGRALAK, A.S., MERNAGH, T.P., Composition, provenance and timing of hydrothermal fluids in the Tanami–Arunta Regions, Tech. Rep. GS2008-004, Northern Territory Geological Survey (2008).
[3.349] AHMAD, M., WYGRALAK, A.S., Calvert Hills, Northern Territory 1:250 000 Metallogenic Map Series, sheet SE53-8. Northern Territory Geological Survey, Map and Explainatory Notes, Government Printer of the Northern Territory (1989).
[3.350] MCKAY, A.D., MIEZITIS, Y., Australia’s uranium resources, geology and development of deposits, Mineral Res. Report 1, AGSO–Geoscience Australia (2001).

[3.351] RHEINBERGER, G.M., HALLENSTEIN, C., STEGMAN, C.L., “Westmoreland uranium deposits”, Geology of Australian and Papua New Guinean Mineral Deposits (BERKMAN, D.A., MACKENZIE, D.H., Eds), Austral. Inst. Min., Metall., Melbourne (1998) 807–814.
[3.352] VIGAR, A.J., JONES, D.G., Laramide Recources Limited Westmorland uranium project Redtree Resources update, Mining Associates (2009) 183 pp.
[3.353] FUCHS, H.D., SCHINDLMAYR, W.E., “The Westmoreland uranium deposit Queensland Australia”, Uranium Exploration Case Histories, International Atomic Energy Agency, Vienna, (1981) 59–73.
[3.354] MERNAGH, T.P., WYGRALAK, A.S., A fluid inclusion study of uranium and copper mineral systems in the Murphy Inlier, Northern Australia, Russian Geol. Geophys. **52** (2011) 1421–1435.
[3.355] MIKHAILOV, V.A., KLUEV, N.K., TIKHOMIROV, L.I., KHARLAMOV, M.G., MELNIKOV, E.K., PETROV, Y.V., POLIKARPOV, V.I., SHARIKOV P.I., Metallogeny of uranium of Onega-Ladoga uranium ore province, Reg. Geol. Metall. **8** (1999) 65–82.
[3.356] MATRENICHEV, V.A., VREVSKY, A.V., SERGEEV, S.A., MATUKOV, D.A., The Ludicovian-Kalevian Boundary in the northern Ladoga region: geological relations and isotopic age, Dokl. Earth Sci., **407A** (2006) 388–392.
[3.357] KOTOVA, L.N., KOTOV, A.B., GLEBOVITSKII, V.A., PODKOVYROV, V.N., SAVATENKOV, V.N., Source rocks and provenances of the Ladoga Group siliciclastic metasediments (Svecofennian Foldbelt, Baltic Shield): Results of geochemical and Sm–Nd isotopic study, Stratig. Geolog Correl. **17** (2009) 1–19.
[3.358] NIRONEN, M., The Svecofennian orogeny: a tectonic model, Precamb. Res. **86** (1997) 21–44.
[3.359] BOGDANOVA, S.V., PASHKEVICH, I.K., GORBATSCHEV, R., ORLYUK, M.I., Riphean rifting and major Palaeoproterozoic crustal boundaries in the basement of the East European Craton: geology and geophysics, Tectonophys. **268** (1996) 1–21.
[3.360] AMELIN, Y.V., LARIN, A.M., TUCKER, R.D., Chronology of multiphase emplacement of the Salmi rapakivi granite-anorthosite complex, Baltic Shield: implications for magmatic evolution, Contrib. Mineral. Petrol. **127** (1997) 353–368.
[3.361] BOGDANOVA, S.V., BINGEN, B., GORBATSCHEV, R., KHERASKOVA, T.N., KOZLOV, V.I., PUCHKOV, V.N., VOLOZH, Y.A., The East European Craton (Baltica) before and during the assembly of Rodinia, Precamb. Res. **160** (2008) 23–45.
[3.362] MIKHAILOV, V.A., To the question of the genesis of ores of the unconformity-type deposits in the Karku deposit (Ladoga region), Materials on geology of deposits of uranium, rare and rare-earth metals, Moscow, **143** (2001) 30–39 (in Russian).
[3.363] VELICHKIN, V.I., KUSHNERENKO, V.K., TARASOV, N.N., ANDREEVA, O.V., KISELYOVA, G.D., KRYLOVA, T.L., DOINIKOVA, O.A., GOLUBEV, V.N., GOLOVIN, V.A., Geology and formation conditions of the Karku unconformity-type deposit in the northern Ladoga Region (Russia), Geol. Ore Dep. **47** (2005) 99–126.
[3.364] KUSHNERENKO, V.K., PETROV, YU.V., PICHUGIN, V.A., GROMOV, Y.A., SHURILOV, A.V., POLEKHOVSKY, Y.S., TARASOVA, I.P., BRITVIN, S.N., Geological structure and succession of the epigenetic mineragenesis of the Karku uranium deposit (north-eastern Ladoga area), Materials on Geology of Deposits of Uranium, Rare and Rare-Earth Metals, Issue 146, Moscow, (2004) 11–22 (in Russian).

[3.365] BOGDANOV, YU.B., SAVATENKOV, V.V., IVANIKOV, V.V., FRANK-KAMENETCKY, D.V., "Isotopic age of volcanites of the Salmi suite of the Riphean", Proc. Conf. 2nd Russian Conference on Isotopic Geochronology: Isotopic Geochronology for Solution of Problems of Geodynamics and Ore Genesis, St-Petersburg (2003) 71–72 (in Russian).
[3.366] RAMO, O.T., MANTTARI, I., KOHONEN, J., UPTON, B.G.J., LUTTINEN, A.V., LINDQVIST, V., LOBAEV, V., CUNEY, M., SVIRIDENKO, L.P., "Mesoproterozoic CFB magmatism in the Lake Ladoga Basin, Russian Karelia", Proc. Conf. The Fifth International Dyke Conference, Rovaniemi, Finland 2003, (VUOLLO, J., MERTANEN, S., Eds) (2005) 41–42.
[3.367] SKOROSPELKIN, S.A., Results on the estimation of prospects of uranium deposit discoveries near the pre-Riphean and pre-Palaeoproterozoic surfaces of the structural-stratigraphic unconformities on the base of compilation of geological-prognosis map of the 1:200 000 scale of Onega-Ladoga area, carrying out of specialized geological mapping of 1:50 000 scale in Svyr-Oyat and Ladva areas and reconnaissance drilling, Unpub. Rep. Nevskgeologia, Geological program 2–61 (2002) (in Russian).
[3.368] SHURILOV, A., Métallogenèse de l'Uranium dans la Région de Ladoga (Karélie, Russie), PhD Thesis, Université Henri Poincaré, Nancy (2008).
[3.369] PETROV, Yu.V., Prospecting of the high-profitable uranium deposits of the unconformity-type in the limits of the Karkunlampi ore field (40 km2) and the Salmi area on the base of the drilling and complex of the advance geophysical works, Unpub. Rep. Nevskgeologia (2006) (in Russian).
[3.370] KRANIDIOTIS, P., MACLEAN, W.H., Systematics of chlorite alteration at the Phelps Dodge massive sulfide deposit, Matagami, Quebec, Econ. Geol., **82** (1987) 1898–1911.
[3.371] ZANG, W., FYFE, W.S., Chloritization of the hydrothermally altered bedrock at the Igarapé Bahia gold deposit, Carajás, Brazil, Mineral. Dep. **30** (1995) 30–38.
[3.372] RICE, R., Paragenesis and Fluid History of the Karku Unconformity-Uranium Deposit, Pasha-Ladoga Basin, Western Russia, MSc Thesis, Queen's University, Kingston ON (2012).
[3.373] POLEKHOVSKY, Yu.S., TARASOVA, I.P., BRITVIN, S.N., KOLTSOV, A.B., SHURILOV, A.V., Geology and mineral paragenesises of Karku uranium deposit (North-Eastern Ladoga area, Karelia), Unpub. Rep. St. Petersburg State University (2005) (in Russian).
[3.374] SERGEEV, S.A., LOKHOV, K.I., SERGEEV; A.S., POLEKHOVSKY, Yu.S., "An experience of $^{207}Pb/^{206}Pb$ age determination of accessory minerals with the multichannel mass-spectrometer with ionization in inducted-coupled plasma with local laser ablation, Proc. Symp. XVI Symposium on Geochemistry of Isotopes in the Name of Academic A.P. Vinogradov, Moscow (2001) 225–226.
[3.375] POLLASTRO, R.M., Considerations and applications of the illite/smectite geothermometer in hydrocarbon-bearing rocks of Miocene to Mississippian age, Clays Clay Min., **41** (1993) 119–133.
[3.376] KYSER, T.K., KERRICH, R., "Retrograde exchange of hydrogen isotopes between hydrous minerals and water at low temperatures", Stable Isotope Geochemistry: A Tribute to Samuel Epstein (TAYLOR, H.P., O'NEIL, J.R., KAPLAN, I., Eds), Geochem. Soc. Spec. Pub. **3** (1991) 409–424.
[3.377] LOBAEV, V., Mineralogical and Petrogeochemical Characteristics of the Mesoproterozoic Pasha–Ladoga Volcanic-sedimentary Basin and its Basement (Baltic shield, Russia), Inferences on the Genesis of Unconformity-Related Uranium Deposits, PhD Thesis, Université Henri Poincaré, Nancy, France (2005).

[3.378] DOLGUSHINA I.S., “Geochemical criteria of the prognosis of the uranium deposits of unconformity type (by the example of the Karku deposit)”, Proc. Conf. Geology, Geochemistry and Ecology of the North-West of the Russia (2005) 19–22 (in Russian).
[3.379] DOLGUSHINA, I.S., KUSHNERENKO, V.K., “Geochemical prognostic criteria of unconformity-type uranium deposits (by the example of the Karku deposit)”, Proc. Conf. Materials on Geology of Deposits of Uranium, Rare and Rare-Earth Metals, Moscow **146** (2004) 37–41 (in Russian).
[3.380] POLIKARPOV V.I., About results of the prognostic-geological works of 1:50000 scale, led by the Central Expedition No 2 in the North-Eastern part of the Ladvinsky depression and its surrounding (Salminskaya area) in 1990–1993, Unpub. Rep. Nevskgeologia (1993) (in Russian).
[3.381] ORRELL, S.E., BICKFORD, M.E., LEWRY, J.F., Crustal evolution and age of thermotectonic reworking in the western hinterland of the Trans-Hudson Orogen, northern Saskatchewan, Precamb. Res. **95** (1999) 187–223.
[3.382] CUNEY, M., “World-class unconformity-related uranium deposits: Key factors for their genesis”, Proc. Conf. Society of Applied Geology, 8th biennal meeting, Beijing, China (2005) 245–246.
[3.383] PAGEL, M., Les gisements d'uranium lids spatialement aux discordances.,Géol. Géochim. Uranium, Nancy, Mém. **1** (1983) 380 pp.
[3.384] LÉVÈQUE, M.H., LANCELOT, J.R., GEORGE, E., The Bertholène uranium deposit –mineralogical characteristics and U/Pb dating of the primary U mineralization and its subsequent remobilization: consequences upon the evolution of the U deposits of the Massif Central, France, Chem. Geol. **69**, (1988) 147–163.
[3.385] SCHMITT, J.M., Albitisation Triasique, Hydrothermalisme Jurassique et Alteration Supergène Récente : Métallogénie des Gisements Uranifères du Rouergue, PhD Thesis, University of Strasbourg (1986).
[3.386] GEORGES, E., Les minéralisations uranifères jurassiques liées spatialement à une discordance hercynienne : Pétrographie, minéralogie et géochimie des gisements du Rouergue (Aveyron, France), Géol. Géochim. Uranium, Nancy, Mém. **9** (1985) 219 pp.
[3.387] GEOLOGICAL SURVEY OF INDIA, Geological Map of India, Geological Society of India, Kolkata, India (1998).
[3.388] BHOOPATHI, V., NIRANJAN KUMAR, S., SASTRY, R.S.N., SRINIVAS, B., RAMANA KUMAR, M., Delineation of target zones for detailed uranium exploration using secondary dispersion haloes (Pedogeochemical) as a tool in the NNW parts of Srisailam sub-Basin, Andhra Pradesh (India), Internat. J. of Sci. Res. Pub. **3** (2013b) 1–11.
[3.389] FRENCH, J.E, HEAMAN, L.M., Precise U–Pb dating of Paleoproterozoic mafic dyke swarms of the Dharwar craton, India: Implications for the existence of the Neoarchean supercraton Sclavia, Precamb. Res. **183** (2010) 416–441.
[3.390] MALLIKARJUNA, RAO, J., BHATTACHARJI, S., RAO, M.N., HERMES, O.D., “^{40}Ar-^{39}Ar ages and geochemical characteristics of dolerite dykes around the Proterozoic Cuddapa Basin, South India”, Mafic Dyke Swarms of Peninsular India (DEVARAJU, T.C., Ed.), Geol. Soc. India Memoir **33** (1995) 307–328.
[3.391] PANDEY, B.K., PRASAD, R.N., SASTRY, D.V.L.N., KUMAR, B.R.M., RAO, S.S., GUPTA, J.N., “Rb–Sr Whole rock ages for granites from parts of Andhra Pradesh and Karnataka”, Proc. Symp. Fourth National Symposium on Mass Spectrometry, Indian Institute of Science, Bengaluru (1988) 1–5.
[3.392] PANDEY, B.K., CHHABRIA, T., GUPTA, J.N., Geochemical characterisation of Proterozoic terrains of Peninsular India: relevance to the first order target selection for uranium exploration, Explor. Res. Atom. Miner. **8** (1995) 187–213.

[3.393] NAGARAJA RAO, B.K., RAJURKAR, S.T., RAMALINGASWAMY, G., RAVINDRA BABU, B., Stratigraphy, structure and evolution of the Cuddapah Basin, Purana Basins of peninsular India, Geol. Soc. India Memoir **6** (1987) 33–86.
[3.394] RAMAM, P.K., MURTY, V.N., Geology of Andhra Pradesh, Geol. Soc. India, Bengaluru, (1997) 245.
[3.395] VIMAL, R., BANERJEE, R., GUPTA, S., KRISHNA, V., ACHAR, K.K., RAMESH BABU, P.V., PARIHAR, P.S., MAITHANI, P.B., Geochemistry and Sr and Pb isotope systematics of basement granitoids from north and west of Palnad sub-Basin, Guntur and Nalgonda districts, Andhra Pradesh, J. Appl. Geochem. **14** (2012) 295–315.
[3.396] SHRIVASTAVA, V.K., PARTHASARATHY, T.N., SINHA, K.K., Geochemical study of the uraniferous granites from Lambapur area, Nalgonda district, Andhra Pradesh, India, Explor. Res. Atomic Min. **5** (1992) 41–52.
[3.397] SINGH, A.P., MISHRA, D.C., Tectonosedimentary evolution of Cuddapah Basin and Eastern Ghats mobile belt (India) as Proterozoic collision: gravity, seismic and geodynamic constraints, J. Geodyn. **33** (2002) 249–267.
[3.398] BANERJEE, R., BAHUKHANDI, N.K., RAHMAN, M., ACHAR, K.K., RAMESH BABU, P.V., UMAMAHESWAR, K., PARIHAR, P.S., Lithostratigraphic and radiometric appraisal of deeper parts of Srisailam and Palnad sub-basins in Kottapullareddipuram–Achchammagunta–Rachchamallepadu area, Guntur district, Andhra Pradesh, Explor. Res. Atomic Min. **22** (2012) 55–69.
[3.399] JEYAGOPAL, A.V., DESHPANDE, M.S.M., GUPTA, SHEKHAR., RAMESH BABU, P.V., UMAMAHESWAR, K., MAITHANI, P.B., Uranium mineralisation and association of carbonaceous matter in Koppunuru area, Palnad Sub-basin, Cuddapah Basin, Andhra Pradesh, Indian Mineral **45** (2011) 100–111.
[3.400] VERMA, M.B., GUPTA, SHEKHAR., SINGH, R.V., LATHA, A., MAITHANI, P.B., CHAKI, A., Orebody characterization of Koppunuru uranium deposit in Palnad Sub-basin, Guntur district, Andhra Pradesh, Indian Mineral **45** (2011) 51–61.
[3.401] RAMESH BABU, P.V., BANERJEE, R., ACHAR, K.K., Srisailam and Palnad Sub-basins: potential geological domains for unconformity-related uranium mineralisation in India, Explor. Res. Atomic Min. **22** (2012) 21–42.
[3.402] THOMAS, P.K., THOMAS, T., THOMAS, J., PANDIAN, M.S., BANERJEE, M.S., RAMESH BABU, P.V., GUPTA, S., VIMAL, R., Role of hydrothermal activity in uranium mineralisation in Palnad Sub-basin, Cuddapah Basin, India, J. Asian Earth Sci. **91** (2014) 280–288.
[3.403] BOIRON, M.C., CATHELINEAU, M., BANKS, D.A., BUSCHAERT, S., FOURCADE, S., COULIBALY, Y., MICHELOT, J.L., BOYCE, A., Fluid transfers at a basement/cover interface: part II. Large-scale introduction of chlorine into the basement by Mesozoic basinal brines, Chem. Geol. **192** (2002) 121–140.
[3.404] PANDEY, B.K., KRISHNA, V., PANDEY, U.K., SASTRY, D.V.L.N., "Radiometric dating of uranium mineralisation in the Proterozoic basins of eastern Dharwar craton, South India", Proc. Conf. International Conference on Peaceful uses of Atomic Energy, New Delhi, India, **1** (2009) 116–117.
[3.405] CAILTEUX, J.L.H., KAMPUNZU, A.B., LEROUGE, C., KAPUTO, A.K., MILESI, J.P., Genesis of sediment-hosted stratiform copper–cobalt deposits, central African Copperbelt, J. Afr. Earth Sci. **42** (2005) 134–158.
[3.406] DE WAELE, S., MUCHEZ, P., VETS, J., FERNANDEZ-ALONZO, M., TACK, L., Multiphase origin of the Cu–Co ore deposits in the western part of the Lufilian fold-and-thrust belt, Katanga (Democratic Republic of Congo), J. Afr. Earth Sci. **46** (2006) 455–469.
[3.407] MUCHEZ, P., VANDERHAEGHEN, P., DESOUKY, H., SCHNEIDER, J., BOYCE, A., DE WAELE, S., CAILTEUX, J.L.H., Anhydrite pseudomorphs and the origin of

stratiform Cu–Co ores in the Katangan Copperbelt (Democratic Republic of Congo), Mineral. Dep. **43** (2008) 575–589.

[3.408] HITZMAN, M.W., SELLEY, D., BULL, S., Formation of sedimentary rock-hosted stratiform copper deposits through earth history, Econ. Geol. **105** (2010) 627–639.

[3.409] MENEGHEL, L., The occurrence of uranium in the Katanga System of northwestern Zambia, Econ. Geol. **76** (1981) 56–68.

[3.410] DE WAELE, B., JOHNSON, S.P., PISAREVSKY, S.A., Palaeoproterozoic to Neoproterozoic growth and evolution of the eastern Congo Craton: Its role in the Rodinia puzzle, Precamb. Res. **160** (2008) 127–141.

[3.411] UNRUG, R., The Lufilian Arc: A microplate in the Pan-African collision zone of the Congo and the Kalahari cratons, Precamb. Res. **21** (1983) 181–196.

[3.412] JOHN, T., SCHENK, V., MEZGER, K., TEMBO, F., Timing and PT evolution of whiteschist metamorphism in the Lufilian Arc-Zambezi Belt orogen (Zambia): Implications for the assembly of Gondwana, Geology **112** (2004) 71–90.

[3.413] CAILTEUX, J.L.H., Lithostratigraphy of the Neoproterozoic Shaba-type (Zaire) Roan Supergroup and metallogenesis of associated stratiform mineralization, J. Afr. Earth Sci. **19** (1994) 279–301.

[3.414] PORADA, H., BERHORST, V., Towards a new understanding of the Neoproterozoic early Palæozoic Lufilian and northern Zambezi belts in Zambia and the Democratic Republic of Congo, J. Afr. Earth Sci. **30** (2000) 727–771.

[3.415] COSI, M., DE BONIS, A., GOSSO, G., HUNZIKER, J., MARTINOTTI, G., MORATTO, S., ROBERT, J.P., RUHLMAN, F., Late Proterozoic thrust tectonics, high-pressure metamorphism and uranium mineralization in the Domes Area, Lufilian Arc, Northwestern Zambia, Precamb. Res. **58** (1992) 215–240.

[3.416] DERRIKS, J.J., OOSTERBOSCH, R., “The Swambo and Kalongwe deposits compared to Shinkolobwe: Contribution to the study of Katanga uranium”, Proc. Conf. International Conference on Peaceful uses of Atomic Energy, Geneva (1958) 663–695.

[3.417] FRANÇOIS, A., Stratigraphie, tectonique et minéralisations dans l'arc cuprifère du Shaba (Rép. du Zaïre), Centenaire De La Société Géologique De Belgique, Liège (1974) 79–101.

[3.418] LORIS, N.B.T., Etude des Minéralisations Uranifères du Gisement Cupro-Cobaltifère de Luiswishi (Shaba, Zaïre): Contextes Géologiques et Géochimiques, Discussion des Modèles Génétiques, PhD Thesis, Polytechnic Faculty, Mons, Belgium (1996).

[3.419] CAILTEUX, J.L.H., Minéralisations à U–Pb–Se–Mo–Ni dans le gisement stratiforme cupro-cobaltifère de Kampove-Ouest (Shaba, Rép. Zaïre). Colloque Intern. Cornet : Gisements Stratiformes de Cuivre et Minéralisations Associées. Belgium, (1997) 245–268.

[3.420] LORIS, N.B.T., CHARLET, J.-M., OKITAUDJI, R., La mobilité de l'uranium et des métaux associés en environnement géologique oxydo-réducteur, le cas des minéralisations Cu–Co–Ni–U de Lwiswishi (Katanga, RDC), Acad. R. Sci. Outre Mer **48** (2002) 165–188.

[3.421] RICHARDS, J.P., CUMMING, G.L., KRSTIC, D., WAGNER, P.A., SPOONER, E.T.C., Pb isotope constraints on the age of sulfide ore deposition and U–Pb age of late uraninite veining at the Musoshi stratiform copper deposit, Central Africa copper belt, Zaire, Econ. Geol. **83** (1988) 724–741.

[3.422] DECRÉE, S., DELOULE, É., DE PUTTER, T., DE WAELE, S., MEES, F., YANS, J., MARIGNAC, C., SIMS U–Pb dating of uranium mineralization in the Katanga Copperbelt: Constraints for the geodynamic context, Ore Geol. Rev. **40** (2011) 81–89.

[3.423] EGLINGER, A., ANDRÉ-MAYER, A-S., VANDERHAEGHE, O., MERCADIER, J., CUNEY, M., DECRÉE, S., FEYBESSE, J.-L., MILESI, J.-P., Geochemical signatures of uranium oxides in the Lufilian belt: From unconformity-related to syn-metamorphic uranium deposits during the Pan-African orogenic cycle, Ore Geol. Rev. **54** (2013) 197–213.

[3.424] MERCADIER, J., CUNEY, M., LACH, P., BOIRON, M.-C., BONHOURE, J., RICHARD, A., LEISEN, L., KISTER, P., Origin of uranium deposits revealed by their rare earth element signature, Terra Nova **23** (2011) 264–269.

[3.425] AUDEOUD, D., Les Minéralisations Uranifères et Leur Environnement à Kamoto, Kambove et Shinkolobwe (Shaba, Zaïre): Pétrographie, Géochimie et Inclusions Fluides, PhD Thesis, Claude Bernard Lyon 1 Univ., France (1982).

[3.426] OKITAUDJI, L.R., Géologie Sédimentaire et Concentration Syndiagénétique du Cuivre et du Cobalt dans la "Série des Mines" du Shaba, Zaïre, PhD Thesis, Polytechnic National Institute of Lorraine, France (1989).

[3.427] DEROME, D., CATHELINEAU, M., FABRE, C., BOIRON, M.-C., BANKS, D., LHOMME, T., CUNEY, M., Paleo-fluid composition determined from individual fluid inclusions by Raman and LIBS: Application to mid-proterozoic evaporitic Na–Ca brines (Alligator Rivers Uranium Field, Northern Territories Australia), Chem. Geol. **237** (2007) 240–254.

[3.428] EL DESOUKY, H.A., BANKS, D., DE CLERCQ, F., CAILTEUX, J., MUCHEZ, P., "Chemistry of syn-orogenic copper–cobalt ore-forming fluids in the Katanga copperbelt, Democratic Republic of Congo", Proc. Conf. Geofluids VII, Rueil-Malmaison, France (2012) 83–86.

[3.429] HEIJLEN, W., BANKS, D.A., MUCHEZ, P., STENSGARD, B.M., YARDLEY, B.W.D., The nature of mineralizing fluids of the Kipushi Zn–Cu Deposit, Katanga, Democratic Repubic of Congo: Quantitative fluid inclusion analysis using laser ablation ICP-MS and bulk crush–leach methods, Econ. Geol. **103** (2008) 1459–1482.

[3.430] KOZIY, L., BULL, S., LARGE, R., SELLEY, D., Salt as a fluid driver, and basement as a metal source, for stratiform sediment-hosted copper deposits, Geology **37** (2009) 1107–1110.

[3.431] CHERKASOV, G.N., DOLGUSHIN, A.P., "Peculiarities in the formation uranium deposits of 'unconformity' type in folded regions of southern Siberia", Proc. Conf. 33rd International Geological Congress, Oslo, Norway **33** (2008).

[3.432] GENEST, S., Histoire Géologique du Bassin d'Otish, Protérozoïque Inférieur (Québec), PhD Thesis, Université de Montréal, Montréal, Canada (1989).

[3.433] GATZWEILER, R., Uranium mineralization in the Proterozoic Otish Basin, central Quebec, Canada. Berlin-Stuttgart, Gebrüder Borntaeger, Monograph Series on Mineral Deposits, **27** (1987) 27–48.

[3.434] CHOWN, E.H., CATY, J.L., Diagenesis of the Aphebian Mistassini regolith, Quebec, Canada, Precamb. Res. **19** (1983) 285–299.

[3.435] HAMILTON, M.A., BUCHAN, K.L., A 2169 Ma U-Pb baddeleyite age for the Otish Gabbro, Quebec: implications for correlation of Proterozoic magmatic events and sedimentary sequences in the eastern Superior Province, Can. J. Earth Sci. **53** (2016) 119–128.

[3.436] MILIDRAGOVIC, D., BEAUDOIN, G., HAMILTON, M.A., KING, J.J., The Paleoproterozoic Otish Gabbro suite and coeval dyke swarms of the Superior Province: Probing the c. 2.17 Ga mantle, Precamb. Res. **278** (2016) 126–144.

[3.437] HYNES, A.J., RIVERS, T., Protracted continental collision – evidence from the Grenville Orogen, Can. J. Earth Sci. **47** (2010) 591–620.

[3.438] CHOWN, E.H., Mineralization Controls in the Aphebian formations, Chibougamau; Mistassini and Otish areas, Can. Inst. Min. Metall. Spec. Vol. **34** (1984) 229–243.

[3.439] LESBROS-PIAT-DESVIAL, M., BEAUDOIN, G., MERCADIER, J., CREASER, R., Age and origin of uranium mineralization in the Camie River deposit (Otish Basin, Québec, Canada), Ore Geol. Rev. (in press).
[3.440] HÖHNDORF, A., BIANCONI, E., VON PECHMANN, E., "Geochronology and metallogeny of vein type uranium occurrences in the Otish Basin area, Quebec, Canada", Proc. Conf. Metallogenesis of Uranium Deposits, IAEA, Vienna (1987) 233–260.
[3.441] AUBIN, A., ZALUSKI, G., ROGERS, S., KELLER, C., BORT, E., Cameco Corporation 2011 Explor. Report – Camie River Project. Nov. 2012. Unpub. Cameco Corp. report (2012) 60 pp.
[3.442] BEYER, S.R., KYSER, T.K., HIATT, E.E., POLITO, P.A., ALEXANDRE, P., HOKSBERGEN, K., Basin evolution and unconformity-related uranium mineralization: the Camie River U Prospect, Paleoproterozoic Otish Basin, Quebec, Econ. Geol. **107** (2012) 401–425.
[3.443] RUZICKA, V., LE CHEMINANT, G.M., "Uranium deposit research", Current Research, Part. A, Geological Survey of Canada, Paper **84–1A** (1983) 39–51.
[3.444] AUBIN, A., "The Camie-Beaver and Otish South projects and the uranium potential of the Otish sedimentary Basin, Proc. Symp. Mines Baie-James (2011).
[3.445] ALEXANDRE, P., KYSER, T.K., LAYTON-MATTHEWS, D., BEYER, S., HIATT, E.E., LAFONTAINE, J., Formation of the enigmatic Matoush uranium deposit in the Paleoprotozoic Otish Basin, Quebec, Canada, Mineral. Dep. **50** (2015) 825–845.
[3.447] KISH, L., CUNEY, M., Uraninite – albite veins from the Mistamisk Valley of the Labrador Trough, Québec, Min. Mag. **44** (1981) 471–483.

4. EXPLORATION FOR UNFORMITY-RELATED URANIUM DEPOSITS

4.1. INTRODUCTION

When setting out to explore for Proterozoic unconformity uranium deposits, it is of the utmost importance to integrate both genetic and empirical/descriptive models. These models not only embody a comprehensive description of the selected deposit characteristics but also throw light upon these characteristics in terms of geological processes, as explained in Chapter 3. Both these models influence decisions including where and how to explore. Genetic models can be used to sift through the available information and identify areas that might meet a set of criteria for the potential to host an unconformity deposit. Alternatively, geological observations can be used to decide on the exploration potential of a specific area. Once an area is selected for exploration, both models need to be considered when looking for proxies such as structure and alteration, and can both be used to either predict trends or narrow down the search.

Genetic and empirical models remain relevant through all stages of the exploration process, from initial greenfields to brownfields programmes, and will both influence and be influenced by interpretations and observations. Regardless of the model, exploration programmes focus on proxies for source, transport, trap and fluid-rock interaction — as these have a larger physical footprint than ore bodies, and are thus easier to observe. This Chapter presents the most current geological, geochemical, and geophysical methods used in exploration for unconformity uranium deposits. The selection of the appropriate geological, geochemical, and geophysical exploration techniques presented in this Chapter, and the exploration strategy decided upon, depend ultimately on the characteristics of the ore deposit model.

Although most modern sedimentary basins contain formation waters that can be directly measured and characterized [4.1, 4.2], determining the origin and characteristics of palaeofluids responsible for metallogenesis and diagenesis of sediments in ancient basins is difficult, since traces of original pore waters rarely remain. The movement of fluids over large distances in basins is associated with several distinct geological processes, such as thermal and tectonic events, and the transport and deposition of metals [4.3–4.6]. Paleofluids leave behind vestiges of their existence in the form of diagenetic minerals and fluid inclusions (fossil fluids trapped in minerals) that have resulted from water-rock reactions [4.7, 4.8].

To develop a comprehensive genetic model for ore deposits related to diagenetic brines (e.g. unconformity-related uranium deposits), it is imperative that studies take an integrated approach. This would suggest combining descriptive field observations with quantitative chemical and isotopic analyses on well characterized minerals to provide information about fluid sources, the spatial and temporal extent of fluid events, fluid pathways and related aspects of ancient fluid systems. Results from these types of studies can then be used to develop an overall time-temperature-fluid history and aid in quantitatively assessing the mechanisms associated with the formation of an ore deposit.

The first approach to developing a genetic model for an ore system is to document the geology. For example, exploration for unconformity-related uranium deposits first begins in Proterozoic red-bed basins that unconformably overlie Archean to Palaeoproterozoic basement complexes and source regions characterized by high uranium contents [4.9]. Graphite-rich metasedimentary units and faults rooted in the basement rocks are generally favourable. Faults are the foci of fluid flow and uranium mineral deposition [4.10–4.14]. Zones of clay minerals form proximal to these faults whereas distal to the fault zones, the sandstone rocks have undergone a distinct diagenesis due to the lateral movement of fluids [4.10–4.13], [4.15–4.19].

Based on field observations, samples can be collected that represent different zones proximal and distal to the faults hosting mineralization and barren fault systems.

The usefulness of many of the basin minerals (e.g. uraninite, sulphides, clays) for establishing the timing and origin of major fluid events is limited without detailed knowledge of the chemical and isotopic composition of the mineral, which can only be accomplished by combining the results of detailed petrographic, fluid inclusion, and stable and radiogenic isotopic data from well-constrained samples [4.13, 4.19]. Petrographic examination of these minerals provides a useful and simple approach to developing the relative timing of formation of minerals (i.e. mineral paragenesis) that are associated with mineralized and barren systems. Fluid inclusion analysis provides information on the chemical composition of the fluids [4.20–4.27]. The stable isotopic composition of fluid inclusions and clay, silicate, sulphide and uranium minerals can provide information about the source of the fluids and temperature. For example, numerous studies have utilized oxygen and hydrogen isotopic compositions of diagenetic minerals as tracers for fluids [4.12, 4.15, 4.17, 4.28–4.35]. Stable isotopic studies of diagenetic and hydrothermal minerals from the basins that host high-grade, unconformity-related uranium ore deposits have shown that these deposits formed as a result of transport of metals by diagenetic basinal fluids (brines) and by mixing of the chemically and isotopically distinct diagenetic basin fluids with basement-derived fluids in fault zones at 200°C [4.10–4.12, 4.14–4.17, 4.36–4.38].

The palaeogeographic position and palaeoclimates of Proterozoic basins that host unconformity-related uranium deposits have changed markedly from low-latitude, coastal environments to their present locations [4.39, 4.40]. The large changes in the isotopic compositions and temperatures of the fluids, which have affected the basins, present a unique situation whereby oxygen and hydrogen isotopes can be used to trace specific fluids. Stable isotope analysis of clay and silicate minerals from these basins have been affected by varying degrees of post-crystallization alteration by low-temperature, deuterium-depleted meteoric waters which cannot be detected optically or by other spectroscopic methods such as X ray diffraction (XRD) [4.12, 4.14, 4.17, 4.36, 4.38].

Genetic models are incomplete without the knowledge of both the relative and absolute age of the deposit. Thus, K-Ar, Ar-Ar, Re-Os, Rb-Sr, Sm-Nd and U-Pb isotopic systematics of minerals whose stable isotopic compositions and paragenesis have been established provides insights into the ages and discern sources and pathways of fluid movements in basins [4.12,4.14, 4.17, 4.36, 4.38, 4.41-4.47].

Although determining the age of unconformity-related deposits is not straightforward, recent advances in micro analytical techniques (e.g. SIMS, ICP-MS) and the use of multiple radiogenic isotope systems (e.g. U-Pb, Ar-Ar, Re-Os), have provided researchers with an opportunity to date paragenetically well-characterized uranium minerals, and associated clay and silicate minerals [4.38, 4.47–4.49] precisely. The integration of these age data with other geological factors (e.g. tectonic orogenies) render geochronologic data easier to interpret and incorporate in a meaningful way for exploration purposes. The timing of the mineralizing process is required in exploration, so that the geological, chemical and physical environment conducive to the mineralizing process at a critical time in the evolution of an environment can be realized [4.9]. In addition to the age of the ore minerals, the timing of post-depositional events that have subsequently affected the ores can also reveal when elements were mobilized from the deposits and moved into secondary dispersion haloes that surround the deposit. Elevated concentration of these elements in the surrounding environment can provide additional evidence of the presence of an ore system, with gradients in concentrations as vectors towards a deposit [4.50, 4.51].

In summary, the integration of descriptive and genetic models is the key to developing the next generation of exploration models. Knowledge of the types of fluids involved in the ore-forming process is absolutely critical for refining exploration strategies. The critical factors involved in identifying the fluids include time, temperature, pressure, oxygen fugacity, and chemical and isotopic composition. Without knowledge of these critical factors, it is difficult to identify the correct environment in which to explore [4.9, 4.18]. For next generation exploration models, it is also equally important that a comparison is made between the characteristics of fluids associated with mineralized and barren systems, and to recognize which critical factors are important for ore formation.

4.2. TECHNIQUES USED IN EXPLORATION FOR UNCONFORMITY-RELATED DEPOSITS

4.2.1. Introduction

Proterozoic unconformity-related uranium deposits are rarely exposed at surface because they are located at the unconformity between older basement rocks and the overlying Proterozoic sedimentary cover. Therefore, the probability of discovering a deposit by exploring a rocky outcrop is extremely small, and exploration should be focused on the identification of proxies that can be indicative of the uranium mineralizing processes. The type of proxy will vary based on the style of the mineralization and the geology. Fig. 4.1 is a composite schematic representation of an unconformity-related uranium deposit with associated proxies and geologic environments. A deposit may have one or more of these proxies, based on the geologic environment.

Currently, only two underground mines are in operation worldwide and they contribute over 20% of the world's production [4.52]. The McArthur River and Cigar Lake mines are located in the Athabasca Basin and are approximately 45 km apart. The exploration costs associated with these deposit types range from tens of thousands of dollars for chemical soil survey to millions of dollars for a multi-phase diamond drilling programme. In 2016, exploration expenditures in the Athabasca Basin amounted to Canadian $44.8 million [4.53]. Major uranium companies, such as AREVA and Cameco Corporation, will commit the majority of their annual worldwide exploration budget to the Athabasca Basin. Exploration expenditures in the Northern Territory of Australia have seen a steady decline since 2011, and recorded exploration expenditures of Australian $4 million in 2016 [4.54].

There are many variables to consider when starting an exploration programme within the confines or vicinity of a Palaeoproterozoic basin. The genetic end members of Proterozoic unconformity-related uranium deposits as outlined in Chapter 2 have associated footprints related to primary and secondary alteration halos. The environmental conditions dictate the costs, types of surveys and sample types (e.g. soil, rocks), while the sampling methodology dictates the survey scale. Table 4.1 outlines the common types of samples in relation to a range of environmental conditions such as boreal forest, rain forest, arid or arctic conditions.

Over the last century, exploration geologists have developed a multitude of tools and methods that can be used to explore for unconformity-related uranium deposits. The following sections describe a wide range of methods (geological, geochemical and geophysical) with examples of how and when they can be utilized.

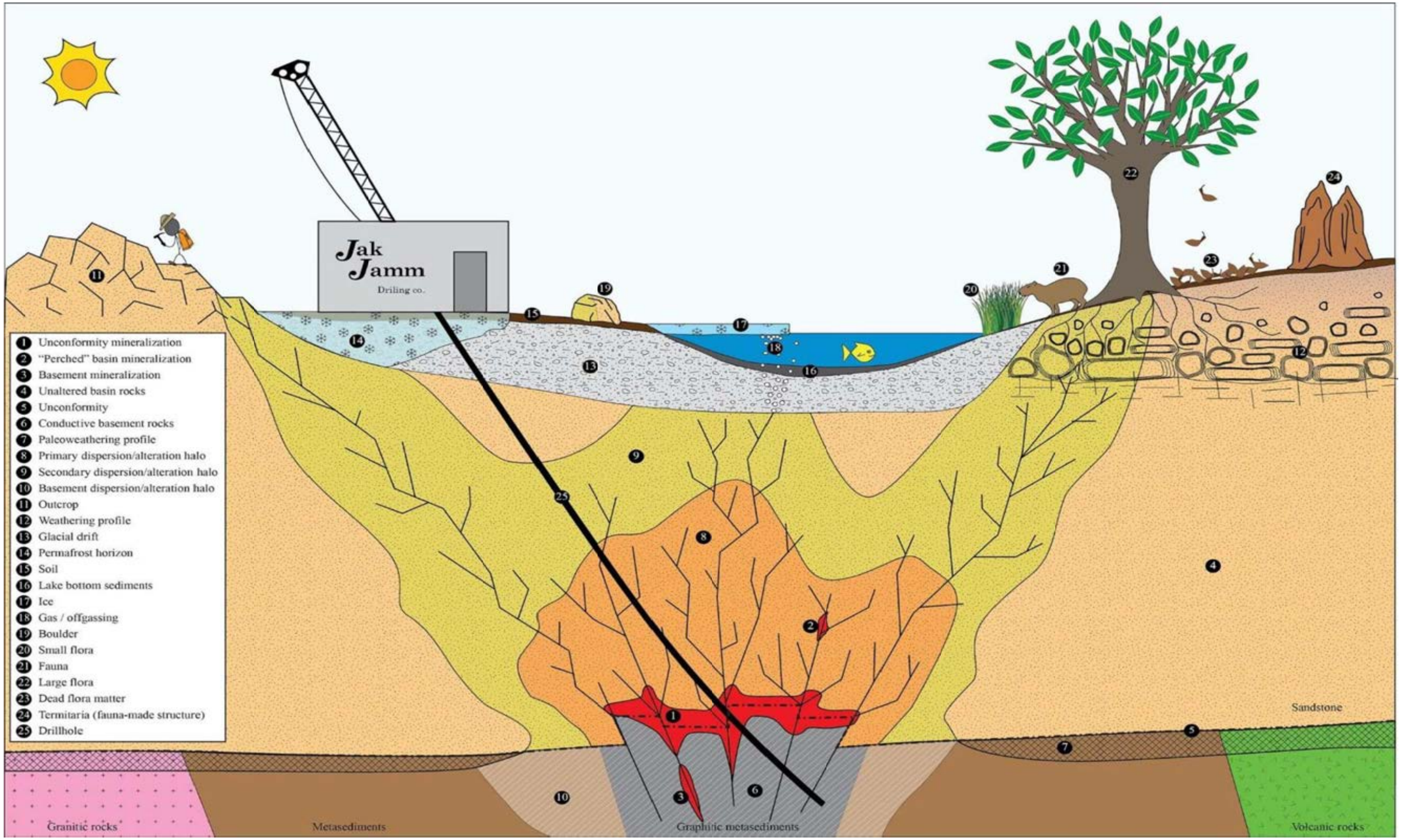

FIG. 4.1. Schematic depiction of a generic Proterozoic unconformity uranium deposit with its principal characteristics and most of the possible environments that can be sampled/imaged/tested for signs of mineralization and/or the dispersion halo associated with the deposits. None of the elements depicted are to scale. Climate on the left side can be interpreted as arctic to boreal, while that on the right can be interpreted as more tropical.

4.2.2. Geography and geology

Detailed knowledge of the geography and geology of an area is critical for any exploration programme and often guides the initial exploration strategies and the selection of methods used to explore for a deposit. The geology can provide important information on the source of the metals, the fluid pathways and the traps necessary to form the ore deposits of interest.

4.2.2.1. Surface cover and overburden

The surface of an area of possible interest for unconformity-related uranium exploration can be covered by soils, unconsolidated sediments, grasses, forests or water, which can range in thickness from millimetres to hundreds of metres. The surface cover type dictates the type of exploration survey that may yield the best results. For example, if an area is covered by lakes, a lake sediment survey may be appropriate. The surface can also host dispersion halos associated with these uranium deposits. Therefore, trace element or isotope geochemistry of the surface soils, vegetation, sediments and water can be used to define these dispersion halos and potentially provide targets for a drilling programme.

The composition of the overburden can also influence geophysical surveys. For example, surface lithologies that contain an abundance of magnetically susceptible minerals can produce geophysical anomalies that can be drilled to explore for mineralization at depth. Boulder trains can often be detected by airborne and magnetic surveys. However, clay-rich lithologies can mask geophysical anomalies and the thickness of the overburden can add to the cost of drilling. Other considerations include access to the site and access to water for drilling.

4.2.2.2. Bedrock mapping

Bedrock mapping is critical to the exploration strategy used to explore for unconformity-related uranium deposits. Quite often, various techniques are required to gain access to the bedrock, such as trenching to remove soil or drilling to determine rock types in the subsurface. Information gained from mapping the bedrock includes the relationship between rock types, distinguishing between barren and mineralized structures, metamorphic grade, and alteration mineralogy. The use of satellite images and multispectral sensors (ground- and satellite-based) are common tools for explorations and have enhanced outcrop mapping.

Most of the unconformity-related uranium deposits in Australia, Canada, India and the Russian Federation occur proximal to the unconformity between flat-lying, late Palaeoproterozoic to Mesoproterozoic unmetamorphosed, intracontinental quartz-rich sandstones [4.55, 4.56] and Archean and Palaeoproterozoic granitoid rocks (commonly called basement rocks). Orebodies often occur in fracture zones and can be hosted by the sediments, basement rocks or both (Fig. 4.1). The basin fill consists of a monotonous package of fluvial and Aeolian sediments that varies in thickness from a few millimeters along the edges of basins to kilometres deep in the centre of the basins.

4.2.2.3. Reverse circulation (RC) drilling and hammers

Reverse circulation drilling, commonly called RC drilling, is a form of bedrock sampling that provides a series of chips and pulverized lithological samples for interpretation and analysis. The drilling technique works by forcing large volumes of air generated by surface compressors through a chambered drill stem. The forced air, in turn, activates a pneumatic reciprocating piston known as a hammer that rotates a tungsten-steel drill bit. The drill bit and drill stem continuously rotate as the rock is being hammered. Pulverized rock and fragments are carried up by the strong airflow through the middle of the bit into an inner chambered drill pipe or, the samples can be forced out of the drill pipe and back to the surface. The air current is strong enough to bring rock material to the surface from a depth of hundreds of metres. When the samples reach the surface, the pulverized rock and fragments are often fed into a cyclone splitter that slows the air flow down and divides the sample into small and large samples. Depending on the importance of the sampling, they can be bagged and stored, so that a portion of the sample may be retrieved for future studies.

The advantage of the RC drilling technique is that it uses forced air rather than water, which is required for diamond drilling operations. Therefore, in arid and artic conditions, RC drilling has advantages over diamond drilling. Other factors to consider are cost and production rates. RC drilling costs are generally lower than diamond drilling and its penetration rates are faster.

The disadvantage of RC drilling is that the samples produced are pulverized rock chips, which makes rock and mineral identification difficult. Also, information regarding the relationship between rock types and structures is lost.

Reverse circulation hammers produce pulverized rock fragments that are returned to the surface inside the drill rod string (Fig. 4.2). Thus, these provide the depth of the downhole sample and shield the samples from contamination with other surrounding lithologies. In comparison, conventional hammers operate in air and the sample return takes place outside the drill string and as such, samples can be contaminated by various lithologies as they travel uphole (Fig. 4.2).

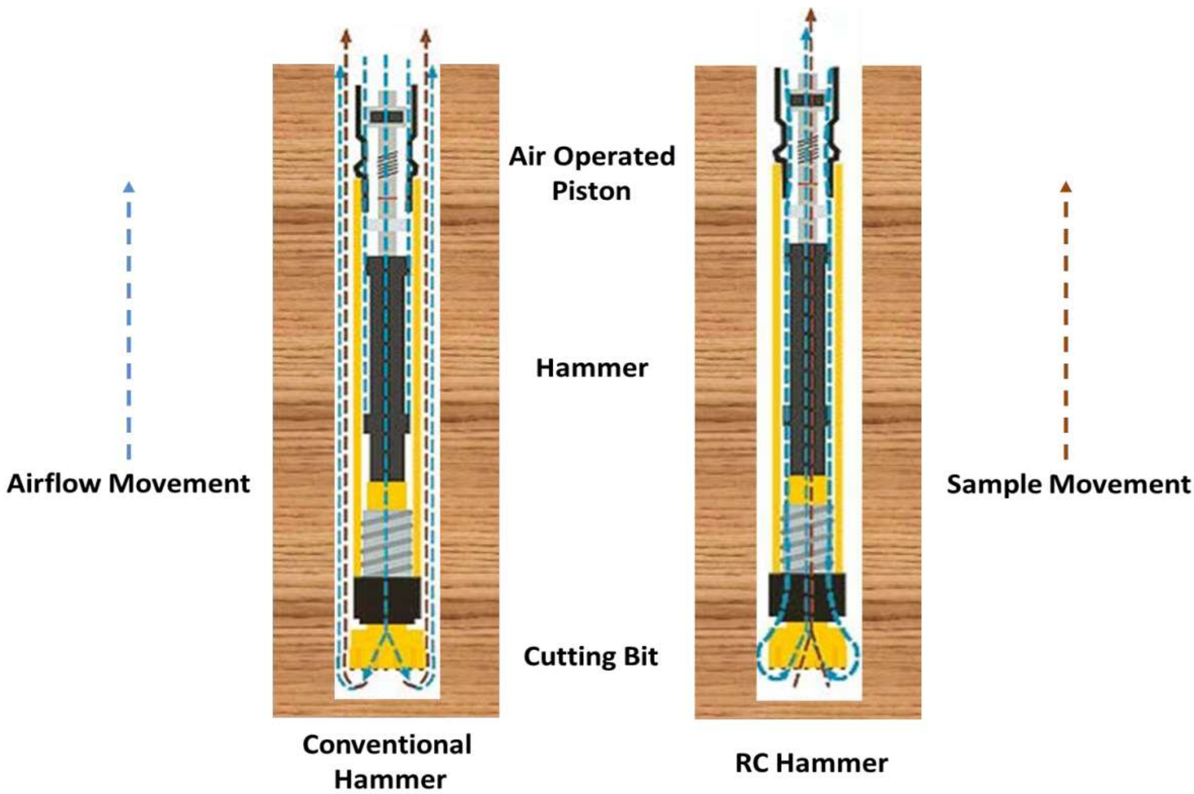

FIG. 4.2. Simplified reverse circulation drilling methodology (modified and reproduced courtesy of Atlas Copco) [4.57].

TABLE 4.1. OVERVIEW OF DIFFERENT EXPLORATION TECHNOLOGIES AND THEIR APPLICABILITY

Scientific field	Method ID	Scale		Detection				Cost of Survey	Personnel Requirements	Computer/Software Requirements
		Regional	Project	Ore	Primary Dispersion	Secondary Dispersion	Geololgy / Structure	$ - $$$$$	👤 - 👤👤👤👤👤	💻 - 💻💻💻💻💻
Geophysics										
Airborne Surveys	Radiometrics	✓	✓	✓				$	👤	💻💻
	Magnetics	✓	✓		✓		✓	$	👤	💻💻
	Electromagnetics	✓	✓				✓	$$$	👤👤	💻💻💻💻
	VLF-EM	✓	✓				✓	$	👤	💻💻
	MT/AMT	✓			✓		✓	$$$	👤👤	💻💻💻💻
	Gravity	✓			✓		✓	$$$	👤👤	💻💻
Ground Surveys	Radiometrics		✓	✓				$	👤	💻💻
	Magnetics		✓		✓		✓	$	👤	💻💻
	Electromagnetics		✓				✓	$$	👤👤	💻💻💻💻
	Resistivity (DCIP)		✓		✓		✓	$$$	👤👤👤	💻💻💻
	MT/AMT	✓	✓		✓		✓	$$	👤👤	💻💻💻💻
	VLF-EM		✓				✓	$	👤	💻💻
	Gravity	✓	✓		✓		✓	$$	👤👤	💻💻
	Seismic	✓	✓				✓	$$$$	👤👤👤👤	💻💻💻💻💻
Borehole Surveys	Radiometrics		✓	✓				$$	👤	💻💻
	Electromagnetics		✓				✓	$$	👤👤	💻💻💻
	Seismic		✓				✓	$$$$$	👤👤👤	💻💻💻💻💻

$ - $$$$$	minimal - expensive
👤 - 👤👤👤👤👤	few - many personnel
💻 - 💻💻💻💻💻	minimal - significant computing
◆ - ◆◆◆◆◆	minimal - significant experience

Scientific field	Method ID	Scale		Detection				Cost of Survey	Personnel Requirements	Computer/Software Requirements
		Regional	Project	Ore	Primary Dispersion	Secondary Dispersion	Geololgy / Structure	$ - $$$$$	👤 - 👤👤👤👤👤	💻 - 💻💻💻💻💻
Geology	Cover mapping	✓	✓		✓	✓		$	👤👤	💻
	Bedrock mapping	✓	✓	✓	✓	✓	✓	$	👤👤	💻
	Prospecting		✓	✓	✓			$	👤👤	💻
Geochemistry	Soil sampling		✓		✓	✓		$	👤👤👤	💻
	Boulder sampling	✓	✓		✓			$	👤👤👤	💻
	Lake sediment	✓	✓		✓	✓		$	👤👤	💻
	Radon survey		✓	✓		✓		$	👤👤👤	💻
	Weathering profile	✓	✓		✓			$$	👤👤	💻
	Hydrogen-Helium survey		✓	✓		✓		$$	👤👤	💻
	Water		✓		✓	✓		$	👤👤	💻
	Animal-derived		✓		✓	✓		$$	👤👤	💻
	Geobotany		✓		✓	✓		$$	👤👤	💻
Mineralogy	Whole-rock analysis	✓	✓	✓	✓	✓		$$	👤	💻💻
	Reflectance spectrometry	✓	✓		✓			$$	👤	💻💻
	X ray diffraction (XRD)		✓	✓	✓			$$$	👤👤	💻💻
	X ray florescence, portable (XRF)	✓	✓	✓	✓			$$	👤	💻💻
Drilling	Diamond		✓	✓	✓		✓	$$$$	👤👤👤👤	💻💻
	Reverse circulation (RC)		✓	✓	✓		✓	$$$	👤👤👤👤	💻💻

$ - $$$$$	minimal - expensive
👤 - 👤👤👤👤👤	few - many personnel
💻 - 💻💻💻💻💻	minimal - significant computing
◆ - ◆◆◆◆◆	minimal - significant experience

4.2.2.4. *Diamond drilling*

The diamond drilling sampling technique provides a continuous rock sample, often referred to as 'drill core' or 'core'. The use of the title 'diamond' in the extraction methodology refers to the diamond encrusted drill bit that is attached to the drill rod stem, providing the cutting and grinding action needed to provide depth advancement into bedrock. Drill bits used today are encrusted with synthetic diamonds emplaced within a hardened matrix. An important component of the methodology is water that is required to reduce the heat generated by the cutting and grinding action of the bit and the removal of drill cuttings from the face of the bit. Diamond drill bits are constructed for a defined rock hardness and daily production rates are based upon (but not limited to) lithology hardness, geological conditions, depth of targets and drill crew experience.

The retrieval of the drilled core (i.e. bringing it back to the surface) can be completed by two means — conventional or wireline. In conventional retrieval, the whole drill string is pulled at determined retrieval intervals. It is considered the least productive method. A wireline assembly involves an inner tube that travels inside the drill rods (Fig. 4.3). The tube is placed inside the rods and allowed to travel to the end of the rod string by means of gravity or pumping with water. The retrieval of a tube consists of a device called an 'overshot' that is lowered or pumped by a wireline on a hoist. Current standard methodology uses a wireline retrieval method after three metres of bedrock advancement; standardized core sample sizes and hole diameters are listed in Table 4.2. The retrieved cores are labelled based on depth, and placed in a systematic order in boxes for geological logging and sampling.

TABLE 4.2. STANDARDIZED CORE SAMPLES SIZE AND DRILL HOLE DIAMETERS

Diamond bit gauges – Q™ wireline				
Imperial measurements				
Size	BQ™	NQ™	HQ™	PQ™
Core diameter (inch)	1.433	1.875	2.500	3.345
Bit OD RSG* (inch)	2.36	2.98	3.78	4.83
Hole volume (gal/100 ft)	22.7	36.3	58.3	95.1
Metric measurements				
Size	BQ™	NQ™	HQ™	PQ™
Core diameter (mm)	36.4	47.6	63.5	85.0
Bit OD RSG* (mm)	59.9	75.7	96.1	122.6
Hole volume (L/100 m)	282	451	724	1180

**Bit Outside Diameter (Regular Standard Gauge)*

The use of diamond drilling provides a representative lithological sample at depth below the surface. Of equal importance, the core can be orientated, meaning the in-situ position of the core can be determined allowing for structural measurements such as foliations, fractures and faults to be recorded and plotted. There are many core orientation devices available on the market that are documented and can be utilized.

The hole produced by either diamond or RC drilling provides an opportunity to obtain additional information in the third dimension such as radiometrics, and lithological properties such as resistivity or acoustic/sonic properties that help define structures within lithologies.

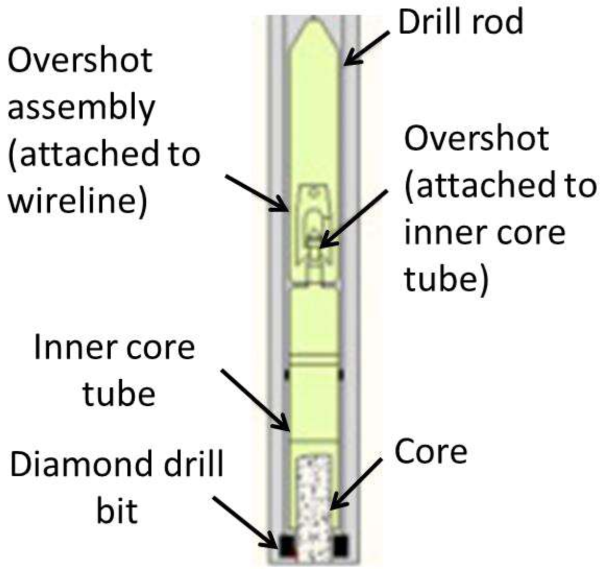

FIG. 4.3. Simplified wireline core retrieve system (modified and reproduced courtesy of Wang [4.58]).

Diamond drilling is one of the most expensive techniques used to explore for unconformity-related uranium deposits. However, this technique is often necessary because it provides a means of verifying the data obtained from other methods such as geophysics, surface mapping and geochemical surface surveys. Proper core storage provides the ability to revisit and sample the core for further investigation (Fig. 4.4).

FIG. 4.4. Photo of diamond drill core in boxes, depth of hole is noted in three metre intervals on the markers inside the boxes.

4.2.3. Geochemistry

4.2.3.1. Radon survey

Radon is a short-lived intermediate daughter product in the radioactive decay series of uranium. This gas can move through soils or can dissolve in water. Bedrock, overburden or spring water are all potential sources of radon [4.59].

Radon sampling along defined grids has evolved from active pump systems to passive detectors. In all systems, the radon sample abundance is measured by the amount of alpha emissions collected either directly or indirectly by a detector. A more common technique used in the Athabasca Basin is a radon flux monitor survey that uses Electret Ion Chamber (EIC) technology [4.60]. Measurements can be made at designated surface locations or from water samples. The methodology allows for sampling and analysis to be completed on the same day and has been credited for the discovery of Fission Uranium Corporation's Triple R unconformity-related uranium deposit in the western Athabasca Basin [4.61].

Other radon surveys in the Athabasca Basin include the research by Devine et al. [4.62], who studied radon emissions over deep-seated unconformity related deposits, located at a depth of more than 500 m with sandstone and overburden cover. They concluded that radon dissolved in groundwater sampled from previously drilled boreholes at varying depths above and away from a known deposit can provide information that is useful when exploring for deep unconformity-related uranium deposits.

4.2.3.2. *Hydrogen-helium survey*

Hydrogen-helium surveys are often conducted in conjunction with radon surveys. The development of helium (^4He) in soil gas is related to uranium radioactive decay and the release of alpha particles. Hydrogen is produced by the radiolysis of water by the radioactive decay of uranium; the interaction of various types of ionizing radiation (α, β, and γ) with water produces molecular hydrogen.

Samples are taken in soils along predefined grids using soil gas probes. Gas analysis is measured using a gas chromatograph. The measurement of helium and hydrogen in soils requires special care because of their volatility [4.63]. A study by Duduk and Hattori [4.64] on the Phoenix deposit, which is 400 m below surface, outlines the complexities of working with this type of survey. Results published by Power et al. [4.65] on Cameco's Millennium deposit, which is located at a depth of approximately 750 m, indicates the possibility of upward migration of helium through faults, producing helium anomalies that can be detected at the surface.

4.2.3.3. *Soil sampling*

The soil sampling technique for unconformity-related uranium deposits is dependent on the type of overburden cover such as soil and Palaeoproterozoic to Mesoproterozoic quartz-rich sandstones. Quaternary geological studies should be conducted prior to soil sampling to determine the areas that would provide best data. In general, soil sampling surveys are limited in size and designed to investigate small areas of interests. The B soil horizon, which occurs directly below the organic rich zone, is typically the best horizon to sample because it has the highest accumulation of minerals.

A recent study by Power et al. [4.66] detected anomalous elements, including uranium, in soils above the Phoenix deposit. Samples were obtained from the humus E-, B- and C-horizons. The humus layer and B-horizon have anomalous pathfinder element concentrations, including uranium, which was up to six times greater than background levels. Power et al. [4.66] postulate that fault zones coinciding with the deposit allow pathways for upward migration of fluids into the upper sedimentary sequences, producing element anomalies in soils.

4.2.3.4. *Boulder sampling*

The method is based on the premise that ore systems with recognizable alteration halos associated with unconformity-related uranium orebodies extend to the surface and that these have been eroded (i.e. glacial processes), resulting in anomalous dispersion trains recognizable within the cobble/boulder component of a ground moraine. Boulders are preferred as a sample medium over the non-boulder part of the till because the large, often relatively angular, boulders likely did not travel as far as the finer till material. The advantage of this type of survey is that the technique provides rapid and inexpensive exploration coverage of large project areas. For example, the discovery of radioactive boulders in the Athabasca Basin directly led to the discovery of the Rabbit Lake, Cluff D Zone, Key Lake and more recently, the Triple R uranium deposits.

As the goal of the boulder sampling programme is to identify the presence of geochemical and/or mineralogical anomalies, both lithogeochemical and mineralogical analysis of boulder samples are carried out. At the very least, the normative clay mineralogy calculations are carried out using the geochemical data. Select samples are analysed by XRD to corroborate the normative data. Short-Wave Infrared Reflectance (SWIR) spectral mineralogical analyses are performed in the field, but care must be taken in sampling, analysis, and interpretation.

4.2.3.5. Weathering

The extent of the weathering profile in basement lithologies below the Athabasca Group sediments is limited to 10–50 m and may be similar to modern-day laterites with a zone of pervasive haematite alteration at the unconformity and grading to illite and chlorite at depth [4.67].

Removal or overprinting of the palaeoweathering profile is normally associated with hydrothermal fluid movement, possibly because of fault reactivation, with a potential link to uranium deposition. Diamond drilling campaigns that identify such areas should be sampled to determine if pathfinder elements or clays are associated with the alteration.

The study of weathering profiles in relation to Proterozoic unconformity-related uranium deposits is typically associated with exploration in Australia. In the regolith, uranium and thorium are associated with more stable weathering products including clay minerals, iron and aluminium oxyhydroxides and resistate minerals (such as monazite and zircon). The presence of organic matter and specific bacteria (for example, sulphate-reducing bacteria) can also influence the distribution of uranium in the regolith. High thorium/uranium ratio values in the weathering profile compared to the underlying bedrock can indicate preferential mobilization and leaching of uranium, and may indicate nearby sources of secondary uranium mineralization.

4.2.3.6. Water

The use of hydrogeochemistry involves the study of ground and surface waters that comes into contact with soluble minerals. Currently, it is not a commonly used survey method to explore for unconformity-related uranium deposits, but should be considered in an exploration programme at either a regional or localized scale. The interpretation of the results can be complicated and involve the potential sources and transportation of elements, seasonal water changes, precipitation, and flow rates. Uraninite and some associated alteration minerals are soluble in most modern-day surface and subsurface waters. Sample locations can include but are not limited to streams, lakes, springs, swamps or wet terrains as well as sampling at depth into overburden or bedrock using previously drilled holes that have remained open or lined to stay open. Sample collections are usually taken at the same time as other previously mentioned surveys in this chapter such as lake or stream sediments, radon surveys and hydrogen-helium surveys. A comparison of results between different types of surveys or using the same sample type can help define anomalies that can be drilled.

4.2.3.7. Lake sediment

Lake sediment surveys are early reconnaissance exploration tools used in grassroots exploration. The density spacing can be highly variable depending on the geographical setting and the area of coverage that is being investigated. For regional surveys, a sample taken every 1 km^2 would be considered dense. The objective of such a survey is to use the sampled medium to identify geochemical anomalies to aid in mineral exploration.

Samples are generally taken in the perceived deeper more ‘quiet’ portions of a lake to gather a sample that is less likely to be disturbed or contaminated by human or industrial sources. A means of transport can vary from using a boat in summer or a snowmobile in winters, but the most cost-effective means of transportation is a helicopter fitted with pontoons. The sampling procedure involves a weighted sampling tube that is attached to a line for retrieval. The sample tube usually has a closure mechanism at the bottom that closes upon sample retrieval to prevent the captured sample from escaping. Observations made during the sampling process consist of location coordinates, depth of sample, vegetation surrounding the lake and water colour. The sample can be stored in simple paper bags with a general description of the sediment colour, texture and composition [4.68].

A study by Davenport et al. [4.69] showed that to avoid sample contamination, the lower portion of a sediment sample should be selected and the removal of the upper 6–12 cm is required. Successful exploitation of this survey in the Athabasca Basin has been documented in the discovery of the Key Lake, Gaertner Deposit [4.70] where chemical dispersions in lake sediments and muskeg are reported up to 6 km SW of the deposit.

4.2.3.8. Portable XRF

The handheld X ray fluorescence (XRF) analyser is a non-destructive elemental analysis technique for the quantification of elements. It provides an immediate chemical analysis of samples (outcrop, drill cores, rock chip, soils). The analyser works by emitting X rays that interact with the sample causing the disruption of electrons within elements of the sample. This disruption is the displacing (or removal) of electrons from the inner orbital shells of an atom, causing the electron configuration to become unstable, after which an electron from a higher orbital valence replaces the displaced electron. Electrons have higher binding energy the further they are from the nucleus of the atom and in turn, release energy moving from a higher valence level to a lower one. This release of energy is called fluorescence; the distances between orbital valences in elements are unique, which produce a unique fluorescence. A detector on the instrument measures the energy release and determines the element [4.71].

4.2.3.9. Whole-rock analysis

Whole-rock analysis of rock samples (diamond drill cores, bedrock grab samples, boulders, tills, sediments) are done to identify the presence of elements associated with alteration envelopes surrounding an unconformity-related uranium deposit. Generally, both major and trace elements are analysed (e.g. major element oxides: Al_2O_3, Fe_2O_3, MgO, K_2O by ICP-OES; Trace elements: As, B, Bi, Co, Cu, Mo, Ni, V, Zn by ICP-OES or ICP-MS; $U_{partial}$ by fluorimetry or ICP-MS; $Pb_{partial}$ by ICP-OES or ICP-MS.

Sample preparation and analytical packages are outlined by the Saskatchewan Research Council [4.72]. Samples are crushed (~ 2mm) and ground (106 microns) prior to analysis. Different types of crushing plates can be used to avoid contamination during sample preparation. For example, steel crushing plates can contaminate a sample with iron and chromium.

Analytical packages include:

1) Partial digestion Inductively Coupled Plasma Mass Spectrometry (ICP-MS) analyses for many trace elements, including lead isotopes;
2) Total digestion ICP-MS analyses for many trace elements, including lead isotopes; and
3) Inductively Coupled Plasma Optical Emission Spectrometry (ICP-OES) analyses for the major element oxides and several minor elements.

The Minimum Detection Limits (MDLs) for elements determined by these analysis packages are presented in Tables 4.3 and 4.4.

The sample digestions used are: 1) partial digestion (sample is digested in a mixture of HCl and HNO3 in a Teflon tube in a hot water bath, then diluted using de-ionized water); and 2) total digestion (sample is digested to dryness in a Teflon tube in a hot block digestion system using concentrated $HClO_4$:HNO_3:HF, with the residue dissolved in dilute HNO_3). Boron is analysed using ICP-OES following a total digestion (NaO2/NaCO3 fusion with dissolution in distilled water).

There are three types of uranium assay data: U-partial and U-total by ICP-MS (or ICP-OES), and U_3O_8 assay:

1) The ICP-MS uranium analysis is essentially equivalent to the formerly-used fluorimetric uranium analysis on the partial digestion with respect to accuracy and precision, and has a similar to slightly better MDL (0.01 ppm U [100 ppb U] versus 0.02 ppm). However, the ICP-MS method has a significantly better MDL (0.01 ppm) than the ICP-OES analysis (0.5 ppm sandstone sample, 1 ppm basement sample);
2) The ICP-MS method using the multi-acid total digestion also has a significantly better MDL (0.02 ppm) than does the ICP-OES analysis (2 ppm) and fluorimetry (0.1 ppm);
3) Uranium (U_3O_8) assay is done on samples containing relatively high uranium content using ICP analysis following sample digestion using Aqua Regia. The minimum reported value is 0.001 wt% U_3O_8 (equivalent to 8.5 ppm U), although the actual MDL is similar to the ICP uranium analysis. In fact, the data are very similar to those produced by the ICP uranium analysis (the values often fall between the partial U and total U values), but the precision is much better (1–2%) because: (a) more sample material is used; (b) less digestion dilution is used, and (c) a more rigorous analysis protocol is followed. These more precise data are useable in grade and tonnage calculations.

TABLE 4.3. MINIMUM DETECTION LIMITS (MDLS) FOR ELEMENTS ANALYSED BY ICP-MS

Partial Digestion Elements ICP-MS	
element	detection limit (ppm)
Ag	0.01
As	0.01
Be	0.01
Bi	0.01
Cd	0.01
Ce	0.01
Co	0.01
Cs	0.01
Cu	0.01
Dy	0.01
Er	0.01
Eu	0.01
Ga	0.01
Gd	0.01
Ge	0.01
Hf	0.01
Hg	0.01
Ho	0.01
Mo	0.01
Nb	0.01
Nd	0.01
Ni	0.01
Pb204	0.01
Pb206	0.02
Pb207	0.02
Pb208	0.02
PbTOTAL	0.02
Pr	0.01
Rb	0.01
Sb	0.01
Sc	0.1
Se	0.1
Sm	0.01
Sn	0.01
Ta	0.01
Tb	0.01
Te	0.01
Th	0.01
U	0.01
V	0.1
W	0.1
Y	0.01
Yb	0.01
Zn	0.1
Zr	0.01

Total Digestion Elements ICP-MS	
element	detection limit (ppm)
Ag	0.02
Be	0.1
Bi	0.1
Cd	0.1
Co	0.01
Cs	0.1
Cu	0.1
Dy	0.01
Er	0.01
Eu	0.01
Ga	0.01
Gd	0.01
Hf	0.01
Ho	0.01
Mo	0.01
Nb	0.01
Nd	0.01
Ni	0.01
Pb204	0.01
Pb206	0.02
Pb207	0.02
Pb208	0.02
PbTOTAL	0.02
Pr	0.01
Rb	0.01
Sc	0.1
Sm	0.01
Sn	0.01
Ta	0.1
Tb	0.01
Th	0.01
U	0.01
V	0.1
W	0.1
Y	0.01
Yb	0.01
Zn	0.1

Note that historical minimum reported assay values have until recently been 0.01 wt% U_3O_8 (equivalent to 84.7 ppm U). The differences in historic MDLs and the current MDL will impact the data analysis of the uranium assay values.

TABLE 4.4. MINIMUM DETECTION LIMITS (MDLS) FOR ELEMENTS ANALYSED BY ICP-OES

Partial Digestion Elements ICP-OES	
element	detection limit (ppm)
Ag	0.1
As	0.2
Bi	0.2
Co	0.1
Cu	0.1
Ge	0.2
Hg	0.2
Mo	0.1
Ni	0.1
Pb	0.02
Sb	0.2
Se	0.2
Te	0.2
U	0.5
V	0.1
Zn	0.1

Total Digestion Elements ICP-OES	
element	detection limit (ppm)
Ag	0.2
Ba	1
Be	0.2
Cd	0.2
Ce	1
Co	1
Cr	1
Cu	1
Dy	0.2
Er	0.2
Eu	0.2
Ga	1
Gd	0.5
Hf	0.5
Ho	0.4
La	1
Li	1
Mo	1
Nb	1
Nd	1
Ni	1
Pb	1
Pr	1
Sc	1
Sm	0.5
Sn	1
Sr	1
Ta	1
Tb	0.3
Th	1
U	2
V	1
W	1
Y	1
Yb	0.1
Zn	1
Zr	1

Total Digestion Elements ICP-OES	
element oxide	detection limit (wt%)
Al2O3	0.01
CaO	0.01
Fe2O3	0.01
K2O	0.002
MgO	0.001
MnO	0.001
NaO2	0.01
P2O5	0.002
TiO2	0.001

4.2.4. Mineralogy

Mineral identification in hand samples and thin sections is important because it is used to identify rock types, ore mineralogy and mineral associations (e.g. differentiate between authigenic and alteration minerals). The development of a mineral paragenesis is also important because it provides a relative mineral chronology (i.e. relative ages of minerals). Mineral identification in hand samples by using an optical microscope is one of the least expensive techniques available to exploration geologists. Many sophisticated mineral identification and analytical techniques are available in the exploration industry. Some notable mineral identification instruments include the scanning electron microscope (SEM) and the electron microprobe (EMP) to determine chemical compositions and provide high resolution images, and Raman spectroscopy to identify mineral spectra. Some of the more common field-related technologies are described in detail below.

4.2.4.1. Reflectance spectroscopy

Reflectance spectroscopy is used to identify the clay minerals in the Palaeoproterozoic to Mesoproterozoic quartz-rich sandstones. Reflectance spectrometers such as the TerraSpec® are sensitive to electromagnetic energy in a wavelength range of 350–2500 nm, including the VNIR (visible/near-infrared radiation 350–1000 nm) range, and the SWIR (short-wave infrared radiation 1000–2500 nm) range [4.73]. The VNIR reflectance spectrometry is sensitive to electronic processes in material that can be related to colour variations or oxidation states. Iron bearing minerals (haematite and goethite), rare earth element bearing minerals, and pyroxenes have prominent spectral features within this range [4.74]. The SWIR reflectance spectroscopy records absorptions related to molecular bond vibrations, particularly those related to H_2O, OH^-, CO_3^{2-}, SO_4^{2-}, and NH_4^+. Because these are commonly found in alteration minerals, SWIR spectroscopy is useful for identifying hydrothermal alteration. Therefore, molecules containing OH, H_2O, AlOH, FeOH, MgOH, CO_2 and NH_3 groups have distinct wavelength absorption features. Minerals with prominent features in this range include phyllosilicates (clays, chlorites, serpentines, biotites), hydroxylated silicates (epidotes, amphiboles, tourmalines), sulphates, carbonates (calcite, dolomite, magnesite, siderite), and ammonium-bearing minerals such as NH_4 illites [4.74].

Reflectance spectroscopy provides more detailed information about the mineralogy of a sample relative to geochemical analysis, and is faster and much less expensive than XRD. A significant advantage of reflectance spectrometry is that it provides immediate results, which can be followed up with additional sampling.

One of the primary advantages of reflectance spectrometry over both XRD and geochemistry is that it allows unequivocal differentiation between the kaolin minerals dickite and kaolinite. This has allowed a clear distinction between the hydrothermal kaolinite spatially associated with the mineralization at Key Lake and the diagenetic dickite, which is a regional feature of the Key Lake area and of much of the rest of the eastern Athabasca Basin. The intense kaolinitization of the sandstone is interpreted as a significant feature of the hydrothermal alteration halo, and is an important exploration criterion in this part of the basin. Another important advantage of reflectance spectrometry is that it can be used in a field-camp setting, and hence the results can be available immediately to guide follow-up exploration.

4.2.4.2. X ray diffraction

X ray diffraction (XRD) is a technique used for the study of crystal structures based upon constructive interference of X rays and a studied sample. The sample consists of a granulated fine powder (usually <1 gram) that is placed in a sample holder. The sample is bombarded with X rays and the interaction of the incident rays with the sample causes diffracted X rays. The detection and processing of the angle between the incident and diffracted rays occurs by means of rotating the sample and detector, allowing for all possible diffraction directions of the sample's crystal lattice to be attained due to the random orientation of the powdered material.

The diffracted X ray only occurs when conditions meet Bragg's Law ($n\lambda=2d \sin \theta$) that relates the wavelength of electromagnetic radiation to the diffraction angle and the lattice spacing (d-spacing) in a sample [4.75]. The measured diffraction peaks are converted to d-spacing and allows for mineral identification because each mineral has a unique set of d-spacings.

The application of XRD is widely used because instruments are readily available, it is a relatively inexpensive technique, and data interpretation is relatively easy. The methodology and sample preparation is well documented and results are generally obtained in less than 20 minutes. The XRD provides characterization of minerals and is used in uranium exploration for detection of fine-grained clays that could be associated with alteration halos. Equally important is the determination of modal amounts of minerals (quantitative analysis).

4.2.5. Other

Exploring for mineral deposits by sampling animal waste and tissue was recently attempted in Australia. Noble et al. [4.76] analysed the chemistry of water, foliage, soil, regolith material and termitaria at the Kintyre uranium deposit in Western Australia. They were able to detect uranium anomalies above the deposit, which below 80 m of cover. Additional work on termitaria sampling in the eastern Alligator regions, Northern Territory, Australia was completed by González-Álvarez et al. [4.77]. They suggest that termitaria are enriched in uranium because of the near surface ferricrete unit located 1–3 m below the surface.

4.2.6. Geobotany

Biogeochemical sampling has been used to explore for uranium exploration in conjunction with other geological, geochemical and geophysical surveys. Extensive regional and localized surveys were conducted in the north-eastern portion of the Athabasca Basin between 1979 — 1982 [4.78] with the sampling of black spruce (Picea mariana) twigs. Black spruce was selected as the preferred vegetation due to its proven ability to concentrate many elements [4.78, 4.79] and widespread availability in both well-drained and poorly-drained areas. Previous studies by Dunn [4.78, 4.79] also identified Jack pine (Pinus banksiana) as a suitable biogeochemical medium. Numerous deposits have been discovered in the north-eastern portion of the Athabasca Basin since the initial surveys. There is no deposit discovery that is directly linked to vegetation sampling surveys, but surveys have highlighted anamolies in the vicinity of several areas. An excellent reference relating to the science of geobotany has been written by Dunn [4.79] entitled "Biogeochemistry in Mineral Exploration".

There are a couple of recent studies that are examining the utility of vegetation sampling in the vicinity of deep (>500 m) unconformity-related deposits in the Athabasca Basin. Stewart et al. [4.80] and Beyer et al. [4.81] studied the relationship between the geochemistry of soils and the geochemistry of tree rings. They conclude that tree roots can source uranium from sandstone related to unconformity-related uranium deposits.

4.2.7. Geophysics

Geophysics is widely used in all forms of mineral exploration. More specifically, for uranium exploration, the ability to directly detect this mineral because of its natural gamma-ray emissions is a fundamental characteristic of the mineral [4.82]. The natural radioactive decay can make remote detection a rapid and effective process when implemented from an airborne platform. However, this efficacy can be quickly moderated by any number of factors such as depth of cover, environmental factors, conductive overburden or cultural constraints, which then have the potential to turn a simple exploration problem into a significantly more complex process. The complexity of the exploration process is further compounded when the target is not exposed on the surface and the means of direct detection is substantially reduced, forcing the use of methods which detect physical property contrast. It is this notion of physical property contrast that is fundamental to all aspects of geophysical exploration. The following discussion is presented as a summary of the various methods used over time in the exploration for Proterozoic unconformity uranium mineralization. It is not intended that this discussion be used as a template for conducting geophysical exploration — rather, the purpose is to demonstrate the application of a method and how the method has aided the exploration objective.

An outcrop of uranium mineralization on the earth's surface is considered a relatively straightforward exploration target where direct detection of gamma-ray emissions from the daughter products of ^{238}U can be measured. However, not all uranium mineralization outcrops. If the uranium target is at depth, and is covered by other non-mineralizing rock types, the application of geophysical methods must move from a focus on direct detection to one of indirect detection. Geophysical methods must now aim to identify an anticipated contrasting physical property between mineralized and non-mineralized elements of the target. Or, as can be the case for unconformity deposits, the focus is on detection of a physical property used as a proxy for the increased likelihood of mineralization. An example would be the detection of graphitic units displaying a conductivity response in the presence of a time varying inducing electromagnetic field.

One limitation with the detection of physical property contrasts is that as the depth increases, the measurable limits of detection decrease substantially. Increasing depth necessitates an increasing physical property contrast as well as an increasing size of target, for although there may be significant differences in properties between two rocks, the actual size of the target may be too small to produce sufficient detectable contrast at the specified depth. Generally, the deeper the target, the greater the physical size and property contrast must be. Increasing depth is always associated with decreasing resolution when considering surface or airborne measurements, so this factor is crucial when planning surveys.

4.2.7.1. Defining the geophysical exploration problem

Before considering a geophysical survey, an understanding of the target geological model is necessary. Models for Proterozoic unconformity deposits vary from country to country, as do the depths at which they are found. Fig. 4.1 depicts a generalized amalgamation of the different facets and properties of these deposits and is based on multiple deposits from different parts of the world. Consequently, it should be noted that while a deposit may have some or many of the features displayed, no one deposit will have all of these features. For an explorer to effectively target aspects of this model using geophysical methods, it is necessary to understand the tenor and spatial distribution of physical property contrasts. Although it may seem counterintuitive, this is achieved by understanding the target purely in terms of its physical property and not in terms of geology. Although the two are related, often a physical property will be transgressive to geology which leads to a very important concept.

Different rock types with similar physical property ranges are indistinguishable on the basis of that property alone.

This point is illustrated in the following model. A generalized cross-section for the Proterozoic unconformity setting in northern Australia is presented in Fig. 4.5. This model corresponds with some aspects on the right-hand side of the model in Fig. 4.1. A sedimentary layer of varying thickness overlies crystalline basement and is separated by a thin palaeo-weathering layer. By proxy, this weathering contact represents a good approximation for the spatial distribution of the unconformity. The weathering layer may extend into both sandstone and basement and as a result, has altered the chemical and physical properties of both rock types. Petrophysical analysis of the different rock types would reveal the following:

1) Both sandstone and crystalline basement are electrically resistive with values of the order of several thousand ohm-metres;
2) Rocks subjected to palaeo-weathering are altered into clay rich forms and display weak electrical resistivity of the order of 10–200 ohm-metres;
3) An extreme resistivity contrast exists between fresh and weathered rocks;
4) The palaeo-weathering layer is not considered 'conductive' in the normal sense of a conductor, rather it is simply less resistive than the surrounding rocks.

It is important to understand that knowledge of rock resistivities is fundamental for establishing the credibility of the electrical model. Without this knowledge, the explorer is taking a speculative risk as to the applicability and outcome of the survey.

The model presented in Fig. 4.6 is intended to display how an unconformity setting may appear when considering only the electrical properties of rocks. From an electrical perspective, both sandstone and basement rocks are highly resistive, leaving the unconformity as the only conductive element in an electrically neutral half-space. This basic model describes gross features of the unconformity setting from which a more complex geological/geophysical model can be built. The model also highlights how indistinguishable a layer of sandstone can be from crystalline basement, when viewed purely in terms of electrical conductivity.

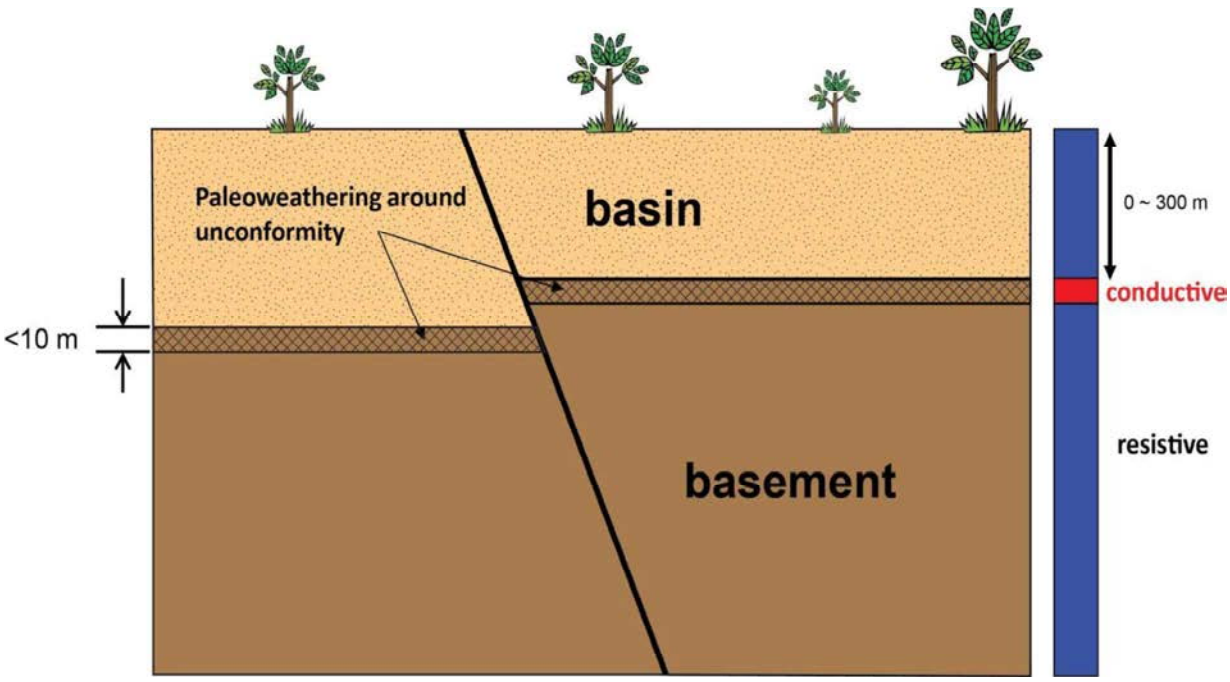

FIG. 4.5. Basic geological model of an Australian Proterozoic unconformity setting.

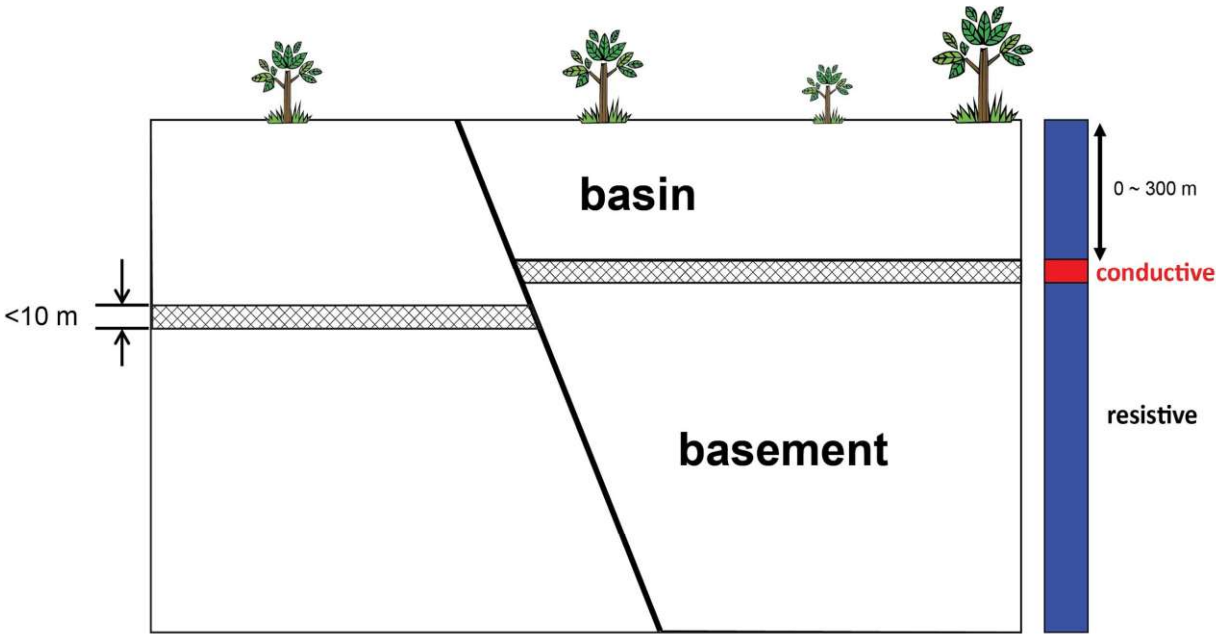

FIG. 4.6. The unconformity model as it appears from an electrical property perspective. The two rock types are indistinguishable in terms of electrical properties, whilst palaeo-weathering around the unconformity produces a thin layer of significantly lower resistance.

The geological settings of Proterozoic unconformity uranium deposits can be much more complex than indicated above. However, starting with this model is a crucial first step towards successfully planning the type of geophysical method that will be used to aid in exploration. Without an understanding of the expected type of geological, geochemical and structural setting, geophysical surveying can be unexpectedly ineffective. As is often the case during early exploration, these factors are unknown, so some effort should be made to understand as much as is possible about the physical properties of the target system before undertaking any form of geophysical survey.

4.2.7.2. Direct versus indirect exploration

This concept is even more crucial when target mineralization occurs under cover, potentially up to 1000 m below surface. In this circumstance, the role of geophysics is one of indirect exploration where it is the anticipated physical property contrast that becomes the target, rather than mineralization itself. Consider the geological situation depicted in Fig. 4.7 where several uranium mineralized targets are depicted as outcropping with varying levels of gamma-ray emission. Ignoring weathering profiles, surface prospecting will likely result in the discovery of all targets, particularly if each has some form of natural radioactive decay. However, consider the impact a few centimetres of soil or solid rock will have on finding each target. A few centimetres (~ 40 cm) of cover is sufficient to block all gamma-ray emissions associated with the uranium [4.83]. Hence, for exploration under shallow cover or at depth, the focus shifts to identifying and mapping changes in physical properties indirectly linked to mineralization, or to at least provide a vector for improving prospectivity.

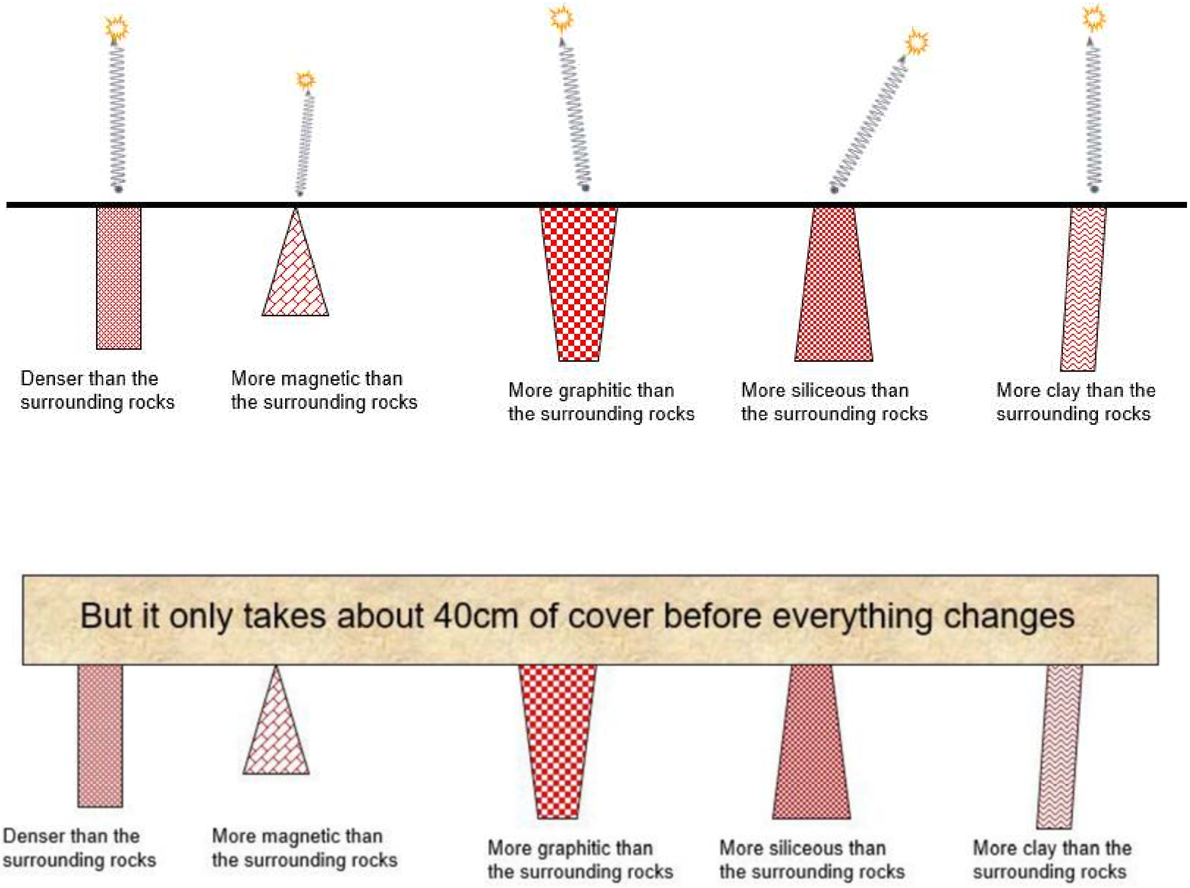

FIG. 4.7. A diagrammatic representation of how exploration for a variety of outcropping uranium targets (top) shifts from direct detection of gamma-ray emissions to other indirect, but still measurable property contrasts with as little as 40 cm of cover (bottom).

Improving a mineralization vector could be as simple as quantifying how deep the unconformity is below surface, identification of strong basement conductors as a proxy for graphitic accumulations, mapping of faults, mapping of alteration effects through changes in electrical resistivity, depth to basement estimates through magnetic modelling or clay alteration mapping through satellite imagery, to name but a few.

When direct detection of uranium mineralization is no longer possible, indirect detection of a physical property associated with the mineralized geological model becomes the primary focus. The explorer should always be aware of the need for physical property contrasts to exist, and more so as depth to target increases.

Having a well-founded geological model is critical for effective geophysical targeting under cover.

4.2.7.3. Target size and depth

Consideration for target size and depth is necessary when planning for geophysical surveys. In relation to the unconformity model, the target can be relatively small at a significant depth.

Increasing depth provides a challenge for all geophysical methods in that the ability to resolve features decreases with increasing depth (Fig. 4.8). Thus, the deeper the target, the greater the physical property contrast must be or the greater the size must be. It is possible to resolve a smaller target at depth so long as there is a corresponding increase in the tenor of physical property contrast. Conversely, an extremely large mineralization system with almost no measurable physical property contrast has a much lower chance of being detected through contrasting geophysical responses.

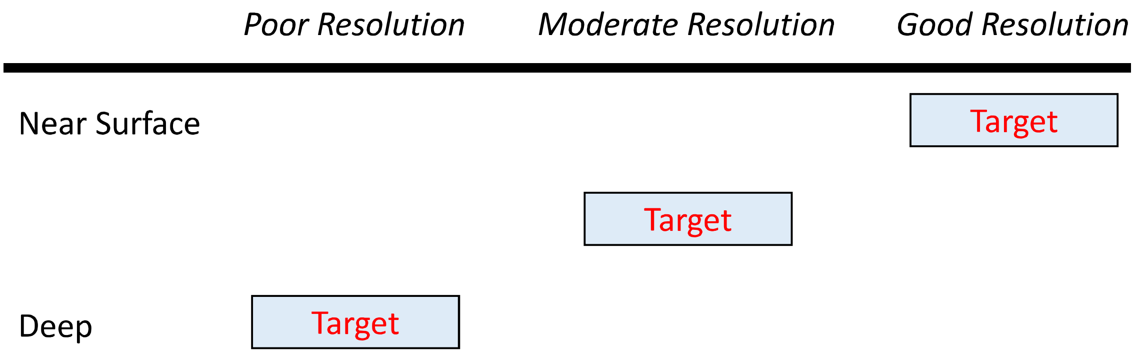

FIG. 4.8. Target resolution decreases with depth and improves as the target becomes shallower.

4.2.7.4. Survey costs

The decision on which geophysical method to use should be made on the basis of technical and geological factors. Unfortunately, survey costs often dictate what method will form a part of the exploration programme with technical and geological factors a necessary secondary consideration.

A large area of prospective ground with little history of exploration can be effectively covered with airborne geophysical surveys as a means of contributing to the initial assessment phase. A certain geophysical method may have more technical merit and thus appeal over another method, making it an attractive first option. However, the choice of which geophysical survey to apply first is rarely achieved on pure technical merit alone. For many operators, the choice of survey is inherently related to the level of available funds. So, whilst it may seem an attractive option to cover large parcels of ground with an airborne electromagnetic survey, the costs associated with such a survey could be substantial.

Whilst survey planning and choice of method is intimately tied to technical factors, it must be balanced against the economic constraints of funding and the longer-term objectives of the operator. An idealized approach is rarely viable in which case, compromise with regard to method, line spacing, survey area and even choice of contractor becomes necessary. Financial constraints often result in a more efficient use of funds, leading to better planning, execution and use of data.

A geophysical survey forms a part of the exploration objective so costs associated with it form a part of the broader budget. As such, proponents of geophysical surveys often find they are in competition with non-geophysical programmes for funding.

4.2.7.5. Interpretation

Modern geophysical surveys can produce large quantities of complex data that require specialist software and expertise to produce an effective interpretation. When planning to acquire geophysical data from any method, a necessary consideration is how the data will be interpreted and by whom. Too often, geophysical surveys are executed with no thought given to the subsequent analysis, resulting in an excess of surveys with unrealized value in many parts of the world. In many instances, if an interpretation is pursued, it lacks the necessary geological value to be meaningful to anyone else except another geophysicist. Interpretation of geophysical data should focus on the desired outcome and clearly identify the target audience (customer) of the interpretation.

There are few resources available to the non-expert that can assist in the interpretation of geophysical data. Generally, an external consultant or in-house geophysicist is required for this work. Interpretation fundamentals are briefly discussed in Dentith and Mudge [4.84], Telford, Geldart and Sheriff [4.85], whilst Isles and Rankin [4.86] provide a more in-depth analysis of aeromagnetic data interpretation.

Once collected, the interpretation of geophysical data is essential, as is the need to present the results in a geologically meaningful way. Given that most geophysical survey data is collected by, or at the request of a geophysicist, it is incumbent upon the geophysicist to assist in the development of a geological interpretation of the data. For example, a 'strong conductor' identified in an electromagnetic (EM) survey must have some geological association, which should be clearly stated (even if it is speculation). However, all users of the data need to understand that an interpretation should always be viewed as just that — an interpretation. It is extremely rare for an interpretation to be 100% accurate as it is subjective and can have errors. It should not be viewed as definitive answer, rather, it adds value to the project's geological understanding. This is important for programme participants and others to understand, and accept.

An example of one type of geophysical interpretation is shown in Fig. 4.9. In this example, gridded magnetic data represents a map of magnetic susceptibility distribution within an Australian Archean domain. The interpretation reflects a geological distribution of magnetite within this domain and is presented to the customer as a geological map. Two different levels of survey resolution highlight the benefit of acquiring detailed (closer line spacing) aeromagnetic data verses regional aeromagnetic data. The interpretation of aeromagnetic data is contrasted against the currently available published geological fact map and demonstrates the significant improvement gained in the understanding of the local geology.

Whatever the source of data, a concerted effort should be made to relate all geophysical data to the geological environment from which it was collected, and this is normally achieved in the form of an interpretation.

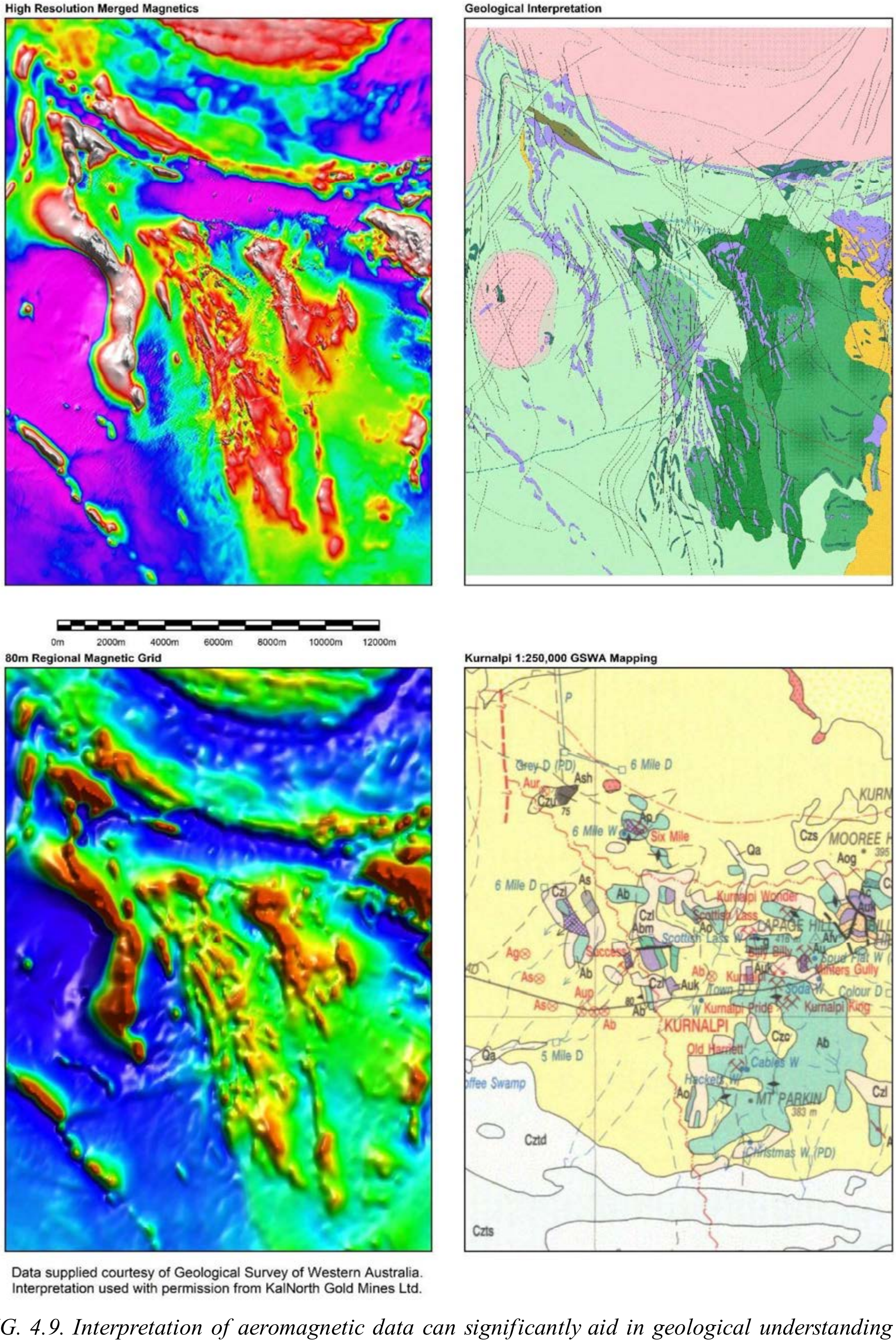

Data supplied courtesy of Geological Survey of Western Australia.
Interpretation used with permission from KalNorth Gold Mines Ltd.

FIG. 4.9. Interpretation of aeromagnetic data can significantly aid in geological understanding as shown here. The acquisition of high resolution magnetic data (top left) significantly improves upon the interpretability of regional survey data (bottom left) and delivers greater geological understanding (top right) in an area with reduced outcrop (bottom right). (Geological mapping and data used with permission and reproduced courtesy of Geoscience Australia).

4.2.7.6. Airborne surveys

The decision to acquire geophysical data utilizing an airborne or ground-based method can depend on a multitude of factors. In the context of an unconformity uranium model, factors that influence the decision include, but are not limited to: total prospective area, surface vegetation and geomorphology, available funds, time constraints for acquisition of data, target physical property and depth to target. All these factors may be better served by data acquisition using an airborne platform. With the primary focus on unconformity uranium exploration, acquisition of data from an airborne platform is generally limited to magnetic, radiometric and electromagnetic data. Airborne gravity has been effective as a targeting mechanism in the assessment of projects for near surface hydrothermal clay-rich alteration halos associated with uranium mineralization, however its use is still relatively minor (Fig. 4.23).

An airborne survey platform allows the efficient and rapid collection of data over a large area and is one of the main reasons for using this method. Most surveys are conducted on a grid-line basis with aircraft following a pre-planned flight path. There are often competing priorities between choosing an appropriate sample and line density that maximizes data coverage, against the cost of a survey constrained to a level insufficient to achieve suitable coverage. The desire is always to collect as much data as possible; however, costs can quickly increase to unrealistic levels, forcing a compromise between obtaining meaningful data and meeting prescribed financial constraints. There is considerable skill and creativity involved in being able to maximize the use of available funding in collecting appropriate exploration data.

When considering an airborne survey, it is necessary to assess the status of the exploration programme in the context of the value such a survey will add to the exploration objective. Questions that need to be asked include how the data that is being collected will aid in advancing the objective, and that depending on the maturity of exploration, whether the survey is appropriate for an advanced programme, or for one in its infancy. The maturity of the exploration process can significantly influence what type of data is required, and hence what type of survey is required.

First and foremost, the geological objective must be clearly understood and communicated before committing to an airborne survey. A decision to acquire airborne survey data of any kind should be justified from a geological perspective, with a clear understanding of how the data will add to understanding the geological problem.

4.2.7.6.1. Airborne magnetics

Understanding the magnetization of rocks and the various chemical and physical properties that influence this property is foundational knowledge that is required by all explorers. A detailed discussion on the basics of rock magnetism, its causes and the interpretation thereof is beyond the scope of this document and the reader is referred to a more comprehensive resource for a process driven description of rock magnetism, its causes and the geological interpretation of aeromagnetic data [4.86]. Readers requiring a basic and easy to understand discussion on magnetism are referred to Dentith and Mudge [4.84], Telford, Geldart and Sheriff [4.85].

For the mineral explorer, magnetic data is primarily concerned with the need to map the distribution and relative abundance of magnetically susceptible minerals within the near surface of the earth's crust, the most significant and abundant being magnetite, a ferromagnetic mineral [4.86]. A magnetically susceptible mineral placed within the geomagnetic magnetic field will introduce perturbations to the local magnetic field. Mapping these magnetic variations is the objective of an aeromagnetic survey.

During the early stages of a uranium exploration programme, it is common to acquire airborne magnetic data of the project, if such data did not already exist. This phase may also include acquisition of airborne radiometrics if the geological model favours the possibility of surficial mineralization. An example of magnetic data from an Australian unconformity setting is presented in Fig. 4.10.

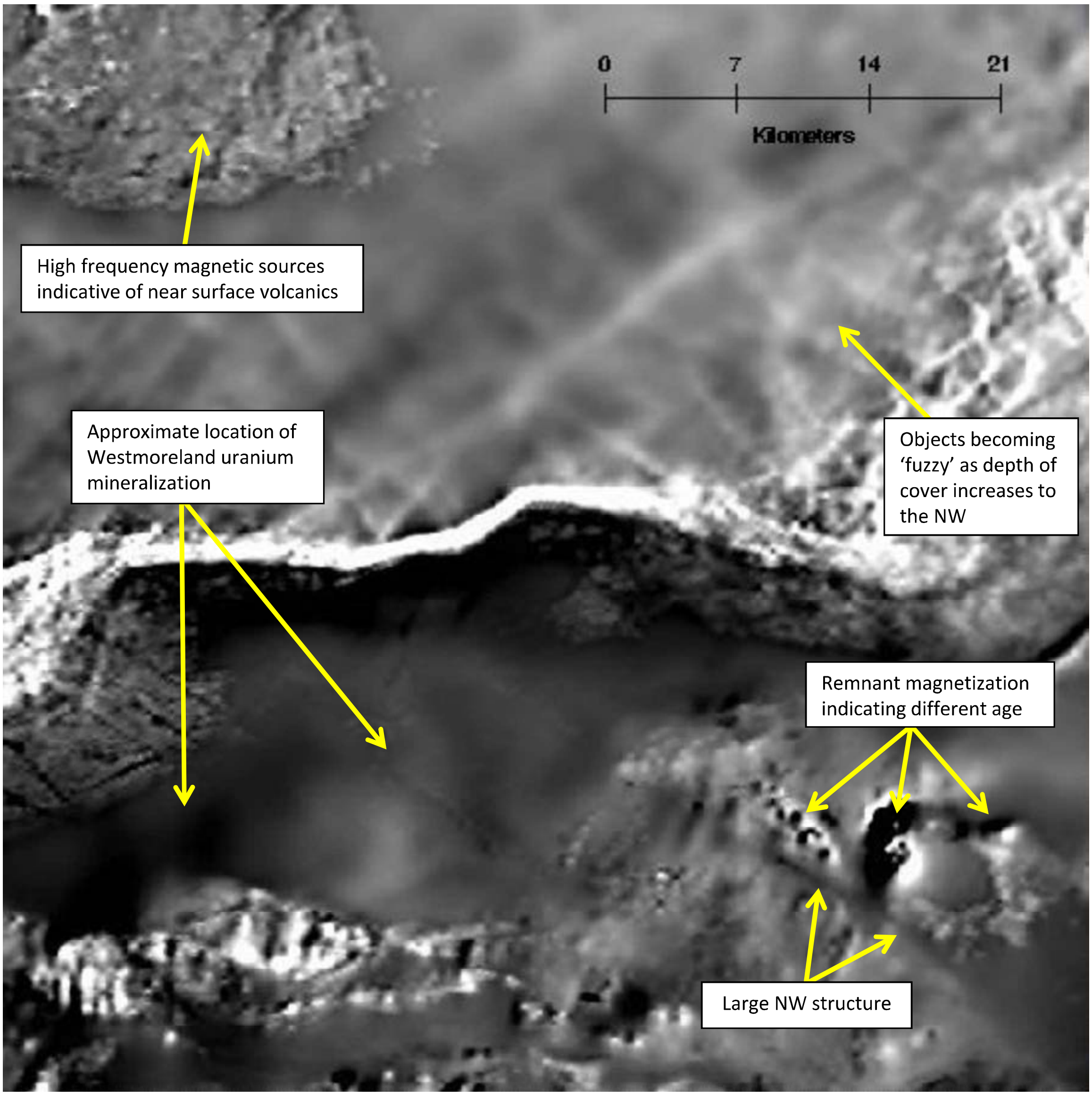

FIG. 4.10. Total magnetic field (reduced to the pole) over the Westmoreland uranium deposit in Queensland, Australia. This data can provide information regarding depth to magnetic basement, major structural elements and the identification of geological components. (Geoscience Australia).

This image highlights several dominant magnetic sources of varying depths which, in this instance, have no direct relationship to the unconformity or to mineralization. However, magnetic data is often used in non-direct targeting by providing information such as depth to basement sources, and, identifying faults and signature specific patterns for evidence of favourable lithologies. Typically, unconformity uranium deposits occur in regions of non-magnetic sedimentary cover. Thus, the expert interpretation of magnetic data will more likely yield a geological framework describing basement structure and composition, which in turn contributes to the exploration process.

The presence of a magnetic source within the area of interest is unlikely to have direct significance in the search for unconformity uranium deposits, unless there is reason to believe some aspect of a mineralized system has a direct association with a magnetic mineral such as magnetite or pyrrhotite. While possible, it is uncommon. Therefore, when acquiring magnetic data, it should be for the purpose of indirect association with some geological aspect that relates to the target of interest. However, in contrast to this, magnetic modelling of the Kintyre Uranium deposit, Australia, has been shown to accurately define altered host rock lithology [4.87].

Global variations in the inducing geomagnetic field mean that an identical magnetic source at differing geographic localities will have a non-characteristic magnetic response, displaying variations in the dipolar nature of the magnetic signal. Understanding this variation is crucial for the proper interpretation and localization of magnetic sources. Reduction to the magnetic pole (RTP) can be calculated to simulate the effect of a vertically inducing magnetic field ($I = 90^{o}$), removing the dipolar nature of magnetic anomalies, placing the peak magnetic value closer to the centre of magnetic source and associating asymmetries in RTP in magnetic images with true dips and plunges [4.86]. Alternative processing methods should be considered when working with survey data collected at very low latitudes [4.88, 4.89].

Fig. 4.11 presents examples of reduction to the pole for survey data from the northern hemisphere, equatorial region and southern hemisphere. Changes in the magnetic image are greatest for the equatorial survey, while the northern hemisphere image shows little change.

Design and acquisition of an aeromagnetic survey requires careful consideration of many factors including climate, access, culture, topography, safety, survey platform, depth to magnetic source, line spacing, cost, line orientation and survey flying height. Before attempting to plan and execute an airborne survey, it is fundamental to understand what the purpose of the survey is and who the target audience is. There are countless examples around the world of surveys being flown with no objective other than to acquire data with the hope that something obvious will become apparent. Such an approach lacks scientific rigour, yet remains widespread. The net result is an accumulation of vast amounts of magnetic data that have served no purpose beyond producing a simple image of the total magnetic field.

Planning and executing an aeromagnetic survey is influenced by numerous interrelated factors. TABLE 4.5 provides an overview of critical factors and the interrelatedness of these factors; however, the table should not be construed as definitive nor does it cover all possibilities. The topics listed are equally relevant to most other forms of geophysical surveying.

In the search for unconformity uranium mineralization, an aeromagnetic survey can significantly aid the exploration initiative so long as due care and planning has been given to the collection of data, and more critically, how and by whom that data is to be used.

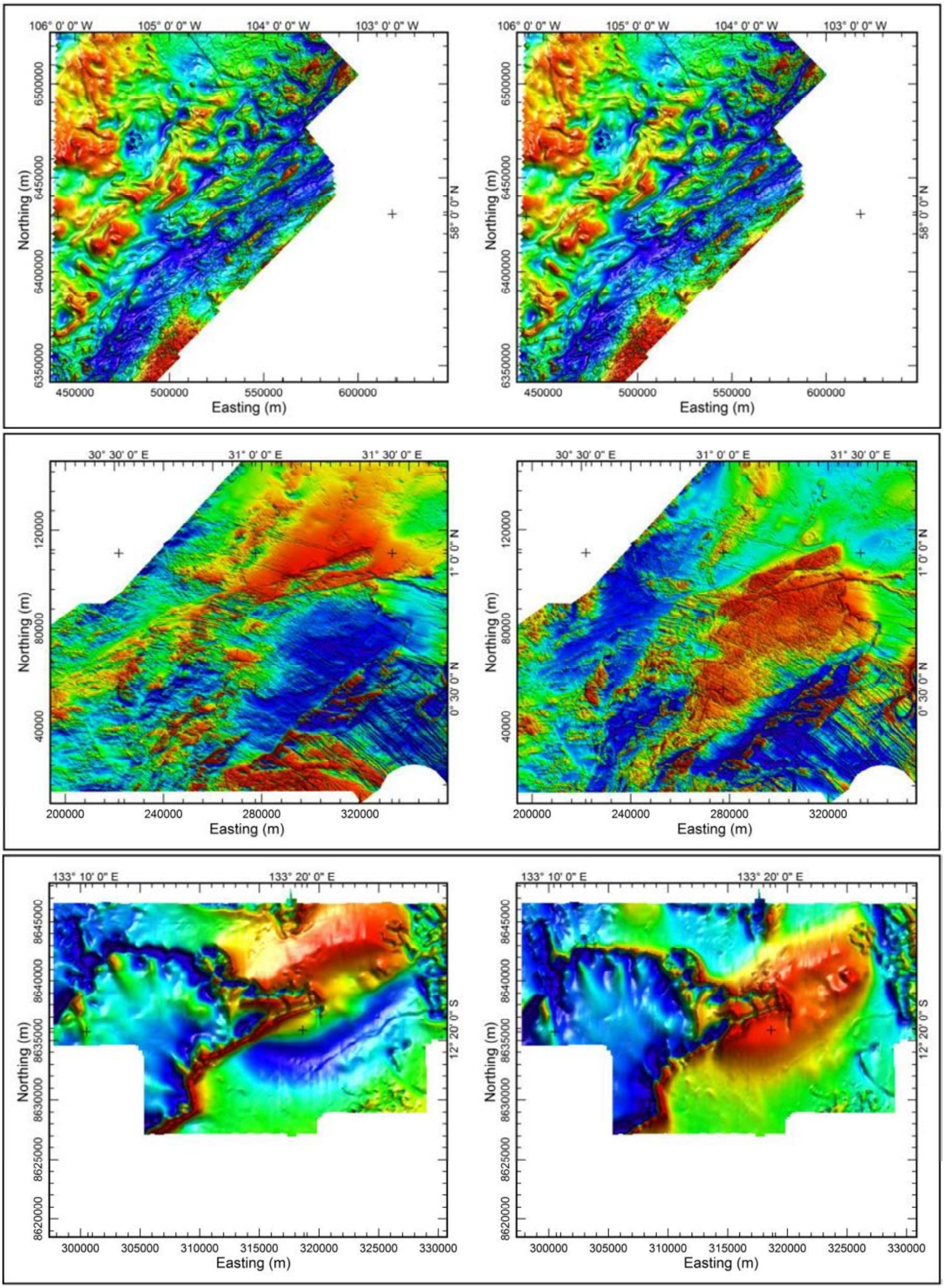

FIG. 4.11. Calculating reduction to the pole for aeromagnetic data has different effects at different latitudes. Three surveys are presented showing data without (left) and with reduction to the pole (right). Surveys are from (top to bottom) northern hemisphere (Athabasca Basin, Canada), equatorial region (Western Uganda) and southern hemisphere (Arnhem Land, Australia). (Data courtesy of Areva Canada, The Republic of Uganda Directorate of Geological Survey and Mines, Northern Territory Geological Survey – Australia).

TABLE 4.5. FACTORS TO BE ASSESSED DURING THE PLANNING AND ACQUISITION OF AEROMAGNETIC DATA

Factor	Consideration
Conceptualization	● Detail the primary reasoning behind why aeromagnetic data is being collected; ● Customer focus; is the customer correctly identified; ● Survey specifications – has expert advice been sought in designing the survey? This is especially important before committing to a formal contract.
Cost	● Does available funding adequately meet the desired survey specifications or will it result in compromises? ● Is pricing competitive? ● Does the delivered product justify the expenditure?
Topography and climate	● Flat and open terrain will suit a fixed-wing aircraft. Hilly and rugged terrain will require a helicopter. There are significant price differences; ● Wet season activity is often associated with thunder and lightning. Such elements may cause extended standby for a survey; ● High temperature air (deserts) can impact the aerodynamic performance of flying aircraft and subsequently impact the ability to meet survey specifications.
Access	● How far can the aircraft fly from the operations base to the survey area? This will affect the survey endurance capabilities; ● If using a helicopter, can fuel be placed close to the survey area to avoid lengthy and costly refueling flights?
Culture	● Is the survey area used by farmers with livestock? Low-flying aircraft can cause significant disruption to livestock; ● Have local residents been advised of the survey and what to expect? ● Are there flying hazards such as power lines, radio towers, uncontrolled airstrips, military installations? ● Are there political or safety restrictions that could be adversely impacted by low-flying aircraft?
Survey shape and flight line orientation	● Avoid odd shaped survey boundaries with many vertices or small segments; ● Slightly extend the survey boundary beyond the central survey area to allow for interpretation of magnetic features close to the survey boundary; ● Where possible, acquire data in a N–S or E–W orientation. Standard practice has been to orient flight lines perpendicular to strike, however it has been shown that this can adversely

	impact an interpreter's ability to recognize strike-perpendicular structures [4.86]; ● At low field inclination, standard practice has been to always fly a N–S orientation. Isles and Rankin [4.86] contest this and advocate that in some circumstances, an E–W orientation is preferred for low magnetic field inclinations; ● Avoid short line lengths (< 5 km fixed wing and <3 km helicopter) due to the large aircraft maneuver required to complete a turn at the end of a line. An over-representation of short lines will incur a significant cost penalty that is already built into the price.
Line spacing	● Choice of line spacing will generally determine survey cost and subsequent resolution. It is generally agreed that a closer line spacing results in greater resolution. However, in the case of an unconformity setting, magnetic sources are often under considerable depths of non-magnetic cover. An increased depth to source lessens the resolving ability of any magnetic survey, regardless of how close lines are flown together. The choice of line spacing will ultimately depend on depth to magnetic sources and an appropriate sample density that will adequately resolve those sources. Each situation will be different so expert advice should be sought when planning the survey.
Flying height	● Safety of the aircraft, pilot and surface inhabitants should always take precedence over any other objective; ● Modern surveys are achieving survey heights as low as 8 m across flat salt lakes [4.86], however this not the norm nor is it necessary for any unconformity uranium setting. The increased depth to magnetic source reduces any benefit from a lower than normal flying height. For the majority of unconformity settings, a 50–60 m flying height should be sufficient. Safety considerations will always dictate the ultimate flying height.

4.2.7.6.2. Airborne radiometrics

The recording of radiometric data is principally concerned with the detection and analysis of natural gamma ray emissions from three of the most abundant radioelements in the upper crust; potassium, uranium and thorium. Details of the radiometric method and theory are documented in earlier IAEA publications [4.82, 4.90–4.93]. Gamma rays can travel large distances through air but are quickly attenuated in rock [4.83]. Therefore, unless mineralization outcrops at the surface, there will be no diagnostic radiometric signature when exploring for the unconformity uranium deposit. Although this limits the benefit of acquiring radiometric data, virtually all modern aeromagnetic surveys incorporate acquisition of radiometric data at the same time, thus making it cost effective and logical to record both magnetic and radiometric data at the same time.

For the most part, airborne radiometric responses over an unconformity_target are going to reflect radioelement distributions from the top few centimetres of the exposed overlying rock type and have no relationship to deeper subsurface rocks. However, the relationship between outcrop and the unexposed unconformity is not always obvious, nor should it be presumed that because an unconformity is known to be at a certain depth, there is no possible relationship between surface radioelement responses and deeper mineralization. Knowledge of the geological environment will enable an explorer to determine the likelihood of subsurface mineralization being expressed at surface, and thus the veracity of any anomalous radiometric responses. For example, an unconformity deposit in the Athabasca Basin (Canada) at a depth of 500 m has a negligible likelihood of any surface expression. In contrast, mineralization within the Ashburton Basin (Australia) with an unconformity less than 200 m below surface has a higher probability of some minor surface expression.

An example of this is presented in Fig. 4.12 which demonstrates two important facets in exploration. The satellite image displayed is from the Ashburton Basin in Western Australia and shows Bresnahan Group sediments unconformably overlying the basement outcrop of the Ashburton Basin. Flight paths from two separate airborne magnetic/radiometric surveys are represented in the image at 400 m and 100 m separation along with profile data for each of potassium, thorium and uranium (Fig. 4.13). Data from the 100-m survey successfully resolved a very small surface fracture in sandstone which contained secondary uranium (Fig. 4.14). No indication of the anomalous radiometric response was recorded in the 400-m survey and this anomalous subcrop would have remained undiscovered without airborne radiometric data at the tighter line spacing.

Selecting the correct flight line spacing was crucial in identifying a localized outcrop of uranium.

There was no assumption made concerning the likelihood of the occurrence of outcropping uranium mineralization, which thus influenced the decision to acquire airborne radiometric data at the same time as magnetic data. In this Australian example, there is a negligible price differential between collecting only magnetic data vs. collecting both magnetic and radiometric data. Acquisition of data in other countries may be subject to a larger price variation, which in turn could be an influencing factor for determination of which data sets to collect. If radiometric data had not been acquired in this situation, then the discovery of a new mineralized outcrop in an unexpected geological setting would have been highly unlikely.

Making early assumptions about what can or cannot be discovered can be a limiting factor in exploration success.

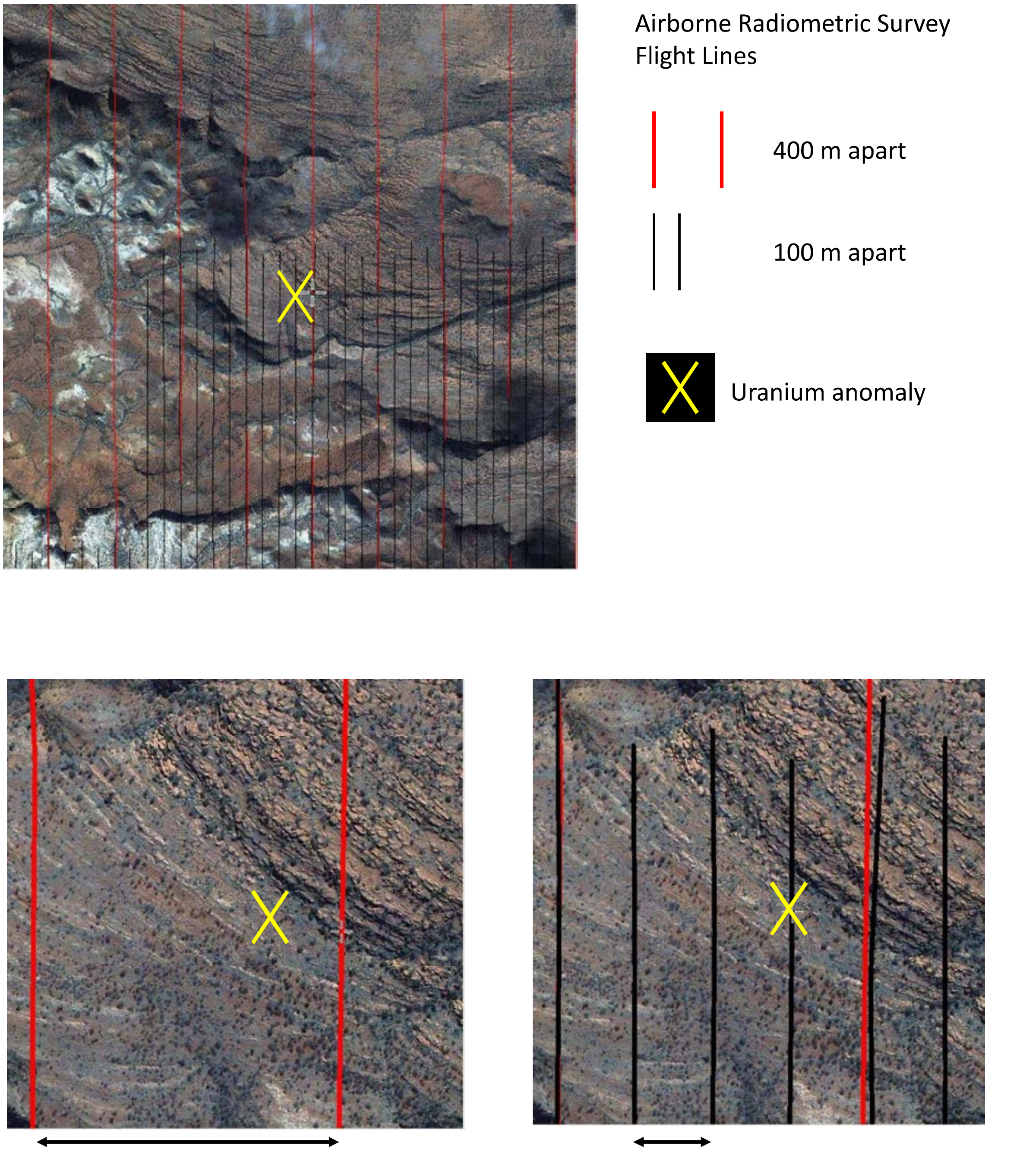

0

FIG. 4.12. Flight path differences can have a significant effect as shown with two surveys flown at 100 m and 400 m line spacing. An outcrop of uranium was missed with a 400-m line spacing, but was detected with a 100-m flight line spacing.

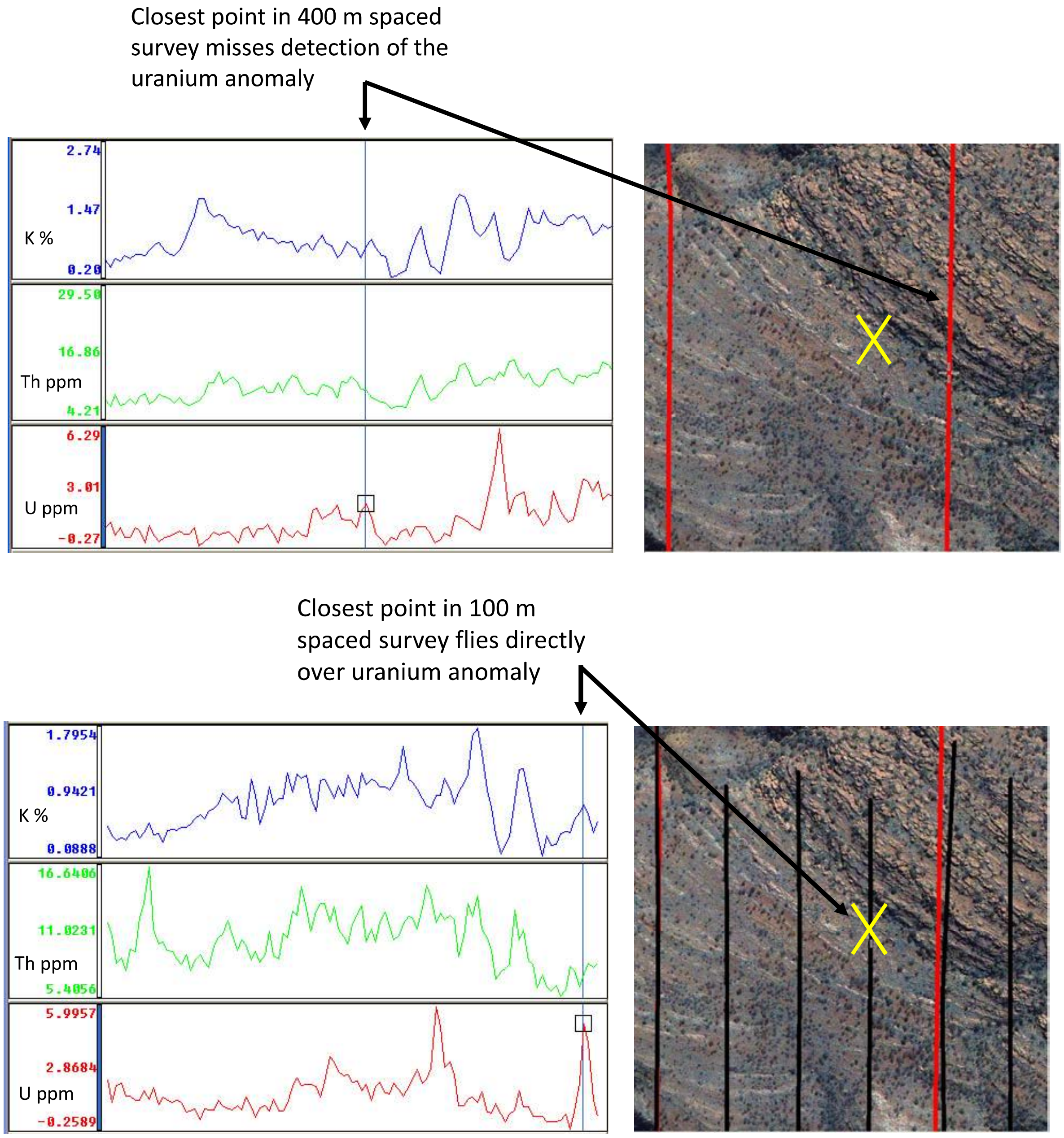

FIG. 4.13. Profile data for potassium, thorium and uranium along each of the closest flight lines from the 400 m (top) and 100 m surveys (bottom).

Fig. 4.15 presents the gridded data from the uranium channel for both surveys and clearly demonstrates the advantages of a higher resolution data set. Note that the discrete uranium anomaly identified in Fig. 4.13 is only visible within the closer spaced data set.

FIG. 4.14. Surface locality for the uranium anomaly presented in Fig. 4.13. The source of the airborne radiometric anomaly remained unclear until a ground radiometric survey was completed.

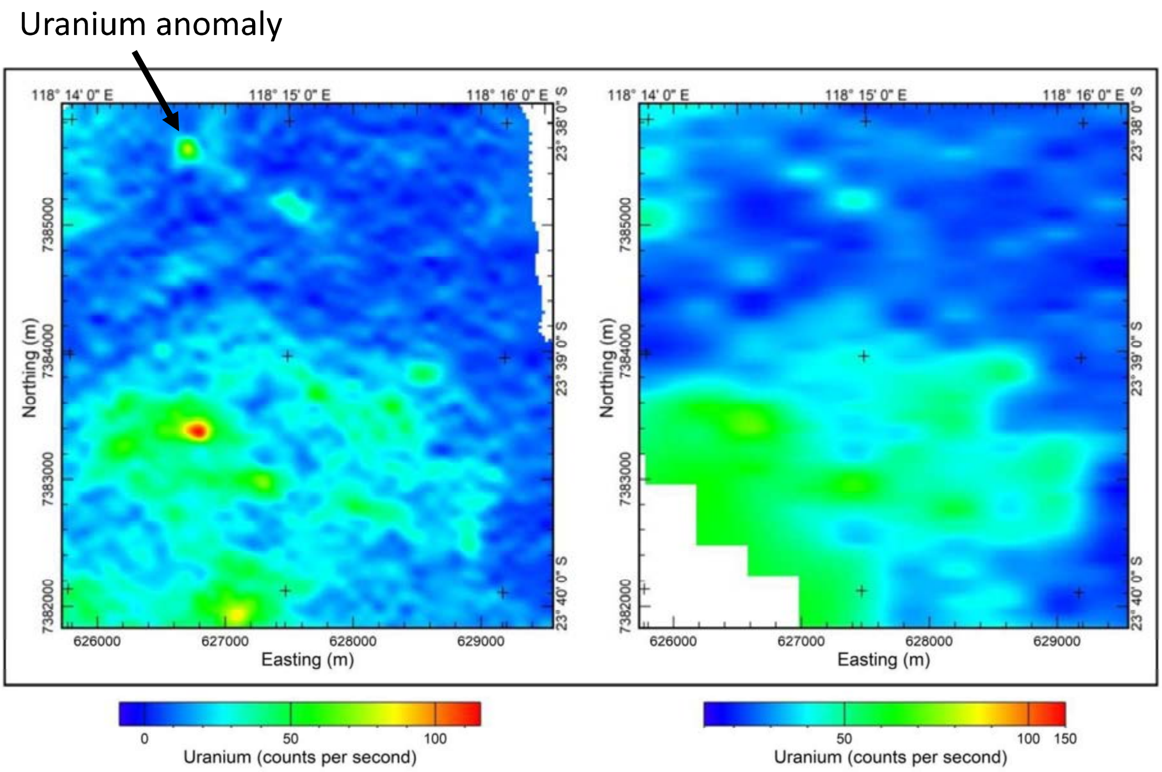

FIG. 4.15. Gridded uranium channel data for the 100 m (left) and 400 m (right) line spaced airborne surveys. A weak, discrete uranium anomaly in the 100-m data was the only indication of undiscovered surface mineralization. (Data supplied by Geological Survey of Western Australia).

4.2.7.6.3. Airborne electromagnetics

The primary aim of an EM survey is to map variations in electrical properties within rocks of potential interest by measuring how easily an electric current can pass through it [4.94]. Electromagnetic surveys in the following discussion are primarily concerned with methods using an active source to generate a time varying electromagnetic field. Historically, a majority of EM surveys were implemented to locate anomalous conductors. However, modern EM surveys can also provide useful information on shallow resistivity mapping, construction of 3-D conductivity models, hydrogeological targeting as well as the effective targeting of deep conductors [4.95]. Application of EM methods in the search for Proterozoic_unconformity uranium mineralization is widespread and driven by the requirement to map a specific electrical property associated with target deposits. Importantly, an EM survey does not directly detect uranium mineralization, rather this method is used to highlight an indirect association between electrical conductivity and some desirable characteristic of the host rock. As with all other geophysical techniques, the method relies on sufficient physical property contrast between the target and surrounding host rocks.

Airborne EM (AEM) surveys fall into two main categories: time domain and frequency domain. A concise and readable description of these two methods can be found in Dentith and Mudge [4.84]. Due to the limited depth of investigation of frequency domain systems, the majority of mineral exploration surveys are time domain [4.84].

The AEM surveys have played a pivotal role in focusing exploration and the subsequent discovery of numerous Proterozoic unconformity uranium deposits within the Athabasca Basin. Conductive graphitic lithologies in the basement were shown to be spatially correlated with uranium mineralization [4.96] which provided an immediate targeting vector for further prospecting. A strong conductor such as a graphitic schist, within a highly resistive environment became an excellent geophysical target and one that suited the widespread application of AEM surveys. Although early work had established the spatial correlation between basement graphitic conductors and uranium mineralization however, after much testing, it is widely acknowledged that a graphitic conductor in no way guarantees uranium mineralization [4.95]. The Centennial uranium deposit displays many characteristics of an unconformity uranium deposit, yet is recognized as atypical in that it has no association with graphitic conductors [4.97]. This fact highlights the need for an explorer to not only maintain an awareness of the preferential geological and geophysical associations based on existing deposits, but also to be acutely aware that variations are likely to occur.

The AEM method has other applications besides direct detection of large conductors. In geological terranes such as the Alligator Rivers Uranium Field of Northern Australia, Archean basement and Proterozoic sandstones lack highly conductive features and are instead characterized by an extreme electrically resistive profile encompassing both basement and overlying sediments. Airborne EM has been applied here to identify weak conductors as a proxy for subtle alteration and structural offsets [4.98] as well as successfully map palaeo-weathering alteration around an unconformable horizon as a direct proxy for a 3-D expression of the unconformity [4.82, 4.99]. The application of this approach is demonstrated in Fig. 4.16 where conductivity depth sections from a Tempest AEM survey have been combined to create a virtual representation of alteration around the unconformity.

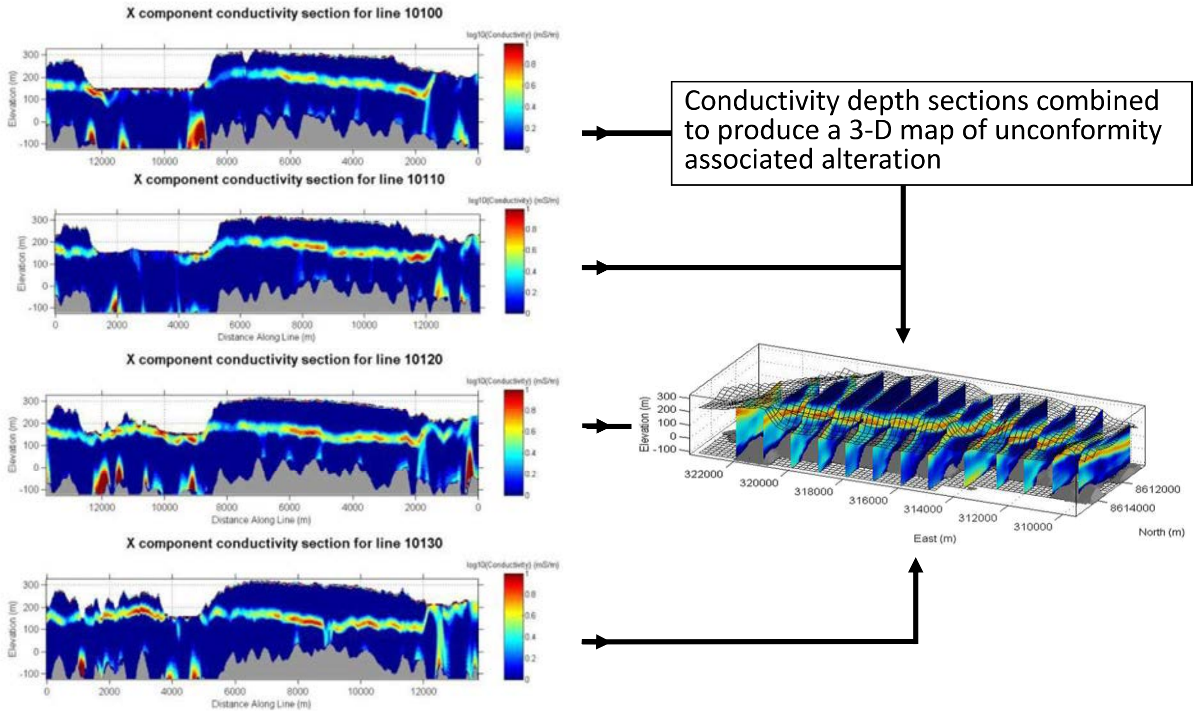

FIG. 4.16. Conductivity depth sections from a Tempest AEM survey are combined to create a pseudo 3-D model of unconformity alteration in this Australian data set.

The design, execution and interpretation of an AEM survey is a specialist process and requires considerable geophysical expertise to ensure the correct choice of system, platform, line spacing and interpretation. The AEM surveys are generally much more expensive than an equivalent aeromagnetic/radiometric survey and therefore represent a considerable monetary investment. Inappropriate selection of system or survey specifications can prove very costly.

TABLE 4.6 summarizes some of the AEM systems currently available that may have applicability in the search for Proterozoic unconformity uranium deposits. The variety of systems is an indication of the range of geological environments for which these systems were devised. Note that not all available AEM systems are listed.

TABLE 4.6. SPECIFICATIONS OF SELECTED AIRBORNE ELECTROMAGNETIC TIME DOMAIN SYSTEMS WITH POTENTIAL APPLICATION IN UNCONFORMITY URANIUM EXPLORATION (MODIFIED AFTER AUKEN, BOESEN & CHRISTIANSEN [4.100]

Name	TEMPEST	$HeliTEM_{30C}$	$HeliTEM_{35C}$	XCITE	AeroTEM	VTEM	VTEM+	$VTEM^{Max}$	ZTEM
Company	CGG	CGG	CGG	NRG	Geotech	Geotech	Geotech	Geotech	Geotech
Method	FTEM	HTEM	HTEM	HTEM	HTEM	HTEM	HTEM	HTEM	HTEM
EM induction	Active	Active	Active	Active	Active	Active	Active	Active	Passive
Base frequency (Hz)	12.5/15, 25/30, 75/90	25/30, 75/90	12.5/15, 25/30	25	90	30	30	30	19-720
Tx area per turn (m^2)	154	706	962	266	110	240	540	960	N/A
Tx turns (#)	1	3	4	4	5	4	4	4	N/A
Waveform	Square	Half Sine & Square	Half Sine & Square	Square	Triangular	Polygonal	Polygonal	Polygonal	N/A
Peak current (A)	560	325	260	235 to 350	410	250	310	335	N/A
Peak moment ($k.Am^2$)	86	688	1000	250 to 372	220	240	625	1300	N/A
Transmitter altitude (m)	120	30	30	30	30	30	30	30	N/A
Receiver altitude (m)	75	30	30	30	30	30	30	30	80
Speed (m/s)	50	25	25	25	21	25	25	25	-
Off-time channels (#)	15	26/15	26/15	Streaming Off-time and On-time	17	32	32	32	N/A
Earliest channel (μs)	7	16	8	6	87	21	21	21	N/A
Receiver component	XYZ	XYZ	XYZ	XZ	XZ	Z	XYZ	XYZ	Z

4.2.7.7. Ground surveys

A ground geophysical survey is one where geophysical measurements or observations are carried out on the Earth's surface. All airborne methods have an equivalent ground survey technique, but not all ground methods can be applied from an airborne platform. There are many factors to be considered before undertaking a ground survey, including choosing the appropriate method to meet the exploration objective. Understanding what that objective is will greatly assist the planning, implementation and interpretation of a ground geophysical survey. In the context of unconformity uranium mineralization, choosing the appropriate ground method can involve many diverse issues such as: cost, topography, access, cultural considerations, target depth, target size, physical property contrast, climate, health and safety risk to name a few. TABLE 4.7 summarizes the above points and should serve to highlight the necessity of considering much more than simply the collection of geophysical data. This Table is not intended to be comprehensive regarding all aspects relating to ground geophysical surveys, and expert advice is encouraged.

TABLE 4.7 FACTORS INFLUENCING THE DECISION TO CONDUCT A GROUND GEOPHYSICAL SURVEY AND SOME POTENTIAL IMPACTS

Factor	Consideration	Potential impact
Cost	● Is the survey cost effective or cost prohibitive? ● Do you need external contractors or can the survey be run in-house? ● Is the equipment available locally or must it be shipped in?	A disproportionate amount of money is used to fund the survey to the potential detriment of other factors.
Topography	● Flat, hilly or mountainous terrain; ● Deeply incised surface topography making movement difficult; ● Sand cover, abundant water, deep rivers, rocky; ● Dense vegetation requiring line clearing.	Potentially a significant impact on the ability to conduct the survey in a time and cost-effective manner.
Access	● Can the survey location be accessed easily and quickly? ● Are there vehicle accessible roads? ● Would air transport be required (e.g. helicopter)? ● Can the survey equipment be transported by hand or is a vehicle mandatory (e.g. generators)?	If access is difficult or impossible, then this can affect cost and time required to complete the work.
Culture	● Are there dwellings within the survey area? ● High voltage power lines impact electrical surveys; ● Major roads with traffic pose a safety risk; ● Water pipes and fences cause false anomalies;	Potential for negative impact upon local populations affected by the survey.

	● Access to culturally sensitive sites may not be possible; ● Extreme risk to local population during electrical surveys; ● Political restrictions.	Potential for false anomalies caused by artefacts like water pipes or power lines.
Target depth	● Is the depth to target beyond the reasonable detection limits of the relevant technique? ● Target depth is intimately tied to physical property contrasts.	If the target depth is unrealistic (too great) there is the danger of a false negative.
Physical property contrast	● At any given depth, is there sufficient contrast in the physical property being measured though the ground survey? ● Note that the ability to resolve a physical property contrast generally decreases with increasing depth; ● Measuring a property that is inappropriate can also lead to false anomalies. For example, an induced polarization (IP) survey is well suited to finding disseminated sulphides, however carbon rich shales are well known for producing very strong IP anomalies which could be misinterpreted as sulphides.	Targeting using a physical property that presents minimal, insufficient or inappropriate contrast can result in poor judgement.
Climate	● Excessive snow will mask surface gamma radiation; ● Excessive heat/cold may cause equipment failure; ● Rain or surface water may interfere with magnetic and electromagnetic readings; ● Climatic extremes can present a significant health risk to field crews.	Climatic extremes can impact equipment operation as well as present significant health and safety risk to personnel.
Health and Safety	● Many ground electrical surveys require high voltage and high current to operate correctly; ● Temperature extremes can affect field crews; ● Attacks by indigenous fauna (polar bears, crocodiles, snakes, spiders, gorillas, lions); ● Operating in remote and isolated areas limit opportunities for urgent medical assistance.	Some types of ground surveys can potentially have a lethal impact. Likewise, environmental, flora and fauna elements have the potential for adverse impact on people.

The need for undertaking a ground geophysical survey should be assessed within the context of the above elements and with a clearly defined objective. It should be evident from the start that the ground survey is targeting a localized, physical property contrast that has a direct or indirect association with the mineralized setting. Generally, most Proterozoic unconformity targets are at depth. Therefore, a ground survey will focus on identifying a specific physical property that is known, or at least theorized as being associated with potential mineralization. To satisfy this, the explorer needs a good understanding of the geological setting and likely mineralization style for the survey area. Additionally, careful assessment is required concerning target depth, target size and the ability to detect the specified property contrast, should it exist.

The following discussion presents a brief review of select methods that are relevant in the search for unconformity related uranium mineralization. It is not an exhaustive list as each geological situation is different and the methods described are often used to satisfy a specific exploration situation. The discussion of each method can be used as a guide for how certain techniques have aided the exploration process. Where possible, example data is included to demonstrate the application in recent exploration programmes.

4.2.7.7.1. Resistivity (DCIP)

Ground direct current (DC) resistivity surveys have been widely used by many Canadian uranium explorers to map lithology, structure and alteration [4.96]. Extensive clay mineral alteration in the sandstone and basement occurs around many of the unconformity uranium deposits [4.101]. The alteration of sedimentary and basement host rocks creates a significant electrical property contrast between fresh and altered rocks, and is an excellent target for detecting with surface resistivity measurements within the highly resistive host rock environment [4.102].

A uranium explorer will generally choose to conduct a DC resistivity survey on the basis that a favourable geological process has resulted in the alteration of target lithologies. Such alteration may increase electrical resistance (silicification) or reduce it (clay-mineral alteration). It is common for such surveys to be used as a follow-up mechanism when targeting and refining airborne electromagnetic anomalies. The AEM survey may indicate a zone of decreased resistivity proximal to a larger conductor or simply a strong basement conductor on its own. However, it is recognized that an alteration halo and a strong graphitic basement conductor are favourable elements that increase the prospectivity for uranium mineralization [4.95], and such a setting can be characterized through its electrical response.

Smith, Wood and Powell [4.95] also highlight the variability in electrical characterization between airborne electromagnetic anomalies and spatially equivalent ground resistivity data. Whilst both methods can be thought of as responding to changes in electrical conductivity, they yield very different results due to different noise levels, coupling mechanisms and sensitivities.

An explorer should be aware that a variety of methods may be used to measure the same physical property, but should not expect the output from each method to be the same.

Fig. 4.17 shows a DC resistivity section from the Wheeler River uranium project where alteration of sandstones within the Manitou Falls formation is characterized by a corresponding decrease in apparent resistivity. The combination of a basement hosted graphitic pelite conductor and sandstone alteration characterizes the uranium mineralization setting at this deposit [4.102].

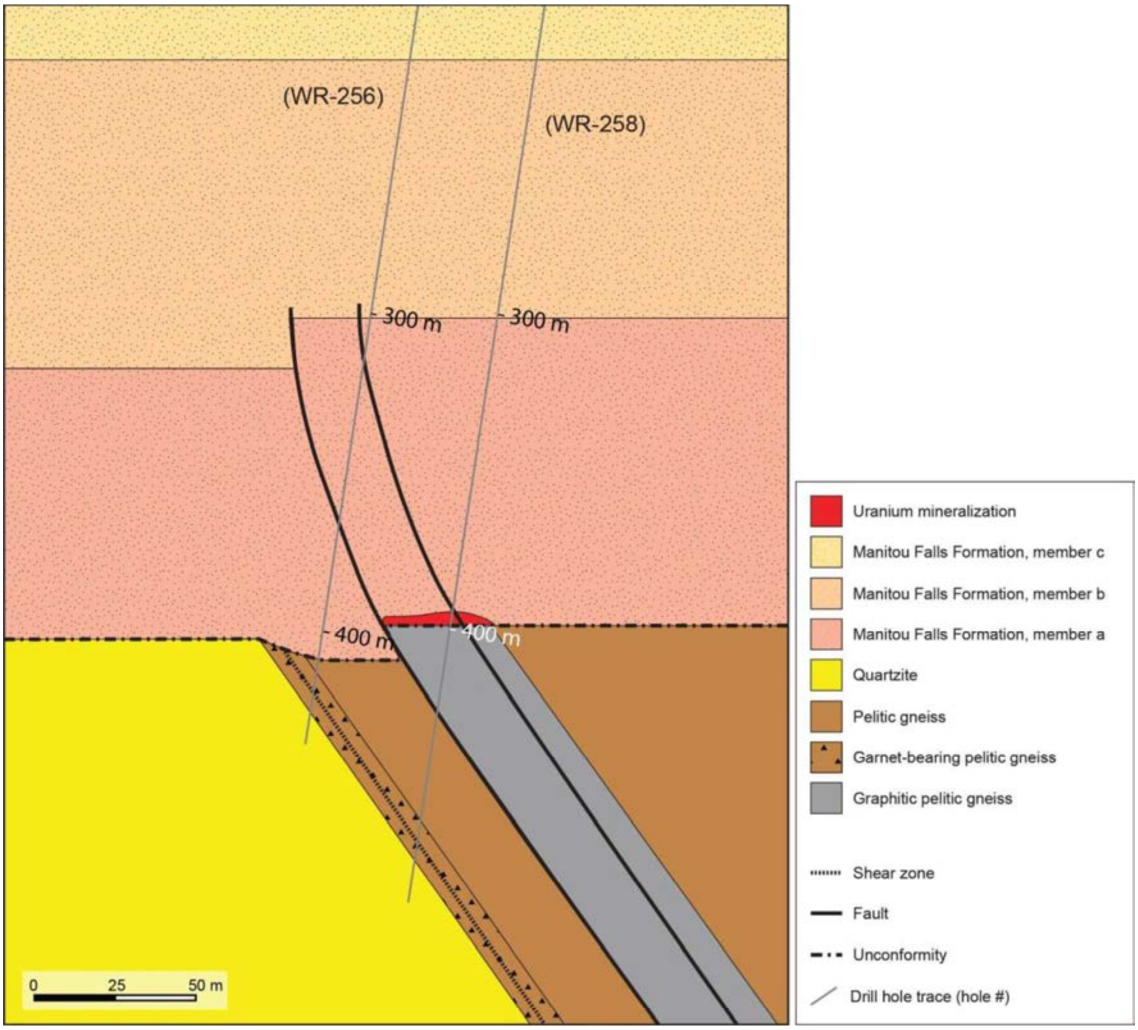

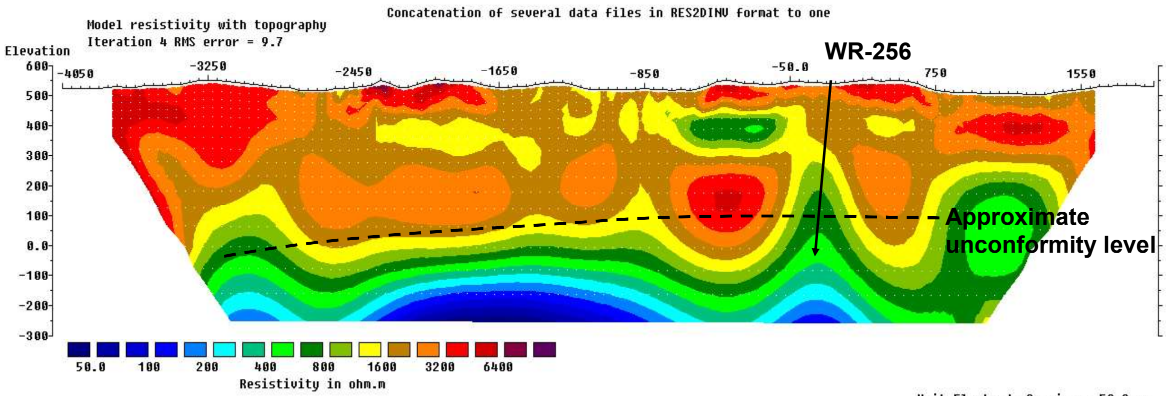

FIG. 4.17. DC resistivity section from the Wheeler River uranium project highlighting the resistivity low associated with mineralizing structures within the Manitou Falls Formation sediments. The interpreted boundary of the unconformity is shown in the resistivity pseudo section (Image reproduced courtesy of Denison Mines Corp.).

4.2.7.7.2. Magnetics

Like its airborne equivalent, a ground magnetic survey samples local variations in the earth's magnetic field, generally with the intent of constructing a spatially representative grid of these localized variations, albeit at a more localized scale. A ground magnetic survey can yield detailed information on shallow magnetic sources and depending on the line/station spacing, provide a higher spatial resolution than an equivalent airborne magnetic survey [4.103].

As with the airborne equivalent, a ground magnetic survey can provide information concerning structural and lithological components over the earth's near surface. The role such information has in the search for unconformity uranium mineralization depends on how the explorer perceives the relationship between mapping magnetically significant minerals and the target deposit type. An observable response between uranium mineralization and magnetization is unlikely due to uranium being a paramagnetic mineral [4.82]. Paramagnetic minerals include pyroxenes, amphiboles and micas and are characterized by a small positive magnetic susceptibility [4.86] which is generally too small to be significant. Thus, the ground magnetic survey helps by mapping structure and magnetic lithology at the prospect scale.

Understanding how magnetism varies at a localized scale can provide information about depth to magnetic sources as well as mapping frequency characteristics of those sources. This can be used to generate a magnetically based geological interpretation. Due to the generally high depths of cover associated with an unconformity geological setting, an airborne magnetic survey will provide comparable geological detail compared to data collected from a ground magnetic survey. The benefit in conducting a ground magnetic survey arises when the target source is relatively shallow. Bringing source and sensor closer together allows the resultant magnetic field to be sampled at a higher spatial density, providing greater resolution for those near surface sources. This benefit diminishes rapidly as the depth to magnetic source increases, resulting in a loss of detail [4.86]. Likewise, conducting a ground survey along widely spaced lines has no advantage over an equivalently spaced airborne survey except where only small numbers of lines are required and there is an obvious cost differential.

The setup, collection and reduction of data from a ground magnetic survey can generally be completed by most competent personal with only a small level of training required. Most modern magnetometers incorporate GPS positioning, permitting accurate synchronization with base stations (Fig. 4.18). A succinct overview of ground magnetic surveying can be found in Brodie [4.103].

FIG. 4.18. Ground magnetic survey in operation (left) and base station (right). Modern ground magnetometers incorporate GPS positioning (left) providing positional accuracy and time synchronization with the base station (Photos courtesy of the Republic of Uganda Directorate of Geological Survey and Mines).

4.2.7.7.3. Radiometrics

The application of gamma ray surveying in the search for unconformity uranium deposits has been discussed previously. Of fundamental relevance is the fact that surface gamma ray emissions correlate with radioelement concentrations from approximately the top 30–40 cm of the earth's surface, predominantly representing the distribution of potassium, uranium and thorium [4.83]. The decision to acquire ground radiometrics in the context of unconformity uranium exploration must therefore have a sound geological basis linking the near surface distribution of radioelements with the often much deeper target horizon.

Instruments used in ground surveys can either be hand-held or vehicle mounted (Fig. 4.19), the main difference being the size of crystal which determines if it can be operator carried or requires vehicle mounting. As a general rule, the larger the detector crystal, the greater the sensitivity. However, as the size increases, so does the weight. Car mounted detectors provide a rapid survey mode, but are limited by a requirement for suitable and safe vehicular access. Hand-held detectors offer more portability with a smaller crystal size (Fig. 4.20). A ground survey will normally be conducted over a regularized grid as follow-up to an airborne anomaly.

The explorer should also be aware of the limitations of using a total count (TC) detector verses a differential spectrometer. A TC instrument provides information on all radiation particle energy above a discrimination threshold whilst a differential spectrometer differentiates particles based on energy and provides a quantitative analysis of the source [4.82]. Wherever possible, all ground prospecting and survey work should always be conducted with a differential spectrometer.

FIG. 4.19. Car-borne radiation detector mounted on top of a vehicle (Picture reproduced courtesy of Radiation Solutions Inc.).

FIG. 4.20. An example of a hand-held portable differential spectrometer (left). The same spectrometer mounted on a backpack provides a convenient survey configuration, freeing up the hands of the operator. In this configuration, the user should be aware of the minimal, but constant signal attenuation caused by the proximity of the operator's body (Pictures reproduced courtesy of Radiation Solutions Inc.).

Acquisition of radiometric data from the ground will nearly always show an improvement over the airborne equivalent; the significant difference in crystal volume between portable ground sensors and an airborne sensor can be advantageous in areas of very low count rates. A ground survey will benefit from higher emission energies related to localized anomalies and therefore a greater signal to noise ratio for weak or small sources. Despite having a significantly smaller crystal size compared to an airborne detector, the slower survey speed has the advantage of longer count times over a source, thus providing greater spatial resolution of potassium, uranium and thorium.

The other main advantage is increased resolution of localized anomalies when compared to an equivalent airborne data set. An airborne detector will typically operate at a 1 Hz or 2 Hz sampling frequency, equating to an average ground distance of approximately 70 m or 35 m respectively. At normal walking pace, a ground survey covers approximately 1.1 m/s (4 km/hr) and depending on sample rate, can result in a greatly improved resolution.

Fig. 4.21 demonstrates the resolution difference between an airborne and ground radiometric survey over an area of outcropping uranium mineralization from the Kimberley region of Western Australia. A coloured U^2/Th ratio grid is overlain on satellite imagery in both images and highlights an area of elevated uranium. This ratio is often used for rapid discrimination of uranium anomalies from those also elevated in thorium. The airborne survey accurately identifies the location of surface anomalism but fails to discriminate the internal variability of the large anomaly. It is only once the ground survey data has been collected that this variability becomes apparent.

When choosing to conduct a ground radiometric survey, several assumptions are made, namely:

- There is sound geological and geophysical reasoning to support the detailed mapping of radioelements on the ground. This is usually because of a known or suspected radiometric anomaly for which detailed mapping of gamma radiation is considered advantageous;
- Surface conditions favour minimal risk and ready access for an operator who will generally walk pre-planned grid lines at a constant speed ensuring a constant sampling rate. Examples of restrictive surface conditions could include heavily vegetated regions, the presence of dangerous flora or fauna, swamps, the risk of unexploded ordinances, abundant water courses, unstable or steep terrain; and
- Systematic prospecting around localized radiometric anomalies which may or may not have been previously detected by an airborne survey.

The processing and correction of ground radiometric data is generally performed by software supplied with the survey instrument. Additional information on the application and interpretation of radiometric data is available in Refs [4.83, 4.90, 4.91, 4.93, 4.104, 4.105].

a)

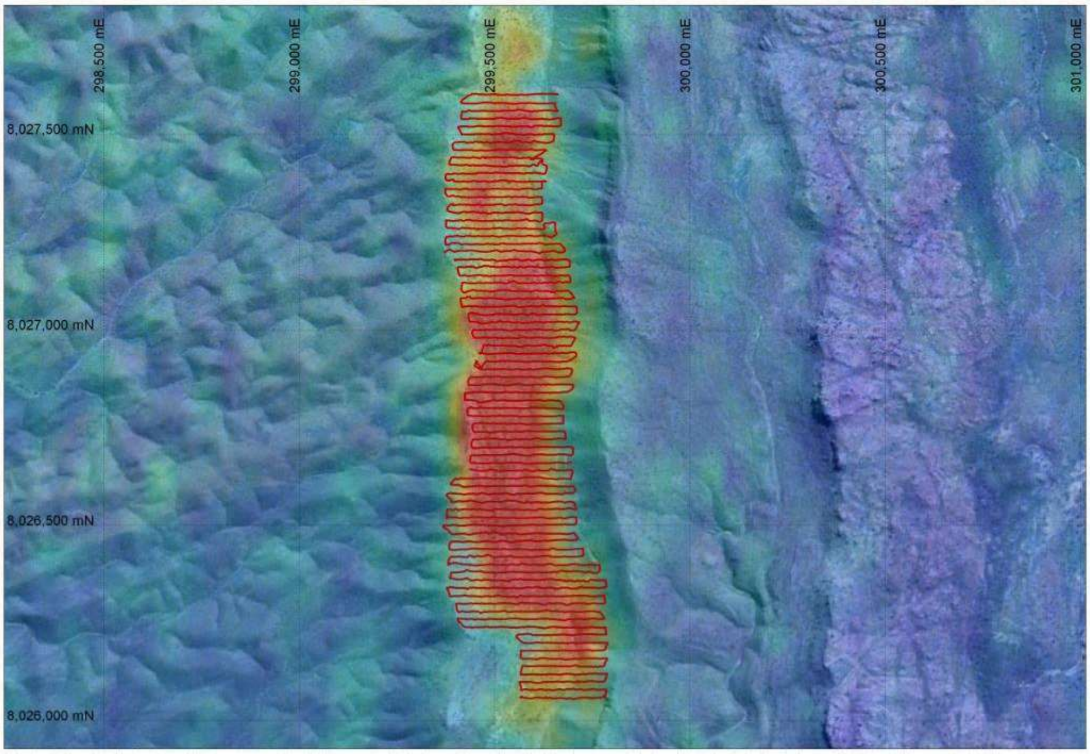

b)

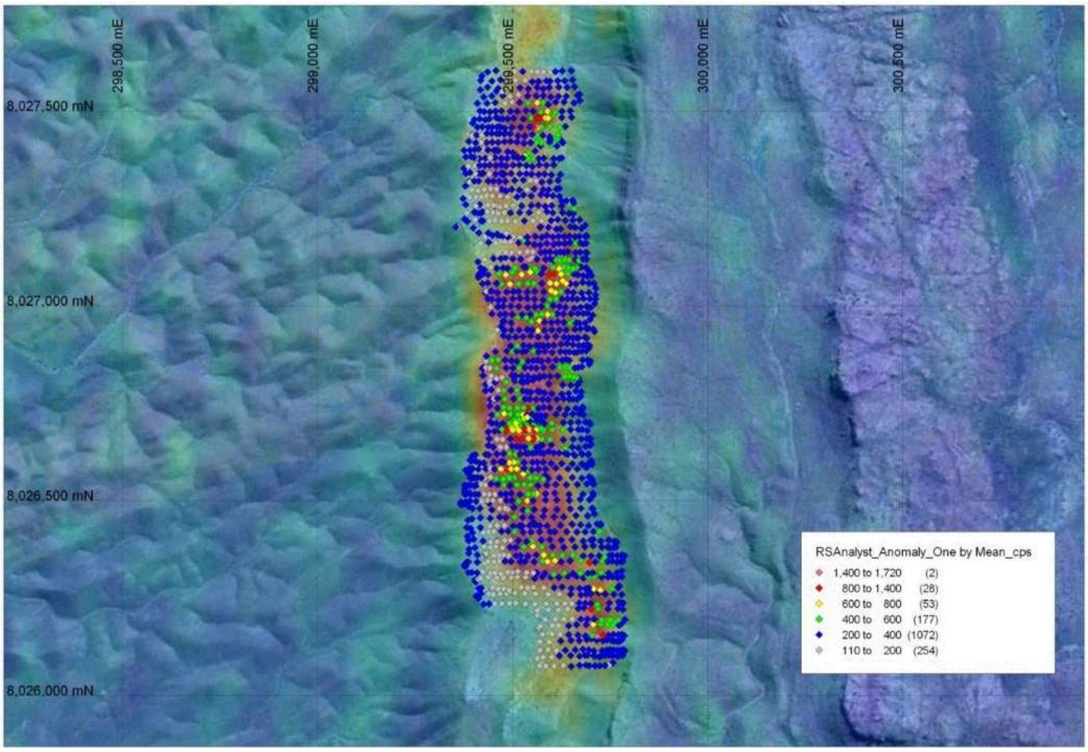

FIG. 4.21. a) An airborne radiometric ratio grid (U^2/Th) draped over high resolution satellite imagery with the ground radiometric survey path. b) 30 sec accumulation values for the uranium channel. Data from the ground survey is noticeably more detailed in mapping the localized distribution of surface anomalism.

4.2.7.7.4. Ground electromagnetics

In general, an EM survey is conducted to target an aspect of the mineralized system that is electrically conductive, and from this information, determine its depth, dip, size and conductivity/resistivity. The interpretation and geological meaning of a conductor needs to be considered within the broader geological setting of the survey area and why locating a buried conductor is relevant to the exploration problem. A uranium explorer searching for an unconformity style deposit may decide to conduct a ground EM survey because:

- There is a sound geological basis for targeting unconformity style uranium mineralization within the target terrain — right age, favourable structures, favourable geochemistry;
- The presence of a conductor has geological significance in locating target mineralization;
- Some other vector (an aem survey) has provided evidence for buried conductors; and
- There is a reduced, or manageable probability for false anomalies arising from unremarkable geology such as carbon rich shales.

Since there are a multitude of ground EM survey systems and loop configurations suitable for use in this context, expert assistance for planning, execution and interpretation of a ground EM survey is advisable.

It is useful for the explorer to have an understanding of the interrelatedness between geological factors and the electrical properties of rocks and to this extent, the following generalizations are made [4.84]:

- Within the geological environment, most substances are semiconductors;
- The common silicate and carbonate minerals are insulators;
- Metallic sulphides are relatively conductive (with the exception of sphalerite);
- Metal oxides are normally less conductive than metal sulphides. The normal range of conductivities overlaps with the main rock types, making detection by physical property contrast less effective;
- The contents of porous rocks can greatly influence their conductivity, with water being a good conductor whilst air and ice are poor conductors;
- Pure water and ice are poor conductors;
- Rising salinity generally correlates with increased conductivity. This has implications for saline water environments where significant attenuation of the inducing electromagnetic wave is often observed;
- A rock type cannot be determined by its electrical resistivity. Many different rock types present with similar electrical properties and the problem is one of non-uniqueness;
- The increased pore space of a sedimentary rock will generally make it more conductive than an igneous rock. It should be noted that the conductivity of a sedimentary rock is strongly influenced by the pore space fluid so that a highly porous sedimentary rock in a fresh water environment will manifest as highly resistive;
- Clay rich minerals are some of the strongest conductors, increasing in conductivity when saturated;
- Graphite is highly conductive, extending the conductivity of rocks in which it forms. It is also highly anisotropic in its electrical properties.

An example of non-standard EM surveying is presented in Fig. 4.22 which shows data from a series of E–W traverses over known mineralization within a shallow unconformity setting of Northern Australia. The data presented are of smooth-model 1-D resistivity inversions. In this example, the objective was not to detect large basement conductors; rather, it was to identify the decrease in resistivity associated with weathering around an unconformity. Extensive drilling at the prospect had confirmed a pervasive clay-mineral alteration associated with a narrow horizon surrounding the unconformity, whilst sediments and basement rocks proximal to the contact remained unaltered and highly resistive. High annual rainfall also contributes to a constant inundation of fresh water within sedimentary pore space and an elevated ground water table. All sections are parallel with a 200-m offset between lines.

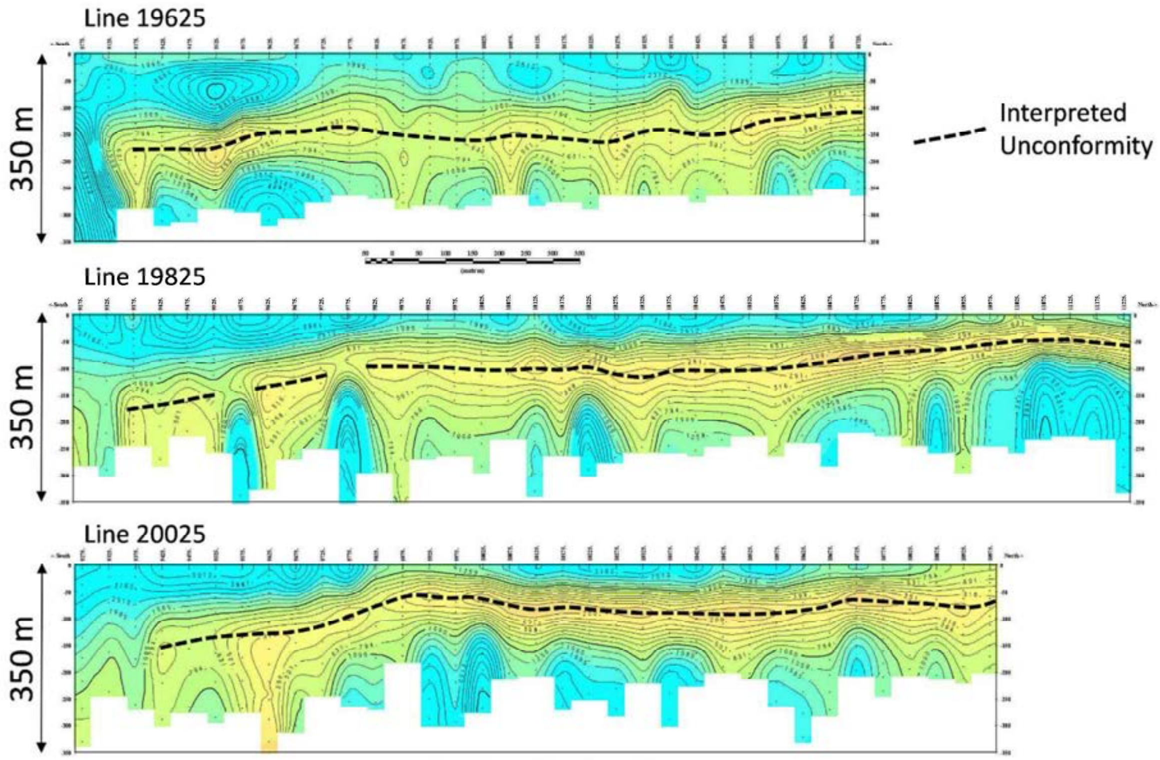

FIG. 4.22. Three parallel pseudo-sections of a 1-D smooth model resistivity inversion recorded over a shallow unconformity setting in Northern Australia. Vertical cross-sections show a laterally extensive horizon of decreased resistivity that corresponds with a zone of increased clay alteration around the unconformity. The precise location of the unconformity is not determined but can be inferred as shown by the dashed lines.

Identifying this characteristic of the unconformity provided an opportunity to test the electrical contrast of the palaeo-weathering layer as a proxy for the actual location of the unconformity. The extremely resistive host rocks and thin, weakly conductive alteration layer was a contraindication for normal EM methods designed to detect strong conductors. Thus, it was necessary to adopt a non-conventional approach and use an engineering-based EM system such as Zonge's NanoTEM. Designed to penetrate no more than several metres in normal operation, NanoTEM was effective at recording decay responses from the weakly conductive alteration layer within a highly resistive half-space.

4.2.7.7.5. Gravity

Gravity surveys conducted for mineral exploration are concerned with mapping relative density differences between a base station and field observations, rather than absolute values [4.84]. Mapping these differences allows the explorer to identify an area of anomalous density variation which can hopefully be related back to a geological causation. The interpretability of gravity data requires an understanding of geological processes that may have contributed to, or caused the observed change in density, while keeping in mind that a variety of geological processes can result in a relative increase or decrease of rock density. It is crucial for the explorer to understand that a change in density can be caused by many different and unrelated geological processes. For this reason, changes in density have a non-unique geological correlation which leads to the phenomenon known as non-uniqueness. This phenomenon also arises in many other types of geophysical data.

A ground gravity survey is carried out using a portable gravity meter, normally along a predetermined grid layout, although it is also common practice to take gravity readings along irregularly spaced points because of physical access restrictions. It is critical to establish a base station for every survey, and reoccupy this point on a regular basis to record instrument drift. Larger surveys make use of multiple base stations tied together. Each reading must be accompanied by a centimeter accurate elevation measurement and geographic location. Data reduction of all measurements is necessary and follows a standard mathematical process. Details of these reductions can be found in Dentith and Mudge [4.84] whilst Murray and Tracey [4.106] provide a comprehensive summary of best practice in gravity surveying.

Within the context of an unconformity model, the explorer must consider what geological aspect of the model can be targeted by the recording of gravity observations. As with all geophysical surveys, an understanding of the relationship between physical property contrast and geological process is fundamental. Of equal importance is the anticipated depth to target since the resolving power of a survey decreases as depth increases. For a gravity survey, increasing depth requires the target to increase substantially in size and density contrast for it to remain detectable. Whilst this can occur to some extent, there are limits to what will form naturally, and consequently, the explorer should be aware of the limitations of being able to detect density changes as depth increases.

Pervasive hydrothermal alteration haloes are associated with uranium mineralization at the Kiggavik uranium deposit where significant geophysical anomalies result due to a lowering of electrical resistivity, density and magnetic susceptibility [4.107]. The hydrothermal clay-rich alteration haloes are characterized by a significantly reduced host rock density, providing an excellent physical property contrast that becomes a prime targeting vector.

Fig. 4.23 presents the results of an airborne gravity survey over the Kiggavik region highlighting numerous gravity lows, each potentially representing a shallow alteration halo. This information was used to direct early investigations towards potential mineralized systems. However, initial drill testing of airborne anomalies (Gzz lows) did not always identify a cause for the anomaly; hence ground gravity surveying was used to follow-up airborne anomalies prior to drill testing. Ground gravity surveying at the Contact prospect (Fig. 4.24) highlights the differences between airborne and ground anomalies with ground data subsequently used to produce a constrained 3-D inversion incorporating drilling information [4.107].

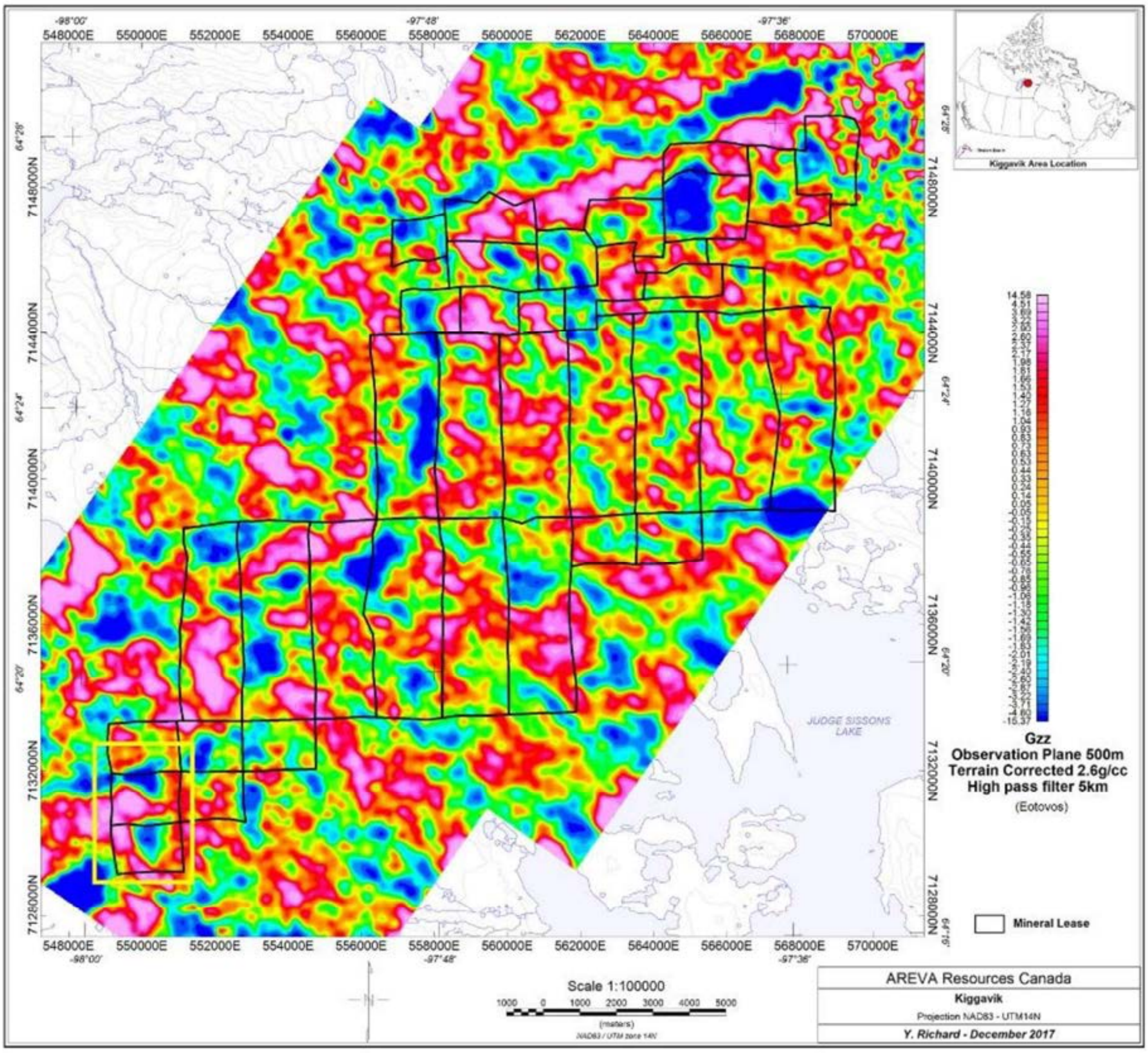

FIG. 4.23. Airborne gravity (Gzz) from the Kiggavik region, Canada, has been used as a vectoring mechanism when searching for shallow alteration haloes indicative of hydrothermal alteration. The haloes formed by the alteration are known to have a significantly reduced density [4.107] (Gravity image reproduced courtesy of Areva).

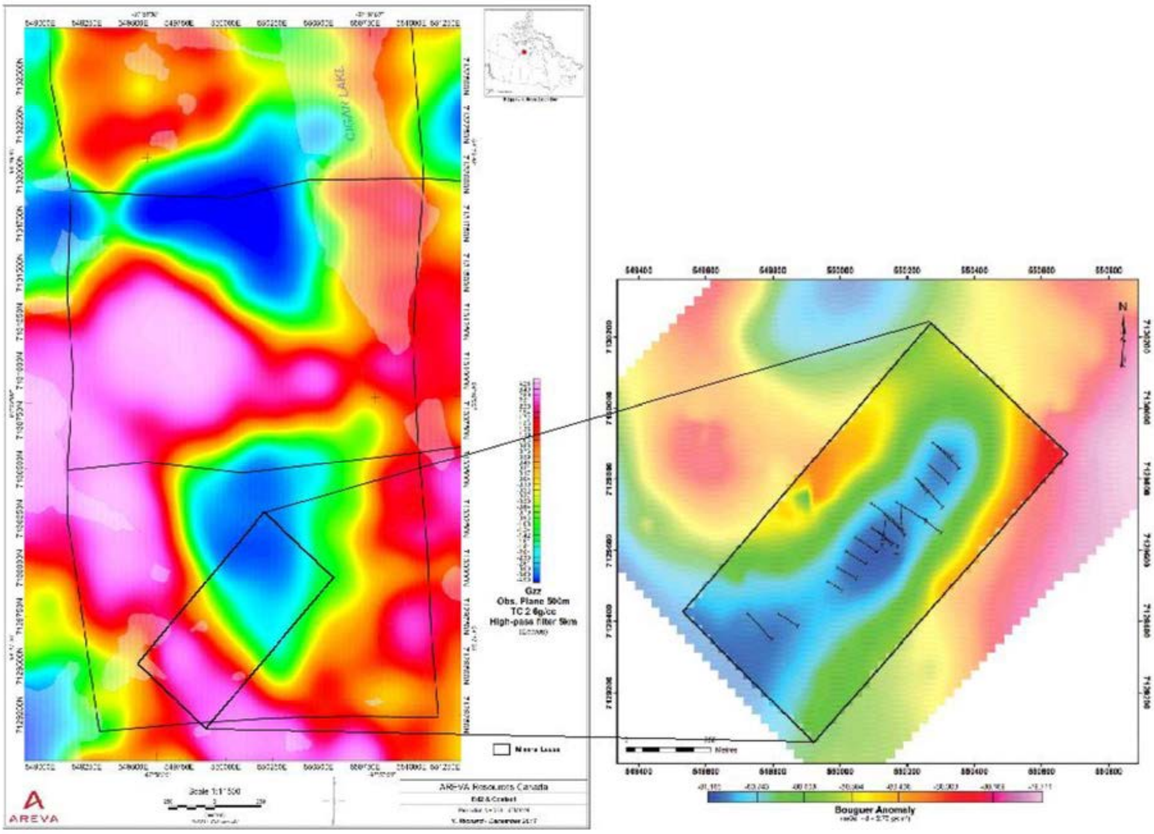

FIG. 4.24. A ground gravity survey (right) at the Contact prospect was used to refine the airborne gravity anomaly (left). A noticeable difference between airborne and ground signatures is apparent. Area presented is outlined by the yellow rectangle in FIG. 4.23 (Images reproduced courtesy of Areva).

4.2.7.7.6. Magnetotelluric electromagnetic surveys

The exploration environment has changed substantially over the past decade, with greater emphasis now placed on understanding the regional setting, and on exploring at ever increasing depths. This has resulted in explorers desiring to revisit deep penetrating geophysical survey methods, ones not typically used for the very fact that they are deep penetrating with limited application in the shallow exploration environment. In countries like Australia and Canada, the search for unconformity uranium mineralization has shifted into geological terrain with increasing depth of cover. Exploration within these terrains has seen operators incorporate magnetotelluric surveys (MT) into programmes that require an effective tool to map resistivity and conductivity at depths that are beyond most active source methods.

The advantage an MT survey has is a large depth of penetration and the ability to map resistors and conductors. Also, an MT survey only requires receivers, making it a very low-cost option.

In Australia, the application of MT has been successfully demonstrated in mapping the unconformable contact between the prospective Pandurra Formation and Gawler Range volcanics, where the presence of a conductive overburden was an impediment to the effectiveness of standard AEM surveys [4.108]. This work also identified deep structures as potential fluid pathways. Audio magnetotelluric surveys (AMT) have been instrumental in identifying deep conductors and sandstone alteration [4.109, 4.110].

Due to the shift of exploration efforts into areas with deeper cover, recent exploration programmes in Canada are making increasing use of ground MT surveys as one method that can effectively and efficiently prospect to great depths. The application of MT has been demonstrated in the Otish Basin, Canada where a transient audio magnetotelluric (TAMT) survey was conducted to delineate shallow and deep conductors, and determine if a link exists with magnetically susceptible sulphides. Fig. 4.25 shows real and imaginary components of Ty confirming a response from two shallow conductors (C1 and C2) identified from VLF work in the 1960s. Deeper conductors C3 and C4 were newly identified from this more recent work. The 2-D inversion of TAMT data shows the responses from all four conductors.

Natural source magnetotelluric measurements are generally acquired on the earth's surface; however recent developments have seen the successful integration of AMT measurements into an airborne platform in the form of the ZTEM system [4.111]. The ZTEM is considered a cost-effective first pass airborne survey capable of providing a deeper penetrating, large scale assessment of conductivity and resistivity, which can then be used to focus more detailed airborne or ground geophysical work. The ZTEM should be viewed as complementary to, rather than competing with other EM methods.

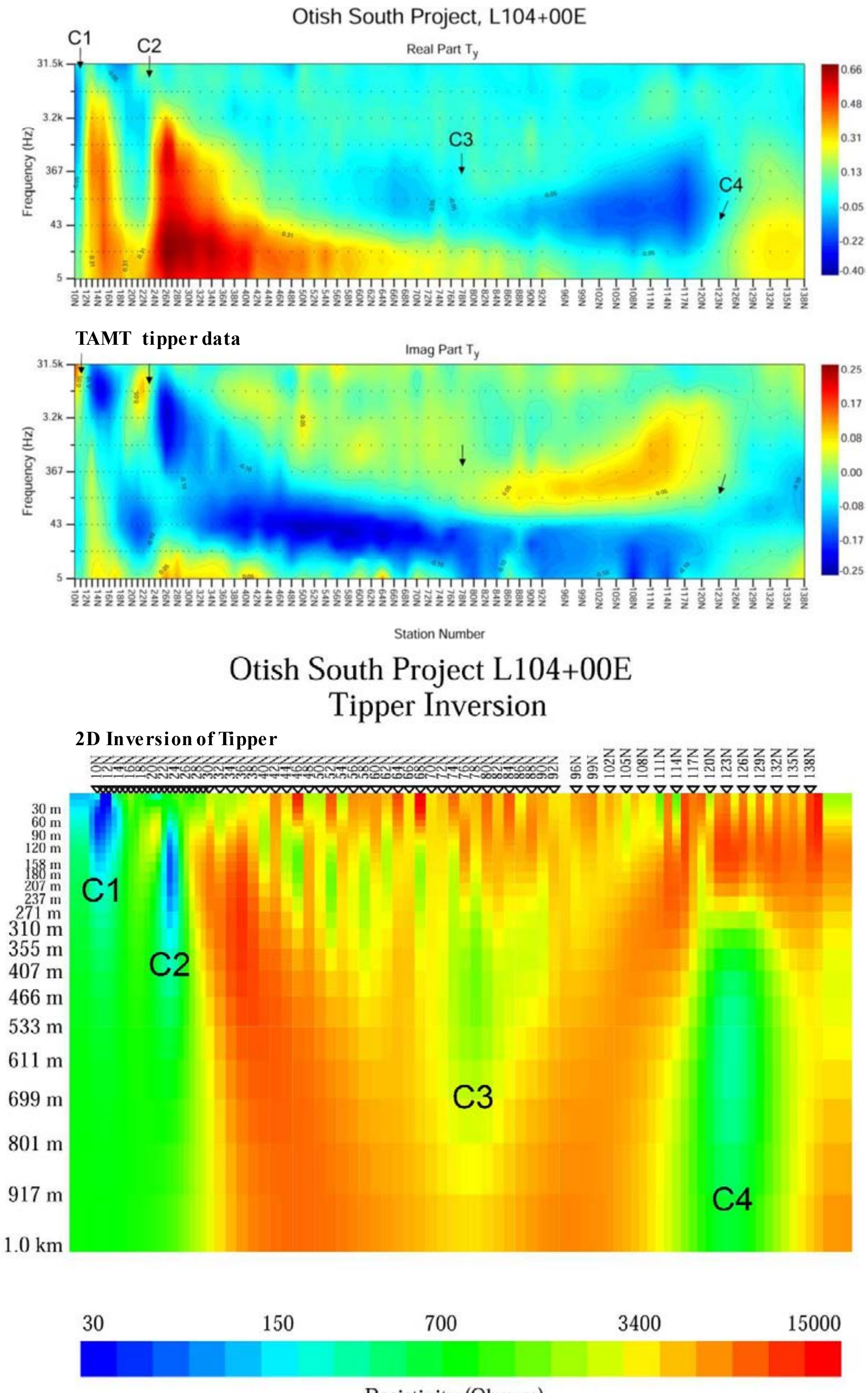

FIG. 4.25. Transient AMT tipper data (Real Ty, Imaginary Ty) from the Otish Basin, Quebec, Canada and the resultant 2-D inversion of tipper data (bottom). Conductors represented in the data are labelled C1-C4, from shallowest to deepest. An increasing depth to basement is represented in tipper data from left to right. C3 and C4 were newly discovered conductors from the AMT survey (Images reproduced courtesy of EMpulse Geophysics Limited).

Fig. 4.26 shows ZTEM resistivity data from the Arrow uranium deposit, Saskatchewan, Canada. A resistivity low corridor joins several deposits and mineralized zones (RRR, Arrow, Cannon, Bow, Harpoon, Spitfire) and in conjunction with prior geological knowledge, can be interpreted as an intercalated package of orthogneiss and paragneiss to granulites that contain anastomosing high strain and shear zones. Within these zones, the graphite/sulphide content and competency contrasts are likely responsible for the resistivity low. Mineralization is often found along this resistivity trend in or proximal to localities where the resistivity low widens or shows a cross-cutting feature.

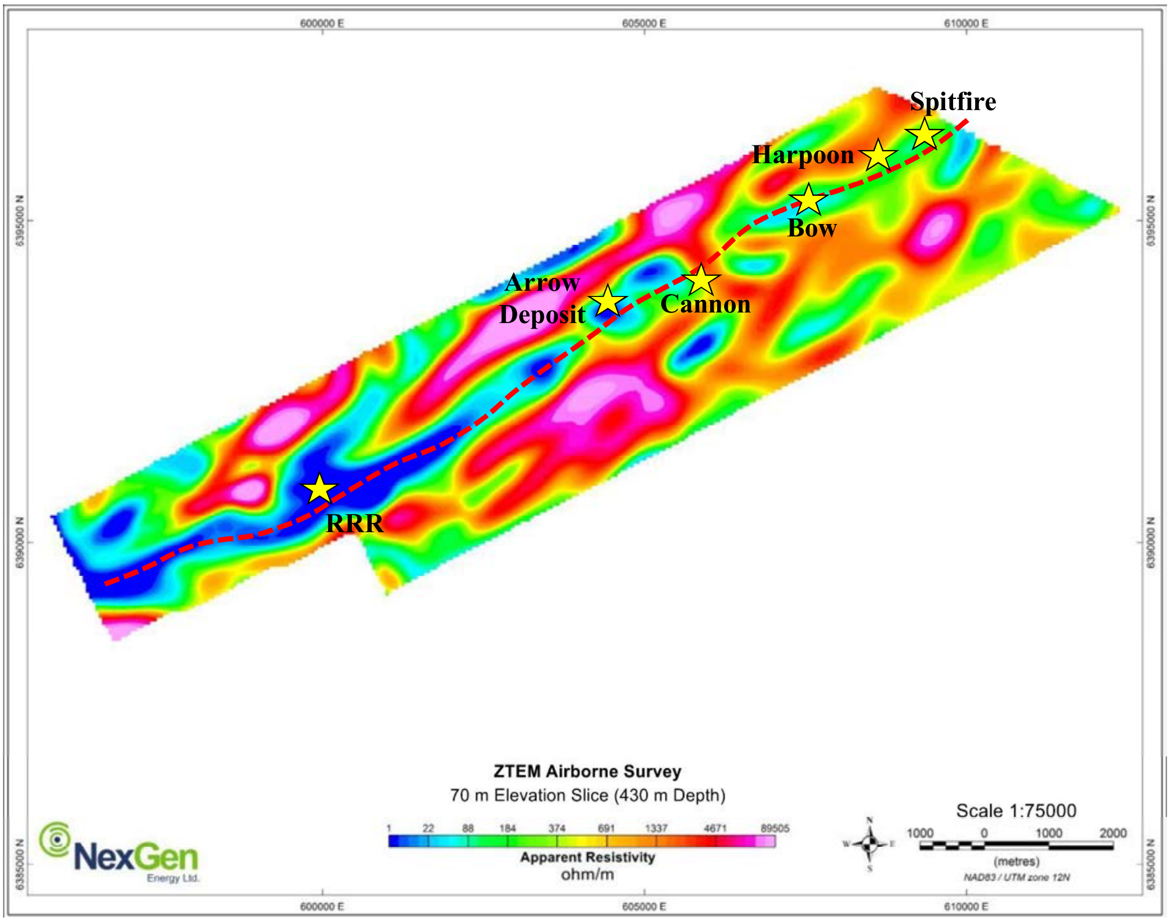

FIG. 4.26. Data from a ZTEM survey highlighting a long corridor of anomalously low resistivity (red dash line) linking several significant uranium deposits and prospects. (Reproduced courtesy of NexGen Energy Limited).

The application of active source MT surveys for unconformity uranium exploration is far less common than is the use of natural source MT surveys, although recent work has demonstrated the relevance of controlled source audiomagnetotellurics (CSAMT) in mapping an unconformity contact between the Kurnool Group and Nallamalai Group of the Cuddapah Basin, India [4.112]. The strong resistivity contrast between sediments and basement was suitably mapped using CSAMT.

The CSAMT was trialled in Arnhem Land, Northern Australia as a means for mapping a thin palaeo-weathering horizon coincident with the sandstone-basement unconformity. Although successful in measuring the decreased resistivity associated with this layer, the vertical resolution was considered insufficient to validate the continued use in this application. The two conductivity pseudosections in Fig. 4.27 present a comparison between moving loop EM (NanoTEM) and CSAMT data along the same transect with alteration around the unconformity manifest as a well-defined undulating horizontal layer of decreased resistivity. Although CSAMT lacked the vertical resolution compared to the NanoTEM, it was successful at detecting a very shallow and thin conductive horizon. The CSAMT could have application in very deep environments, where structural features are of interest or where there is a necessity to detect resistive targets. The relatively fast acquisition of CSAMT compared to MT may be favourable to some explorers.

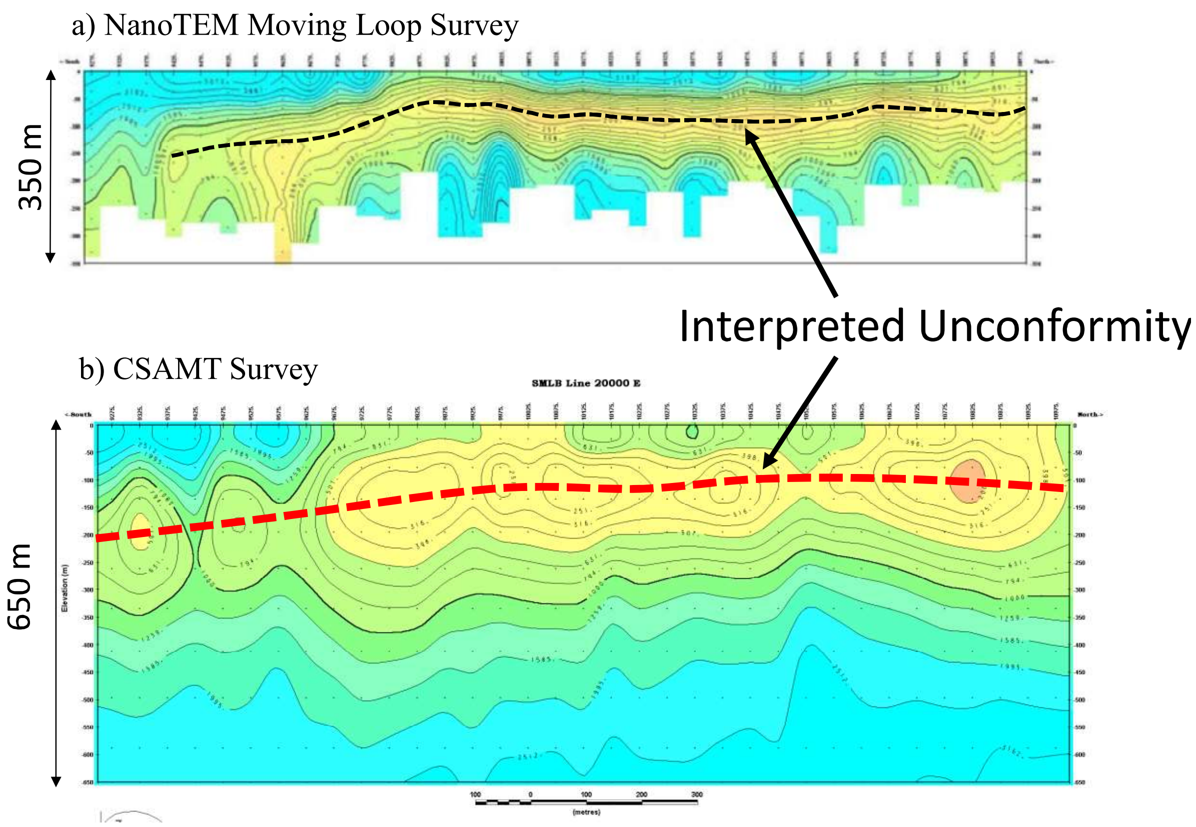

FIG. 4.27. 1D smooth model resistivity inversions of moving loop EM (a) and CSAMT (b) along the same transect. The position of the unconformity is inferred by association with a layer of decreased resistivity resulting from pervasive palaeo-weathering. The CSAMT successfully mapped resistivity changes but lacked vertical resolution. Contour values are in ohm metres.

4.2.7.7.7. Seismic

The acquisition of seismic data in a standard mineral exploration programme is not common [4.84], often finding application in near mine situations or specific focus problems. The cost of a seismic survey can be substantially greater than other types of mineral focused geophysical methods; hence the method is mostly used around existing mines or deposits where there is justification for the increased expenditure.

Within the context of unconformity uranium mineralization, seismic reflection studies have successfully imaged the unconformity and fault offsets at McArthur River [4.113, 4.114], expanded the understanding of crustal links to the Athabasca Basin deposits and demonstrated the applicability of 3-D surveys in detailed mapping of the unconformity and structural controls on mineralization [4.115–4.117]. Three-dimensional seismic reflection surveys have been instrumental in mine planning at the Millennium uranium deposit, Canada [4.118] and in identifying uranium bearing structures at the Ranger 3 Deeps deposit, Australia [4.119]. Examples of near mine seismic surveying in the unconformity environment are presented in Ref. 4.82.

Due to the costs and complexities of modern seismic reflection surveys, it is recommended to engage the service of an expert consultant in the planning, acquisition and interpretation of a survey.

4.2.7.7.8. Wireline logging

Wireline logging refers to the acquisition of data using slimline instruments specifically designed to be lowered down a drill hole. Depending on the physical property being measured, the instrument may be lowered down the inside of a steel drill stem, down a plastic (polyvinyl chloride) cased hole or down an open hole with no rods or casing. The user should be aware of the impact on measurements that can occur in relation to whether a hole is cased or not, as well as the type of casing used. For example, downhole magnetic measurements would never be taken inside a steel drill rod, nor would a galvanic resistivity survey be attempted within sections of a drill hole lined with solid plastic or steel casing. In both these examples, an uncased hole is preferable for measurements. In contrast to this, downhole gamma ray measurements are routinely acquired through steel drill rods as there is only minor attenuation of the signal and it can be more efficient and safer to have drill rods in place. The cost of a downhole probe can be considerable, so there is a relatively high risk for loss of equipment when running probes down uncased holes.

With respect to the unconformity uranium target, the principal logging tools used by explorers include natural gamma ray, inductive resistivity, acoustic televiewer/sonic and electromagnetic. Specialized borehole seismic surveys such as 3-D vertical seismic profiling and side-scan seismic profiling have been used in near mine geotechnical surveys at the Millennium mine [4.82].

The benefit of acquiring borehole logging data is that it provides bulk in situ physical property measurements that can be used for interpretation and modelling of potential field, seismic and electrical data [4.120].

A downhole log of gamma radiation (total count) provides the explorer with a continuous trace for the length of the hole. Depending on the type of stratigraphy drilled and the dips of units, these logs may be used to identify and correlate characteristic gamma responses between different drill holes, which in turn may establish geological equivalency between holes. A gamma log also provides an immediate visual/quantitative assessment of radiation variability down hole, making it easy to identify an anomalous peak.

Downhole resistivity logging can be used as follow-up to drill testing of a surface DC resistivity anomaly. As discussed previously, hydrothermal clay alteration associated with mineralization can produce a corresponding resistivity low, so the logging of a drill hole designed to test a resistivity anomaly can provide confirmation of the geophysical target intersection.

The role of acoustic tele viewer logging has increased over recent years due to the ability to extract information about rock structure and fabric. The information from this probe provides a quantitative analysis of structural elements, and when combined with other logging information, can be presented into a concise summary plot as shown in Fig. 4.28.

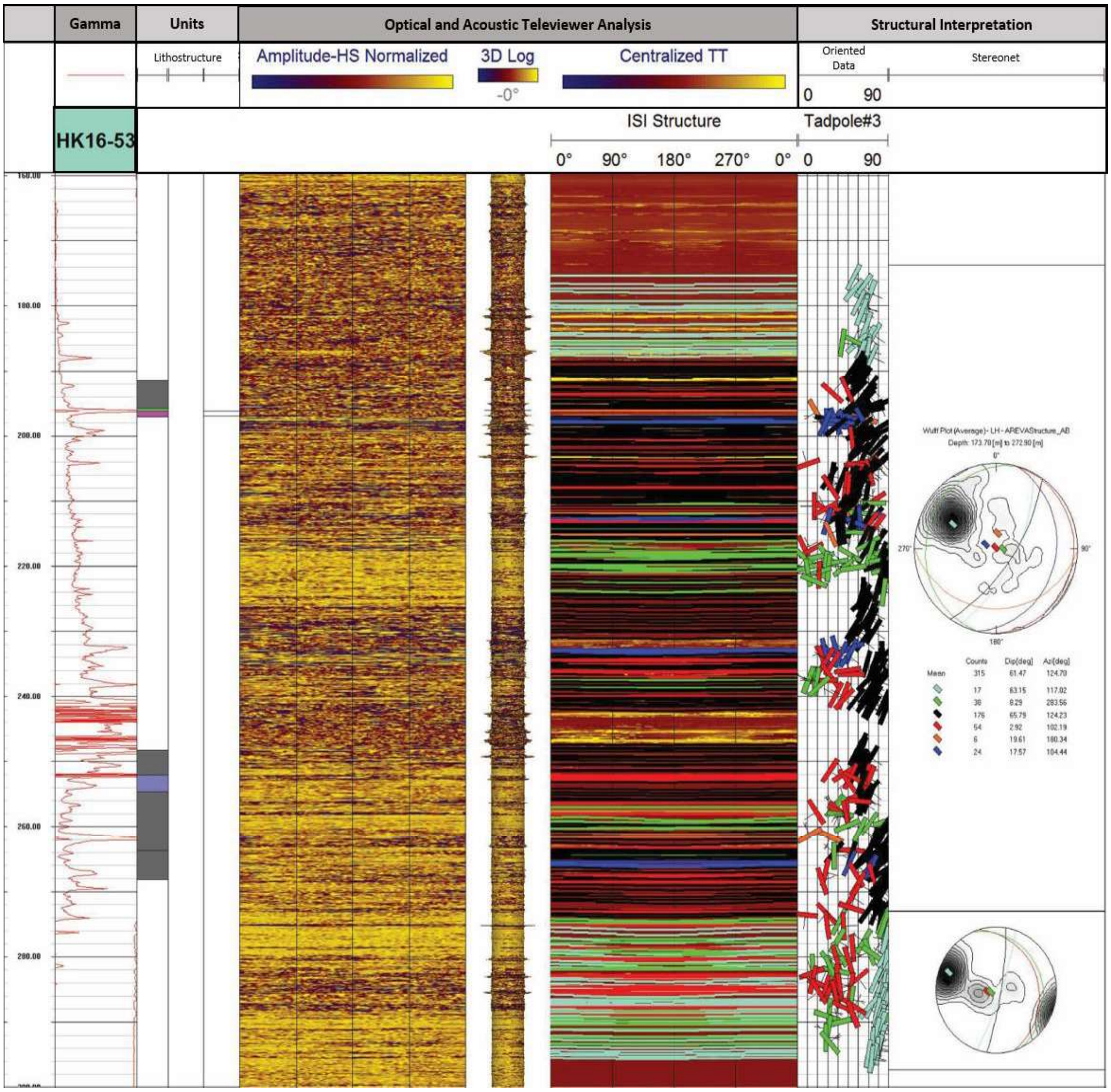

FIG. 4.28. An example of combining a gamma log with a borehole acoustic tele viewer log and the subsequently derived structural components. Orientation data are used to construct 3-D stereo nets as shown.

Drill testing of a buried conductor can be quantified with a downhole electromagnetic (DHEM) survey. A distinction should be made between two types of downhole electromagnetic surveying. The first uses a large surface loop with measurements made from a probe as it is lowered into the drill hole. This is the most commonly used method to accurately delineate conductors surrounding the drill hole. The second method known as induction logging, has a combined transmitter and receiver in the logging probe and measures the wall rock conductivity in the immediate vicinity of the probe [4.84]. Due to the limited depth of investigation, this method would never be recommended for the quantitative determination of how effectively a conductor has been tested through drilling. Drill testing of a conductor may be assessed with a suitably designed DHEM survey since this will provide information on the location and orientation of the conductor, whether a larger portion of the conductor is located off the drilling axis and how extensive the conductor may be away from the drill hole [4.84].

4.2.7.8. Other methods

As has already been discussed, the application of geophysical methods in the search for unconformity uranium deposits is nearly always concerned with indirect targeting. If successful, a method will provide the explorer with an improved targeting vector, thereby reducing risk and improving prospectivity. As technology improves, it is incumbent upon the explorer to be aware of advancements in established methods as well as newly developed methods that can be applied as a direct or indirect targeting tool.

Due to its very low power, ground penetrating radar (GPR) surveys are normally reserved for very shallow civil engineering investigations. However, advances in radar technology have seen an increasing acceptance and use of such systems in the mineral exploration environment [4.121]. The use of GPR in the search for unconformity uranium mineralization, often buried under hundreds of metres of sedimentary cover, may seem an obvious incompatibility, yet GPR has recently been tested to solve a specific exploration problem for some explorers. In this situation, the GPR method was applied in an attempt to map cover thickness and spatially locate large boulders within a glacial till environment, both of which can present difficulties when drilling. Surveying with GPR potentially allows the operator to position a drill hole and avoid the unnecessary expense of drilling through problematic areas.

Passive seismic has been used within the mineral exploration industry as a rapid and cost-effective means for mapping cover thickness and depth to basement [4.122]. This method relies upon ambient (natural) surface waves travelling through the ground, creating a resonant frequency which can characterize the overburden layer, provided there is sufficient contrast in shear wave velocities between the overburden layer and underlying basement rocks. The technique has been used to map thickness of tillite cover in the Athabasca Basin and depth of cretaceous cover in Arnhem Land, Australia.

4.3. CONCLUSIONS

With advances in technology, new exploration methods will be developed for unconformity-related uranium deposits. However, there will always be a need to decide which method is best suited for a specific area based on: 1) the genetic model for the deposit; 2) the proxies for mineralization; 3) the stage of exploration and 4) the environment and available sample types (e.g. outcrop). Only by considering all these factors will an exploration programme be successful and efficient.

A successful exploration programme also requires a combination of geoscientific surveys that are tailored to the geography and geology of the area of interest. These surveys include geophysical, geochemical, and lithological mapping techniques. A combination of data from disparate surveys may identify coincident anomalies representing potential drill targets.

Field and laboratory based instrumentation are required to accurately identify the mineralogy associate with unconformity-related deposits, as well as provide quality control on interpretations. Unique mineralogy associated with large and diffuse alteration halos can be used to vector towards a deposit or identify drilling targets.

The utilization and visualization of large datasets in exploration using software packages and GIS based methodologies have been instrumental in reviewing and compiling new and historical results. Due to database sizes and the identification of minute anomalies, the use of prospectivity analysis is becoming a key tool used by exploration geologists. Signature analysis takes a different approach than the conventional targeting methods. The goal is to characterize areas that are known for hosting deposits and then apply those characteristics to prospective areas. Both conventional and signature analysis will continue to evolve.

Geophysical surveys provide important data sets that can be used to explore for unconformity-related uranium deposits. Data manipulation can produce potential targets for drilling that can be corroborated by geochemical methods and field mapping.

4.4. REFERENCES

[4.1] CLAYTON, R.N., FRIEDMAN, I., GRAF, M.D., MAYEDA, T.K., MEENTS, W.F., SHIMP, N.F., The origin of saline formation waters, I. Isotopic composition, Journal of Geophysical Research **71** (1966) 3869–3882.

[4.2] FISHER, J.B., BOLES, J.R., Water-rock interaction in Tertiary sandstones, San Joaquin basin, California, USA: Diagenetic controls on water composition, Chemical Geology **82** (1990) 83–101.

[4.3] GARVEN, G., The role of regional fluid flow in the genesis of the Pine Point deposit, Western Canadian Sedimentary Basin, Economic Geology **80** (1985) 307–324.

[4.4] BETHKE, C., Hydrologic constraints on the genesis of the upper Mississippi Valley mineral district from Illinois Basin brines, Economic Geology **81** (1986) 233–249.

[4.5] BETHKE, C.M., RERD, J.D., OLTZ, D.F., Long-range petroleum migration in the Illinois Basin, Bulletin of the American Association of Petroleum Geologists **75** (1991) 925–945.

[4.6] BREDEHOEFT, J.D., BELITZ, K., SHARP-HANSEN, S., The hydrodynamics of the Big Hom Basin: A study in the role of faults, Bulletin of the American Association of Petroleum Geologists **76** (1992) 530–546.

[4.7] BATH, A.H., MILODOWSKI, A.E., STRONG, G.E., "Fluid flow and diagenesis in the East Midlands Triassic sand–stone aquifer" (Goff J. and Williams B., (Eds)), Fluid Flow in Sedimentary Basins and Aquifers. Geological Society, London, Special Publications **34** (1987) 127–140.

[4.8] BETHKE, C., MARSHAK, S., Brine migrations across North America - The plate tectonics of Groundwater. Annual Review of Earth and Planetary Sciences **18** (1990) 287–350.

[4.9] KYSER, T.K., CUNEY, M., "Unconformity-related uranium deposits", , Recent and not-so-recent developments in uranium deposits and implications for exploration (Cuney M., Kyser K. (Eds), Mineralogical Association of Canada, Québec, Short Course Series **39** (2008) 161–219.

[4.10] HOEVE, J., SIBBALD, T., On the genesis of Rabbit Lake and other unconformity-type uranium deposits in northern Saskatchewan, Canada, Economic Geology **73** (1978) 1450– 1473.

[4.11] HOEVE, J., QUIRT, D., Mineralization and host rock alteration in relation to clay mineral diagenesis and evolution of the middle-Proterozoic Athabasca Basin, northern Saskatchewan, Canada, Saskatchewan Research Council Technical Report **187** (1984) 187.

[4.12] KOTZER, T., KYSER, T.K., Fluid history of the Athabasca Basin and its relation to diagenesis, uranium mineralization and paleohydrology, Chemical Geology, **120** (1995) 45–89.

[4.13] CUNEY, M., KYSER, T.K., Recent and Not-So-Recent Developments in Uranium Deposits and Implications for Exploration GAC–MAC 2008, Quebec, Short Course 39 (2008).

[4.14] SHEAHAN, C., FAYEK, M., QUIRT, D., JEFFERSON, C.W., A Combined Ingress-Egress Model for the Kianna Unconformity-Related Uranium Deposit, Shea Creek Project, Athabasca Basin, Canada, Economic Geology **111** (2016) 225–257.

[4.15] WILSON, M.R., KYSER, T.K., Stable isotope geo-chemistry of alteration associated with the Key Lake uranium deposit, Economic Geology **82** (1987) 1450–1557.

[4.16] KOTZER, T.G., KYSER, T.K., “The use of stable and radiogenic isotopes in the identification of fluids and processes associated with unconformity-type uranium deposits”, Modern Exploration Techniques, Saskatchewan Geological Society Special Publication **10** (1990a) 115–131.

[4.17] FAYEK, M., KYSER, T.K., Characterization of multiple fluid-flow events and rare-earth-element mobility associated with formation of unconformity-type uranium deposits in the Athabasca Basin, Saskatchewan, Canadian Mineralogist **35** (1997) 627–658.

[4.18] MERCADIER, J., CUNEY, M., CATHELINEAU, M., LACORDE, M., U redox fronts and kaolinisation in basement-hosted unconformity-related U ores of the Athabasca Basin (Canada), Late U remobilization by meteoric fluids: Mineralium Deposita **46** (2011) 105–135.

[4.19] CUNEY, M., KYSER, T.K., Geology and Geochemistry of Uranium and Thorium Deposits GAC–MAC 2015, Quebec, Short Course 46 (2015).

[4.20] DEROME, D., CATHELINEAU, M., LHOMME, T., CUNEY M., Fluid inclusion evidence of the differential migration of H_2 and O_2 in the McArthur River unconformity-type uranium deposit (Saskatchewan, Canada). Possible role on post-ore modifications of the host rocks, Journal of Geochemical Exploration **78–79** (2003a) 525–530.

[4.21] DEROME, D., CUNEY, M. CATHELINEAU, M., DUBESSY, J., BRUNETON, P., A detailed fluid inclusion study in silicified breccias from the Kombolgie sandstones (Northern Territory, Australia): application to the genesis of Middle-Proterozoic unconformity-type uranium deposits, Journal of Geochemical Exploration **80** (2003b) 259–275.

[4.22] MERCADIER, J., RICHARD, A., BOIRON, M.C., CATHELINEAU, M., CUNEY, M., Brine migration in the basement rocks of the Athabasca Basin through microfracture networks (P-Patch U deposit, Canada), Lithos **115** (2010) 121–136.

[4.23] RICHARD, A., PETTKE, T., CATHELINEAU, M., BOIRON, M.C., MERCADIER, J., CUNEY, M., DEROME, D., Brine-rock interaction in the Athabasca basement (McArthur River U deposit, Canada): consequences for fluid chemistry and uranium uptake, Terra Nova, **22** (2010) 303–308.

[4.24] RICHARD, A., BANKS, D.A., MERCADIER, J., BOIRON, M.C., CUNEY, M., CATHELINEAU, M., An evaporated seawater origin for the ore-forming brines in unconformity-related uranium deposits (Athabasca Basin, Canada): Cl/Br and δ37Cl analysis of fluid inclusions, Geochimca et Cosmochimica Acta **75** (2011) 2792–2810.

[4.25] RICHARD, A., ROZSYPAL, C., MERCADIER, J., BANKS, D.A., CUNEY, M., BOIRON, M.C., CATHELINEAU, M., Giant uranium deposits formed from exceptionally uranium-rich acidic brines, Nature Geoscience **5** (2012) 142–146.

[4.26] RICHARD, A., BOULVAIS, P., MERCADIER, J., BOIRON, M.C., CATHELINEAU, M., CUNEY, M., FRANCE-LANORD, C., From evaporated seawater to uranium mineralizing brines: isotopic and trace element study of quartz dolomite veins in the Athabasca system, Geochimca et Cosmochimica Acta **113** (2013b) 38–59.

[4.27] RICHARD, A., KENDRICK, M.A., CATHELINEAU, M., Noble gases (Ar, Kr, Xe) and halogens (Cl, Br, I) in fluid inclusions from the Athabasca Basin (Canada): implications for unconformity-related U deposits, Precambrian Research **247** (2014) 110–125.

[4.28] TAYLOR, H.P., Oxygen and hydrogen isotope studies of plutonic granitic rocks, Earth and Planetary Science Letters **47** (1978) 255– 262.

[4.29] CRISS, R.E., LANPHERE, M.A., TAYLOR, H.P., Effects of regional uplift, deformation, and meteoric-hydrothermal metamorphism on K-Ar ages in the southern half of the Idaho Batholith, Journal of Geophysical Research **87** (1982) 7029–7046.

[4.30] CHIVAS, A.R., O'NEIL, J.R., KATCHAN, G., Uplift and submarine formation of Melanesian porphyry copper deposits: stable isotope evidence, Earth and Planetary Science Letters **68** (1984) 326–334.

[4.31] WHITNEY, G., NORTHROP, H., Diagenesis and fluid flow in the San Juan Basin, New Mexico- Regional zonations in mineralogy and stable isotopes of clay minerals in sandstone, American Journal of Science **287** (1987) 353–382.

[4.32] BIRD, M.I., CHIVAS, A.R., "Stable isotope evidence for low-temperature kaolinite weathering and post-formational hydrogen-isotope exchange in Permian kaolinites", Isotopes in Palaeo-environments, (Chivas, A.R., Guest Ed.), Chemical Geology: Isotope Geoscience section **72** (1988) 249–265.

[4.33] LEE, M., ARONSON, J.L., SAVIN, S.M., Timing and conditions of Permian Rotliegende sandstone diagenesis, southern North Sea: K/Ar and oxygen isotopic data, Bulletin of the American Association of Petroleum Geologists **73** (1989) 195–215.

[4.34] LONGSTAFFE, F., AVALON, A., Hydrogen-isotope geochemistry of diagenetic clay minerals from Cretaceous sandstones, Alberta: Evidence for exchange, Applied Geochemistry **5** (1990) 657–668.

[4.35] GIRARD, J., DEYNOUX, M., Oxygen isotope study of diagenetic quartz overgrowths from the upper-Proterozoic quartzites of western Mali, Taoudeni Basin: Implications for conditions of quartz cementation, Journal of Sedimentary Research **61** (1991) 406–418.

[4.36] ALEXANDRE, P., KYSER, K., THOMAS, D., POLITO, P., MARLATT, J., Geochronology of unconformity-related uranium deposits in the Athabasca Basin, Saskatchewan, Canada and their integration in the evolution of the basin, Mineralium Deposita **44** 1 (2009) 41–59.

[4.37] CLOUTIER, J., KYSER, K., OLIVO, G.R., ALEXANDRE, P., Contrasting patterns of alteration at the Wheeler River area, Athabasca Basin, Saskatchewan, Canada: Insights into the apparently uranium-barren Zone K alteration system: Economic Geology **105** (2010) 303–324.
[4.38] SHARPE, R., FAYEK, M., QUIRT, D., JEFFERSON, C.W., Geochronology and Genesis of the Bong Uranium Deposit, Thelon Baisn, Nunavut, Canada, Economic Geology **110** (2015) 1759–177.
[4.39] RAMAEKERS, P., "Hudsonian and Helikian basins of the Athabasca Region, northern Saskatchewan", Proterozoic Basins of Canada (Campbell, F.H.A., Ed.) Geological Survey of Canada, Paper, **81–10** (1981) 219–233.
[4.40] KOTZER, T.G., KYSER, T.K., IRVING, E., Paleomagnetism and the evolution of fluids in the Proterozoic Athabasca Basin, northern Saskatchewan, Canada, Canadian Journal of Earth Sciences **29** (1992) 1474–1491.
[4.41] LIEWIG, N., CLAUER, N., SOMMER, F., Rb-Sr and K-Ar dating of clay minerals in Jurassic sandstone oil reservoir, North Sea, Bulletin of the American Association of Petroleum Geologists **71** (1987) 1467– 1474.
[4.42] MCNUTT, R.H., "$^{87}Sr/^{86}Sr$ ratios as indicators of water rock interactions: applications to brines found in Precambrian ages rocks from Canada", (Fritz, P., Frape, S.K., Eds), Saline Water and Gases in Crystalline Rocks. Geological Association of Canada Special Paper **33** (1987) 81–88.
[4.43] KESSLER, S.E., LONES, L.M., RUIZ, J., Strontium isotope geochemistry of MVT deposits, East Tennessee: Implications for age and source of mineralizing brines, Bulletin of the Geological Society of America **100** (1988) 1300–1307.
[4.44] MORGAN, D.S., HASZELDINE, R.S., FLLICK, A.E., Linear coupling of carbon and strontium isotopes in Rotliegend Sandstone, North Sea: Evidence for cross-formational fluid flow, Geology **18** (1990) 1215–1218.
[4.45] SMALLEY, P., LONOY, A., RILHEIM, A., Spatial $^{87}Sr/^{86}Sr$ variations in formation water and calcite from the Ekofisk chalk oil field: implications for reservoir connectivity and fluid composition, Applied Geochemistry **7** (1992) 341–350.
[4.46] SAINTILAN, N.J., CREASER, R.A., BOOKSTROM, A.A., Re-Os systematics and geochemistry of cobaltite (CoAsS) in the Idaho cobalt belt, Belt-Purcell Basin, USA: Evidence for middle Mesoproterozoic sediment-hosted Co-Cu sulfide mineralization with Grenvillian and Cretaceous remobilization, Ore Geology Reviews **86** (2017) 509–525.
[4.47] SHABAGA, B.M., FAYEK, M., QUIRT, D., JEFFERSON, C.W., Mineralogy, Geochronology, and Genesis of the Andrew Lake Uranium Deposit, Thelon Basin, Nunavut, Canada, Canadian Journal of Earth Sciences, in press, (2017).
[4.48] RIEGLER, T., LESCUVER, J-L., WOLLENBERG, P., QUIRT, D., BEAUFORT, D., Alteration related to uranium deposits in the Kiggavik-Andrew Lake structural trend, Nunavut Canada: New insights from petrography and clay mineralogy, Canadian Mineralogist **52** (2014) 27–45.
[4.49] SHARPE, R.W., FAYEK, M., Mass bias corrections for U-Pb isotopic analysis by secondary ion mass spectrometry: Implications for U-Pb dating of uraninite, Rapid Communications in Mass Spectrometry **30** (2016) 1601–1611.
[4.50] HOLK, G.J., KYSER, T.K., CHIPLEY, D., HIATT, E.E., MARLATT, J., Mobile Pb-isotopes in Proterozoic sedimentary basins as guides for exploration of uranium deposits, Journal of Geochemical Exploration **80** (2003) 297–320.

[4.51] KISTER, P., CUNEY, M., GOLUBEV, V.N., ROYER, J-J., LE CARLIER DE VESLUD, C., RIPPERT, J.C., Radiogenic lead mobility in the Shea Creek unconformity-related uranium deposit (Saskatchewan, Canada): migration pathways and Pb loss quantification, Comptes Rendus Geoscience **336** (2004) 205–215.

[4.52] WORLD NUCLEAR ASSOCIATION, www.world-nuclear.org (2017)

[4.53] SASKATCHEWAN MINING ASSOCIATION, Uranium in Saskatchewan, Facts on the Industry for 2016, SMA (2017), retrieved from www.saskmining.ca

[4.54] ABS, 2017. Australian Bureau of Statistics, 8412.0–Mineral and Petroleum Exploration, Australia, ABS (September 2017), retrieved from www.abs.gov.au

[4.55] RAMAEKERS, P., Geology of the Athabasca Group (Helikian) in northern Saskatchewan, Saskatchewan Energy and Mines, Saskatchewan Geological Survey Report 195 (1990) 49p.

[4.56] NEEDHAM, R.S., Geology of the Alligator Rivers Uranium Field, Northern Territory, Bureau of Mineral Resources, Australia, Bulletin 224. (1988b).

[4.57] ATLAS COPCO, www.atlascopcowelltech.se/english/exploration/exploration

[4.58] WANG, J., CAO, P., LIU, C., TALALAY, P., Comparison and analysis of subglacial bedrock core drilling technology in polar regions, Polar Science **9**, i.2, (2015) 208–220.

[4.59] POWELL, B., "Case histories of the radon tube sampler in the Carswell Structure", The Carswell Structure Uranium Deposits, Saskatchewan, (9th edn) R. Laine, D. Alonso and M. Svab; Geological Association of Canada, Special Paper 26, (1985) 189–201.

[4.60] RADONEX, "Advances in Radon Surveys: The Evolution of RadonEx Survey Techniques", Presentation at Saskatchewan Geological Open House, November 2016.

[4.61] RPA, Technical Report on the Patterson Lake South Property, Northern Saskatchewan, Canada, NI 43–101 Report, (February 12, 2015).

[4.62] DEVINE, M., HATTORI, K., CORNETT, J., KOTZER, T., "Detection of deeply buried uranium deposits using radon gas dissolved in groundwater: a case study in the Athabasca Basin", Joint Annual Meeting of the Geological Association of Canada and Mineralogical Association of Canada, Fredericton, NB (2014).

[4.63] LAFLEUR, P., Cost-Effective Helium Surveys in Uranium Exploration, (n.a.), retrieved from www.gasoilgeochem.com

[4.64] DUDEK, N., HATTORI, K., Radon and helium distribution and concentrations above buried uranium ore: the Phoenix deposits, Saskatchewan. Geological Survey of Canada Scientific Presentation 033 (2015) doi: 10.4095/296515.

[4.65] POWER, M., HATTORI, K., PINTI, D., POTTER, E.G., Anomalous abundances of He and mobile metals in surface media over the deeply buried Millennium U deposit, Athabasca Basin, Canada, 2013 Goldschmidt Conference. Mineralogical Magazine, Volume 77 (5) (2013)

[4.66] POWER, M.J., HATTORI, K., PINTI, D.L., SORBA, C., KOTZER, T., POTTER, E., "Surface media expressions of buried uranium deposits: The Phoenix and Millennium deposits, Athabasca Basin, Saskatchewan, Canada", 12th Biennial meeting of Society for Geology Applied to Mineral Deposits, Uppsala, Sweden (2013).

[4.67] SIBBALD, T.I.I., "Geology and genesis of the Athabasca Basin uranium deposits", Summary of Investigations 1985, Saskatchewan Geological Survey; Saskatchewan Energy and Mines, Miscellaneous Report 85–4. (1985), retrieved from www.publications.gov.sk.ca

[4.68] MCCONNELL, J.M., RICKETTS, M.J., Current Research Newfoundland and Labrador Department of Natural Resources Geological Survey, Report 08–1, (2008) 1–12.

[4.69] DAVENPORT, P.H., FRISKE, P.W.B., AND BEAUMIER, M., "The Application of Lake Sediment Geochemistry to Mineral Exploration: Recent Advances and Examples from Canada", "Proceedings of Exploration 97: Fourth Decennial International Conference on Mineral Exploration", Gubins, A.G., (Ed.) (1997) 261–270.

[4.70] GATZWEILLER, R., SCHMELING, B. AND TAN, B., "Exploration of the Key Lake uranium deposits, Saskatchewan, Canada" (IAEA-AG-250/5), Proceedings of an Advisory Group Meeting Vienna, 26–29 November 1979 jointly organized by IAEA and NEA (OECD), Uranium Exploration Case Histories (1981).

[4.71] BRUKER, How Handheld XRF Works: A Step-by-Step Guide, retrieved from www.bruker.com/products/x-ray-diffraction-and-elemental-analysis/handheld-xrf/how-xrf-works.html (2017).

[4.72] SRC, Saskatchewan Research Council Geoanalytical Laboratories, Service Schedule, retrieved from www.src.sk.ca (2017).

[4.73] ASD TerraSpec® User Manual, ASD Document 600541 Rev.G © 2008 by Analytical Spectral Devices, Inc. (2008a).

[4.74] EWINGTON, D., "Advanced SWIR Reflectance Interpretation". AREVA Resources Canada Inc. Internal Training Presentations–Advanced spectral analysis Ewington 2007-05-24.ppt (2017).

[4.75] DUTROW, B., CLARK, C., X-ray Powder Diffraction (XRD) (2017), retrieved from serc.carleton.edu/research_education/geochemsheets/techniques/XRD.html.

[4.76] NOBLE, R., STEWART, A., PINCHAND, T., ROBSON, T., ANAND, R., Integrated studies of soil, termites, vegetation and groundwater to understand metal migration at the Kintyre U deposits, Western Australia, Geochemistry: Exploration, Environment, Analysis. **17** 2 (2017) 143–158. doi.org/10.1144/geochem2016–439

[4.77] GONZÁLEZ-ÁLVAREZ, I., STEWART, A., ANAND, R., SINCLAIR, P., SALAMA, P., LAIRD, J.S., IBRAHIMI, T., PINCHAND, T., "Termitaria Geochemistry for Uranium Exploration in Arnhem Land, Northern Territory, Australia", Conference: Society of Economic Geologists at Tasmania, Australia. Projects–CSIRO Nuclear Microprobe User Papers September (2015).

[4.78] DUNN, C.E., Uranium biogeochemistry of the NEA/IAEA Athabasca Test Area, in: E.M. Cameron, (Ed.), "Uranium Exploration in Athabasca Basin, Saskatchewan, Canada, Geological Survey of Canada", Paper **82** 11 (1983a) 127– 132.

[4.79] DUNN, C.E., Biogeochemistry in Mineral Exploration, Vol. 9, 1st Edn. Elsevier Science, New York (2007).

[4.80] STEWART, P., KYSER, T. K., GRIFFITHS D., LAHUSEN L., Dendrochemistry and soil clay geochemistry applied to exploration for deep U mineralization at the Halliday Lake Prospect, Athabasca Basin, Canada, Geochemistry: Exploration, Environment, Analysis **17** i.2, (2016) 164–181.

[4.81] BEYER, S.R., KYSER, K., KOTZER, T.G., ANSDELL, K., WASYLIUK, K., AND QUIRT, D.H., "Expression of the McArthur River Uranium deposit footprint in diverse surficial sampling media (POSTER)", GAC-MAC 2017, Abstracts Volume **40** (2017) 26

[4.82] INTERNATIONAL ATOMIC ENERGY AGENCY, Advances in Airborne and Ground Geophysical Methods for Uranium Exploration, Nuclear Energy Series No. NF-T-1.5, Vienna (2013).

[4.83] DICKSON, B.L., SCOTT, K.M., Interpretation of aerial gamma-ray surveys - adding the geochemical factors, AGSO Journal of Australian Geology and Geophysics, **17** 2 (1997) 187–200.
[4.84] DENTITH, M., MUDGE, S.T., Geophysics for The Mineral Exploration Geoscientist, Cambridge University Press, New York (2014).
[4.85] TELFORD, W.M., GELDART, L.P., SHERIFF, R.E. Applied geophysics (Vol. 1), Cambridge University Press, New York (1990).
[4.86] ISLES, D.J. RANKIN, L.R., Geological Interpretation of Aeromagnetic Data, (1st edn), CSIRO Publishing, Collingwood, Australia (2013).
[4.87] FITZPATRICK, A., LARGE, P., "Magnetic modelling and geological modelling come together at the Kintyre uranium deposit", ASEG Extended Abstracts (2015) 1–4. doi.org/10.1071/ASEG2015ab049
[4.88] GUNN, P.J., An algorithm for reduction to the pole that works at all magnetic latitudes, Exploration Geophysics **26** (1995) 247–254. doi.org/10.1071/EG995247
[4.89] RAJAGOPALAN, S., "Analytic Signal vs. Reduction to Pole: Solutions for Low Magnetic Latitudes", ASEG Extended Abstracts (2003) 1–4. doi.org/10.1071/ASEG2003ab136
[4.90] INTERNATIONAL ATOMIC ENERGY AGENCY, Guidelines to Radioelement Mapping Using Gamma Ray Spectrometric Data, IAEA-TECDOC-1363, IAEA, Vienna (2003).
[4.91] INTERNATIONAL ATOMIC ENERGY AGENCY, The Use of Gamma Ray Data to Define the Natural Radiation Environment, IAEA-TECDOC-566, IAEA, Vienna (1990).
[4.92] INTERNATIONAL ATOMIC ENERGY AGENCY, Airborne Gamma Ray Spectrometer Surveying, Technical Reports Series No. 323, IAEA, Vienna (1991).
[4.93] INTERNATIONAL ATOMIC ENERGY AGENCY, Radioelement Mapping, IAEA Nuclear Energy Series No. NF-T-1.3, Vienna (2010).
[4.94] LANE, R., "Ground and airborne electromagnetic methods", Geophysical and Remote Sensing Methods for Regolith Exploration, CECLEME open file report **144** (2002) 53–77.
[4.95] SMITH, R.S., WOOD, G.R., POWELL, B., Detection of alteration at the Millennium uranium deposit in the Athabasca Basin: a comparison of data from two airborne electromagnetic systems with ground resistivity data, Geophysical Prospecting, **58** 6 (2010) 1147–1158. doi:10.1111/j.1365-2478.2010. 00880.x
[4.96] MATTHEWS R., KOCH R., LEPPIN M., "Advances in integrated exploration for unconformity uranium deposits in western Canada", Proceedings of Exploration 97: Fourth Decennial International Conference on Mineral Exploration (Gubins, A.G., (Ed)), (1997) 993–1002.
[4.97] ALEXANDRE, P., KYSER, K., JIRICKA, D., WITT, G., (2012), Formation and evolution of the centennial unconformity-related uranium deposit in the south-central Athabasca Basin, Canada, Economic Geology **107** 3 (2012) 385–400. doi:10.2113/econgeo.107.3.385
[4.98] BECKITT G. (2003) Exploration for unconformity uranium in Arnhem Land (NT), Exploration Geophysics **34** (2003) 137–142. doi.org/10.1071/EG03137
[4.99] BISSET, A., "Detecting unconformity related alteration with TEMPEST- an example from Arnhem Land", NT, Australia, International Conference on Uranium Geochemistry (2003).

[4.100] AUKEN, E., BOESEN, T., CHRISTIANSEN, A.V., "A Review of Airborne Electromagnetic Methods with Focus on Geotechnical and Hydrological Applications From 2007 to 2017", Advances in Geophysics **58** (2017) doi.org/10.1016/bs.agph.2017.10.002

[4.101] LONG S., SMITH R., HEARST R., Ground resistivity method and DCIP2D forward and inversion modelling to identify alteration at the Midwest uranium deposit, northern Saskatchewan, Canada, Exploration Geophysics **48**, (2016) 383–393. doi.org/10.1071/EG15059

[4.102] LEGAULT, J.M., CARRIERE, D., PETRIE, L., Synthetic model testing and distributed acquisition dc resistivity results over an unconformity uranium target from the Athabasca Basin, northern Saskatchewan, The Leading Edge **27** 1 (2008) 46–51.

[4.103] BRODIE, R.C., "Airborne and Ground Magnetics", Geophysical and Remote Sensing for Regolith Exploration, CRCLEME open file report 144 (2002) 33–45.

[4.104] MATOLIN, M., MINTY, B., "Levelling airborne and ground gamma-ray spectrometric data to assist uranium exploration" (2009), in IAEA-TECDOC-1730, IAEA, Vienna (2014).

[4.105] WILFORD, J.R., BIERWIRTH, P.E., & CRAIG, M.A., Application of airborne gamma-ray spectrometry in soil/regolith mapping and applied geomorphology. AGSO Journal of Australian Geology and Geophysics, **17** 2 (1997) 201–216.

[4.106] MURRAY, A.S., TRACEY, R.M., Best Practice in Gravity Surveying (2001), retrieved from www.data.gov.au/dataset/best-practice-in-gravity-surveying

[4.107] ROY, R., BENEDICTO, A., GRARE, A., BEHAEGEL, M., RICHARD, Y., HARRISON, G., Three-dimensional gravity modelling applied to the exploration of uranium unconformity-related basement-hosted deposits: The contact prospect case study, Kiggavik, northeast Thelon region (Nunavut, Canada), Canadian Journal of Earth Sciences **54** 8 (2017) 869–882. doi:10.1139/cjes-2016-0225

[4.108] CROWE M., HEINSON G., DHU T., "Magnetotellurics and Airborne Electromagnetics– a combined method for assessing basin structure and exploring for unconformity related uranium", ASEG Extended Abstracts (2013) 1–5. doi.org/10.1071/ASEG2013ab225

[4.109] LEPPIN, M., GOLDAK, D., "Mapping deep sandstone alteration and basement conductors utilizing audio magnetotellurics: exploration for uranium in the Virgin River area, Athabasca Basin, Saskatchewan, Canada", Society of Exploration Geophysicists, SEG Technical Program Expanded Abstracts (2005) 591-594.

[4.110] TUNCER, V., UNSWORTH, M.J., SIRIPUNVARAPORN, W., CRAVEN, J.A. Exploration for unconformity-type uranium deposits with audiomagnetotelluric data: A case study from the McArthur River mine, Saskatchewan, Canada, Geophysics **71** 6 (2006) B201–B209.

[4.111] LO B., LEGAULT J., KUZMIN P., COMBRINCK M., "Z-TEM (airborne AFMAG) tests over unconformity uranium deposits", ASEG Extended Abstracts (2009) 1–6.

[4.112] KUMAR, I., KUMAR, S.V., BABU, V.R., KUMAR, B.V.L., DASH, J.K., CHATURVEDI, A.K., Controlled Source Audio Magneto Telluric (CSAMT) studies for uranium exploration in Durgi area, Palnad sub-basin, Cuddapah basin, India", Journal of the Geological Society of India **89** 1 (2017) 12–20.

[4.113] WHITE, D.J., HAJNAL, Z., ROBERTS, B., GYÖRFI, I., REILKOFF, B., BELLEFLEUR, G., MUELLER, C., WOELZ, S., MWENIFUMBO, C.J., TAKÁCS, E., SCHMITT, D.R., BRISBIN, D., JEFFERSON, C.W., KOCH, R., POWELL, B., ANNESLEY, I.R., Seismic methods for uranium exploration: an overview of EXTECH IV seismic studies at the McArthur River mining camp, Athabasca Basin, Saskatchewan. Bulletin-Geological Survey of Canada, **588** (2007) 363.

[4.114] GYÖRFI, I., HAJNAL, Z., WHITE, D.J., TAKÁCS, E., REILKOFF, B., ANNESLEY, I.R., POWELL, B., KOCH, R., High-resolution seismic survey from the McArthur River region: contributions to mapping of the complex P2 uranium ore zone, Athabasca Basin, Saskatchewan. Bulletin-Geological Survey of Canada, **588** (2007) 397.

[4.115] HAJNAL, Z., WHITE, D. J., TAKACS, E., GYÖRFI, I., ANNESLEY, I. R., WOOD, G., ODOWD, C., NIMECK, G., Application of modern 2-D and 3-D seismic-reflection techniques for uranium exploration in the Athabasca Basin, [This article is one of a series of papers published in this Special Issue on the theme Lithoprobe - parameters, processes, and the evolution of a continent], Canadian Journal of Earth Sciences **47** 5 (2010) 761–782.

[4.116] HAJNAL, Z., TAKACS, E., PANDIT, B., ANNESLEY, I.R., Uranium mineralization indicators from seismic and well log data in the Shea Creek area at the southern margin of the Carswell impact structure, Athabasca Basin, Canada. Geophysical Prospecting, **63** 4 (2015) 861–880.

[4.117] JUHOJUNTTI, N., WOOD, G., JUHLIN, C., O'DOWD, C., DUECK, P., COSMA, C., 3D seismic survey at the Millennium uranium deposit, Saskatchewan, Canada: Mapping depth to basement and imaging post-Athabasca structure near the orebody. Geophysics **77** 5 (2012) WC245–WC258.

[4.118] WOOD, G., O'DOWD, C., COSMA, C., ENESCU, N., An interpretation of surface and borehole seismic surveys for mine planning at the Millennium uranium deposit, northern Saskatchewan, Canada, Geophysics **77** 5 (2012) WC203–WC212.

[4.119] MCCOY, A., "Application of 3D seismic in the delineation of U bearing structures at Ranger 3 Deeps", Australian Society of Exploration Geophysicists (ASEG), ASEG Extended Abstracts (2010) 1–1.

[4.120] MWENIFUMBO, C.J., ELLIOTT, B.E., JEFFERSON, C.W., BERNIUS, G.R., PFLUG, K.A., Physical rock properties from the Athabasca Group: designing geophysical exploration models for unconformity uranium deposits, Journal of Applied Geophysics **55** 1 (2004) 117–135.

[4.121] FRANCKE, J., A review of selected ground penetrating radar applications to mineral resource evaluations, Journal of Applied Geophysics **81** (2012) 29–37. doi: 10.1016/j.jappgeo.2011.09.020

[4.122] SCHEIB, A.J., The application of passive seismic to estimate cover thickness in greenfields areas of Western Australia — method, data interpretation and recommendations. Geological Survey of Western Australia, Record 2014/9 (2014).

5. EXPLORATION STRATEGY

5.1. INTRODUCTION

This section focuses on the description of strategic aspects of uranium exploration for the discovery of the next generation of economic deposits. It includes an overview of the global distribution of economic uranium resources, a description of the exploration process, the identification of exploration risk factors, and an illustration of an approach for exploration in frontier environments.

Uranium exploration is a complex high-risk high-reward business activity focused on the discovery of economic uranium deposits. The exploration process involves many stakeholders who take on different roles to support the activities of exploration and mining companies. Stakeholders involved in the process include the IAEA, geological survey organizations, consultants, researchers, exploration service providers, and exploration company managers and workers.

Uranium exploration requires long time-frames and sustained funding to identify economic resources and to develop these resources into mines. Exploration companies invest in exploration after assessing a variety of factors including the prospectivity and explorability of the geological environments, and understanding potential social, environmental and economic risks associated with future mine development.

Prospectivity assessments are based upon models of uranium ore formation and involve the disciplines of geology, geochemistry, and geophysics. The goal is to identify the potential for the occurrence of economic uranium deposits within a specific geological environment. The assessment of prospectivity focuses on identifying exploration methods that are suitable for the environment under evaluation. The goal is to identify approaches to exploration that will confirm the presence of uranium mineralization in an efficient and cost-effective manner.

Economic unconformity uranium deposits have been discovered in Australia and Canada. Other jurisdictions that are known to host Proterozoic sandstone basins and that are deemed to be prospective and explorable, could potentially host new deposits.

5.2. EXPLORATION AND THE NUCLEAR FUEL CYCLE

Uranium exploration is an activity located at the front end of the nuclear fuel cycle (Fig. 5.1). It is a high-risk high-reward business activity that is analogous to a research and development process. Exploration can lead to the discovery of economic uranium resources that are exploited through mining developments. Uranium ores are processed, converted, and enriched, for fuel fabrication and the generation of electricity in nuclear power reactors [5.1].

A description of the global distribution of uranium resources is regularly prepared jointly by the NEA and IAEA and published by the OECD [5.2, 5.3]. In 2016, total global identified resources (reasonable assured and inferred) were 5 718 400 tonnes of uranium metal (tU) in the <US $130 /kgU category. The estimate includes 3 458 400 tonnes of reasonably assured resources. From 2014 to 2016, identified resources increased by 0.1%. The lack of growth in the resource base was attributed to lower levels of investment in exploration due to depressed conditions in the uranium market.

The distribution of global reasonably assured resources are illustrated in Fig.s 5.2–5.4 [5.1–5.3]. Significant economic Proterozoic unconformity uranium deposits have been developed in Australia and Canada by open-pit and underground mining methods.

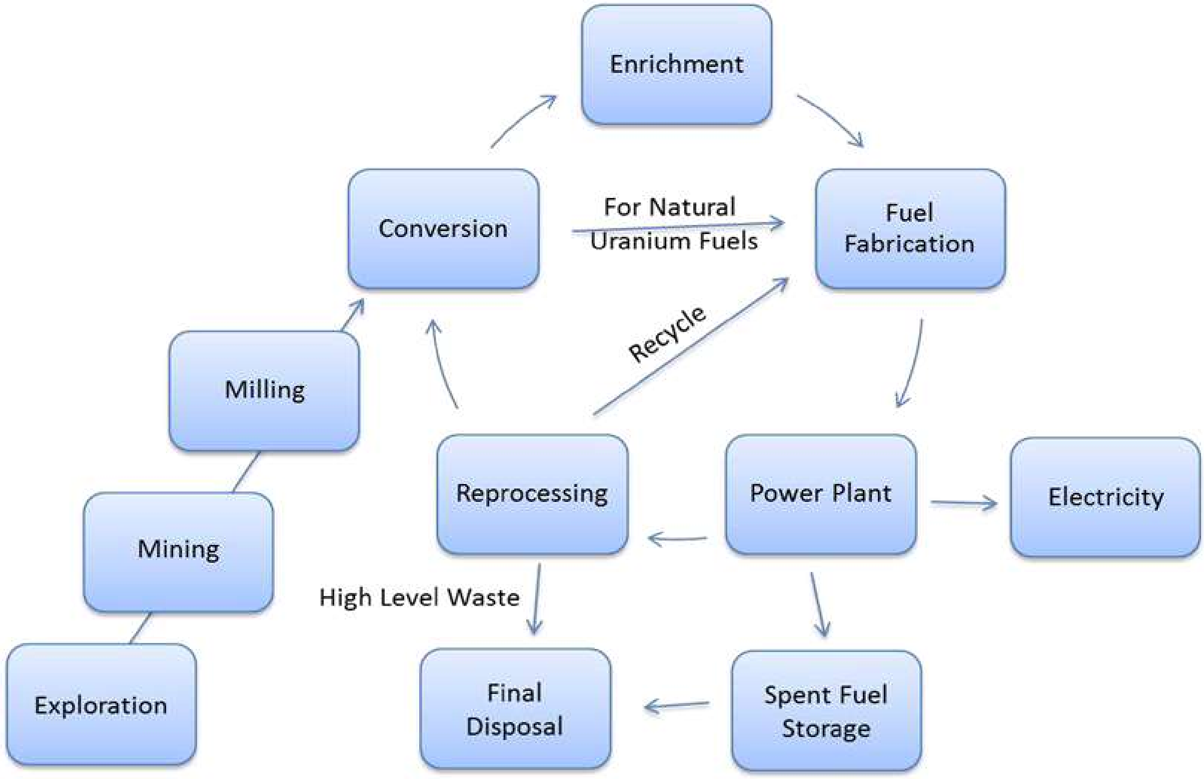

FIG. 5.1. Situating exploration in the nuclear fuel cycle (reproduced courtesy of IAEA [5.4]).

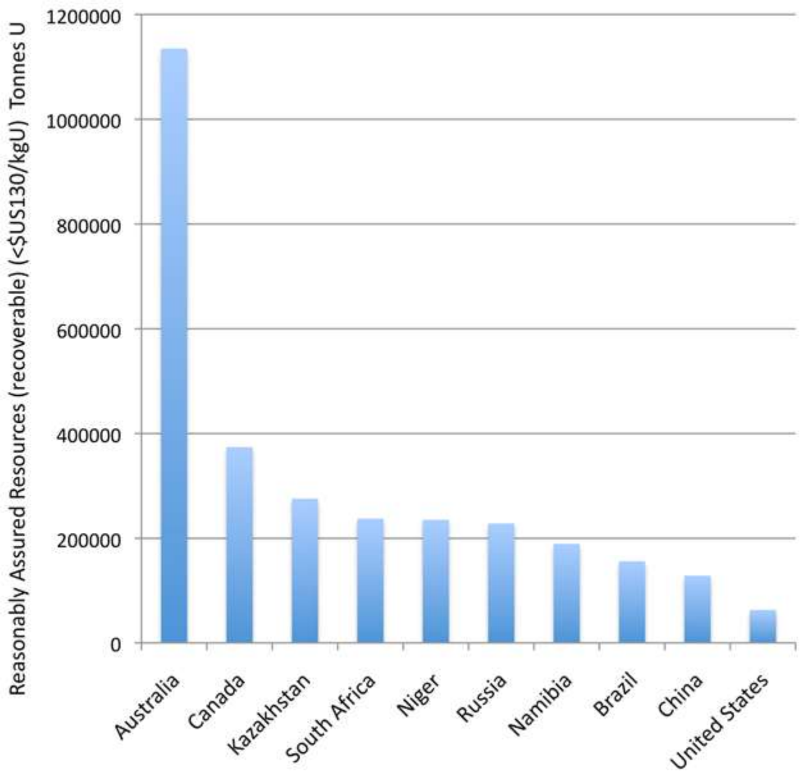

FIG. 5.2. Reasonably assured uranium resources by countries with significant resources (data from OECD/ NEA-IAEA [5.2]).

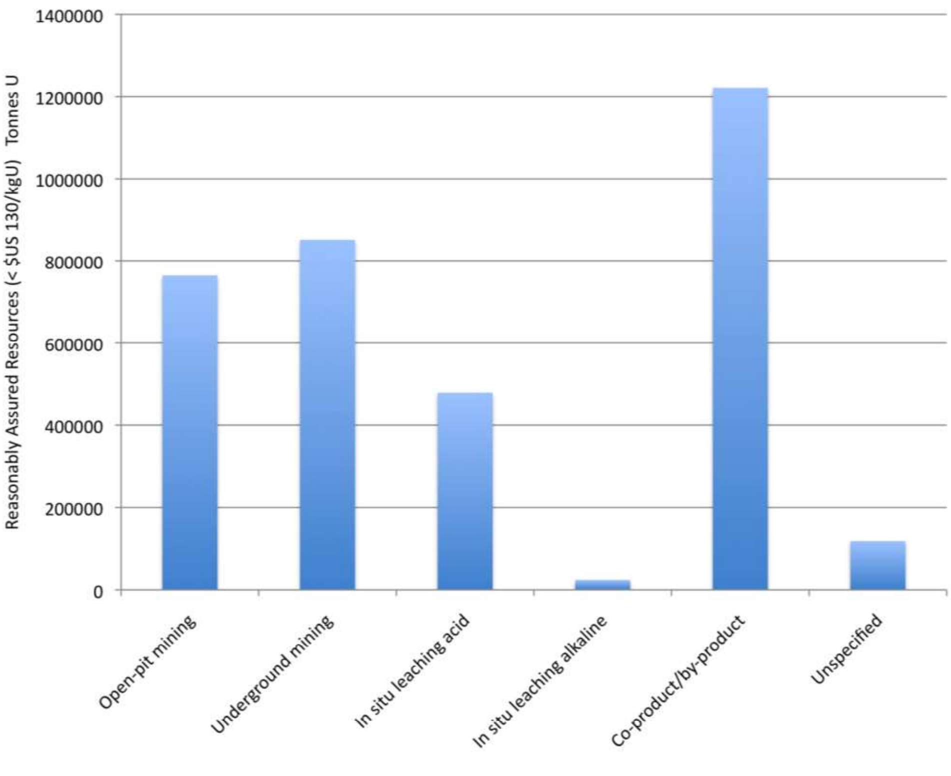

FIG. 5.3. Reasonably assured uranium resources by production method (data from OECD/NEA-IAEA [5.2]).

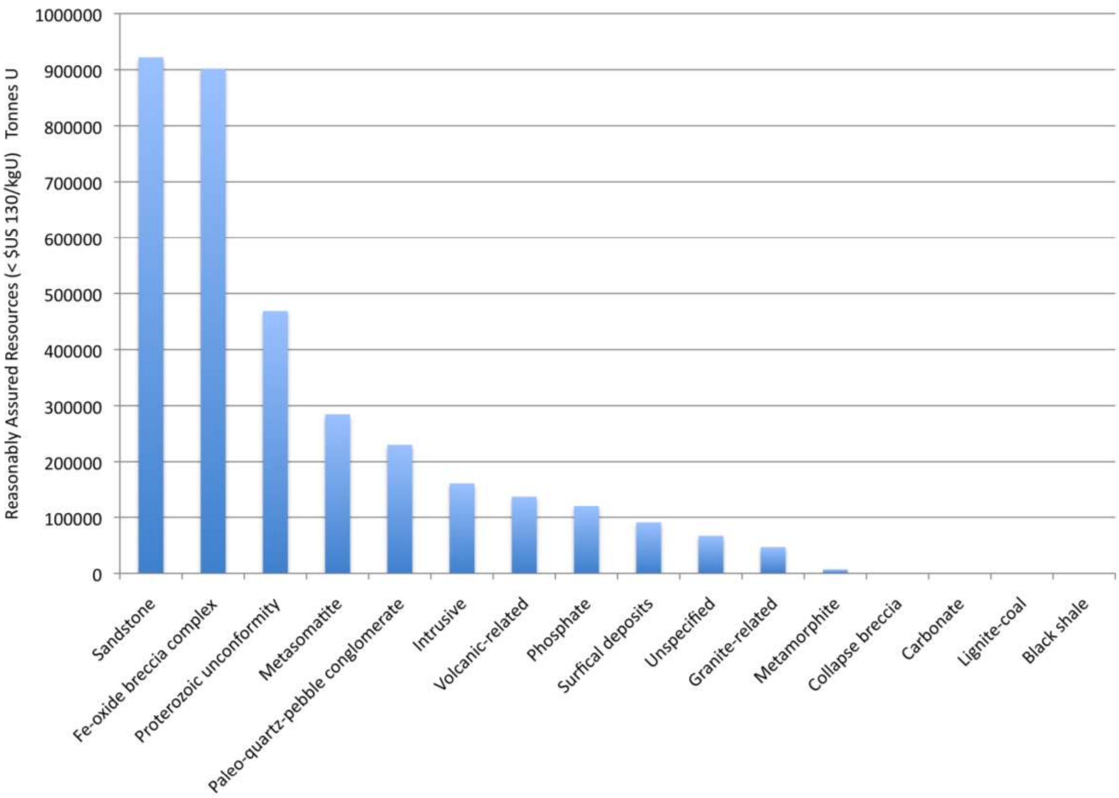

FIG. 5.4. Reasonably assured uranium resources by deposit type (data sourced from OECD/NEA-IAEA [5.2]).

The "Red Book Retrospective" report provides an historical profile of the world uranium industry for the period 1965 to 2004, with a focus on uranium resources, exploration and production [5.5]. Annual production of uranium (1945–2016) peaked at 70 000 tU around 1980, and decreased to 30 000 tU around 1995. Current annual production levels are approximately 60 000 tU (Fig. 5.5) [5.1, 5.3].

World recoverable reasonably assured uranium resources (<US $130/kgU) are estimated to be 6 263 532 tU (2015) (Fig. 5.6). Historical production of uranium is approximately 2805 132 tU. The inventory of recoverable reasonably assured resources (<US $130/kgU) is 3 458 400 tU (2015). Statistics for Canadian and Australian uranium deposits suggest that less than one half of these RAR will eventually be exploited by mining operations (<1 729 000 tU). This equates to 30 years of production at a rate of 60 000 tU/year [5.1].

World historical uranium exploration expenditures are illustrated in Fig. 5.7. Levels exceeded US $3 billion in 1976, and declined below US $500 million in the 1990s, rebounding to US $2 billion in 2007. As of 2016, expenditures were declining. Uranium exploration expenditure and the price of uranium are positively correlated.

From 1970–2015, US $53.5 billion (constant dollars) were expended on world uranium exploration resulting in the addition of 4 410 991 tU of RAR (<US $130/kgU) to the world inventory at a cost of >US $12.13/kgU (equivalent to >US $4.66/lb U_3O_8) [5.1].

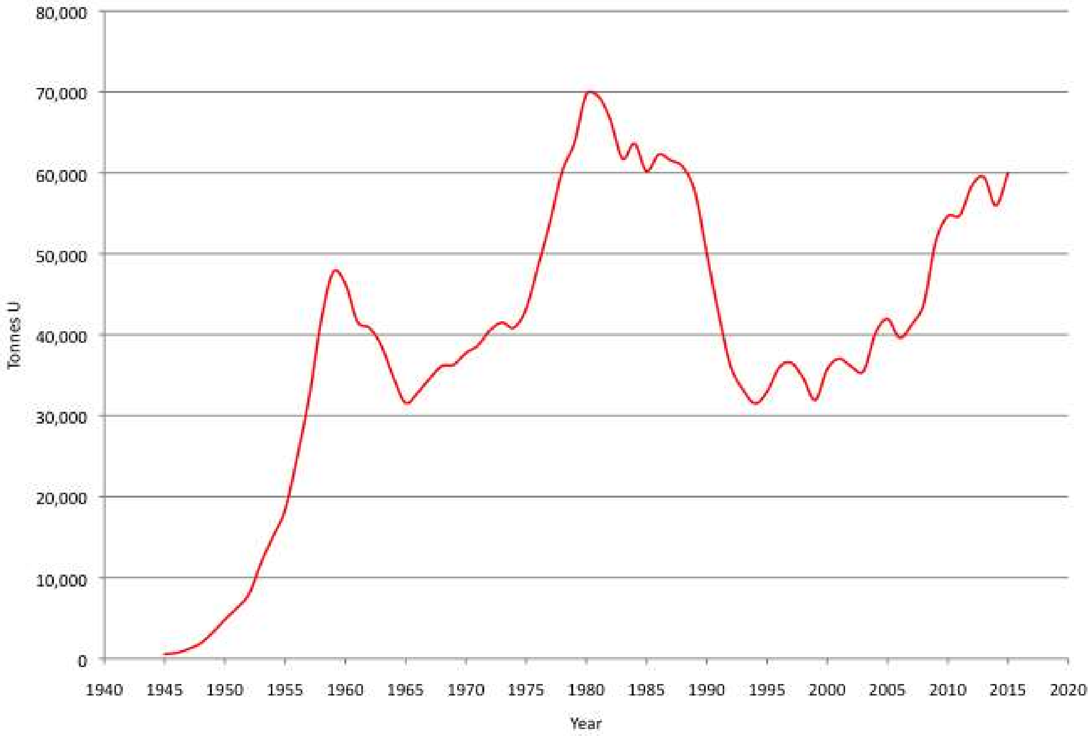

FIG. 5.5. Global uranium production (1945–2015 data from [5.2, 5.3 and 5.5]).

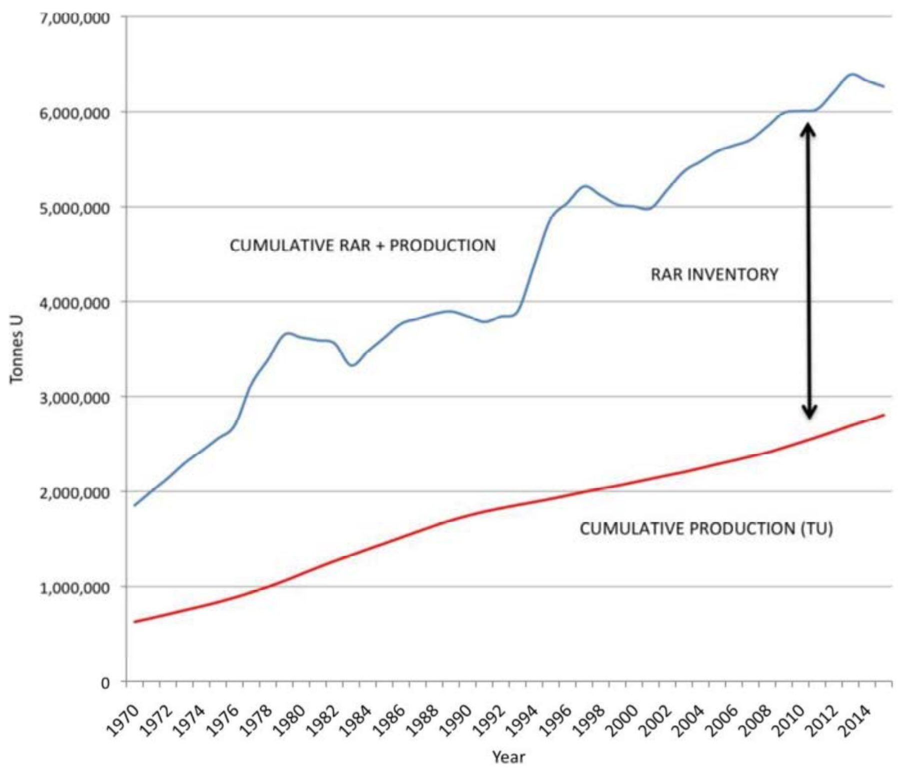

FIG. 5.6. Global cumulative historical uranium production and historical cumulative reasonably assured resources (<US $130/kgU) 1970–2015 data from [5.2, 5.3 and 5.5]).

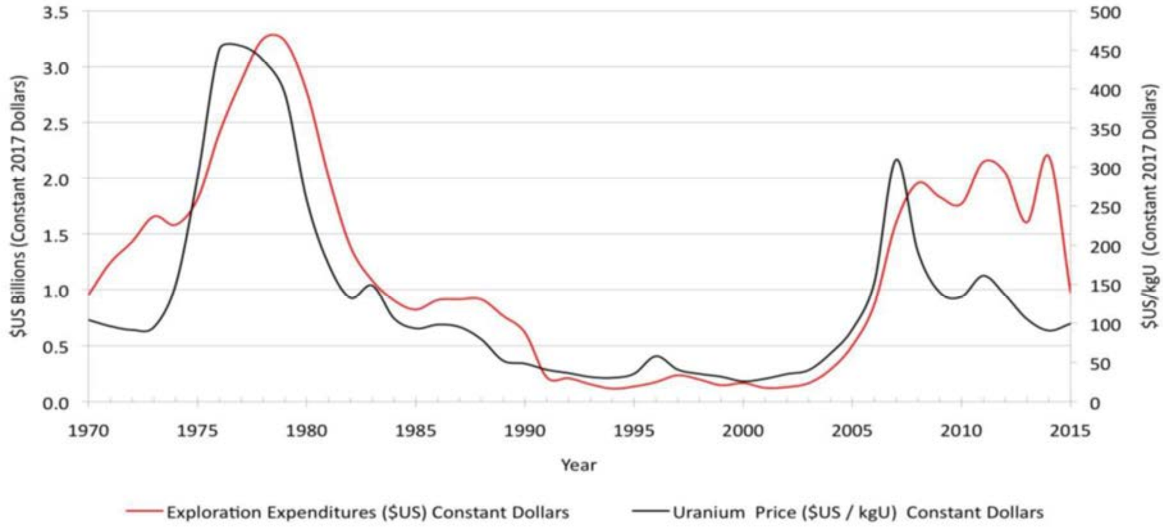

FIG. 5.7. Global uranium exploration expenditures and uranium price (constant 2017 dollars) 1970–2015 data from [5.2, 5.3 and 5.5]).

The IAEA combined a uranium deposit classification scheme used for the 'Red Book' publication since 1991, with Dahlkamp's uranium deposit classification scheme [5.6, 5.7]. The revised scheme defines 15 types of uranium deposits worldwide (Table 5.1). Unconformity-related deposits make a large contribution to global reasonably assured resources (Fig. 5.4).

TABLE 5.1. URANIUM DEPOSIT CLASSIFICATION SCHEME [5.2, 5.8]

Worldwide uranium deposit types
1. Intrusive
2. Granite-related
3. Polymetallic hematite breccia complex
4. Volcanic-related
5. Metasomatite
6. Metamorphite
7. Proterozoic unconformity
8. Collapse breccia pipe
9. Sandstone
10. Paleo-quartz pebble conglomerate
11. Surficial
12. Coal-lignite
13. Carbonate
14. Phosphate
15. Black shales

The sales price of uranium determines the viability of a uranium mining operation. A cost curve for uranium production is presented in Fig. 5.8. World mining operations are depicted by deposit type. Low cost uranium production may be found in situ-acid-recovery roll-front uranium deposits in Kazakhstan and Proterozoic unconformity deposits in Saskatchewan. The world annual uranium production capacity in 2013 was 80 million pounds (approximately 30 000 tU) U_3O_8 at <US $30/lb, and 120 million pounds (approximately 45 000 tU) U_3O_8 at <US $40/lb [5.9]. The weighted average sales price for US production is shown for two uranium operations in the United States of America along with short- and long-term spot market prices [5.1].

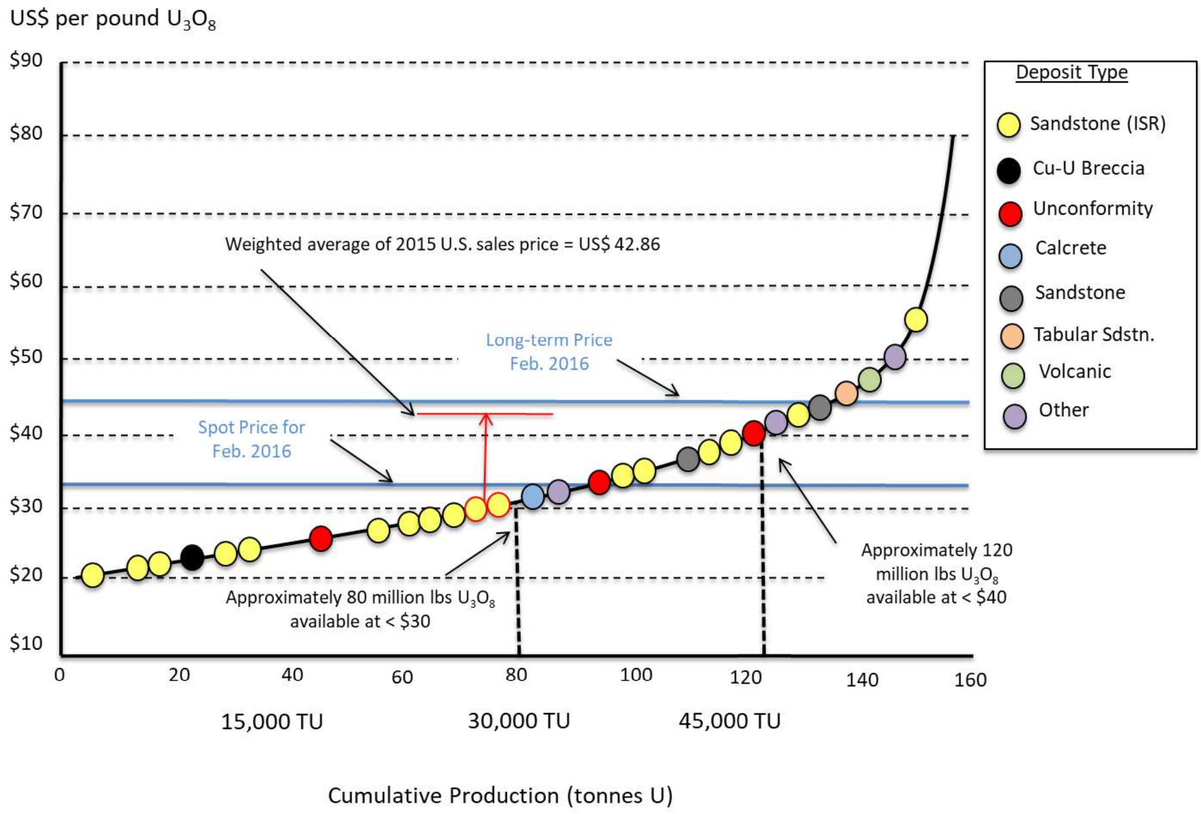

FIG. 5.8. Uranium mining production cost curve (modified from Carter [5.9], Botsov [5.10], and the US Energy Administration [5.11]).

5.3. EXPLORATION BUSINESS DEVELOPMENT

The discovery and development of economic mineral deposits requires long time-frames and sustained funding. Sources of funding are impacted by uranium supply and demand factors as expressed in the uranium price.

Stakeholders in the uranium exploration business have different motivations (Fig. 5.9). Governments are involved in supporting domestic nuclear energy programmes, and generating royalties and employment opportunities from the mining sector. Larger mining companies focus on generating corporate profits and increasing shareholder value. Junior exploration companies look to increase company share price through promotional activities in the stock market. They are generally interested in discovering an economic deposit and selling it to a major mining company. Sometimes junior and major mining companies enter joint exploration ventures and alliances with a major company which acts as a funding partner [5.1].

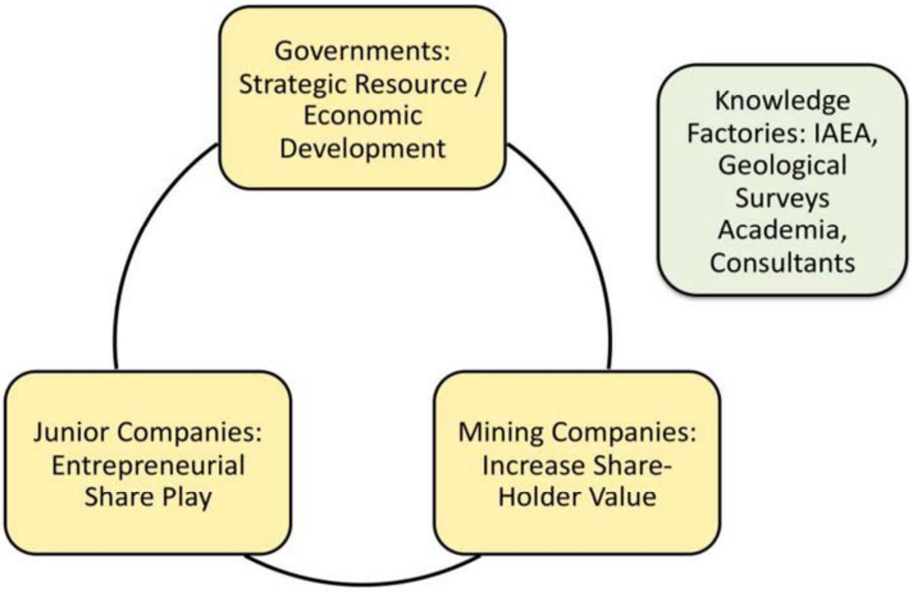

FIG. 5.9. Rationale for uranium exploration.

The IAEA, geological survey organizations, university researchers, consultants, and contractors act as knowledge brokers in the exploration process. They provide expertise in the areas of geoscience, exploration technology, and mining. Exploration and mining companies also employ geoscientists to expedite their exploration programmes [5.1].

Exploration companies compete for limited sources of funding in the market place. They must carefully select projects and jurisdictions for investment in exploration. These decisions are driven by an assessment of the economic mineral potential, and the identification of suitable exploration technologies.

Junior exploration companies often face challenges in raising money through private and public sources to sustain their exploration programmes. Funding is sympathetic with the price of uranium that responds to new production entering the market [5.12].

The roles and interests of stakeholders in the uranium exploration business are illustrated in Table 5.2. Exploration companies are interested in conducting exploration in countries that have prospective terrains and that have a favourable business environment, attractive policies and a reliable mineral tenure system. Geological survey organizations and consultants act to reduce technical risk associated with investment decisions through the provision of pre-competitive geoscientific data sets and expertise.

Governments and geological survey organizations can use competitive benchmarks such as the Fraser Institute annual rankings on perceptions of investment attractiveness and policy perceptions as a gauge. Transparency International's anti-corruption index is another benchmark of investor attractiveness. Measures of annual exploration expenditures, exploration drilling statistics, and discovery statistics provide additional measures (Table 5.3) [5.1, 5.13, 5.14].

TABLE 5.2. FACTORS INFLUENCING URANIUM EXPLORATION AND MINING INVESTMENT DECISIONS

Factors Influencing Investment Decisions in Various Jurisdictions	Role of Governments & Ministries	Role of Agencies, & Geological Survey Organizations	Role & Needs of Consultants / Academics Involved in Supporting Uranium Exploration	Needs of Junior Uranium Exploration Companies	Needs of Uranium Exploration & Mining Companies	Needs of Multi-Commodity Exploration & Mining Companies
Motivation of Organizations, Consultants & Academics	Attract Investors	Provide Information and Expertise	Provide Specialist Expertise	Share Price Escalation	Increase Shareholder Value	Increase Shareholder Value
Exploration Investment Risk Tolerance	Risk Mitigation Role	Risk Mitigation Role	Technical Risk Mitigation Role	Higher	Moderate	Lower
At the Exploration Stage						
Higher level of security	x				?	x
Favourable uranium exploration & mining policies	x	x		x	x	x
Lower level of corruption	x	x		?	?	x
Advocate for Best Practice	x	x				x
Availability of local logistical experts		x		x	x	
Safe working conditions				?	x	x
Access to senior government officials	x	x		x	x	x
Easy/free access to high-quality geoscientfic databases	x	x	x	x	?	?
Availability of local geoscientific experts/consultants/academics		x	x	x	?	
Advice on uranium prospectivity and explorability		x	x	x		
Certainty around the application of regulations*	x	x		?	x	
Cost effective land tenure and reporting system*	x	x		x	x	
Timely granting of exploration land holdings	x	x		x	x	
Ability to import scientific equipment	x	x	x	x	x	
Ability to export rock, soil, vegetation, water and other samples	x	x	x	x	x	
Reporting on the status of mineral resources (i.e. 43-101)			x			
Exploration agreements with consultants, experts, & academics				?	?	x
Exploration agreements with junior exploration companies					x	x
Development of stakeholder relationships	x	x	x	x	x	x
At the Mining Stage						
Higher level of security	x			A common strategy is to develop a resource and sell the company to a major mining company.	x	x
Lower level of corruption	x				x	x
Political stability*	x				x	x
Fair legal system*	x				x	x
Clear taxation regime*	x				x	x
Understanding trade barriers*	x				x	x
Certainty around the application of regulations*	x	x			x	x
Minimal regulatory duplication and inconsistency*	x	x			x	x
Certainty around environmental regulations*	x	x			x	x
Clear understanding of socioeconomic stakeholder agreements*	x	x			x	x
Clear land claim dispute mechanism*	x	x			x	x
Infrastructure to support mining development*	x				x	x
Understanding labour regulations*	x				x	x
Availability of labour/skills*	x				x	x
Worker health & safety	x				x	x

** Factors adapted from the Fraser Institute Annual Survey of Mining Companies 2016 [5.14].*

TABLE 5.3. A COMPARISON OF URANIUM EXPLORATION AND MINING INVESTMENT ATTRACTIVENESS BY COUNTRY

Country	State / Province	Economic Deposit Models	Economic Uranium Prospectivity	Transparency International Corruption	Fraser Institute Investment Attractiveness	Fraser Institute Policy Perception	Factors impacting Uranium Exploration and Mining Investment Decisions
Uzbekistan		ISR Sandstone	moderate	19	?	?	
Ukraine		ISR Sandstone	depleted	27	?	?	
Kazakhstan		ISR sandstone	high	28	75	70	State controlled; acid leach permitted
Guyana		Unconformity-related?	low (under-explored)	29	51	60	permitting timelines
Russia		Various	moderate	29	66	52	
Niger		Sandstone	high	34	46	30	Threat of terrorism.
Gabon		Unconformity-related?	low	34	?	?	Under-cover exploration in a tropical environment.
China		ISR Sandstone	moderate	37	58	46	State controlled
Brazil		By-product	by-product	38	61	57	
Mongolia		Sandstone	low	39	50	37	
South Africa		By-product	low	44	58	52	Permitting challenges; no new discoveries.
Namibia		Calcrete	moderate	53	70	30	Namibian state firm has exclusive rights to future uranium developments
United States	New Mexico	ISR Sandstone	low	76	61	77	Permitting challenges
United States	Wyoming	ISR Sandstone	moderate	76	78	97	Acid leach prohibited
Australia	Queensland	Volcanic	low	79	78	79	History of back-flipping on uranium mining policy/ Uranium exploration permitted but mining is not.
Australia	South Australia	ISR Sandstone; By-product	high	79	80	86	High level of government support. Excellent pre-competitive databases.
Australia	Northern Territory	Unconformity-related	moderate	79	82	85	Koongarra deposit incorporated into Kakadu National Park; Jabiluka mine on care and maintenance; NT government opposes Angela-Pamela uranium mine.
Australia	Western Australia	Calcrete	high	79	87	92	History of back-flipping on uranium mining policy
Canada	Northwest Territories	Unconformity-related	low	83	69	65	Remote, expensive, exploration, and permitting challenges.
Canada	Nunavut	Unconformity-related?	low	83	74	69	Uranium mining developments impeded by process
Canada	Newfoundland / Labrador	Volcanic-related	low	83	74	88	New deposits have not been discovered.
Canada	Quebec	Dyke-related	low	83	81	85	Uranium exploration and mining prohibited
Canada	Saskatchewan	Unconformity-related	moderate (depleted)	83	86	95	Economic deposits are taking longer to find.
Finland		U-Au and hydrothermal vein type	low	90	84	95	Anti-uranium politics. Uranium-specific permitting requirements.

Selected Rankings after Transparency International [5.13] and the Fraser Institute [5.14]. (Higher values are more favourable).

5.4. THE EXPLORATION PROCESS

The goal of uranium exploration is the discovery of economic concentrations of mineralization that can be mined [5.1]. Exploration begins with the study of historical data to determine the investment worth of exploration, with the focus on the potential for the discovery of economic concentrations of uranium within the geological terrain. The identification of suitable exploration technologies is another focus [5.15].

Exploration programmes typically involve both regional and detailed exploration phases leading to the drill testing of promising targets. Economic concentrations of uranium mineralization are developed into orebodies through intensive follow-up work. The IAEA publications provide additional descriptions of the exploration process and exploration methods [5.16].

The exploration process is depicted in Fig. 5.10 [5.1]. An exploration rule-of-thumb suggests that about 1 in 1000 exploration projects will lead to the discovery of an economic uranium deposit. And one in three discoveries will advance from the mining feasibility stage to the mining stage. Expenditures increase from the exploration to mining stage. Large expenditures are required at the mining stage for the pre-development, development, production, and ultimately decommissioning phases (Fig. 5.11). The return on investment is realized after long lead times.

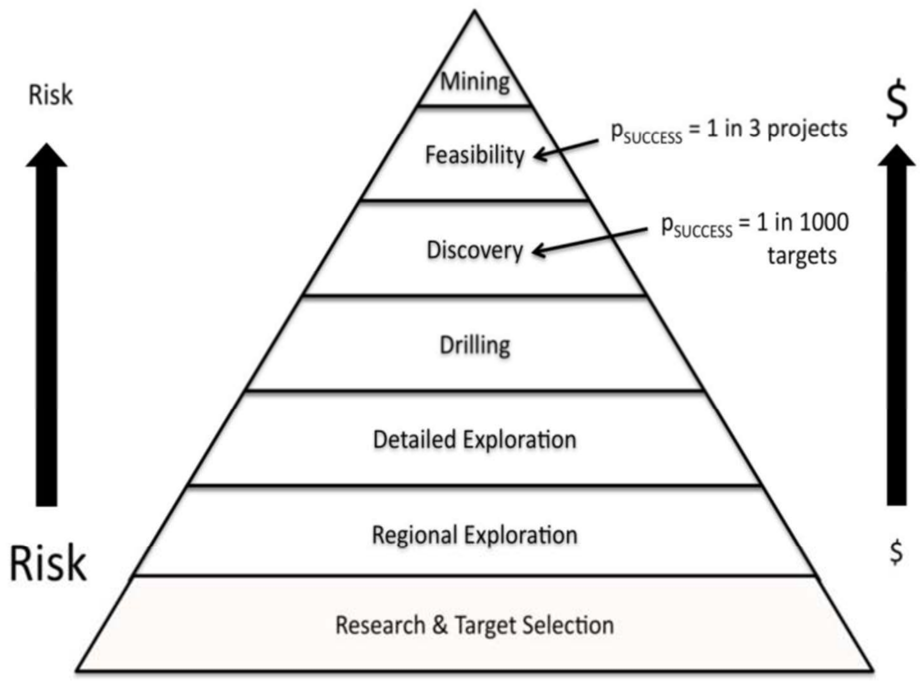

FIG. 5.10. The exploration process.

The Canadian Institute of Mining and Metallurgy lists factors that can impact the viability of mining developments [5.18]. These include risks associated with reserves, political and country risk, social and environmental risk, metal price, and operating costs (Fig. 5.12). The quality of ore reserve grade and tonnage is a critical factor.

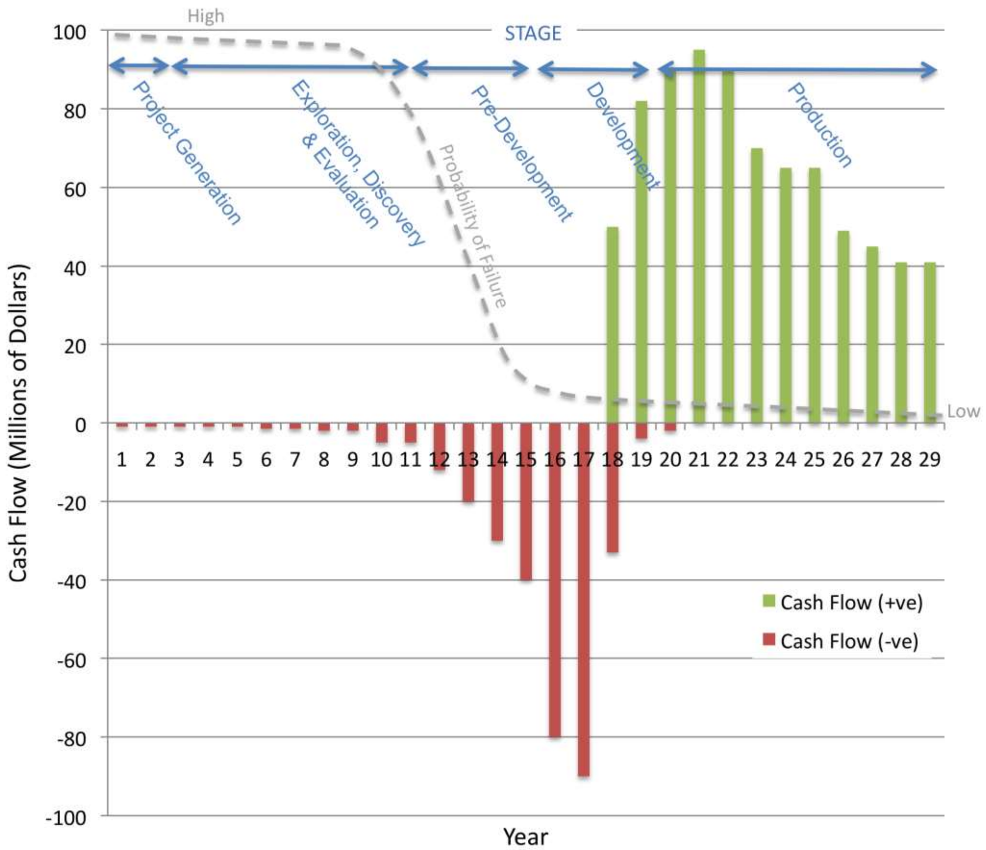

FIG. 5.11. Hypothetical cash flow associated with exploration and mining development (modified from Smith and Tauchid [5.17]).

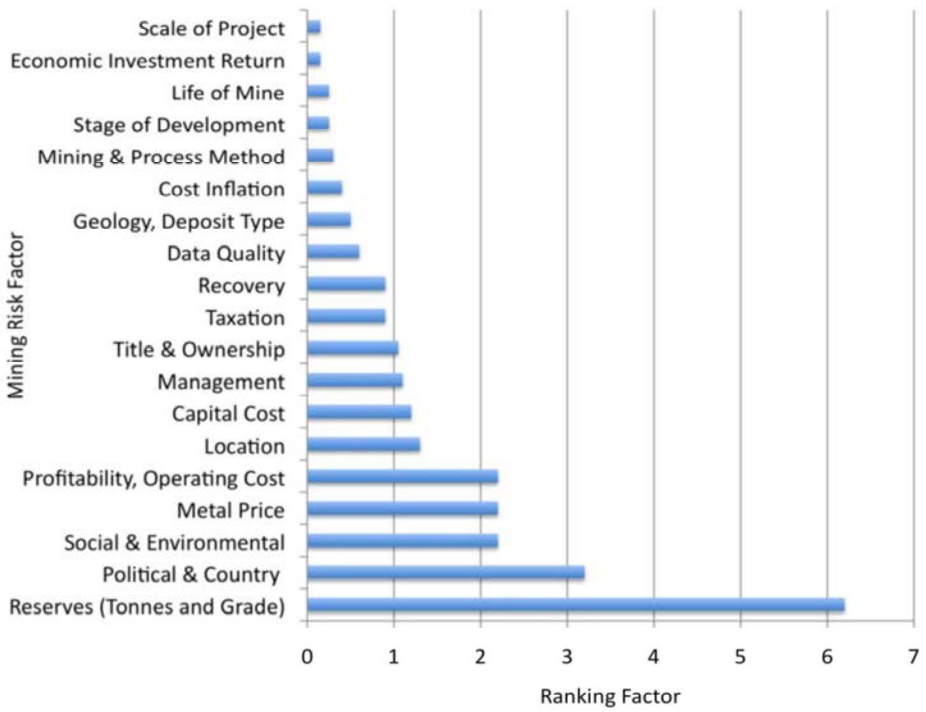

FIG. 5.12. Ranking of principal mining project risks (modified from CIMM [5.1, 5.18]).

The Australian and Canadian uranium deposit size distribution is presented in Fig. 5.13 to illustrate some of the risks associated with uranium exploration. Many of the uranium deposits that are discovered are sub-economic or not deemed to be viable due to social, environmental, and political factors. For example, the Kintyre and Millennium deposits are sub-economic under current price conditions. The Rabbit Lake mine was closed due to the depressed uranium market. The Koongarra deposit may never be developed given its inclusion into the Kakadu National Park. The Jabiluka uranium deposit was discovered in 1971 and has been placed on long-term care and maintenance in response to socio-political factors. Not all discoveries result in a mine development.

Long time-frames are required from the start of exploration to discovery and mining. The time from exploration discovery to mining production for Canadian and Australian uranium deposits is illustrated in Fig. 5.14 [5.19]. About one half of the significant discoveries in these countries have been brought into production (Fig. 5.15). The historical data show that the process has taken up to 33 years. The sub-economic deposits have been inventoried from 30 years to 60 years. In most cases, advanced exploration to improve these resources has been unsuccessful [5.1].

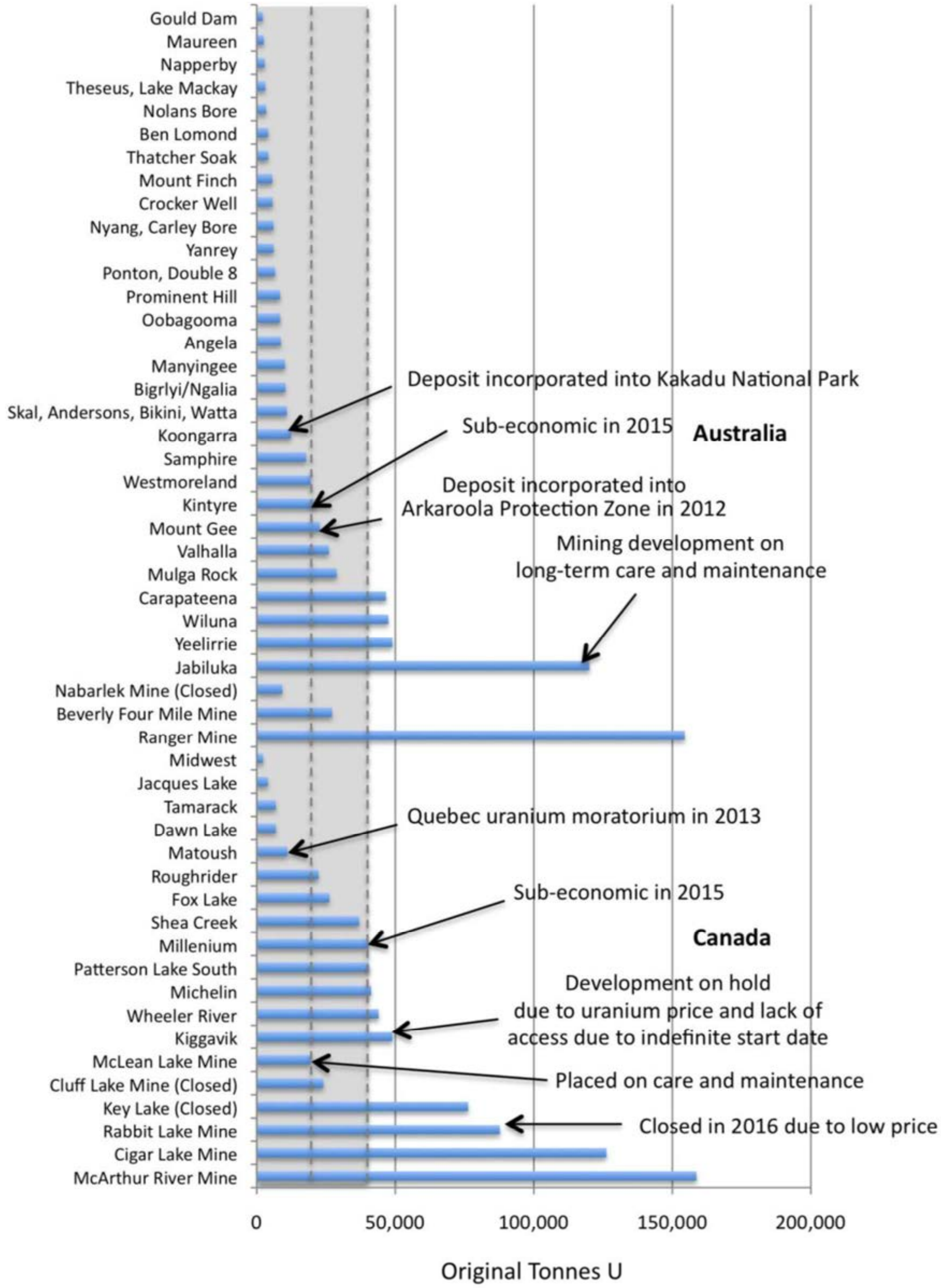

FIG. 5.13. Status and size distribution of uranium deposits in Australia and Canada. Australia size data from McKay and Miezitis [5.19]. 'Sub-economic' deposits fall in gray shaded area [5.1].

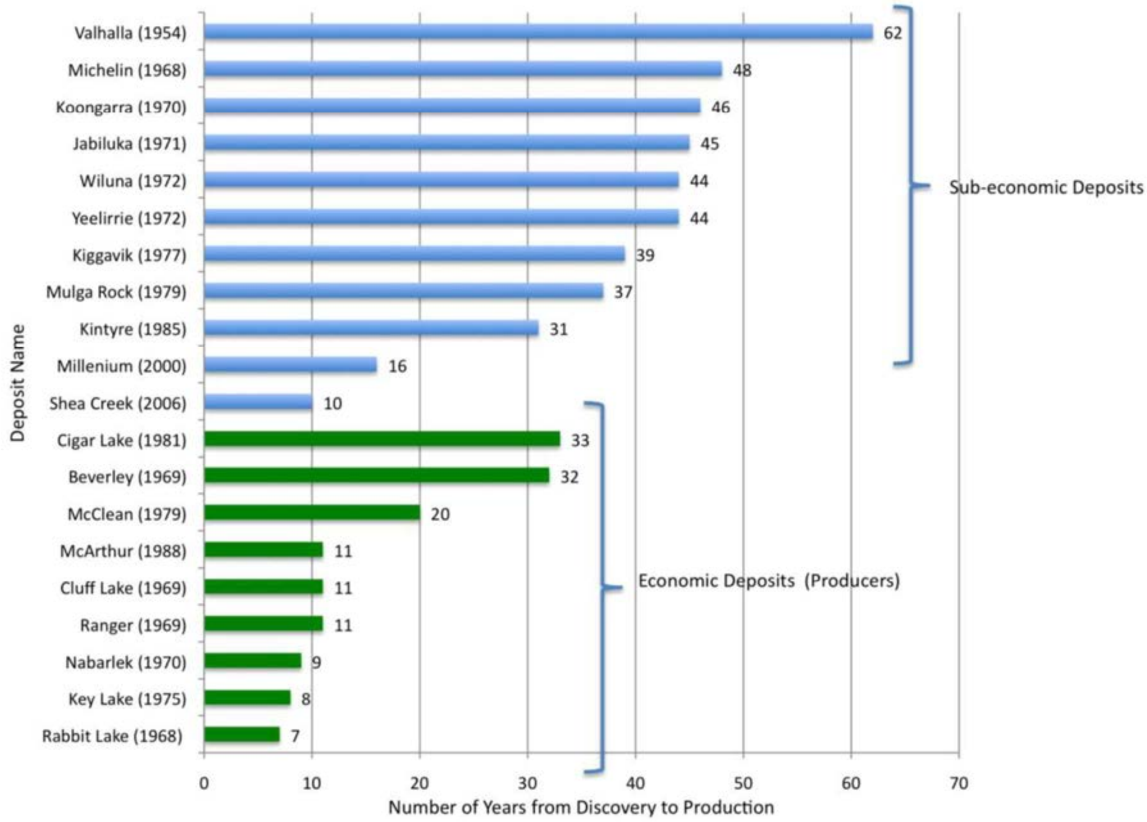

FIG. 5.14. Number of years from discovery to production for selected Australian and Canadian uranium deposits (as of 2016). Australian data from McKay and Miezitis [5.19]. For sub-economic deposits, the number of years are illustrated from discovery to 2016 without a production decision.

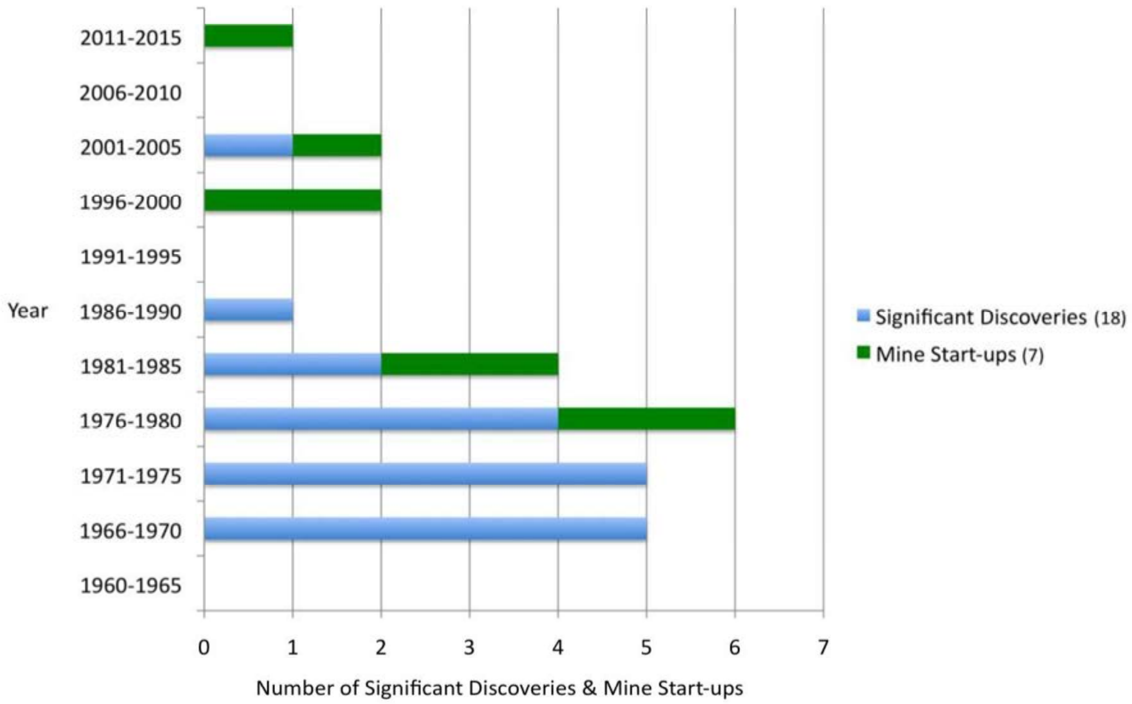

FIG. 5.15. Conversion of significant discoveries to mines for Australian and Canadian uranium deposits.

5.5. ECONOMIC RESOURCE DEPLETION AND FUTURE DISCOVERY

There are enough uranium resources to supply the nuclear power industry for the foreseeable future [5.1, 5.20]. Future supply gaps will be filled by new discoveries and the re-categorization of sub-economic resources to economic status in response to changes in the price of uranium. The development of innovative exploration and mining technologies, exploration discoveries based on new deposit models [5.21, 5.22], and uranium from secondary sources will also contribute to supply security [5.23].

The relationship of exploration risk, average discovery costs, and time associated with exploration discovery is presented in Fig. 5.16. There are only so many economic deposits in the geological environment that are available for discovery. After each economic discovery, the number of economic deposits is reduced. With each discovery, the exploration environment becomes depleted of economic deposits. In addition, large economic deposits are typically discovered earlier in the history of exploration. Average discovery costs increase with time, as the probability of economic discovery decreases with each discovery in a depleting exploration environment. Eventually, discovery rates decrease to a point when explorers abandon exploration and explore in other areas. Exploration technology innovations can extend the life of exploration programmes in some instances.

Given future exploration expenditure in an exploration environment, the magnitude of future discovery can be predicted through the development of a 'learning curve'. A learning curve is a mathematical model that relates exploration expenditure to the magnitude of economic resource discovery. The analysis can lead to a better understanding of the role of technology in reaching discovery and the nature of economic resource depletion. A learning curve can be developed for an exploration environment where economic deposits have been discovered and where the history of exploration expenditure, or a proxy for this expenditure, is known. The learning curve is constructed by plotting the cumulative exploration expenditure against the cumulative magnitude of economic resources discovered [5.1, 5.21, 5.24].

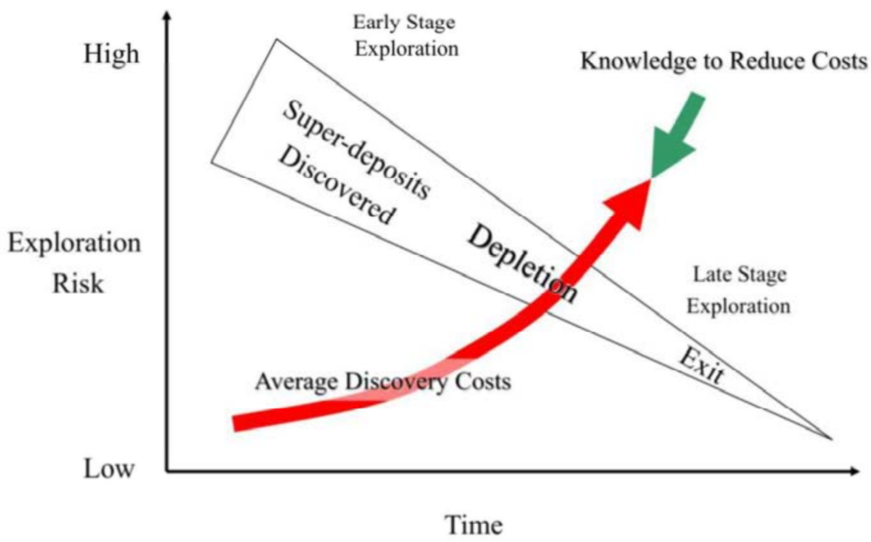

FIG. 5.16. Relationship of exploration risk of failure, average discovery costs, and time associated with exploration [5.1].

Harris et al. [5.1, 5.24] developed a learning curve for Canada's Athabasca Basin (Fig. 5.17). The Basin has experienced two periods of exploration defining a prospector-driven and a deposit model-driven technology phase. In addition, large high-grade deposits were discovered earlier in the history of each of the exploration phases. Additional economic discoveries have not yet been made during the second exploration phase despite significant expenditures, suggesting that a technological breakthrough will be required to reach future discovery. That is, future discoveries can be anticipated during a third phase of exploration. Relying on existing modes of exploration and deposit models will be less efficient or effective. Marlatt and Kyser [5.21] describe the Athabasca learning curve in more detail.

A learning curve for economic uranium deposits discovered in Australia is depicted in Fig. 5.18 [5.1]. The curve is defined by statistics for seven deposits that were discovered from 1969–1985. Between 1967 and 2015, more than 3.5 billion Australian dollars was spent on uranium exploration across Australia resulting in the identification of approximately 400 000 tU. It is estimated that one-half of these resources can be reasonably assumed to be mineable at this time due to economic or political constraints. Less than one-half of the deposits have been mined.

Discoveries in Australia were made early in the history of exploration by prospecting and through radiometric prospecting and surveys. Additional discoveries have not been made despite large exploration expenditures. This suggests that the current technology is not effective and that additional discoveries using traditional exploration technologies will be limited. The learning curve analysis suggests that future discoveries could be achieved through some sort of technological innovation leading to discoveries that will plot on a second learning curve.

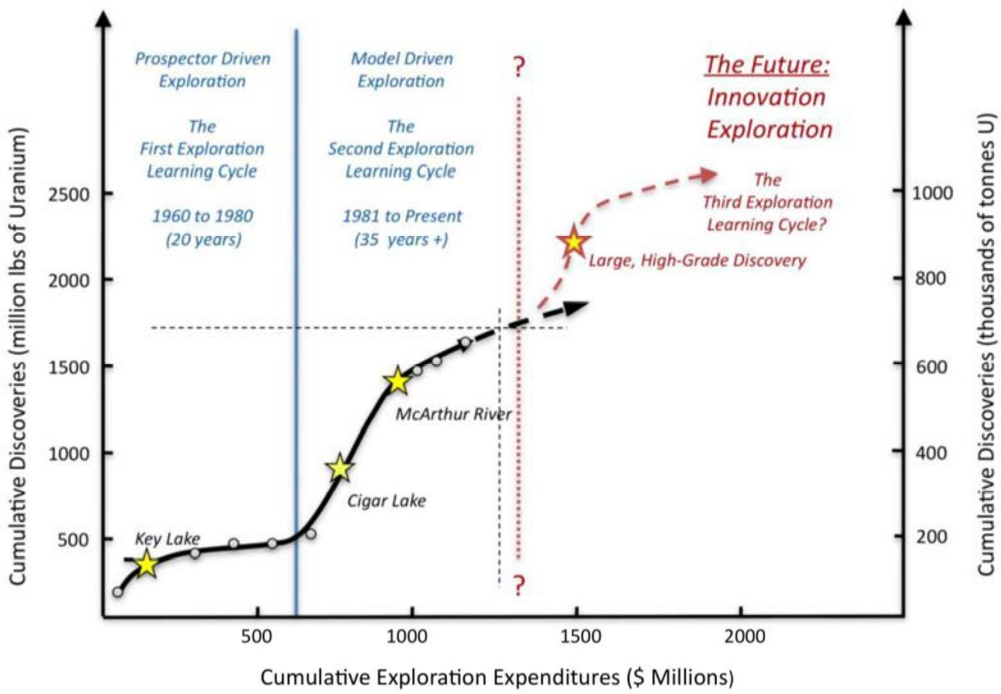

FIG. 5.17. Athabasca Basin learning curve for the discovery of economic unconformity uranium deposits (constant dollars). Modified from Marlatt and Kyser [5.21].

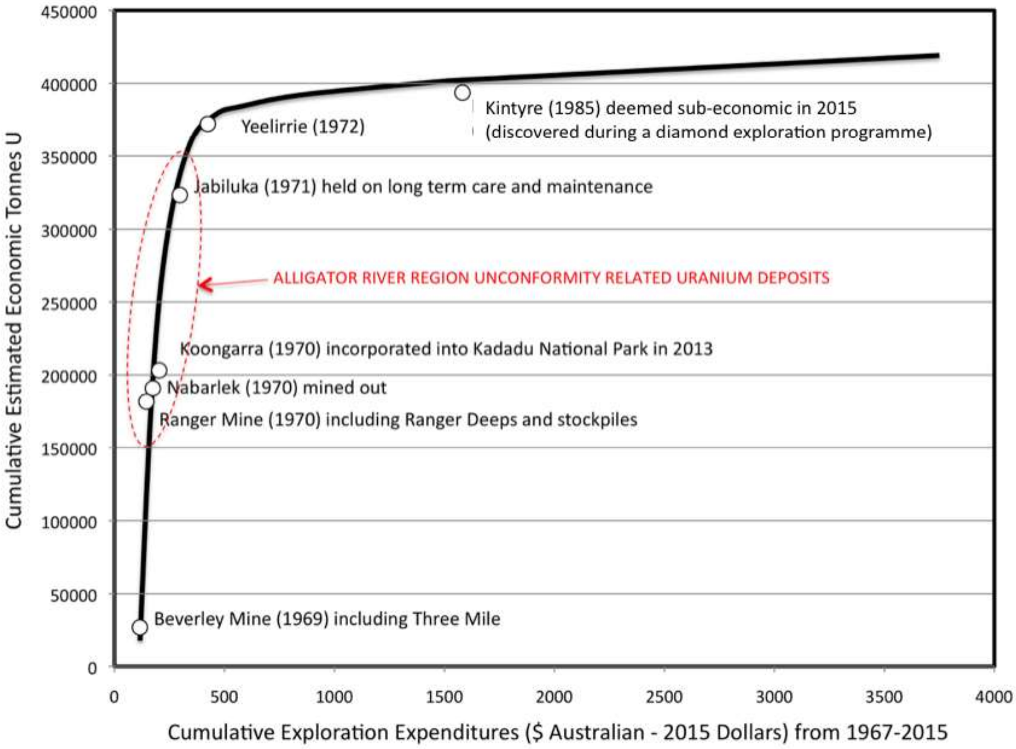

FIG. 5.18. Australia learning curve for the discovery of economic uranium deposits (excluding Olympic Dam). Based on data from MacKay and Miezitis [5.19] and the Australian Bureau of Statistics [5.25]. The Alligator River Region unconformity deposits are highlighted.

Exploration in the Athabasca Basin from the 1960s through to mid-2000 is characterized by an increased depth of discovery (Fig. 5.19) [5.1]. Prospectors who tracked radioactive glacial boulder trains to their origin over orebodies made the earliest discoveries. Later discoveries are attributed to the evolution of genetic models of uranium mineralization, innovations in ground and airborne geophysical technology, and innovations in exploration geochemistry. These developments have led to discoveries at greater and greater depths under sandstone cover rocks. Current exploration is limited by the capacity of geophysical tools to resolve targets at greater depths, and by the high cost and the time it takes to drill test these deep targets. New geochemical technologies are being developed to identify deep, blind deposits [5.15].

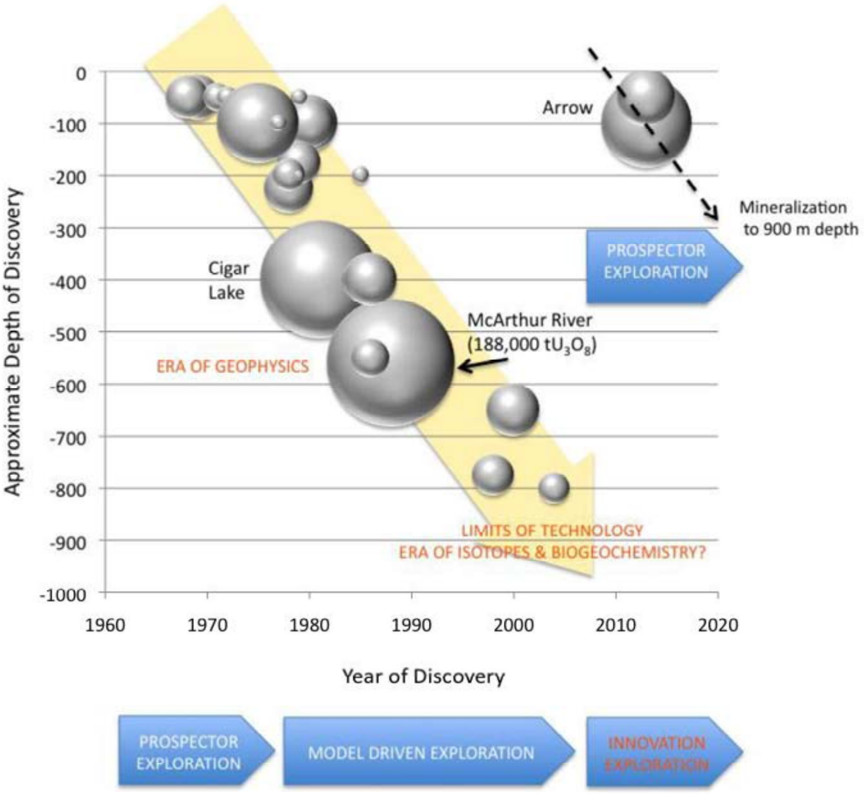

FIG. 5.19. History of Athabasca Basin unconformity uranium deposit discoveries by year of discovery, size, and depth [5.1].

5.6. ASSESSING PROSPECTIVITY, EXPLORABILITY AND OTHER RISK FACTORS

Exploration companies make investment decisions based on the technical assessment of the prospectivity and explorability of project areas. Additional strategic and operational risk factors associated with exploration activities are also considered. These include assessments of the investment risk associated with working in foreign jurisdictions, and the potential impact of future mining operations, viewed from social and environmental impact perspectives (Fig. 5.20). A description of some of these investment risk factors follows [5.1].

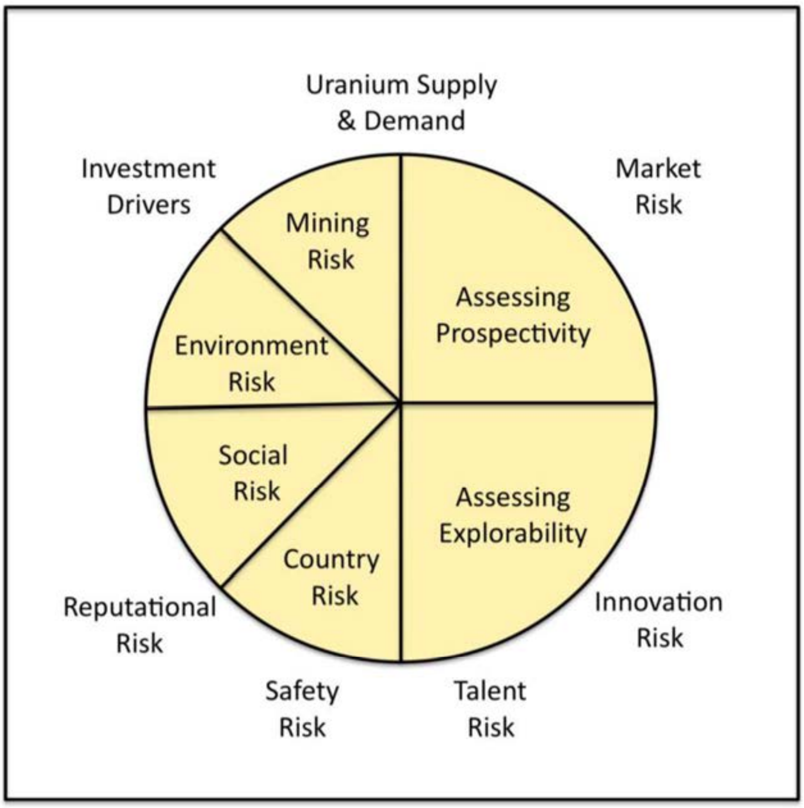

FIG. 5.20. Uranium exploration risk factors [5.1].

5.6.1. Prospectivity

Understanding the prospectivity of an exploration environment is a crucial element when making a decision to conduct exploration in a project area. The economic potential for mineral occurrences in the project area is estimated on an assessment of technical and economic factors. These include the historical rate of discovery, historical exploration expenditures, the grades and tonnages of deposits that have been discovered, the maturity of the exploration play, mineral resource depletion, the anticipated value of these orebodies, and the availability of prospective lands.

The selection of the correct deposit model for exploration is on a robust geoscientific evaluation of the mineral potential. This involves the ranking of technical factors pointing to favourable ore-forming processes in the project area, based upon descriptive and genetic deposit models. Quantitative estimates of mineral resource potential can also be made, in addition to qualitative estimates, through the use of spatial and geomathematical methods [5.1].

5.6.2. Explorability

Exploration project managers assess the explorability of a new project area. They determine if exploration can be conducted in an economical and efficient fashion using existing exploration technologies, or if innovative technologies need to be developed. Exploration technology includes the tools and methods associated with applied geology, geochemistry, geophysics, and drilling.

5.6.3. Mining risk

Mining risk refers to changes in economic, geopolitical, and geoenvironmental factors which affect business environment, which in turn can impact the likelihood of the mineral deposit being developed [5.26].

5.6.4. Country risk

Country risk refers to changes in the business environment (political, economic and financial) that could increase the cost of doing exploration in a country or prohibit exploration [5.27]. Special planning is required when there is potential for political instability and violence that could affect the safety and security of the exploration team and operations [5.28].

5.6.5. Environmental risk

Exploration companies need to be sensitive to the risk of conducting exploration activities in close proximity to environmentally sensitive areas, near parks and reserves, or traditional lands. Changes in the business environment can stem from calls from social and political arenas to limit development in these localities. This can lead to an increase in cost of doing exploration in a country. In some cases, exploration can be prohibited.

5.6.6. Social risk

Changes in the socio-political environment can lead to increases in the cost of exploration or the prohibition of exploration. The uranium business is particularly susceptible to the impact of concerns related to land rights and uranium project development.

5.6.7. Assessing prospectivity

A framework for assessing prospectivity is presented in Fig. 5.21. Activities include the assessment of strategic risks, the assessment of existing mineral occurrences from IAEA and other sources, the selection of appropriate uranium deposit models, the assessment of economic mineral potential, the development of conceptual targets for exploration, and the acquisition of exploration permits [5.1].

Exploration geologists analyse geological, geochemical, and geophysical data sets with a goal of identifying patterns indicative of ore formation. Fieldwork involves the evaluation of historical mineralized showings to confirm the deposit model and intensity of metallogenic processes. These expert assessments validate the deposit model and provide evidence of mineralizing potential.

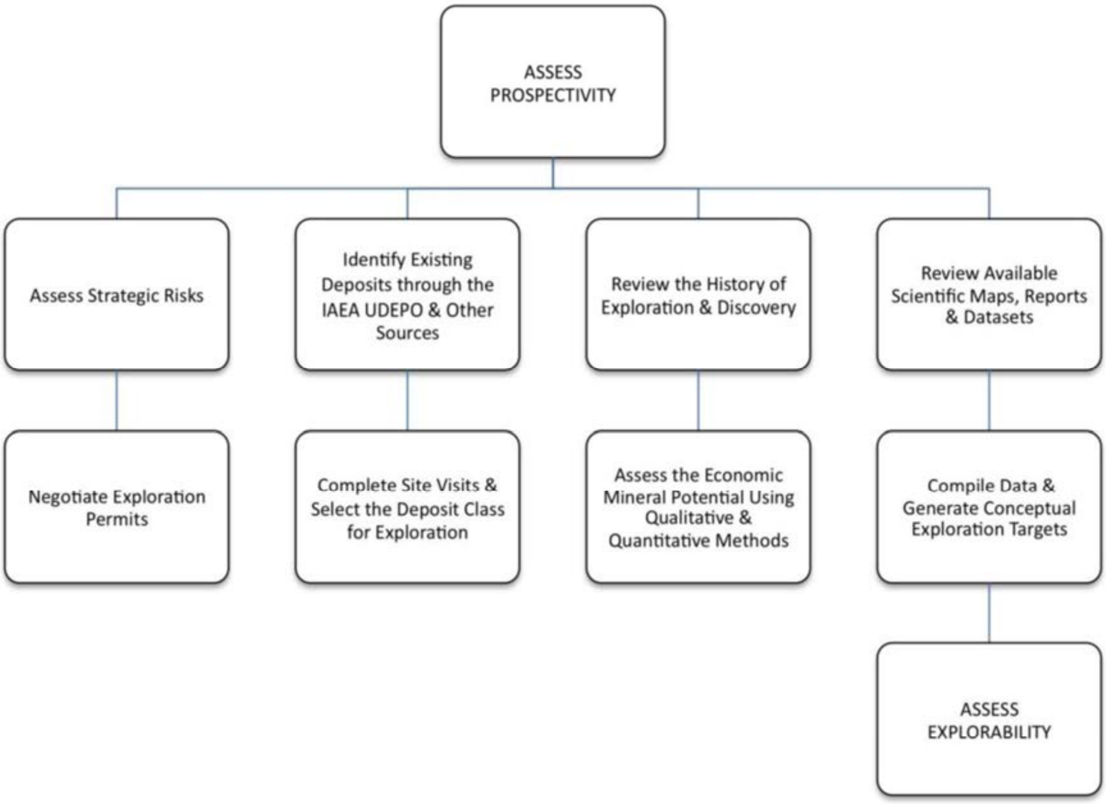

FIG. 5.21. A basic framework for assessing prospectivity [5.1].

5.6.8. Assessing explorability

A framework for assessing explorability is presented in Fig. 5.22. This assessment includes the evaluation of physical access and logistics associated with working within the permit area. Service providers that can support activities in the field are identified. Geoscientific baseline data and historical reports by exploration companies are assessed to understand past methodologies, successes and failures. Depth to target is estimated. Discussions with resident experts are conducted to better understand the geology of the project area. Data is compiled and conceptual exploration targets are generated. Programme proposals and budgets are established and the investment worth of exploration is determined [5.1].

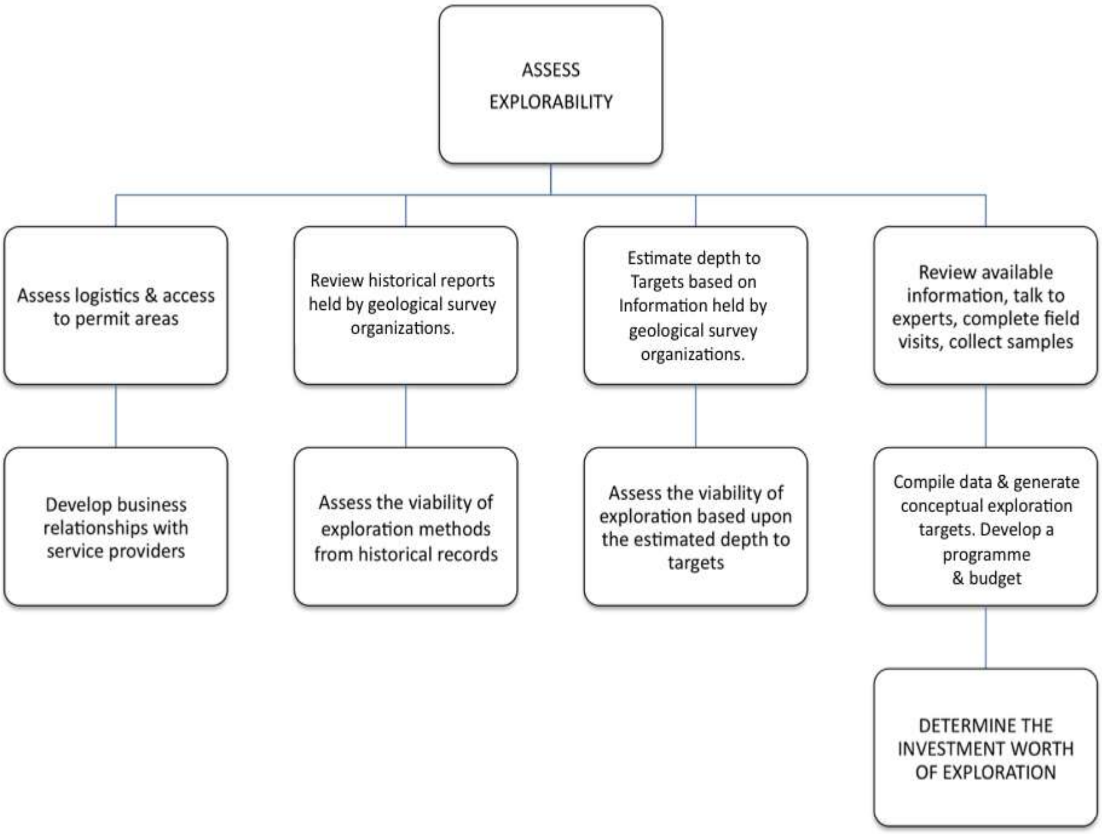

FIG. 5.22. A basic framework for assessing explorability [5.1].

5.6.9. Exploration methods

A variety of methods are available for the exploration of uranium deposits. These survey methods are used to identify anomalous geological, geochemical and geophysical signatures that are indicative of ore-forming processes. Surveys are completed in an iterative manner from regional to local scales. When significant anomalies are located, they are tested by diamond or rotary drilling techniques to identify expressions of mineralization.

Uranium exploration methods and associated cost estimates are illustrated in Fig. 5.23. The survey methods focus on the evaluation of the geological, geochemical, geophysical characteristics of exploration project areas. Geophysical methods include magnetic, gravimetric, electromagnetic, radiometric, seismic methods. Exploration programme managers carefully assess the feasibility of deploying specific survey methods and their cost, when developing programmes and budgets. More detailed information about exploration methods can be found in this volume and other IAEA publications such as a recent publication on innovations in geophysical methods [5.1, 5.29].

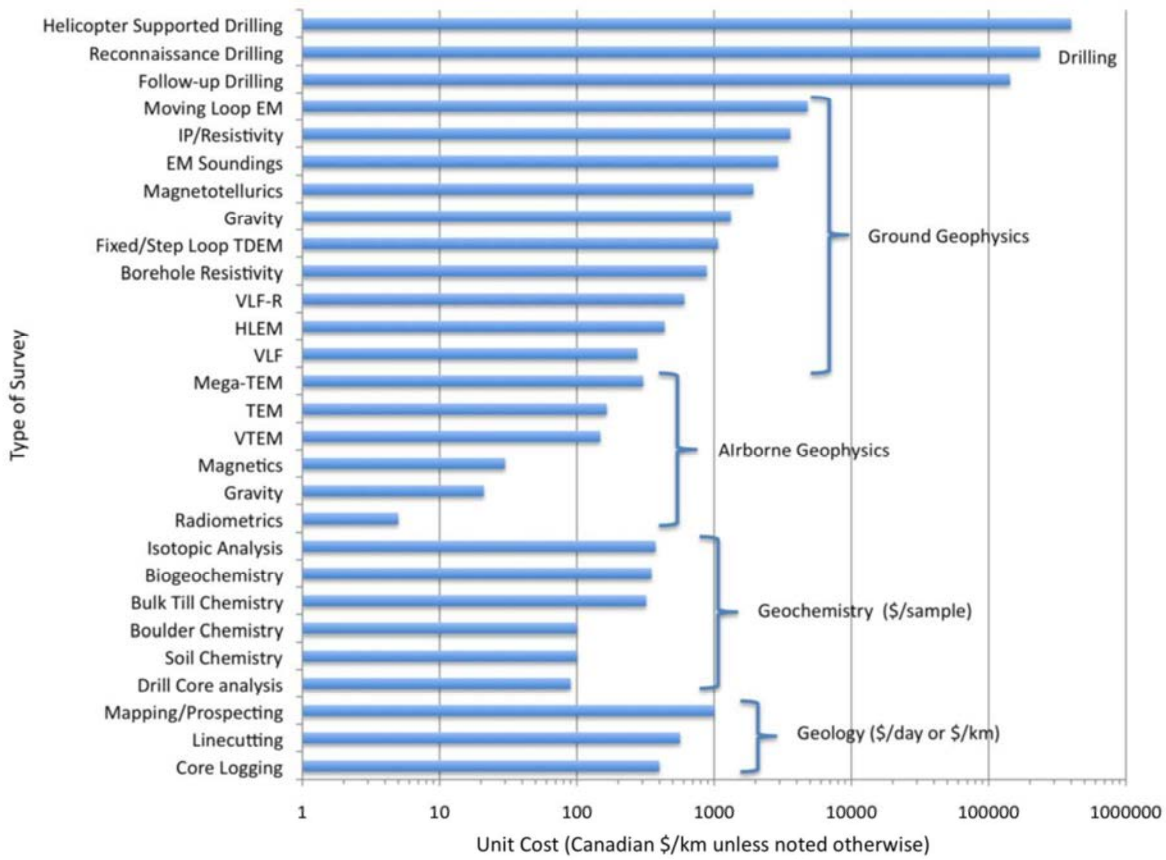

FIG. 5.23. Approximate unit cost of exploration by type of survey [5.1].

5.7. ROLE OF AGENCIES, GOVERNMENTS, CONSULTANTS AND ACADEMIA

There are many stakeholders who support the uranium exploration process. These include the IAEA, geological survey organizations, independent consultants, geoscientists from exploration companies, and researchers in university and government organizations [5.1]. The uranium exploration technology system consists of these experts, exploration techniques, and the programme managers responsible for funding the business of uranium exploration (Fig. 5.24).

Exploration managers have the responsibility of assessing the investment worth of exploration. Exploration programmes and budgets are developed, exploration methods are selected, and contractors are hired to collect data through work in the field.

The IAEA provides baseline data and education and training opportunities in the field of uranium exploration and mining. The goal is promoting the peaceful and sustainable use of nuclear energy. The IAEA also engages consultants in the field of uranium geology and exploration to support some of their programmes.

Geological survey organizations play an important role in the uranium exploration process as sources of administrative and technical expertise. They also supply pre-competitive technical data sets to exploration companies. Geological survey organizations act to attract exploration investment by providing easy and low-cost access to information that companies can use to support their investment decisions. The geological survey organizations in South Australia, Saskatchewan, and Finland, among others, are good examples of such service providers.

Independent consultants can offer unique managerial and technical expertise in the field of uranium exploration. They can support the IAEA and Member States through participation in education and training programmes and as authors of technical publications. Independent consultants can also provide specialized services to exploration companies. Other consultants can work with researchers to develop innovative methods in uranium exploration.

Some university researchers focus on pure and applied research projects in the field of uranium ore deposits and uranium exploration technology development. They leverage funds from government grants, university–company–government collaboration programmes, and contracts with exploration companies. Occasionally, other researchers act as independent consultants in addition to their university teaching positions.

Contractors provide for-fee services including the acquisition, interpretation and reporting of survey data collected for their clients. Some contractors focus on the development and sale of new exploration technologies in the area of remote sensing, geological, geochemical, geophysical and drilling methods.

Exploration companies hire programme managers who develop, implement and assess their exploration programmes and budgets. Exploration managers are responsible for technical teams that can range in size and experience and sophistication. Organizations that do not have a great depth of experience with uranium exploration can rely on the expertise of uranium consultants to support their exploration programmes.

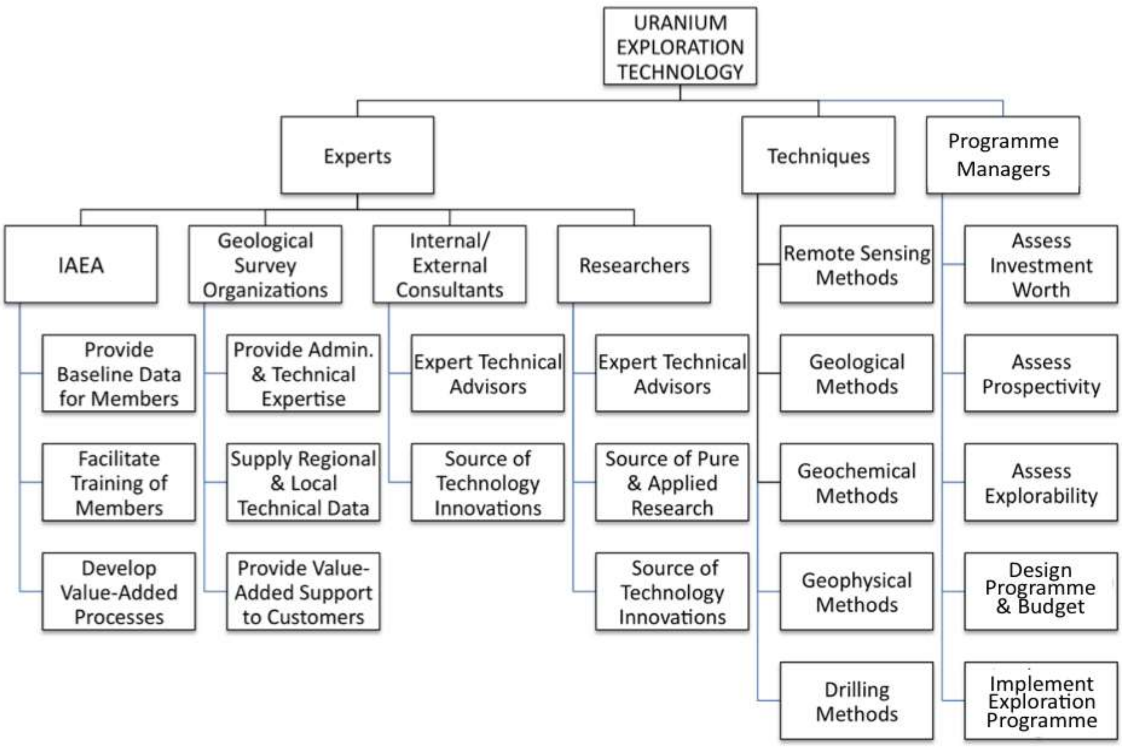

FIG. 5.24. The uranium exploration technology system [5.1].

5.8. FRONTIER EXPLORATION FOR PROTEROZOIC UNCONFORMITY-RELATED URANIUM DEPOSITS

Undiscovered economic uranium deposits and resources may exist within under-explored localities that have received limited exploration expenditure in the past or where efforts have been focused on near-surface exploration [5.1]. The development of exploration programmes in frontier areas is one of the riskiest forms of exploration due to the uncertainty associated with explorability and prospectivity. Exploration within these environments can be classified as high risk and high reward. Proterozoic basins occur in many countries and represent the necessary target for the exploration for unconformity deposits (Fig. 5.25). Several IAEA and OECD publications focus on the exploration for unconformity deposits [5.30–5.33].

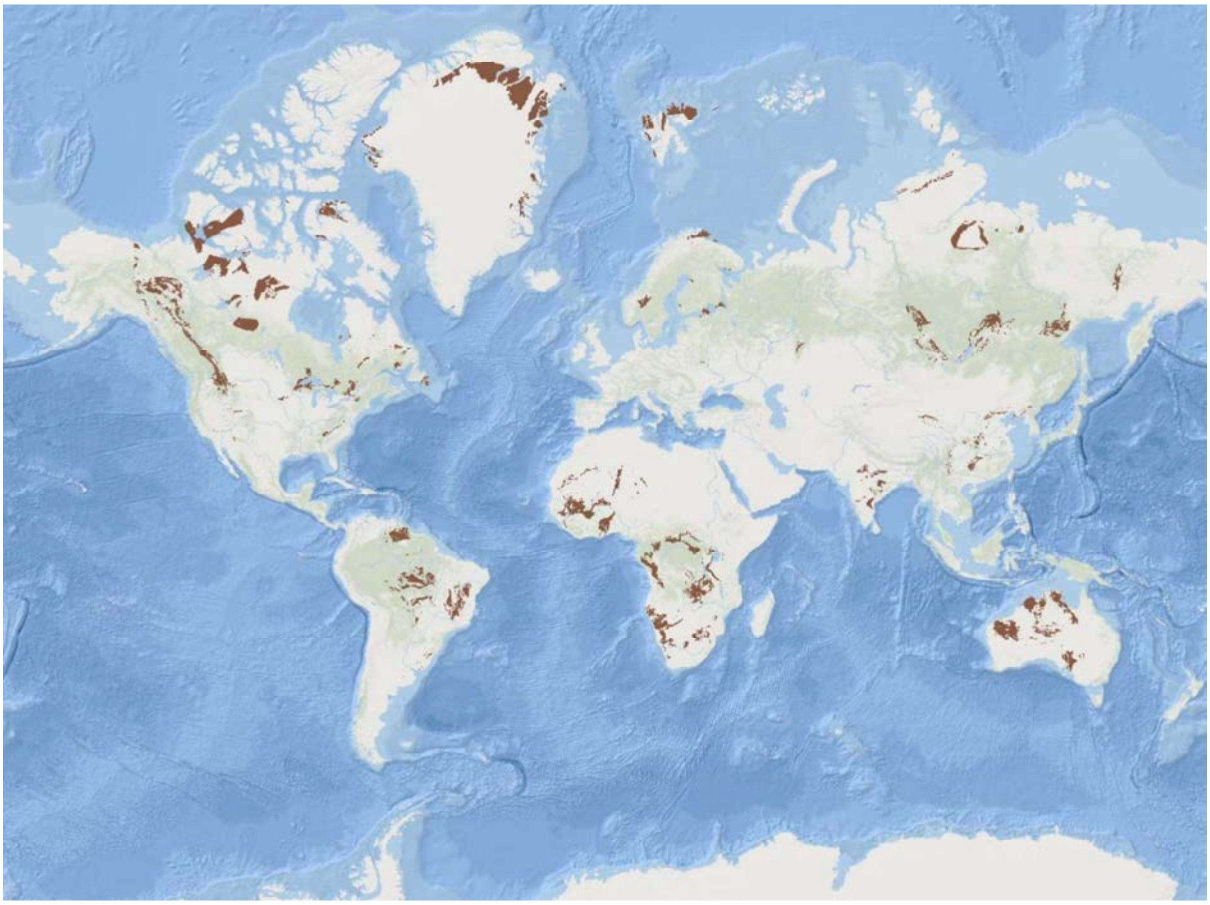

FIG. 5.25. Global distribution of Proterozoic basins representing potential targets for exploration for unconformity deposits.

5.8.1. Uranium deposit models

Exploration managers rely on uranium deposit models to guide their exploration programmes. Models are developed through the description and identification of characteristics such as tectonic settings, rock type, and the age of deposit formation, among other factors. Geochemical and geophysical signatures are also relied upon as exploration guides. Models are used as the basis for interpreting geological data collected during exploration programmes [5.34].

Dahlkamp [5.7] provides descriptive models of uranium deposits. His deposit classification scheme was combined with the IAEA uranium deposit classification scheme used for the 'Red Book' publication since 1991 [5.6]. The revised IAEA scheme depicts 15 types of uranium deposits that are known from around the world (Table 5.6).

As ore formation processes become understood through exploration practice and research, the descriptive models evolve into genetic models. Genetic models are created to explain the sources of mineralizing fluid sources, fluid transportation in the geosphere, and the trapping and preservation mechanisms that lead to economic ore concentrations.

Another way to understand ore deposits is through the mathematical distribution of their grade and tonnage characteristics. The economics of discovery can be evaluated through grade–tonnage plots. These plots can be used to understand the likelihood of discovering large or high-grade deposits and offers another way to evaluate investment worth.

The range of deposit models used in exploration is depicted in Fig. 5.26. Another framework is described by Cox and Singer along with some descriptions and examples [5.34]. Elements of the unconformity uranium deposit model are illustrated in Fig. 5.27 showing the relationship of uranium mineralization to lithologies, structure, and hydrothermal alteration.

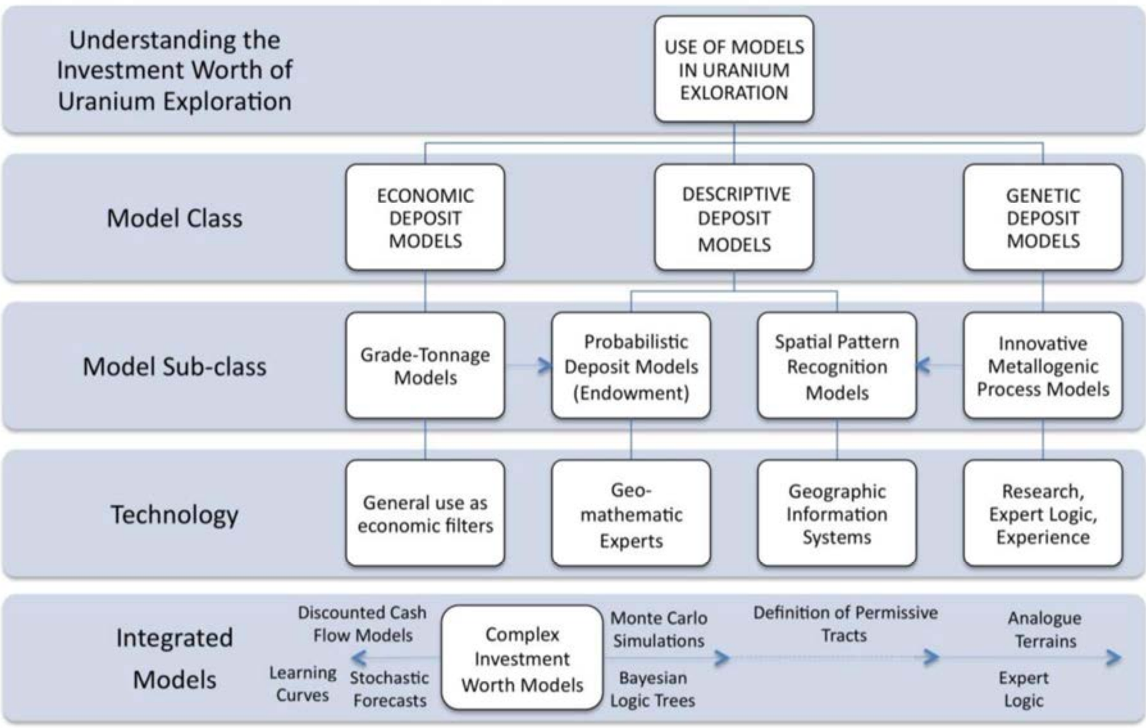

FIG. 5.26. Deposit models used in uranium exploration [5.1].

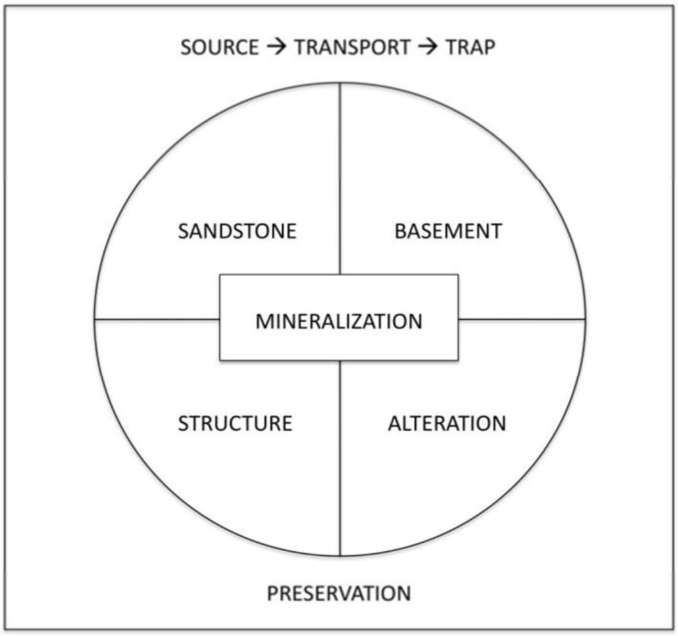

FIG. 5.27. Basic elements of the unconformity uranium deposit model.

The U.S. Geological Survey (USGS) provides an example of descriptive and grade–tonnage models for unconformity uranium–gold deposits [5.34]. Additional information about genetic models for uranium deposits can be found in publications by Cuney and Kyser [5.35, 5.36].

The demand for more reliable approaches for the assessment of the economic mineral potential of exploration areas has led to the development of probabilistic and spatial recognition models. These models rely upon specialists in mathematical geology and geographic information systems. Examples of spatial and quantitative models are presented in a report published by the IAEA [5.1]. The spatial models rely on data sets depicting topography, geology, geochemistry, geophysics, and drilling results and an understanding of deposit models.

An example of a quantitative investment worth model for unconformity uranium deposit exploration is presented by Harris et al. [5.24]. The comprehensive model estimates the economic value of an exploration programme, given exploration expenditure. The model relies on descriptive and genetic deposit models, grade–tonnage models, probability distributions and simulations, engineering costs estimates, stochastic price forecasts, and discounted cash flow and risk adjustment techniques, guided by expert judgements.

Adams and Cramer developed a data–process–criteria model for unconformity sandstone roll-type deposits [5.37]. This is a qualitative predictive model that can be used to identify exploration potential. It is based on the recognition of geological data, genetic processes and the criteria that are favourable for the occurrence of ore deposits. The model can be deployed at scales ranging from regional to local and identifies geological factors that are necessary for the occurrence of a deposit.

Fig. 5.28 illustrates the elements of a data–process–criteria model for Proterozoic unconformity deposits. These models can be used to assess the uranium potential of frontier environments. Such models are useful when spatial and other data are limited.

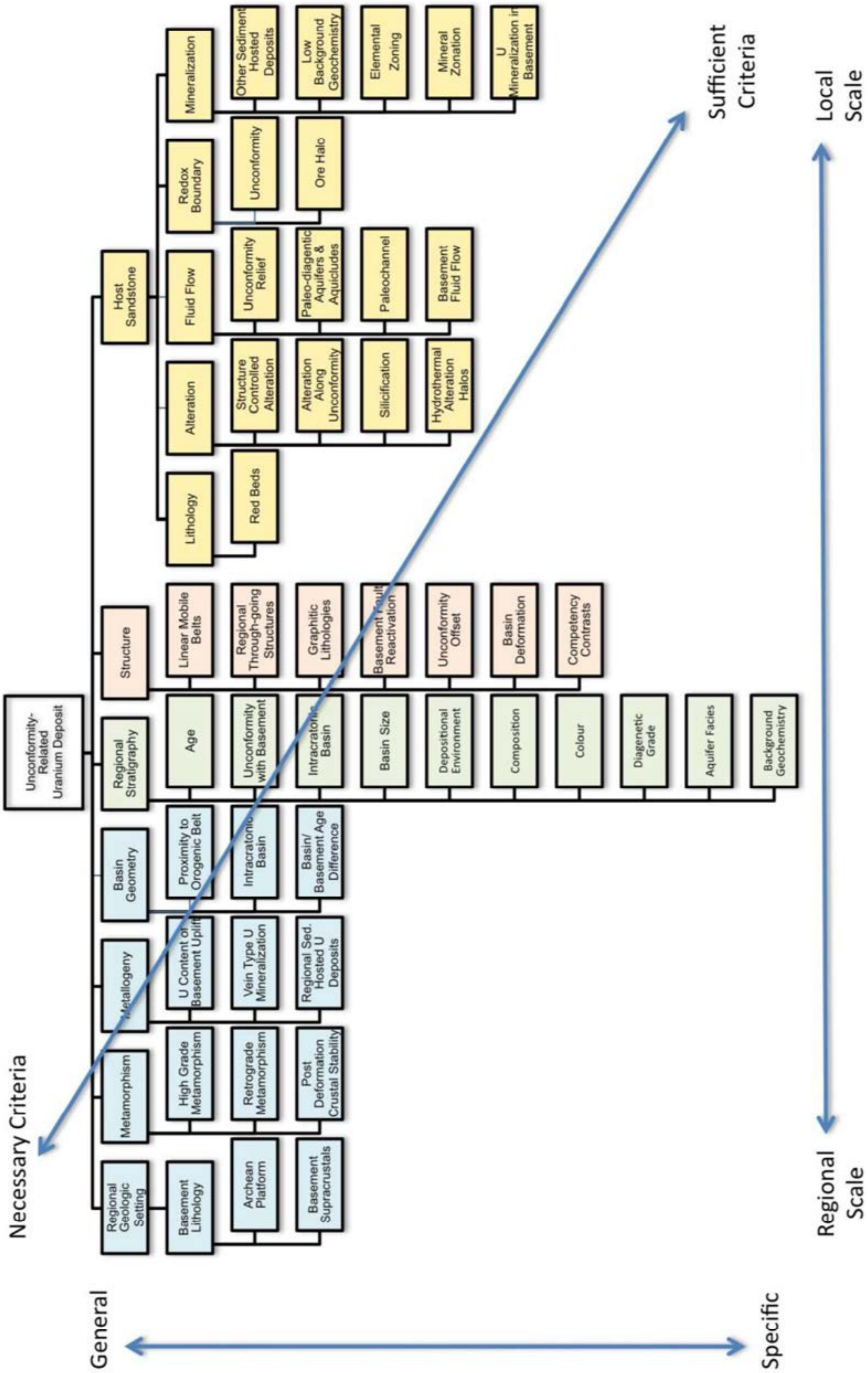

FIG. 5.28. Data-process-criteria model for unconformity uranium deposits.

5.8.2. Exploration frontiers

There are several types of exploration frontiers and they can be classified as geological, technological, depth-related, and data-related in nature (Table 5.4). The characteristics of the first three types of frontiers can be used to inform explorability, while the fourth informs prospectivity [5.1]. While the uranium potential of frontier exploration environments can be assessed, this may be particularly challenging when baseline data is unavailable and ore deposits have not yet been identified.

TABLE 5.4. EXPLORATION FRONTIER TYPES

Frontiers	Description	Example
Geographical	Exploration project areas are difficult to access and explore.	Working in remote equatorial rainforest or desert environments, with poor infrastructure and logistics.
Technological	Exploration targets are difficult to identify or resolve by existing exploration methods.	Geochemical haloes over economic unconformity uranium deposits may not be detectable at >1000 m.
Depth	Exploration targets are anticipated to be too deep and expensive to explore.	Drilling programme for targets >1000 m is too expensive and takes too long to complete.
Data	Data sets, reports and drill cores are not available to companies considering exploration investment.	Some geological survey organizations do not have adequate regional data and do not offer easy and low-cost access to historical data submitted by explorers.

An exploration project located in a *geographical frontier* such as a rainforest covered area that cannot be easily accessed by road, air, or foot, and characterized by limited bedrock exposure and dense vegetation cover can make geological mapping and sampling difficult. If 'classic' geochemical methods do not work, the same area could be classified as a *technological frontier*. Technology may also be limited if geophysical methods cannot resolve targets adequately because of poor contrasts in the physical properties of rocks associated with ore deposits based on models. Thick cover rocks may also indicate that the exploration area is too deep to explore in an economical fashion with exiting technology.

Mature exploration environments that host economic deposits can also encounter *depth frontiers* associated with increasing depths to targets. For example, geochemical and geophysical technologies cannot adequately resolve targets at depths in excess of 1000 m in the Athabasca Basin, Saskatchewan, Canada. Testing targets at these depths is too expensive and takes too much time. The technological and economic risks of potentially mining at greater and greater depths can negatively impact exploration investment decisions.

Exploration companies assess available geoscientific data when evaluating the prospectivity of a project area. This data can include regional geology maps, and topographic, cadastral, aeromagnetic, radiometric, gravimetric, and multi-element geochemical survey data. Some geological survey organizations organize this data so that it is easily available to exploration companies online. In some jurisdictions, it is a requirement for exploration companies to file activity reports to fulfil obligations set out in exploration permits.

There is a shortage of data in many parts of the world for explorers to examine. Geological survey organizations may not be adequately funded, or have not invested in the collection of regional data sets, data libraries, technical staff and infrastructure to promote and support investment in exploration. These situations can be classified as *data frontiers*. As a result, assessing the worth of investing in exploration in frontier project areas with limited data and limited or no discoveries can be challenging. In data-poor jurisdictions, quantitative models can be developed based on making analogies with other jurisdictions areas that yielded economic deposits [5.24]. However, the current use of these methods is not common. Innovative qualitative assessments can also be used in these settings.

Two approaches to assessing the investment worth of exploration in a frontier project environment characterized by limited data are presented in Fig. 5.29. The conventional approach in the frontier area involves an assessment of existing spatial data sets provided by geological survey organizations. This approach is fundamentally a pattern recognition exercise designed to identify areas that exhibit characteristics associated with deposits as defined from descriptive deposit models. Exploration programmes involve regional, local, and detailed geophysical, geochemical and geological survey programmes that lead to drilling programmes to test significant anomalies. Programmes for unconformity deposit exploration can typically last over four to five years, and can cost up to US $5 million. After a few drilling programmes, a decision to continue with, or abandon, the project is based upon the presence or absence of mineralizing signatures.

An alternative approach to evaluating a frontier area is to focus on a rapid qualitative assessment of economic uranium potential by relying on the knowledge of experts. This approach focuses on evaluating prospectivity through a holistic and evidence-based analysis of mineralizing potential. In addition, the identification and development of uranium exploration technologies that are best suited to the local geological environment are identified and developed. Collaborations with company geoscientists, consultants and applied academic researchers, are key to this process. The goal is the exchange of knowledge for better decision-making. Discussion around the critical questions for ore formation, the development of genetic deposit models, holistic prospectivity analysis, and the development of new technologies, are central to the collaborative effort.

The prospectivity of Proterozoic basins for their uranium deposit potential can be understood through holistic basin analysis. The analysis includes the assessment of palaeohydraulic systems during basin evolution. It involves the synthesis of information about the tectonic, sedimentological, stratigraphic, diagenetic, geochemical, geochronological, geophysical, and geological nature of the basin under assessment (Table 5.5) [5.38].

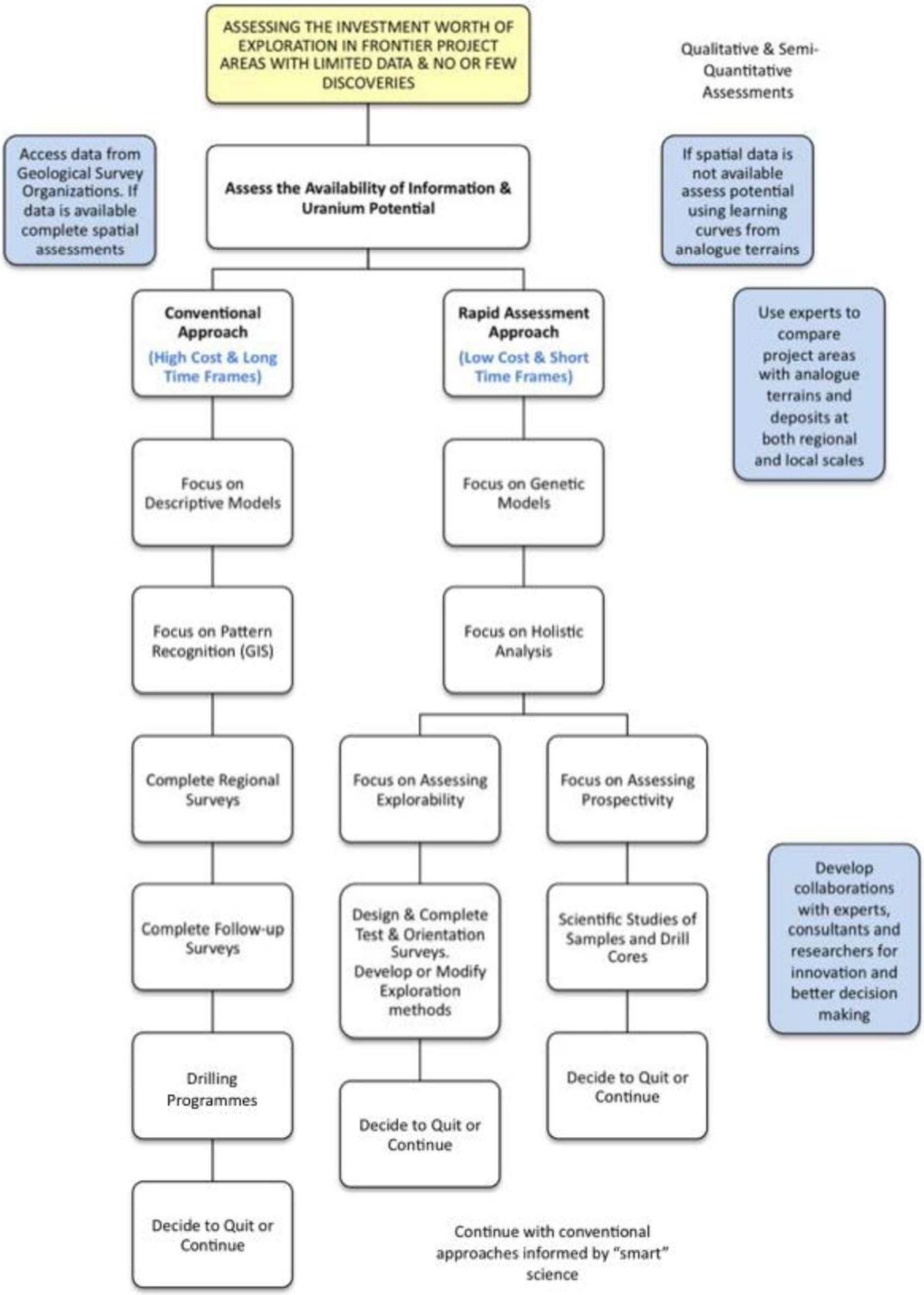

FIG. 5.29. A comparison of conventional and rapid approaches to assessing the investment worth of uranium exploration for unconformity deposits in frontier project areas with limited data [5.1].

TABLE 5.5. COMPONENTS OF HOLISTIC BASIN ANALYSIS USED TO ASSESS BASIN PROSECTIVITY [5.38]

Sub-discipline	Expected result
Tectonics	Structure, type and fluid flow mechanism of basin.
Sedimentology Stratigraphy	Characterizing lithofacies, sequences, sequence boundaries, location of possible palaeoaquifers, and possible metal sources.
Petrography	Identify detrital and authigenic phases, fluid inclusions, and paragenesis of diagenetic minerals and reactions.
Geochemistry	Constrain pressure, temperature, composition, origin and evolution of basin fluids and fluids associated with ore deposits.
Geochronology	Determine the timing of fluid events, and specify the critical time when deposits formed.
Modelling	Integrate all of the data to validate the processes involved.

Beyer et al. [5.39] present an example of the rapid assessment of the Roraima sandstone basin in Guyana through a holistic basin assessment. The exploration frontier is host to challenging logistics, geography, technology, target depth and a lack of baseline data. The collaborative exploration team consisted of an exploration manager, researchers, geophysical and geophysicists. The team assessed the uranium potential of the basin from the perspective of a holistic basin analysis, relying on expert judgement. They concluded that there was a low potential for uranium occurrences associated with the basin and that the technology to search for such deposits was not available due to excessive depth-to-target, and other reasons. The programme involved an expenditure of US $2 million over two to three years to reach a conclusion.

5.9. CONCLUSIONS

Uranium exploration is a high-risk high-reward business. The business drivers of exploration include uranium supply and demand, the sales price of uranium, and the capacity of companies to fund exploration programmes. The technical drivers of exploration include the selection of exploration targets based on an assessment of their prospectivity and explorability, and other risk factors.

Stakeholders involved in supporting uranium exploration include the IAEA, geological survey organizations, consultants, researchers, exploration service providers, and exploration company managers and workers.

Geological survey organizations can support the establishment of favourable business environments within their respective jurisdictions. They can provide access to pre-competitive geoscientific data that can be used by companies to assess the investment worth of exploration.Rapid and cost-effective approaches to identifying the potential for the discovery of uranium deposits in frontier project areas provide an alternative to more conventional approaches, which are more costly and time consuming.

5.10. REFERENCES

[5.1] INTERNATIONAL ATOMIC ENERGY AGENCY, Spatial and Quantitative Modelling of Undiscovered Uranium Resources, IAEA, Vienna (in preparation).

[5.2] ORGANISATION FOR ECONOMIC CO-OPERATION AND DEVELOPMENT/ NUCLEAR ENERGY AGENCY–INTERNATIONAL ATOMIC ENERGY AGENCY, Uranium 2014: Resources, Production and Demand, 2014 Red Book, NEA No. 7209 (2014) 504 pp.

[5.3] ORGANISATION FOR ECONOMIC CO-OPERATION AND DEVELOPMENT/ NUCLEAR ENERGY AGENCY–INTERNATIONAL ATOMIC ENERGY AGENCY, Uranium 2016: Resources, Production and Demand, 2016 Red Book, NEA No. 7301 (2016) 550 pp.

[5.4] INTERNATIONAL ATOMIC ENERGY AGENCY, The Nuclear Fuel Cycle, IAEA, Vienna (2011) https://www.iaea.org/sites/default/files/nfc0811.pdf.

[5.5] ORGANISATION FOR ECONOMIC CO-OPERATION AND DEVELOPMENT/ NUCLEAR ENERGY AGENCY, Forty Years of Uranium Resources, Production and Demand in Perspective, NEA, Paris (2006).

[5.6] INTERNATIONAL ATOMIC ENERGY AGENCY, World Distribution of Uranium Deposits, IAEA, Vienna (2016) https://infcis.iaea.org/UDEPO/About.cshtml.

[5.7] DALHKAMP, F., Uranium Deposit Models, Springer-Verlag, Berlin (1993) 460 pp.

[5.8] FAYEK, M., "Uranium ore deposits – a review," Uranium – Cradle to Grave (BURNS, P.C., SIGMON, G.E., Eds) Min. Assoc. Can. Short Course **43** (2013) 121–146.

[5.9] CARTER, N., "A market in transition," IAEA International Symposium on Uranium Raw Material for the Nuclear Fuel Cycle, Vienna (2014).

[5.10] BOYSTOV, A., "Worldwide ISL uranium mining outlook",International Symposium on Uranium Raw Material for the Nuclear Fuel Cycle , Vienna (2014).

[5.11] U.S. ENERGY INFORMATION ADMINISTRATION, 2015 Domestic Uranium Production Report, U.S. Department of Energy, Washington (2016) 15 pp.

[5.12] WORLD NUCLEAR ASSOCIATION, Uranium Market (updated February 2015), WNA (2015) http://www.world-nuclear.org/information-library/nuclear-fuel-cycle/uranium-resources/uranium-markets.aspx.

[5.13] TRANSPARENCY INTERNATIONAL, Corruptions Perceptions Index 2015, TI (2015) http://www.transparency.org/.

[5.14] JACKSON, T., GREEN, K., Annual Survey of Mining Companies, Fraser Institute, Toronto (2016).

[5.15] KYSER, T.K., "Exploration for uranium", Uranium for Nuclear Power (HORE-LACEY, I., Ed.) Woodhead, Swaston (2016) 468 pp.

[5.16] INTERNATIONAL ATOMIC ENERGY AGENCY, Uranium Exploration Planning and Practice, IAEA-TECDOC-583, IAEA,Vienna (1991).

[5.17] SMITH, A., TAUCHID, M., "Uranium exploration planning and practice", Uranium Exploration Planning and Strategy, IAEA-TECDOC-583, IAEA, Vienna (1991).

[5.18] CANADIAN INSTITUTE OF MINING AND METALLURGY, Survey of Principal Mining Risks, CIMM, Toronto (2000).

[5.19] MCKAY, A., MIEZITIS, Y., Australia's Uranium Resources, Geology and Development of Deposits, – Geosc. Austral. (2001) 184 pp.

[5.20] POOL, T.C., "Uranium supply to 2060", IAEA International Symposium on Uranium Raw Material for the Nuclear Fuel Cycle , IAEA, Vienna (2014).

[5.21] MARLATT, J., KYSER, T.K. Paradigmatic shifts in the uranium exploration process: knowledge brokers and the Athabasca learning curve, Soc. Econ. Geol. News. **84** (2011) 1.
[5.22] CRANSTONE, D., WHILLANS, R., "The analysis of uranium discovery in Canada, 1930–1983: rates of discovery, exploration expenditures, discovery costs and geological deposit types", Uranium Resources and Geology of North America, IAEA-TECDOC-500, IAEA, Vienna (1989).
[5.23] MACDONALD, C., Uranium: Sustainable Resource or Limit to Growth? Proc. Symp. WNA 2003, World Nuclear Association, London (2003).
[5.24] HARRIS, D., ZALUSKI, G., MARLATT, J., A method for the selection of exploration areas for unconformity uranium deposits, Nat. Res. Research (2009).
[5.25] AUSTRALIAN BUREAU OF STATISTICS, Mineral and Petroleum Exploration, Statistics Report 8412.0, ABS, Australia (2015).
[5.26] SMITH, L., "Discounted cash flow analysis methodology and discount rates, mineral valuation proceedings", Mining Millenium 2000 Symposium, Canadian Institute of Mining, Metallurgy and Petroleum, Toronto (2000).
[5.27] THE PRS GROUP INC., Country Risk, International Country Risk Guide, XXI, 9, (2001).
[5.28] CENTER FOR STRATEGIC AND INTERNATONAL STUDIES, High Country Risk Definition (2012) http://www.csis.org/energy/ga120601mamae/sld004.htm.
[5.29] INTERNATIONAL ATOMIC ENERGY AGENCY, Advances in Airborne and Ground Geophysical Methods of Uranium Exploration, IAEA Nuclear Energy Series No. NF-T-1.5, IAEA Vienna (2013).
[5.30] INTERNATIONAL ATOMIC ENERGY AGENCY, Proterozoic Unconformity and Stratabound Uranium Deposits, IAEA, Vienna, (1984).
[5.31] INTERNATIONAL ATOMIC ENERGY AGENCY, Uranium Resources and Geology of North America, IAEA Vienna, (1989).
[5.32] NUCLEAR ENERGY AGENCY, OECD, World Uranium Geology and Resource Potential, Miller Freeman, San Francisco (1980) 524 pp.
[5.33] INTERNATIONAL ATOMIC ENERGY AGENCY, Uranium in the Pine Creek Geosyncline, IAEA, Vienna (1980).
[5.34] COX, D., SINGER, D., Mineral Deposit Models, U.S. Geological Survey Bulletin 1693, United States Government Printing Office, Washington (1992).
[5.35] CUNEY, M., "Geology of uranium deposits", Uranium for Nuclear Power (HORE-LACEY, I., Ed.), Woodhead, Swatson (2016) 468 pp.
[5.36] CUNEY, M., KYSER, T.K., (Eds) Recent and Not-So-Recent Developments in Uranium Deposits and Implications for Exploration, Min. Assoc. Can. Short Course **39** (2009) 258 pp.
[5.37] ADAMS, S.S., CRAMER, R.T., "Data-process-criteria model for roll-front deposits", Geological Environments for Sandstone Uranium Deposits, IAEA, Vienna (1985) 383–400.
[5.38] KYSER, T.K., Fluids, basin analysis, and mineral deposits, Geofluids **7** (2007) 238.
[5.39] BEYER, S., HIATT, E., KYSER, K., DREVER, G., MARLATT, J., Stratigraphy, diagenesis and geological evolution of the Palaeoproterozoic Roraima Basin, Guyana: links to tectonic events on the Amazon Craton and assessment for uranium mineralization, Precam. Res. **267** (2015) 227.

6. OVERALL CONCLUSIONS

1) Unconformity-related uranium deposits are a significant source of uranium because ores are both high grade and have among the largest global uranium inventories. These characteristics make these deposits a highly strategic resource, especially given the minimal environmental impact and relatively economical mining cost compared to many other deposit types;
2) Empirical parameters tabulated from a global inventory of Proterozoic unconformity-related uranium deposits illustrate the variability of geometric and geological attributes that characterize the deposits' footprints. Nevertheless, a number of generalizations can be made in terms of the variations in geological settings and geometric attributes observed (e.g. basement, unconformity-contact, wedge-type settings), resource size and grades (e.g. high, moderate, low grade; large, moderate, small resource size), size of associated alteration envelop relative to the ore body and styles of mineralization (e.g. broad versus narrow), and the spatial relationship to mineralization controlling structures (e.g. footwall, hanging wall, amount of unconformity offset). Based on the variability of lithostructural attributes of the deposit footprints, a classification was developed around four representative end members from the Athabasca Basin, the type area for unconformity-related uranium deposits; Cigar Lake, McArthur River, Eagle Point, and Millennium deposits. The proposed tetragonal based classification captures the range of structural settings represented by deposits (e.g. basement, unconformity-contact, structural wedge), the characteristic alteration footprints (e.g. extensive and broad halos versus tight and narrow halos), the variability in relative grade and resource size (e.g. high grade-large resource, low grade-large resource, or moderate grade-moderate resource). Other aspects captured as a corollary of the classification and background data are the geometric shape and 3-D orientation of the orebody footprints (e.g. cylindrical, tabular, prismatic versus horizontal, vertical or inclined). The intent of this classification is that it will better assist and guide exploration teams in developing targeting strategies for Proterozoic unconformity associated uranium mineralization, not only in those basins with identified deposits, but in under-explored basins elsewhere in the world;
3) There are numerous uranium deposits worldwide that were classified as unconformity-related in the literature, largely because they are located at or near an unconformity between basement rocks and basin fill. However, many of these deposits do not share the main physiochemical and geological characteristics that are typical of the classical, Proterozoic unconformity-related uranium deposits from Canada and Australia (e.g. 200°C, basinal brine fluids at pressures of ~5 kbars). The classification of an ore occurrence as unconformity-related in some cases has been rather broadly and liberally applied, therefore some deposits designated as unconformity-related are better interpreted as a different uranium model type;
4) Advances in technology will provide rapid and cost-effective approaches to identifying the potential for the discovery of uranium deposits in frontier project areas. These methods will eventually replace more conventional approaches, which are costlier and time consuming. However, a successful exploration programme will always require a combination of geotechnical surveys that are tailored to the geography and geology of the area of interest. These surveys include geophysics, geochemistry, and lithological mapping techniques, and can lead to the discovery of deposits at increasing depth;
5) Uranium exploration is a high-risk, high-reward business. The business drivers of exploration include uranium supply and demand, the sale price of uranium, and the capacity of companies to fund exploration programmes. The technical drivers of

exploration include the selection of exploration targets based on an assessment of their prospectivity and explorability, and other risk factors. Uranium exploration is usually initiated by private sector companies, although other stakeholders including the IAEA (e.g. this publication), geological surveys and academia can provide access to pre-competitive geoscientific data, such as maps, geophysical surveys, geochemical data sets, and local expertise that can be used by companies to assess their exploration investments.

ABBREVIATIONS

APS	aluminum phosphate sulphate mineral
AEM	airborne electromagnetic
AMT	Audio magnetotellurics
ASL	Above Sea Level
cm	centimetre
CSAMT	controlled source audiomagnetotellurics
1-D	one dimensional
2-D	two dimensional
3-D	three dimensional
D_1	first deformation phase
D_2	second deformation phase
D_3	third deformation phase
D_4	fourth deformation phase
D_5	fifth deformation phase
D_6	sixth deformation phase
DC	direct current
DCIP	direct current induced polarization
det.	detection
DHEM	downhole electromagnetic
DRC	Democratic Republic of Congo
EM	electromagnetic
E	east
EIC	Electret Ion Chamber
EM	electromagnetic
EMP	electron microprobe
ENE	east-northeast
EW	east-west
fO2	oxygen fugacity
Gal	United States gallon
GMCL	Gulf Mineral Resources Company
GPS	Global Positioning System
GPR	ground penetrating radar
Gzz	rate of change of vertical gravity (gz) with height (z)
Hz	hertz
HREE	heavy rare earth elements
IAEA	International Atomic Energy Agency
ICP-MS	Inductively coupled plasma mass spectrometry
ICP-OES	Inductively coupled plasma - optical emission spectrometry
ID-TIMS	isotope dilution thermal ionization mass spectrometry
INPUT	Induced Pulse Transient System
IP	induced polarization
KALST	Kiggavik-Andrew Lake structural trend
km	kilometre
km/hr	kilometre per hour
km^2	square kilometre
L	litre
LA-HR-ICP-MS	Laser Ablation High-Resolution Inductively Coupled Plasma Mass Spectrometry

LA-ICP-MS	Laser Ablation Inductively Coupled Mass Spectrometry
LA-MC-ICP-MS	Laser Ablation Multiple Collector Inductively Coupled Plasma Mass Spectrometry
LIBS	Laser Induced Breakdown Spectroscopy
Lw	Liquid-vapor aqueous fluid inclusions
Lwh	Liquid-vapor aqueous fluid inclusions containing halite crystals
LREE	light rare earth elements
m	metre
Ma	million years
MDLs	Minimum Detection Limits
MF	Manitou Falls Formation
MFc	Collins Member of the Manitou Falls Formation
MFd	Dunlop Member of the Manitou Falls Formation
m/s	metre per second
MT	magnetotellurics
N	north
NCO	New Continental Oil Company of Canada Ltd.
NE	northeast
nm	nanometre
NE	northeast
NNE	north-northeast
NNW	north-northwest
NS	north-south
NW	northwest
ppm	part per million
ppb	part per billion
RC	reverse circulation
REE	Rare Earth Elements
RTP	Reduction to the magnetic pole
S	south
SIMS	secondary ion mass spectrometer
SEM	scanning electron microscope
SE	southeast
SW	south west
SWIR	Short-Wave Infrared Reflectance
SWIR	short-wave infrared radiation
TAMT	transient audio magnetotellurics
TEM	Transient electromagnetic
VNIR	visible/near-infrared
S_0	lithologic layering
S_1	first planar fabric
S_{1g}	first planar fabric, gneissic
S_2	second planar fabric
S_3	third planar fabric
S_4	fourth planar fabric
SW	southwest
tU	tonnes of uranium
TDEM	time-domain electromagnetic
VLF	very-low-frequency

W	west
wt%	weight percent
XRD	X-ray diffraction
XRF	X-ray florescence
UEM	Uranerz Exploration and Mining Ltd.
UTEM	University of Toronto TDEM System
VLF	very low frequency
WNW	west-northwest
ZTEM	Z-Axis Tipper Electromagnetic

CONTRIBUTORS TO DRAFTING AND REVIEW

Aubin, A.	Cameco Corporation, Canada
Bissett, A.	Consultant, Australia
Cuney, M.	Consultant, France
Hanly, A.	International Atomic Energy Agency
Fayek, M.	University of Manitoba, Canada
Kyser, K.	Queen's University, Canada
Ledru, P	Orano, Canada
Marlatt, J.	Consultant, Canada
Robbins, J.	Orano, Canada
Quirt, D.	Orano, Canada
Thomas, D.	Cameco Corporation, Canada

Consultants Meetings

Vienna, Austria: 2 October 2015; 12-15 December 2016; 4–7 December 2017
Saskatoon, Canada: 17-20 July 2017

IAEA
International Atomic Energy Agency

No. 25

ORDERING LOCALLY

In the following countries, IAEA priced publications may be purchased from the sources listed below or from major local booksellers.

Orders for unpriced publications should be made directly to the IAEA. The contact details are given at the end of this list.

CANADA

Renouf Publishing Co. Ltd

22-1010 Polytek Street, Ottawa, ON K1J 9J1, CANADA
Telephone: +1 613 745 2665 • Fax: +1 643 745 7660
Email: order@renoufbooks.com • Web site: www.renoufbooks.com

Bernan / Rowman & Littlefield

15200 NBN Way, Blue Ridge Summit, PA 17214, USA
Tel: +1 800 462 6420 • Fax: +1 800 338 4550
Email: orders@rowman.com Web site: www.rowman.com/bernan

CZECH REPUBLIC

Suweco CZ, s.r.o.

Sestupná 153/11, 162 00 Prague 6, CZECH REPUBLIC
Telephone: +420 242 459 205 • Fax: +420 284 821 646
Email: nakup@suweco.cz • Web site: www.suweco.cz

FRANCE

Form-Edit

5 rue Janssen, PO Box 25, 75921 Paris CEDEX, FRANCE
Telephone: +33 1 42 01 49 49 • Fax: +33 1 42 01 90 90
Email: formedit@formedit.fr • Web site: www.form-edit.com

GERMANY

Goethe Buchhandlung Teubig GmbH

Schweitzer Fachinformationen
Willstätterstrasse 15, 40549 Düsseldorf, GERMANY
Telephone: +49 (0) 211 49 874 015 • Fax: +49 (0) 211 49 874 28
Email: kundenbetreuung.goethe@schweitzer-online.de • Web site: www.goethebuch.de

INDIA

Allied Publishers

1st Floor, Dubash House, 15, J.N. Heredi Marg, Ballard Estate, Mumbai 400001, INDIA
Telephone: +91 22 4212 6930/31/69 • Fax: +91 22 2261 7928
Email: alliedpl@vsnl.com • Web site: www.alliedpublishers.com

Bookwell

3/79 Nirankari, Delhi 110009, INDIA
Telephone: +91 11 2760 1283/4536
Email: bkwell@nde.vsnl.net.in • Web site: www.bookwellindia.com

ITALY

Libreria Scientifica "AEIOU"

Via Vincenzo Maria Coronelli 6, 20146 Milan, ITALY
Telephone: +39 02 48 95 45 52 • Fax: +39 02 48 95 45 48
Email: info@libreriaaeiou.eu • Web site: www.libreriaaeiou.eu

JAPAN

Maruzen-Yushodo Co., Ltd

10-10 Yotsuyasakamachi, Shinjuku-ku, Tokyo 160-0002, JAPAN
Telephone: +81 3 4335 9312 • Fax: +81 3 4335 9364
Email: bookimport@maruzen.co.jp • Web site: www.maruzen.co.jp

RUSSIAN FEDERATION

Scientific and Engineering Centre for Nuclear and Radiation Safety

107140, Moscow, Malaya Krasnoselskaya st. 2/8, bld. 5, RUSSIAN FEDERATION
Telephone: +7 499 264 00 03 • Fax: +7 499 264 28 59
Email: secnrs@secnrs.ru • Web site: www.secnrs.ru

UNITED STATES OF AMERICA

Bernan / Rowman & Littlefield

15200 NBN Way, Blue Ridge Summit, PA 17214, USA
Tel: +1 800 462 6420 • Fax: +1 800 338 4550
Email: orders@rowman.com • Web site: www.rowman.com/bernan

Renouf Publishing Co. Ltd

812 Proctor Avenue, Ogdensburg, NY 13669-2205, USA
Telephone: +1 888 551 7470 • Fax: +1 888 551 7471
Email: orders@renoufbooks.com • Web site: www.renoufbooks.com

Orders for both priced and unpriced publications may be addressed directly to:

Marketing and Sales Unit
International Atomic Energy Agency
Vienna International Centre, PO Box 100, 1400 Vienna, Austria
Telephone: +43 1 2600 22529 or 22530 • Fax: +43 1 2600 29302 or +43 1 26007 22529
Email: sales.publications@iaea.org • Web site: www.iaea.org/books

18-04121

International Atomic Energy Agency
Vienna
ISBN 978–92–0–92–0–108518–4
ISSN 1011–4289